University of Nottingham
UK | CHINA | MALAYSIA

CLIC1 and CLIC4 ion channels as therapeutic targets for tumour treating fields in paediatric high-grade glioma.

Michaela Louise Griffin
BSc(hons), MRes

Thesis submitted to the University of Nottingham for the degree of Doctor of Philosophy
April 2023

Declaration

I confirm that the work presented in this thesis is my own work except where stated in the text. The material and figures included in Sections 1.4 and 3.3 draw heavily on my previously published literature review (Griffin et al., 2020) and are presented in line with the article reuse permissions policies of MDPI journals. I understand the nature of plagiarism and that it is a serious academic offence. I confirm that no material in this project has been plagiarised.

Name: Michaela Louise Griffin

Signed: 

Date: 13th April 2023

Abstract

Background: The lack of treatments for paediatric high-grade glioma represents one of the most significant unmet clinical needs in paediatric cancers. pHGGs form a subset of lethal brain tumours with a median overall survival of only 14 months; forming the leading cause of CNS cancer-related death in children. Optune™, a non-invasive electrotherapy device that delivers alternating electric fields – coined tumour treating fields (TTFields) – into the tumour. Despite success in adult trials, TTFields treatment is currently not approved in the paediatric population. Increasing evidence show that ion channels not only regulate electrical signalling of excitable cells, but also play a pivotal role in the development and progression of brain tumours. Membrane potential is a crucial biophysical signal that modulates the malignant processes via a plethora of tightly controlled ionic exchange processes. We aim to identify potential targets for TTFields and provide a proof-of-principle to elucidate the role of ion channels for multimodal therapies for paediatric high-grade gliomas.

Methods: Widescale literature and genomic analysis of adult and paediatric HGG tissue was used to characterised CLIC channel expression via multivariate analysis. To understand the functional role of CLIC1 and CLIC4, siRNA depletion, or pharmacological targeting via IAA94/metformin was assessed using cell cycle, clonogenic, invasion and proliferation assays. The potential for multimodal therapies was interrogated by combining *in vitro* TTFields with CLIC inhibition. Whole cell and cell attached patch clamp protocols, along with Cl- ion tracking was used to assess ion channel activity in pHGG and normal astrocytes. To build a global understanding of TTFields and HGG recurrence, 3’ mRNA sequencing was carried out across three recurrent tumours following TTFields treatment.

Results: We have demonstrated an elevated expression of CLIC1 and CLIC4 in HGG, which

is significantly associated with poor overall survival in patient cohorts. siRNA/pharmacological depletion of CLIC1 or CLIC4 propagates a reduction in the proliferation and invasion of pHGG associated with cell cycle arrest. Furthermore, combination of CLIC inhibition and TTFields revealed that CLIC1 and CLIC4 deficiency exacerbated the killing capacity of TTFields, and sufficiently re-sensitised TTFields tolerant cells. Furthermore, electrophysiology experiments reveal increasingly depolarised membrane potential in pHGG compared to astrocytes. RNA sequencing of recurrent GBM tissues revealed that *in situ* TTFields treatment is indeed associated with decreased CLIC1 and CLIC4 expression. Moreover, *in vivo* TTFields exposure is associated with a downregulation in DNA repair and increase neurodegenerative pathways.

Conclusions: This study characterised CLIC1 and CLIC4 expression in pHGG, finding they have clear implications in HGG and are prognostic indicators for OS of patients. We provide evidence that CLIC channels provide mechanistic insight into TTFields success. These data provide rationale that genetic, electrical, and pharmacological manipulation of ion channels can reduce the capacity of pHGGs to proliferate and invade and that CLIC channels may be a suitable target for combination therapy to enhance the treatment efficacy of TTFields.

Acknowledgements

This PhD has been the most challenging yet rewarding experience of my life. I have truly loved my PhD and I am so grateful that I have been able to spend the last 3 years researching something that I am so passionate about. To everyone who has contributed to making this experience so incredible, thank you.

Firstly, I'd like to extend my gratitude to my supervisors Dr Stuart Smith and Prof Raheela Khan for their support, advice, and guidance throughout this project. A particular thank you to Stuart for allowing me to work independently as a researcher, and for providing invaluable patient samples. To Dr Paul Smith, thank you for saving the day with the electrophysiology!

Secondly, I'd like to thank everyone in the CBTRC, I am incredibly privileged to have worked within such a highly skilled and wonderful research group. A particular thank you to Phoebe, Louisa, Alina, Harry, and Louise. Your friendship, support and encouragement has meant the world to me.

To the 'BDI babes' Eva, Kathryn, Zarah, Grace and George. Thank you for always brightening my day and providing me with sufficient beverage breaks, be it coffee or wine.

To Pippa and James, my PhD would not have been what it is without you; I have gained two wonderful lifelong friends and I am so lucky to have met you both. Thank you for keeping me grounded, the endless laughs and the constant reassurance. I am sure none of the maths in my project would be right without you.

Next, I would like to thank my amazing family, specifically my dad, my grandparents and my incredible sisters Laura, Kirstie, and Ava. There is no doubt in my mind that I would not be where I am without you all. Thank you for the constant love and support, comedic breaks,

and all-round Griffin craziness. I cannot put into words how much I value you all. I hope to make you as proud of me as I am of all of you.

Finally, to my incredible partner Cameron. Thank you for always allowing me to chase my dreams and being a never-ending source of love and encouragement. Thank you for always believing in me, especially when I did not believe in myself.

Dedications

I dedicate this thesis to all of the patients and families that have been affected by brain tumours, without your bravery and selflessness, this project would not have been possible.

Most importantly, I dedicate this thesis to my amazing mum, Wendy Griffin, who sadly died from a brain tumour in December 2020. You have been and will always be my biggest motivator, my constant source of love and my best friend. You are the driving force behind my ambition and my dedication, and this work is a product of the love and encouragement I received from you throughout my life. You helped me to believe that I am capable of anything I put my mind to. I am so proud to have been able to research brain tumours in your honour, and I will continue in this fight, because this fight is personal**.**

Table of Contents

List of Figures

List of Tables

List of common Abbreviations

aHGG	Adult high-grade glioma
ANOVA	Analysis of variance
BBB	Blood brain barrier
cDNA	Complimentary DN
CLIC1	Chloride intracellular channel 1
CLIC4	Chloride intracellular channel 4
CNS	Central nervous system
DDR	DNA damage repair
DNA	Deoxyribonucleic acid
EGFR	Epidermal growth factor receptor
EMT	Epithelial to mesenchymal transition
FDR	False discovery rate
GBM	Glioblastoma multiforme
GCE	Primary cells derived from the GBM core
GIN	Primary cells derived from the GBM invasive edge
GLUT	Glucose transporter
IAA94	Indanyloxyacetic acid-94
ICG	Ion channel gene
IC50	half-maximal inhibitory concentration
IDH	Isocitrate dehydrogenase
IHC	Immunohistochemical
KEGG	Kyoto encyclopaedia of genes and genomes
KD	Knock down
LGG	Low-grade glioma
MAPK	Mitogen-activated protein kinases
MGMT	O-6-methylguanine-DNA methyltransferase
MMP	Matrix metalloproteinase
mTor	Mechanistic target of rapamycin kinase
NGS	Normal goat serum
NT	Non-targeting
O/S	Overall survival
PCA	Principal component analysis
PCR	Polymerase chain reaction
PET	Positron emission tomography
PFS	Progression free survival
pHGG	Paediatric high-grade glioma
PI3K	Phosphatidylinositol 3-kinase
PTEN	Phosphatase and tensin-homolog
QC	Quality control
RNA	Ribonucleic acid
ROS	Reactive oxygen species
siRNA	Small interfering RNA
TMA	Tissue microarray
TMZ	Temozolomide
VEGF	Vascular endothelial growth factor
WHO	World health organisation
WT	Wildtype

1 Introduction

1.1 Childhood cancer

Childhood cancers are rare; around 1600 cases of paediatric (0-14 years) cancers are diagnosed every year in the UK (1,2). This accounts for 0.5% of all annual cancer diagnoses, representing the lowest childhood cancer rate in Europe and amongst the lowest of industrialised Western countries (3). Comparatively, the US and Australia have some of the highest rates. In the UK, around 250 children lose their lives to cancer each year, and an estimated 50 young adults (15-19 years) die from cancers that are diagnosed in childhood (4).

1.1.1 Paediatric Brain Tumours

Tumours forming in the central nervous system (CNS) are the second most common neoplasm found in paediatric patients - second only to leukaemia (3)- and represent the most common solid tumour type (4). Unlike the diagnosis, management and treatment of adult brain tumours, there are radical implications for treatment and diagnosis methods in children. Brain tumours such as high-grade gliomas (HGG) claim more paediatric lives than any other type of cancer, yet there has been little to no advancements in treatment of this disease (5), often due to the lack of progressive treatments. These treatment boundaries arise due to the sensitive nature of the developing brain, potential toxicities, and long-term effects of mainstay therapies (6,7). Every effort is made to preserve neurocognitive function whilst ensuring that maximum treatment consequence is reached; despite this, 60% of survivors are left with pronounced disability (8). These secondary effects are often as a direct result of treatments such as radiotherapy, and as such, it is standard for

radiotherapy omission in patients less than 3 years old (9). Nonetheless, radiotherapy remains a critical element of the therapeutic strategy for brain tumours and is undergoing constant re-evaluation alongside targeted therapies (9). There are more than 120 recognised subtypes of brain and CNS malignancies, all of which have unique characteristics (CRUK, 2022), varying outcomes and distinct pathologies.

Research has claimed that paediatric brain tumours arise as a product of embryological mutations, with clear corelation to both age and neuroanatomical location (10). Despite this, there is no known cause for the majority of paediatric brain tumours with most occurring sporadically. Even so, a small percentage of paediatric brain tumours have been associated with genetic and developmental syndromes that arise from germline mutations (11). For example, several familial mutations cancer predispositions syndromes have been associated with brain tumours, such as Turcot's syndrome, Li-Fraumeni syndrome and neurofibromatosis (12,13). In these syndromes, a germline mutation in a tumour suppressor gene is inherited, and upon silencing or mutation of the remaining copy tumour are established. Table 1.1 details the known brain tumour susceptibility diseases and syndromes (13).

Table 1.1 Brain tumour susceptibility syndromes and their associated mutations. Description of brain tumour disorders with gene location, and associated resulting tumour (Adapted from Ostrom et al., 2019 (13))

Gene (chromosome location)	Disorder/Syndrome	Mode of Inheritance	Associated Brain Tumours
APC, MMR (5q21)	Familial adenomatous polyposis, Turcot's syndrome type 2	Dominant	Medulloblastoma, glioma
ATM (11q22.3)	Ataxia-telangiectasia	Autosomal recessive trait	Astrocytoma and medulloblastoma
CDKN2A (9p21.3)	Melanoma-neural system tumour syndrome	Dominant	Glioma
IDH1/IDH2 (2q33.3/15q26.1)	Ollier disease	Dominant with reduced penetrance	Glioma
MLH1, PMS2	Turcot's syndrome type 1	Autosomal recessive trait	Medulloblastoma, glioma,
MSH2,MLH1,MSH6,PMS2	Lynch syndrome, biallelic mismatch repair deficiency, constitutional MMR *deficiency*	Dominant	Glioblastoma, other gliomas
MSH2,MLH1,MSH6,PMS2	Mismatch repair deficiency syndrome	Recessive	Glioma
NF1 (17q11.2)	Neurofibromatosis 1 (NF1)	Dominant	Astrocytoma, schwannomas, optic nerve glioma
NF2 (22q12.2)	Neurofibromatosis 2 (NF2)	Dominant	Acoustic neuromas, meningiomas, Ependymoma
RB1 (13q14)	Retinoblastoma	Dominant	Retinoblastoma, Pineoblastoma, Malignant glioma
TP53 (17p13.1)	Li–Fraumeni syndrome	Dominant	Glioblastoma, other gliomas
TSC1,TSC2 (9q34.14,16p13.3)	Tuberous sclerosis (TSC)	Dominant	Giant cell astrocytoma

As such, through these brain tumour predisposition syndromes, many pathways are implicated. Mutations in checkpoint genes such as *CHECK2* and *TP53* are the drivers in Li-Fraumeni syndrome, whereas aberrant DNA repair mechanisms due to mutations in DNA repair genes are responsible for Turcot's syndrome (13,14). Furthermore, pathways associated with the promotion of growth signalling are associated with tuberous sclerosis and neurofibromatosis, leading to aberrant transduction pathways and likely priming cells for excessive growth. This risk is elevated in paediatric brain cells due to increase growth kinetics.

Paediatric tumours can be classified by location into two subsets: infra and supratentorial tumours (5), with tumours forming in the supratentorial region informing poorer cognitive function. Brain tumour subtypes are often limited to specific neuroanatomical regions as demonstrated in figure 1.1. The prognosis of CNS tumours can depend on a multitude of factors including histological type, age at presentation and extent of surgical resection – with this being a main predictor of outcome and survival (15,16). Advancements in molecular biology, imaging, neurosurgical techniques, and genetic analysis correlate with an increasing number of paediatric brain tumours being diagnosed at an earlier stage, as well as improved classification for subgrouping, with targeted therapies becoming an option (17). As a result, the 5-year survival of children with brain tumours in the UK is now 75%, amongst the highest globally, but varied greatly, with tumours such as DIPG and HGG having dismal survival rates (NCRAS, 2020). Owing to the variability of symptoms, and relative rarity of paediatric brain tumours, the diagnoses of CNS tumours is often delayed, affecting treatment options and ultimately, the prognosis of these tumours (8,18).

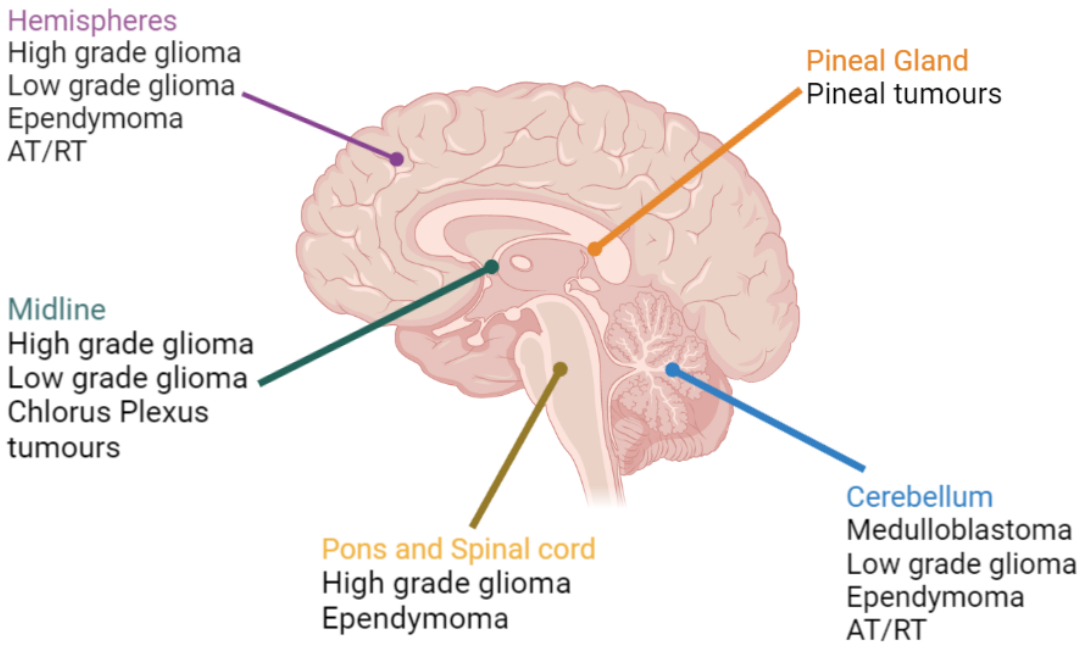

Figure 1.1 Common paediatric brain tumours and their neuroanatomical regions. The hemispheres of the brain commonly harbour high- and low-grade gliomas, ependymoma, AT/RT tumours. The Pineal gland is associated with pineal tumours, whereas medulloblastoma occurs in the cerebellum along with low grade gliomas, ependymomas and AT/RT.

1.1.1.1 Paediatric High-Grade Gliomas

Gliomas arise from their glial precursor cells of both the brain and the spinal cord (19). Glial cells include oligodendrocytes, astrocytes, ependymal cells, Schwann cells, microglia, and satellite cells – all of which have known related malignancies (20–22). These glial neoplasms encompass a sizable group of tumours that range in histological and clinicopathologic subtype (5) and make up over 50% of all paediatric CNS tumours. Gliomas are classified as low grade (WHO grade I/II) and high grade (WHO grade III/IV); glioblastoma (multiforme) is an aggressive malignant tumour, classified as WHO grade IV astrocytoma. During this project, the WHO 2021 CNS5 classification of CNS tumours was released, featuring substantial changes to enhance the role of molecular diagnostics in CNS tumours. As such, the previously known entity, paediatric glioblastoma multiforme (Grade IV) has now been re-classified, and unlike their adult counterparts (GBM IDH wildtype),

other molecular factors influence diagnosis as well as IDH status (10,21). For the purpose of clarity and aligning to literature cited that was published prior to the WHO 2021 update, the entity formerly known as paediatric glioblastoma will be referred to henceforth as paediatric high-grade glioma (pHGG), with specific subcategorising based on molecular diagnostics being stated where relevant.

1.1.1.2 Epidemiology

The incidence of paediatric brain tumours is around 5 cases per 100,000 population, over 50% of which are classified as gliomas (23). Gliomas comprise the most common CNS tumour in both children and adults; 30% of these paediatric gliomas are defined as high grade (WHO grade III/IV) malignant tumours (23). Characterised by an aggressive phenotype; both adult and paediatric HGGs are synonymous with low survival rates, poor prognosis, and limited therapies (24). Paediatric HGGs are usually aggressive astrocytomas, comprising 60% of all high-grade gliomas, and are diffuse and infiltrative in nature. As per the Central Brain Tumour Registry of the United States (CBTRUS) 2019 data, the incidence of pHGG is approximately 0.85 per 100,000 (25).

Currently, the overall median survival of pHGG patients is 14 months, with an average 1-year survival of 58%, and 5-year survival of 17%. Children aged 0-5years were found to have 1- and 5-year survival rates of 52.2% and 29.8% respectively. The 6-10-year group 1- and 5-year survival of 51.2% and 14.1% respectively, and 11-19-year group had 1- and 5-year survival rates of 64.3% and 13.2% (26). The recently defined HGG entity, diffuse midline glioma H3K27M- mutant (grade IV) has a notedly worse prognosis, with less than 10% of patients surviving more than 2 years (27). Further to age, factors that were significantly associated with poor survival were tumour location and ethnicity. Black

patients demonstrate significantly lower 5-year survival rates, despite non-Hispanic White patients having a higher incidence of the disease (28–30).

It is well understood that the molecular biological features of pHGG are distinct from those in adults, and therefore, adult clinical trial data cannot necessarily be extrapolated to children (29). Compared to adult HGG, pHGG is characterised by more frequent mutations in PDGFRA, TP53 and recurrent K27M and G34R/V mutations on histone H3 (31,32). In younger children, pHGG is associated with H3F3A mutations at K27 that correlate to poor prognosis (32). These tumours typically originate in the midline i.e., upper spinal cord, pons, and thalamus (32) whereas other genetic mutations are archetypally observed in other distinct brain regions, for example, the G34 histone mutations occur most often in the cerebral hemisphere of teenagers (33). In adolescent HGG with mutations in the IDH 1 or IDH2 genes prevail, customarily affecting the hemispheric regions of the brain. Whilst a mutual mutation is observed in both adolescent and adult GBMs, IDH mutants present as unique subtypes diverging in prognostic, biological and growth patterns dependant on age (26). Mutations occur during cell division in all somatic lineages, including glial cells. As a consequence of a degree of neurogenesis persisting throughout human life, somatic mutations in the brain can arise throughout development and therefore accumulate with the aging process, thus creating these distinct special and neuroanatomical differences in adult and paediatric glioma biology (34).

1.1.1.3 Classification

1.1.1.3.1 Molecular Biology

Molecularly defined diagnostic criteria of paediatric brain tumours was introduced in the WHO 2016 CNS4 (35) and has been largely expanded on in the recent release of the WHO 2021 CNS5 (10). For some tumours, classification by defining molecular characteristics is consistent, yet for other tumours we cannot readily diagnose with molecular features

alone, with certain subsets of tumours never using a molecular diagnostic approach. Because of this, a combined approach of histology and molecular biology is required (21). Over the last 30 years there have been many advances in diagnostics and tumour grading, with the last few years showing an expansion in the capacity to use molecular techniques for grading. RNA and DNA sequencing have been key in the delineation of molecular subgroups of high-grade glioma, allowing mutational status to act as a primary prognostic and diagnostic indicator, and enhancing the capacity for personalised medicine in gliomas. Table 1.2 details the key molecular features of gliomas, summarising both adult and paediatric tumours (21,36).

Methylome profiling is a powerful approach in determining tumour status, with most CNS tumours being accurately classified using their methylome profile. Furthermore, copy number such as 1p/19q, homozygous deletions and amplifications can be identified using this approach. Methylome array data may be useful as a surrogate marker for genetic events where molecular testing is not possible, however this approach is not appropriate for targeted therapies and patient specific approaches (32,36).

Table 1.2 The defining molecular features of gliomas according to WHO 2021 CNS5. Description of the classification of brain tumours, including molecular features and identifiers. Adapted from Louis et al, 2021 (10)

Tumour Type	Molecular Features
Astrocytoma, IDH-mutant	IDH1, IDH2, ATRX, TP53, CDKN2A/B
Oligodendroglioma, IDH-mutant, and 1p/19q-codeleted	IDH1, IDH2, 1p/19q, TERT promoter, CIC, FUBP1, NOTCH1
Glioblastoma, IDH-wildtype	IDH-wildtype, TERT promoter, chromosomes 7/10, EGFR
Diffuse astrocytoma, MYB- or MYBL1-altered	MYB, MYBL1
Polymorphous low-grade neuroepithelial tumour of the young	BRAF, FGFR family
Diffuse low-grade glioma, MAPK pathway-altered	FGFR1, BRAF
Diffuse midline glioma, H3 K27-altered	H3 K27, TP53, ACVR1, PDGFRA, EGFR, EZHIP
Diffuse hemispheric glioma, H3 G34-mutant	H3 G34, TP53, ATRX
Diffuse paediatric-type high-grade glioma, H3-wildtype, and IDH-wildtype	IDH-wildtype, H3-wildtype, PDGFRA, MYCN, EGFR (methylome)
Infant-type hemispheric glioma	NTRK family, ALK, ROS, MET
Pilocytic astrocytoma	KIAA1549-BRAF, BRAF, NF1
High-grade astrocytoma with piloid features	BRAF, NF1, ATRX, CDKN2A/B (methylome)
Pleomorphic xanthoastrocytoma	BRAF, CDKN2A/B
Subependymal giant cell astrocytoma	TSC1, TSC2
Chordoid glioma	PRKCA
Astroblastoma, MN1-altered	MN1
Ganglion cell tumours	BRAF
Dysembryoplastic neuroepithelial tumour	FGFR1
Papillary glioneuronal tumour	PRKCA
Rosette-forming glioneuronal tumour	FGFR1, PIK3CA, NF1
Myxoid glioneuronal tumour	PDFGRA
Diffuse leptomeningeal glioneuronal tumour	KIAA1549-BRAF fusion, 1p (methylome)
Multinodular and vacuolating neuronal tumour	MAPK pathway
Supratentorial ependymomas	ZFTA, RELA, YAP1, MAML2
Posterior fossa ependymomas	H3 K27me3, EZHIP (methylome)
Spinal ependymomas	NF2, MYCN

Atypical teratoid/rhabdoid tumour	SMARCB1, SMARCA4

Paediatric HGG may be classified on the basis of gene expression as four distinct subgroups: proneural, neural, classical, and mesenchymal (37). Further delineation can be provided by genome wide approaches such as utilising DNA methylome arrays (31,32). Paediatric gliomas are a heterogenous group of tumours, which through molecular grouping, can be divided into 3 main molecular categories: H3.3 mutant, IDH mutant, and H3.3/IDH wild type (38). Paediatric brain tumours have been proven to be a fundamentally different disease to that of their adult counterparts, and as such, demand their own unique classification system. It is apparent that different genetic pathways hold varying degrees of importance in different age groups of pHGG patients. IDH-1 mutations are often associated with secondary GBM in adults, but typically absent in paediatrics (32,39). Smith *et al* found that 1q gain is found in 30% of paediatric patients and 9% of adults respectively, whereas 80% of adult GBM patients harbour 10q loss, compared to 35% of paediatrics (39).

To summarise, diffuse gliomas have now been classified according to 'adult type' or 'paediatric type,' where some 'paediatric type' tumours arise in adulthood particularly adolescents and young adults, whereas 'adult type' rarely occur in paediatrics (10,13). Paediatric-type diffuse gliomas are notably uncommon, with circumscribed gliomas and glioneuronal tumours being more prevalent. The recent advances in molecular subtyping have allowed for lineage determination, finding that diffuse gliomas have astrocytic and oligodendroglial differentiation (table 1.3). These high-grade diffuse gliomas are IHD-wildtype, and as such, harbour no mutations in the IDH-1 or IDH-2 gene unlike their low-grade counter parts, and are therefore delineated according to their MYB/MYB1 and MAPK

pathway status (11). pHGG is characterised by mutations in PDGFRA, TP53 and recurrent K27M and G34R/V mutations on histone H3, with around 40% of pHGGs possessing mutations the histone H3 gene (38). Of these H3 variants, a majority are observed on position 27, whereby a lysine is substituted with methionine (Lys27Met) at the h3.3 (H3F3A) gene or h3.1 gene (38,40). Additionally, a substitution of glycine to arginine or valine can occur at the Gly34 position, these H3G34 mutations are associated with an increased occurrence of O6-methylguanin DNA methyltransferase (MGMT) methylation, which may guide prognosis and drug response (41). Diffuse midline glioma by definition required a diffuse infiltrative growth across the midline structures, and harbours H3K27 mutations. In high grade hemispheric tumours of the young adult and adolescent, a H3G34 mutation is often observed (10).

BRAF and CDKN2A/B mutations are associated with pleomorphic-xantoastrocytoma (PXA) like HGGs, resulting in RAS and MAPK pathway alterations (42). Finally, MYCN-amplified gliomas show the poorest prognosis, whereas amplification in PDGFRA show a better prognosis, and the EGFR-amplified gliomas demonstrate an intermediate prognosis (38).

Table 1.3 Common genetic mutations found in pHGG and the function of the translated protein.

Mutation	Function
IDH 1/2	Catalytic isozymes that reduce NADPH and NADP+. Directly linked to prognosis in adults, less prevalent in paediatrics. WHO 2016 changes denote IDH as a classification factor and can determine tumour grade.
HIST1H3B	Histone. Very common in the paediatric population. WHO 2016 classification denotes that p.K27M mutation status can change glioma grade classification
TP53	Tumour suppressor acts in cell cycle regulation. Mutations in P53 indicate high grade malignant tumour behaviour
Histone H3	Histone involved in the structure of chromatin in eukaryotic cells. G34 mutation in the histone 3 gene are extremely malignant tumours.
BRAF	Viral oncogene homolog functioning in the RAS/MAPK pathway. Mutations in BRAF are associated with poor prognosis is LGG
FGFR	Code for signal transduction surface receptors, commonly mutated in diffuse LGG

MYB/MYBL1	Transcription fact functions in cell cycle and apoptosis. Viral oncogene analogue, present in 25% of grade II gliomas

1.1.1.3.2 Histopathology

Diffuse paediatric-type high-grade gliomas, H3-wildtype and IDH-wildtype demonstrate glioblastoma-like features microscopically. Their histopathology can vary but they are often characterised by necrosis, brisk mitotic activity, microvascular proliferation, and high cellularity (43). Infant-type hemispheric gliomas demonstrate fascicles or sheets of astrocytic cells that possess mild to moderate pleomorphism and palisading necrosis with mitotic activity (43). Histologically, diffuse midline gliomas (H3 K27 altered) appear as astrocytic tumours, despite being WHO grade IV, a minority of cases may lack characteristic microvascular proliferation, necrosis, and mitotic figures, however these attributes are ordinarily present. The H3 G34 mutant diffuse midline gliomas are astrocytic with glioblastoma like features, including high cellularity, infiltrative growth, and mitotic activity, with microvascular proliferation and necrosis sometimes present. These tumours can be characterised by the presence of hyperchromatic nuclei and embryonal-like appearance of the cells (44,45). High grade (grade III) oligodendrogliomas contain high levels of cellular density, necrosis, microvascular proliferation and increased mitotic activity, with nuclear anaplasia being a common feature (46).

1.1.1.4 Aetiology and Risk factors

Despite advancements in research, there is very little known about the cause of paediatric brain tumours, especially pHGGs. As previously mentioned, in some cases glioma may be familial and has been associated with several predisposition syndromes. Alterations found in the p53 gene are responsible for Li-Fraumeni syndrome (LFS) a known predisposition for

brain tumours, research has shown that CNS tumours related to LFS have a prevalence ranging from 9 to 14% (47,48). Similarly, neurofibromatosis 1 and 2 arises as a result of mutations in NF1 and NF2 respectively and are linked to the development of optic pathway gliomas (15–20%) and brainstem -gliomas (1–2%) (49). Turcot's syndrome (type 1) is caused by alterations in mismatch repair (MMR) genes, malignant gliomas are the most frequent MMR associated tumours (25–40%) (50,51), whereas APC is implicated in Turcot's syndrome (type 2). Finally, BRCA syndrome, cause by mutations on BRCA1 and BRCA 2 is seen in glioma patients (52).

In addition to the familial predisposition syndromes previously described, data has revealed that gliomas may cluster within families. An in-depth review of familial glioma by Malmer *et al* (53) found that both genetic and environmental factors resulted in familial clustering of gliomas. The GLIOGENE consortium, consisting of a genome-wide single-nucleotide polymorphism approach aimed to identify route of gliomagenesis by way of distinguishing new genomic regions of interest. Around 5% of all glioma cases are suggested to be familial, with most of these families not being ascribed to predisposition syndromes (53). Genome wide homozygosity marking of Swedish families identified geographical clustering of glioma, associated with allele sharing LOD score of 1.05 for D1S196 on chromosome 1q23 (54). Furthermore, exposure to ionising radiation therapy during the treatment of other childhood cancer types is a significant risk factor for the development of a CNS tumour (55).

1.1.1.5 Pathology

In terms of physical occupancy, gliomas are unique. They are the only cancers that grow in a defined space: the cranium - rarely progressing to the spinal cord. Thus, to grow and expand, gliomas need to overcome these spatial constraints (56). Cancerous glial cells actively release high concentrations of glutamate into their immediate vicinity, killing

neurones in the surrounding space. Glutamate activates NMDA receptors on neurones and the prolonged activation of these receptors results in peritumoral seizures trigging excitotoxic cellular death. Similarly, this cell death pathway is found in various neurological/neurodegenerative disorders such ALS and stroke. However, despite the resemblance in the final death pathway, gliomas synthesise glutamate differently to the cells implicated in neurodegeneration (57).

Unlike other cancers that disseminate themselves via the vasculature, gliomas do not metastasise haematogenously, giving explanation as to why they are rarely found to metastasise to other sites. They do, however spread through the brain successfully, migrating along the path of neurones or blood vessels (57). When compared to their normal counterparts, glioma cells are characteristically resistant to cell death. This resistance is vital to the core region of the tumour that is subject to a lack of renewable nutrients and hypoxia and therefore typically display a necrotic phenotype. This resistance is attributed to P13 kinase activation and the subsequent downstream phosphorylation of AKT (58,59).

1.1.1.6 Clinical Symptoms

Patients diagnosed with pHGG can present with a variety of symptoms, ordinarily influenced by the location of the tumour and age. Initial symptoms such as nausea, behavioural issues, headaches, and lack of co-ordination are often mistaken for those of more common, less serious disease (18). These symptoms can worsen to give rise to features that are more notable such as seizure, macrocephaly, papilloedema, spinal deformity and impaired consciousness (8). Focal neurological signs and seizures generally accompany hemispheric tumours, whereas symptoms related to intracranial pressure are associated with posterior fossa tumours (60). A higher risk of seizures is associated with cerebral hemisphere tumours and are generally more prevalent in low-grade gliomas (LGG)

(60). Increased skull elasticity in infants allows delay in pressure related symptoms but may present as increased head circumference and nonspecific clinical symptoms such as general irritability and lack of feeding (61). Low-grade tumours present with chronic symptoms, whereas acute symptom duration is associated with higher-grade lesions (62). The development of the HeadSmart campaign based on the Diagnosis of Brain Tumours in Children guideline (produced by the Children's Brain Tumour Research Centre (CBTRC) in Nottingham) has led to improved guidance for healthcare professionals has had an impact on timeframe, enabling earlier diagnosis, bettering prognostic outcome (18). Additionally, the diagnosis time for children with brain tumours has markedly reduced since the accreditation of HeadSmart, decreasing from 12-13 weeks to 6.5 weeks to diagnosis (18,63).

1.1.1.7 Treatment Strategies

Despite its aggressive nature, an optimal therapy for the treatment of paediatric GBM (pHGG) is yet to be well defined. As standard, pHGG treatment regimen consists of maximal surgical resection (where practicable) followed by adjuvant chemo-radiation at 50-60Gy fractionated over 6 weeks (64). In the youngest patients, chemotherapy is the preferred treatment after surgery and is employed to delay the need for radiation. In infants, radiotherapy is often deferred in an effort to prevent additional brain injury and preserve neurocognitive function in the developing brain. Conversely, older paediatric patients are given radiotherapy treatment, followed by a Temozolomide regimen (26). CCNU (chloroethyl-cyclohexyl nitrosourea) and vincristine are alternative chemotherapeutic agents that have been utilised in clinical trials. Similarly, PCV (procarbazine, lomustine, and vincristine) has also been reported to improve survival in

paediatric gliomas (65). There is a desperate call for new and improved treatment strategies for pHGG, particularly with the failure of the HERBY trials where the addition of bevacizumab to conventional TMZ + RT treatment did not reduce death, and was instead, found to increase serious adverse events (66). Although immunotherapy seems to be a promising approach in other cancers, both the ACT IV (67) and CHECKMATE (68) trials failed to show any significant improvement in overall survival.

1.2 Electrotherapy

It is clear that there is a desperate need for the improvement of treatment for both adult and pHHGs. The scarcity of current effective therapies had led to new treatment options being the focal point of many research groups. Electrotherapy is one such treatment option that is being widely explored, with treatments currently approved across Europe and the U.S.

1.2.1 Optune™

The Optune™ system developed by Novocure Ltd (Israel) is a novel FDA approved electrotherapeutic treatment for primary and recurrent adult GBM. The Optune™ device is indicated for patients 22 years and older that have a histologically confirmed case of supratentorial GBM (WHO Grade IV astrocytoma) (69). The use of Optune™ as a therapy is approved in combination for patients who have received maximal surgical resection and with those who have received concomitant TMZ and radiotherapy (69,70). The Optune™ device works by generating alternating electric fields delivered directly to the patient – coined tumour treating fields (TTFields). The device consists of four transducer arrays (to be attached to the patient's scalp), a field generator and power pack that can be carried in a portable backpack.

The first-generation Optune™ system weighed approximately 2.7 kg. The second-generation redesigned Optune™ system weighs 1.2 kg conferring significant improvement to patient wearability (69,71). The field generator delivers alternating electric fields at a recommended 200kHz (72) through the insulated transducer arrays (attached to the patient's shaved scalp) with a minimum field intensity of 1.0V/cm (73,74). These tumour fields are delivered throughout the tumour in a non-invasive manner. The optimal array

placement is calculated by a purpose made tool, NovoTAL™ (Novocure, Ltd, Israel) which uses simulation software to optimise the field intensity within the tumour, accounting for variables such a head size and shape, resection cavity and swelling (71,73,74).

Each transducer array is composed of 9 insulated ceramic discs and a conductive hydrogel is applied to the patient's shaven scalp to prevent direct contact between the discs and patient's skin. Head shaving is imperative to allow optimal contact between the arrays and the patient's head, therefore delivering complete TTFields (71). Two transducer arrays are attached to pre-mapped locations on the scalp and are held in place by medical bandage. Each array is connected to a single wire, which connects to the field generator (figure 1.2) (75). Research has found that the efficacy of TTFields is influenced by compliance to treatment, including treatment hours per day (>18h/day), electrical field intensity and electrical field frequency.

Figure 1.2. Representative image of a patient wearing the Optune Tumour treating fields device. Transducer arrays attach to the patient's shaved scalp, and the generator is carried in the portable backpack as shown.

1.2.1.1 Mechanism of Action

Tumour treating fields act via alternating electrical field therapy, and exert biophysical forces on charged, polarisable molecules known as dipoles. The biological effects of the alternating electric fields are dependent on their frequency (73). Electrical fields at low frequencies (<1kHz) have the ability to affect the polarisation of the cell membrane, altering excitable cell behaviour. Conversely, high frequency electrical fields (>500kHz) cause vibrational movements in charged and polar molecules in cells, transferring kinetic energy between molecules and therefore causing tissues heating. The electrical field used in TTFields treatment are of the intermediate frequency range (100-500kHz) (76) and avoid the issue seen in low and high frequency fields. They do not cause heating of tissues or action potential firing in excitable cells but can interfere with microtubule polymerisation in rapidly diving cells (72).

1.2.1.1.1 Antimitotic effects

One of the proposed mechanisms of Optune is via the antimitotic effects of TTFields. Polar molecules are susceptible to electrical manipulation, and it is thought that TTFields interact and exert their effect on these polar molecules during mitosis (77,78). At the start of metaphase pairs of centromeres are captured by microtubules, orienting them towards their specific poles. Sister chromatid separation (via cytokinesis) (79) is a direct result of Securin and Cyclin B mediated degradation by Cdc20 and APC (80). The formation of this destruction complex is wholly dependent on correct localisation and function of microtubules at both anaphase and metaphase (77,79). Errors in this intricate process, particularly errors following anaphase are irrevocable. Cancer cells depend on mitotic competency and when this is compromised i.e., by errors committed in anaphase due

TTFields exertion, a multitude of cell fates i.e. aberrant mitotic exit (81), apoptosis and mitotic catastrophe can occur (77,82).

A key process that TTFields target is tubulin polymerisation, a process by which microtubules undergo constant cycles of polymerisation and depolymerisation. Tubulins are amongst some of the most polar molecules, possessing a large dipole moment, and are highly susceptible to disruption by TTFields, promoting consistent depolymerisation (83). When applied to a cancer cell, TTFields force polar molecules to align with the electric field, causing misalignment of the individual tubulin subunits resulting in microtubule disruption (Figure 1.3) (77,84). In turn, this results in abnormal spindle formation, which may lead to arrest in mitosis, leading to mitotic cell death. Additionally, failure at the spindle assembly checkpoint may lead to aberrant exit at metaphase, and abnormal chromosome segregation (85).

In normal cells, the electrical field is uniform, unlike their malignant counterparts. TTFields capitalise on this non-uniform characteristic of dividing cells that arises due to the 'hourglass' structure observed post anaphase. This generates dielectrophoresis, whereby during cytokinesis, the field intensity is elevated at the furrow, resulting in the accumulation of polar molecules (81). TTFields have been shown to prevent the recruitment and localisation of the septin complex – a complex involved in limiting contraction and cross-linking actin, helping to provide contractive forces for cytokinesis. Incorrect localisation of the septin complex results in abnormal chromosome segregation, morphological changes in cell membrane including blebbing and rupturing and extended mitotic duration (77).

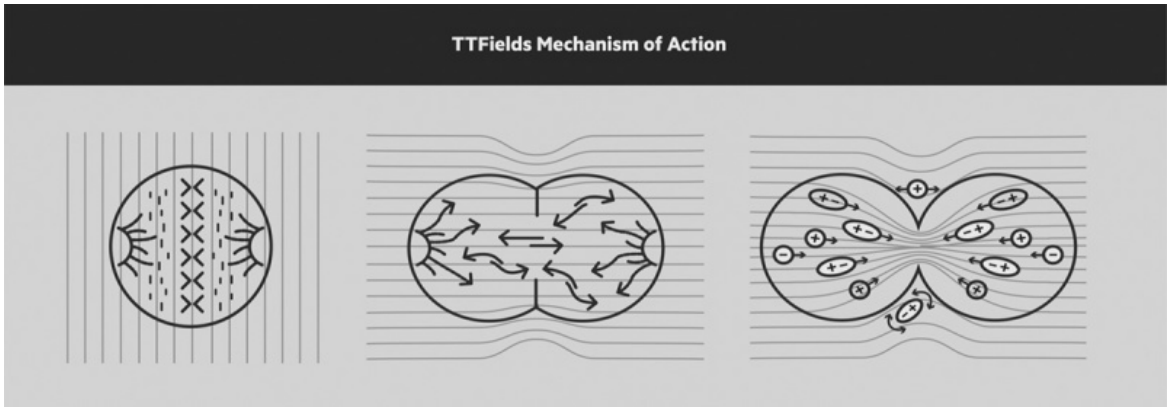

Figure 1.3. Alternating electric fields interfere with mitosis leading to apoptosis and cell death. The alternating electric fields effects are interference and prolongation of cell division, and disruption of cytokinesis in rapidly dividing cells, (Novocure)

1.2.1.1.2 Alternative mechanism for TTFields

Although the antimitotic effects observed post TTFields treatment are noted to be the key mechanistic driver behind cell death, this is yet to be conclusively proved and does not accurately account for some of the other changes i.e., gene expression that are observed. Branter et al. found that following TTFields treatment genes associated with mitochondrial and ER functioning, including, electron transport, metabolism, ion signalling, and protein folding were significantly differentially expressed (86).

TTFields has been found to sensitise glioma cells to radiotherapy, with studies finding that exposure to TTFields before radiotherapy treatment causing a delay in the DNA damage repair mechanisms (85,87), a reduction in survival and an increase in mitotic catastrophe. Furthermore, when combining TTFields with radiotherapy there has been found to be an increased number of γH2AX foci – a marker of DNA damage – than with either TTFields or radiotherapy alone (85,88). Other studies have identified a significant down regulation of DNA damage repair genes such as *BRCA1, FANCM, FAND2 and MLH1*, and that this down regulation was more prominent in cell lines that demonstrated higher sensitivity to TTFields (89).

Other studies have noted that TTFields have the capacity to enhance the permeability of cell membranes and therefore affect intracellular drug concentration. Analysis via scanning electron microscopy found that exposure to TTFields resulted in an increase in both the size and number of the holes present in the membrane of glioma cells, with these effects being absent in healthy human fibroblasts. This increase in number and size was associated with a marked increase in cellular uptake in a reversible manner (90). These data suggest that TTFields delivered prior to other therapies may be beneficial in enhancing the concentration of drugs within glioma cells.

HGGs are unique in that they are extremely locally invasive, with extensive infiltration into the surrounding healthy brain, as such, cancer cell migration is a key mechanism in glioma progression and poor outcome. Glioma cells treated with TTFields have been shown to possess reduced capacity to invade (via transwell assays) (91) and that this inhibited infiltrative capacity is associated with a downregulation of the PI3K/AKT and NFκB and MAPK signalling pathways.

1.2.1.2 Clinical trials

The EF-14 trial was a landmark study, being the first phase 3 trial since the addition of TMZ to standard care to show an increase in overall survival in patients with newly diagnosed GBM. In this phase III clinical trial, significant improvements in both overall and progression free survival when TTFields was used in combination with maintenance Temozolomide (TMZ) when compared with TMZ alone (70). The median overall survival increased by 4.9 months (20.9 vs 16.0 months with TMZ alone). Better clinical outcome was associated with compliance of patients (the average monthly use of the device) (69) and importantly, the addition of TTFields to standard of care TMZ maintenance was not

associated with a significant increase in systemic adverse effects (70). The data from this trial was imperative in the approval of TTFields as a treatment for newly diagnosed GBM. Similarly, the NovoTTF vs 'physician's choice chemotherapy' trial revealed that although there was no significant improvement in overall survival with the use of TTFields in the absence of chemotherapy, TTFields did produce comparable efficacy and activity to standard chemotherapy regimens, with toxicity and quality of life clearly favouring TTFields (92).

Further to this, the EF-11 phase III trial explored TTFields as a monotherapy. There was no significant difference found in overall survival (6.6 months vs 6.0 months) or progression free survival (2.2 vs 2.1 months) when comparing TTFields alone to chemotherapy alone. A review by Branter et al 2018 reveals that there are clear indications for TTFields as a combinatorial therapy with both mainstay and novel therapeutics, however there is limited efficacy when used as a monotherapy. Despite there being some descriptive mechanistic preclinical evidence there is a significant lack of study into the mechanism of TTFields in complex models (86).

1.2.1.2.1 Paediatric trials

The efficacy and safety profiles of TTFields as a treatment in paediatric brain tumours have not been extensively investigated, and as such, data is very limited.

A multicentre clinical trial [NCT03033992] sought to investigate the device related toxicities and feasibility use of TTFields in a cohort of 20 children (5-21 years) diagnosed with recurrent HGG and ependymoma. The device was used for >18 hours a day, and patients completed at least 23/28 days of cycle one. The treatment continued for up to a maximum of 26 cycles. Of these patients 11 were diagnosed with HGG (4 male/7 female)

and one patient had an ependymoma. Ten patients were evaluable during the feasibility period, and of these patients and 4 remained on study for 4 cycles of treatment, with one patient on Cycle 14. Noted adverse events include one grade 5 intracranial haemorrhage that was found to not be associated with the device. No grade IV toxicities were observed, 3 patients had seizures, fatigue, scalp pain, localized rash, and headache (none greater than grade 3). Of the 10 evaluable patients, 7 satisfied the feasibility criteria for the Optune therapy, therefore preliminary results indicate feasibility with minimal toxicity (93,94).

There a limited case reports of TTFields treatment in the paediatric population, this small retrospective review of the feasibility of TTFields in paediatric patients was carried out (Table 1.4). In this limited cohort of patients, it was found that adjuvant therapy with TTFields (over treatment periods of a maximum of 4 months), TTFields was well tolerated and there were no device related toxicities. Despite these data being consistent with findings in previous case reports, limited conclusions can be drawn due to the nature of heavy pre-treatment in these children (95).

Table 1.4 Patient data for small scale study of TTFields in paediatric patients (Crawford et al., 2020) (90)

Age	Gender	Initial presentation	Treatment prior to TTFields	TTFields Treatment	Compliance	Device related toxicity	Outcome
15	Female	High-risk acute pre-B Cell lymphoblastic leukaemia, 24 months later GBM diagnosis	Whole brain photon irradiation (1800cGy), TMZ	TMZ TTFields	47.4%-67.8%	No	Progression after 2 months of TTFields, death 2 months after progression
9	Male	Large posterior parietal neoplasm spanning the corpus callosum - GBM	TMZ	TTFields TMZ Everolimus, Bevacizumab	52.2%-68.9%	No	Progression after 2 months of TTFields, death 2 months after progression
4	Male	Left frontal temporal lobe - GBM	Failed: carboplatin, vincristine, TMZ, RT, bevacizumab, irinotecan, and vorinostat	TTFields	91.2% to 92.1%	No	Patient died of disease three months after initiation of TTFields.
16	Male	Known germline p53 mutation - anaplastic astrocytoma	Radiation therapy, TMZ, bevacizumab, PDL-1 inhibitor	TTFields TMZ	Not available	No	TTFields therapy was discontinued 3 months after initiation and the patient died of disease six months later

A study looking at post-marketing surveillance safety data from paediatric patients were obtained and analysed from Novocure's safety data base. Eighty-one paediatric patients were included in this analysis. A large majority of patients had HGGs and consisted of newly diagnoses (51%) and recurrent (47%) tumours. In total, 170 adverse events were recorded, with frequency and type of event being consistent across age groups, however these events were recorded at a slightly higher rate in newly diagnoses tumours (68%) compared to recurrent (58%). In 11 patients (14%) serious adverse effects were seen including seizure (5%), brain oedema (2%) and infection (4%). These serious adverse effects were not associated with TTFields use. In the total cohort 52% of patients experienced effects potentially related to TTFields, with skin reaction being the most common. All effects were non serious and included headache (36%), heat sensation (10%) and fatigue (6%). The data presented in this analysis suggest a favourable safety profile for TTFields treatment, with predominantly mild, localise skin effects in paediatric patients (93).

1.2.2 Deep Brain Stimulation (DBS)

Deep brain stimulation (DBS) is a powerful clinical therapy that aims to control the electrical activity of the brain. It is effective in the treatment of severe neurological movement disorders that are unresponsive to pharmacological intervention. There are clear indications in the use of DBS to treat tremor associated with Parkinson's disease and dystonia (96). DBS is also indicated in the treatment of pain syndromes such as cluster headaches and neuropathic pain, dystonia (97) and essential tremor (94).

1.2.2.1 Clinical use

Typically, a DBS device consists of an implantable pulse generator (IPG) that is implanted into the area of therapeutic interest. The electrical setting of the DBS device is either current or voltage, which can be manipulated through an electrical source (98). A DBS device can deliver either uni-lateral or bi-lateral stimulation depending on the number of implanted electrodes connected to the IPG, which can target multiple brain regions (99). It is essential that the DBS electrical field is precisely configured to enable a localised neuronal response, with configuration being the main indicator for efficacy of treatment (100). Neuronal function and signalling pathways are known to be influenced by electrical stimulation; with each structure being differentially sensitive to varying influences including geometry of electrical field and target structure and the electrophysiological properties of the target (101,102).

1.2.2.2 DBS and brain tumours

The co-occurrence of gliomas and having an implantable neuromodulation device is markedly low with publications noting only 3 confirmed cases (101) which leads to the hypothesis of a neuro-protective property of DBS devices against treatment. Although the occurrence of brain tumour and neurological disorders are relatively low, and such co-morbidities might seem unlikely, there are already described effects of intratumoral modulation therapy; diffuse intrinsic pontine glioma cells exhibited robust and consistent susceptibility to IMT fields, resulting in a significant reduction in viability.

In this study, the impact of using IMT as a monotherapy yielded results comparable to dual TMZ and radiotherapy treatment. Further to this, when IMT was used in combination with TMZ-RT, cell viability reduced drastically to 20% (103). DBS devices

exist to modulate the electrical activity of excitable cells, however non-excitable cells also exhibit significant electrical activity, and in cancer cells, this bioelectrical activity is dysregulated (104). Therefore, there is rationale in exploring the use of DBS treatment for brain tumours by modulating electrical activity. DBS treatment suggest that tumours are sensitive to electrical signals at a cellular level.

1.3 Membrane potential

Mammalian cells are encompassed in a plasma membrane, consisting primarily of phospholipids and proteins. The primary purpose of the cell membrane is to modulate the entrance and exit of ions into and out of the cell, thus being essential to the life of the cell. Across the plasma membrane of every cell in the body, there is an electrical energy gradient, which is the driving factor for the movement of water, nutrients, and salt (105). This electrical gradient is the consequence of two key physiological factors: the presence of a large Na^+ and K^+ gradient and the permeability of the membrane to these ions, conferring a large outward K^+ and an inwards Na^+ cellular current. A primary active ion pump – Na^+K^+ATPase is ubiquitously expressed across the membrane of mammalian cells and is the main modulator of gradient maintenance (106). In order to sustain a persistent gradient, electrogenic Na^+K^+ATPase pumps 3 Na^+ ions out of the cell for every 2 K^+ ion pumped in: hydrolysing 1 molecule of ATP per transport cycle, therefore the pump is not electroneutral (107). There is an ionic imbalance between the intra and extracellular spaces, with K^+ concentration high inside the cell and low outside with the converse being true for Na^+ concentration. The

K^+ ion is the predominant permeant ion, with the membrane classically exhibiting an open channel at the resting state (108).

The plasma membrane potential (Vm) exists due to the presence of cellular ion channels and transporters each with varying permeability to distinct ions i.e., K^+, Na^+, Cl^- and $Ca2^+$. Due to the non-uniform distribution of these mono and divalent ions an electrical gradient is established between the cytoplasm of the cell and the extracellular environment (106). Thus, Vm is expressed in terms of relativity to the charge of the extracellular space. A cell is considered depolarised when its Vm measures less negative than that of the extracellular environment, conversely a hyperpolarised cell displays a more negative Vm (104). Alterations in the conductivity of each ion leads to fluxes in Vm, as such seminal work performed by Goldman, Hodgkin and Katz demonstrated that Vm depends on the permeability (P) of said ions with the following equation (109,110).

$$V_m = \frac{RT}{F} \ln \left(\frac{P_{Na^+}\left[Na^+\right]_o + P_{K^+}\left[K^+\right]_o + P_{Cl^-}\left[Cl^-\right]_o}{P_{Na^+}\left[Na^+\right]_i + P_{K^+}\left[K^+\right]_i + P_{Cl^-}\left[Cl^-\right]_i} \right)$$

Here R is the ideal gas constant, T the temperature, and F the Faraday constant. Changes in Vm underpin the control of action potentials in excitable cells, closely regulated by key ion transporters such as voltage gated K^+ and Na^+ channels.

1.3.1 Membrane potential in cell cycle control

Increasing data from bioelectric studies have revealed the imperative nature of membrane potential in the control and progression of the cell cycle (111). This unique and powerful signalling system holds the key to coordinated cellular interactions and is well conserved, however poorly understood. Nevertheless, it is well known that the control of the cell cycle is responsible for the proliferative capacity of a cell, thus stringent regulatory measures are employed (112).

A series of seminal experiments observed that sarcoma cells underwent hyperpolarisation before entering M phase, indicating that membrane potential may harness a key role in cell cycle progression (113). To consolidate this evidence, a later study (114) revealed that hyperpolarisation blocked mitosis and subsequent DNA synthesis in a reversible manner. Further to this it was then postulated that the Vm of a cell was correlated to its state of differentiation, for example, terminally differentiated cells such as epithelial cells possessed a hyperpolarised Vm (115). These experiments provided a platform for further investigation into a now well understood phenotype: highly plastic cells such as tumour cells and embryonic cells retain a depolarised state, whereas quiescent cells tend to be hyperpolarized (116).

Studies quickly established that there is significant depolarisation of the Vm during malignant transformation of normal cells. Akin to Cone's theory of cellular Vm (114) many *in vivo* and *in vitro* studies including those of normal breast and breast cancer cells (117) normal hepatocytes versus hepatocellular carcinoma (118) demonstrated that cancer cells tend to be more depolarized than their normal counterparts.

Demonstrated in figure 1.4, a multistep and rhythmic pattern of hyper and depolarisation of cellular Vm is crucial for cell cycle progression. A cell undergoes

hyperpolarisation at the G1/S transition point as a result of K^+ efflux via K^+ channels, suggesting that hyperpolarisation of Vm acts as an instructive cue in initiating the cycle (figure 1.5 4,5). Conversely the cell is subject to Cl- efflux at the transition to M phase and is accompanied by membrane depolarisation (104). The exact threshold value that needs to be met to drive progression can vary and is heavily dependent on the type of cell, its level of differentiation and if cultured, the density of the monolayer (112).

A recent study on endometrial stem cells found that the presence of membranous BK (voltage gated K^+) was (despite their minor role in Vm) cell-cycle dependent and that their number was significantly decreased in G2/M phase transitions, depolarising the cell (119). However, when subjected to BK channel inhibitors (Iberiotoxin and charybdotoxin) there was no effect on cell cycle transitions, suggesting whilst the presence of BK channels might be an indicator of proliferation, cell cycle transition is not BK channel dependant (119).

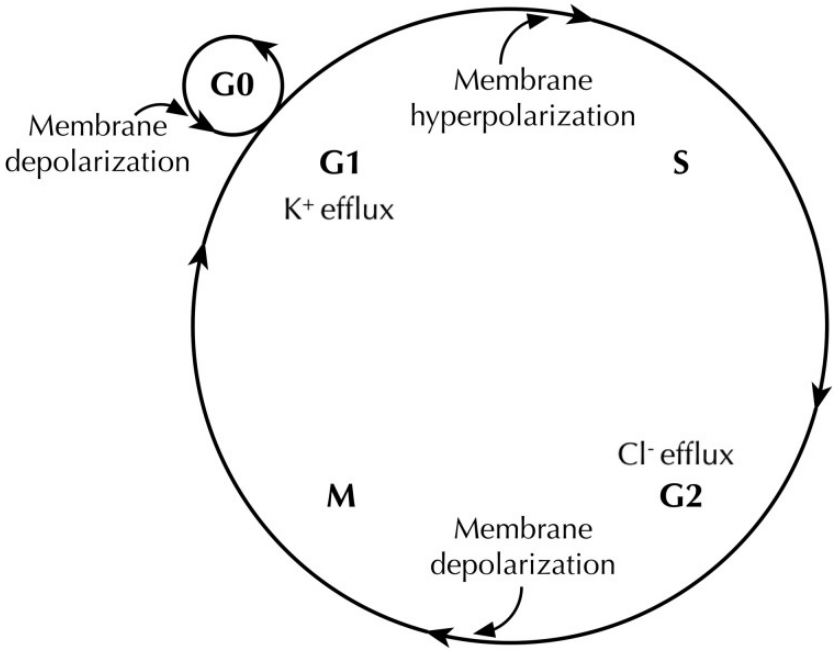

***Figure 1.4. Schematic representing the ionic fluxes across the membrane during the cell cycle**. Membrane potential (Vm) hyperpolarises and depolarises throughout the cell cycle. (Cone and Cone, 1976).*

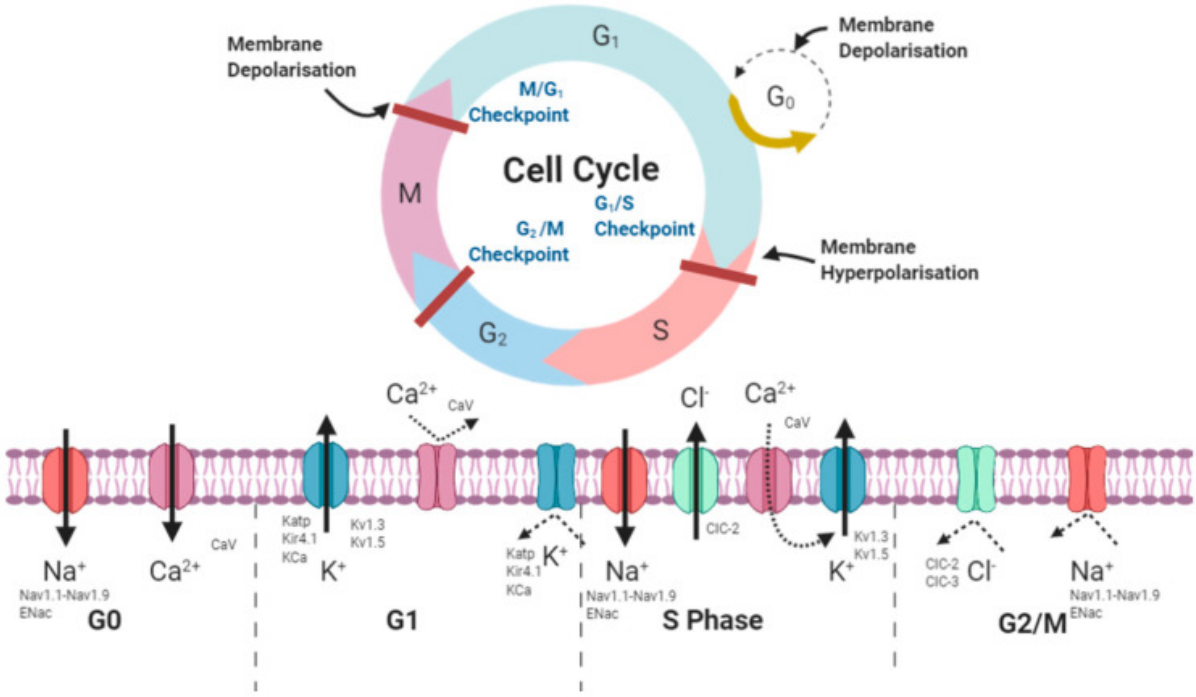

Figure 1.5 Ion channels associated with the cell cycle. Schematic representing the ion channels active during different phases of the cell cycle. Taken from the authors previous publication in line with MDPI guidelines (120). During G0 Na+ (red) and Ca2+ (pink) flow into the cell (downwards arrow) across the cell membrane causing depolarisation. Voltage gates K+ channels (blue) open in G1 to allow K+ ions to flow out of the cell (upwards arrow) with inwardly rectifying channels closing. Following membrane hyperpolarisation, during S phase Na+ flows into the cell, whilst Cl- and K+ (activated by inward Ca2+) flow out of the cell. Finally, membrane depolarisation occurs in G2/M with Cl- and Na+ channels closing to prevent movement of ions.

1.4 Ion channels and cancer

Cancer genotypes translate into several common features; defined in 2000 by Hanahan and Weinberg and coined the 'Hall marks of cancer' (121). Later revisited by in 2011 (122), these ever-expanding clinicopathologic hallmarks have become the backbone of much cancer research. Although not recognised as a hall mark, amongst the genes linked to cancer, those encoding ion channels stand out. The dysregulation of the homeostatic maintenance of intracellular ionic function underpins many of the pathophysiological events defining these hallmarks (123). As previously noted, ionic exchange processes are responsible for proliferative activity, apoptosis, and migration

of cells. The role that ion channels play in carcinogenesis was first understood when small cell lung cancer cell lines were observed to exhibit unusual patterns of sodium ion channel functions (124) and that, when subjected to pharmacological intervention by tetrodotoxin a sodium channel inhibitor, cancer cell growth was inhibited (125). This provided evidence that disordered function or expression of ion channel genes contributed widely to neoplastic progression of cells, triggering a new milieu of research.

Physiological Vm can range from −90 to −10 mV, depending on the cell type and physiological state (104). It is worth noting that the previously discussed rhythmic fluctuations of membrane potential do not stand as contradictory evidence to the fact that depolarised Vm is a hallmark of cancer cells. Whilst cancer cells still undergo the pattern of hyperpolarisation and depolarisation as the cell cycle progresses, the mean Vm value of cancers cells are consistently depolarised when compared to their somatic counterparts (126). Figure 1.6 demonstrates that the rapidly proliferating cancer cells harness on average a more depolarised Vm, whilst quiescent cells such as the glia, smooth muscle and neurones reflect a more negative Vm. Somatic cells with proliferative capacity also permit a depolarised Vm, suggesting a functionally instructive nature of Vm supporting a proliferative phenotype (104).

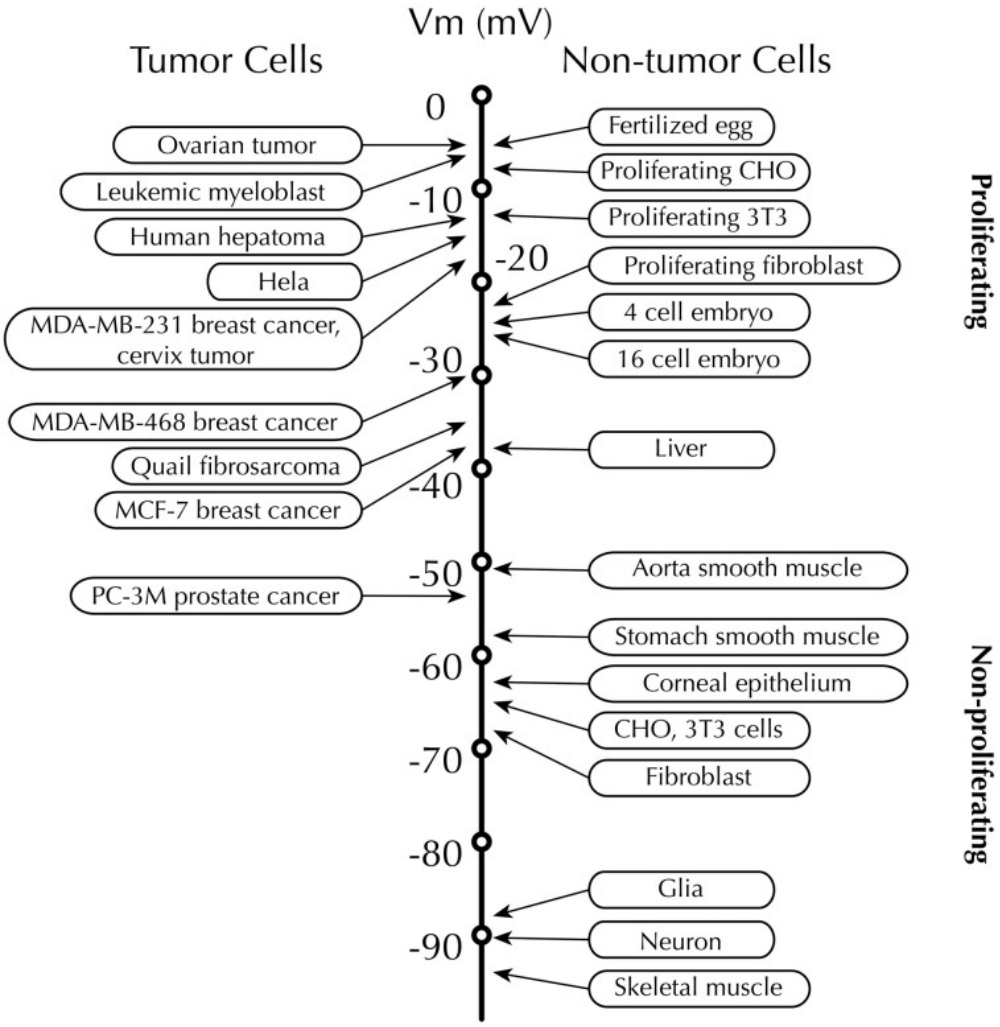

Figure 1.6 Malignant cells are on average, more depolarised than their malignant counterparts. Membrane potential in tumour and non-tumour cells. On average cancer cells and proliferating cells have a less negative membrane potential when compared to somatic and non-proliferating cells. (Yang and Brackenbury, 2013)

It is well known that the intracellular concentration of $Ca2^{+}$ is integral in regulating cell volume, cytoskeletal function, and cellular pH, therefore being intrinsic in the metastasis of a cell. Cancer cells exhibit dysregulated $Ca2^{+}$ channels and thus aberrant $Ca2^{+}$-binding, resulting in $Ca2^{+}$ flux modifications. Furthermore, activation of oncogenes results in remarkable changes in $Ca2^{+}$ signals, causing amplification of mobilisation (127). One of the major $Ca2^{+}$ channels classes involved in metastasis is the voltage gated channels. Studies have shown that in melanoma cells that these

channels have a fundamental role in regulating motility through instructive cues in the tumour microenvironment to generate a calcium signal (127,128).

Transient receptor potential channels (TRP) are a family of widely versatile $Ca2^{+}$ permeable ion channels that are sensitive to a multitude of micro-environmental factors and demonstrate complex supervisory roles. TRPC1 has been found to play an important role in a variety of cancer processes, and these roles differ depending on the stage of the cancer. TRPC1 has pro-proliferative effects in normal tissues, however in tumours TRPC1 shows pro-apoptotic activity (129).

1.4.1 Ion channels In Glioma

1.4.1.1 Sodium channels

Epithelial sodium channels (ENaC) are a class of amiloride-sensitive sodium channels that have been linked to sustained proliferation and invasion in many cancers (130,131). Psalmotoxin-1 (PcTX-1) and benzamil are amiloride analogs and that act to block ENaC. When targeted by these inhibitors, D-54-MG glioma cells underwent cell cycle arrest at G0/G1 and reduced the S and G2/M accumulation, suggesting that sodium influx is essential for cell cycle progression in glioma cells (132). This inward Na^{+} current found in GBM is absent in low grade glioma and normal astrocytes (133,134).

A gene expression study of the tumours of 21 GBM patients revealed that nearly 90% of the tumours showed at least one ion channel gene mutation (135). Sodium channel genes were most often subject to missense mutations and were significantly associated with shorter survival (168 days) compared to those who had no Na^{+} channel mutations (689 days)(135). However, when K^{+} and $Ca2^{+}$ channels with a similar mutational status were assessed, there was no significant survival differences

observed. Similarly, preferential cytotoxicity was demonstrated in U-87 GMB cell lines when targeted with digoxin when compared to somatic astrocytes. Interestingly, the patients harbouring IDH mutations did not have any mutations in the sodium channel genes (135). These data should be considered with caution due to the small sample size, however they tend to support the trend of sodium channels being crucial in glioma progression.

Further sequencing studies by Pollak and colleagues using RNAseq identified 18 ion channel genes with clear associations in glioma stem cell (GSC) malignancy when compared to the genome of normal astrocytes. Of these genes SCNA8 was highly enriched in bulk tumour samples and demonstrated obvious implications in malignant progression of these cells. siRNA knock down of SCN8A sodium channel gene conferred reduced viability (55-62% less growth) in GSC (136).

1.4.1.2 Potassium channels

Voltage-gated potassium channels (Kv) are the largest group of ion channels; it is widely recognised that Kv channels control proliferation by allowing cell cycle progression. The expression of Kv channels is altered in many cancers, and their participation in neoplastic progression is well marked (137). Three potassium channel genes KCNN4, KCNB1 and KCNJ10 have been identified to be significantly correlated with malignant progression and associated with overall survival in pGBM (138). KCNN4 is upregulated and KCNB1 and KCNJ10 are downregulated. Based on this genetic signature, patients were classified into high risk (three gene signature) and low risk (no signature), and findings demonstrated that pGBM patients who had a high risk of unfavourable outcome were sensitive to chemotherapy. Finally, molecular analysis of

the tumours revealed that this ion channel signature was associated with a mesenchymal subtype and wild-type IDH1 expression (138).

Various studies have focused on the part that ion channels can play in neoplastic development, progression, and invasion in brain cancers. Such studies include those by Weaver, Sontheimer and colleagues, evaluating the role of BK channels in gliomas. Voltage-dependant large conductance $Ca2^{+}$ activated K^{+} channels, also known as BK channels, are unique ion channels that are involved in both electrical and chemical signalling. An upregulation in the expression of these channels has been observed in human glioma biopsies, with expression level positively correlating with malignant grade of the tumour (57). BK channels in glioma cells form their own specific subclass – glioma BK channels (gBK) and are characterised by heightened sensitivity to $Ca2^{+}$ ions. Iberiotoxin (ibTX) is a selective pharmacological inhibitor of BK channels which has been shown to cause a dose/time dependant decrease in glioma cell number in survival assays. Further to this, inhibition of BK channels via ibTX results in S phase arrest and cellular death (58,59).

1.4.1.3 Chloride channels

Chloride channels are a functionally and structurally diverse group of selective channels, associated with cell volume regulation and excitability in cardiac, neuronal, and smooth muscle cells. Due to their relationship with cell volume regulation, they have been proven to be interesting targets in the mobility of cancer cells (139). ClC-2 and ClC-3 are Cl^{-} channels that are identified to be specifically upregulated in the membranes of gliomas cells. Increased expression of these channels endows glioma

cells with an enhanced route of Cl^- transport; in turn facilitating changes in cell shape and size during division and invasion (140).

A study utilising a gene expression array data set (accession number: GSE3289) identified 18 ion channel genes that are differentially expressed. Of the 18 channel genes identified, 16 were down regulated in hGG including epithelial sodium channel SCN1A, anion channel VDAC, potassium channel KCNJ10 and purinoreceptor P2RX7 (141). However, the chloride channels CLIC1 and CLI4 were both upregulated in the high-grade cohort. A second microarray data set was employed to validate these findings (accession number: GSE4290) and the results were mirrored. Kaplan Meier analysis confirmed that tumours that had the ion channel genetic signature described were associated with decreased overall survival in the cohorts compared to tumours with ion channel signature (141). Moreover, CLIC1 is found to be over expressed in GBM samples and is implicated widely in the tumorigenic capacity of GBM cells, with CLIC1 silencing by shRNA reducing the proliferative and clonogenic capacities of GBM derived stem cells. Further to this, clinical correlation reveals that high expression of CLIC1 is significantly associated with worse overall survival (142).

In an invasive context, glioma cells appear to adapt to spatial constraints and take on an elongated spindle like morphology. This mechanism of cellular shrinkage requires a Cl^- and K^+ mediated efflux of water (143). During apoptosis, a cell undergoes cell shrinkage, this hallmark is known as apoptotic volume decrease (AVD). Altered regulation of cell volume and morphology is associated with apoptosis in both normal and malignant cells. The mechanism of AVD is reliant on concomitant cellular loss of Cl^- ions, K^+ ions and water. Studies have shown that a down-regulation of these channels is associated with the ability of cancer cells to evade apoptosis (144).

1.4.1.4 Calcium channels

In human HGG, inhibition of TRPC1 via pharmacological inhibitors such as SKF96365 and MRS1845 or siRNA diminished the proliferative capacity of the cells and arrested the cell cycle. Interestingly, when stimulated with epidermal growth factor (EGF), TRPC1 relocated to the leading edge of migratory glioma cells (D54MG), suggesting a growth factor mediated role for TRPC1 in the migration of cancer cells (145,146). Moreover, suppression of TRPC1 via siRNA in a lung carcinoma cell line conferred a significant decrease in cell growth associated with cell cycle arrest at G0/G1 (147).

1.4.2 Targeting ion channels

Ion channels present as attractive druggable targets in the treatment of a multitude of disorders. They are particularly appealing as anti-cancer agents, as molecules inhibiting the mechanism of these channels act from the extracellular space, and do not necessarily require entry into the cell. Thus, rendering one protective capacity of tumour cells–expressing drug pumping carriers–ineffective (148). A multitude of studies have confirmed the inhibitory effect of ion channel blockers on cancer cell progression and invasion. Despite the focus of the review being specifically on high grade gliomas, evidence from studies thus far demonstrates that ion channels present as a tumour agnostic approach to most cancer therapies. However, when it comes to the utilisation of ion channel inhibitors there are grave concerns regarding the potential toxicities associated with these drugs, especially on the cardiac and nervous systems (149). One predominant issue that arises when searching for treatments for brain cancer is over-coming the blood brain barrier (150). The repurposing of currently available drugs is particularly appealing, table

1.5 summarises some commercially available ion channel inhibitors and biological toxins and their therapeutic/experimental effect on patients and cell lines.

Table 1.5 Ion channels and their respective drug inhibitors. Repurposed from the author's previous work

Repurposing ion Channel Inhibiting Drugs in Glioma Treatment		
Channel	**Tumour**	**Drug**
$Ca_v3.2$	GSC	Mibefradil
$Ca_v1.1$, $Ca_v1.2$, $Ca_v1.3$, $Ca_v1.4$	Rat Derived GBM GBM mouse models GBM cell lines	Pimozide Pimozide Fluspirilene
$Na_v1.1$ and $Na_v1.2$.	Human GBM	Valporate levetiracetam
$Na_v1.4$ and $Na_v1.5$	GBM cell line	Riluzole
Kv1.4	GBM cell line	Tamoxifen
Kv1.3	Human and mouse GBM biopsies	Clofazimine
EAG1	Glioma	Imipramine
KCa3.1	GBM cell lines Mouse GBM xenografts	Clotrimazole
CLIC1	GSC GBM cell lines	Metformin
Biological Toxins as Novel ion Channel Inhibitors in Cancer Treatment		
Channel	**Tumour**	**Toxin**
ClC-3	GBM, AA, Xenografts	Chlorotoxin
VGSC	GBM, HGG cell lines	Tetrodotoxin
ENaC/ASIC	GBM cell lines	Psalmotoxin

1.5 Hypothesis and aims.

The purpose of the project/hypotheses are as follows:

1) That the cellular membrane potential (Vm) exhibits differences between normal human astrocytes and pHGG cell lines.
2) That specific and unique ion channel expression patterns exist in paediatric brain tumours.
3) That genetic, electrical, and pharmacological manipulation of ion channels will reduce the capacity of childhood brain tumours to proliferate and invade.

The aims of this study are:

1) We aim to develop and validate a comprehensive understanding of ion channels and their role in the invasion, proliferation, and migration of childhood brain tumour cells.
2) We aim to investigate the expression and prognostic significant of candidate ion channel genes coupled with a functional analysis of electrical behaviour of pHGG cell lines, patient tissue, and publicly available data sets.
3) We aim to develop electrical and pharmacological methods of manipulating ion channels and consequently membrane potential, with the aim of providing new candidate therapies for clinical trials.
4) To develop an understanding of ion channels as bioelectric targets for combination with TTFields as a dual therapy
5) To assess the global effect of TTFields in the patient, including differential gene expression and functional capacity.

2 Materials and Methods

2.1 Identification of candidate ion channel genes in high grade glioma

2.1.1 Systematic literature review

A systematic review of available literature was performed using the NCBI PubMed data base to find appropriate candidate ion channel genes. Full details of papers included in this review can be found in the appendices.

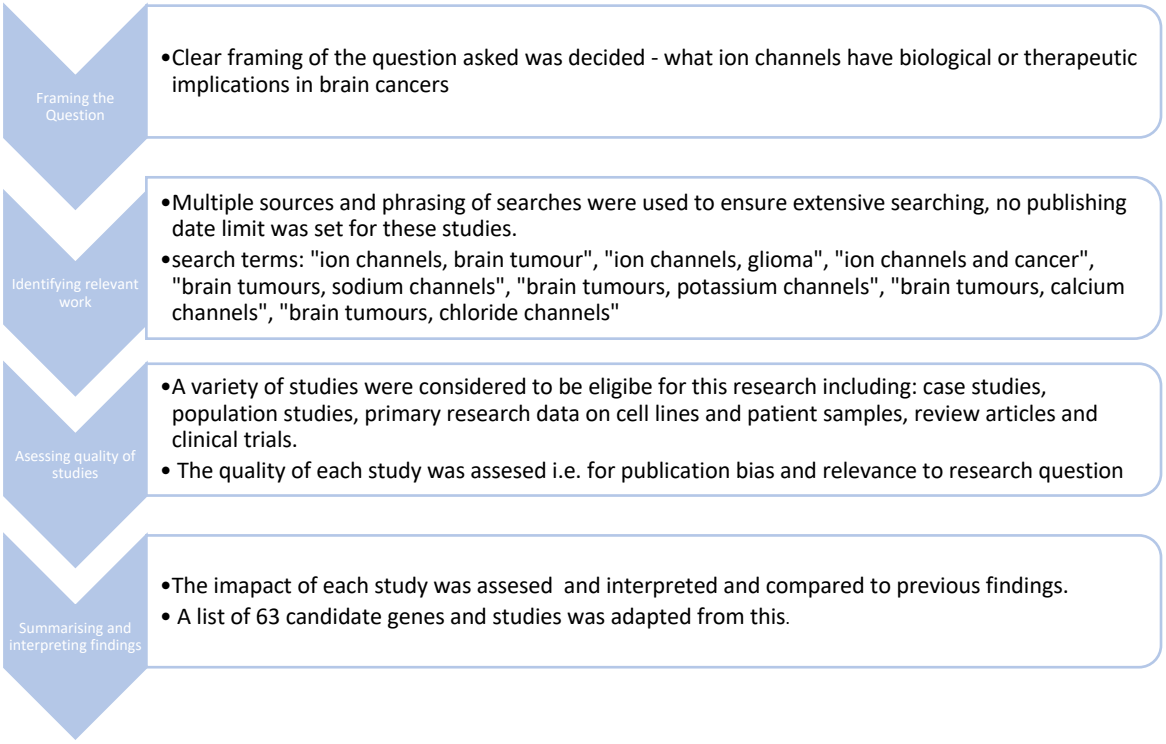

The 63 candidate ion channel genes found in this literature search were then used to progress to database analysis.

2.2 Analysis of in-house adult RNA sequencing data

RNAseq data (previously performed by the CBTRC) was kindly provided by Mr Stuart Smith. RNAseq data was acquired from the core, rim, and invasive regions of 10 adult human high grade glioma samples extracted during tumour removal by Mr Stuart Smith at Queen's Medical Centre, Nottingham with full ethical approval (REC: 11/EM/0076).

This data was used for crude analysis (by averaging the RPKM of each sample) to identify expression patterns of the 63 candidate genes taken from literature searches. The panel of ion channels were selected based on a Reads per kilo base of transcript per Million reads mapped (RPKM) of over 1 as 'expressing' the gene, with further segregation based on percentage of 'FACS positive cells' and overall, highly expressing RPHM. This group of cells were fluorescently sorted using FACS (Work performed by Jonathan Rowlinson and Dr Maria Cerebro-Estevez) (151) and were selected as positive for 5-aminolevulinic acid (5ALA), indicating a population of pure tumour cells. Therefore, high average RPKM values in the FACS positive population, suggest an increased expression in a pure tumour population, vs normal brain tissue.

This analysis was used to narrow the initial 63 candidate genes down. Criteria for candidacy included genes found to be significantly up or down regulated, clinical data indicating survival association and mechanistic links to glioma progression. Additionally, ion channels across families and types were included. VDAC, CLIC1, CLIC4, P2RX4, P2RX7, SCNN1A, TRPM2 and KCNJ10 were selected as the candidate panel.

2.3 Genomic analysis of wide-scale publicly available data sets

Genomic analysis was carried out using the R2 genomics analysis and visualisation platform of publicly available data sets (http://r2.amc.nl) of both paediatric HGG and adult HGG as well as various other glial tumours such as ependymoma and oligodendroglioma. Table 2.1

details information for each data set used, including sample size and sequencing platform. Genes of interest were searched against each data set to determine overall expression, and this expression was compared between normal brain regions and HGG. These searches were then further refined by specific tracks such as age of patient, gender, WHO grade or overall survival, significant differences in gene expression between groups were calculated using the Kruskal-Wallis test.

Table 2.1 Patient data sets analysed on the R2 genomics analysis and visualisation platform

Author	Tumour	Sample Size	Normalisation	Platform	Reference
Paugh	Paediatric glioma	53	MAS5.0	u133p2	(Paugh *et al*., 2010)
Roth	Normal cerebellum (adult)	9	MAS5.0	u133p2	(Roth *et al*., 2006)
Harris	Normal brain (adult -prefrontal cortex)	44	MAS5.0	u133p2	n/a
French	Adult glioma	284	MAS5.9	U133p2	(Gravendeel *et al*., 2009)

2.3.1 Survival analysis of public data sets

The R2 genomic analysis platform was then used to assess candidate ion channel genes (as previously selected via in-house RNA sequencing data) in wide scale publicly available glioblastoma data sets. Data sets without clinical information available were disregarded. Both adult and paediatric data sets were assessed for expression levels of candidate genes and compared to normal brain data. Kaplan-Meier analysis was employed as a non-parametric statistic to estimate the survival function from patient glioblastoma data in

comparison to the expression level of selected candidate genes. The Mantel-Haenszel long-rank test was employed to determine the statistically significance of high vs low expression and overall survival. A P-value of <0.05 was considered statistically significant.

2.4 Cell culture

2.4.1 Cell lines used and associated clinical data

Three paediatric cell lines KNS42, SF188 and GCE62 were selected for the initial screening process and their use was continued for subsequent experiments. KNS42 and SF188 are established commercial cell lines with recognised STR profiles and GCE62 is an in-house tumour derived sample originating from the core tumour region of a teenage patient. KNS42 cells were derived from a primary GBM presenting in the fronto-parietal lobe of a 16-year-old male (gifted to the CBTRC by Dr Stewart Martin, University of Nottingham) and SF188 cells were derived from a right frontal lobe GBM of an 8-year-old male (Merck, Germany). Normal human astrocytes (ScienCell, CA) derived from the cerebral cortex were used as an anatomically matched healthy control for human high-grade glioma cells. The adult patient lines GIN98 and GCE98 were derived from different tumour regions of a 47 year old male patient G(INvasive margin)98 and G(Core Enhanced)98 who had received TTFields as part of their treatment regimen. All in-house patient derived cell lines were acquired by routine surgical resection by Mr Stuart Smith, Neurosurgical Department, Queens Medical Centre, Nottingham. All commercial cell lines were subject to STR testing (table 2.2).

Table 2.2 Cell lines and associated patient information. Note: * indicates matched cell line derived from different regions of the same patient's tumour

Cell Line	Origin	Age	Sex	Brain Region	Histology
SF188	Merck, Germany	8	Male	Right frontal lobe tumour	Glioblastoma multiforme (WHO 2021, paediatric high grade glioma)
KNS42	Gifted by Stewart Martin, University of Nottingham	16	Male	Right fronto-parietal lobe	Glioblastoma multiforme (WHO 2021, paediatric high-grade glioma)
GCE62	Patient derived by Mr Stuart Smith, Neurosurgical unit, Queens Medical Centre, Nottingham	19	Male	Right temporal lobe	Glioblastoma multiforme (WHO 2021, paediatric high-grade glioma)
GIN98*	Patient derived by Mr Stuart Smith, Neurosurgical unit, Queens Medical Centre, Nottingham	47	Male	Temporal lobe	Glioblastoma multiforme
GCE98*	Patient derived by Mr Stuart Smith, Neurosurgical unit, Queens Medical Centre, Nottingham	47	Male	Temporal lobe	Glioblastoma multiforme
Human Astrocytes	ScienCell™, California (1800)	-	-	-	Cerebral cortex astrocytes

Table 2.3 Cell culture specific media. Note: * indicates matched cell line derived from different regions of the same patient's tumour

Cell Line	Culture Media	Split Ratio	Doubling time
SF188	DMEM F12 (Gibco™), 10% FBS (Hyclone™), 1% PenStrep (Sigma-Aldrich), 1% L-Glutamine (Sigma-Aldrich),	1:15	26 hours
KNS42	DMEM F12 (Gibco™), 10% FBS (Hyclone™), 1% PenStrep (Sigma-Aldrich), 1% L-Glutamine (Sigma-Aldrich),	1:10	48 hours
GCE62	DMEM (Gibco™), 10% FBS (Hyclone™), 1% PenStrep (Sigma-Aldrich)	1:10	36 hours
GIN98*	DMEM (Gibco™), 10% FBS (Hyclone™), 1% PenStrep (Sigma-Aldrich)	1:8	48 hours
GCE98*	DMEM (Gibco™), 10% FBS (Hyclone™), 1% PenStrep (Sigma-Aldrich)	1:5	~50 hours
Human Astrocytes	Astrocyte media (ScienCell™), 1% Astrocyte Growth Serum 1% (ScienCell™), 10% FBS (Hyclone™),	1:4	50 hours, increasing with passage number. Astrocytes senesce after 14 population doublings.

2.4.2 Culturing adherent cells

The cell lines KNS42 and SF188 were maintained in Dulbecco's modified Eagle's medium (DMEM)/F12 (Gibco, USA), while GCE62 was maintained in Dulbecco's modified Eagle's medium (DMEM) (Gibco, USA). All media was supplemented with 10% (*v/v*) foetal bovine serum (FBS, HyClone), 100 IU/ml penicillin (Sigma-Aldrich) and 100 µg/ml streptomycin (Sigma-Aldrich), with the addition of 1% (v/v) L-Glutamine in the KNS42 and SF188 cells. Cell lines were cultured in humidified incubators at a constant temperature of 37°c at 5% CO_2 atmosphere. Culture environment was maintained to be completely sterile, and each cell line handled individually within a biohazard hood (class 2) with laminar airflow to prevent contamination. Each cell line was grown in specifically selected media (as stated above) in a culture flask (without the presence of special matrixes) to encourage optimal growth conditions. Cells were checked microscopically daily.

To split or collect the cells, media was aspirated and discarded in order to remove any non-adherent (dead cells) leaving the remaining (live) cells attached to the substrate present in the flask. The cell monolayer was then washed with phosphate buffered solution (Thermofisher Scientific) without $Mg2^+$ or $Ca2^+$. To detach cells, 0.5mg/ml trypsin-EDTA (Sigma-PAA, UK) was added to disrupt the monolayer (with volume used dependent on culture vessel), and incubated at 37°c for ~3minutes. The detachment was then visually analysed microscopically to observe free cells. Following this, selected serum containing media was added in excess of the volume of trypsin, to the flask to inhibit the activity of the trypsin. The cell suspension was collected and then centrifuged at 1000 rpm (800xg) to collect a cell pellet. The supernatant was discarded, and the pellet re-suspended in specified volumes of media depending on the appropriate split ratio. According to the desired cell number, the cell suspension was transferred to a new flask along with media.

This was then incubated in the above conditions and cells left to grow until around 60-80% confluency where they are at a suitable level for experimentation. Alternatively, cell pellets were collected after centrifugation and re-suspended in experiment specific buffers for downstream application, or frozen as described in 2.4.

2.4.2.1 Astrocyte cell culture

Human derived Astrocytes (ScienCell™, Cat. No. 1800) were seeded at 5000 cells/cm^2 onto flasks coated in 2µg/cm^2 Poly-L Lysine (ScienCell™). Cells were incubated at 37 °C, 5% CO_2 in astrocyte medium containing 2% FBS, 1% astrocyte growth supplement and 1% Pen./Strep. (v/v, ScienCell™).

2.4.3 Neurosphere culture

For 3D culture of HGG cells, a neurosphere culture method was employed. Neurosphere cell culture consists of plating cells on a non-adherent surface in stem-like culture medium (table 2.4) to allow free forming 3D neurospheres to develop.

Cells were counted and plated at the densities described in table 2.5 to ensure that growth kinetics remained steady, and the spheres reached no more than 85% confluency by experiment end point. The 3D neurospheres were observed microscopically (via a phase-contrast light microscope) daily to assess their shape, consistency, and size. The development of a dark necrotic core indicated the need to passage the neurospheres. To passage cells, the cell suspension spheres were collected centrifuged at 300xg for 2 minutes. The pellet was then washed 2x with PBS. To disaggregate the neurospheres, 500µL Trypsin-EDTA was used to re-suspend the cell pellet, pipetting up and down every 30 seconds to break apart clumps of cells. The cell suspension was then centrifuged at

300xg for 5 minutes, washed 2x with PBS and re-suspended in appropriate serum free media and plated in ultra-low attachment 6 well plates (Corning).

Table 2.4 Neurosphere culture media recipe

Reagent	Final concentration	Stock Concentration	Source
DMEM/F12 or DMEM	1X	1X	Gibco 17504044
B-27 supplement	1X	50X	Gibco 17502048
N-2 supplement	1X	100X	Stem Cell Technologies 07980
Heparin	2µg/mL	2mg/mL	Gibco PHG0315
EGF	20ng/mL	0.1mg/mL	Gibco PHG0266
FGF	10ng/mL	0.1mg/mL	Corning 7007

Table 2.5 Cell seeding densities for neurosphere culture.

Cell Line	Seeding density (6 well plate)
SF188	10,000
KNS42	15,000
GCE62	15,000
GIN98	15,000
GCE98	10,000

2.4.4 Hypoxic cell culture

Each cell line was cultured in duplicate to give two flasks. Upon reaching 55% confluency, experimental flasks were transferred to a hypoxic chamber maintained at 37°C and 1% oxygen. As a control, a paired flask was maintained at 37°C atmospheric oxygen % (~21%). The flasks were put into their respective conditions at the same time and left to incubate for 24 hours. Pellets could then be collected for downstream experiments.

2.4.5 Acidotic cell culture

Cell lines were grown as previously stated in adherent vessels and incubated at 37 °C, 5% CO_2. In order to expose cell lines to acidosis, a media with a pH of 6.7 was made (table 2.7). As a control, a non-acidotic media was also made at a pH of 7.4 for control conditions (table 2.6). This was to confirm that potential differences were indeed a result of exposure to acidosis, and not to deviation from commercial cell culture media. Cells were incubated in acidotic (pH 6.4) or neutral media (pH 7.4) for 72 hours and were then subsequently used for downstream assays. The respective media recipes were optimised by the McIntrye Lab, University of Nottingham,

Table 2.6 Recipe for pH 7.4 media. Media was used as a control in acidosis experiments.

Medium pH 7.4	Final concentration	for 100 ml
DMEM 10X	1x	84.7ml
Hepes 1M	30mM	3ml
FBS	10%	10ml
Glutamine	1%	1ml
Pen/Strep	1%	1ml
Hypoxanthine (100mM)	0.1mM	100µl
UTP (1OOmM)	0.1mM	100µl
Folic acid (4g/L)	0.004g/L	100µl
H2O	-	-

Table 2.7 Recipe for pH 6.7 media.

Medium pH 6.7	Final concentration	for 100 ml
DMEM 10X	1x	84.7ml
Mes 1M	30mM	3ml
FBS	10%	10ml
Glutamine	1%	1ml
Pen/Strep	1%	1ml
Hypoxanthine (100mM)	0.1mM	100µl
UTP (1OOmM)	0.1mM	100µl
Folic acid (4g/L)	0.004g/L	100µl
H_2O	-	-

2.4.6 Cell dissociation from solid CNS tumours for the generation of primary cell lines

CNS tissue samples were collected from NUH Histopathology department or directly from operating theatre and transported on ice to human tissue culture facilities. The tumour specimen was cleaned by removing visible blood clots, vessels, gross necrosis, or any other contaminating material with a sterile scalpel, briefly washing with HBSS to remove blood. The tissue was then weighed and minced using a single edged blade or scalpel. 10x stock enzyme solution (table 2.8) was diluted 1:10 in HBSS and the minced tissue suspended in 1x enzyme solution at a volume 10ml/g. The specimen was then transferred to a sterile rotation culture flask and placed in an orbital shaker/incubator at 37°C, 70rpm for 30-60 minutes or until the majority of the visible solid material had disappeared. The disaggregated cells were then collected, passed through a 40µm cell strainer into a 50ml falcon tube, and rinsed with 5ml media. The specimen was then centrifuged at 800rpm (180xg) for 5 minutes at room temperature. The disaggregated cells were then re-suspended in 1ml of tumour media and transferred to a t25 cell culture flask containing 5ml of culture media. The cells were then incubated for 24 hours at 37 °C, 5% CO_2 in a

human cell culture incubator. The cells were microscopically assessed daily to ensure attachment.

Table 2.8 Enzymes used for the tissue disassociation.

Product	Supplier	Cat #	Amount	Final conc.
DNase Type 1 (3190U/mg)	Worthington	LS002139	12.6mg (0.0126g)	1.26mg/ml (4000U/ml)
Neutral Protease (Dispase) (9.5U/mg)	Worthington	LS002100	5.3mg (0.0053g)	0.3mg/ml (5U/ml)
Collagenase Type 1a (345U/mg)	Worthington	LS004194	14.5mg (0.0145g)	1.28mg/ml (500U/ml)
Hyaluronidase (630U/mg)	Worthington	LS002592	100mg/ml (Worthington sell 300,000U = 300kU) (0.1g)	10mg/ml (6300U/ml)
HBSS (calcium magnesium free)	Fisher	VX14170-088	10ml	-

2.4.7 Cell counting

Cells under both control and treatment conditions were counted manually using a haemocytometer. Growth medium was removed from cell flasks, cells were washed and then trypsinised as described previously. After trypsin neutralisation with an equal volume of growth media, cells were centrifuged at 120xg for 5 minutes. The supernatant was then removed, and cell pellet resuspended in 3ml of fresh growth medium. Following this 100 µL of cells were transferred into a new Eppendorf tube and 400 µL 0.4% Trypan Blue was added. 100 µL of the Trypan Blue-treated cell suspension was then applied to the haemocytometer and under a 10x object lens, the live, unstained cells were counted in one set of 16 squares and repeated until all 4 corners counted.

$$average\ count\ viable\ cells = \frac{\text{cell count 1+cell count 2+cell count 3+cell count 4+cell count 5}}{5}$$

$$cells\ /\ ml = average\ count\ viable\ cells \times dilution\ factor \times 10^4$$

Where the dilution factor has a value of 2 and 10^4 represents the counting chamber value.

$$total\ cell\ number = cell\ concentration \times volume\ of\ cell\ suspension$$

To calculate the viability of cells in suspension, the following equation was used:

$$cell\ viability\ (\%) = \frac{\text{average count viable cells}}{\text{average count of all cells (dead+viable}} \times 100$$

2.4.8 Cell storage

Upon reaching 70-80% confluency, cells were frozen in 10%DMSO + specific media for long term storage in a Brooks BioStore™ III (Select Science). For this, growth medium was removed from cells, and they were washed in PBS and trypsinised at 37°c for 5-10minutes according to the method above. Cell suspension was centrifuged at 1000rpm, and the supernatant removed, leaving a cell pellet, which was then resuspended in 1ml of 10%DMSO and specific media. Cells were frozen at a density of 1million cells in 500µl of 10% DMSO:Media suspension.

2.4.9 Revival of cells

To revive cells from frozen, cryovials were retrieved from storage and kept on ice. They were then rapidly thawed by partially submerging the body of the vial into a 37°c water-bath for ~1 minute or until visibly defrosted. Cells were then plated at high confluency (1 million cells) into a new T25 flask and left to incubate at 37°c for 24 hours. Following this, microscopic analysis to check for cellular adherence and a subsequent media change was performed to remove any traces of DMSO.

2.4.10 Mycoplasma testing

Routine mycoplasma testing was performed on a monthly basis using a PlasmoTest™ Mycoplasma Detection kit (InvivoGen; rep-pt1). Cells were cultured for a minimum of 7 days in antibiotic free media and collected media had been in contact with cells for 48 hours prior to testing.

2.5 Drug Assays

2.5.1 Presto blue viability assay

Cells under treatment conditions had their viability assessed using PrestoBlue™. Following various experimental time points, cell flasks had their growth medium removed and were washed in PBS. 1mL of PrestoBlue™ diluted 1:10 with growth medium was added to the flasks, and the flasks were transferred to a 37°c incubator (in the case of cells plated directed into clear bottom, black walled plates, the PrestoBlue™ reagent was added directly to the wells) for 30 minutes – 2 hours (cell dependant). Following incubation, 100ul of the presto blue solution was transferred to a black-bottomed 96 well plate for analysis via UV/Vis Spectroscopy at 560/590nm on the FLUOstar Omega plate reader (BMG Labtech). If a viability reading was taken at a mid-point of an experiment, excess presto blue was removed from the culture flask, cells were washed with PBS and fresh growth media was added.

2.5.2 IC_{50} calculation of drug response in adherent and neurosphere culture

An IC_{50} calculation was used to determine cellular response to various chemotherapeutics, via a viability measurement using PrestoBlue (Thermo Fisher; A13262) reagent. Cells were plated in clear-bottomed, black-walled 96-well plates (Greiner; 655096) at appropriate densities to allow no more than 80% confluency after 72 hours. Cells were then treated with the chemotherapeutic of interest, at range concentrations determined via assessment of the literature, and incubated at 37°C and 5% CO_2 for 72 hours. Unless otherwise stated, cekk growth media was not changed during the 72-hour incubation period. Post-treatment, the surviving cells were assayed using PrestoBlue as described in section 2.5.1. The half maximal inhibitory concentration (IC_{50}) was then calculated by normalising fluorescent measurements for each sample against a media only control and viability of the cells was then calculated as a percentage relative to the vehicle control samples. The relative values were then transported for analysis in GraphPad Prism 9.3, whereby drug concentrations were transformed into log form, and a dose response curve generated by non-linear regression.

Table 2.9 Seeding density of cell lines for IC50 experiments at 72 hours in 96 well plates.

Cell Line	Seeding Density/Ml
SF188	7,500
KNS42	15,000
GCE62	15,000
GIN98	15,000
GCE98	15,000
Astrocytes	20,000

Table 2.10 Drugs used in this study.

Drug	Stock Concentration	Vehicle	Product Details
Metformin (1,1-Dimethylbiguanide hydrochloride)	1M	Cell culture grade water	Sigma, D150595
Indanyloxyacetic acid 94 (IAA94)	1M	DMSO	Sigma, I117
Puromycin	10mg/ml	Cell culture grade water	Sigma, P8833
Doxycycline	10mg/ml	Cell culture grade water	Sigma, D5207

2.6 Electrotherapy treatment of pHGG

2.6.1 Inovitro - Tumour treating fields.

To deliver tumour-treating fields *in vitro*, the Inovitro TTFields (Novocure, Israel) device was used. The parameters for treatment were selected based on previous work by Dr Joshua Branter (152) .

2.6.1.1 Base plate and Dish Maintenance

Before use, the dishes and covers were rinsed under tap water, following this, they were rinsed with deionised water and placed face down to air dry. If chemotherapeutics or inhibitors had previously been used, a light detergent was used for the initial cleaning step, followed by tap water and deionised water before air drying.

To ensure aseptic working, dishes and covers were then sealed in autoclave bags with dishes being place face down. An autoclave program of <120°c for 60 minutes was then ran. Plates were removed from autoclave and dried for a minimum of 30 minutes before use.

2.6.1.2 Experimental Procedure

Previously sterilised base plates, dishes and covers were used in all experimental set ups. Sterile 22mm coverslips were inserted into the circular dishes, where a 200µl cell

suspension was transferred onto the cover slips and covered with the dish lid. The cells were then incubated overnight at 37°c to allow for cell adherence to the cover slips. Cells were seeded at appropriate numbers to allow for no more than 90% confluency to be reached after a 72-hour period. Following incubation, the dishes were then inserted into provided base plates and rotated until locked into place. Any media remaining on the cover slips was aspirated and replaced with 2ml of fresh culture media (specific to each cell line).

Table 2.11 Seeding densities for TTFields experiments.

Cell Line	Seeding Density
SF188	25,000/ml
KNS42	50,000/ml
GCE62	50,000/ml
GIN98	50,000/ml
GCE98	50,000/ml
Human Astrocytes	50,000/ml

2.6.1.3 Application of TTFields

The application of TTFields via Inovitro generates heat, therefore, to compensate for the warming of the media beyond optimal cell culture conditions, all applications of TTF were completed in a specialist cooling incubator which was maintained between 18-22°c. The temperature of the culture media was tracked by the Inovitro software was maintained at 37°c.

The baseplate and attached dished were connected via flat cables to the TTFields generator (cables were fed through the incubator door and caused no issue with incubator closing). The experimental parameters were then defined on the Inovitro system software, whereby experiments could be named and the frequency of the TTFields defined. The treatment was delivered at low intensity 1-3 v/cm and intermediate frequency was 200kHz for experiments. Verification of the connection of the dishes to the base plates is done

automatically via the Inovitro software, with successfully connected plates appearing as light blue. If connection is unsuccessful, dishes can be slowly and carefully disconnected and reconnected to the base plate. The application was then run for 24 hours, if 24hours signalled the end point of the experiment 'END EXPERIMENT' was selected on the software and the experiment can be continued i.e., by assessing viability. If this was not the endpoint, baseplates were disconnected from the generator and transferred to a laminar flow hood, where media was aspirated and replaced. Baseplates were then reconnected, and experiment application was continued. This was to be repeated every 24hours until experiment end point was reached to avoid evaporation of media.

Control samples were generated by using the same cell line in parallel to the TTFields experiments. As with the TTFields condition, 200µl of cells were plated onto cover slips in Inovitro dishes and left overnight to adhere, media was then aspirated and replaced with 2ml of growth media. The dishes were then transferred to a standard CO_2 incubator at 37°c, with media being replaced every 24 hours to replicate conditions of experimental group.

2.6.2 Application on Deep Brain Stimulation for pHGG

2.6.2.1 DBS Lead Maintenance

Before experiments leads were soaked in light detergent for 30 minutes, before then being soaked in 70% ethanol for a further 30 minutes, and thereafter exposed to UV light in a cell culture hood for 20 minutes. Leads were dried and wiped clean before beginning the experiment. DBS field treatment was achieved by delivering electric fields from Neurostimulators via low impedance leads, programmed with N'Vision programmer, with a bipolar configuration and one anode contact (+ve).

2.6.2.2 Deep brain stimulation protocol

Cells were cultured as per the standard protocol defined in section 5.1. Cells were designated to one of four groups: IAA94 100µM with DBS treatment, IAA94 100µM without DBS treatment, no drug and no DBS treatment or no drug and DBS treatment. Cells were seeded at the appropriate seeding density (SF188 5,000 cells/ml, KNS42 8,000cells/ml, GCE62 8,000 cells/ml) in 5ml into a T25 flask. The cell densities were selected to ensure that the control (no DBS treatment) flasks did not reach any higher than 90% confluency by the end of the experiment. Cells were left to adhere overnight, and then topped up to a volume of 20ml of media per flask. This volume of media was selected to ensure enough to cover DBS wired throughout the experiment. Following thorough sterilisation, the DBS electrode leads were pierced through the filter paper in the cap of the culture flask and submerged in the media. The electrode was directed towards the back corner of the flask to ensure contact with the cells. The wires were then fed through the back of the incubated and programmed using a neurostimulator. Control samples receiving no DBS treatment also had leads inserted into the media, but were not connected to the neurostimulator.

2.6.2.3 Programming the Neurostimulator

Before programming the pulse generator, contact between the stimulator and the programmer must be established. The programmer was connected to the back of the generator. The program was set by selecting 'Program MyStim' where the parameter of each lead can be programmed independently for example, a program of (voltage, frequency, and pulse width) 10v, 130hz, 450µs can be used. The parameters used in these experiments were previously optimised by Dr Branter (152). The lead configuration must contain at least one cathode (negative) and one anode (positive) contact to complete the circuit. Resistance of the experiment can be measured to ensure the experiment is running properly and the

leads are fully submerged. Electrode impedance should also be checked, a reading of <500 is considered acceptable.

2.6.2.4 Analysis of DBS treatment and Experiment Endpoints

Following experimental time i.e., 5 days, the program was stopped and leads were removed from the flasks. Growth media was removed and presto blue (1:10 media) was added and incubated for 30 minutes to perform a viability assay. 100µl of prestoblue:media was then transferred to a black well plate and read on a FLOUstar omega. At this point experiment can resume by removing excess presto blue, washing, and adding fresh growth media. Alternatively, cells can be trypsinised and a cell pellet collected.

Cell counts were also performed as described in section 2.4.7.

2.6.3 Partek analysis of electrotherapy associated genes.

The Human Clariom^{TM} S array was used for whole transcriptome gene expression analysis of paediatric GBM cell lines treated with electrotherapy via DBS or TTFields (Data sets were kindly provided by Dr Josh Branter). Bioinformatic analysis was carried out using Partek by Dr Marcos Costellanos.

2.7 Generation of CLIC1 and CLIC4 deficient cell lines

2.7.1 siRNA of CLIC1 and CLIC4

Silencing RNA (siRNA) is a class of 20-25 base pairs of double stranded RNA that operate within the RNA interface pathway (RNAi). The siRNA interferes with specific sequences of complementary nucleotides, therefore degrading mRNA post transcriptionally, preventing translation of the target gene, and reversibly knocking it down.

A SMARTpool methodology was employed to ensure maximum knock down efficiency.

SF188, KNS42, GCE62 and normal human astrocytes were seeded overnight to allow for

adherence to the flask. Seeding density was calculated individually for each cell line to allow for no more than 70% confluency at the point of transfection. Following this, cells were transfected with 20 nM of either CLIC1 siRNA oligonucleotide (ON-TARGET plus siRNA, Dharmacon) or CLIC4 siRNA oligonucleotide (ON-TARGET plus siRNA, Dharmacon) or a negative control siRNA (AM4611, Invitrogen™) that has no known complimentary target sequence. Target sequences can be found in table 2.12.

Table 2.12 Target sequences of pooled siRNAs in CLIC1 SMARTpool (Dharmacon, UK)

ON-TARGETplus SMARTpool siRNA	Target sequence	Molecular weight
J-009530-05, CLIC1	GGAGAUCGAGCUCGCCUAU	13,460.1 (g/mol)
J-009530-06, CLIC1	CAUCGGUACUUGAGCAAUG	13,430.1 (g/mol)
J-009530-07, CLIC1	GGCAAAGGCCCUCAAAUAA	13,430.1 (g/mol)
J-009530-08, CLIC1	GGACCGAGACAGUGCAGAA	13,460.1 (g/mol)

Table 2.13 Target sequences of pooled siRNAs in CLIC4 SMARTpool (Dharmacon, UK)

ON-TARGETplus SMARTpool siRNA	Target sequence	Molecular weight
J-013553-05, CLIC4	CCAAAAGACUCACCAAGUA	13,415.1 (g/mol)
J-013553-06, CLIC4	CCUCAUAGCUUAAAGUAUA	13,385.1 (g/mol)
J-013553-07, CLIC4	UGACUUAGCUAUAGCAGUA	13,400.1 (g/mol)
J-013553-08, CLIC4	GACAAAAGCUAGCUAGUAA	13,400.1 (g/mol)

The selected transfection reagent was Lipofectamine 3000™ (L3000008, Invitrogen™) due to supporting literature (146) suggesting that this had the highest success rate in

transfection of the commercial cell lines KNS42 and SF188. Prior to transfection Lipofectamine 3000™ was diluted in optiMEM (Gibco™) growth medium and left to incubate for 5 minutes at room temperature, the specific volumes of each reagent are dependent on the size of the transfection vessel, suggested volumes can be found via ThermoFisher™ . Each siRNA oligo (20nM) was then incubated with an equal volume of OptiMEM that was used to dilute the Lipofectamine3000™, and the two dilutions were combined 1:1 and left to incubate at room temperature for 15 minutes to allow complexes to form. The media was then removed from the cells and replaced with the Lipofectamine, OptiMEM and siRNA mix, and left to incubate for 24 hours, at which stage the transfection mix was replaced with whole media. A non-targeting (NT) siRNA scramble sequence was employed as a control.

2.7.1.1 Confirmation of CLIC1 and CLIC4 knock down.

To optimise and guarantee transfection efficiency cell pellets were collected from each cell line with each knock down after 24, 72, and 120 hours and the knockdown was verified by both qrt-PCR and western blot analysis to observe the effect on protein cycling. A suitable experimental window was then selected for each gene and cell line.

2.7.2 CRISPR-Cas9

CRISPR-cas9 induced SF188 (iCas9) and GCE28 (iCas9) cell lines were kindly gifted by Dr Alan McIntyre, University of Nottingham. Generation of a stable knock out of CLIC1 and CLIC4 was carried out via CAS-9 mediated lentiviral silencing. CLIC1 and CLIC4 lentiviral particles were purchased from SigmaAldrich, and their sequences are below. The following protocol was optimised by the Hypoxia and Acidosis Group, ran by Dr Alan McIntyre, University of Nottingham.

Cells were initially transduced with Dharmacon Edit-R Inducible Lentiviral hEF1a-Blast-Cas9 Nuclease Particles to introduce an inducible Cas9. Prior to transfection with gRNA, cells were retrieved from liquid nitrogen and grown until 70% confluent. A cell suspension was prepared by trypsining and centrifugation. Cells were then counted to give a final seeding density of 20,000 cells per well in 200μl of media.

Each cell line was plated into 5 wells of a 24 well plate: 1 well for each gRNA plus 2 control wells per cell line, these will be for un-transduced cells + and – puromycin, and a nontargeted gRNA control). Transfection is carried out under the presence of polybrene (final concentration 8ug/mL polybrene).

Following this this the volume of virus needed for transfection is calculated. The MOI provided on the data sheet is the number of viral particles per cell. Prior optimisation by McIntyre group has determined that an MOI of 5 is sufficient to ensure an efficient transduction. For non-targeting gRNA virus and MOI of 0.5 was used. The equation below is used to calculate the volume of virus to use for each transfection, where the VP/ml is the specific titre of each virus and is batch specific.

$$\boldsymbol{ul\ virus} = \left(\frac{\boldsymbol{MOI} * \boldsymbol{no.of\ cells}}{\boldsymbol{VP/ml}}\right) * \mathbf{1000}$$

Table 2.14 CRISPR-CAS9 target sequences. Lentiviral backbone, LV04.

Gene	Clone ID	Target sequence	Titre (VP/Ml)
CLIC1 G1	HSPD0000007695	AATGGGCAGTTCCCAATCT	$8.0x10^6$
CLIC1 G2	HSPD0000007696	TTCATGGTACTGTGGCTCA	$7.4x10^7$
CLIC4 G1	HSPD0000076598	CCCGGGAGCCAAGTTCTGC	$7.2x10^6$
CLIC4 G2	HSPD0000076599	GAGGCTCTTCATGATTCTT	$9.0x10^6$
-ve control	NEGATIVECONTROL1	CGCGATAGCGCGAATATATT	$8.0x10^7$
+ve control	HSCONTROL_AAVS1	GGGGCCACTAGGGACAGGAT	$7.9x10^6$

The viral gRNA was then added to the bottom of a well (24 well plate) and the polybrene/cell suspension added and swirled gently to mix. The plate was then incubated for 24 hours. Following this, cells were gently washed with PBS to removed live virus and 300ul of fresh medium added, and incubated until they reached 70% confluency.

2.7.2.1 Puromycin selection

Once 70% confluent puromycin selection can begin. Prior to investigation, a puromycin kill curve was carried out on each cell line to determine the optimum concentration of puromycin for selection. Selection of transfected cell lines was carried out by dosing cells with 1ug/ml puromycin every 48 hours. This was completed over several passaged to ensure selection. The media was removed and replaced with media containing 1ug/ml puromycin. Puromycin was added to all wells except from the 'minus puromycin' control wells. Cell growth in wells dosed with puromycin was compared to the untransduced +

puromycin control, and – puromycin conditions. Selection was continued for 7-10 days or until all of the untransduced cells treated with puromycin are dead.

2.7.2.2 Doxycycline induction of CAS9

Following puromycin selection, doxycycline (4μg/ml) was used to induce CRISPR-Cas9 activity. Cells were dosed with 4μg /ml doxycycline for 48hours, washed, and re-dosed for a following 48hours prior to experimentation.

2.7.2.3 Validation of CRISPR-CAS9 knock out of

Validation of CRISPR-cas9 knock out of CLIC1 and CLIC4 was carried out by western blotting technique as described in section 2.11.5 and analysis carried out as described in section 2.11.6.

2.8 Assessment of invasive and proliferative capacity of HGG

2.8.1 Modified Boyden chamber assay as a measurement of invasion of HGG cells

A modified Boyden chamber assay was utilised to assess the invasive capacity of HGG cell lines. In this transwell based assay, cells are seeded onto the upper surface of a polycarbonate membrane consisting of randomly distributed pores coated in ECM component in this case, Collagen IV was used to mimic the basement membrane.

Prior to experimentation, the upper surface of the ThinCertTM (Corning, 8μm pore size) transwell was coated with 0.5mg/ml mouse Collagen IV (Cultrex), and left to dry overnight in a shaker incubator at 37°C in a 24 well plate. Cells were harvested and counted following either drug treatment, siRNA transfection or non-treatment conditions, and re-suspended in cell culture media containing no FBS. 200μL of cell suspension (1x10^4 cells) was seeded onto the upper surface of the transwell. Following this, 600μL of complete cell culture media (containing 10% FBS) was placed in to the well to create a chemo-attractant gradient for the cells to invade towards. The cells were then left to invade overnight at 37°C, 5% CO_2.

Following incubation for 24 hours, the non-invading cells and residual collagen IV was removed from the upper surface of the transwell by scrubbing with cotton bud. The invading cells (on the lower surface of the transwell) were fixed for 50 minutes using 100% ice cold methanol (VWR chemicals) and subsequently stained for 20 minutes using a 0.5% crystal violet stain.

2.8.1.1 Quantification of cell invasion

Quantification was performed using a light microscope by counting invading cells from 4 pre-selected microscopic fields (40x magnification). The number of invading cells in treatment conditions was then normalised to their control conditions, and data presented at percentage of invading cells. Statistical analysis was carried out by using a student's T-Test on GraphPad Prism 9, a p value of <0.05 was considered significant.

2.8.2 Clonogenicity of HGG

A clonogenic (colony forming assay) was used in analysis of the clonogenic survival capacity of HGG cells subject to drug treatment, TTFields or siRNA transfection. This assay provides real-time insight into the proliferative capacity of a cell line and reproductive death, thus the cytotoxicity of treatment of interest.

To assess cell sensitivity to drugs, cell lines were plated in a 6 well plate or t25 flask at a pre optimised cell density in standard cell culture media and left to adhere overnight at 37°C in5% CO_2. Following adherence cells were treated with the chemotherapeutic of interest, with maintenance doses given every 72 hours via media change. The cells were then left to form colonies for 10 days or until the cells present in the control plates (Vehicle control) had formed visible colonies of a substantial size (50 cells per colony). Subsequently, the cells were washed with PBS and fixed in 1:1 methanol (100%):saline for 15 minutes. The

cells were then fixed in 100% methanol for 20 minutes. Post fixation, the cells were then stained with a 0.5% crystal violet stain.

For cultures subject to TTFields or siRNA transfection, cells were either pre-treated with TTFields for 72 hours and harvested before plating for colony analysis, or subject to reverse transfection with siRNA (as described in section 2.7). Transfected cells were left to adhere for 24 hours, with a subsequent media change to remove any toxic Lipofectamine3000™. The protocol was then followed as previously described in this section.

2.8.2.1 Quantification of clonogenic capacity

To quantify colony forming units (clonogenic capacity) stained cells were manually counted, taking the average number of colonies formed per replicate of each condition. The data was then normalised to a percentage of colony forming units by normalising each treatment condition to the relevant control.

2.9 Assessment of ion channel activity in pHGG

2.9.1 Chloride efflux assay

Assessment of the chloride flux into and out of the cells was performed using the Abcam Chloride Channel Assay Kit (Colorimetric) (ab176767). This protocol was optimised with some deviation from the original protocol. Cells were seeded overnight into a black walled clear bottom 96-well plate, according to the adherent cell protocol. Seeding densities were as followed: SF188 40,000 cells/well, KNS42 60,000 cells/well and GCE62 60,000 cells/well, GIN98 60,000/well, GCE98 60,000/well and astrocytes 60,000/well. Prior to experiment, all reagents were warmed to room temperature.

2.9.2 Iodide efflux assay

Following overnight incubation, the growth media was removed from the cells and 100 µL/well of I-loading buffer was applied to each well and incubated for 4 hours at 37°C.

Following this, the loading buffer was aspirated, and the cells were then treated with either IAA-94 in media (100µM) or metformin (10mM) and controlled via media + vehicle (0.1% DMSO or and water respectively) for 48 hours. For TTFields and siRNA transfection, treatment protocols were carried out as previously descried, and cells harvested prior to experimentation. The cells were then washed 3 times with HBSS and lysed by adding 50µL/well of 1x cell lysis buffer.

2.9.3 Iodide assay

Following cell lysis, 50µL of Iodide Sensor Blue Dye was added to each well, followed by 50µL for the 1x Iodide Sensor Enhancer. The absorbance was then measured at 405nm on the FLUORstar Omega plate reader, and results visualised in GraphPad Prism 9.0.

2.9.4 Membrane potential assay

The FLIPR® membrane potential assay (Molecular devices, RED (R8126) kit was used as a high throughput fluorescent based assay to assess changes in membrane potential. This assay detects bidirectional gradient changes in fluorescence, allowing monitoring of both variable and control conditions within a single experiment. This assay is able to detect voltage-based changes across cellular membranes.

Prior to experimentation $5x10^4$ Cells were seeded into clear bottom, black walled 96-well plates and left to adhere overnight in 100µl of media. Following this, the FLIPR Membrane Potential Assay reagent (Red) was dissolved completely in 10ml of the 1x Assay buffer from the kit and mixed well to ensure residual dye was dissolved. An equal volume of Loading Buffer was added directly to the cells without removing the media or washing (100µl) and the cells were incubated at 37 °C for 30 minutes.

Where membrane potential was being assessed in siRNA knock down of CLIC1 or CLCI4, TTFields or in response to IAA94 or metformin, the cells were pre exposed to the experimental conditions (as described previously) before starting experimentation.

2.9.4.1 Analysis of membrane potential activity via Flexstation

Following incubation with Loading Buffer/Membrane Potential Assay reagent, the relative fluorescence was measured using a Flexstation plate reader (Molecular Devices) with the parameters stated in tables 2.16 and 2.17 and analysis was performed using the SoftMax Pro 5.4 software.

To measure a cellular response to voltage changes, an injection of KCl (0.5M) was performed at 20 seconds into the read to elicit a membrane potential response, with each well of the plate being read independently.

Table 2.15 Wavelength parameters for Flexstation

Parameters	Wavelength (nm)
Excitation wavelength (nm)	530
Emission wavelength (nm)	565
Emission cut-off (nm)	550

Table 2.16 Experimental parameters for Flexstation

Parameters	Addition
Pipette Height (µL)	230
Transfer Volume (µL)	50
Compound Concentration	5x
Addition Speed (Rate)	2-3
Compound addition	20s

2.9.4.2 Flexstation data analysis via SoftMax Pro 5.4

To analyse membrane potential assay data, fluorescent values were exported to the SoftMax Pro 5.4 software (Molecular devices). The values for each well were reduces using the reduction function, and a numerical value assigned to each well. Data was then normalised via the 'area under curve' function and exported to GraphPad prism 9.0. Fluorescent values were taken from the point following depolarisation via KCl injection at 20s and the individual readings were normalised as a percentage change when compared to the un-treated samples.

2.9.5 Patch clamping

Patch clamp experiments were kindly carried out by Dr Paul Smith, University of Nottingham.

Pipettes were pulled from Harvard GC150TF-15 thin-walled borosilicate glass capillaries (Harvard Apparatus, Cambridge, UK) using a PC-10 dual-stage glass micropipette puller (Narishige International, London, UK) and the tips coated in sticky wax (Kerr Dental, Peterborough, UK). Prior to experiments pipettes were fire polished using a MF-900 microforge (Narishige) to a resistance between 3-5 MΩ.

For cell-attached recordings pipettes were filled with a high KCl solution which contained (in mM): 146 KCl, 2.6 CaCl2, 1.1 MgCl2 and 10 HEPES (pH 7.4, free [Ca2+]> 1.5 mM) and cells were bathed in Hanks which contained (in mM): 143 KCl, 1.2 NaH2PO4, 1.2 MgCl2, 2.6 CaCl2, 4.2 NaHCO3,10 HEPES, (pH 7.4 with NaOH) and 10 glucose. Following formation of a gigaohm seal, currents were recorded with a pipette potential of +70 mV, digitised at 10 KHz and filtered at 2 kHz with an 8 pole Bessel. For single-channel current amplitude voltage

relationships, the pipette was held at potentials in 10 mV incremental steps, each of 1 minute duration.

Whole cell recordings were made using Hanks solution in the bath either with the high KCl ([Cl-] = 153.4 mM) high free free [Ca2+] solution in the pipette or a low Cl ([Cl-] = 16 mM) low free [Ca2+] (45 nM) low Cl solution which contained (in mM): 130 KGluconate, 10 NaCl, 2 MgCl2, 1 CaCl2, 3 EGTA, 10 HEPES, (pH 7.4 with NaOH) and 10 glucose. Voltage-gated currents were elicited by a voltage step protocol, with the membrane potential increased by 10 mV increments, from a holding potential of -70 mV at a frequency of 0.1 Hz and step duration of 240ms. Currents were filtered at 5 kHz. No leak subtraction was used.

Recordings were made using an Axopatch-1D (Axon Instruments, Scottsdale, AZ, USA) patch clamp amplifier and a Digidata 1440A low-noise digitizer controlled by PClamp 11 software (Molecular Devices, Sunnyvale, CA, USA). All electrophysiology experiments were performed at room temperature (20-25°C).

Data was then exported and analysed in GraphPad prism 9.0.

2.10 Cell Cycle Analysis

Cell cycle analysis of pHGG cell lines was performed using flow cytometry with propidium iodide staining and analysed using Kaluza.

Following 72 hours of treatment with IAA94 or transfection of CLC1 or CLIC4 siRNA, cells were trypsinised and counted (seeding density $1x10^5$ cells). Cells were then centrifuged at 1500rpm for 5 minutes to collect a pellet, and the media supernatant was removed. The cell pellet was then re-suspended in ice cold PBS via pipetting, and the fixed with ice cold 70% ethanol and fixed overnight at 4°C. Following incubation, the cells were then centrifuged at 1500rpm (800xg), re-suspended in PBS and re-centrifuged to remove traces of ethanol. The

supernatant was then aspirated, and the pellet re-suspended in DNase-free RNase A (100ug/ml in cold PBS) and propidium iodide (PI) (0.1% triton-x, 10ug/ml PI), and incubated in the dark, at room temperate for 30 minutes. The cells were then analysed using SONY ID7000. The cell cycle fit curve was then analysed using Kaluza, and the percentage of cells present under the curve was used to determine the percentage of cells present in each stage of the cell cycle.

2.11 Molecular biology

2.11.1 Immunohistochemistry

IHC analysis was used to assess clinical correlations and significance of experimental results. Immunohistochemical labelling of formalin-fixed paraffin embedded tissue micro array sections and surgically retrieved glioblastoma tissue, temporal lobe tissue and control tissue was carried out. Initially the concentration of antibodies and incubation time was optimised, and appropriate conditions selected. Slides were placed on a hotplate at 60°C for 10minutes in order to fully melt the wax on the sections before proceeding with removal of paraffin wax.

Slides were dewaxed by fully submerging the sections in the following series of reagents: xylene for 10 minutes, xylene 5 minutes, 100% ethanol 5 minutes, 100% ethanol 5minutes, 95% ethanol 5 minutes, 80% ethanol 5 minutes and 70% ethanol 5 minutes. Following the final ethanol bath slides were rinsed thoroughly in deionised water, ensuring the water ran clear.

The antigen retrieval method utilised was heat exposure via pressure cooker. Sodium citrate buffer (pH 6.0) was poured into a pressure cooker and brought to a boil on a hot plate. Slides were then placed into the pressure cooker and the lid secured safely; slides were treated for 7 minutes once full pressure reached. The pressure cooker was then left to depressurise and then slides were cooled.

Following antigen retrieval, slides were washed in PBS with agitation or 2 minutes and which time a humidified staining box was set up. Sections were then outlined with a hydrophobic barrier pen to prevent any loss of reagent during the staining process. Sections were then covered with 20% NGS in PBS and left to incubate at room temperature for 20 minutes. The sections were then washed in PBS for 5 minutes with agitation. Slides were then covered with 200μL-400μL of blocking solution from the Dako Chemate Envision Kit and left to incubate for 5 minutes. A subsequent 5-minute wash with PBS then followed. Primary antibodies diluted in antibody dilutant (Chemate Envision Kit, Dako) were then applied to the sections and left to incubate for 2 hours at room temperature (incubation times were decided after experiment optimisation. For antibody dilutions see below table. Following incubation of primary antibody, the slides were then washed 2x for 5 minutes in PBS with gentle agitation. The sections were then covered with secondary antibody (Chemate Envision Kit, Dako) and incubated at room temperature for 30 minutes. This was then followed by a final wash in PBS. A 200μL of DAB (1ml PBS to 20μL of DAB) was applied to each section and incubated for 15 minutes. The slides were then rinsed gently with distilled water and then placed in a rack and agitated gently in Harris Haematoxylin (10-60 second) to counterstain. The slides were washed in running water until no colour was visible and then returned briefly to each of the xylene and ethanol series as follows: 70% ethanol, 80% ethanol, 95% ethanol, 100% ethanol, 100% ethanol, xylene, xylene. The slides were then left in the final xylene ready for mounting.

Table 2.17 Antibodies used for immunohistochemistry – species, dilution and incubation time. Positive control as per manufacturers recommendation. Incubation and dilution time selected following optimisation protocols.

Name	Species	Clone	Company	Positive Control Tissue	Incubation Time	Dilution
CLIC1	Mouse	356.1	Santa Cruz (sc-81873)	Kidney Tissue	120 minutes	1:200
CLIC4	Mouse	45.42	Santa Cruz (sc-135739)	Duodenum	120 minutes	1:200
ZEB1	Rabbit	-	Invitrogen	Glioma	60 minutes	1:500

Tissue sections were then viewed under a light microscope and observed for staining intensity, to optimise the protocol the staining quality was assessed, and incubation times and antibody dilutions were reassessed. To image tissues an Olympus DP25 light microscope was used.

2.11.1.1 Scoring of tissue staining

Stained TMAs were scanned and visualised using NDP.View2 (Hamamatsu). Each TMA was aligned to a specific sample using a TMA map of historical glioblastoma specimens collected at Queens Medical Centre. The TMA was created in-house by the CBTRC whereby PFFA fixed tissue blocks were carefully assessed by a trained pathologist, and appropriate cores selected for the TMA generation.

Each core was carefully examined, and the extent of staining assessed. A score based on relative staining intensity was assigned to both the cytoplasmic and nuclear elements of the tissue core. A score of 0 = no staining, 1+ = weak staining, 2+ = moderate staining and 3+ = strong staining. All staining was double scored by an independent individual.

2.11.1.2 Patient clinical data analysis

For the purpose of analysis, cores staining 2+ and 3+ were considered CLIC1 and CLIC4 positive. The upper and lower quartiles of the staining scores were taken from all the cores to split the data into CLC1/CLIC4 + and CLIC1/CLIC4 – i.e., cores expressing high or low levels of the chosen ion channel proteins. This exclusion was carried out relative to positive control tissue, or normal temporal lobe tissue.

Graph pad prism was then used to generate Kaplan-Meier curves for survival analysis of protein expression vs survival in months for each of the patients. Statistical analysis on these data included log rank and chi^2 tests.

2.11.2 Immunofluorescence

For fluorescent staining, cells were seeded overnight and left to adhere to an 8 well staining chamber slide (Merck). 400µl of cell suspension was applied to each well at a seeding density of 15,000 (GIN98, GCE98, Astrocytes KNS42 and GCE62) or 10,000 (SF188) cells per well. Following overnight incubation, the media was aspirated, and the cells were washed in PBS. Following washing and removal of PBS the cells were fixed at room temperature with 200µl of 4% paraformaldehyde (PFA) for 10-15 minutes. The PFA was aspirated, and the cells were washed with PBS, and at this stage the chambers were either filled with PBS, covered in parafilm, and stored at 4°C or the experiment was continued. The cells were then permeabilised in (0.1%) Triton-x PBS and incubated for 30 minutes at room temperature. Dependant on cell adherence, the slides were then rinsed in PBS, if cells were semi-adherent this stage was skipped to retain cell number. The cells were then blocked in 10% normal goat serum in PBS for one hour in a humidity chamber. Following this, blocking solution was tipped off and the slides were incubated with primary antibody (CLIC1 1:50, CLIC4 1:50, Santa Cruz) diluted in 10% NGS for 1 hour at room temperature in the humidity chamber. Next, 5, 10 and 15-minute washes were carried out with PBS-T (0.1% tween). The secondary

antibody was then applied to the cells (anti-Mouse Alexa Flour-488, Thermofisher) at a dilution of 1:100, diluted in 10% NGS for 1 hour at room temperature. Washes of 5, 10 and 15 minutes were repeated with PBS-T. The cells were then counterstained with DAPI (300nm) (Thermofisher, USA) and incubated at room temperature for 10 minutes. The chamber slide plastic was then carefully removed, and slides were mounted with Fluoromount-G™ (Thermofisher, USA) and left to dry in the dark. Slides were imaged with a Leica DMR microscope within a week of initial staining, and stored in the dark at 4°C. Immunofluorescent staining of neurospheres was completed in an Eppendorf after collecting neurospheres grown for four days as previously explained in 2.4.3. Neurospheres were briefly centrifuged between each of the above steps to ensure spheres were not lost.

2.11.2.1 Analysis of immunofluorescence

Slides were imaged using a Leica SPEII Confocal Microscope with a 20x air lens and 488 nm, 633 nm, and 405 nm lasers. All images were taken at 1024 x 1024-pixel resolution. The resulting images were then viewed and analysed using Fiji (ImageJ) software.

In order to quantify the cytoplasmic and overall staining intensity of multi-channel immunofluorescence images, Fiji (ImageJ) software was employed. A binary-mask generation method was employed to assess fluorescent intensity. The multi-channel images were opened and converted to single channel images by splitting the 405 and 488 channels. Next, either the 488 channel (conjugated secondary antibody; protein of interest) or the 405 channel (DAPI nuclear stain) was selected and the “mean” threshold function was used to isolate the overall staining of the region of interest. This was repeated for each channel used. Alternatively, regions of interest ROIs were generated using the “analyse particles” function, and the “measure” command was executed, displaying a relative fluorescent signal

for the ROI. These data were normalised to background signal reads, and significant differences were analysed in GraphPad Prism 9 via a t-test. The antibodies used for this experiment are the same as described above in section 2.18.

2.11.3 qRT-PCR

2.11.3.1 RNA Extraction

RNA was extracted from each cell lines and neurospheres using the mirVana miRNA isolation Kit (Ambion, TX), whereby cell pellets were re-suspended in 300µl lysis/binding buffer, breaking up the pellet by pipetting. Following this, 30µl of miRNA homogenate additive was added to the lysate, vortexed and incubated on ice for 10 minutes. After incubating on ice, 300µl of Acid-Phenol:Chloroform (Ambion, TX) was added to the lysate and vortexed for 1 minute. After vortexing the samples was centrifuged at 10,000xg for 5 minutes allowing for the upper aqueous phase (nucleic acids) to form. The aqueous phase was removed and pipetted into a clean Eppendorf tube along with 375µl of 70% EtOH. The ethanol/lysate mixture was then vortexed and pipetted into a filter cartridge inside a collection tube (MirVana miRNA extraction kit) and centrifuged for 1 minute. Flow through was discarded. 700µl of miRNA wash solution 1 was added onto the cartridge and again centrifuged at 10,000xg for 1 minute, discarding flow through. This was repeated two times with wash buffer 2/3. Finally, the cartridge was centrifuged a final time to remove any remaining wash buffer. The filter cartridge was then transferred into a new Eppendorf tube. Nuclease-free water was pre-heated to 95°C and used as an elution agent. 50µl was pipetted onto the filter cartridge and left for 1 minute before centrifuging at 10,000xg for 1 minute to collect RNA. Nanodrop readings were then taken to determine RNA concentration and The RNA was stored at -80°C.

2.11.3.2 Spectrophotometric Analysis

Spectrophotometric analysis is essential for determining biomolecules concentration. The concentration of RNA and DNA was quantified using the NanoDrop 2000 (ThermoFisher Scientific, USA). Prior to its use, the instrument was calibrated with sterile NFW to clear any previous sample spectrum and provide a blank reading. Absorption ratios of 260/280 and 260/230nm were quantified to assess the extent of protein and organic contaminants (chaotropic salts) respectively. Absorbance ratios between 1.8-2.2 and 2.0-2.2 for 260/280 and 260/230nm ratios respectively were considered acceptable for subsequent cDNA synthesis.

2.11.3.3 cDNA synthesis

cDNA was synthesised from RNA in volumes of 20μl reactions using a High-Capacity cDNA reverse transcription kit and a BioRad T100 Thermo cycler (BioRad laboratories, UK). All samples were transcribed at a concentration of 1200ng RNA. All cDNA samples were stored at -80°C until qPCR analysis. Samples and all reagents were kept on ice at all times unless otherwise stated and prior cleaning of lab space with RNA-Zap and IMS was carried out to prevent contamination.

Initial RNA denaturation was prepared with the following master mix (MIX1) for (n x 2)+1=y where n = number of samples. Nuclease free water (y x 3.2 µl) and Random Primers (y x 2.0 µl) were aliquoted into an Eppendorf to make up MIX1. Following this, 10.4 µl of MIX1 was aliquoted into tubes labelled with RNA samples, and 20 µl of total RNA was pipetted into each tube containing MIX1. Following resuspension, the RNA+MIX1 solution was incubated on a heat block at 70°C for 10 minutes. Denatured RNA samples were transferred to ice immediately after.

Using the denatured RNA, the following cDNA synthesis reaction was set up. Each reaction was carried out in 20 µl final volume, containing 10 µl of RNA at 120ng/µl concentration i.e. each RT is done using 1200ng total RNA (totRNA). The following table denotes the total volume of reagents per reaction.

Table 2.18. rtPCR master mix recipe

Reagent	Volume (µl)
10XRT Buffer	2.0 µl
dNTP mix	0.8 µl
Random Primers	2.0 µl
RNAse inhibitor	1.0 µl
Nuclease free water	3.2 µl
Reverse Transcriptase	1.0 µl
RNA (120ng/µ)	10 µl

Table 2.19 Thermocycler parameters for cDNA generation

Temperature (°C)	Time (minutes)
25	10
37	120
85	5

Each RT reaction was completed in duplicate: one containing the RT enzyme (+RT) and one where RT is substituted with water (-RT). This is to control for any genomic contamination in RNA samples as well as other reaction components.

2.11.3.4 qRT-PCR

qPCR experiments were assessed using Taqman probes (Thermofisher). Assay efficiencies were generated for all reference and target genes using the respective cell lines. Standard curves were assessed on each group. Five 1:10 serial dilutions from the initial cDNA sample.

Table 2.20 Gene probes used for qrt-PCR (TaqMan)

Gene	Purpose	TaqMan assay
CLIC1	Target gene	Hs00559461_m1
CLIC4	Target gene	Hs00749895_s1
P2RX4	Target gene	Hs00902156_g1
P2RX7	Target gene	Hs00902156_g1
SCNN1A	Target gene	Hs00168906_m1
SCNN1D	Target gene	Hs00936289_m1
GAPDH	Reference gene	Hs00939621_m1
HPRT1	Reference gene	Hs02800695_m1
Actin	Reference gene	Hs00939627_m1

qPCR of each sample was performed in triplicate containing 2μL cDNA solution, 10μL 2x TaqMan Universal MasterMix, 0.7μL TaqMan Gene Expression Assay and 7.3μL H2O. Reactions were performed by initial denaturation at 95°C for 10 min followed by 50 cycles of denaturation at 95C for 15s and annealing/ extension at 60C for 1min.

2.11.4 RNA extraction from FFPE patient tissue

To extract RNA from patient FFPE tissue, a column extraction method was employed. Prior to extraction, 10µm sections were taken from patient tissue of interest. No more than 4 x 10µm sections were used per extraction, and each replicate was carried out using consecutive sections on from the same block.

Initially dewaxing was carried out as per the AllPrep DNA/RNA FFPE (Quiagen, Germany) kit instructions, however the dewaxing proved to be insufficient, and RNA yield was <2ng/µl. Subsequently, dewaxing of the FFPE sections was carried out as follow: 4x10µm sections were dewaxed with 1ml of 100% xylene (VWR chemicals) and agitated at high speed for 15 minutes. The samples were then centrifuged at full speed (>20,000 rpm) for 5 minutes. The excess xylene was removed from the tissue pellet, and 1ml of 100% Ethanol (VWR chemicals, UK) was added to extract residual xylene from the tissue, with agitation for 10 minutes. The tissue was again centrifuged at >20,000 rpm for 5 minutes, and excess ethanol removed. The tissue was then left to air dry at 37°C for 15 minutes to allow any residual ethanol to evaporate.

RNA extraction was then performed according to the manufacturer's handbook, whereby the lysate was lysed via proteinase K. The RNA was then separated from the DNA pellet, and heated to 80°C. The total RNA was then bound using a column, treated with DNAse, washed and eluted. RNA concentration was then determined via NanoDrop.

2.11.5 Immunoblotting

2.11.5.1 Protein extraction

Cells were washed, trypsinised and collected according to the method described in section 2.4. Cell pellets were resuspended in up to 500μL of RIPA buffer with protease inhibitors (volume of lysis buffer added was dependant on cell pellet size and cell number). Samples were then incubated on ice for 20 minutes and high molecular weight DNA was sheared using a needle and syringe. Samples were then transferred into a sonicator where high frequency waves were applied for 15 minutes. Following sonication, the samples were again sheared 20 times with a needle and syringe and then centrifuged at 13,000xg for 60 minutes at 4°C.

2.11.5.2 Protein concentration quantification

The concentration of the protein present in the sample was calculated via standard BCA assay (Walker, 1994), whereby known concentrations of BSA standards were compared to sample values using an y=mx+c line equation.

A protein standard curve was created by dissolving bovine serum albumin (Sigma, UK) in homogenisation buffer to obtain the following standards (mg/ml): 0.1, 0.2, 0.4, 0.6, 0.8, 1mg/ml. 10μl of each standard or protein lysate was applied in triplicate to the well of a 98 well plate (Greiner, UK) placed on a cool block to prevent protein degradation. Immediately after, 90 μl of BCA assay reagent (Bicinchoninic acid: 4% copper II sulphate pentahydrate (50:1)) was added to the respective wells and incubated at 37°C for 30 minutes. Following incubation, absorbance was read at 562nm in an plate reader (Thermo, UK).

2.11.5.3 Immunoblotting

Electrophoretic blotting of protein samples was carried out on a 10-12% gel using 20μg overall protein concentration. 10μL of sample was loaded into a pre-cast gel (Mini-Protean, Biorad) and ran against a protein ladder of known molecular weights (Precision Plus Protein Dual Colour, Biorad). Samples were run at 40mA for 60minutes or until complete separate of bands observed on reference ladder in western blot running buffer (100ml 10x Running buffer (Pierce, ThermoFisher) and 900ml dH2O).

Subsequently, transfer of the proteins onto a 4.5μm nitrocellulose membrane (ThermoFisher) was performed at 100v for 50 minutes in transfer buffer (100ml 10x Transfer buffer (Pierce, ThermoFisher), 200ml Methanol (VWR chemicals) and 700ml dH2O).

The membrane was then blocked in 5% milk in TTBS (0.05%Tween20) for 60minutes at room temperature on a shaker. Blocking solution was removed and the membrane was incubated with the primary antibody diluted in TBS-T for 60minutes at room temperature or overnight

at 4°C with gentle agitation. Following incubation, the primary antibody was removed, and the membrane was washed in TBS-T for 5x10 minute under strong agitation at room temperature. After washing, the membrane was incubated with secondary antibody (1:50,000-1:250,000) in TBS-T for 60mins at room temperature. Following incubation, the secondary antibody was removed, and the membrane was washed in TBS-T for 5x10 minute under agitation at room temperature. Blot development was followed according to the Immun-Star™ AP Chemiluminescence Kits, luminol/enhancer and peroxide buffer were mixed 1:1 with 125ul of substrate solution. (12ml total for one membrane) and the membrane was incubated in the solution for 3-5 minutes. Following incubation excess substrate was drained off, and it was the processed for camera detection and semi-quantitative analysis.

2.11.5.4 Analysis of Immunoblots

Semi quantitative analysis of immunoblots was performed via the "Gels" analysis tool from Fiji, ImageJ software. The band of interest was selected using the rectangular selection tool, generating a histogram and raw number indicating the intensity of the band. To calculate the relative densities of each band, the area of the peak of the histogram was measured, and normalised by the area of the relative control band peak. This was repeated across blots, and values normalised to housekeeping control. Significance was calculated using a paired and unpaired T-Test (GraphPad Prism 9).

2.12 RNA sequencing

RNA was extracted from FFPE patient tissue as described in section 2.11.4. Prior to sequencing, RNA integrity and concentration was assessed via a Qubit (ThermoFisher, UK) and Tapestation (Agilent, UK) and exclusion of genomic DNA contamination of the samples was carried out via PCR.

2.12.1 Lexogen sequencing pipeline

Nine RNA samples submitted for 3' RNA Seq using the Lexogen QuantSeq 3' mRNA-Seq library prep kit. RNA concentrations and integrity assessed using the Agilent TapeStation 4200 and the Agilent RNA ScreenTape Assay Kit (Agilent; 5067-5576 and 5067-5577).

2.12.2 Library Prep

For all samples, cDNA was generated from 50-100ng of total RNA using the QuantSeq 3' mRNA-Seq library prep kit for Illumina (FWD) (Lexogen; 015.96) - Low Input/Low Quality/FFPE RNA Protocol.

Indexed sequencing libraries were prepared using the Lexogen i7 6nt Index Set (Lexogen; P04496). For samples ds1166_1 to ds1166_6 - 17 cycles of PCR. For samples ds1166_7 to ds1166_9 – 20 cycles of PCR.

2.12.3 Library QC

Libraries were quantified using the Qubit Fluorometer and the Qubit dsDNA HS Kit (ThermoFisher Scientific; Q32854). Library fragment-length distributions were analyzed using the Agilent TapeStation 4200 and the Agilent High Sensitivity D1000 ScreenTape Assay (Agilent; 5067-5584 and 5067-5585). Libraries pooled in equimolar amounts and final library quantification performed using the KAPA Library Quantification Kit for Illumina (Roche; KK4824)

2.12.4 Sequencing

Library pool sequenced on the Illumina NextSeq 500 Platform, on a NextSeq 500/550 Mid Output v2.5 150 cycle kit (Illumina; 20024904), to generate approximately 5 million 75bp single end reads per sample.

Sample QC, library preparation and QC, and sequencing RNA concentrations and integrity was assessed by the DeepSequencing facility (University of Nottingham) using the Agilent TapeStation 4200 and the Agilent RNA ScreenTape Assay Kit (Agilent; 5067-5576 and 5067-5577). For all samples, cDNA was generated from 50-100ng of total RNA using the QuantSeq 3' mRNA-Seq library prep kit for Illumina (FWD) (Lexogen; 015.96) - Low Input/Degraded RNA Protocol. Indexed sequencing libraries were prepared using the Lexogen i7 6nt Index Set (Lexogen; P04496). For samples ds1166_1 to ds1166_6 - 17 cycles of PCR. For samples ds1166_7 to ds1166_9 – 20 cycles of PCR. Libraries were quantified using the Qubit Fluorometer and the Qubit dsDNA HS Kit (ThermoFisher Scientific; Q32854).

Library fragment-length distributions were analyzed using the Agilent TapeStation 4200 and the Agilent High Sensitivity D1000 ScreenTape Assay (Agilent; 5067-5584 and 5067-5585). Libraries pooled in equimolar amounts and final library quantification performed using the KAPA Library Quantification Kit for Illumina (Roche; KK4824). Library pool sequenced on the Illumina NextSeq 500 Platform, on a NextSeq 500/550 Mid Output v2.5 150 cycle kit (Illumina; 20024904), to generate approximately 5 million 75bp single-end reads per sample. Bcl2fastq basecaller version 2.20 used.

2.12.5 Analysis of RNA sequencing

2.12.5.1 Bioinformatic pipeline

Data analysis for RNASeq Raw reads were processed using Lexogen QuantSeq pipeline. In brief, reads were trimmed to remove sequencing adapters, reads shorter than 20 bp and of quality less than Q20 using cutadapt. Trimmed reads were aligned to the Homo sapiens GRCh38 ensembl release 107 reference genome using STAR aligner [2]. Uniquely aligning reads were retained for gene quantification, which was carried out using featureCounts. Differential gene expression analysis was carried out using DESeq2 [4]. Details of each step are explained in the pipeline's github repository (https://github.com/Lexogen-Tools/quantseqpool_analysis). Heatmaps were generated using R packages gplots and heatmaply. Package versions are given in the accompanying .html document containing the heatmaps.

Pathway enrichment analysis was carried out using the R package gprofiler2. An unordered list of up-regulated and down-regulated genes is analysed, separately. All other parameters are set to DeepSeq default. Only statistically significant results are reported where p-value is set at 0.1.

2.13 Statistical analysis

All statistical analysis was undertaken using GraphPad Prism 9. Unless otherwise specified, population data are presented as mean ± SD (standard deviation) of n observations of x independent experiments, where n refers to the number of individual cells/experiments. Significant differences between sample/treatment groups were assessed using the students t-test (paired or unpaired specified in the relevant results sections) or one-/two-way ANOVA for two or more groups, respectively. When comparing 3 or more groups to a control condition with ANOVA, Dunnett's post-hoc test was used. When expressing differences

between samples, data was expressed as the mean value with 95 % confidence intervals; mean [95% LCI , 95% UCI] (LCI, lower confidence interval; UCI, upper confidence interval). Normality tests were performed on data when using parametric tests. Values of $p < 0.05$ were assumed to describe significance in all tests.

3 Characterisation of ion channel expression in adult and paediatric high-grade glioma

3.1 Introduction

Brain tumour research, with high grade glioma research in particular, is met with many limitations and issues arising from the anatomical location of the tumour, aggressiveness of the disease and 'immune cold' status of HGG (153). As such, areas of research that are well explored or up-and-coming in other cancers, remain poorly assessed in both adult and paediatric HGGs. The role of ion channels in cancers has been explored but not thoroughly defined, however many studies have linked the aberrant expression of various ion channels to malignant processes in other cancers. As previously described, dysregulation of ion transport mediated through ion channels and the maintenance of ionic function across the cell membrane underpins a large number of the pathological events that encompass the hallmarks of cancer (147). Specifically, ion channel expression and function is linked to cell cycle progression, invasion, migration, morphology, apoptosis, and proliferation of cancer cells, with certain studies identifying a role for ion channels in angiogenesis and immune response of tumour cells (154).

Here we aim to exploit an under-reviewed area of research and apply it to the brain tumour realm. There is currently no curative treatment for HGG, and one of the main treatment boundaries facing researchers is developing drugs that can cross the blood brain barrier. The brain itself is intrinsically electrically active and as such, harbours cells that are heavily regulated via ion channel function. Ion channel inhibiting drugs are a large class of drugs, that make up 15% of all small molecule drugs on the market to date (155). These clinically available drugs have known safety profiles and are in use for a myriad of diseases and disorders. It is well understood that drugs targeting ion channels such as anti-

depressants and antiepileptics have the capacity to cross the blood brain barrier and act on brain cells. Therefore, ion channels present as viable and logical targets for brain tumour therapeutics, as drug repurposing is a sound possibility, and unlike transcription factors etc. they are easily druggable. The dire overall survival rates of HGG arise as a direct result of the lack of progressive treatment; hence, identifying new drug targets such as ion channels is imperative in developing research and extending survival times in these patients.

During the process of this project, three review publications (including one published by the author) have explored the role of ion channels in gliomagenesis and progression[1] (120,156,157), all of which conclude that gliomas possess aberrant ion channel expression and that ion channels are viable targets for treatment.

Chapter Aims:

1) To identify aberrantly expressed ion channel genes in HGG via systematic review and to use this data combined with publicly available data sets to determine a panel of candidate ion channel genes.
2) To assess the expression of candidate ion channel genes in pHGG cell lines and in house patient derived HGG tissue.
3) To determine the clinical significance of candidate ion channel genes via in-house patient tissue and publicly available data sets
4) To assess the spatial expression of ion channel genes in response to tumour microenvironment.

[1] During the process of this project the author published a review exploring the role of ion channels in high grade gliomas. Some of the work in the chapter draws heavily on this published work, this work d is presented in line with the article reuse permissions policies of MDPI journals.

3.2 Identification of aberrantly expressed ion channels in HGGs via systematic literature review.

As described in section 2.1.1 a systematic literature review was carried out to determine ion channels of noted significance in adult and paediatric gliomas. Unlike many other tissue types, neural tissue is intrinsically electrically active and reliant on ion channels. Ion channels are essential in cell cycle control, invasion and migration of cancer cells and therefore present as valuable therapeutic targets. Through this literature review, a wide range of ion channel targets were identified.

The epithelial sodium channel (ENaC) family of channels was identified as potential targets in this review. Studies have found that these channels are upregulated in GBMs and are significantly associated with shorter overall survival times (158). Furthermore, when targeting glioma cells with ENaC specific inhibitors, cell undergo cell cycle arrest at GO/G1. Voltage-gated sodium channels, highly expressed in gliomas have also been implicated in the malignant progression of brain tumours (159).

Potassium channels are responsible for the selective facilitation of K^+ movement, and have been implicated in the neoplastic development of several solid tumours (111,160). Like their Na^+ counterparts, the voltage gated K^+ channels are also seen to exhibit aberrant expression in gliomas, with *KCNB1* and *KCNJ10* being down regulated in glioma samples (137). Calcium activated potassium channels also known as BK channels have been widely assessed in the glioma landscape, with studies finding upregulation in glioma biopsies. Selective inhibition of BK channels such as KCa1.1 sensitises glioma cells to standard of care chemotherapeutics, and results in cell death as a monotherapy (161).

Chloride channels are associated with the regulation of cell volume and as such, are interesting targets for inhibiting cell invasion. Chloride intracellular channels (CLICs) have

been found to be upregulated in glioma biopsies, with one study showing an association between these channels and patient prognosis, with CLIC4 specifically linked to glioma cell invasion (138). Similarly, transient receptor potential cation channels (TRPC) and aqua-porins such as AQP1 have been implicated in glioma motility and invasion, with silencing of these channels resulting in G1 arrest (162).

Following the generation of a panel of candidate channel targets, we sought to assess available data confirming expression levels of channels in cell lines and tissues. Interrogation of Human Genome Atlas (https://www.humancellatlas.org/) found that CLIC1, CLC4 and VDAC were the most highly expressed ion channels in cell lines (U-251, U-87), whereas the aqua-porins AQP4 and AQP1 were the most highly expressed in tissue samples. Expression data can be found in table 3.1 and 3.2.

Table 3.1 Ion channel genes and their role in glioma pathogenesis. A systematic review was carried out using PubMed to assess the current literature exploring ion channels and ion channel genes associated with the malignant status of glioma, including their association with ion channel inhibiting drugs or standard of care chemotherapy. Key: bold typeface and * indicate candidates used for further investigation.

Gene	**Role**	**Tumour Type**	**Clinical/ experimental association**	**Reference**
Eag1	Cell-cycle regulated channel, relevant in the process of myoblast fusion	HGG	Suppression sensitises GBM to TMZ. Gliomas, despite of their grade, tend to overexpress.	(131,154,157)
SCN8A	Voltage-gated Na+ channel	HGG / GSC	High expression compared to NGC. KD decreases viability. Enriched in GSC but low in bulk GBM	(131,151)
KCNB1 (Kv21)	Potassium voltage-gated channel	HGG / GSC	High expression compared to NGC. KD decreases viability	(131)
GRIA3	AMPA-sensitive	HGG / GSC/pancreatic cancer	High expression compared to NGC.	(131,158)

	glutamate receptor		KD decreases viability	
KCNH1 (Kv10.1)	Ether a go-go K+ channel (hEAG1)	Gliomas, breast carcinoma	Aberrant expression linked to increase in proliferation. Over-expression in 85.3 % of the brain metastases and in 77.5 % of GBMs	(159–161)
GRIK4	Glutamate receptor	HGG / GSC	Enriched in GSC but low in NGC. Enriched in GSC but low in bulk GBM	(162)
GABRG3	GABAA receptor-γ3	HGG	High expression compared to NGC. High expression = increased survival	(131,163)
CNGA3	Cyclic nucleotide gated (CNG) channel	HGG	High expression compared to NGC. High expression = Decreased median survival	(131,151)
TRPM3	Calcium channel mediating constitutive calcium ion entry	HGG / GSC	High expression compared to NGC. High expression = Decreased median survival	(131,151)
P2RX4*	Purinergic Receptor	HGG / GSC/ micro glia/ Prostate cancer	High expression compared to NGC and decreased median survival. Involved in chemotaxis and morphine-induced migration.	(164–166)
KCNC3	Potassium Voltage-Gated Channel	GSC	Enriched in GSC but low in bulk GBM and NGC	(131)
SCN11A*	Voltage-gated sodium channel	GSC	Enriched in GSC but low in NGC	(131,167)
ASIC3 (ACCN3)	neuronal voltage-insensitive sodium channels	GSC	Enriched in GSC but low in bulk GBM	(131)

CLCN3	Voltage gated Cl- channel	Glioma	Reduced expression inhibits migration. Associated with drug resistance	(168)
CACNA1D	Ca2+ channel, voltage dependent, L type alpha 1D subunit	HGG	Down regulated, significant increased risk of death.	(169)
CLCN6	Cl- channel, voltage sensitive 6	HGG	Down regulated, significant increased risk of death.	(135)
CLIC1*	Cl- intracellular channel	HGG	Up regulated in glioma, increases risk of death	(135,136,170)
CLIC4*	Cl- intracellular channel	HGG	Up regulated in glioma, increases risk of death. Associated with glioma cell invasion.	(135,171)
GRIA2	Glutamate receptor, inotropic, AMPA2	HGG	Down regulated, significant increased risk of death.	(135,158)
GRID1	Glutamate receptor, inotropic delta 1	HGG	Down regulated, significant increased risk of death.	(135)
KCNAB1	K+ voltage gated channel	HGG	Down regulated, significant increased risk of death.	(135)
KCND2	K+ voltage gated channel	HGG	Down regulated, significant increased risk of death.	(135)
KCNJ10 (KIR4.1)	K+ inwardly rectifying channel	HGG/ Glioma/NGC	Down regulated, significant increased risk of death. Overexpression stops glioma cells proliferating	(135)
KCNMA1	K+ large conductance Ca2+ activated channel	HGG	Down regulated, significant increased risk of death.	(135)
KCNN3	Potassium intermediate/small conductance calcium-	HGG	Down regulated, significant increased risk of death.	(135)

	activated channel			
KCNQ5	Potassium voltage-gated channel	HGG	Down regulated, significant increased risk of death.	(135)
NALCN	Sodium leak channel, non-selective	HGG	Down regulated, significant increased risk of death.	(135)
P2RX7*	Purinergic receptor P2X, ligand-gated ion channel,	HGG	Down regulated, significant increased risk of death.	(135)
SCN1A	Sodium channel, voltage-gated	HGG	Down regulated, significant increased risk of death.	(135)
VDAC2	Voltage-dependent anion channel 2	HGG	Down regulated, significant increased risk of death.	(135)
NKCC1 (SLC12A1)	(SLC12A) Na-K-Cl cotransporter	Glioma	Highly expressed in glioma tissues	(56)
Kv1.3 (kcna3)*	K+ channel	Melanoma/ rodent glia	interacts with β1-integrins of adhering melanoma cells. Increases as cells progress from g0-g1 in rodent glial cells – increase in g1 K+	(167,172)
Kv3.1 (KCNC1)	K+ Channel	Oligodendrocyte progenitor, chicken neuroblasts	Blockade inhibits glioma cell migration	(167,173)
Kv11.1 (KCNH2)	K+ channel	Melanoma, AML, neuroblastoma, colon cancer	Melanoma: inhibition inhibits migration, AML-confers promigratory phenotype, NB-inhibition regulates integrin signalling, CC- modulates invasiveness	(167,174)

Kca1.1 (KCNMA1)*	K+ channel	Glioma	Over expressed in glioma, alters radiosensitivity of glioma cells	(155,167,173,175)
Kca2.3 (KCNN3)	K+ channel	Melanoma, BC, neuronal progenitor cells	M- enhances motility by hyperpolarising membrane potential, BC – KD inhibits migration, NPC – channel activation induces filopodia formation.	(155,167,175)
Kca3.1n (KCNN4)	K+ channel	Microglia, melanoma, GBM	Microglia and melanoma – blockade slows down growth, GBM - contributes to chemotactic response to CXCL12; inhibition blunts migratory response of U87-MG cells to FCS	(167,176)
Kir4.2 (KCNJ15)	K+ channel	Glioma	colocalization with α9β1 integrins and spermidine/spermine acetyltransferase (SSAT) increases persistence of migration	(121,177)
NaV1.2 (SCN2A)	Voltage gated sodium channel	Microglia	NaV1.6 required for ATP-induced migration	(167,178)
NaV1.6 (SCN8A)	Voltage gated sodium channel	Microglia	NaV1.6 required for ATP-induced migration	(167,178)
ENaC (**SCNN1A***, SCNN1B, SCNN1G, and **SCNN1D***)	Epithelial sodium channel	HGG	Knockdown impairs migration	(167,179)
ASIC1 (ACCN2)	Acid sensing, neuronal voltage-	HGG, Astrocytes	Enhances motility. Toxin inhibits whole cell current in GBM cells	(167,180,181)

	insensitive sodium channels			
VRAC	Cl- channel	Glioma cells	Cell shrinkage enhances invasive capacity	
CIC3	Cl- channel	Glioma cells, HeLa, nasopharyngeal carcinoma	Internalisation inhibits migration, regulated by CaMKII, HeLa- KD impairs migration. Cltx), a scorpion toxin that binds a membrane-bound metallopro-teinase. The former can diffuse within the plasma membrane and thus inhibit ClC-3.	(134,170,182)
TRPC6	Transient receptor channel	GBM cells	KD inhibits invasion	(183)
AQP1*	Aqua porin 1	Glioma cells	Expression enhances migration	(184,185)
AQP4	Aqua porin 4	Astroglial cells, adult neural stem cells	AGC – promotes glial scar formation and enhances protrusive activity, ANSC – knock out impairs migration by altering intracellular Ca2+ signalling	(186,187)
ASIC2	Acid sensing channel 2	Glioma	Down regulated in glioma	(167,179,181,188)
Cav1.2 (CACNA1C)	Ca2+ channel	HGG	Negative biomarker for patient survival. TTFields activate Cav1.2 channels in GMB	(189,190)

Table 3.2 Table describing the expression of ion channel genes in publicly available cell line data and tissue. Data from the human genome atlas and the expression of RNA found in the TCGA data set.

Gene	Cell Line RNA NX		Tissue Expression	TGCA - Glioma
	U-251	U-87		
CLIC4	27.1	40.7	136.4 pTPM - cerebellum	N/A
VDAC2	58.1	43.1	219.4 pTPM	24.9 FPKM
CLIC1	37.6	14.7	5.2 pTPM	124.9 FPKM
AQP4	0.0	1.7	774.2 pTPM	180.1 FPKM
AQP1	0.3	0.1	120.8 pTPM	240.2 FPKM
TRMP2	0.3	0.0	7.4 pTPM	2.5 FPKM
SCN1A	0.00	0.00	11.2 pTPM	1.6 FPKM
KCNJ10	0.00	0.2	117.1 pTPM	22.8 FPKM
GRIA2	0.00	0.7	247.9 pTPM	5.6 FPKM

3.3 Identification of candidate ion channel gene expression in glioma

3.3.1 Analysis of candidate ion channel genes using publicly available data sets

Ion channels have not been widely explored as candidates for therapeutics or biomarkers across glioma data sets, and consequently we sought to assess the expression of candidate ion channel genes (identified via systematic literature review) across publicly available glioma datasets. These data were used to further elucidate promising ion channel targets, and the association between their expression and survival in patient cohorts and narrow down our panel.

The statistical analysis platform R2: Genomics Analysis and Visualisation Platform (http://r2.amc.nl) was utilised as a tool to assess the expression of candidate ion channel targets: P2RX4, SCNN1A, Kv1.3, SCNN1D, AQP1, KCa1.1, CLIC1, CLIC4 and P2RX7. These targets were selected as they are relatively underexplored in gliomas, and indeed brain tumours as a whole. The paediatric glioma data set (Paugh *et al*., 2010(163)), adult glioma dataset (French *et al*., 2011(164) and Kawaguchi *et al*., 2013 (165)) and normal brain data sets (Harris *et al*., 2008, and Berchtoldt *et al*., 2008 (166)) were utilised in this analysis. Candidate ion channel genes were found to be expressed across all data sets (Figure 3.2). When compared to normal brain the highest overall expression was found in CLIC1, CLIC4 and P2RX7, aligning with literature citing that these channels are often over expressed in glioma. Conversely, SCNN1D, SCNN1A and KCa1.1. appear to be down regulated when compared to normal brain.

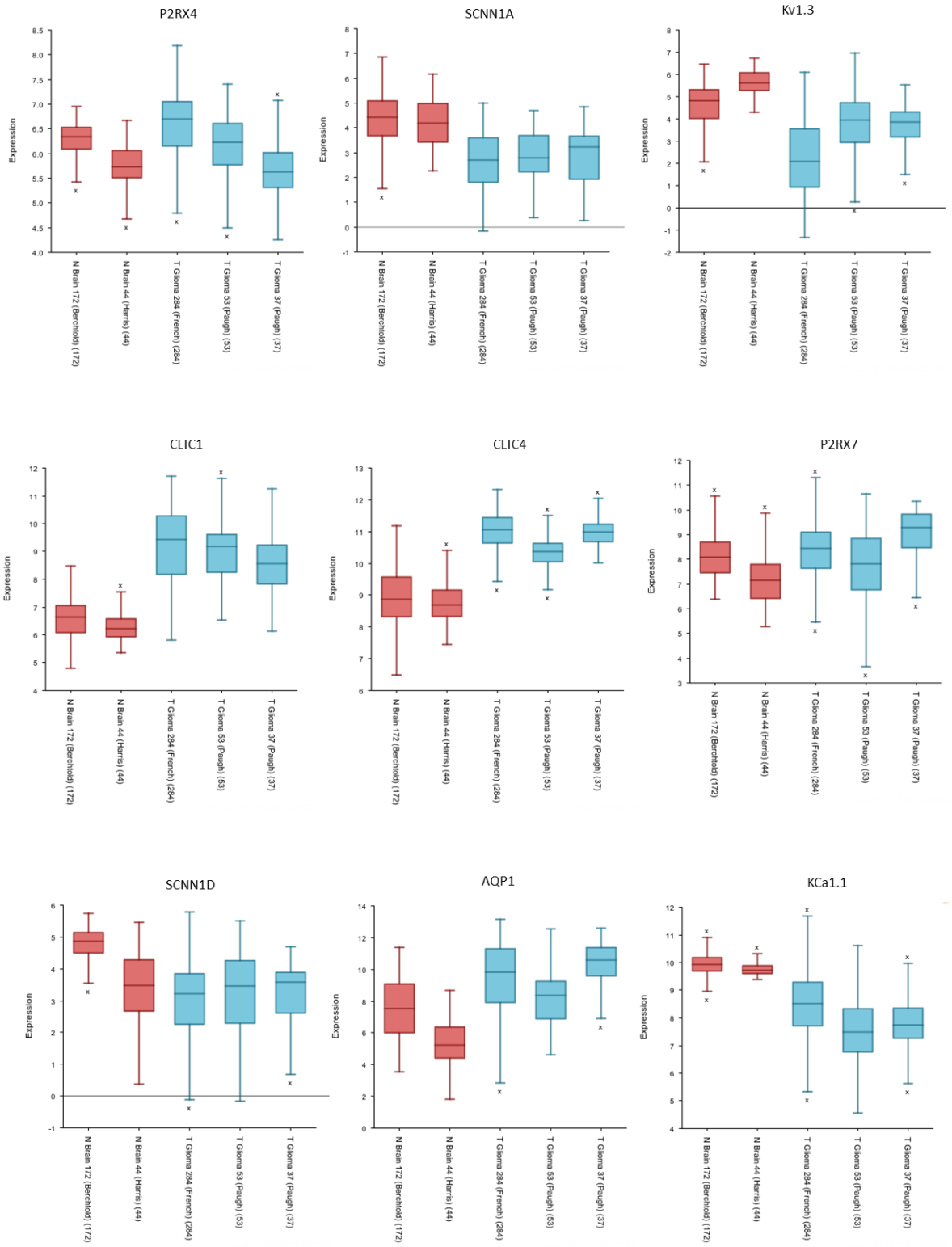

Figure 3.1 Ion channel expression across publicly available data sets. R2 Genomic Analysis was utilised to analyse differences in ion channel expression in glioma data sets. Normal brain (Harris dataset) n = 44; Normal Brain (Berchtold dataset) n = 172; paediatric glioma (Paugh dataset) n = 53; adult glioma (French dataset) n=284. Significance was assessed by Brown-Forsythe and Welch ANOVA analyses with Dunnett's T3 multiple comparison test.

Furthermore, we sought to assess the clinical association between expression of candidate ion channel genes and overall survival in these data sets. Figure 3.2a describes Kaplan-Meier survival curves for the Paugh paediatric HGG data set and the correlation between overall survival and gene expression. Here none of the candidate ion channel genes had a significant correlation with overall survival (p=>0.05). However, some (non-significant) trends were observed. For CLIC1, CLIC4, SCNN1A and SCNN1D high expression levels appeared to be unfavourable and shorter overall survival times were observed. Conversely, there is a trend of low expression of P2RX7 and KCa1.1 and informing lower overall survival rates. Interestingly, data found by way of systematic literature review confirms the role of low P2RX7 expression as a prognostic factor for poor overall survival. Furthermore, these trends were mirrored in the adult HGG dataset (Kawaguchi) whereby the survival curves were not statistically significant, but nodded at trends towards low expression of P2RX7 and KCa1.1 being unfavourable. As this data set is smaller in scale, all results need to be interpreted with caution. Despite this, the expression of CLIC1 was found to be statistically significantly associated with overall survival in this cohort, with high CLIC1 expression conferring poor overall survival (p= 2.2e-07). Likewise, a chloride intracellular channel from the same family, CLIC4 was also found to be unfavourable for survival when highly expressed (p=0.02). These data confirm findings from the literature, stating that CLIC1 and CLIC4 overexpression is associated with poor overall survival. CLIC1 and CLIC4 are also statistically associated with higher WHO grade, with increasing CLIC1 and CLIC4 levels being associated with WHO IV tumours. Interestingly, despite implications in the literature focusing on both clinical and cell line data, there was no significant association between the majority of ion channels in this panel and survival outcome.

Due to no significance being found in the expression of any of the candidate ion channel genes when compared to normal brain, and all genes but CLIC1 and CLIC4 holding no significant correlation with overall survival, it was decided that further analyses using in-house data sets would be carried out to select a suitable target to take forward for the studies.

A

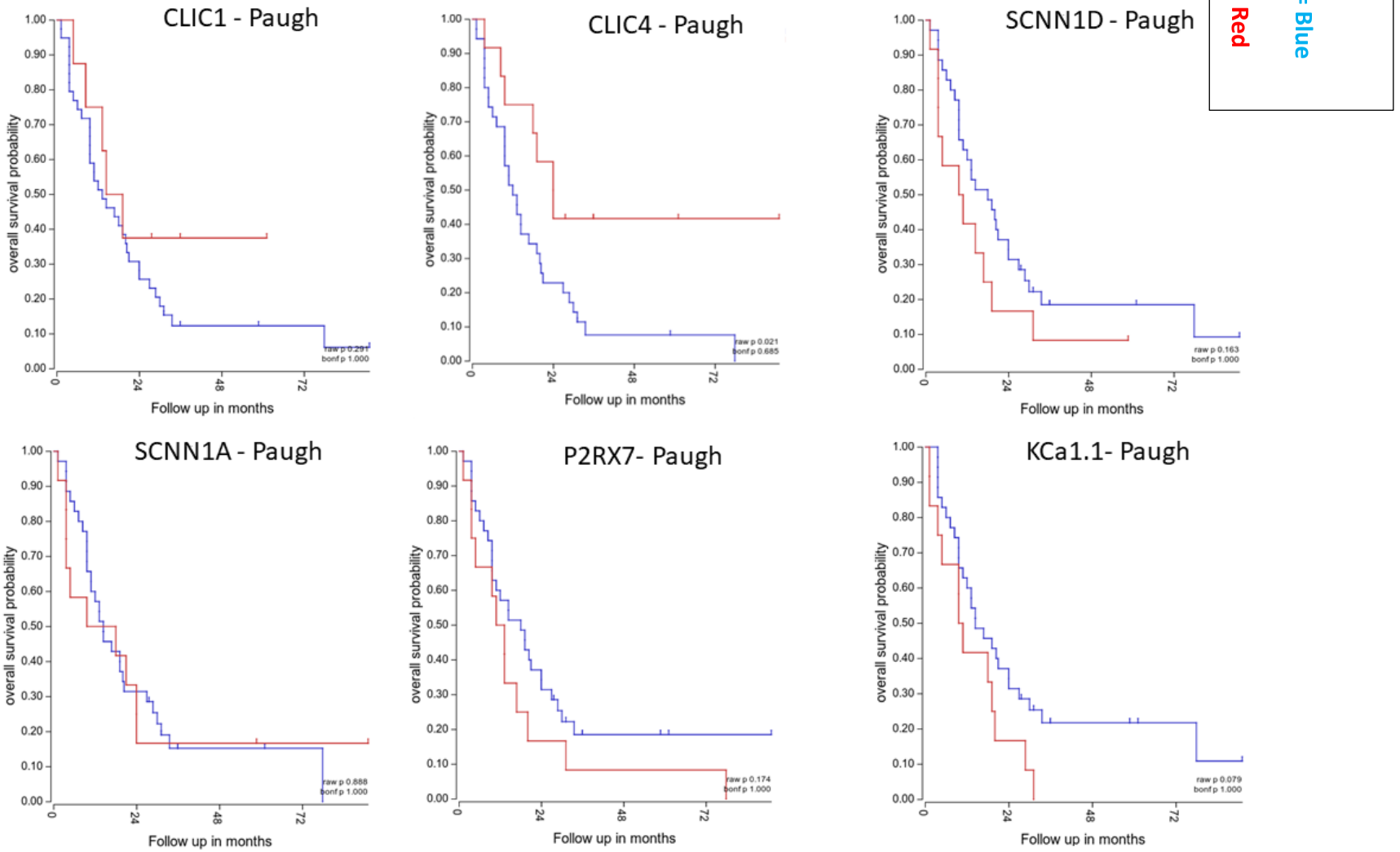
Key:
High = Blue
Low = Red
CLIC1 - Paugh
CLIC4 - Paugh
SCNN1D - Paugh
SCNN1A - Paugh
P2RX7- Paugh
KCa1.1- Paugh
overall survival probability
Follow up in months
raw p 0.291
bonf p 1.000
raw p 0.021
bonf p 0.685
raw p 0.163
bonf p 1.000
raw p 0.888
bonf p 1.000
raw p 0.174
bonf p 1.000
raw p 0.079
bonf p 1.000

B

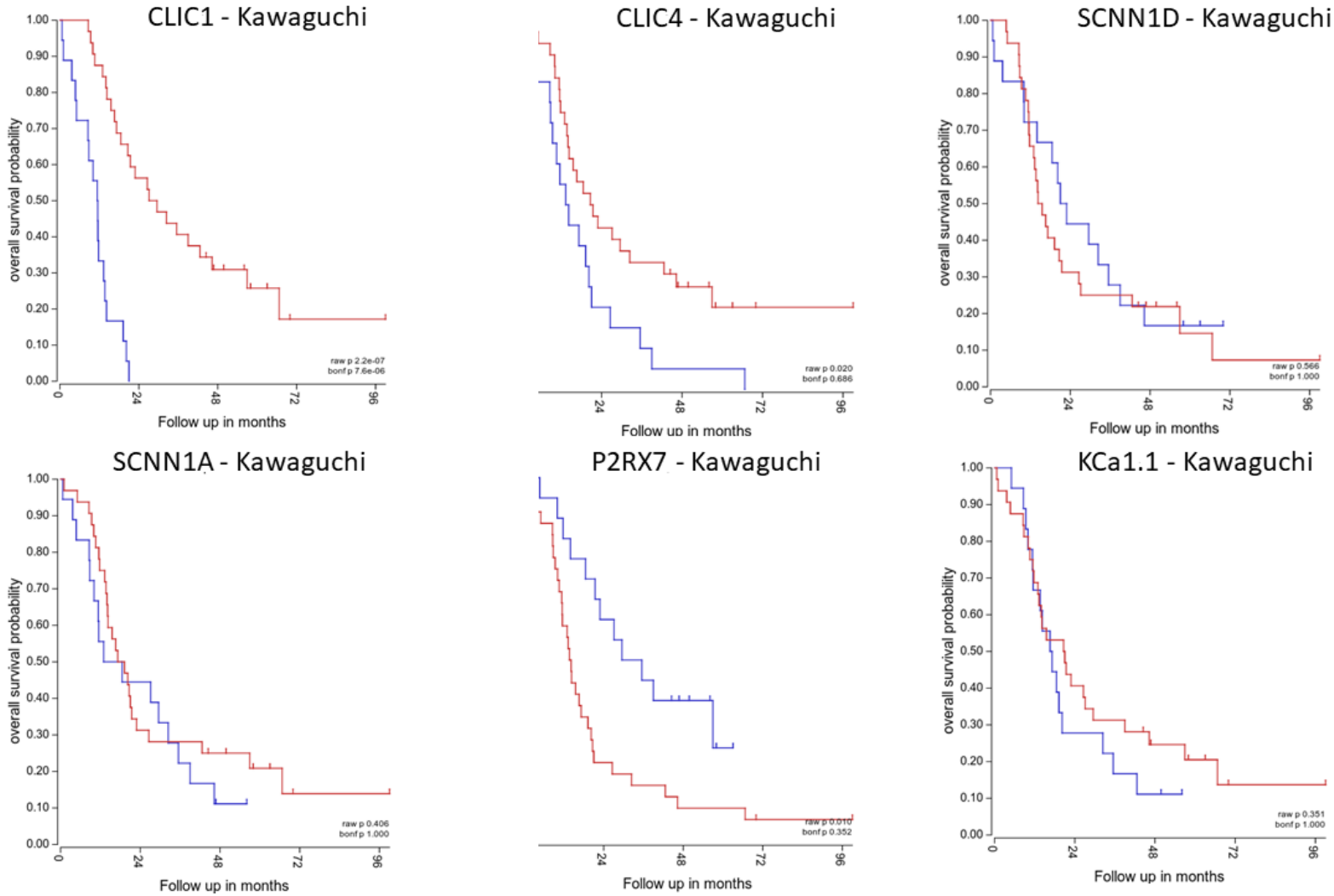
CLIC1 - Kawaguchi
overall survival probability
Follow up in months
raw p 2.2e-07
bonf p 7.6e-06
CLIC4 - Kawaguchi
Follow up in months
raw p 0.020
bonf p 0.686
SCNN1D - Kawaguchi
overall survival probability
Follow up in months
raw p 0.566
bonf p 1.000
SCNN1A - Kawaguchi
overall survival probability
Follow up in months
raw p 0.406
bonf p 1.000
P2RX7 - Kawaguchi
Follow up in months
bonf p 0.352
KCa1.1 - Kawaguchi
overall survival probability
Follow up in months
raw p 0.351
bonf p 1.000

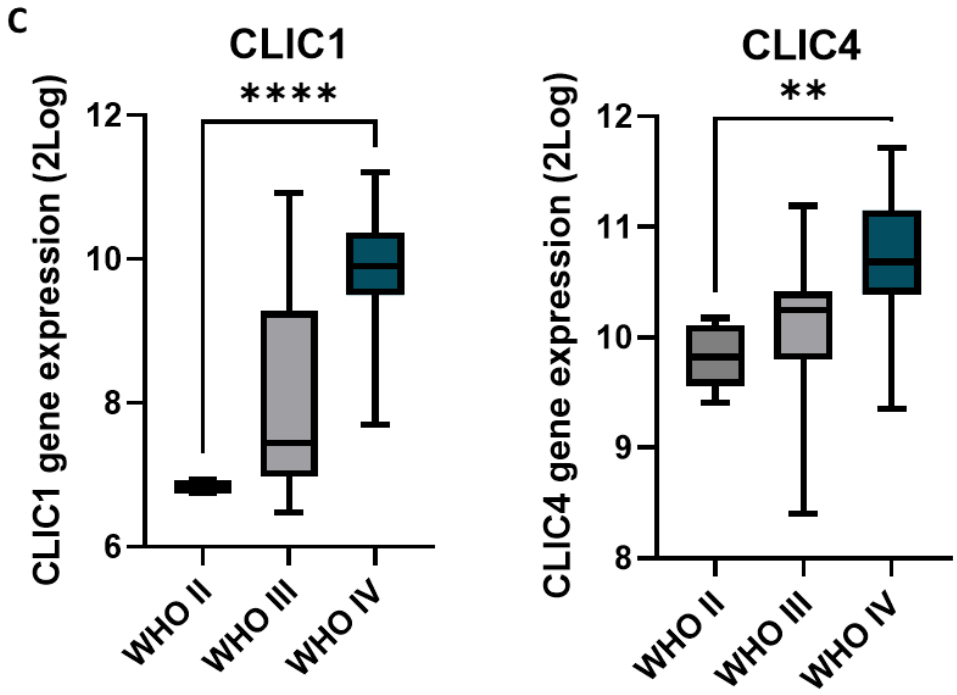

Figure 3.2. High CLIC1 and CLIC4 expression correlates with poor overall survival in adult HGG data set. R2 genomics analysis platform was employed to assess the correlation between the expression of a panel of candidate ion channel genes and overall survival in paediatric and adult high grade glioma data sets. A) No significant association was found between the expression of candidate ion channel genes and overall survival in the Paugh paediatric HGG dataset. B) CLIC1 (p= 2.2e-07) and CLIC4 (p=0.02) overexpression is linked to decreased overall survival in the Kawaguchi adult HGG dataset. Key: High expression is represented by the blue line, low expression is represented by the red line. Survival curves compared using the Log-rank (Mantel-cox) test. C) Express ion values (2Log) of CLIC1 and CLIC4 vs WHO grade. Statistical analysis with unpaired t-test with Welch's correction.

3.3.2 Analysis of candidate ion channel gene expression in pHGG cells and in-house patient derived tissue

Analysis of publicly available datasets found that candidate ion channels are expressed across normal brain, adult, and paediatric glioma. To further this exploration, qrt-PCR of in-house paediatric glioma cell lines, and screening of adult glioma RNA sequencing was carried out. As expected, the 9 candidate channels were expressed across all of the cell lines, with the highest overall expression being found in P2RX7. Interestingly statistical testing via 1-way ANOVA found that there were no significant differences in the expression of P2RX7 across the cell lines, or compared to normal human astrocyte mRNA. The same was found to be true for KCa1.1, however these data align more closely with that found in the Paugh and

French datasets, where no downregulation was found. The most significantly expressed ion channel candidates were CLIC1 and CLIC4, with statistically significant elevation in all cell lines when compared to astrocyte controls. Intriguingly, the highest expression level for both CLIC1 and CLIC4 was observed in the primary line, GCE62, and is comparable to tissue expression data, suggesting that this line is remaining closer to its primary tissue origin. Furthermore, figure 3.3 shows a panel of all of the ion channels that were positive for expression across our in-house adult glioma patient samples (RPKM >1). Here we find the highest expression in AQP1, AQP4, CLIC1 and CLIC4, however the range of expression values for both AQP1 and AQP4 are vast, potentially highlighting the cause for differing results across data sets and qrt-PCR experiments. The potassium channels reflect the lowest expression values across the cohort, with KCNB1, KCNAB1, KCNJ16 and KCNJ10 of note.

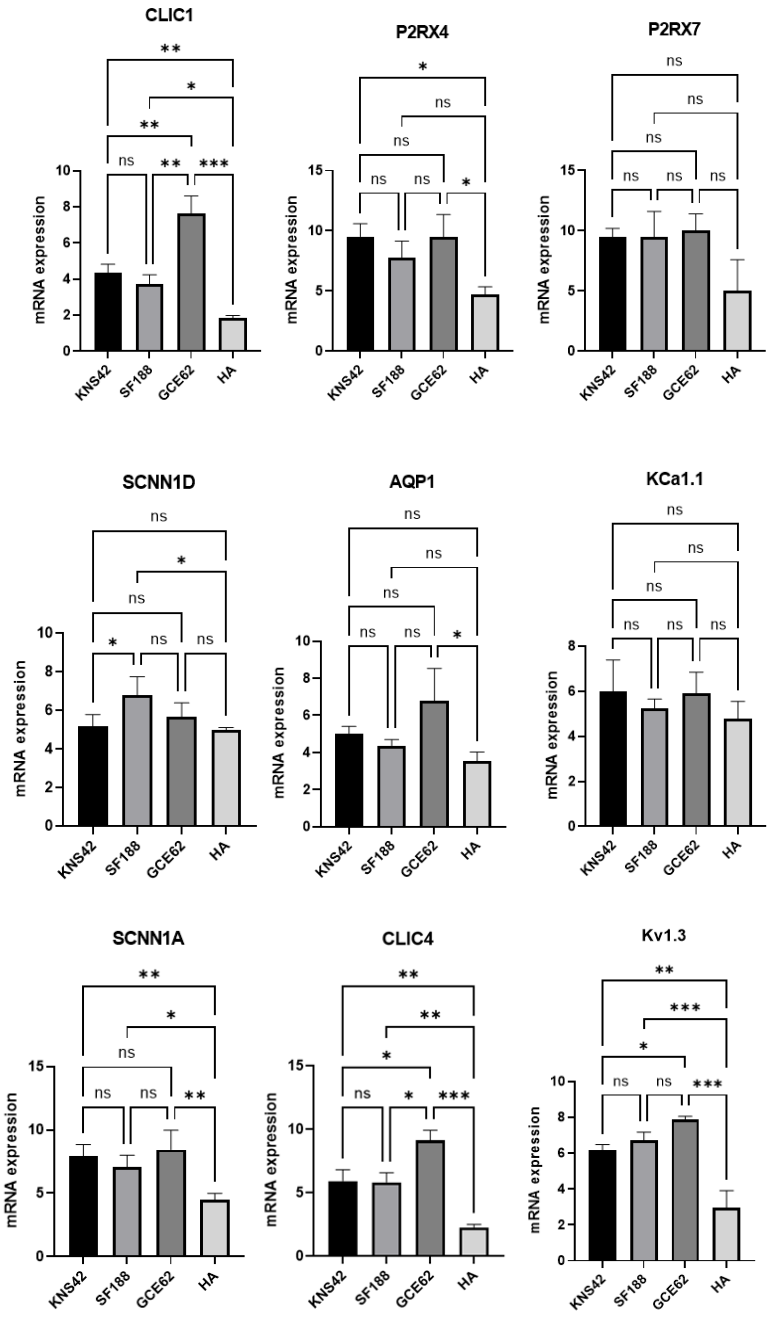

Figure 3.3. Ion channels are expressed across paediatric glioma cells. rtPCR of candidate ion channel genes across two commercial and one primary paediatric high grade glioma cell lines. 2-way ANOVA with multiple comparisons.

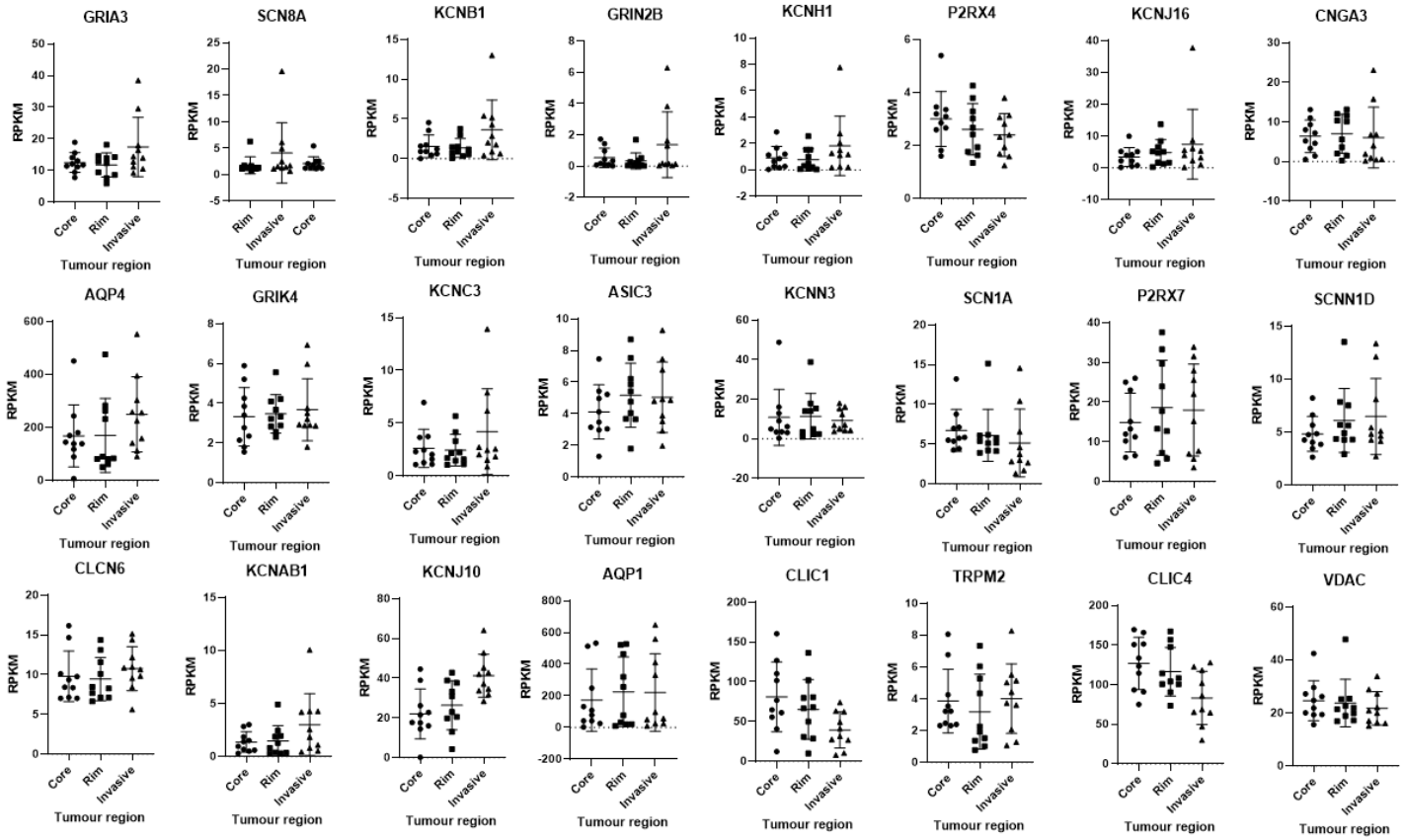

Figure 3.4. Candidate ion channels express in aHGG. Expression of ion channels across in house adult high-grade glioma samples via RNA sequencing. – Patient g expression of ion channel genes. A) In-house RNA sequencing data on core, rim and invasive regions of patient glioma tissues was analysed to determine average associated with malignant glioma status. Expression of ion channel gene and therefore inclusion in the panel was defined as a RPKM >1. N=10 patients, n=3 tech repeats

3.4 CLIC1 and CLIC4 ion channels in HGG

3.4.1 CLIC1 and CLIC4 are overexpressed at the mRNA and protein level in HGG

Following the exploration of candidate ion channel genes across the available literature, publicly available datasets, and our inhouse RNA sequencing data, CLIC1 and CLIC4 were chosen as the primary targets for this study. This is due to the fact that they hold promise as prognostic biomarkers (as seen in aforementioned database studies), have proven track record as targets in other cancers (167–172) and are comparatively understudied in brain cancers, and indeed, gliomas. Large potassium channels were excluded due to their well-researched role in gliomas, and as such the characteristics of channels such as BK channels are well understood (161). The role of sodium channels and aquaporins in cell cycle and invasion of glioma cells have also been widely studied (173–175) and therefore contributions to the wider understanding of ion channels in glioma would be limited. A key focus of this study was to identify novel ion channel targets in HGGs that hold therapeutic promise and are candidates for repurposing of FDA approved drugs. Chloride channels are proven widely druggable targets (176), and accordingly present themselves as viable candidates for this study.

To further elucidate candidate gene expression across in house cell lines and patient tissue, CLIC1 and CLIC4 expression was analysed via qrt-PCR, and RNA sequencing (figure 3.5). At mRNA level, CLIC1 and CLIC4 was seen to be expressed across all samples in a blindly selected panel of adult HGG tissues. Furthermore, compared to normal temporal lobe tissue, CLIC1 was significantly over-expressed in all samples, whereas CLIC4 was significantly over expressed in the majority (67%) of the patient samples. Interestingly, the overall expression levels of both CLIC1 and CLIC4 appears to be similar across the samples. To further this analysis, RNA sequencing data on the full adult patient tissue cohort (40

samples) previously performed by the group was utilised. Panel B represents the average RPKM of patient tissue samples performed in triplicate (an RPKM of >1 was considered positive). CLIC1 and CLIC4 were seen to be expressed across all samples, with average expression of CLIC4 (108.86 RPKM) being higher than CLIC1 (61.76 RPKM).

As the primary focus of this project is paediatric HGG, three pHGG cell lines were utilised to validate this data. Likewise, KNS42, SF188 and GCE62 all expressed CLIC1 and CLIC4 at mRNA level, with significant overexpression found when compared to human astrocyte mRNA. Interestingly, the primary in-house paediatric line, GCE62 had the highest expression of both targets. In this context, expression data may be indicative of GCE62 being closer to the parent tumour, and maintaining native mRNA transcription more so than commercial lines. GCE62 is a cell line derived from the core region of a pHGG sample, the overexpression in this cell line aligns with RNA sequencing data demonstrating an accumulation of target expression in the core region of adult tumours. The mRNA expression of these targets is consistent with cell line and expression data found in the literature and large-scale datasets.

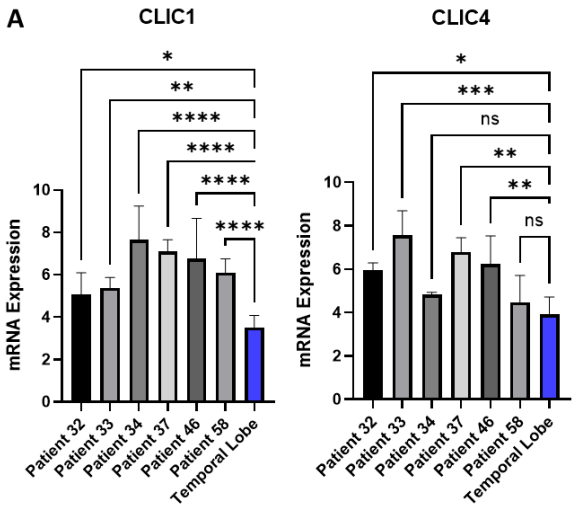

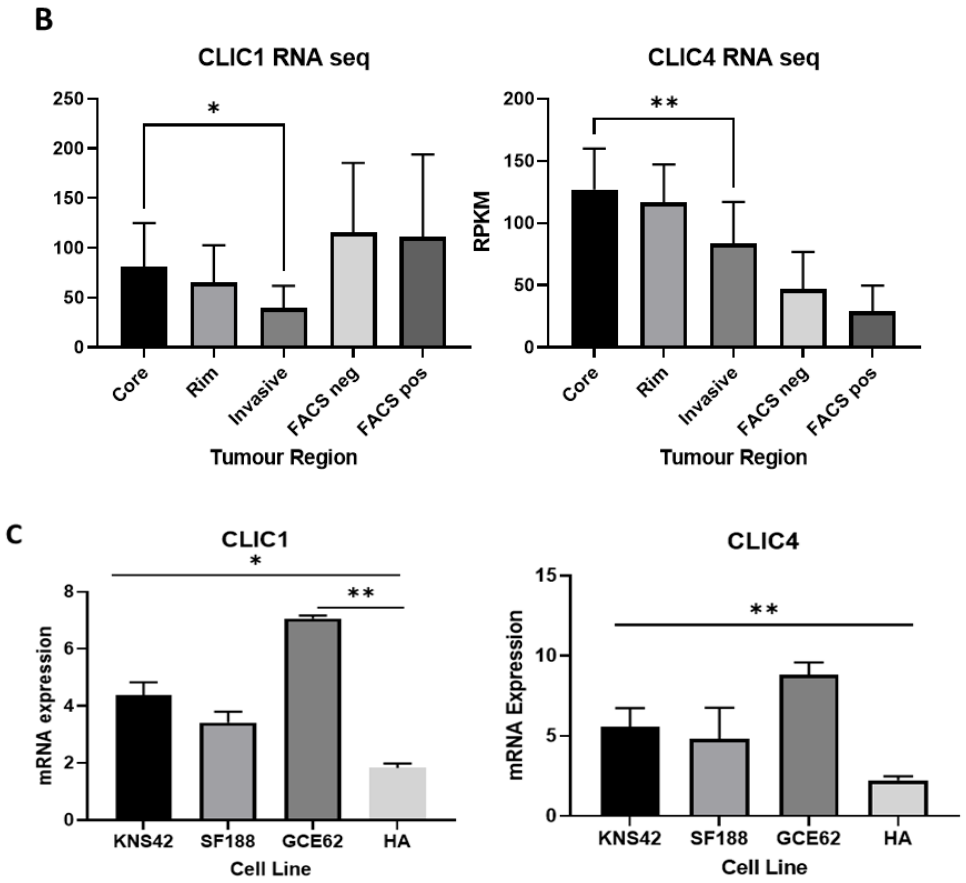

Figure 3.5. CLIC1 and CLIC4 are overexpressed in adult and paediatric HGG at an RNA level. A) Analysis of CLIC1 and CLIC4 expression in aHGG tissue via rtPCR reveals an over expression of CLIC1 and CLIC4 compared to normal brain tissue B) In-house RNA sequencing data of adult glioblastoma samples reveals an over expression of CLIC1 and CLIC4 particularly in the core region of the tumour when compared to the invasive margin. C) rtPCR of paediatric HGG cell lines demonstrates overexpression of CLIC1 and CLIC4 across all cell lines compared to normal human astrocytes.

In the same degree, the protein expression of CLIC1 and CLIC4 was measured in both cell lines and tissue. Analysis at the protein level via western blotting of whole cell protein extracts yielded similar results, with expression of CLIC1 and CLIC4 observed across all pHGG cell lines (figure 3.6). At the time of these experiments, protein extracts from normal human brain were not available as a control. As such, placental tissue was used as a positive control, as it is known to express nearly all ion channels (194). Significant upregulation of CLIC1 and CLIC4 was seen across all cell lines compared to placental

control, with overall expression of CLIC4 being more highly expressed in all cell lines compared to CLIC1. Intriguingly, SF188 exhibited the highest expression of CLIC1 protein, compared to GCE62 harbouring the highest expression at mRNA level. This may be indicative of differences in translational control across the cell lines.

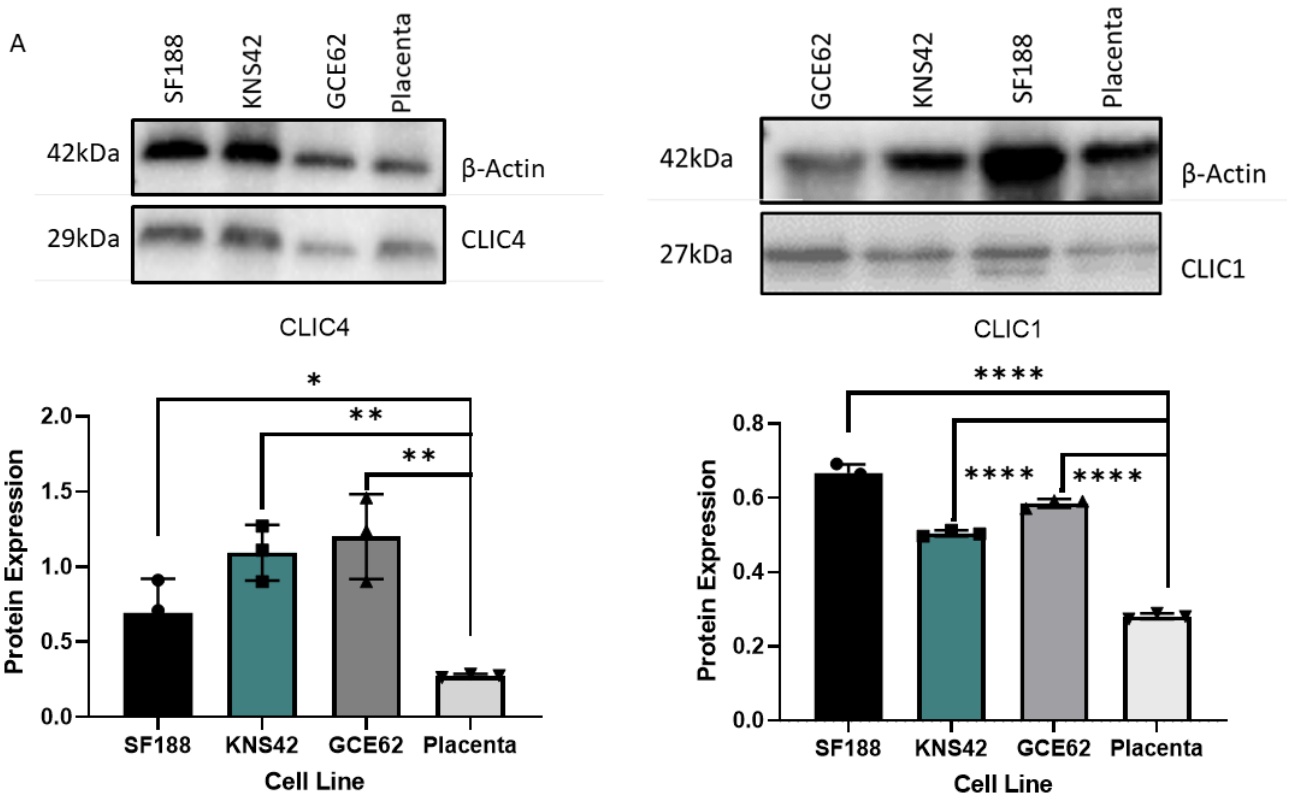

Figure 3.6 CLIC1 and CLIC4 are over-expressed in whole cell protein extracts. A) Representative image of western blot analysis reveals an overexpression of CLIC1 and CLIC4 cell lines compared to placental tissue. Densitometry of bands assessed and normalised to house-keeping control, statistical analysis performed via t-test. N=3.

3.4.2 CLIC1 and CLIC4 exhibit cytoplasmic localisation in pHGG cell lines and HGG tissues

We have demonstrated that CLIC1 and CLIC4 are overexpressed at both protein and mRNA level via analysis of systematic literature review, publicly available data and inhouse patient samples and cell lines, therefore presenting as viable targets in this study. To elucidate the role of CLIC1 and CLIC4 in HGG localisation studies were performed. Previous studies have identified multifunctional roles for CLIC proteins, as they are a structurally and functionally diverse group of proteins and can either present as monomeric soluble proteins, or integral membrane proteins, key in the regulation of membrane potential (177). Membrane insertion of CLIC1 and CLIC4 is rarely seen under physiological pH, and can be triggered by redox and acidic pH changes (178), whereas cytoplasmic localisation appears to be the native state of CLIC proteins, rarely appearing in the nuclei. Immunofluorescent staining against CLIC1 and CLIC4 was employed to visualise protein localisation. Cells were plated into staining chambers, at a seeding density designed to reach no more than 70% confluency. Figure 3.7 details representative images of cells stained against CLIC1 and CLIC4 (green - anti-mouse-488 Alexa Fluor) and DAPI (blue 504nm). As informed by previous data, all pHGG cells that were imaged were positive for CLIC1, however several GCE62 cells were negative for CLIC4 (panel B). This result may be due to technical artefact. GCE62 cells grow in close proximity and often overlap; whilst these areas of cells were avoided for analysis, it may have resulted in reduced antibody penetration. Interestingly, as shown in representative panel A and B, several astrocytes are negative for both CLIC1 and CLIC4. Despite this, image analysis reveals overexpression of CLIC1 and CLIC4 across all cell lines compared to astrocytes. The only exception to this was in GCE62 cells, where CLIC4 expression was not significantly higher than in the astrocytes.

Cytoplasmic localisation of CLIC1 and CLIC4 is confirmed by staining in this compartment, observed in all cell lines. GCE62 cells appear to have an accumulation of CLIC1 in the membranous region of the cells, suggesting functional integral membrane proteins being present in this cell line. Nuclear staining across all cell lines is almost completely absent as confirmed in the literature.

Not only was the compartmentalisation of the cells identified, confocal microscopy also revealed stark morphological differences between the three cell lines. KNS42 are the largest cells of the cohort, possessing a diffuse and spindle-like morphology, whereas representative images of GCE62 portray clusters of cells, with a dense nuclear population. SF188 cells possessed minimal cytoplasm compared to KNS42 cells. Negative controls were completed by staining in the absence of a primary antibody, instead incubating the cells with NGS.

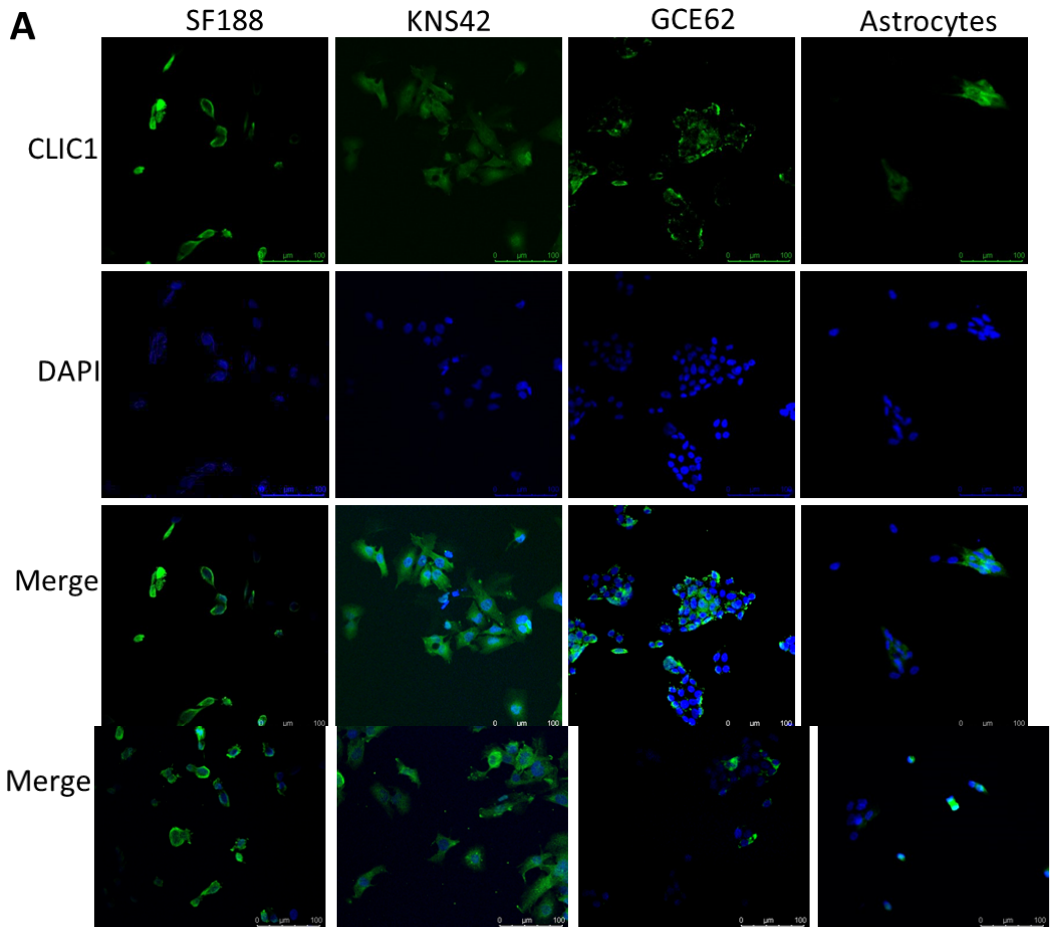

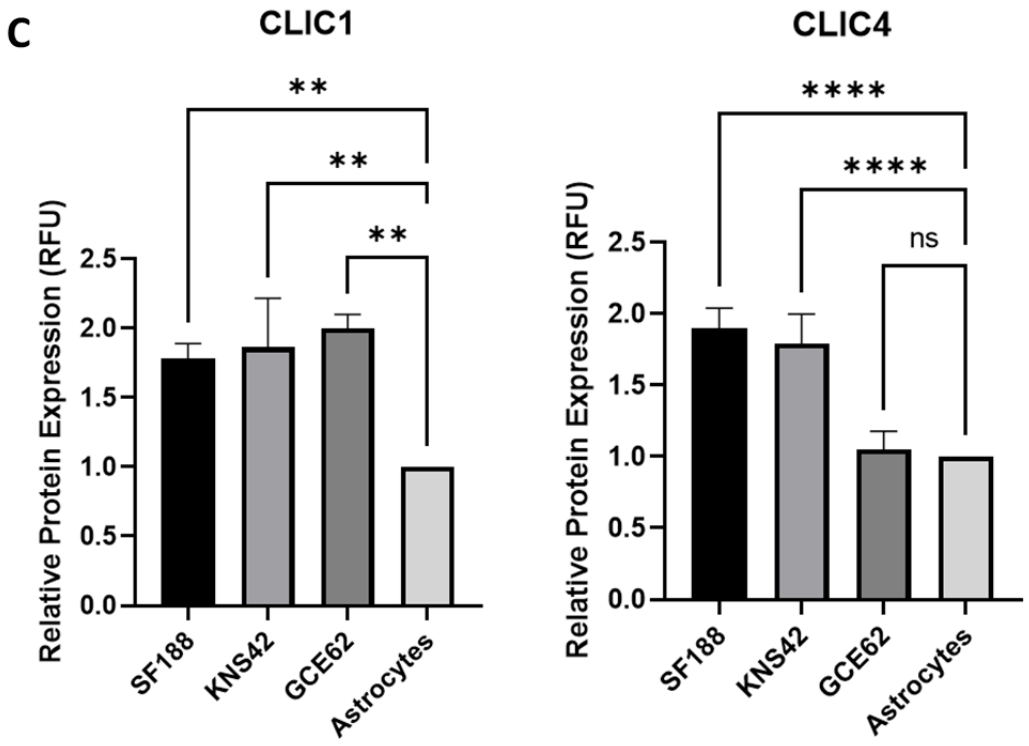

Figure 3.7. CLCI1 and CLIC4 are overexpressed compared to astrocytes. Immunofluorescent staining against mouse CLIC1 and CLIC4 antibodies and anti-mouse-488 Alexa Fluor measured at 488 and 504nm (DAPI) via confocal microscopy. A) Representative images of CLIC1 staining in pHGG. CLIC1 is over expressed in pHGG when compared to normal human astrocytes and harnesses cytoplasmic and membranous staining. B) Representative images of CLIC4 staining in pHGG. CLIC4 is over expressed in SF188 and KNS42 cells when compared to human astrocytes, demonstrating cytoplasmic staining. C) Quantification of Immunoflourescent staining. Image analysis also did not reveal significant differences in CLIC1 and CLIC4 expression compared to normal human astrocytes. n=3. Mean ± SEM; ns = not significant. Significance assessed by unpaired t-test analysis. Scale bar = 100uM, 40x magnification

To further support our data confirming the cytoplasmic localisation of CLIC proteins and inform future work, staining was carried out in patient samples to assess cytoplasmic and nuclear expression in a biologically relevant setting of tumour sections. Figure 3.8a represents immunohistochemical staining against CLIC1 and CLIC4 in adult HGG tumour sections. CLIC1 and CLIC4 are heavily expressed in adult HGG samples when compared to temporal lobe, with HGG showing high positive (2+) staining of CLIC1 and CLIC4 and temporal lobe possessing low positive (<1.5) staining. CLIC1 has both cytoplasmic and nuclear localisation in representative images, whereas nuclei are negative for CLIC4 expression. This was then assessed in paediatric HGG tissues, all samples were positive for CLIC1 and CLIC4, with overall CLIC1 scoring higher (score of 2.5+) on average than CLIC4

(score of 2). The cytoplasm was positive for CLIC1 and CLIC4 with a low proportion of nuclei being positive for these proteins.

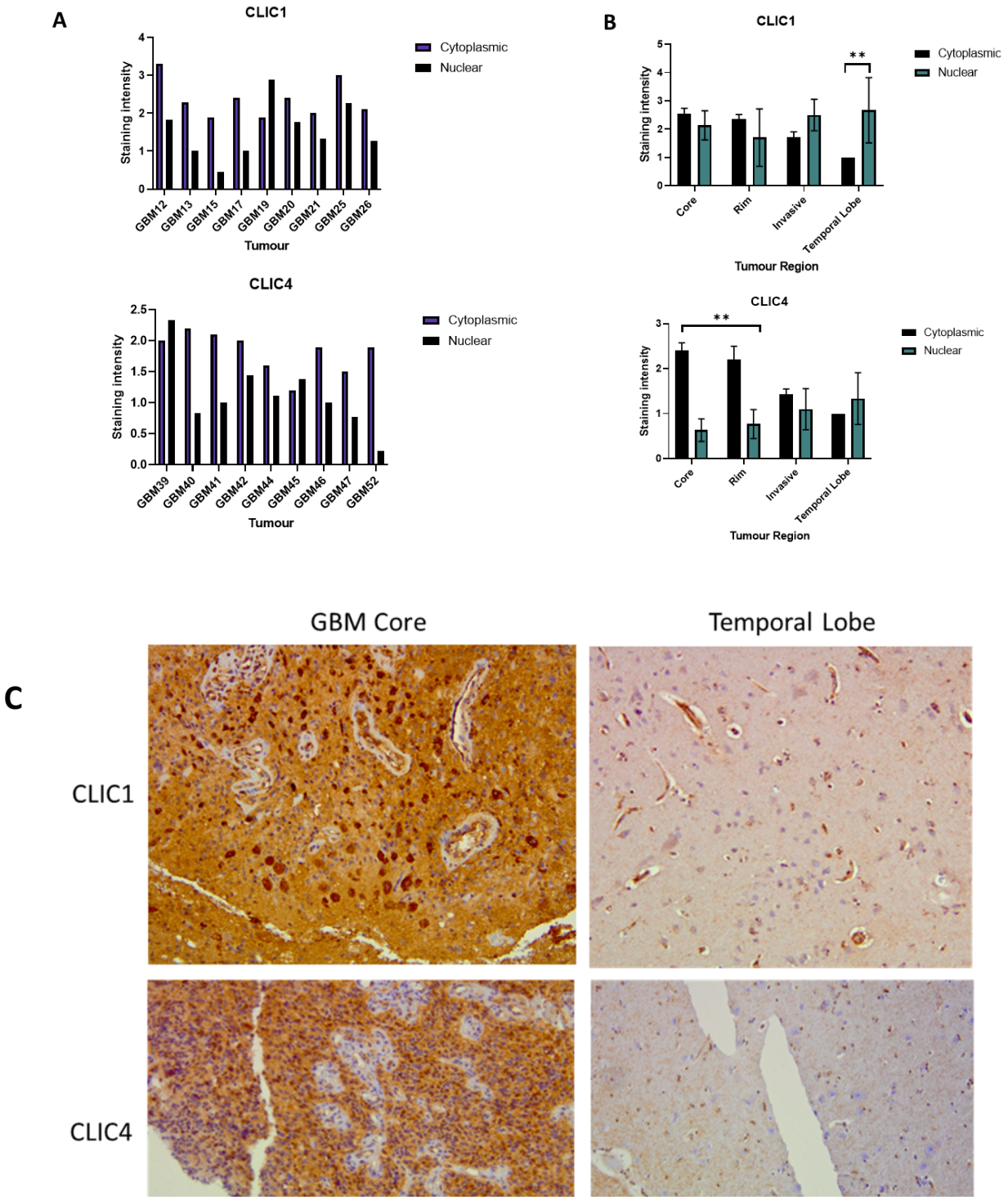

Figure 3.8. CLIC1 and CLIC4 are over-expressed in adult GBM and associated with cytoplasmic localisation. A) IHC analysis of adult glioblastoma tissue. Representative sections from the core, rim an invasive region of 40 glioma patients were compared. Staining against CLIC1 and CLIC4 reveals a high expression of CLIC1 and CLIC4 in the cytoplasmic region vs the nuclear region, and an over expression of CLIC1 and CLIC4 in glioma tissue compared to temporal lobe tissue.

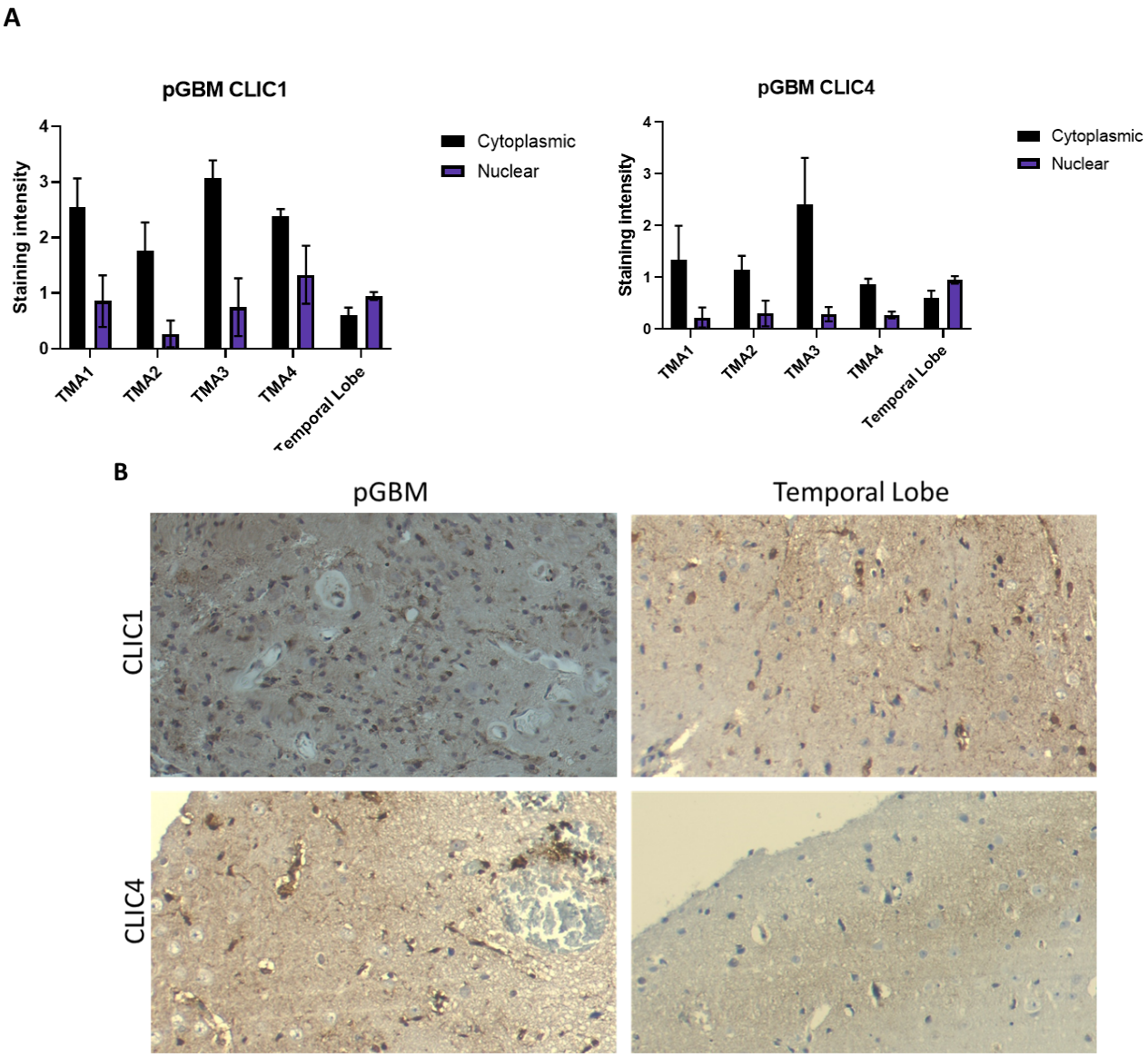

Figure 3.9. CLIC1 and CLIC4 are over-expressed in paediatric HGG and associated with cytoplasmic localisation. A) Quantification of IHC analysis of 16 paediatric glioma patients were compared. Staining against CLIC1 and CLIC4 reveals a high expression of CLIC1 and CLIC4 in the cytoplasmic region vs the nuclear region, and an over expression of CLIC1 and CLIC4 in glioma tissue compared to temporal lobe tissue. B) representative images of CLIC1 and CLIC4 staining of pHGG tissue sections

3.4.3 Clinical correlations of CLIC1 and CLIC4 across in house adult and paediatric HGG tissue micro arrays

Unlike other cancers, there are no clear biomarkers for HGG, and therefore finding biomarkers of prognosis is of high significance. In order to assess the localisation and significance of CLIC1 and CLIC4 expression in the patient, inhouse tissue microarrays (TMA)

of both adult and paediatric with histopathological diagnoses of high-grade gliomas were utilised. The adult microarray is comprised of regional sections of 40 patients who were resected and diagnosed in Nottingham between 2012 and 2019. The paediatric TMA is comprised of a multicentre cohort of 17 paediatric HGG gliomas (total n = 40 however due to depletion, a majority of the cores were unsuitable for inclusion in the analysis). As such, a total of 17 patient samples were deemed suitable for adequate scoring. In both cohorts clinical and survival data is provided, however the molecular detailing of the paediatric cohort is limited. Prior to the use of TMA, the antibodies were optimised on control tissue (intestine and kidney, appendix A2) and normal brain tissue to avoid wastage of precious samples.

To avoid bias, samples on each TMA are anonymised from their clinical data, and each core was scored in triplicate, with double scoring to ensure results were replicable. Manual scoring from 0-3 as described in section 2.11.1 was carried out following training from a pathologist, and samples were double scored to avoid bias. Each core was then averaged to give an overall score. The numerical scores were then used to assign the samples to high positive expression (upper 50th percentile) or low positive expression (lower 50th percentile) groups. Image analysis revealed that all of the adult and paediatric samples were positive for both CLIC1 and CLIC4 expression.

3.4.3.1 CLIC1 and CLIC4 overexpression is associated with poor overall survival in in-house adult HGG cohorts

As anticipated, and previously noted on individual aHGG sections, there was significantly higher staining of CLIC1 and CLIC4 in the cytoplasm of the cores when compared to the nucleus. This finding also aligned with the immunofluorescence data shown in section 3.4 where CLIC1 and CLIC4 expression was principally localised to the cytoplasm. Due to the

primary localisation of functional CLIC proteins being within the cytoplasm and membranous compartments (179,180), all further clinical analyses were performed using the CLIC1 or CLIC4 cytoplasmic scoring data.

It was found that CLIC1 was significantly overexpressed in all distinct spatial regions of the tumours when compared to normal temporal lobe, with the patient cores derived from the core and rim of the tumour harnessing the highest expression of CLIC1. Comparatively, CLIC4 expression was only significantly upregulated in the core and rim regions when evaluated against normal temporal lobe scoring (Figure 3.10 panel A).

Kaplan-Meier analyses were performed as previously described. Unfortunately, up to date clinical data was only available for 37 of the 40 patients on the TMA, and adequate staining in triplicate was only completed in 27 of the 40 patients due to loss of cores. Thus, clinical analyses were performed on the 27 patient samples listed in table 3.3. When split into upper and lower percentiles there was a significant correlation found between the CLIC1 high group and overall survival of the patient, with high CLIC1 expression conferring poor overall survival ($p=0.037$), with a hazard ratio indicating that time to death is half than in the CLIC1 low group (HR= 2.85). Similarly, the CLIC4 high group was also associated with poor overall survival in this cohort, but this was not statistically significant ($p=0.053$) (HR= 1.83), despite this, there is a trend observed, with individuals in the CLIC4 high group having an overall survival of <20 months, compared to the CLIC4 low group overall survival of >30 months. The data presented here align with the data found using publicly available data sets (R2 genomics analysis), whereby high CLIC1 and CLIC4 expression were significantly associated with poor overall survival. The lack of statistically significant association between CLIC4 in this cohort may be an artefact of small sample size.

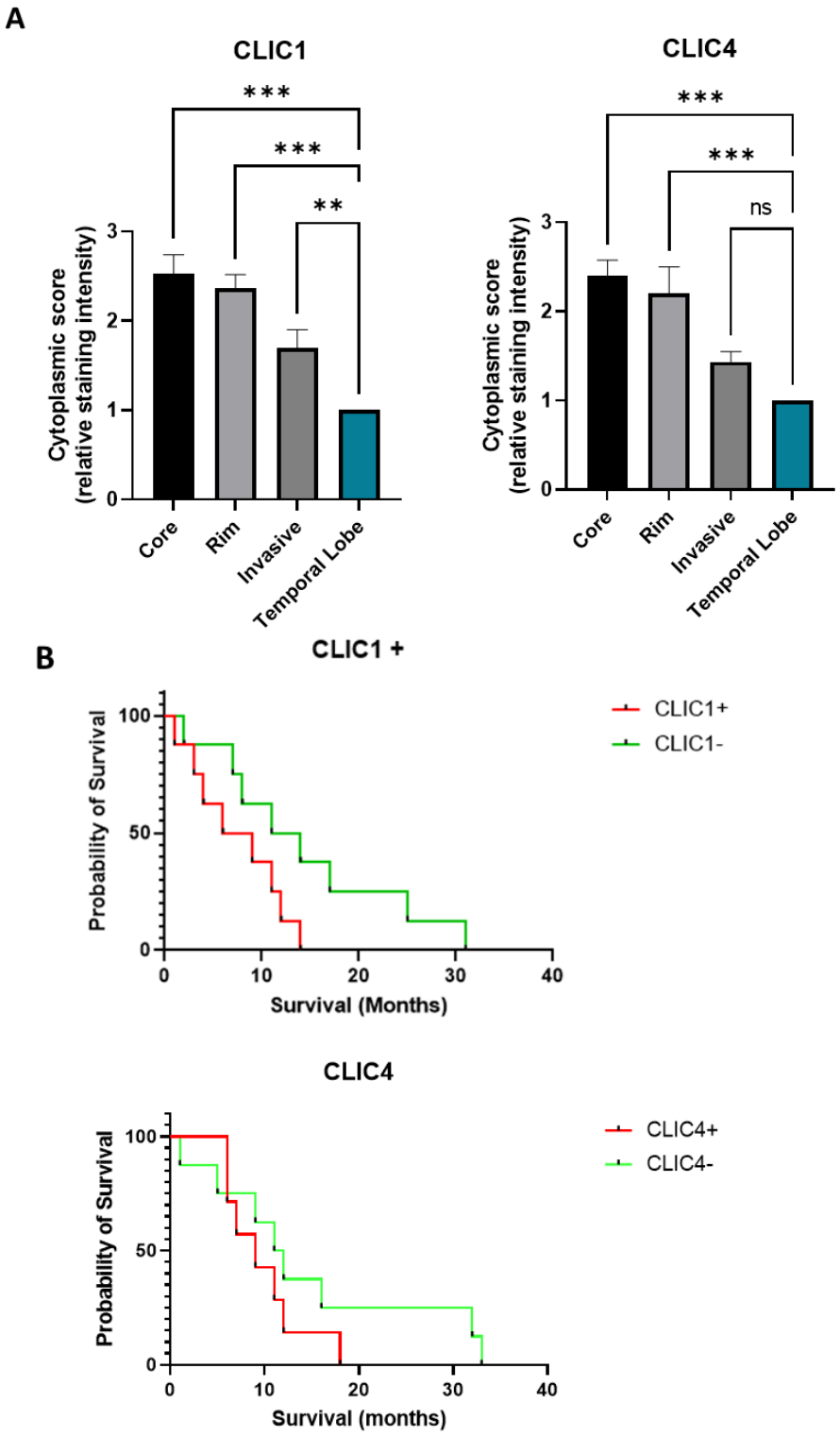

Figure 3.10 CLIC1 and CLIC4 are harness cytoplasmic expression in adult TMAs and overexpression confers poor overall survival. A) Quantification of the staining intensity in the cytoplasmic compartments of CLIC1 and CLIC4 as assessed via IHC analysis of in house adult HGG TMAs compared to temporal lobe. There is an accumulation of staining of CLIC1 and CLIC4 in the cytoplasmic area of cells of aHGG tissues. B) Clinical correlations of CLIC1 and CLIC4 expression of adult HGG TMAs. Kaplan Meier analysis shows that high expression of both CLIC1 and CLIC4 is associated with poor overall survival in patient cohorts CLIC1 p=0.037, CLIC4 p=0.053. Survival curves compared using the Log-rank Mantel Cox test.

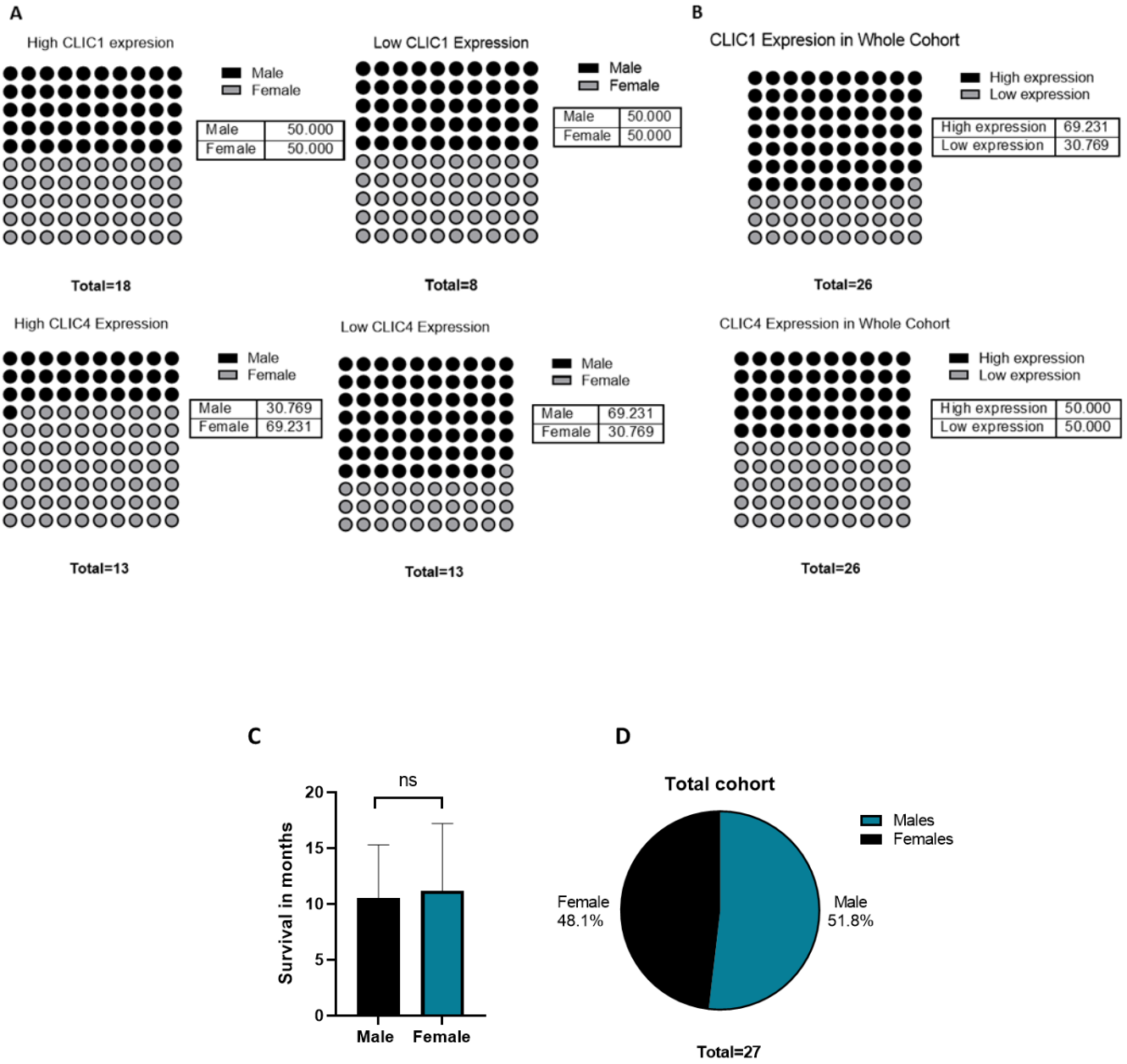

Figure 3.11. Distribution of CLIC1 and CLIC4 expression across patient cohort. A) in aHGG high CLIC1 expression is equally distributed amongst males (50%) and females (50%), whereas males are more likely to have low CLIC4 expression. B) CLIC1 expression is more likely to be high across the whole cohort (69.231% high vs 30.796 low), whereas CLIC4 is equal across the whole cohort (50% high vs 50% low). C) Overall survival in months of males and females in the cohort. D) Overall percentage of males vs females in the cohort. Data analysed in GraphPad prism 9.5 using the 'fraction of whole' analysis function.

In order to further extrapolate the data, the overall expression of CLIC1 and CLIC4 was assessed in the cohort. Overall expression in adult HGG cohorts revealed that both CLIC1 and CLIC4 are expressed in 100% of the patients with 69.3% of patients falling into the CLIC1 high category (upper percentile) and 30.7% falling into the CLIC1 low category (lower percentile), and 50% falling into the CLIC4 high category, and 50% into the CLIC4 low category (Panel B). We then sought to assess whether biological sex of the patient had a bearing on the relative expression of CLIC1 and CLIC4 (figure 3.11A). High CLIC1 (50%) and Low CLIC1 (50%) expression is equally distributed amongst both males and females within the cohort, whereas high CLIC4 expression is significantly associated with female patients (69.231%) as opposed to their male counterparts (30.769%). Interestingly, females are not significantly more likely to have a worse overall survival when compared to males as previous findings would suggest (figure 3.11C). Epidemiology studies have found that there is a higher incidence and worse survival in males with HGG than in females (181), however this difference in incidence is slight, aligning with the data on sex related incidence shown in this study.

It is well known that adult and paediatric gliomas have unique molecular biology; in order to assess whether the CLICs could be molecular markers, a non-parametric linear regression analysis was performed on CLIC1 and CLIC4 expression vs the age of the patient (Figure 3.12). Although not statistically significant, there appears to be a downward trend in expression vs age. The highest expression levels of CLIC1 cluster amongst the youngest patients in the cohort, whereas the lowest expression value is seen in the eldest patient, with the majority of patients showing intermediate levels of expression. Furthermore, the data was stratified according to the molecular diagnoses of the patient. Of the total cohort, only one patient was identified as having an IDH mutation (R132H), whereas the rest of the

cohort was IDH wild type. According to the 2021 WHO classification, these high-grade tumours that would previously have been classified as glioblastomas, are now classified as IDH mutant grade IV astrocytomas, and as such will still be included in the analysis. As there was only one patient with IDH mutation, statistical analysis could not be performed to assess the expression levels of CLIC1 and CLIC4 against the mutation status of the IDH genes. However, analysis was carried out on MGMT methylated (MGMT+) vs MGMT unmethylated patients (MGMT-). Methylation of the O6-methylguanine DNA methyltransferase (MGMT) promoter is recognised as a strong prognostic factor in the therapy of glioblastoma multiforme, and as such guides treatment response and overall survival (182). There was no statistically significant difference found between CLIC1 or CLIC4 expression and MGMT methylation status, however the MGMT methylated (MGMT+) patients clustered more tightly compared to MGMT unmethylated (MGMT-) with the average CLIC1 score of the MGMT+ and MGMT- groups being 1.94 and 2.250, respectively. The average CLIC4 score of the MGMT+ and MGMT- groups were 2.1 and 2.276, respectively.

As all of the tumours were originally classified at GBM grade IV no analyses were carried out on expression vs WHO grade.

A

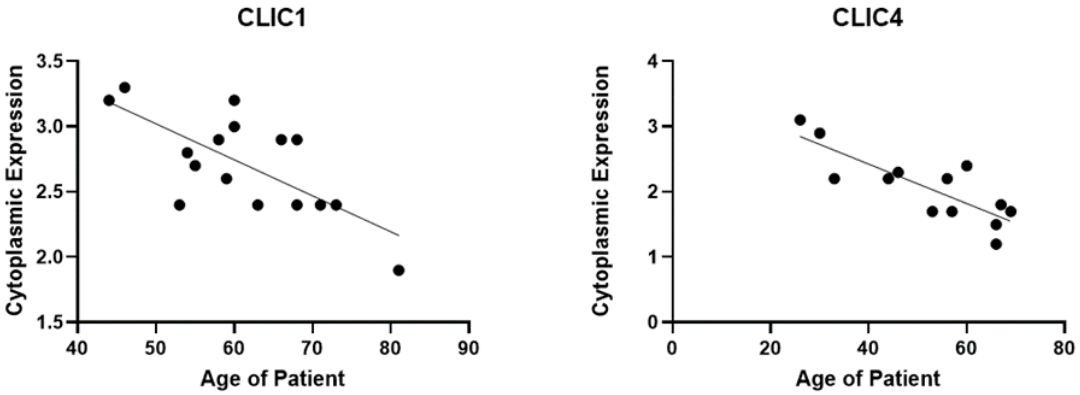

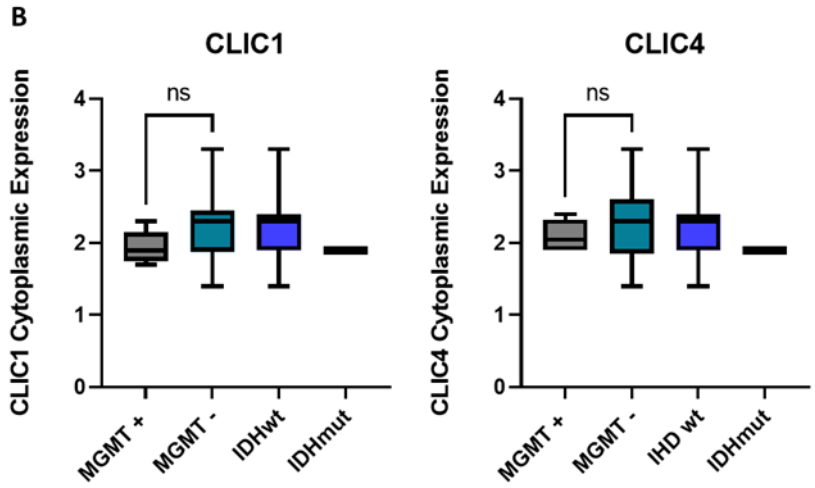

Figure 3.12. Analysis of CLIC1 and CLIC4 expression vs Age and molecular status of patients in aHGG TMAs. There appears to be a downwards trend in age vs CLIC1 and CLIC4 expression. Analysis carried out on GraphPad prism, non-parametric linear line regression analysis using Spearman's correlation test. B) Analysis of CLIC1 and CLIC4 expression vs molecular subtypes of aHGG.

Table 3.3 Clinical details of patient and CLIC1 staining. Clinical details of in-house adult HGG patient samples present on TMA. Tissue sections on TMA were stained via immunohistochemistry with CLIC1 antibody at 1:200 for 2 hours at room temperature. All patients are anonymised.

Sample	CLIC1 Cytoplasmic score	CLIC1 Nuclear score	Histology	IDH-1	MGMT status	ATRX	Tumour Site	Treatment RT/CT	Survival (months)	Age	Sex
GBM12	3.3	1.8	GBM	WT	Hypo		Left parietal	60/TMZ	6.9	46	F
GBM13	2.3	1	GBM	WT			Right Parietal	60/TMZ	9.7	26	M
GBM15	1.9	0.4	GBM	R132H	Interme d		Right temporal	60/TMZ	25.7	33	F
GBM17	2.4	1	GBM	WT	<10% methylation		Left frontal	30	4.4	73	F
GBM19	1.9	2.9	GBM	WT	0% methylation		Left parietal	60/TMZ	14.7	68	M
GBM20	2.4	1.8	GBM	WT	0% methylation		Left parietal	60/TMZ	14.7	68	M
GBM21	2	1.3	GBM	WT	75%		Right temporal	60/TMZ	12.5	67	F
GBM25	3	2.3	GBM	WT	0	WT	Left parietal	60/TMZ	12.9	60	F
GBM26	2.1	1.3	GBM	WT	0	WT	Left temporal	60/TMZ	6.8	56	F
GBM27	2.3	1.1	GBM	WT	75	Mut	Right temporal	60/TMZ	18.7	30	F
GBM28	2.4	2	GBM	WT	0	WT	Right frontal	BSC	3	71	M
GBM29	2.3	2.6	GBM	WT	0	WT	Left frontal		19	67	F
GBM30	2.4	1.7	GBM	WT	0	WT	Left frontal	BSC	9.3	53	M

GBM 31	2.3	2	GBM	WT	0	WT	Right temporal	60/TMZ	16.1	57	F
GBM 32	1.9	2.8	GBM	WT	25%+	WT	Right parietal	60/TMZ	17.7	54	F
GBM 33	2.1	2	GBM	WT	0	WT	Right parietal		11.6	70	M
GBM 37	1.4	2.4	GBM	WT	0%	WT	Right parietal	60/TMZ	12	63	F
GBM 38	2	2.8	GBM	WT	0%	WT	Right frontal	60/TMZ	5.9	69	M
GBM 39	2.9	3	GBM	WT	0%	WT	Right frontal	60/TMZ	14.6	58	F
GBM 40	1.7	3	GBM	WT	0%	WT	Right frontal	30	7.2	44	M
GBM 41	1.4	2.7	GBM	WT	0%	WT	Left temporal	BSC	2.8	55	F
GBM 42	1.7	1.9	GBM	WT	10%	WT	Right temporal		6.8	81	M
GBM 44	2.6	2.7	GBM	WT		WT	Right temporal		1		M
GBM 45	2.1	2.5	GBM	WT	25%	WT	Right parietal	60/TMZ	12.1	66	M
GBM 46	3	2.9	GBM	WT	0%	WT	Right frontal	60	11.5	60	M
GBM 47	1.8	2.9	GBM	WT	0%	WT	Left temporal		11.7	66	M
GBM 52	2.6	2.9	GBM	WT	0	WT	Right frontal	40/TMZ	14.1	59	M

Table 3.4 Clinical details of patients vs CLIC4 staining. Clinical details of in-house adult HGG patient samples present on TMA. Tissue sections on TMA were stained with CLIC4antibody at 1:200 for 2 hours at room temperature. All patients are anonymised.

Sample	CLIC4 Cytoplasmic score	CLIC4 Nuclear score	Histology	MGMT status	IDH-1	ATRX	Tumour Site	Treatment RT/CT	Survival (months)	Age	Sex
GBM12	3.3	1.8	GBM	Hypo	WT		Left parietal	60/TMZ	6.9	46	F
GBM13	2.3	1	GBM		WT		Right Parietal	60/TMZ	9.7	26	M
GBM15	1.9	0.4	GBM	Interme d	R132H		Right temporal	60/TMZ	25.7	33	F
GBM17	2.4	1	GBM	<10% methylation	WT		Left frontal	30	4.4	73	F
GBM19	1.9	2.9	GBM	0% methylation	WT		Left parietal	60/TMZ	14.7	68	M
GBM20	2.4	1.8	GBM	0% methylation	WT		Left parietal	60/TMZ	14.7	68	M
GBM21	2	1.3	GBM	75%	WT		Right temporal	60/TMZ	32.5	67	F
GBM25	3	2.3	GBM	0	WT	WT	Left parietal	60/TMZ	12.9	60	F
GBM26	2.1	1.3	GBM	0	WT	WT	Left temporal	60/TMZ	6.8	56	F
GBM27	2.3	1.1	GBM	75	WT	Mut	Right temporal	60/TMZ	18.7	30	F
GBM28	2.4	2	GBM	0	WT	WT	Right frontal	BSC	3	71	M
GBM29	2.3	2.6	GBM	0	WT	WT	Left frontal		19	67	F
GBM30	2.4	1.7	GBM	0	WT	WT	Left frontal	BSC	9.3	53	M
GBM31	2.3	2	GBM	0	WT	WT	Right temporal	60/TMZ	16.1	57	F

GBM 32	1.9	2.8	GBM	25%+	WT	WT	Right parietal	60/TMZ	17.7	54	F
GBM 33	2.1	2	GBM	0	WT	WT	Right parietal		11.6	70	M
GBM 37	1.4	2.4	GBM	0%	WT	WT	Right parietal	60/TMZ	12	63	F
GBM 38	2	2.8	GBM	0%	WT	WT	Right frontal	60/TMZ	5.9	69	M
GBM 39	2.9	3.5	GBM	0%	WT	WT	Right frontal	60/TMZ	14.6	58	F
GBM 40	1.7	3.2	GBM	0%	WT	WT	Right frontal	30	7.2	44	M
GBM 41	1.4	2.7	GBM	0%	WT	WT	Left temporal	BSC	2.8	55	F
GBM 42	1.7	1.9	GBM	10%	WT	WT	Right temporal		6.8	81	M
GBM 44	2.6	2.7	GBM		WT	WT	Right temporal		1		
GBM 45	2.1	2.5	GBM	25%	WT	WT	Right parietal	60/TMZ	12.1	66	M
GBM 46	3.2	2.9	GBM	0%	WT	WT	Right frontal	60	11.5	60	M
GBM 47	1.8	2.9	GBM	0%	WT	WT	Left temporal		11.7	66	M
GBM 52	2.6	2.9	GBM	0	WT	WT	Right frontal	40/TMZ	14.1	59	M

3.4.3.2 *CLIC1 and CLIC4 overexpression is associated with poor overall survival in in-house paediatric HGG cohorts*

As with the adult data, we sought to explore the clinical associations and intracellular regional expression of CLIC1 and CLIC4 in our in-house paediatric cohort. As previously confirmed in the adult cohort, and Immunofluorescent staining of paediatric HGG cell lines, we found a significant increase of CLIC1 and CLIC4 protein expression in the cytoplasmic region compared to nuclear in our pHGG TMAs (Figure 3.13). When this data was compared to overall staining in the temporal lobe (healthy brain) the overall staining of both proteins was significantly upregulated in the tumour cores. To then assess the clinical association Kaplan-Meier analyses were performed as previously described. In the paediatric cohort high CLIC1 expression was significantly correlated with a decrease in survival time ($p= 0.049$) whereas high CLIC4 ($p=0.7$) was not significantly associated with overall survival. These results support the data found in our adult cohort and the data found in publicly available datasets, and again may be skewed due to small sample size. Of particular note, there is one long term survivor present in the high CLIC4 group, with a survival time of 89 months, this compares dramatically to the median overall survival of 18 months. Hazard ratios for the CLIC1 and CLIC4 high groups were 1.72 and 0.95, respectively.

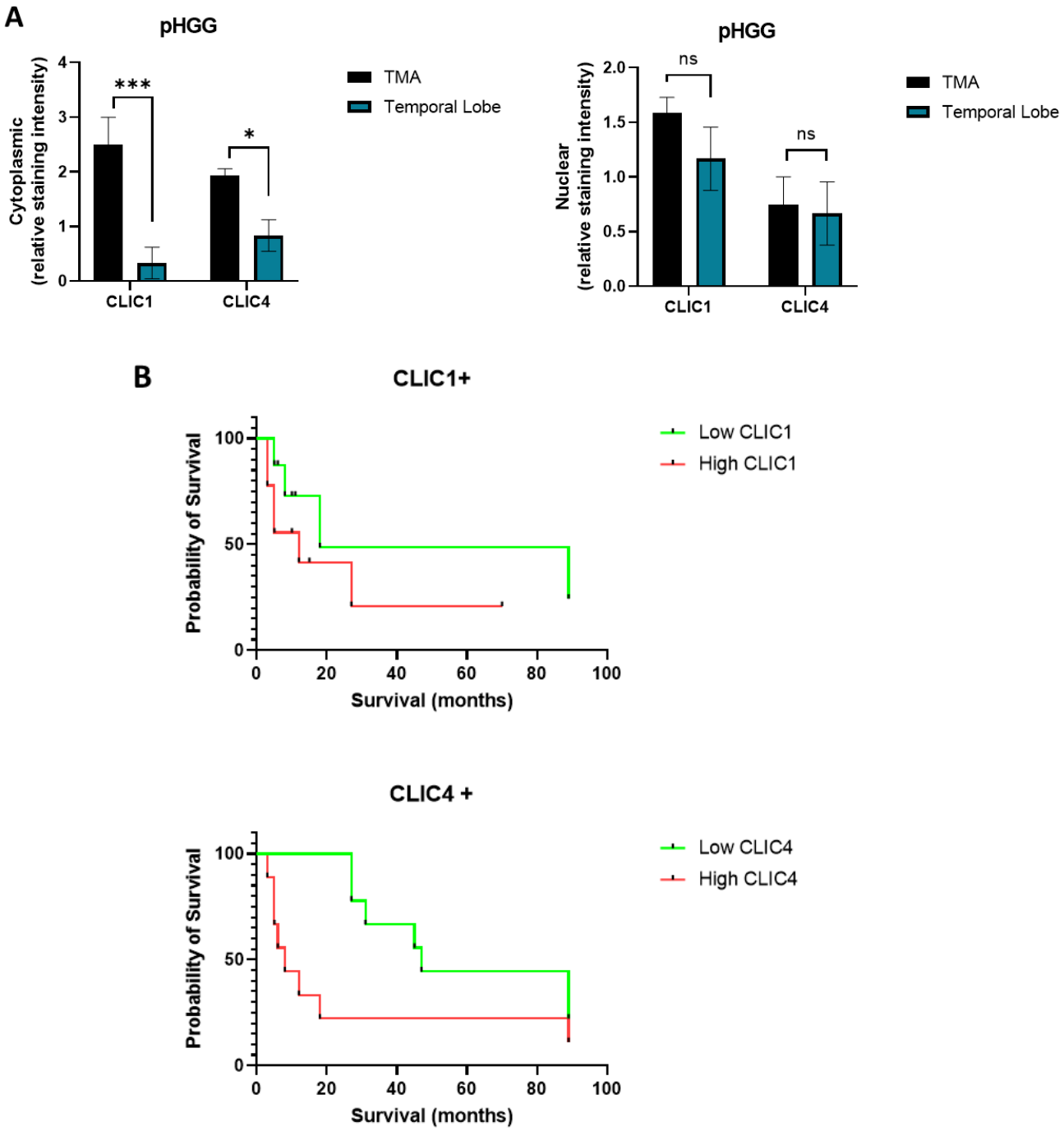

Figure 3.13 CLIC1 and CLIC4 show strong cytoplasmic expression in paediatric TMAs and overexpression confers poor overall survival. A) Quantification of the staining intensity of CLIC1 and CLIC4 in the cytoplasmic and nuclear compartments of pHGG tissue vs temporal lobe, as assessed via IHC analysis. Data represents patient tissue samples falling into the upper quartile of the data. There is an accumulation of staining of CLIC1 and CLIC4 in the cytoplasmic area of cells of pHGG tissues. B) Clinical correlations of CLIC1 and CLIC4 expression of pHGG TMAs. Kaplan Meier analysis shows that high expression of both CLIC1 and CLIC4 is associated with poor overall survival in patient cohorts CLIC1 p=0.049 * HR = 1.72, CLIC4 p=0.072 HR = 0.95 ns. Survival curves compared using the Log-rank Mantel Cox test.

As seen in the adult dataset, 100% of the samples were CLIC4 positive, with only one sample being CLIC1 negative score in 2 out of 3 cores (overall score 0.5). Interestingly, this patient was the long-term survivor, with an overall survival of 89months. Figure 3.14 represents the relative expression of CLIC1 and CLIC4 across the whole cohort and split by sex. There was high CLIC4 expression found in 68.7% of the cohort, with males making up 68% of the CLIC4 high group. Similarly, high CLIC1 expression was found in 56% of the cohort, with male patients making up 75% of this total. These data mirror findings in the adult cohort.

Linear regression analysis of the relative staining of CLIC1 and CLIC4 against age revealed no statistical association, and no trend in age was observed. Due to the lack of molecular diagnostic data, the paediatric cohort was unable to be further stratified according to mutational status, however histopathological diagnosis was performed and determined a range of grade III and grade IV tumours. An un-paired t-test revealed that patients in the WHO grade IV cohort was significantly more likely to have increased CLIC1 cytoplasmic expression, whereas CLIC4 expression was not statistically associated with WHO grade. Clinical association between CLIC1 and CLIC4 expression was explored in the adult cohort on R2, whereby high CLIC1 and CLIC4 were both significantly associated with WHO grade IV tumours. This data is indicative of CLIC1 holding potential as a biomarker of poor overall survival and WHO grade in adult and pHGG, and CLIC4 as a potential marker in aHGG.

As previously found in the adult cohort, biological sex was not an indicator of overall survival in the paediatric population. This was despite the incidence being slightly higher in males (53.3%) compared to females (46.6%).

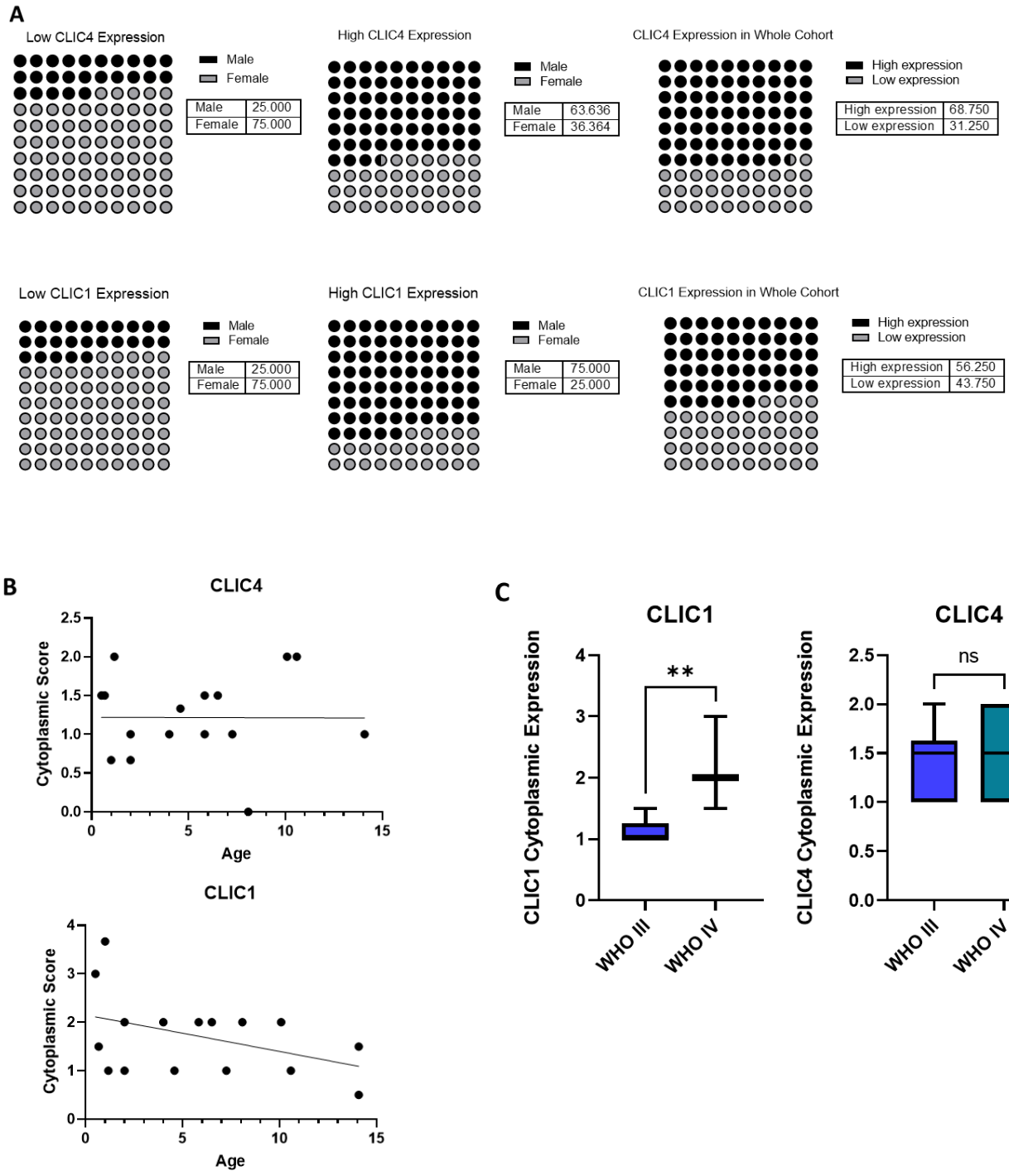

Figure 3.14 Analysis of CLIC1 and CLIC4 expression vs gender and age of patient in pHGG TMAs A) in pHGG high CLIC1 expression is more common in males (75%) and females (25%), whereas males are more likely to have low CLIC4 expression. Data analysed in GraphPad prism 9.5 using the 'fraction of whole' analysis function B) There is no associate between age and CLIC1 and CLIC4 expression. Analysis carried out on GraphPad prism, non-parametric linear line regression analysis using Spearman's correlation test. C) assessment of the correlation between CLIC1 and CLIC4 cytoplasmic scoring and the WHO grade of the tumour, unpaired t-test.

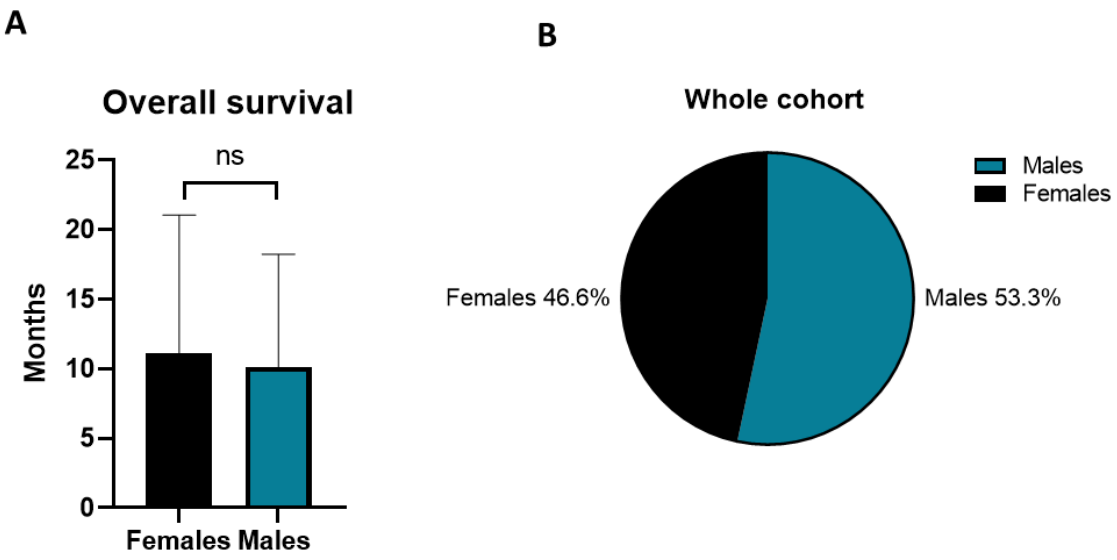

Figure 3.15. **Males have a higher incidence of pHGG but is not associated with worse overall survival.** A) Overall survival in months of males and females in the cohort. B) overall percentage of males vs females in the cohort. Data analysed in GraphPad prism 9.5 using the 'fraction of whole' analysis function and t-test.

Table 3.5 Clinical data of pHGG patients used in this study. All patients are anonymised. Samples collected at Queens medical centre, Nottingham. Patients underwent molecular diagnostics as part of routine diagnoses.

Patient	CLIC1 expression	CLIC4 expression	Diagnosis	Sex	Age at diagnosis	Treatment	Survival months
89/12837 GBM	0.5	2	GBM	M	1	B 7 courses of 8 in 1 CT; hypersensitive: started modified baby brain protocol	89
87/15184 AA	2	1.5	GBM	M	5.83333	cisplatinum x2 + local RT	5
90/6570 2nd look surgery GBM	2	1	GBM	M	5.83333	cisplatinum x2 + local RT	5
00/20847 Recurrent GBM	2	1	GBM			PCV x6 cycles	
90/13949 GBM	2	1	GBM	F	8.08333		2
94/3421 GBM	2	1	GBM	M	4	Thiotepa	10
94/15011 GBM	3	1.5	GBM	M	0.5		3
95/9504 GBM	2	1.5	GBM	M	6.5	previous RT + CT; SIOP protocol then RT	12
99/+S3:T1014974 AA	1.5	2	GBM after non-Hodgkin lymphoma	M	14.08333	RT (55Gy in 30 fractions)	9
01/10325 AA	1	2	AA	F	2	CT (8 in 1).	5
90/6551 GBM	1	2	GBM post ALL	M	7.25	previous UKALL schedule C (1988); RT with relapse	6
87/708 GBM	0.5	1	GBM	F	14.08333	8 in 1 chemo + RT A	8
91/9809 PF GBM	1.5	1.5	AA	F	0.666667	RT + 8 in 1 CT	29

91/16645 BS AA	1	1	GBM	F	1.166667	baby brain; oral VP16	14
93/15148 AA	1	1.5	AA	F	10.58333	cisplatinum x2 + RT; thiotepa	18
87/14535 AA	1	1.5	small cell GBM	F	4.583333		

3.5 Spatial expression of CLICs in neuroanatomical regions

As previously shown, there appears to be spatial differences in the expression of both CLIC1 and CLIC4 in paediatric glioma cell lines, versus patient tissue. There appears to be an accumulation of CLIC proteins in the core region of the tumours, with heavy cytoplasmic staining, whereas cell lines reveal an additional accumulation in the membrane. Gliomas are highly heterogenous tumours, with spatial temporal analyses revealing significant molecular differences, histopathological subtypes, and dynamic spatial transcriptomic signatures across tumours. This heterogeneity may be a major limiting factor in glioma treatment efficacy, with populations of treatment resistant and treatment sensitive cells residing throughout the tumour and therefore drive glioma recurrence (183,184).

Here we sought to assess the spatial expression of CLIC1 and CLIC4 proteins across our in-house adult glioma tissue (section 3.4.3.1). Due to lack of regional sampling for the paediatric tissue samples, this study was not able to be completed in the paediatric setting.

To assess expression levels of CLICs RNA sequencing data (panel A) was utilised by using the average RPKM expression of each sample (10 patients, ran in triplicate). Tumour samples from the core, rim and invasive regions of patient tumours was assessed. Here, CLIC1 expression is seen to be significantly higher in the core region of the tumour when compared to the invasive region (t-test p=0.01). Similarly, CLIC4 expression is accumulated in the core region vs the invasive region of the tumour (t-test p= 0.00175). The overall tumour expression levels of CLIC4 are higher than CLIC1, with average CLIC4 RPKM of 126.0 and 83.28 in the core and invasive regions respectively, compared to 80.89 and 39.30 in the core and invasive regions, respectively. To recapitulate this using rtPCR (panel B), RNA was extracted from 6 matched core and invasive regions of adult HGG samples. CLIC1 accumulation in the core region of the tumour was observed in 5 patients (* = $P \leq 0.05$, **

P ≤ 0.01), showing significantly increased CLIC1 core expression in 83% of patients in this select panel. Interestingly, although significant upregulation of CLIC4 was observed in 3 patient samples (* = P ≤ 0.05, ** P ≤ 0.01), the overall percentage of CLIC4 accumulation in the core region was 50% of patients in the panel. Additionally, staining against CLIC1 and CLIC4 via IHC (panel C) was carried out on adult HGG TMAs to assess regional differences between core, invasive and rim regions of the tumour (n=40, each region in triplicate). CLIC1 accumulation was again observed in the core region of the tumour when compared to the invasive region (unpaired t-test, P=0.0462), however there was no significant difference observed in CLIC4 expression. Intriguingly, the regional expression of CLIC1 appears to be consistent across techniques, whereas the only the most sensitive technique (RNA sequencing) found consistent significant differences in CLIC4 expression. This may be due to the protein cycling of CLIC4 or increasing role of CLIC4 in sustained invasion in actively invasive glioma cells (185). It is noteworthy that there were no significant differences observed between the expression of CLIC proteins when comparing the core region to the rim, or invasive region to the rim. When assessing ion channels, it is important to note that there are significant differences in role of the functional membrane embedded protein, and the nuclear/membrane bound organelle proteins. As such, RNA expression may not be indicative of a functional protein.

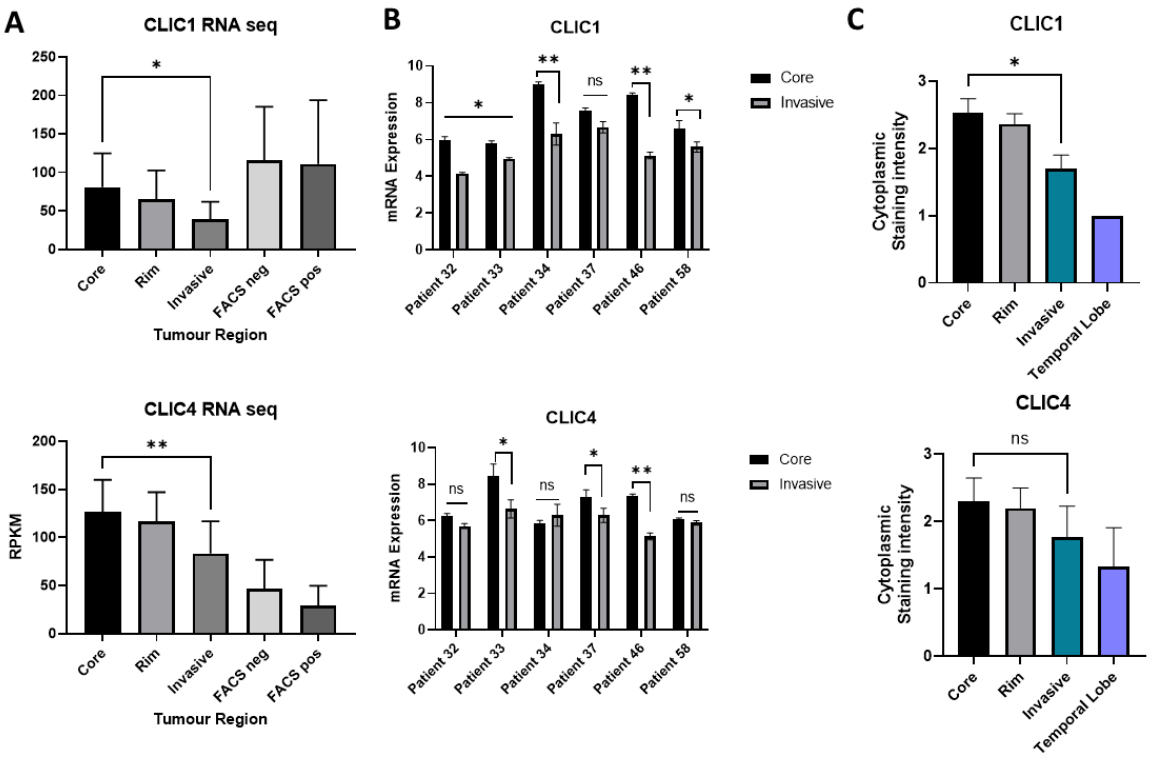

Figure 3.16. Spatial analysis of CLIC1 and CLIC4 expression. A) in-house RNA sequencing of adult high grade glioma tissue reveals a significantly higher expression of CLIC1 and CLIC4 in the core region of the tumour compared to the invasive margin. B) rtPCR of adult glioma tissue reveals significant increase in CLIC1 and CLIC4 expression in 50% of the cohort. C) Staining of adult tissue via IHC reveals no difference in CLIC4 expression between region, but a significant difference between the core and invasive regions for CLIC1. Paired t test * = p <0.05

3.5.1 Hypoxia and acidosis may be associated with re-localisation of CLIC proteins.

It is well known that gliomas are hypoxic tumours, with the core region encompassing the most highly necrotic areas with high levels of hypoxia (186). To investigate the cause of staining differences observed in patient tissue versus cell lines, and a molecular role for spatial differences in expression we sought to assess the potential for microenvironmental re-localisation of CLIC proteins. This high CLIC expression may be associated with an inherent drive for these cells to migrate and invade further into the cranial space, and as such an increased expression of CLIC proteins used to promote morphological changes that are associated with glioma cell invasion. Although it may be expected that the cells residing in the invasive margin would have the higher expression of CLIC proteins as they are actively invading, it may be the case that the functional protein is not being cycled as the

initial drive towards resources has been complete, thus resulting in higher overall expression in the core region. Previous studies on our in-house patient derived adult lines have defined intra-tumour heterogeneity, with a distinct proliferating rim, necrotic core, and oxygen tension gradient (187).

Immunofluorescent staining and imaging via confocal microscopy were used to assess the relationship between exposure to hypoxia (1% oxygen) or acidosis (media pH 6.7). Cells were exposed to microenvironmental changes for 24 hours (hypoxia) or 72 hours (acidosis) prior to experimentations. SF188 cells were exposed to hypoxia and acidosis and stained against CLIC1 (Panel A), had a significant overall reduction in the relative CLIC1 expression was observed following exposure to both hypoxia ($p=0.0364$) and acidosis ($p= 0.009$). Despite the overall reduction in staining intensity, image analysis using ImageJ region of interest tool revealed that SF188 cells exposed to hypoxia had a significantly higher accumulation of CLIC1 in the membranous region of the cell ($p= 0.0087$) as shown by increased staining intensity. Similarly, acidosis appears to be associated with re-localisation of CLIC1, with an accumulation in the nuclear region post exposure to acidotic media ($p=0.001$), suggesting that different microenvironmental change can trigger re-localisation of CLIC1 proteins. SF188 cells were also stained against CLIC4 (panel B). In comparison to CLIC1, the protein localisation of CLIC4 did not significantly change upon exposure to hypoxia ($p =<0.05$) or acidosis ($p=<0.05$) with relative staining intensity remaining consistent across different experimental conditions. However, the overall expression of CLIC4 did decrease when SF188 cells were exposed to acidotic media for 72 hours ($p= 0.0096$), whereas there were no significant changes upon exposure to hypoxia.

Panel C explores the expression of CLIC1 expression associated with the exposure of KNS42 to the same conditions as above. Unlike SF188 cells, acidosis did not significantly alter

overall expression ($p<0.05$) or protein localisation of CLIC4. Interestingly, the induction of hypoxia in these cells resulted in a significant increase in CLIC1 expression ($p= 0.037$), with and elevated accumulation in the cytoplasmic region of the cells (0.0082). Additionally, the cytoplasmic staining appeared to be granular in the hypoxic condition, suggesting either metabolism, or transport of CLIC1. Finally, KNS42 cells were stained against CLIC4 following induction of hypoxia and acidosis (Panel D) significant upregulation of CLIC4 is seen in normoxic conditions ($p= 0.00091$), with accumulation in the membranes of cells ($p=0.01$). Furthermore, acidosis triggers a down regulation of CLIC4 protein expression ($p=0.0071$) associated with cytoplasmic accumulation ($p=0.0471$). No significant morphological changes were observed SF188 cells, however KNS42 cells appear to alter morphology post hypoxia and acidosis, with cells appearing smaller and less diffuse.

Although these data do not draw any conclusive conclusions about the role of hypoxia and acidosis in CLIC1 and CLIC4 localisation, they do provide evidence that these proteins may be regulated by microenvironmental factors, such as oxygen and pH. CLIC4 has been highly implicated in the regulation of pH in a variety of models (205–207), and CLIC1 and CLIC4 are implicated in the redox pathway in ovarian (191) and colon cancers (208). Insertion of CLIC1 into the membrane is redox dependant, and likely mediated by Cys24 and C24A mutations, altering its electrophysiological characteristics. Furthermore, CLIC channel activity at physiological pH has been suggested to be minimal, with changes in pH resulting in increasing membrane expression of CLIC proteins (177).

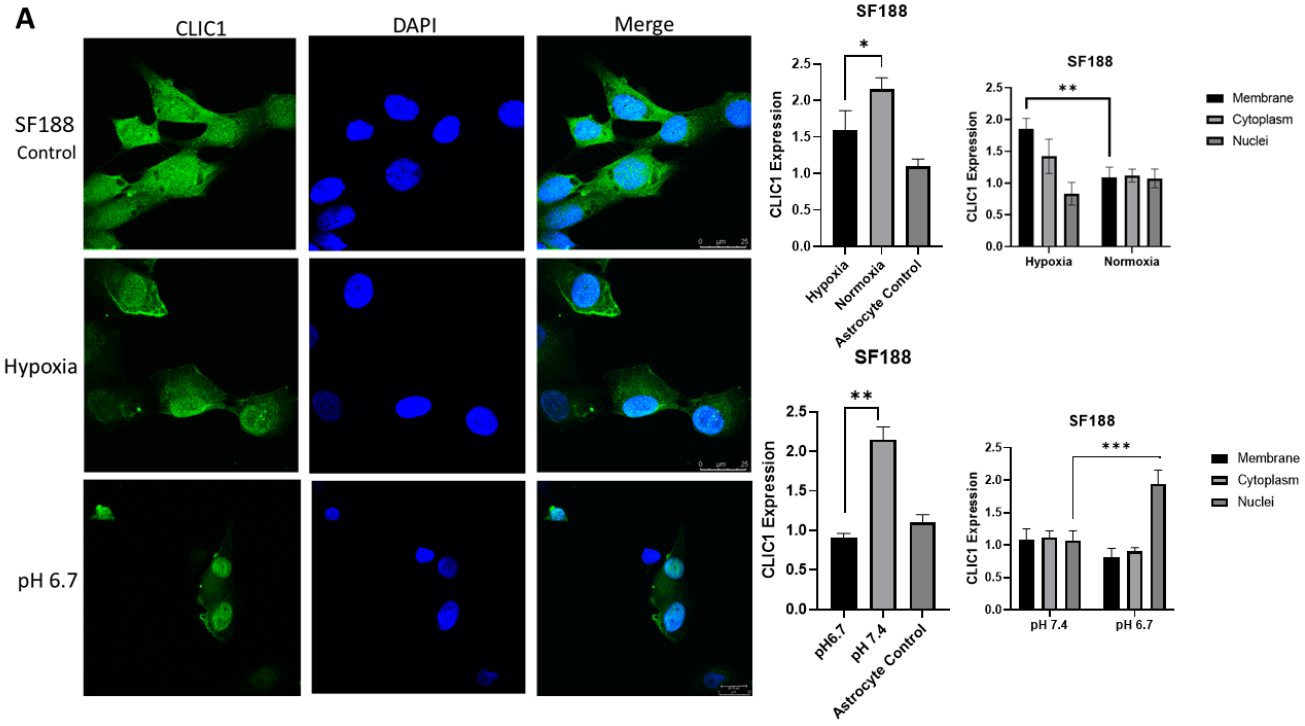
A
CLIC1
DAPI
Merge
SF188
Control
Hypoxia
pH 6.7
SF188
CLIC1 Expression
Hypoxia
Normoxia
Astrocyte Control
SF188
CLIC1 Expression
Hypoxia
Normoxia
Membrane
Cytoplasm
Nuclei
SF188
CLIC1 Expression
pH6.7
pH 7.4
Astrocyte Control
SF188
CLIC1 Expression
pH 7.4
pH 6.7
Membrane
Cytoplasm
Nuclei

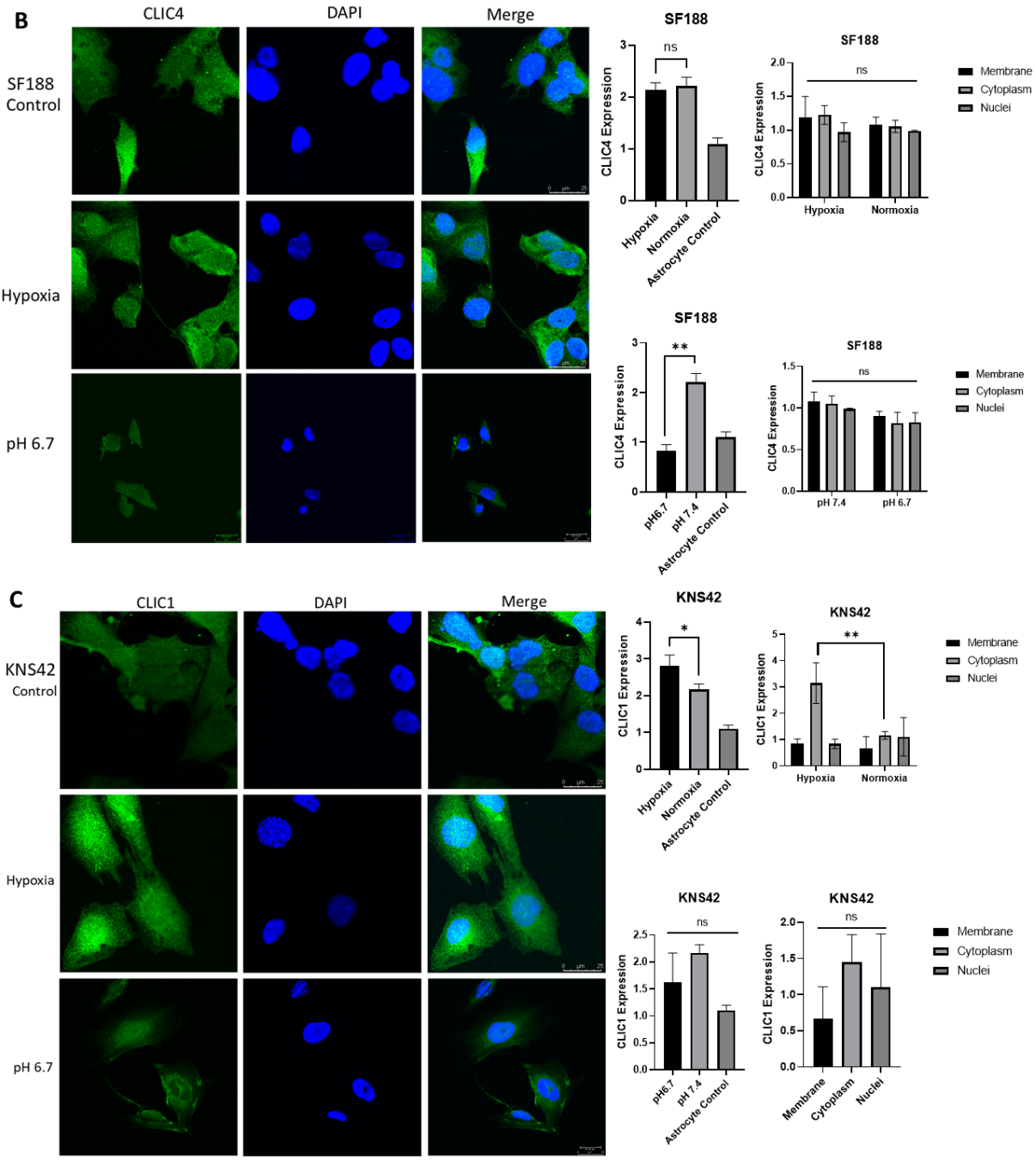
B
CLIC4
DAPI
Merge
SF188
Control
Hypoxia
pH 6.7
SF188
ns
CLIC4 Expression
Hypoxia
Normoxia
Astrocyte Control
SF188
ns
CLIC4 Expression
Hypoxia
Normoxia
Membrane
Cytoplasm
Nuclei
SF188
**
CLIC4 Expression
pH6.7
pH 7.4
Astrocyte Control
SF188
ns
CLIC4 Expression
pH 7.4
pH 6.7
Membrane
Cytoplasm
Nuclei
C
CLIC1
DAPI
Merge
KNS42
Control
Hypoxia
pH 6.7
KNS42
*
CLIC1 Expression
Hypoxia
Normoxia
Astrocyte Control
KNS42
**
CLIC1 Expression
Hypoxia
Normoxia
Membrane
Cytoplasm
Nuclei
KNS42
ns
CLIC1 Expression
pH6.7
pH 7.4
Astrocyte Control
KNS42
ns
CLIC1 Expression
Membrane
Cytoplasm
Nuclei
Membrane
Cytoplasm
Nuclei

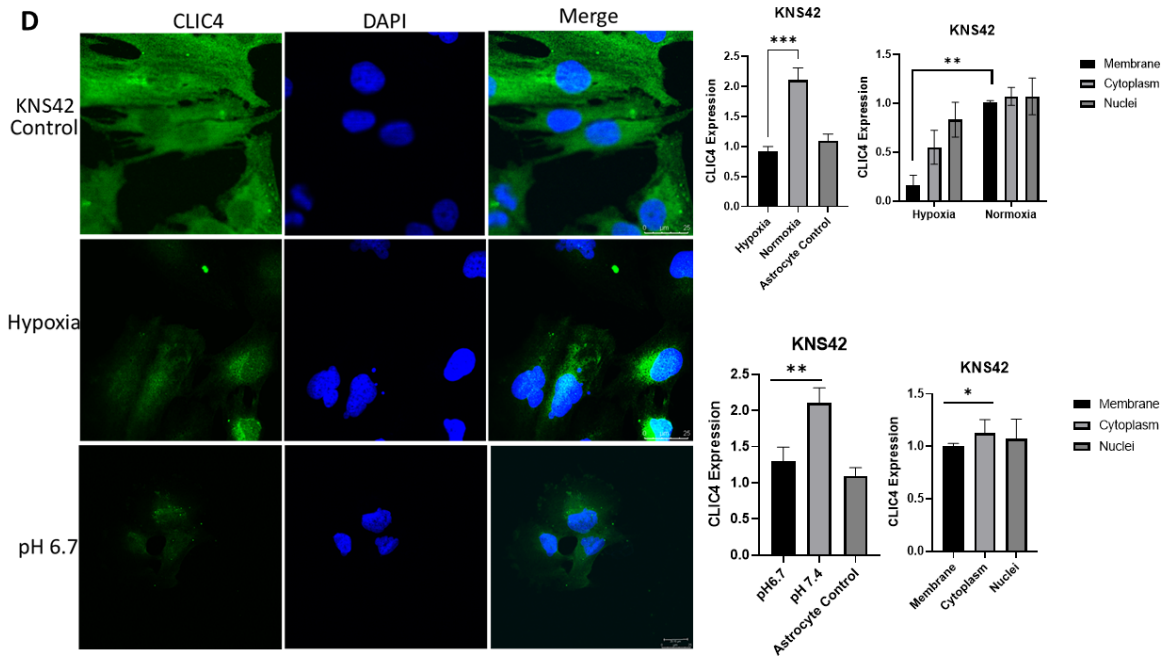

Figure 3.17 Hypoxia and acidosis is associated with re-localisation of CLIC proteins. Representative images of cells exposed to hypoxia, normoxia or acidotic media conditions. Representative astrocyte control data was collected in previous experiments, and as such are not shown as part of this figure. Data collected with the help of undergraduate research student King Yeung. Project design, optimisation, protocol writing, analysis and creation of figures was carried out by myself. Statistical analysis performed via t test. Representative images at X40 magnification. n=3. Scale bars represent 25 μm.

A clear limitation of the above work is the lack of a cytoplasmic or membrane marker as a co-stain to confirm the presence of CLIC1 and CLIC4 in those specific regions. This research was carried out as part of an undergraduate research project, and King Yeung performed some of the lab experiments used to create these figures. As such, there were time and technical constraints in this piece of work. Imaging software such as ImageJ was exploited in this case to use tools to assess specific regions of interest, the protocol for this is described in section 2.11.2 Statistical analyses were carried out, but despite this, conclusive associations cannot be drawn at this time. The GCE62 cell line was established in house from a 16-year-old patient, whereas KNS42 and SF188 are both commercial lines. Further work would include the exploration of this work in our primary lines, as well as

exposing the cells to chronic hypoxia for 48-72 hours, as well as more specific region analysis via fractional protein extraction and western blotting.

3.6 Chapter summary

In this chapter, we have assessed and characterised the expression and clinical associations of ion channels across adult and paediatric glioma datasets. We have utilised inhouse patient samples, cell lines and tissues along with publicly available datasets to investigate and determine a panel of ion channel candidates. Via interrogation of these data sets, the intracellular chloride channels CLIC1 and CLIC4 have been selected as candidates for this study and were taken forward for further analysis. Expression patterns of CLIC1 and CLIC4 including protein localisation was assessed across patient tissue samples, and pHGG cells lines, combined with RNAseq and qrtPCR interrogation of the mRNA expression. We have manipulated the microenvironment of pHGG cells by inducing either hypoxia or acidosis and observing expression patterns of CLIC1 and CLIC4 in pHGG cells. Finally, we have assessed CLIC1 and CLIC4 as potential glioma biomarkers, via determining the clinical significance of CLCI1 and CLIC4 expression and overall survival of in-house adult and paediatric patients.

Chapter outcomes:

1) A widescale literature review has identified that Ion channels are implicated in the malignant progression of a variety of cancers and demonstrate clinical and experimental associations with glioma.
2) CLIC1 and CLIC4 ion channels are overexpressed in adult and paediatric HGG.
    - RNA sequencing reveals that CLIC1 and CLIC4 is overexpressed at the RNA in adult patient tissue samples.

- Paediatric HGG cell lines SF188, KNS42, GCE62 overexpress CLIC1 and CLIC4 mRNA compared to astrocyte controls.

3) Analysis of protein localisation reveals over expression of CLIC1 and CLIC4
   - CLIC1 and CLIC4 are preferentially expressed in the cytoplasm of glioma tissue and pHGG cells.
4) Overexpression of CLIC1 and CLIC4 is associated with poor overall survival in adult and paediatric cohorts.
   - Overexpression of both CLIC1 and CLIC4 results in significantly reduces overall survival in adult and paediatric in-house patient samples.
   - Overexpression of CLIC1 confers poor overall survival in paediatric publicly available data sets.
   - There is no significant associate between CLIC expression and age, gender, or methylation status, but is significantly associated with higher WHO grade in adult patients.
5) There are expression differences of CLIC1 and CLIC4 in neuroanatomical regions, with preferential expression observed in the core region of tumours.
6) Hypoxia and acidosis may influence localisation of CLIC1 and CLIC4

4 Chapter 4: The role of CLIC1 and CLIC4 in glioma pathogenesis

4.1 Introduction

In the previous chapter we demonstrated that CLIC1 and CLIC4 are overexpressed in adult and paediatric high-grade gliomas at both a protein and mRNA level. We found that this overexpression is clinically associated with poor overall survival in adult and paediatric cohorts, and that high levels of CLIC1 and CLIC4 are linked to higher WHO grade tumours. As discussed, there are limited treatment options for HGGs, with proven treatment options in the paediatric population being even more scarce. Clinical trials for HGG fail regularly, and new treatment modalities are met by significant limitations.

One such limitation is the availability of drugs that can successfully cross the blood brain barrier. Ion channel inhibiting drugs are used in a myriad of neurological and psychological disorders, and many are well proven to be able to cross the blood brain barrier (188). Consequently, targeting ion channels such as CLIC1 and CLIC4 is attractive as a new treatment modality for pHGG. Recent advances in brain tumour research suggests that gliomas are able to integrate into neural networks (189), evoking non-synaptic activity-dependant ion channel currents. Similarly, gliomas can integrate electrically into the surrounding brain, creating complex networks (190) and as such, harnessing the brain's intrinsic electrical activity and repositioning it as a defence against HGG progression may provide novel and efficacious.

A plethora of anti-cancer agents target the cell cycle in its various stages. CLIC1 and CLIC4 have both been implicated in the cell cycle, and therefore the replicative, proliferative, and apoptotic properties of cancer cells. CLIC1 expression is associated with multiple cell cycle stages and inhibiting CLIC1 and CLIC4 has been demonstrated to disrupt cell cycle

progression, preventing membrane depolarisation associated with G2/M in gastric cancers (170).

Furthermore, invasion is a significant hallmark of cancer, and indeed, chloride channels are strongly implicated in successful invasion of HGG cells. Chloride channels are associated with apoptotic volume change, via the dual efflux of water and chloride ions, a mechanism essential for morphological changes required for glioma cell invasion and migration (126,179).

Here we seek to underpin the significance of CLIC1 and CLIC4 ion channels in HGG hallmarks, via genetic and pharmacological targeting.

Chapter aims:

1) Assess the role of CLIC1 and CLIC4 as druggable targets via clinically and non-clinically available drugs.
2) To generate CLIC1 and CLIC4 knock out cell lines.
3) To assess the role of genetic and pharmacological inhibition of CLIC1 and CLIC4 in pHGG cell proliferation and viability.
4) To assess the invasive capacity of CLIC1 and CLIC4 deficient cell lines in combination with siRNA and drug targeting.
5) To investigate the effect of CLIC1 and CLIC4 targeting on the cell cycle of pHGG.

4.2 3D culture of pHGG

It is well understood that there are several limitations to the use of 2D culture to assess cellular mechanisms and cancer pathology. To recapitulate the cell state and tumour environment, a 3D culture technique was employed. First, we sought to assess the ability of pHGG cell lines to form neurospheres, using a free forming neurosphere assay. This additionally has the benefit of measuring the stemness of the cells. Studies have suggested that invitro neurosphere formation correlates with poor overall survival and glioma progression, independent of the tumour grade (191).

4.2.1 Paediatric HGG cells readily form neurospheres.

SF188, KNS42 and GCE62 were grown in a stem enriched media (described in chapter 2.4.3) and plated in non-adherent 6 well plates. The growth of the cells was observed microscopically daily, the neurospheres imaged, and then measured using ImageJ. To determine the average size of neurospheres, cells were plated in triplicate, and all neurospheres present on 3 selected regions of each well were measured. Figure 4.1 exhibits representative images of neurospheres grown over a period of 3 days compared to standard monolayer culture. At day 1, SF188 and GCE62 cells form neurospheres of varying sizes, appearing to favour multiple smaller neurospheres as opposed to larger spheres. In comparison, KNS42 forms large neurospheres, even at early time points. Interestingly at day 1 and day 2, there was a high volume of free-floating GCE62 cells that had not yet formed neurospheres. By day 3, GCE62 had formed tight spheres with solid margins, which was often followed by degeneration of the sphere at day 4. Panel B demonstrates representative images of single neurospheres across the time points and is indicative of the average neurosphere size and type of sphere that would be measured. KNS42 and SF188 neurospheres often exhibited necrotic cores at late time points, indicative of a hypoxia

gradient throughout the sphere. This may be a result of the high metabolic activity of the cells and resource restriction in the centre of the neurosphere. As previously discussed in chapter 3, this necrotic centre accurately recapitulates what is typically observed in the core of gliomas, as the core area is usually exposed to hypoxic stress. All three cell lines were able to form consistent spheres with tight margins and would re-form these spheres post passage. Cells maintained the capacity to re-attach and form a monolayer when plated in serum containing media on high attachment plates. KNS42 cells formed the largest neurospheres of all of the lines, which was anticipated due to the large cell size. The size of the SF188 and GCE62 neurospheres were more variable, with less consistency seen between wells.

The ability of these cells to form neurospheres is indicative of their ability to return to a 'stem-like' state i.e., glioma stem cells (GSCs). Some studies claim that GSCs are the population of cells that harness the ability to proliferate indefinitely (142) and are responsible for tumour aggressiveness and subsequently resistance of gliomas. These data suggest that selection pressures, such as low attachment plates and stem inducing media can trigger SF188, KNS42 and GCE62 to transform to this 'stem-like' state, suggesting aggressive and high-risk tumours. All three cell lines were derived from grade IV gliomas, in which the patient had poor overall survival.

To further assess the sphere forming capacity of these cells additional measuring methods could be employed such as isolating individual spheres and performing a cell count accompanied by assessment of live to dead ratio.

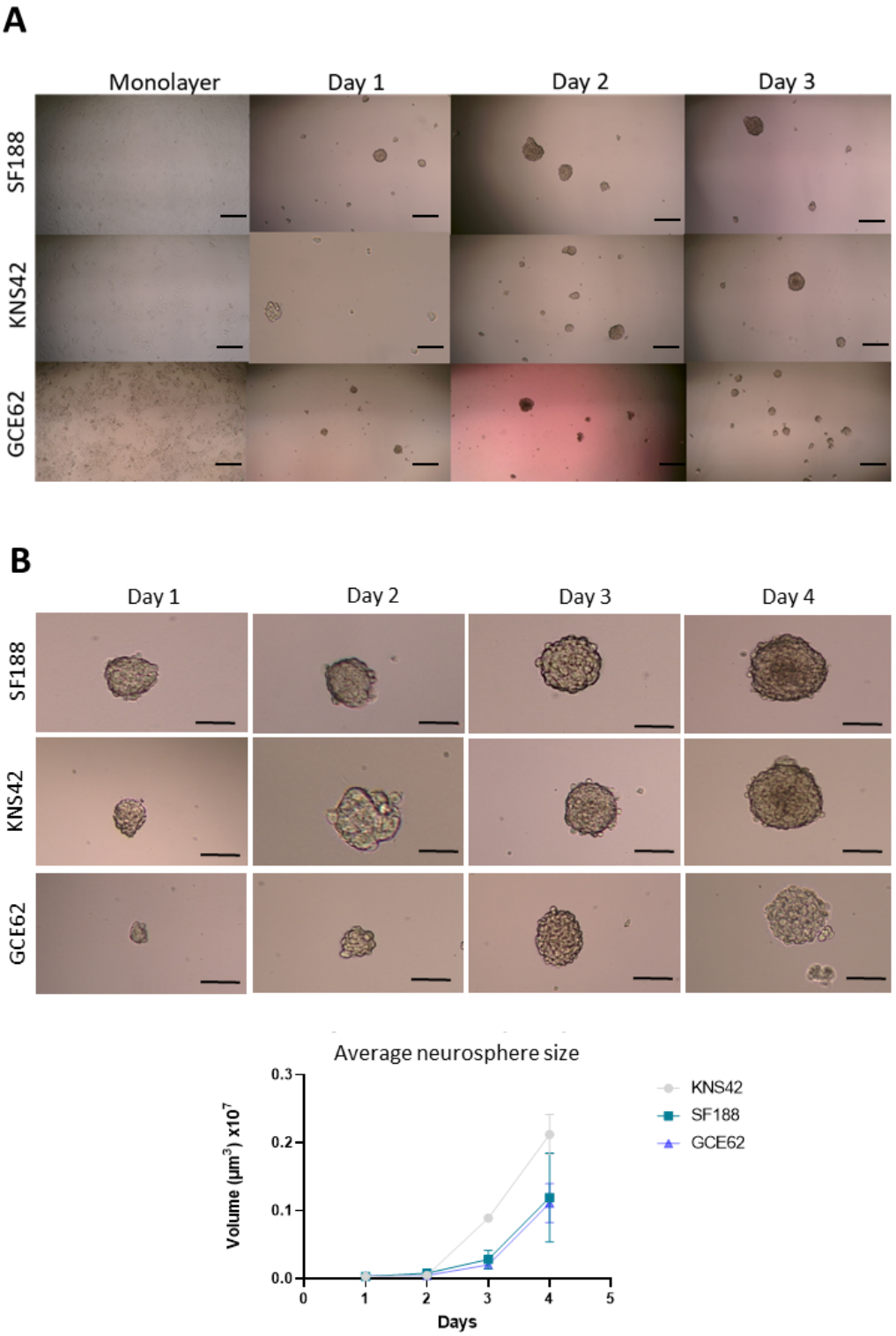

Figure 4.1. pHGG cell lines readily form neurospheres. A) A visual representation of the morphological differences between adherent cell culture of SF188, KNS4 and GCE62 compared to neurospheres across 3 days. Magnification 10x. B) Representative images of neurospheres at each time point. C) Graph showing the average size of neurospheres. Cells were cultured in non-adherent flasks in stem cell media for 4 days. Average neurosphere size was imaged daily and measured using ImageJ. N= 3**.** Scale bar = 250µM

Glioma stem cells refer to a population of tumour originating cells that harness the capacity to self-renew and differentiate. Evidence suggests that these GSCs are linked to resistance to treatment but are widely debated and controversial across the literature. It is cited that neurosphere cell culture is an indirect measurement of the stemness of tumour cells, with this enriched population possessing an increased expression of stem markers such as SOX2, Olig2, Nestin and Oct4 (192).

To assess the relative stemness of pHGG, qrt-PCR was employed to investigate mRNA expression levels of stem markers in 2D monolayer culture vs 3D neurosphere culture. Figure 4.2A details mRNA expression levels of CLIC1, CLIC4, SOX2 and NESTIN across 2D and 3D culture. Stem markers SOX2 and Nestin are expressed across all cell lines tested when cultured in 2D or 3D, with significant increases observed when comparing 2D culture to neurosphere culture. The expression of Sox2 and Nestin are consistent across all cell lines, with the highest expression values observed in SF188 cells.

As studies have suggested that stemness and the capacity to form neurospheres is linked to tumour aggression, we investigated the association between 3D neurosphere culture and expression of CLIC1 and CLIC4. We have previously demonstrated that high expression of both CLIC1 and CLIC4 is clinically linked to poor overall survival and higher tumour grade, and as such hypothesise that CLIC1/4 expression may be associated with stemness. We found that culturing our paediatric lines as neurosphere lead to an increase in CLIC1 and CLIC4 expression, which may be associated with the stem-like state of the cells. An exception to this was the expression of CLIC4 in GCE62 neurospheres, as results obtained were variable across replicates, resulting in no significant changes in expression. This may be a result of the necroses found in the centre of GCE62 neurospheres, meaning that cells

in the centre had varying levels of viability, and therefore differing expression levels. KNS42 had the largest fold change in the expression of both the stem markers and CLIC1/4 mRNA when comparing neurospheres to monolayer culture. The same amount of RNA was used for all experiments, so this excludes results being an artefact of the increasing cell number associated with neurospheres. These findings align with literature confirming that CLCI1 and CLIC4 are both upregulated in GSCs and associated with increased expression of stem markers (179).

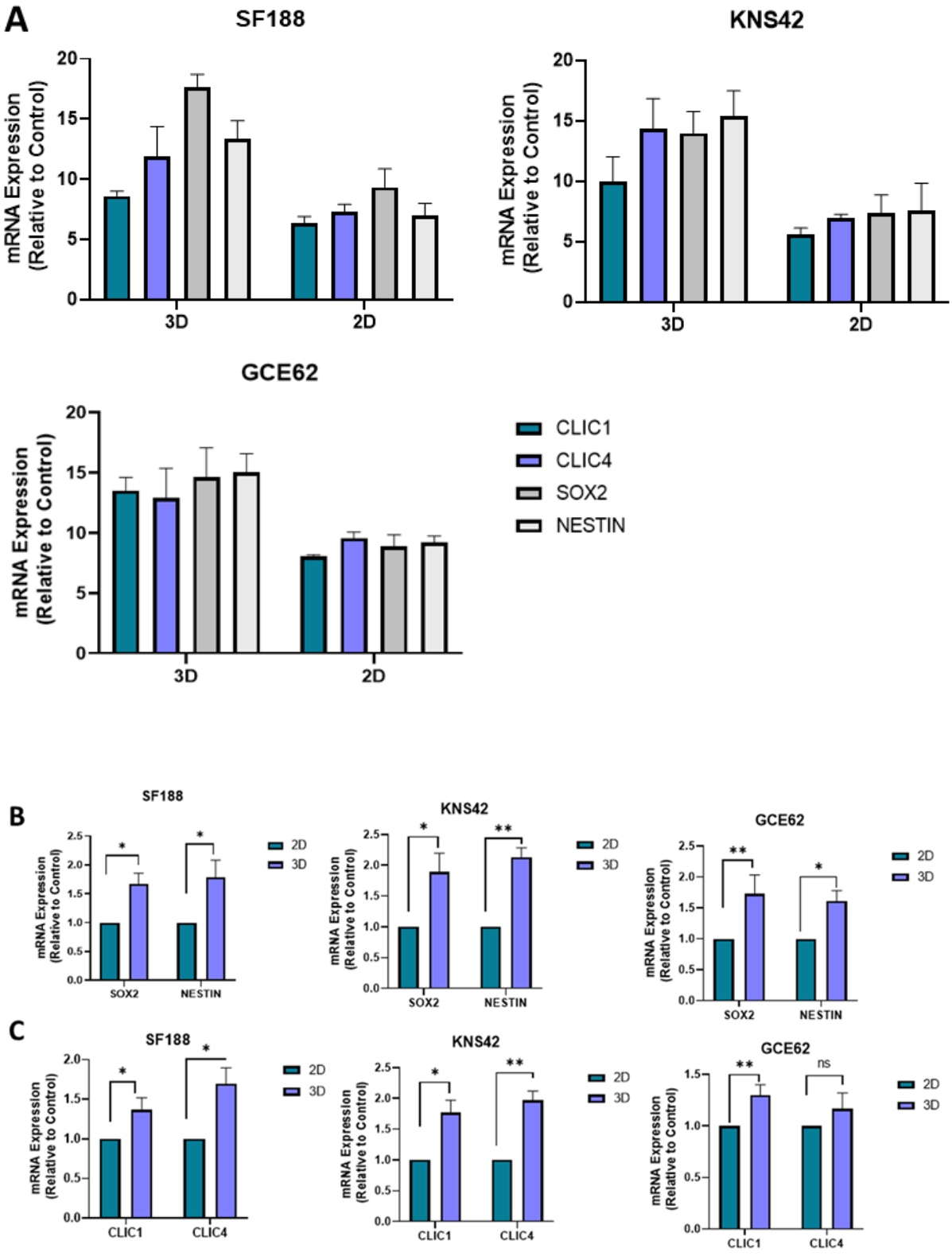

Figure 4.2. 3D culture increases expression of stem markers and CLIC1 and CLIC4. A) rtPCR analysis of overall expression levels of stem markers SOX2 and Nestin in 2D and 3D culture compared to expression of CLIC1 and CLIC4. B) Elevated levels of stem markers are observed in 3D culture when compared to 2D culture. C) Expression of CLIC1 and CLIC4 in 2D culture vs 3D neurospheres. Equal amounts of cDNA were loaded to allow for loading control. mRNA expression normalised to GAPDH. Statistical analysis via paired t-test.

Chapter 3 describes the localisation of CLIC1 and CLIC4 protein using various methods. Here we found a significant cytoplasmic localisation of the proteins in 2D culture and patient tissue. As previously discussed, mRNA expression does not always correlate with protein expression due to translational and transcriptional differences. As a result, we assessed the expression levels and localisation of CLIC1 and CLIC4 in the pHGG neurospheres in order to compare expression between 2D and 3D. Neurospheres were fixed, permeabilised and stained as per the protocol described in section 2.4.3 and were then imaged using confocal microscopy. Due to the size and 3D nature of the neurospheres and to ensure that the full landscape was captured, a z-stack method of imaging was selected. The images were then processed, and the internal 30 Z images were used for analysis. This was decided as the external images only demonstrated a small circumference of the spheres and was not representative of the staining as a whole. Additionally, the images from the middle of the z plane (and therefore the centre of the sphere) were assessed to ensure sufficient antibody penetration and confirm that data were not an artefact of poor antibody penetrance. Neurospheres were observed using brightfield microscopy beforehand, and any spheres that had a significant necrotic core were disregarded as to not skew the data.

Representative images of CLIC1 staining are shown in figure 4.3. We find that there is strong staining of CLIC1 across all three cell lines in 3D culture and is comparable to the staining found in 2D culture. The staining across all cell lines demonstrates that CLIC1 is preferentially expressed in 3D cultures, with accumulation in the outer region of the sphere.

One sphere in the field of view has consistent CLIC1 expression throughout the sphere, with no accumulation in a particular region. Conversely, one sphere appears to have minimal CLIC1 expression on the border of the sphere, and two of the neurospheres demonstrated a ring-like expression of CLIC1 in the outermost border. These findings were somewhat mimicked in the expression of CLIC4 in the GCE62 neurospheres, albeit less significant.

This image was selected to give an accurate overview as this was what was consistently found across the GCE62 neurospheres. As described above, the GCE62 neurospheres often formed necrotic cores by day 4 and were by far the most inconsistent in growth kinetics. This being the case in the low passage primary line is interesting, as it would be presumed that the cell state would be closest to the tumour of origin when compared to the commercial lines.

Additionally, this data conflicts with previous findings on expression patterns across patient tissue, whereby both CLIC1 and CLIC4 appear to accumulate in the core region of the tumour. It could be considered that this is due to the sustained hypoxia found *in vitro*, stimulating CLIC1 and CLIC4 expression, and thus the eventual migration of these cells from the core of the tumour outwards. Whereas the neurospheres were cultured in normoxic conditions, were only grown for 72 hours prior to staining, and are significantly smaller than tumours, thus not experiencing selection pressures such as pH changes, hypoxia, and depleted nutrients. These data provide interesting considerations for future experiments. Interestingly, the expression of CLIC4 in SF188 cells is in fact strongly accumulated in the core region, with intermediate accumulation of CLIC4 found in the KNS42 neurosphere cores, thus recapitulating the data found in patient tissue.

In terms of their morphology, SF188 make the most consistent neurospheres, often demonstrating solid margins. KNS42 neurospheres are more diffuse, likely due to their large size and rapid recruitment of cells into the sphere.

To confirm the data found at PCR level, we stained KNS42 and SF188 neurospheres with Nestin (figure 4.4). Expression of Nestin was found across both cell lines, with representative images showing a higher expression across the SF188 cell line compared to KNS42. This differs from data found in qrt-PCR experiments where KNS42 was found to have the highest expression level of Nestin.

These data need to be interpreted with caution as this experiment is n=1 and there was poor DAPI staining found across the SF188 neurospheres and are included to provide a basis of evidence to support rtPCR data.

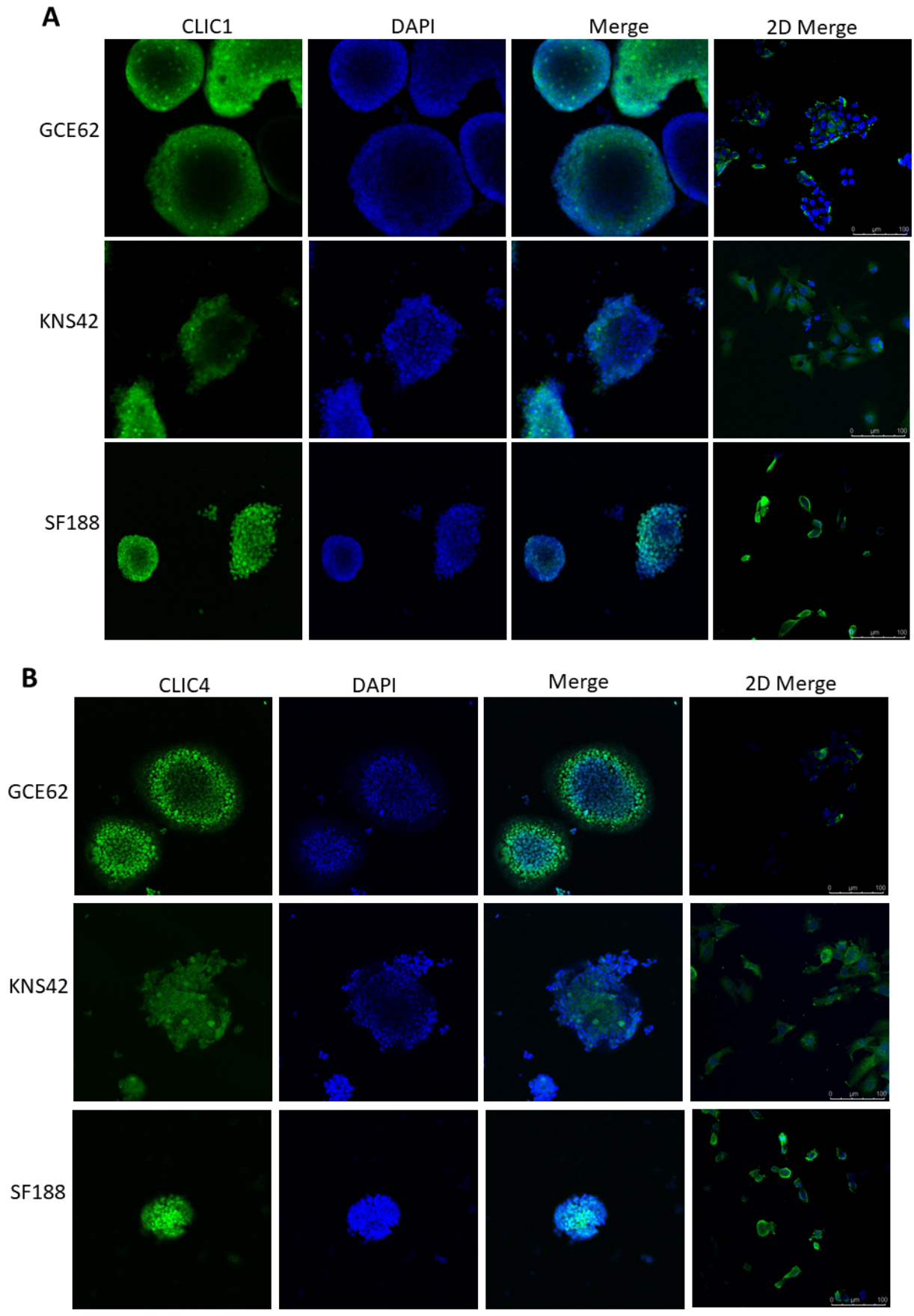

Figure 4.3. CLIC expression is upregulated in neurosphere culture A) Immunofluorescent staining of CLIC1 in SF188, GCE62 and KNS42 neurospheres. B) Immunofluorescent staining of CLIC4 in SF188, GCE62 and KNS42 neurospheres. Imaged by confocal microscopy, via z-stacking. Internal 30 images are show, magnification x40, scale bar = 100uM (2D merge) and 250uM (3D images). N=3

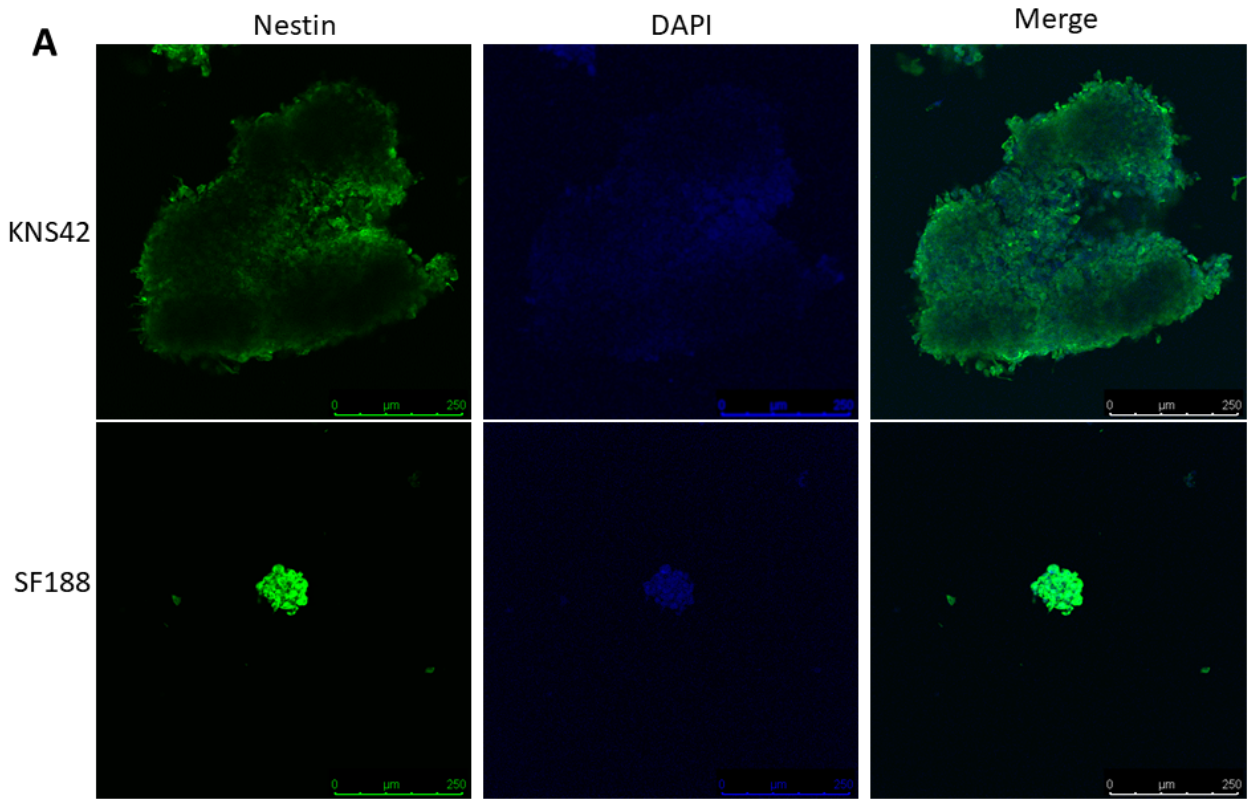

Figure 4.4 Immunoflourescent staining of Nestin in KNS42 and SF188 neurospheres reveals high expression. Imaged by confocal microscopy, magnification x40, scale bar = 250uM. N=1

4.3 Pharmacological targeting of CLIC1 and CLIC4

4.3.1 Overall metabolic activity of cell lines used in this study.

There are several modalities to measure cell viability, all of which have slightly different mechanisms, and thus benefits and draw backs. The presto blue assay is a fluorometric resazurin based assay that can sensitively measure the ability of metabolically-active cells to enzymatically reduce resazurin to resorufin. The relative amount of resorufin produced following incubation with the presto blue reagent is proportional to the viable cells in the sample (193).

To first gain an idea of the metabolic activity of the cell lines under control conditions, a presto blue assay was performed on cells following 72 hours in culture. This was repeated

(n=3) to ensure that baseline readings for the cell lines remained consistent. SF188 harnesses the highest metabolic activity of all cell lines, with GCE62 and KNS42 demonstrating similar activity.

4.3.2 IC50 analysis of chloride channel inhibitors

4.3.2.1 IC50 of IAA94

To assess the effect of CLIC specific inhibition on paediatric HGG cell lines, an IC50 analysis was carried out. First an appropriate range of drug concentrations was found by assessing the literature, and cells were exposed to increasing concentrations of IAA94 for 72 hours. Here we see that the there is little cytotoxic effect via the treatment of IAA94, with the most sensitive cell line being SF188 (IC50 90.45µM).

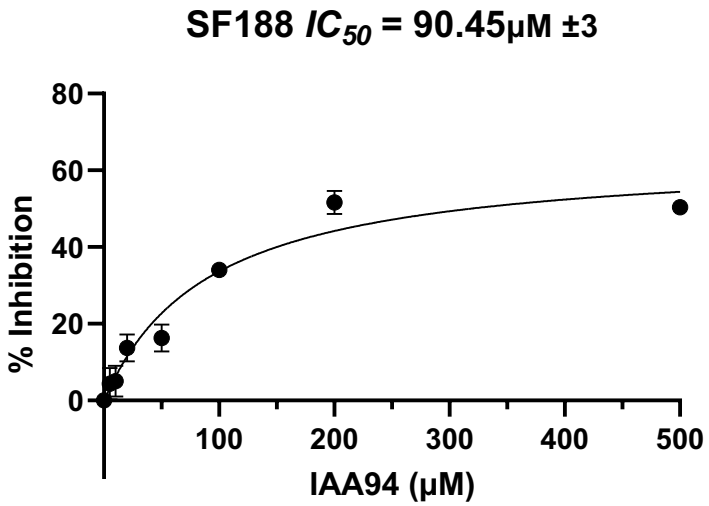

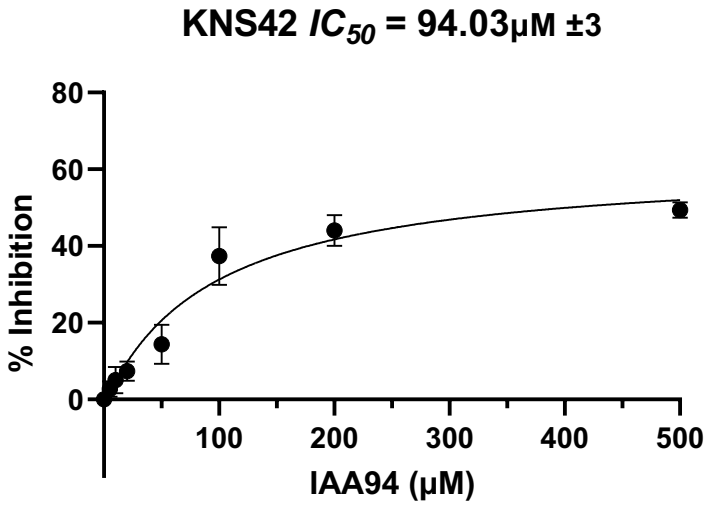

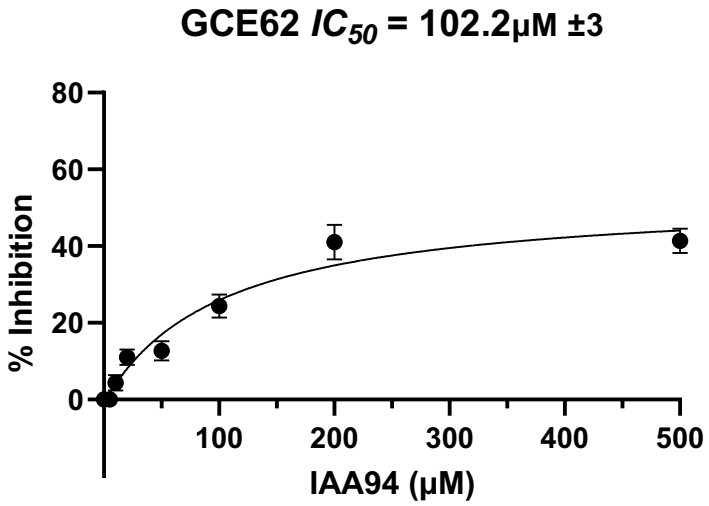

Figure 4.5 IC50 of IAA94. Cell lines were treated with increasing concentrations of IAA94 for 72 hours. PrestoBlue cell viability assays were performed to compare response and viability was calculated as a percentage of the vehicle-treated control. Mean ± SEM plotted; n = 3. Dose response curves were generated using non-linear regression analyses and IC50 values calculated accordingly.

4.3.2.2 IC50 of Metformin

As described above, an IC50 analysis was carried out on KNS42, SF188 and GCE62. cell lines. GCE62 was the most sensitive to Metformin with an IC50 value of 8.9mM with KNS42 being the least sensitive to Metformin treatment (IC50 10.44mM). These values are in line with some of the literature published, and to avoid any unwarranted off target effects an experimental concentration of 10mM was selected.

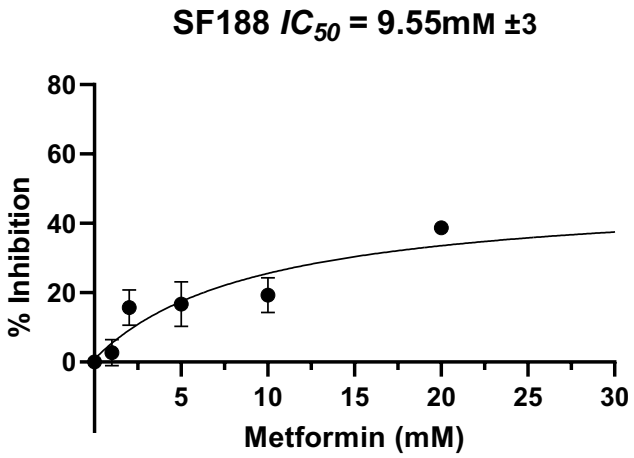

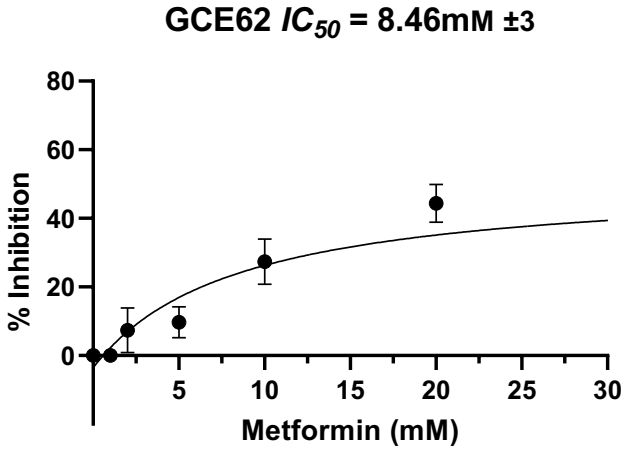

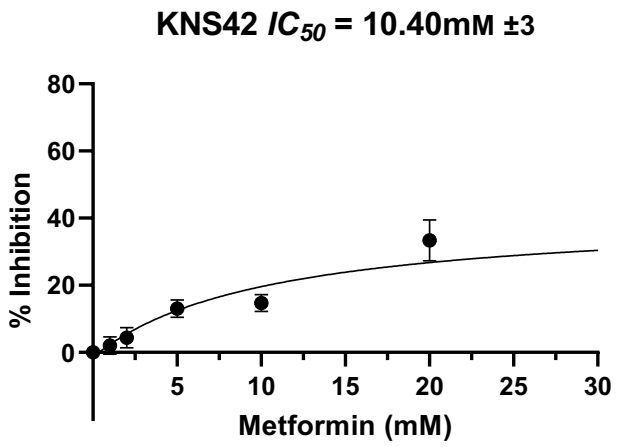

Figure 4.6 IC50 of Metformin. Cell lines were treated with increasing concentrations of Metformin for 72 hours. PrestoBlue cell viability assays were performed to compare response and viability was calculated as a percentage of the vehicle-treated control. Mean ± SEM plotted; n = 3. Dose response curves were generated using non-linear regression analyses and IC50 values calculated accordingly.

4.3.3 CLIC specific targeting by IAA94 reduces cell viability and cell count.

Indanyloxyacetic acid 94 (IAA94) is an inhibitor that binds directly to chloride channels and specifically blocks the ion channel activity of CLIC1 and more widely the CLIC family. Previous studies have reported the efficacy in pharmacologically targeting CLIC1 in various solid cancers (194) including glioblastoma stem cells but is yet to be explored in the paediatric population, and as such presents as an interesting inhibitor of the targets of choice.

Detailed above in section 4.3.2, there is a lack of overall cytotoxicity of IAA94 exhibited by IC50 analysis. Because of this, a review of the relevant literature was completed to identify an appropriate treatment concentration. It has been well reported that treatment of cells with 100µM of IAA94 can completely block CLIC1 ion channel activity in patch clamp experiments and was consequently selected as the treatment dose for further experimentation. Initial experiments sought to assess the effect of IAA94 on overall cell viability. Cells were exposed to 50µM and 100µM IAA94 for 72 hours, and viability

measured via presto blue assay, 0µM represents the DMSO vehicle control condition to control for DMSO related toxicity. Data is presented as both raw values for presto blue fluorometric reading (520nm) figure 4.7A and data normalised as a percentage of the vehicle contro (figure 4.7B). There was no significant decrease in cell viability when treating the cell lines with 50µM IAA94. The viability of SF188 and GCE62 cells were statistically significantly decrease following treatment with 100µM IAA94 (figure 4.7), with a mean decrease of 40% and 30% respectively. KNS42, by contrast was not statistically less viable, with an average of 15% decrease in viability compared to control. Astrocytes were used as an anatomical control for these experiments, and it was found that there was not significant reduction in cell viability at either 50µM or 100µM treatment. This observation is important as it indicative that toxicities to the healthy brain are unlikely, with maximum decrease in viability being 10%. It is notable however, that the result for the astrocyte cell line were the most variable. This may be a product, despite them not being myc-transformed, these astrocytes have a population that are actively proliferative. Data on post mitotic astrocytes confirms limited toxicity via IAA94 (195).

Following presto blue assay, cells were washed, and overall cell count performed. Interestingly, despite no significant reduction in viability, the cell count of KNS42 cells was significantly decreased following 100µM treatment. A possible explanation for this is the lack of cytotoxicity of the drug, but instead alteration in the cell cycle, whereby IAA94 is preventing G1 progression, and thus preventing cellular replication. Similarly, GCE62 and SF188 cell count was significantly decreased, with no decrease in astrocyte cell number observed. This data indicates that IAA94 may be a suitable candidate for pHGG treatment via CLIC1/4 specific targeting, with a potential therapeutic dosage window with normal non-neoplastic brain cells.

To avoid bias in the data reflecting a decrease in viability that is associated not with treatment efficacy, but instead a decrease in cell count, all experiments are normalised as a percentage decrease to a control. The vehicle for IAA94 is DMSO, to avoid any vehicle related cytotoxicity, the final concentration of DMSO did not exceed 0.5%, with the majority of experiments having a final DMSO concentration of 0.1%.

Future work would include combining CLIC1 and CLIC4 knock down with pharmacological inhibition. This would be valuable to recapitulate the effect of drug targeting of CLIC1 and CLIC4 in patients with lower expression of these genes. Low expression of CLIC1 and CLIC4 is favourable for overall survival.

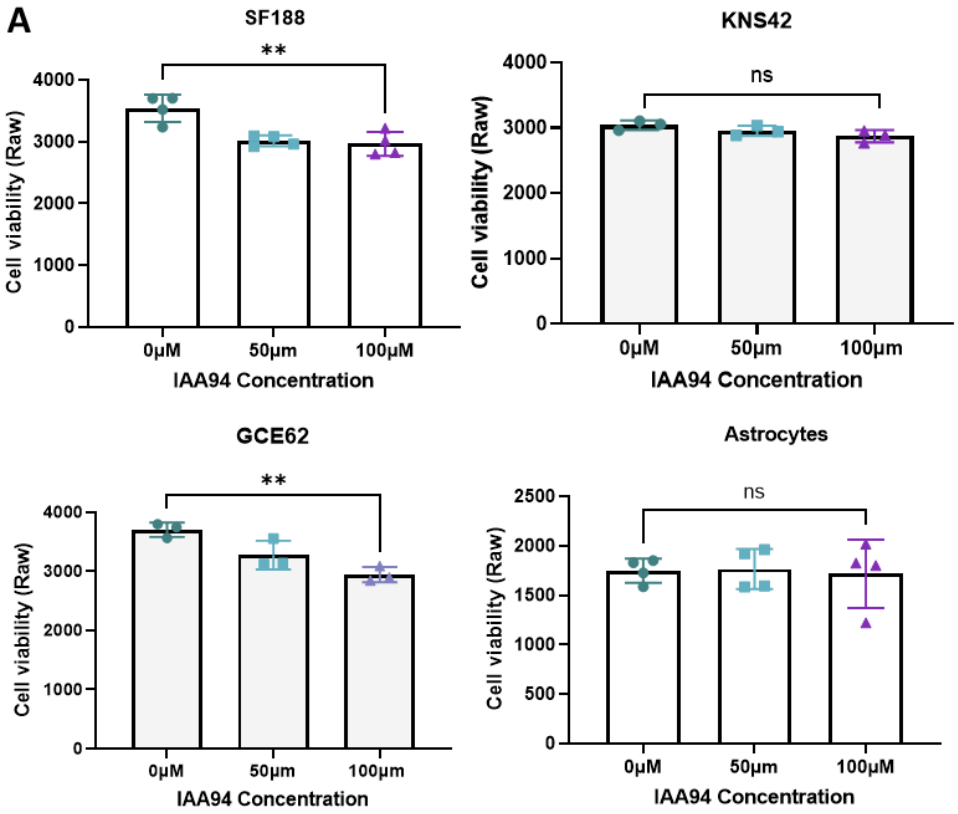

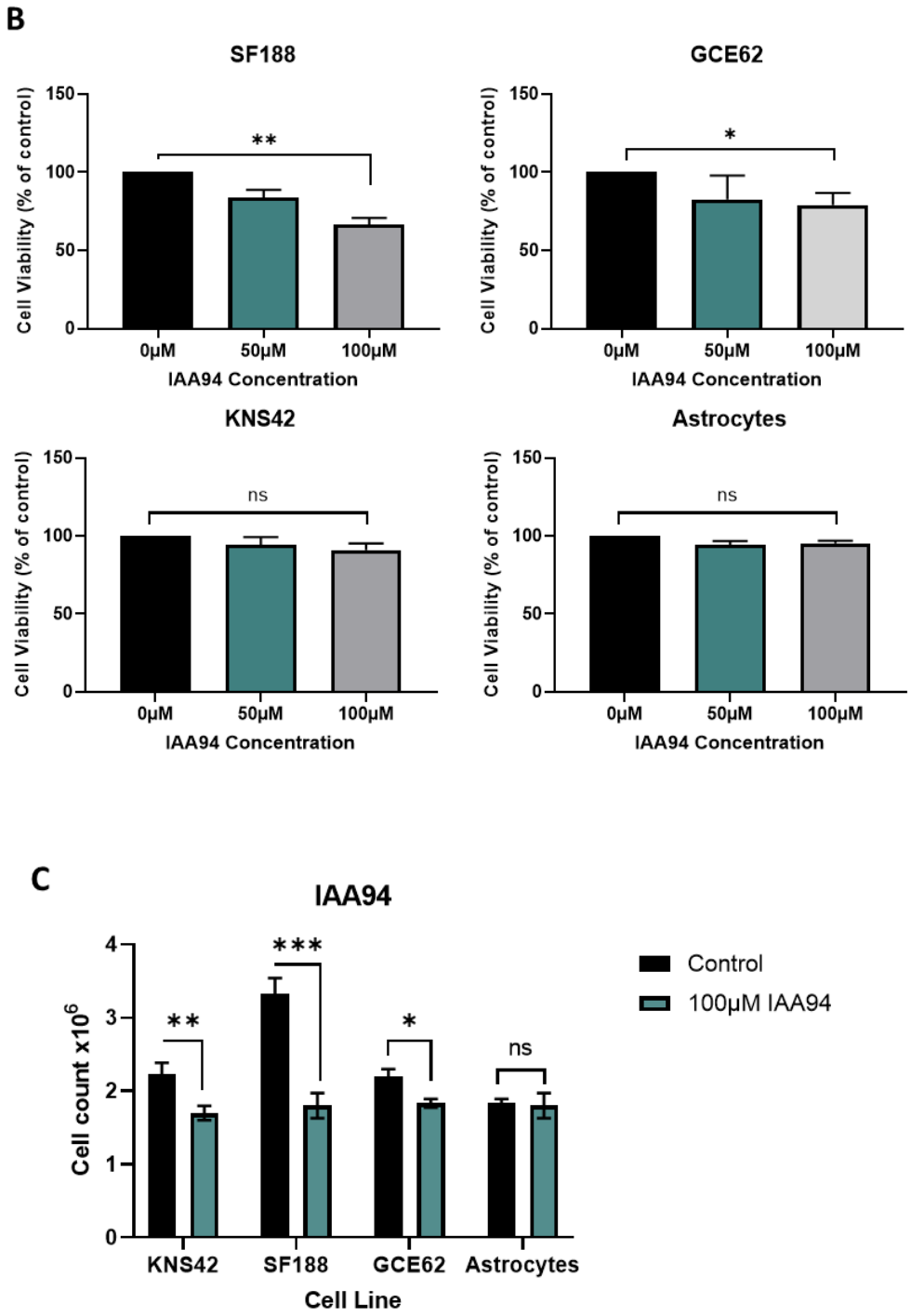

Figure 4.7. IAA94 reduces cell viability and cell count A) measurement of cell viability via presto blue metabolic assay. Significant reduction in the viability of SF188 and GCE62 cells following 72 hours treatment with 100uM IAA94. T-test. B) cell viability normalised as a percentage of untreated cells. C) cell count of cells treated with 100uM IAA94 2-way ANOVA.

4.3.4 Colony formation of KNS42 and GCE62 cells is significantly reduced following IAA94 treatment.

Clonogenic assays are used as *in vitro* cell survival assays, measuring response to various treatment and the ability for cells to proliferate and form colonies. Cells are seeded at very low densities and left to grow over an optimised time period, colonies are then fixed, stained, and counted. Clonogenic growth has also been suggested to be an alternate measure of stemness, as stem cell populations are long living cells that harness the potential for ongoing proliferation. As such, we utilised a colony forming assay to assess the ability of pHGG to retain their proliferative capacity and reproductive integrity over a prolonged period of time. Additionally, this sustained exposure to pharmacological inhibitors more accurately captures the drug exposure in the patient. Due to the highly proliferative nature of our cells, each cell line was left for 10 days for colonies to form following initial seeding densities described in section 2.8.2.

Here we find that treatment with 100µM of IAA94 can significantly reduce the clonogenic capacity of KNS42 cells (figure 4.8). SF188 fail to create tight defined colonies but do however group across the surface of a flask, with cell numbers >50, and as such were considered colonies. There was no significant decrease in the colony forming units of SF188 cells. Interestingly, GCE62 cells formed significantly less colonies post IAA94 treatment, but did show some variability in results. Future work would include increasing replicates to ensure reproducibility of the experiment.

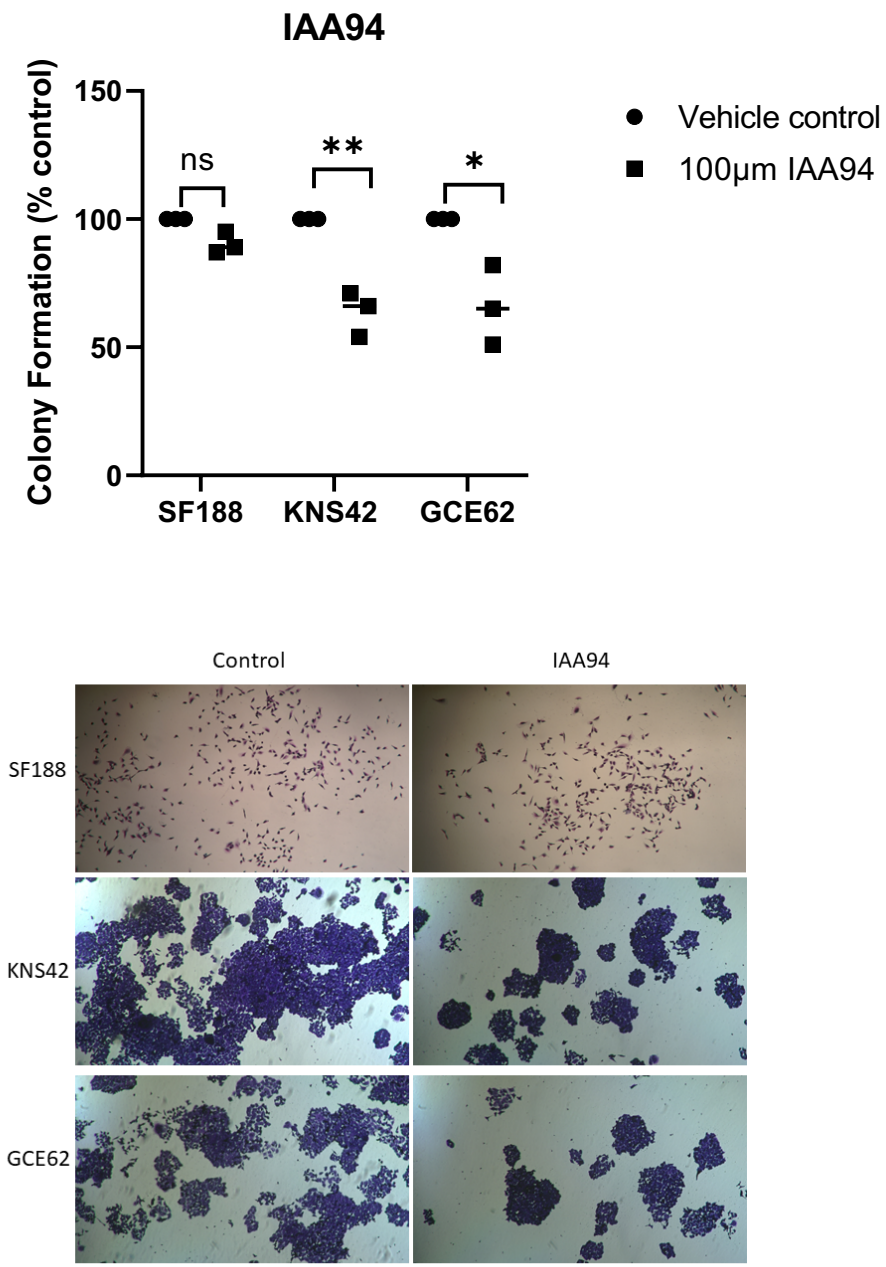

Figure 4.8. IAA94 reduces proliferative capacity of KNS42 and GCE62. A) Representative crystal violet staining of fixed cells following clonogenic assay (10 days) of cell lines treated with 100uM IAA94. Colonies defined as >50 cells and were counted from 4 different fields of view, in triplicate n=3. 10x magnification. B) Quantification of clonogenic assay via colony forming units of vehicle control v 100uM IAA94. Statistical analysis by 1-way ANOVA

4.3.5 CLIC1 and CLIC4 pharmacological inhibition reduces invasive capacity of pHGG.

Previous research has identified a fundamental role of CLIC1 in the invasive capacity of

HGG cells and other tumours, finding that upregulation of CLIC1 is linked to an increased

invasive capacity (196). As such, targeting these cells endowed with an increased intrinsic mechanism favouring invasion is vital in future treatment strategies. Accordingly, we sought to investigate if CLIC1 and CLIC4 pharmacological targeting via IAA94 would affect the invasive capacity of pHGG cells.

Boyden chambers were coated in Collagen IV to simulate a simplified brain extracellular matrix. Cells were pre-treated with 100µM of IAA94 for 24 hours and seeded in serum free, drug containing media into the upper compartment of the chamber and incubated for 24 hours. Cells were left to invade towards complete media (containing 10% FBS) along a chemotactic gradient. Cell seeding density was optimised prior to final experimentation and normalised to a control (no chemotactic gradient).

All cell lines were found to invade through the Collagen IV coating and the transwell, signifying inherent invasive capacity in the cells (figure 4.9). Treatment with IAA94 significantly reduced the invasive capacity across both KNS42 and SF188 cell lines. SF188 cells exhibited a 31% reduction in invasion ($p=0.027$) compared to untreated controls. Similarly, invasion was inhibited by 20% in KNS42 cells ($p=0.041$). Given that IAA94 has been seen to reduce the viability of cells at 72 hours treatment, a shorter overall treatment period (48 hours) was selected as we have identified that at this time point there is no significant reduction in cell viability. As such, it can be assumed that the significant reduction in invasion observed, is in fact due to inhibition of the invasive process, and not an artefact of reduced cell viability or cell number.

Comparatively, there was no significant reduction in the invasive capacity of GCE62 cells (12% reduction). This is interesting as previous experiments revealed that there is a significant reduction in viability when treating GCE62 with IAA94, suggesting alternate mechanisms being at play. This is likely due to compensation of other CLIC ion channel

proteins, aiding in the dual efflux of Cl- and water to promote morphological changes needed for invasion across the Collagen IV membrane. Similarly, whilst KNS42 cell invasion was significantly reduced, we did not observe significant reduction in viability.

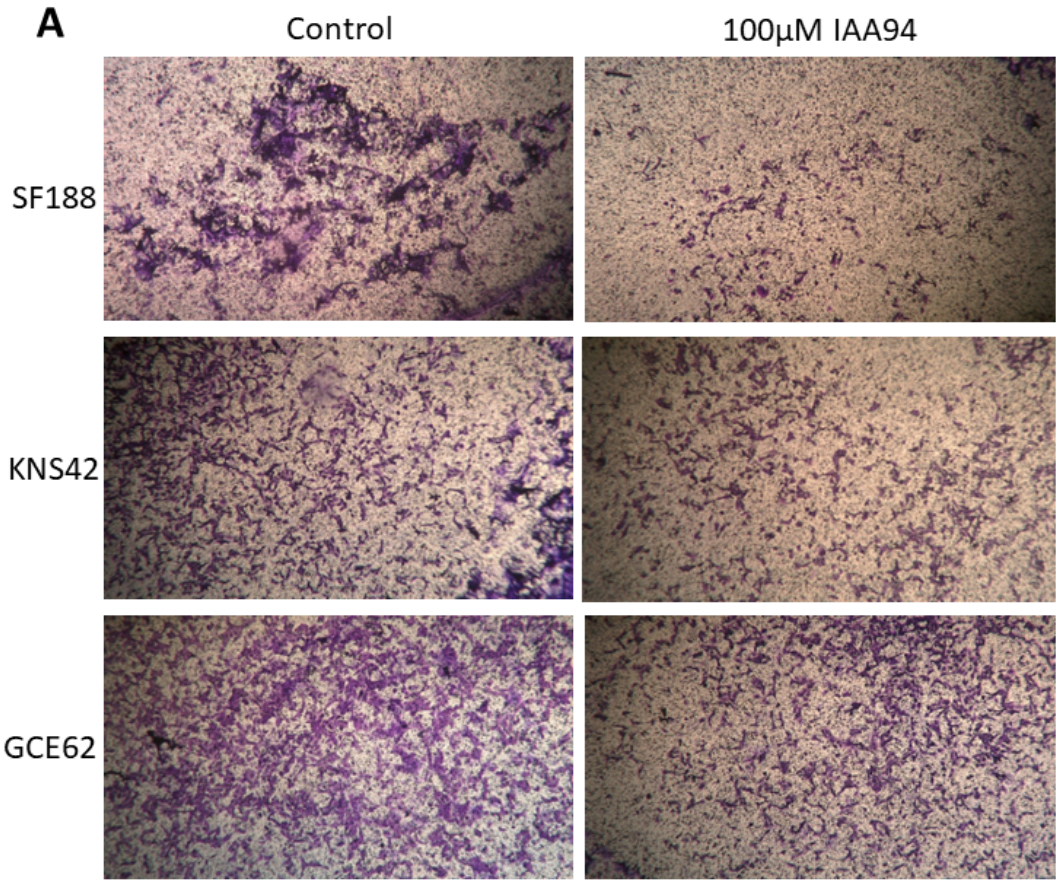

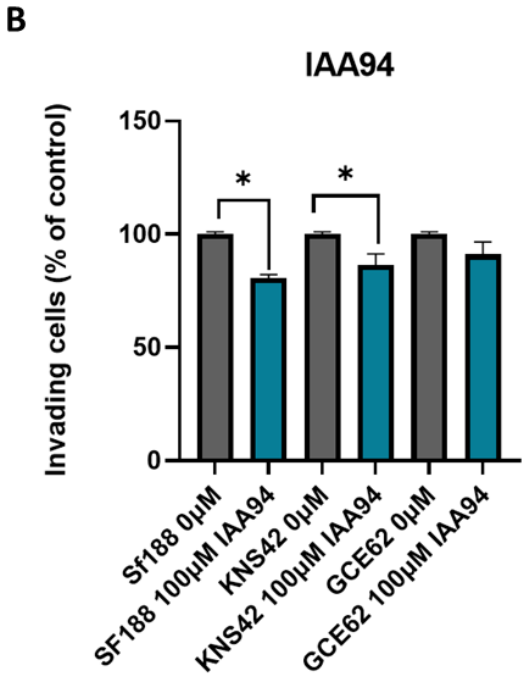

Figure 4.9. Treatment with 100uM IAA94 significantly reduces the invasive capacity of SF188 and KNS42 cells. A) Representative images of invading cells as measured via a modified Boyden chamber assay through Collagen IV coated inserts along a FBS gradient. Staining with crystal violet. 10x magnification. 4 representative areas were selected per field of view and all invading cells counted. N=3 B) Quantification of invading cells in control (0uM) vs treated (100uM) cell lines. statistical analysis via paired t-test. P= <0.05 *

4.3.6 IAA94 causes aberrant cell cycling in pHGG.

As ion channels are implicated in cell cycle control, we sought to investigate the effect of pharmacological targeting of CLIC channels on the cell cycle. Studies indicate that CLIC1 is preferentially active during the transition from G1-S phase of the cell cycle due to its transient insertion into the membrane. However, the current literature is conflicting and a clear role of CLIC1 and CLIC4 in the cell cycle has not been identified.

In order to elucidate this, we exposed cells to 100µM of IAA94 for 72 hours and then carried out cell cycle analysis via propidium iodide staining and flow cytometry. All cell lines demonstrated a significant increase in percentage of cells in the G0/G1 phase of the cell cycle in the treatment condition compared to control (figure 4.10). This increase was observed with a simultaneous significant decrease in the percentage of cells present in the

S-phase in the treatment group across all cell lines. Accumulation in this phase, accompanied by a significant decrease in S phase in the treatment group is suggestive of failure to pass restriction point in G1, and thus cell cycle arrest.

Following treatment with IAA94 GCE62 was subject to significant changes in all phases of the cell cycle when compared to untreated cells, whereas KNS42 and SF188 had no significant changes in the number of cells found in sub G1 or G2/M phase. GCE62 is a low passage primary cell line, and this ability to continue to pass through to various stages of the cell cycle, but maintain some viability as described in section 4.3.2 may be a result of the intrinsic capability of the tumour to bypass cell cycle check points.

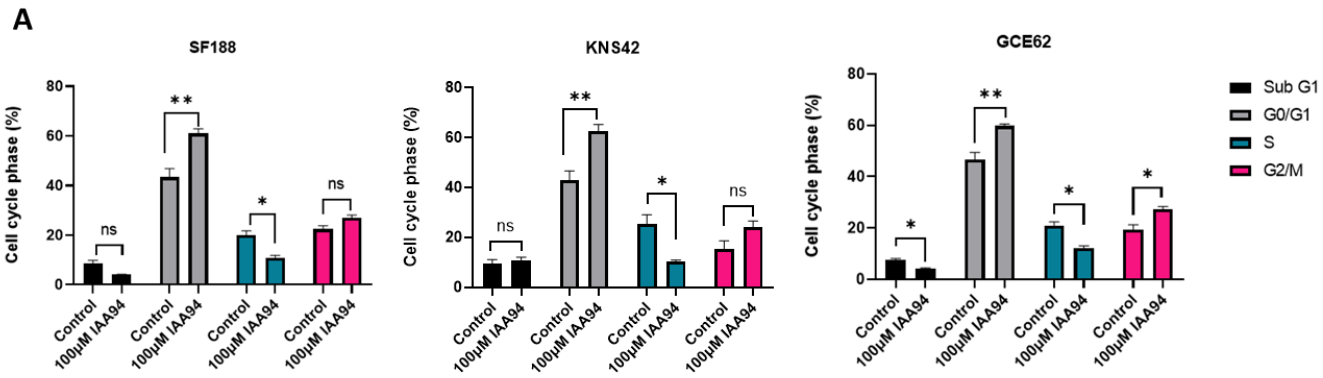

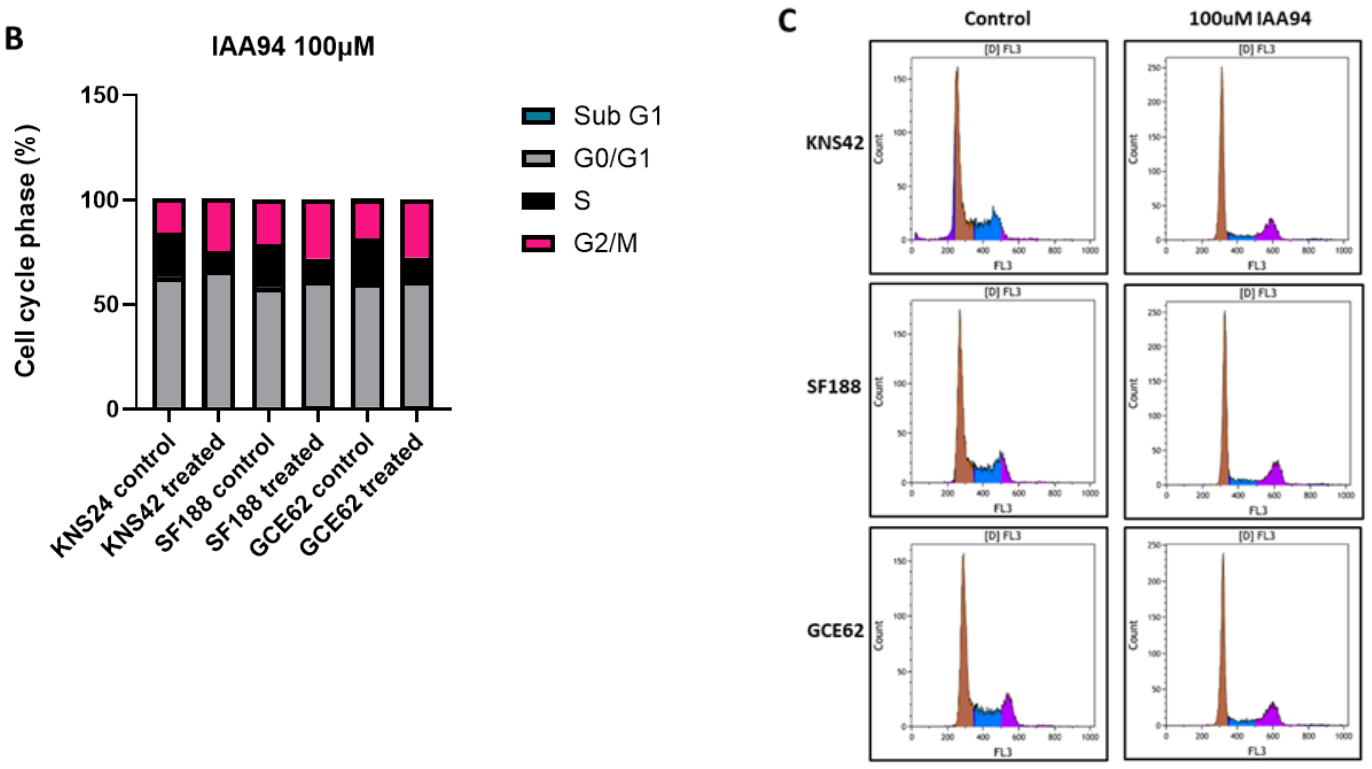

Figure 4.10. Treatment with IAA94 results in aberrant cell cycling. A) Two-way ANOVA, multiple comparisons between percentage of cells in each stage of the cell cycle and each experimental condition. Cells treated with 100uM IAA94 for 72 hours prior to experimentation. B) summary data of percentage cell cycle stage in treated vs untreated cell lines. C) representative histogram images of cell cycle.

4.3.7 IAA94 does not inhibit neurosphere formation.

This chapter describes the ability of pHGG to freely form neurospheres, and the effect of treatment with IAA94 on monolayer viability. To assess the efficacy of IAA94 treatment in a more biologically relevant setting, neurospheres were cultured for 72 hours in the presence of 100µM of IAA94. Despite seeing promising results in 2D cell culture there was no significant reduction in ability of SF188 or KNS42 cells to form neurospheres following treatment with IAA94. However, there was a significant difference in the size of KNS42 neurospheres at day 2 only (p=0.031). As shown in the representative image (figure 4.11) there was a marked number of cellular debris and detached cells present in the flask at day 3 of treatment with IAA94 in KNS42 cell, suggesting that spheres were beginning to break

down, and more apparent effects may have been observed following longer exposure to IAA94 (data not shown). The sizes of SF188 neurospheres in the experiment were extremely variable across all triplicates and therefore results should be taken with caution. It is understood that the ability to form neurospheres is not a direct measure of the viability of the culture, and as such cannot be compared to viability of the 2D culture. However, despite attempts of optimisation, sufficient penetrance of the presto blue reagent into the spheres was not possible, thus rendering any fluorometric readings unreliable.

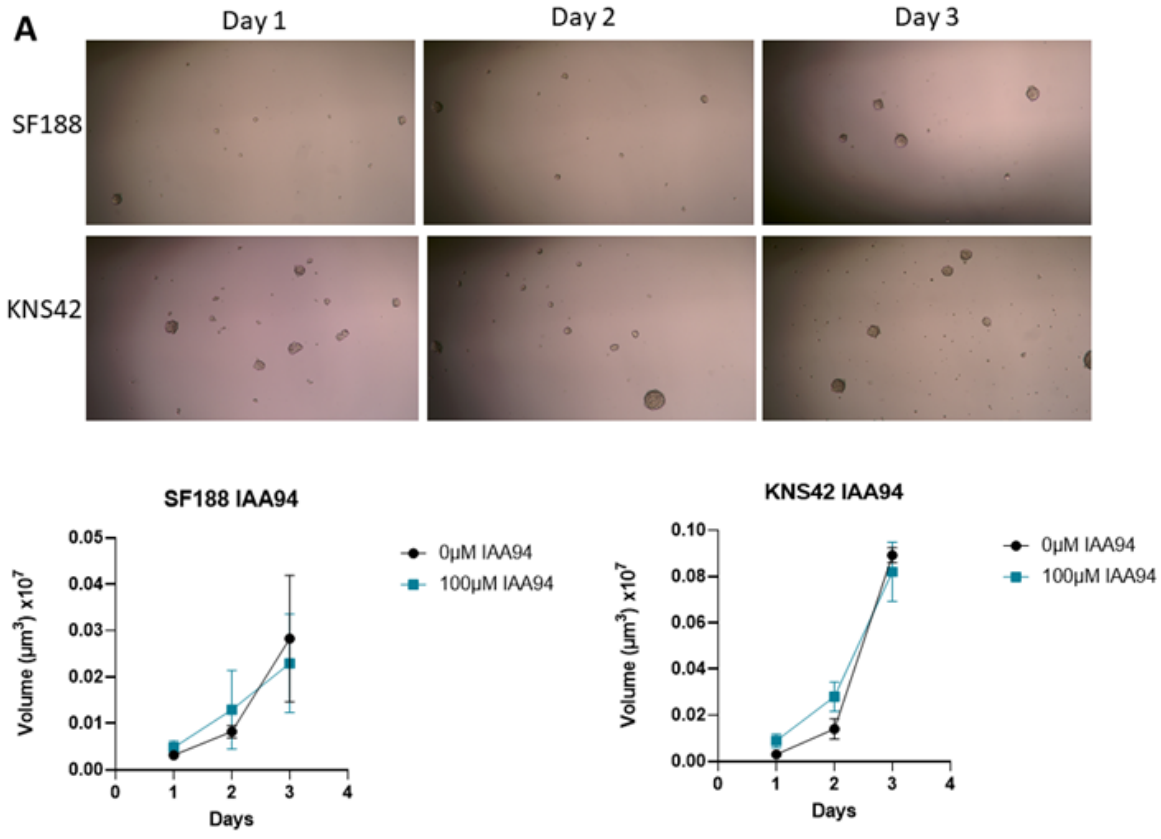

Figure 4.11. Treatment with 100uM IAA94 does not inhibit neurosphere formation. Representative images are of neurospheres treated with 100µM metformin over a 72-hour period. Treatment with IAA94 for 72 hours prior to neurosphere assay does not inhibit neurosphere formation in pHGG, sf188 p = 0.489, kns42 p=0.085

4.3.8 Pharmacological inhibition of CLIC1 and CLIC4 via clinically relevant Cl- channel blocker metformin

Metformin has been used clinically for over a century and is implicated in many disease treatments. Functionally, it is a biguanide hyperglycaemic drug that is the first in line therapy for type 2 diabetes. This is due to the profound inhibition of hepatic glucogenesis, thus promoting a glucose lowering effect (197). Recently, studies have been exploring the anti-tumoural capacity of the biguanide class of drugs, with specific focus on metformin. We have previously described that IAA94 shows a marked decrease in the proliferative and invasive capacity of three paediatric HGG cell lines, and we seek to elucidate if a clinically relevant drug with a similar proposed mechanism of action will exhibit the same efficacy for HGG.

Metformin hydrochloride is not a cytotoxic drug and is therefore subject to high IC50s, as such, a concentration of 10mM was selected for future experimentation.

To assess the consequence of CLIC targeting via metformin cells were incubated in media containing 10mM metformin or a vehicle control (sterile cell culture grade water) for 72 hours. Following incubation viability was measured using presto blue reagent, and then the cells were subsequently washed, trypsinised and counted. At a concentration of 10mM metformin exhibited significant effects on cell viability across all cell lines ($p = <0.01$ **) figure 4.12a.

As the vehicle for this drug is water, any potential DMSO related toxicities can be discounted. The highest decrease in viability was seen in the primary cell line GCE62, with an average of 40% viability post treatment. Notably, there was no significant decrease in viability or cell count of normal human astrocytes, suggesting that this treatment is only

cytotoxic to actively proliferating malignant cells. Likewise, cell count was decreased post treatment in a statistically significant manner across all cell lines.

Furthermore, cell proliferation was measured via clonogenic assay, whereby SF188 and KNS42 colony formation was significantly inhibited (p=>0.05) (figure 4.12c), but there was no significant effect on GCE62 colony count.

These data are comparable to treatment with 100µM of IAA94, with an overall reduction in viability higher across all cell lines when treating with 10mM of metformin. However, the range in dose concentrations between the two drugs is markedly different.

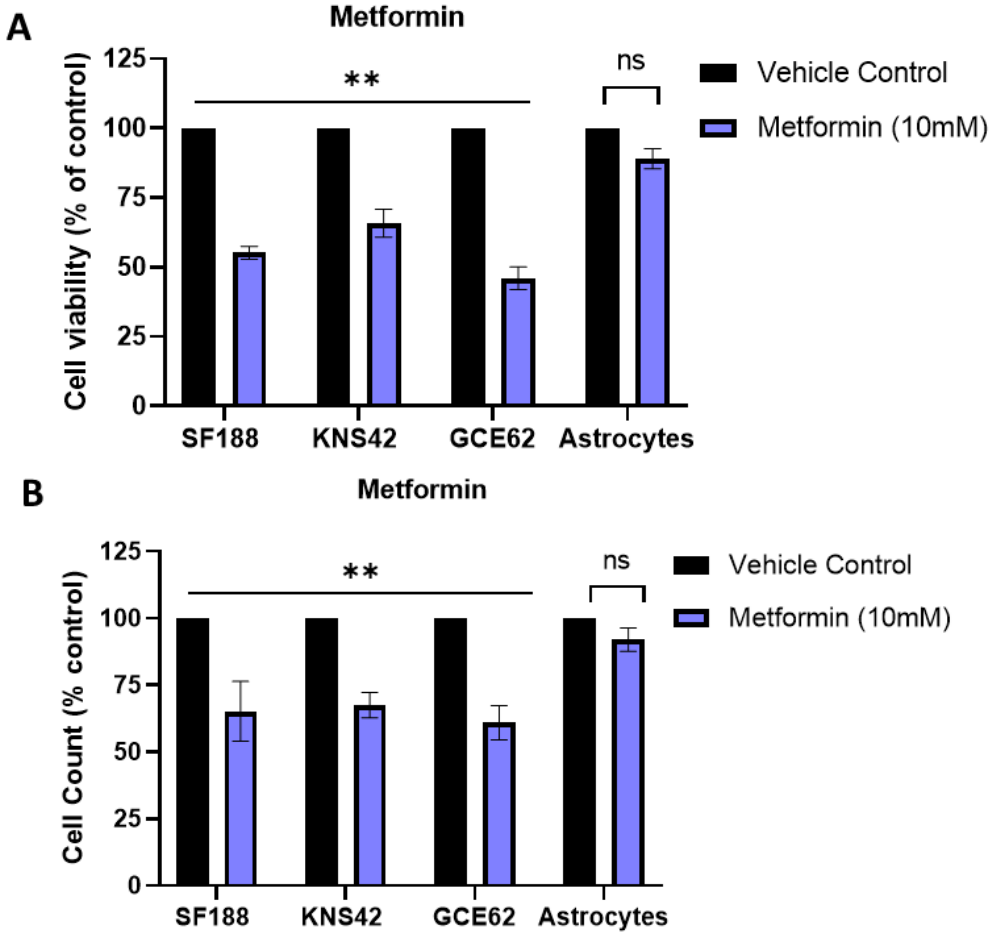

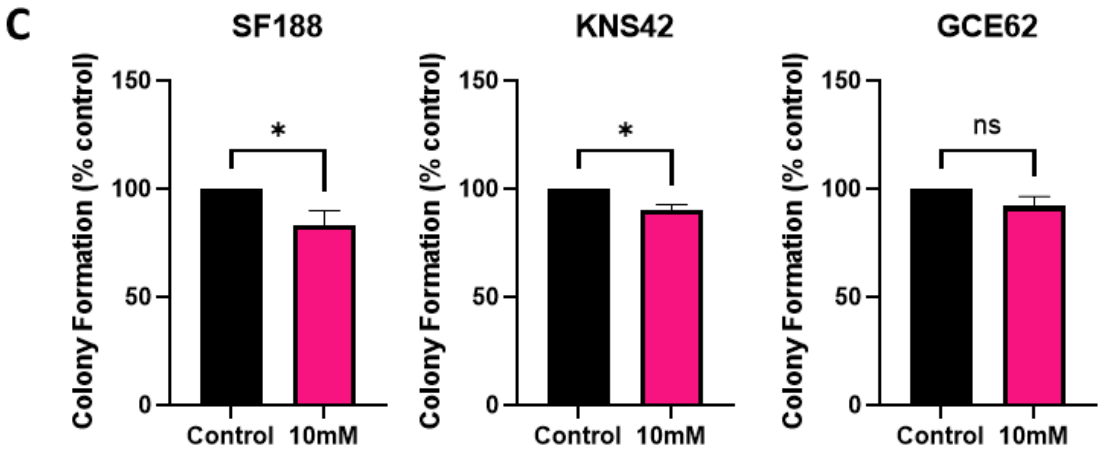

Figure 4.12. Treatment with 10mM of metformin for 72 reduces pHGG proliferation. A) cell viability of pHGG cells (as measured by presto blue assay). B) Cell count of cells treated with 10mM of metformin (percentage of control). Paired t-test. C) Colony forming assay of control vs treated cells

Despite promising results, treatment with metformin at concentrations as high as 10mM is not clinically feasible due to the action of the drug. The molecular weight of metformin is 129.164 g/mol, and the clinical concentration of metformin to treat diabetes is 2.5 g (35 mg/kg body weight) (197), thus a concentration of 10mM far exceeds this recommended dose and would put patients at risk of significant off target effects including hypoglycaemia and cardiac abnormalities. To assess the effect of metformin treatment in a more clinically feasible range, the drug concentration was decreased to 100µM. Cells were treated for 72 hours, and their viability measured via a presto blue assay as previously described. Significant decrease in both viability and cell count was observed in the SF188 cell line, ($p=0.037$), with an average decrease in viability and cell count of 15 and 20% respectively (figure 4.13). There were no significant decreases in viability for KNS42 and GCE62, however there was a significant decrease in cell count in the GCE62 line (20% mean decrease). These results indicate that metformin may not be suitable for a monotherapy in HGG as it fails to be effective in reducing viability in a clinically achievable range. Metformin has a less significant effect on the viability of cells at the same concentration of the CLIC1 specific inhibitor, IAA94, with mean reduction in viability of SF188 being

significantly less when treated with metformin. This is not to say that metformin is not still an attractive candidate in the treatment of gliomas, and it may hold promise as a dual therapy. Often brain tumours require prolonged exposure to chemotherapeutics for efficacy of treatment to be seen. Further analysis would look to explore the effect of long-term exposure to metformin on the viability of pHGG cells.

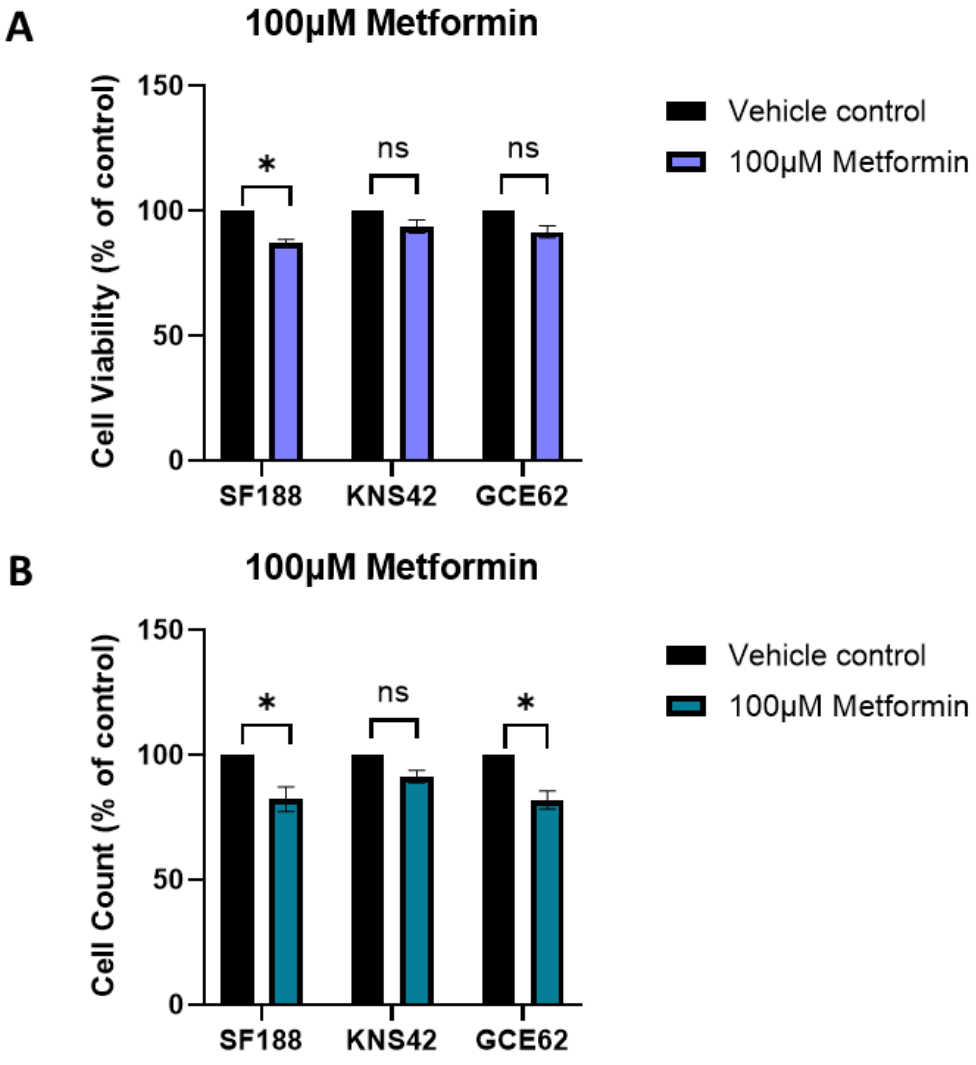

Figure 4.13. Treatment with 100μM metformin decreases viability in SF188 cells. A) Cells treated with 100μM of metformin for 72 hours and their viability (as normalised to vehicle control) was calculated using a presto blue assay. B) Cell count (% of vehicle control) in pHGG cells. P = >0.05 ns, P = <0.05 *, p= <0.01 **. Statistical test via paired t-test. Vehicle control = water.

4.4 Genetic targeting of CLIC1 and CLIC4

In order to further investigate the role of CLIC1 and CLIC4 in glioma pathogenesis, we sought to create a knock down model of CLIC1 and CLIC4 independently across the pHGG cell lines. All cell lines were selected for these experiments as they all expressed CLIC1 and CLIC4 at both the protein and mRNA level. Here, we utilised small interfering RNA (siRNA) to generate transient knock down models. SiRNA is a short double stranded (20-25 nucleotides long) which induces mRNA cleavage, and consequent degradation in the region of interest, resulting in no translation of the respective protein. We selected a pooled siRNA approach, utilising an siRNA pool of 3 siRNAs targeting alternate regions to ensure knock down and reduce off target effects.

4.4.1 siRNA efficiency

Prior to experimentation the transfection efficiency of the siRNA was measured to ensure sufficient knock down levels. Transfection reagent, Lipofectamine3000™ (Sigma Aldrich) was employed to increase transfection efficiency, following review of the literature stating this reagent holding high levels of success in glial cells including HGG.

CLIC1 and CLIC4 expression was quantified at mRNA across SF188, GCE62, KNS42 and normal human astrocytes following incubation with respective siRNAs at 24-, 72- and 120-hours post transfection (n=3). These time periods were selected to ensure that knock down remained sufficient for downstream experimental procedures. Cells were also transfected with a non-targeting control to ensure no off-target effects from the addition of transfection reagent to the cells.

Sufficient knock down of both CLIC1 and CLIC4 was observed across all cell lines, with highest percentage of KD at 24 and 72 hours, confirming an appropriate experimentation

window (figure 4.14). As anticipated, there was also ample knock down observed at protein level across all of the cell lines.

Transfection of normal human astrocytes was included to ensure that there was no reduction in viability or lethality in normal cells as a consequence of CLIC1 or CLIC4 deficiency.

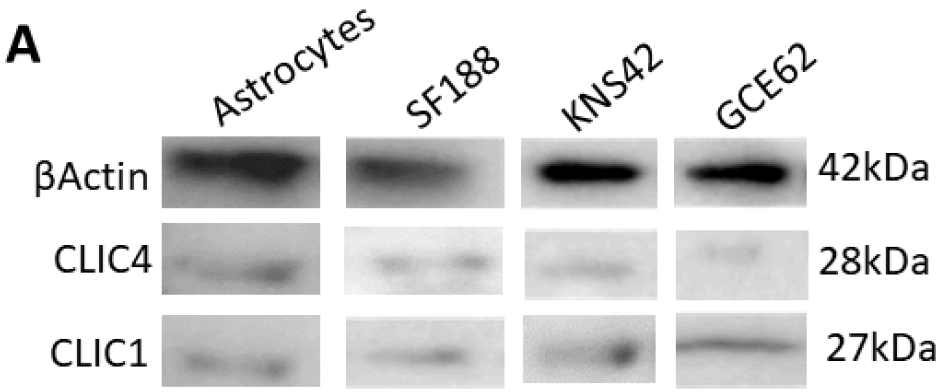
A
Astrocytes
SF188
KNS42
GCE62
βActin
CLIC4
CLIC1
42kDa
28kDa
27kDa

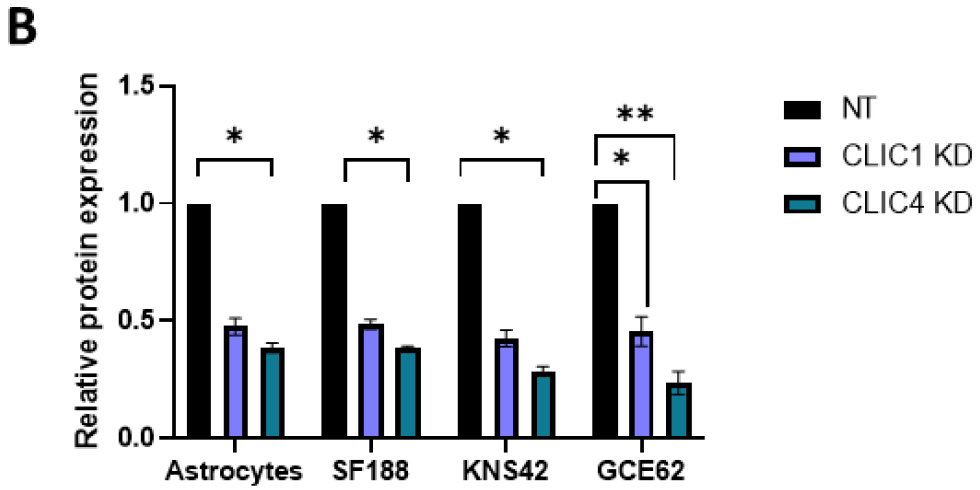
B
Relative protein expression
1.5
1.0
0.5
0.0
*
*
*
**
*
Astrocytes
SF188
KNS42
GCE62
NT
CLIC1 KD
CLIC4 KD

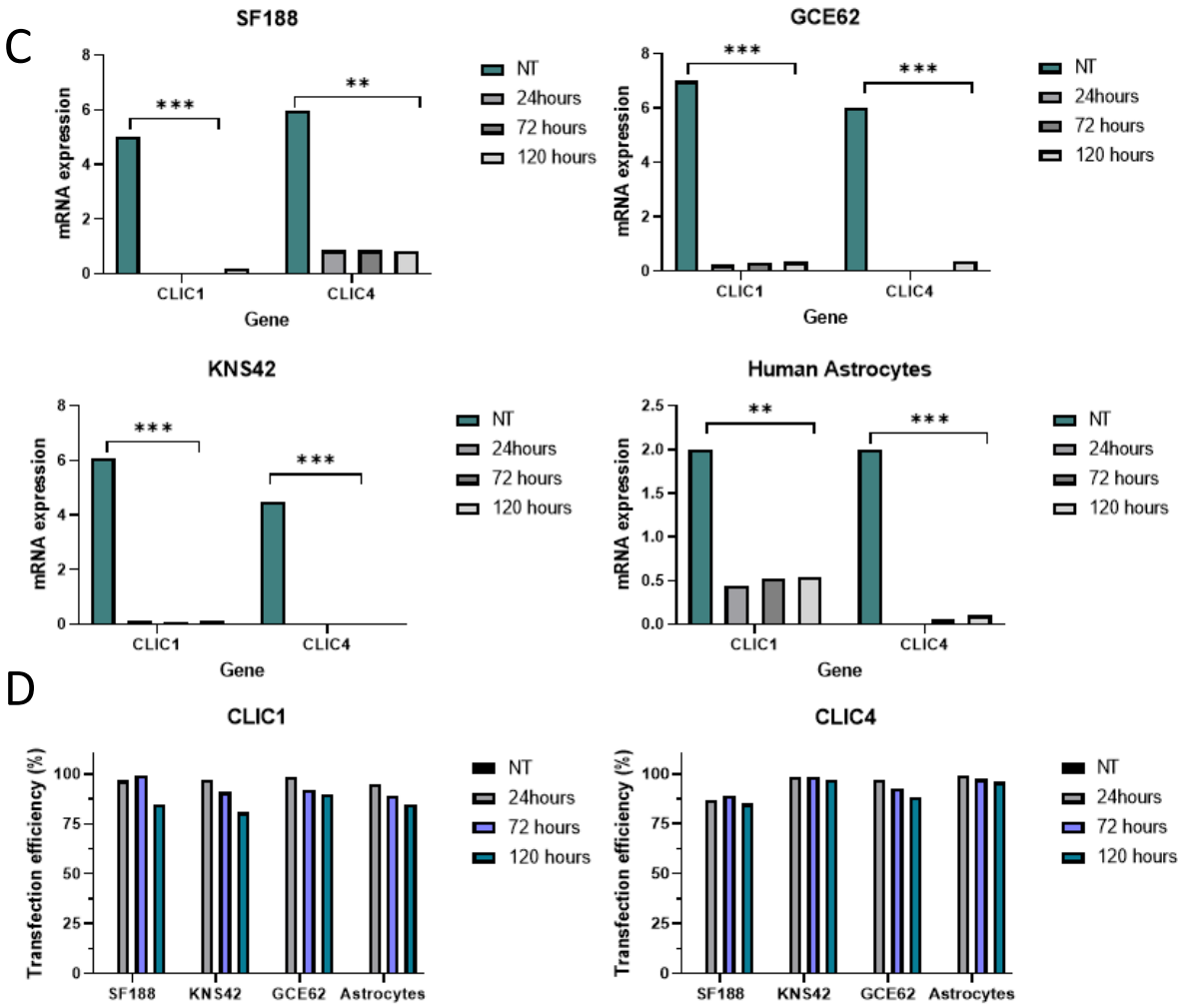

Figure 4.14. **Conformation of siRNA knock down of CLIC1 and CLIC4**. A) Representative western blot bands confirming successful reduction in CLIC1 and CLIC4 protein via siRNA. B) Quantification of western blot bands using optical density image analysis. C) Conformation of siRNA KD via qrtPCR (*2-ΔΔCq)* at 24, 72 and 120-hour time points relative to non-targeting control. Significance assessed by ordinary one-way ANOVA. N=3 D) Transfection efficiency as measured as percentage of non-targeting control taken from qrtPCR analysis.

4.4.2 CLIC1 and CLIC4 knock down reduces the capacity of pHGG to proliferate and invade.

4.4.2.1 CLIC1 and CLIC4 knock down reduces cell viability and cell count.

Prior to downstream functional analysis of CLIC1 and CLIC4 deficiency in pHGG it was fundamental to assess cell viability in KD cell lines. The aim of this was to firstly assess whether a knock down of CLIC1 or CLIC4 would be lethal to the cells, and secondly to see what effect, if any, was had on the overall proliferative capacity of the cells.

A presto blue assay was performed to investigate the viability the cell lines, whereby a significant decrease was observed. It is of note that around ~50% viability was maintained across each of the three pHGG cell lines, confirming that CLIC silencing is not lethal, and therefore appropriate for further experimentation. Significantly, there was no association between CLIC1 or CLIC4 deficiency and reduced viability in the astrocyte control line, confirming that this approach may be viable for clinical use in the future (figure 4.16b). Here we find that genetic targeting of CLIC1 and CLIC4 has a more profound effect on the viability and overall cell count of the cells when comparing to pharmacological targeting via either IAA94 or metformin. This was as hypothesised as it has been previously reported that silencing of the CLIC family of protein significantly diminished proliferative capacity of cancer cells, and that targeting via IAA94 can provide variable results (198).

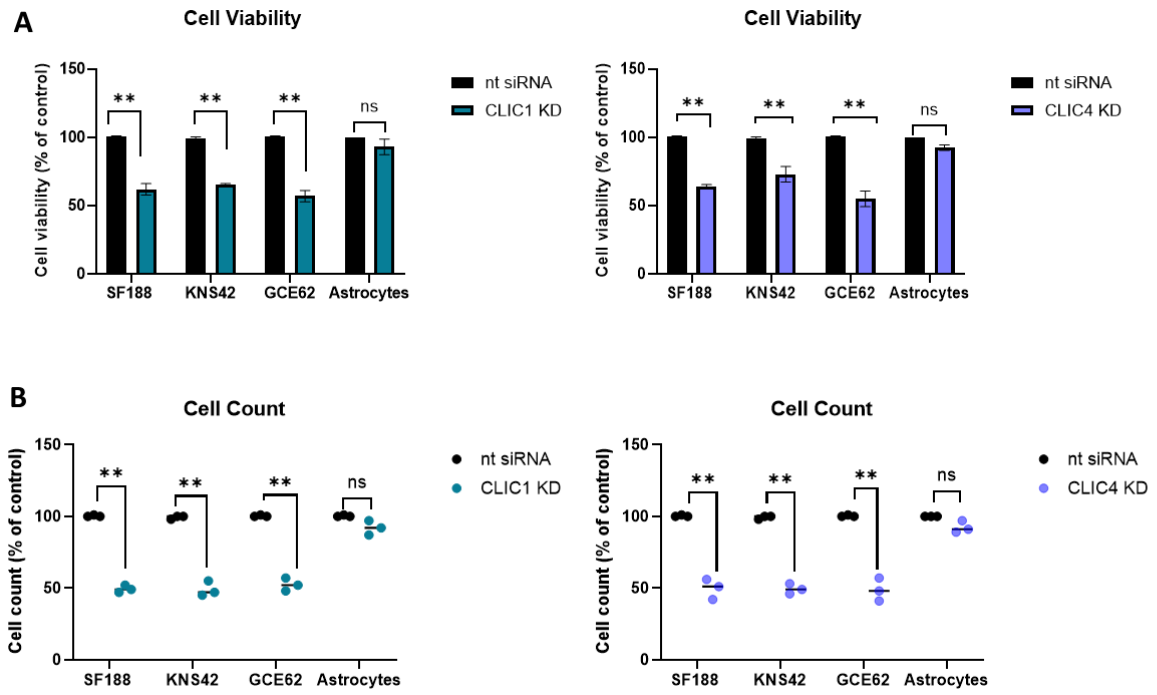

Figure 4.15. siRNA targeting of CLIC1 and CLIC4 reduces cell viability in pHGG. A) Cell viability (as measured by presto blue assay) is significantly reduced across all pHGG cell lines following CLIC1 and CLIC4 KD. B) Cell count (normalised to a control) is significantly reduced following siRNA targeting of CLIC1 and CLIC4 in pHGG.

4.4.2.2 siRNA targeting of CLIC1 and CLIC4 reduces invasive and clonogenic capacity in pHGG.

As previously described in this chapter, clonogenic assays are a well-used methodology to assess response to treatment and cell proliferation under prolonged growth. To investigate the effect of CLIC1 and CLIC4 deficiency on overall growth kinetics, cells were transfected with either CLIC1 or CLIC4 siRNA, and plated at low densities for clonogenic assay for 10 days.

As siRNA knockdown is transient, this model is not suitable for performing long term assays. As such, clonogenic assays were completed for both 10 days (as described when investigating IAA94) and for 5 days post transfection. Data gained form qrt-PCR confirms that CLIC1 and CLIC4 is still knocked down by a minimum of 80% 5 days post transfection, confirming that this would be an appropriate treatment window. To optimise, a clonogenic assay was ran for 5 days and 10 days to assess whether there were any significant differences in the clonogenic capacity of the cells. Importantly, there were no significant differences found at day 10 compared to day 5, and as such, confirming that the transient nature of CLIC1 and CLIC4 siRNA did not affect the results found in this time period.

SF188, as demonstrated previously, do not form tight colonies, instead creating diffuse groups of cells across the well, as these groups were isolated in nature, and contained >50 cells, these were accepted at colonies. We found that there was a significant reduction the colonies formed across SF188, KNS42 and GCE62 cell lines following CLIC1 KD. On average, CLIC1 and CLIC4 KD had similar capacity to inhibit proliferation in all three cell lines, demonstrating consistent decreases in colony counts. GCE62 cells formed the largest colonies in both control and siRNA targeted conditions. This was anticipated as these cells clearly favour close proximity even at low confluency, an explanation possibly due to the low passage primary nature of the cell line.

These data combined with viability and cell count data confirm that deficiency of CLIC1 or CLIC4 is sufficient to significantly inhibit the proliferative capacity of SF188, KNS42 and GCE62 pHGG cells.

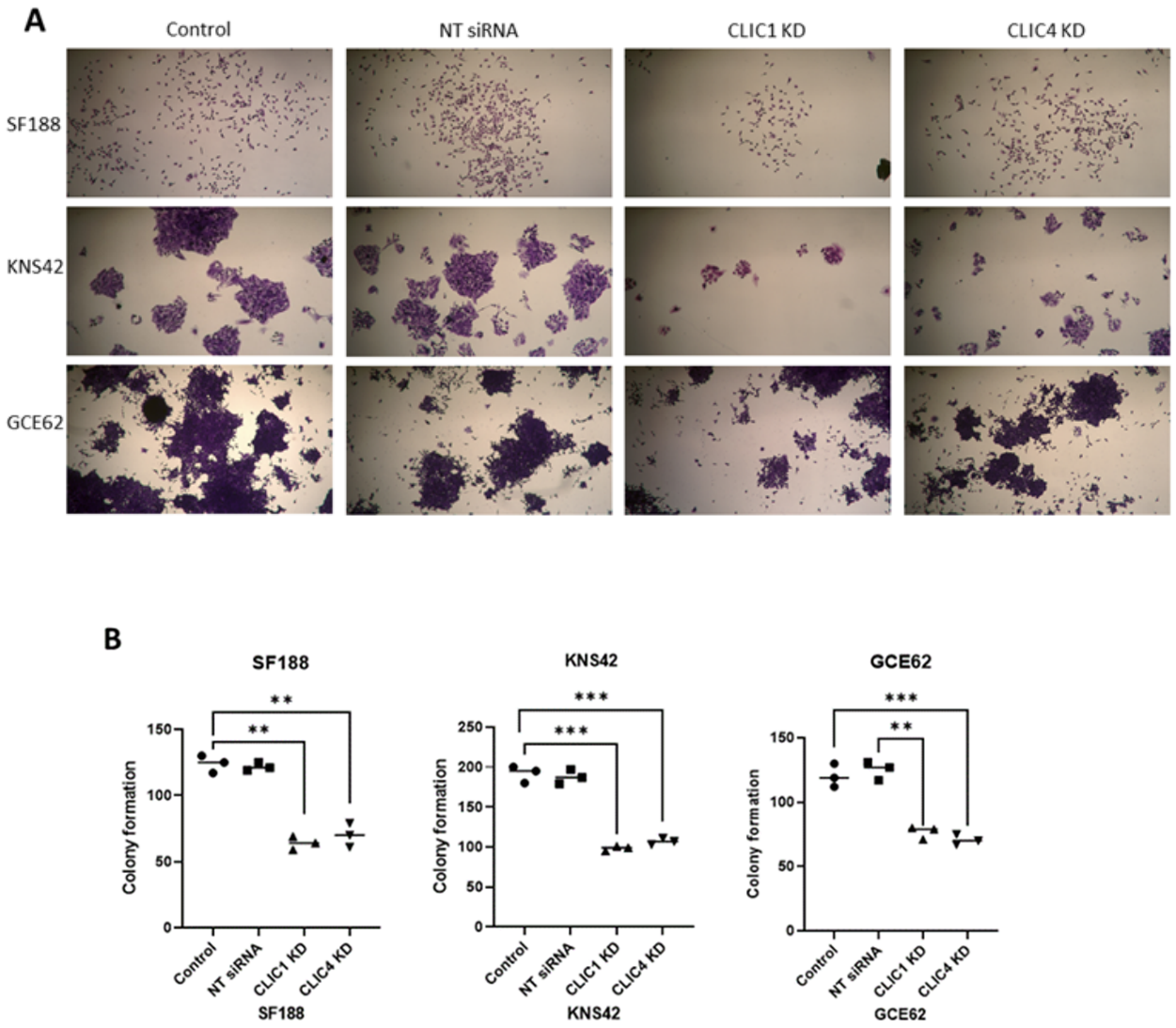

Figure 4.16. CLIC KD reduces proliferative capacity of pHGG. A) Representative crystal violet staining of fixed cells following clonogenic assay (10 days) of CLIC1 or CLIC4 deficient cell lines. Colonies defined as >50 cells and were counted from 4 different fields of view, in triplicate n=3. 10x magnification. B) Quantification of clonogenic assay via colony forming units of non-targeting siRNA vs CLIC1 or CLIC4 knock down. Statistical analysis by 1-way ANOVA.

Furthermore, in order to elucidate the role of CLIC proteins in the invasive capacity of glioma we performed a modified Boyden chamber assay to measure cell invasion following CLIC1 or CLIC4 KD. Cells were transfected and seeded into Boyden chambers 48 hours after transfection.

siRNA targeting of CLIC1 resulted in a marked decrease in invasion in SF188, KNS42 and GCE62 cell lines. SF188 CLIC1 deficient cells had the most significant reduction in the percentage of invading cells (45%) when compared to control.

The overall reduction in invasion across all cell lines was higher following genetic silencing of CLIC1 and CLIC4 (SF188-CLIC1$^-$ 45%, SF188-CLIC4$^-$ 40%, KNS42-CLIC1$^-$ 30%, KNS42-CLIC4$^-$ 33%, GCE62-CLIC1$^-$ 43%, GCE62-CLIC4$^-$ 35%) when compared to pharmacological targeting via IAA94 (SF188 30%, KNS42 20%, GCE62 10%). Interestingly, the decrease in invasion observed in GCE62 cells was 4.3 and 3.5 more in CLIC1 and CLIC4 KD respectively when compared to the decrease in invasion observed following IAA94 treatment. This suggests that pharmacological targeting and mere inhibition of CLIC1/4 in GCE62 is not sufficient to prevent invasive mechanisms, but depletion of the protein over the same time period does in fact contribute to reducing the capacity of these cells to invade.

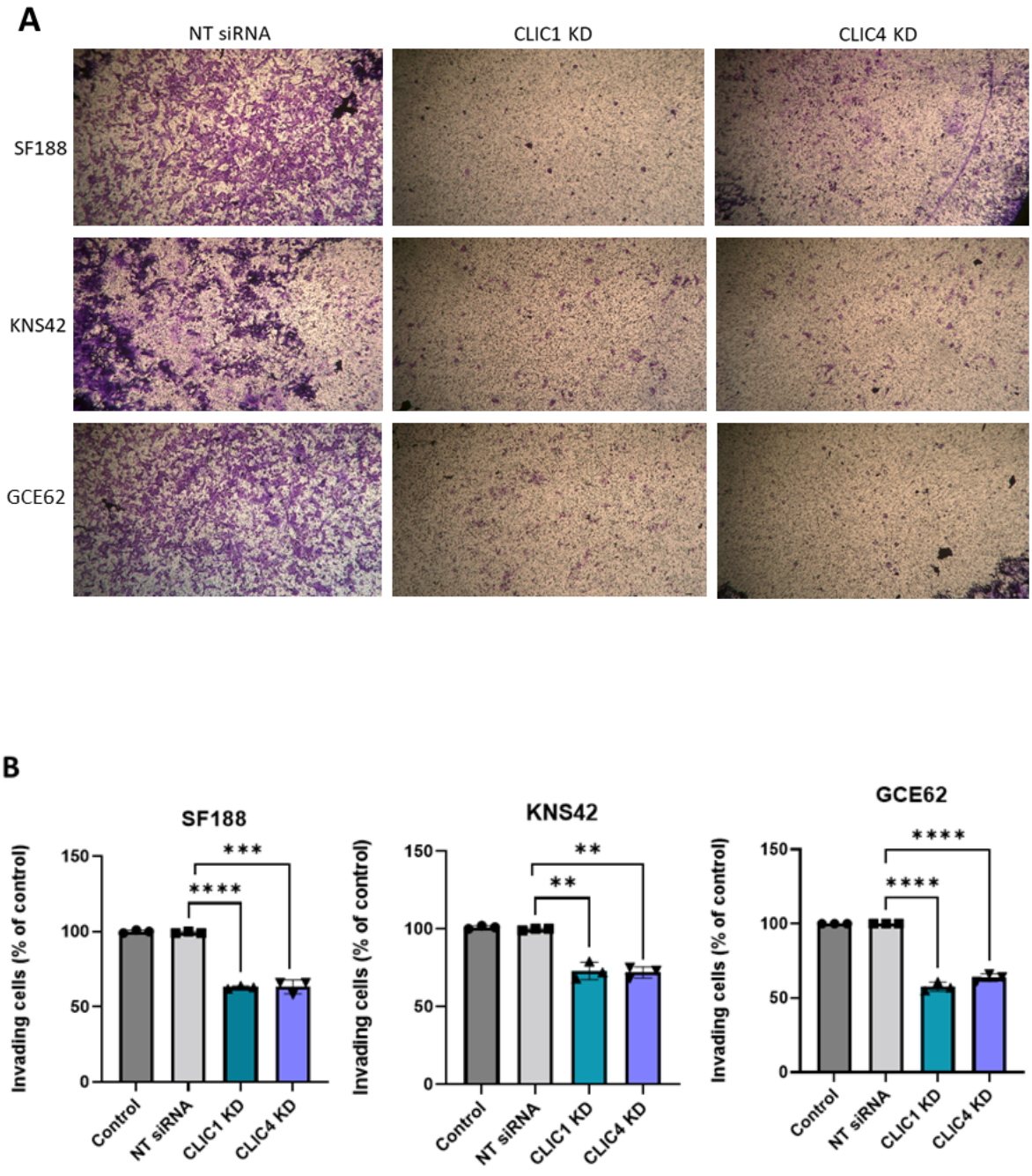

Figure 4.17. CLIC1 and CLIC4 knock down reduces invasive capacity of pHGG cells. A) Representative images of the invasion of SF188, KNS42 and GCE62 cells through a transwell coated with collagen IV. Magnification 10x. N=3 B) Quantification of cell invasion. Statistical analysis via unpaired t-test. Sf188 CLIC4 p= 0.0002, CLIC1 p= <0.0001. KNS42 CLIC4 p=0.0002, CLIC1 p=0.0012. GCE62 CLIC4 p= <0.0001 CLIC1 p= <0.0001

4.4.2.3 CLIC1 and CLIC4 deficiency is associated with aberrant cell cycling.

We have previously described the role of chloride channels in the cell cycle, and the elusive role that the CLIC proteins may play in regulating transition through various stages of the cell cycle. We found that when inhibiting CLIC channels via treatment of IAA94, there was dysregulation of the cell cycle compared to controls, and this was related to accumulation in G1, and a reduction of cells found in s-phase post treatment. To further investigate, we performed cell cycle analysis of CLIC1 and CLIC4 deficient cells (72 hours post transfection). Deficiency of CLIC1 and CLIC4 in causes significant alterations to the cell cycle of all cell lines investigated. We find that CLIC1 deficiency is associated with a significant increase in the percentage of cells present in G1 phase (57%), accompanied by a significant decrease in S phase (12%). Similarly, SF188 cells deficient for CLIC4 possess a lower percentage of cells in S phase (6%) but this is not associated with an accumulation in G1. Both CLIC1 and CLIC4 deficiency results in a higher percentage of cells present in G2/M (CLIC1 25%, CLIC4 19%) compared to control NT-SF188 cells (16%).

KNS42 deficiency of CLIC1 is associated with a significant reduction in both G1 and S phase (35% and 6% of total cells respectively). Both CLIC1 and CLIC4 knock down results in KNS42 cells accumulating in G2/M with 23% ($CLIC1^-$) and 19% ($CLIC4^-$) of total cells in this phase compared to control (13%).

A significant increase in CLIC1 (20%) and CLIC4 (18%) deficient GCE62 cells was found in G2/M phase compared to control cells (12%), and similar to SF188 and KNS42, there was a decrease in cells populating S-phase. Additionally, this was not associated with an increase in G1 cells, as there was a significant decrease in the percentage of cells held in G1 phase following both CLIC1 (35%) and CLIC4 (34%) knock down v NT control (44%).

Interestingly, these data seem to confirm what has been cited in the literature and demonstrate that knock down of CLIC proteins can have varying effects on the cell cycle, particularly associated with G1 and G2/M phase. Changes to the cell cycle observed post genetic targeting of CLIC1 and CLIC4 vary greatly compared to pharmacological targeting via IAA94. Drug targeting appears to be associated with G1 accumulation, whereas cells transfected with CLIC1 and CLIC4 consistently accumulate in G2/M phase.

In these experiments a portion of control SF188 cells were observed in the sub-G1 phase. This is unusual as it indicates cells that have undergone apoptosis, or a population of fragmented cells present in the samples. Although experiments were performed over multiple passages, this may be indicative of cellular stress relating to high passage number. Records indicate that the SF188 cells were several passages above the normal maximum, and therefore results must be interpreted with caution. Interestingly, this sub G1 population seen in the SF188 NT siRNA cell line decreased upon CLIC1 knock down. Overall, these data signify that the alterations to the cell cycle are not associated with apoptosis as there are no significant increase in the population of cells found in sub-G1 in CLIC1 or CLIC4 deficient cell lines.

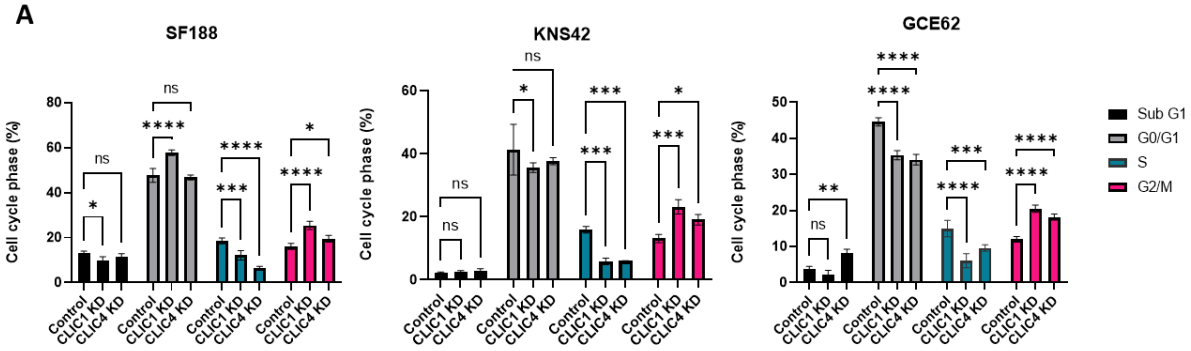

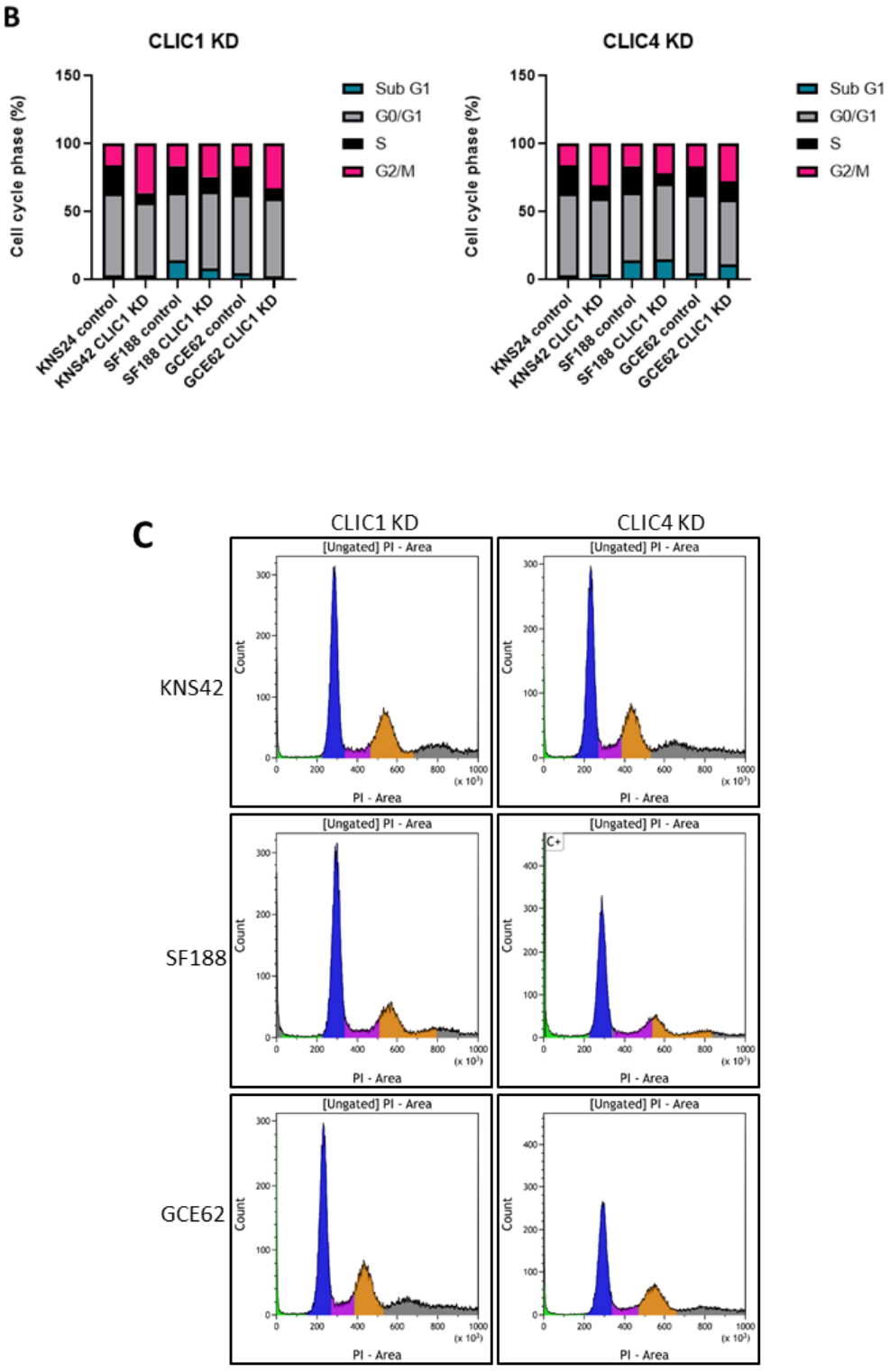

Figure 4.18. CLIC KD results in abnormal cell cycling. A) Two-way ANOVA, multiple comparisons between percentage of cells in each stage of the cell cycle and each experimental condition. CLIC1 and CLIC4 targeting with siRNA for 72 hours prior to experimentation, control = NT siRNA. B) summary data of percentage cell cycle stage in NT vs KD cell lines. C) representative histogram images of cell cycle.

4.4.3 Knock down of CLIC1 and CLIC4 reduces neurosphere formation.

Inhibition of CLIC proteins via IAA94 did not significantly reduce the capacity of pHGG cells to form neurospheres, however we wanted to investigate whether knock down of the proteins would affect sphere formation.

Cells were transfected with CLIC1 and CLIC4 siRNA and plates for sphere forming assays as previously described. CLIC1 knock down significantly inhibits neurosphere formation at day 3 in SF188 and KNS42 cells. This reduction in size was associated with an increased population of small and single cell suspension and cellular debris in SF188 cells.

CLIC4 knock down failed to significantly reduce neurosphere size in KNS42, but was significantly associated with a reduction in size of SF188 neurospheres.

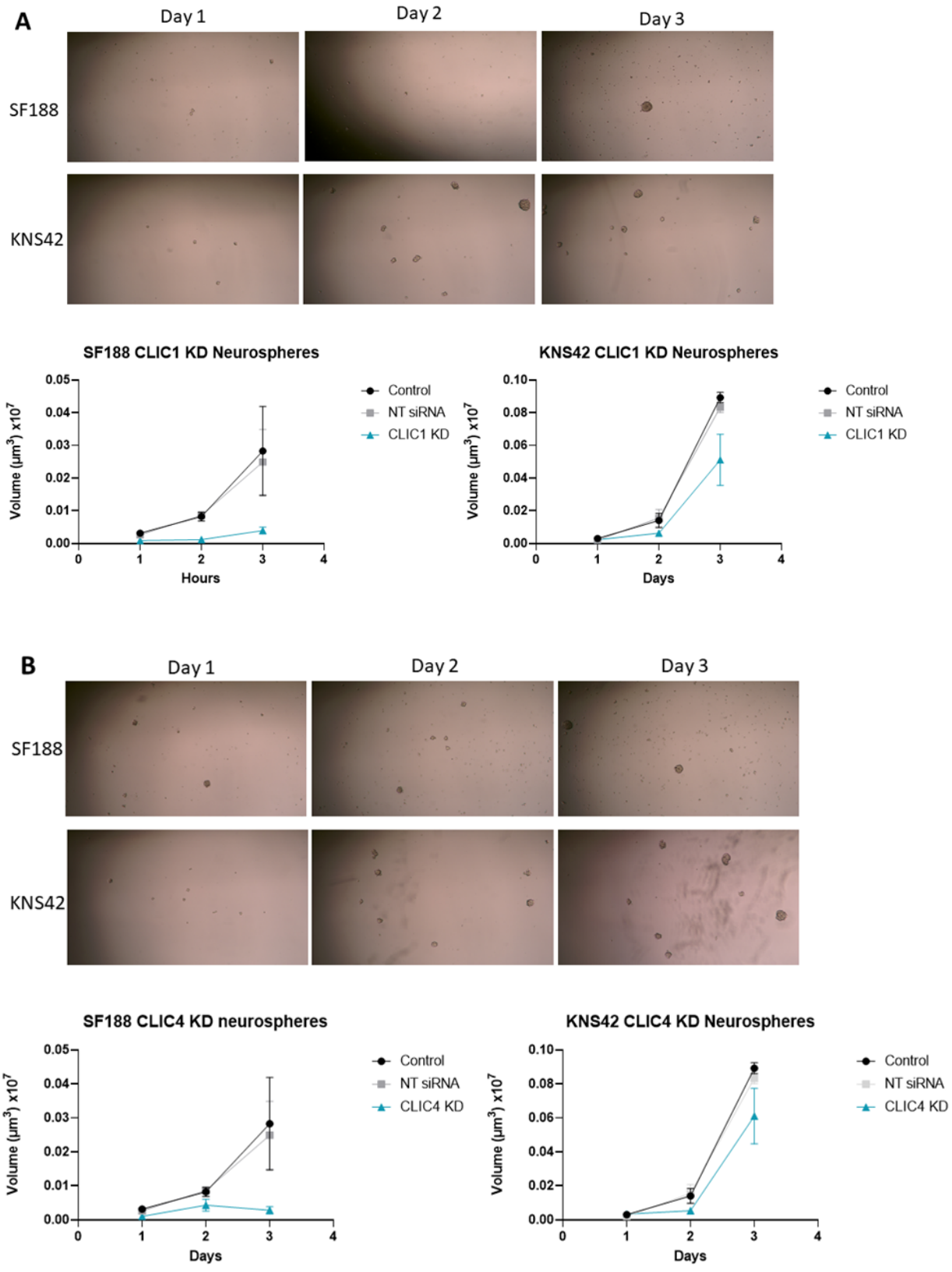

Figure 4.19. CLIC inhibition reduces neurosphere formation in SF188 and KNS42. A) CLIC1 knock down inhibits neurosphere formation of SF188 pHGG cells at all time points, but has only significant reduction in neurosphere size at day 3 in KNS42 cells. SF188 p= 0.0129, KNS42 0.01 2-way ANOVA. B) CLIC4 knock down inhibits neurosphere formation of pHGG cells in SF188 cells but has no significant affect in KNS42 cells. SF188 p =0.0042 **, kns42 p=0.609 ns. Cells were imaged daily for 3 days, and their size measured using ImageJ – statistical analysis via 2-way ANOVA. Magnification x10

4.5 Generation of a stable knock out of CLIC1 and CLIC4 via CRISPRcas9

To further open up the experimental pipeline to long term experiments, we sought to generate a stable knock out model of HGG cell lines. Adult glioma cells lines U87 and GCE28 were previously Cas-9 induced by the lab of Dr Alan McIntyre, University of Nottingham, and as such were selected to perform cas9 induced, lentiviral mediated knock out of CLIC1 and CLIC4.

GCE28 (low passage primary line) and U87 (commercial cell line) were transfected with lentiviral guide RNAs targeting either CLIC1, CLIC4 or a non-specific scramble region. Two gRNAs were selected per gene target to assess efficiency of transfection of different coding areas. Transfection was completed according to a pre-optimised MOI viral titre (McIntrye Lab) described in section 2.7.2 in the presence of polybrene. Cells were then selected with puromycin to generate pure a knockout population over several passages.

Following selection, doxycycline was used to induce the drug inducible promotor, and cells were exposed for 2 cycles of 48 hours prior to experimentation.

Cells were collected and assessed via western blot analysis to confirm knock out of CLIC1 or CLIC4 in U87 or GCE28 cell lines.

Unfortunately, despite optimisation attempts we were unable to produce sufficient knock down using this methodology for either of our targets in any of the cell lines. The highest transduction efficiency observed was total of 30% knock out of CLIC1 in U87 cells, and 33% knock out of CLIC4 in GCE28 cells. These values were significantly lower than the transfection efficiencies observed with siRNA, and as such, it was decided to not pursue this line of investigation.

4.6 Chapter summary

Throughout this chapter we have investigated the role of CLIC1 and CLIC4 in paediatric high-grade gliomas and assessed their candidacy as targets for future novel therapeutics. The effect of the CLIC specific inhibitor IAA94 was assessed alongside the clinically available drug metformin. We sought to gain an overall understanding of the role that CLIC1 and CLIC4 play in glioma cell proliferation via pharmacological and genetic inhibition combined functional proliferative assays. The invasive capacity of SF188, KNS42 and GCE62 was assessed using modified Boyden chambers, coated with Collagen IV to simulate brain extracellular matrix. These assays were performed in tandem drug inhibition via IAA94 and genetic silencing of CLIC1 and CLIC4 via siRNA. The ability of pHGG cell lines to form neurosphere was examined and the function of CLIC1 and CLIC4 in forming said neurosphere was studied. Finally, we assessed the outcome of CLIC targeting on the cell cycle of pHGG cells in order to elucidate the functional mechanism of CLIC1 and CLIC4 ion channels in the cell cycle.

Chapter outcomes:

1) Paediatric high grade glioma cell lines SF188, KNS42 and GCE62 have the capacity to readily form neurospheres.
    - This ability is associated with an increase in the stem markers SOX2 and NESTIN, and an overall increase in CLIC1 and CLIC4 expression was observed at the mRNA level when comparing 2D monolayer culture to 3D neurosphere culture.
    - Neurosphere formation is variable across the cell lines and is linked to cell size and growth kinetics observed in monolayer culture.

2) Pharmacological inhibition of CLIC1 and CLIC4 via IAA94 reduces the capacity for pHGG to proliferate and invade:
    - IAA94 treatment is seen to significantly reduce cellular proliferation, and results in a reduction in cell count (SF188 and GCE62). Importantly this reduction in cell viability and cell count is not mimicked in normal human astrocyte cells. Furthermore, treatment with IAA94 significantly reduces the invasive capacity of KNS42 and SF188 cells.
    - Treatment with IAA94 results in aberrant cell cycling associated with accumulation in G1 and reduction in S-phase.
    - Neurospheres treated with IAA94 retain the ability to proliferate and form solid spheres. IAA94 has no significant effect on the size of SF188, KNS42 or GCE62 neurospheres.
    - Treatment with IAA94 is not associated with astrocyte toxicity and is therefore an appealing candidate for HGG treatment.
3) siRNA knock down of CLIC1 and CLIC4 reduces proliferation, invasion and clonogenicity of pHGG cells.
    - siRNA knock down of CLIC1 and CLIC4 was successful and highly efficient in SF188, KNS42 and GCE62 cell lines.
    - CLIC1 and CLIC4 deficiency is associated with a significant decrease in the viability and overall cell count of pHGG cells. This decrease in cell count and viability was not observed. This marked decrease in proliferation was also observed via colony forming assay, whereby deficiency of both CLIC1 and CLIC4 resulted in significant reduction in colony formation across all cell lines.

- Invasive capacity was significantly reduced in CLIC1 and CLIC4 knock down cell lines compared to NT controls.
- CLIC1 and CLIC4 may be implicated in the control of the cell cycle in pHGG. Deficiency resulted in numerous changes to the cell cycle, particularly associated with an accumulation in G2/M phase.
- CLIC1 knock down inhibits neurosphere formation in SF188 and KNS42 cells. CLIC4 knock down did not reduce neurosphere size in KNS42 but was significantly associated with a reduction in size of SF188 neurospheres.

4) CRISPR-Cas9 mediated silencing of CLIC1 and CLIC4 was unsuccessful in HGG cell lines.

These data suggest are indicative of the feasibility of targeting CLIC1 and CLIC4 as an anticancer agent. Additionally, the lack of toxicity observed in human astrocytes suggests that CLIC1 and CLIC4 are not essential for the survival of normal cells, but are however, essential in maintaining proliferation and invasive capacity in malignant cell lines.

5 Assessing the potential of CLIC1 and CLIC4 as bioelectric targets for electrotherapy in paediatric high-grade glioma

5.1 Introduction

Bioelectricity and bioelectric signalling are emerging fields in cancer research. At the very basis of bioelectricity lies membrane potential, an intrinsic property of all living cells. Research has found that the bioelectric processes of cancer cells is different to those of normal cells, causing dysregulation in homeostatic mechanisms, signalling pathways and communication between cells. Recently, pioneering work has demonstrated that glioma cells integrate themselves into neural networks, relying on synaptic connections with neurones and other tumour cells (189,199,200). Through this, an intra-tumoral electrical network is formed, exposing a therapeutic window for manipulation via exogenous currents.

As previously discussed, TTFields is the first novel treatment for aHGG in over a decade shown to significantly increase overall survival in phase 3 clinical trials and is one of very few novel treatments exploiting bioelectricity to target cancer. Despite this, the mechanism of TTFields is yet to be fully elucidated, with the proposed antimitotic effects failing to successfully explain the myriad of other changes found following TTFields treatment. The brain itself, is intrinsically electrically active, and we propose that one mechanistic factor behind the success of TTFields may be the dysregulation or aberrant expression of ion channel genes therefore further disrupting the cell cycle and potentiating TTFields antimitotic effects.

TTFields is not currently approved in the treatment of paediatric tumors due to the suggested treatment burden of daily head shaving and wearing the device for 18+ hours a day. As such, identifying alternative, minimally invasive electrotherapies or increasing efficacy of TTFields for pHGG is emerging as an important area of research.

A study by Branter et al has demonstrated the efficacy *in vitro* of DBS in inhibiting the growth of adult GBM cells (152). In contrast to TTFields, deep brain stimulation (DBS) therapy uses implantable electrodes to stimulate specific brain regions, and has shown significant success in the treatment of movement disorders. DBS delivers targets electrical fields to specified anatomical regions such as the subthalamic nucleus, and is well tolerated and safe to implant (98,100,101,201). With well known safety profiles, this therapy is attractive for repurposing as a novel therapy for pHGG. Again, the mechanism of DBS is not fully understood, and elucidation of this may unlock therapeutic success in gliomas (101). We seek to assess if electrical therapies such as DBS and TTFields hold efficacy in the treatment of pHGG cell lines, and if ion channel targeting holds potential as the mechanism of action. We will investigate this via the combination of CLIC inhibition, both genetically and pharmacologically, as previously described in chapter 4, with TTFields and DBS treatment.

Chapter aims:

1) To assess CLIC1 and CLIC4 as bioelectric targets via interrogating the electrical activity of these ion channels.
2) To investigate membrane potential across pHGG cell lines, compared to human astrocytes.
3) To investigate the efficacy of TTFields and DBS therapy in pHGG cell lines.
4) To assess the role of CLIC targeting as a dual therapy with TTFields.
5) To establish the consequence of long term TTFields treatment on pHGG cells.

5.2 CLIC1 and CLIC4 are electrically active in pHGG cells.

As described previously, the CLIC family of proteins are a structurally and functionally diverse group, operating within multiple processes as either monomeric soluble proteins, or integral membrane proteins that are crucial in cell cycle control. We have already demonstrated in chapter 4 that the inhibition of CLIC1 or CLIC4 via IAA94 or cellular deficiency via siRNA caused marked alterations to the cell cycle. As a result, we hypothesise that CLIC channels are in fact exerting their influence on glioma pathology as functional ion channels, as opposed to monomeric soluble proteins.

To elucidate the functional state of the CLIC proteins identified in our cohort of tissues and cells, we employed several bioelectrical assays to investigate the movement of chloride ions across the cell, and if these protein harness bioelectric capacity, and as such, are acting as ion channels.

5.2.1 Chloride efflux across pHGG cells

Chloride intracellular channels 1 and 4 are responsible for the movement of chloride ions across the plasma membrane of the cell(142,202,203) in aid of maintaining physiological conditions. Membrane potential is often altered to accommodate function, as such, phenotypic changes in Vm in cancer cells arise. Previous work in this project identified that genetic and pharmacological targeting of CLICs reduces proliferation, invasion and clonogenicity of pHGG cells. In order to assess the functionality of these CLIC proteins and elucidate if they are indeed acting as Cl- channels, including the passive permeability of Cl^- ions across the membranes of pHGG cells, a shadow ion (surrogate tracer) assay was employed, whereby iodide ions are used to track chloride channel opening and closing. Abcam's Chloride Channel Assay Kit (Colorimetric) (ab176767) uses a proprietary iodide indicator (Iodide Sensor Blue dye) to measure iodide concentration, with as low as 30nM of

iodide able to be detected. Iodide Sensor Blue dye forms a blue complex with iodide, which has an absorption spectra spanning from the UV to 700 nm. The principle is that if treating with an antagonist, Cl- channels will be blocked, iodide ions remain in the cell as efflux is prevented, and upon cell lysing, there is increased iodide to dye binding and therefore a higher absorbance reading. Figure 5.1 demonstrates the workflow of this assay.

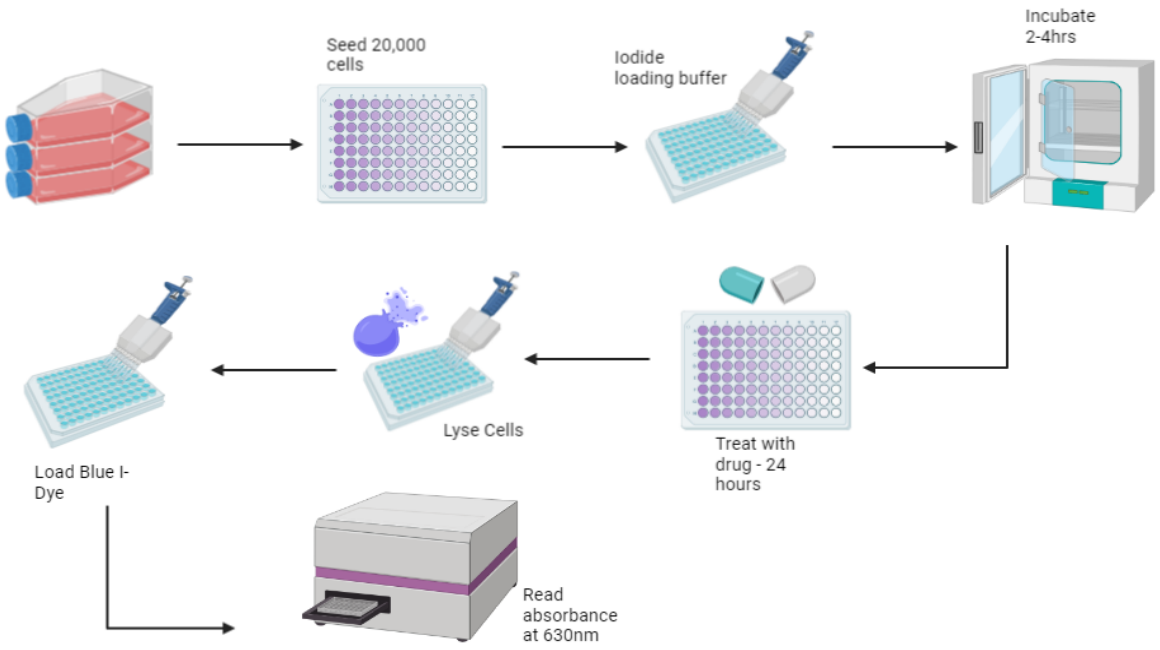

Figure 5.1 Workflow schematic of chloride efflux assay (Abcam). Assessment of the chloride efflux capacity of cells was carried out using the Abcam colorimetric assay in a 96-well plate format by means of shadow ion assay.

Initial experiments were to assess if there was any significant difference in the movement of Cl^- across the cell membrane of astrocytes compared to pHGG. Cells were left untreated and plated to be no more than 80% confluency on the day of experimentation. Figure 5.2 shows that there were no significant differences when comparing normal astrocytes to pHGG cells, and that there were not significant differences in the chloride content of pHGG compared to

normal astrocytes. These data suggest that the basal efflux of chloride was comparable across all control cell lines. It is important to note that this is not a CLIC1 or CLIC4 specific assay, nor a measure of general chloride channel activity, chloride activity and movement is inferred via the movement of iodide ions acting as a surrogate tracer. As such the relative expression levels of CLIC1 and CLIC4 specifically in these cell lines does not hold significant bearing on the results found.

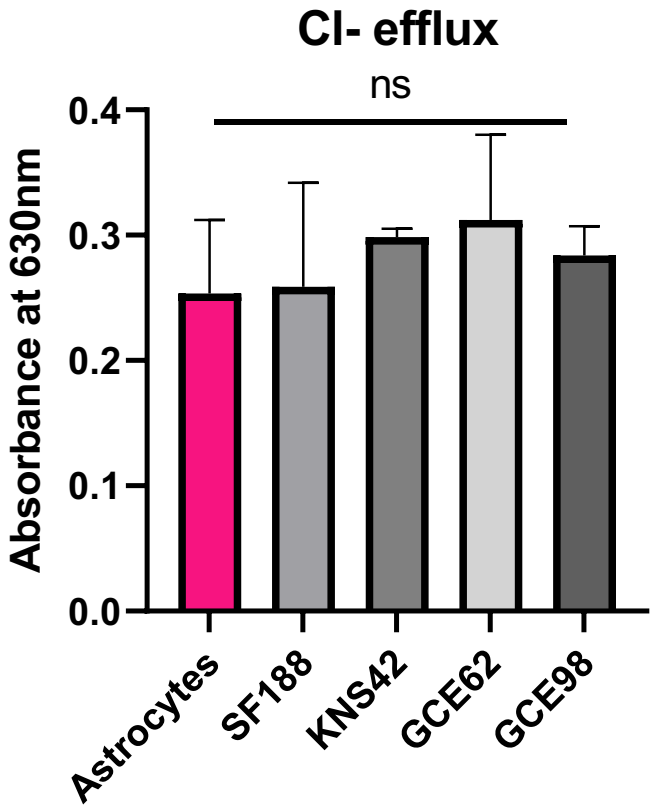

Figure 5.2 There is no significant difference in the Cl- efflux activity across pHGG cells and astrocytes. The iodide efflux across pHGG cell lines and normal human astrocytes was measured via the Abcam colorimetric Cl- efflux kit. Chloride activity is inferred via surrogate tracer assay. N= 3 statistical tests via 1-way ANOVA with multiple comparisons, error bars represent mean + SEM.

5.2.1.1 Drug targeting of CLIC channels reduce chloride efflux in pHGG

Next, we wanted to assess whether the reduction of proliferation and invasion found when siRNA targeting CLIC1 and CLIC4 was associated with a decrease in ion channel activity, and

as such a decrease in Cl- efflux. When performing these experiments there were various optimisation steps, including a pre-incubation with the drugs of choice. We found that pre incubating the cells with either IAA94 or metformin for 72 hours prior to Cl- assay did not yield any valuable results as the data harvested was variable and not replicable. This is likely to be due the antagonist effect of IAA94 and metformin, meaning that a number of channels were blocked prior to iodide loading, and therefore inconsistent permeability into the membrane. Instead, cells were seeded, loaded with iodide buffer, and then incubated with respective drugs for 24 hours, and the assay continued.

Figure 5.3A shows that specific targeting via treatment with 100µM IAA94 resulted in a significant decrease in the movement of chloride ions across SF188 ($p=0.03$) and KNS42 ($p=0.0162$) cells compared to vehicle control, whereas no statistically significant changes in chloride efflux were observed in GCE62 and GCE98 cells. This data is comparable to that found in drug sensitivity assays, whereby we found that GCE62 was the least sensitive cell line to IAA94, perhaps suggesting that sensitivity to IAA94 could be mediated via the movement of chloride ions.

When assessing whether broad chloride channel blocking (via treatment with 10mM of Metformin) influenced the efflux of HGG cells, a significant decreased in chloride ion efflux was observed in three cell lines KNS42, GCE62 and GCE98 when compared to vehicle control. The most significant decrease (and therefore highest absorbance value) was observed in the adult GBM line GCE98 ($p=0.0053$) (figure 5.3b). It is important to note that this primary patient derived line is very early passage (p7) and the patient had received TTFields treatment prior to surgical removal of this tumour. This patient will be discussed in more depth in chapter 6. It is an interesting observation that a cell line with prior exposure to bioelectric manipulation appears to be the most sensitive to chloride channel

inhibition via metformin and has the most pronounced effect on cellular Cl^- efflux.

Treatment with metformin did not result in any statistically significant changes in chloride efflux in SF188 cells. This may be an artefact of the control cells having a high level of variability, and therefore large standard deviation.

Interestingly significant Cl- efflux reduction was observed in opposing cell lines for each drug condition. This is likely due to the broad acting effect of metformin, having an overall more potent effect on the movement on chloride ions in the cell.

It is worth noting that in previous experiments cells were exposed to IAA94 and metformin for 72 hours prior to experimentation, and that the decreased exposure time in this assay may not be reflective of effects previously seen at longer treatment times. We did not incubate drugs for 72 hours due to the observed instability of the iodide loading buffer when optimising at this time point.

These data indicate that drug targeting of chloride channels has a variable effect across our panel of HGG cells, and that both IAA94 and metformin have the capacity to alter chloride channel activity.

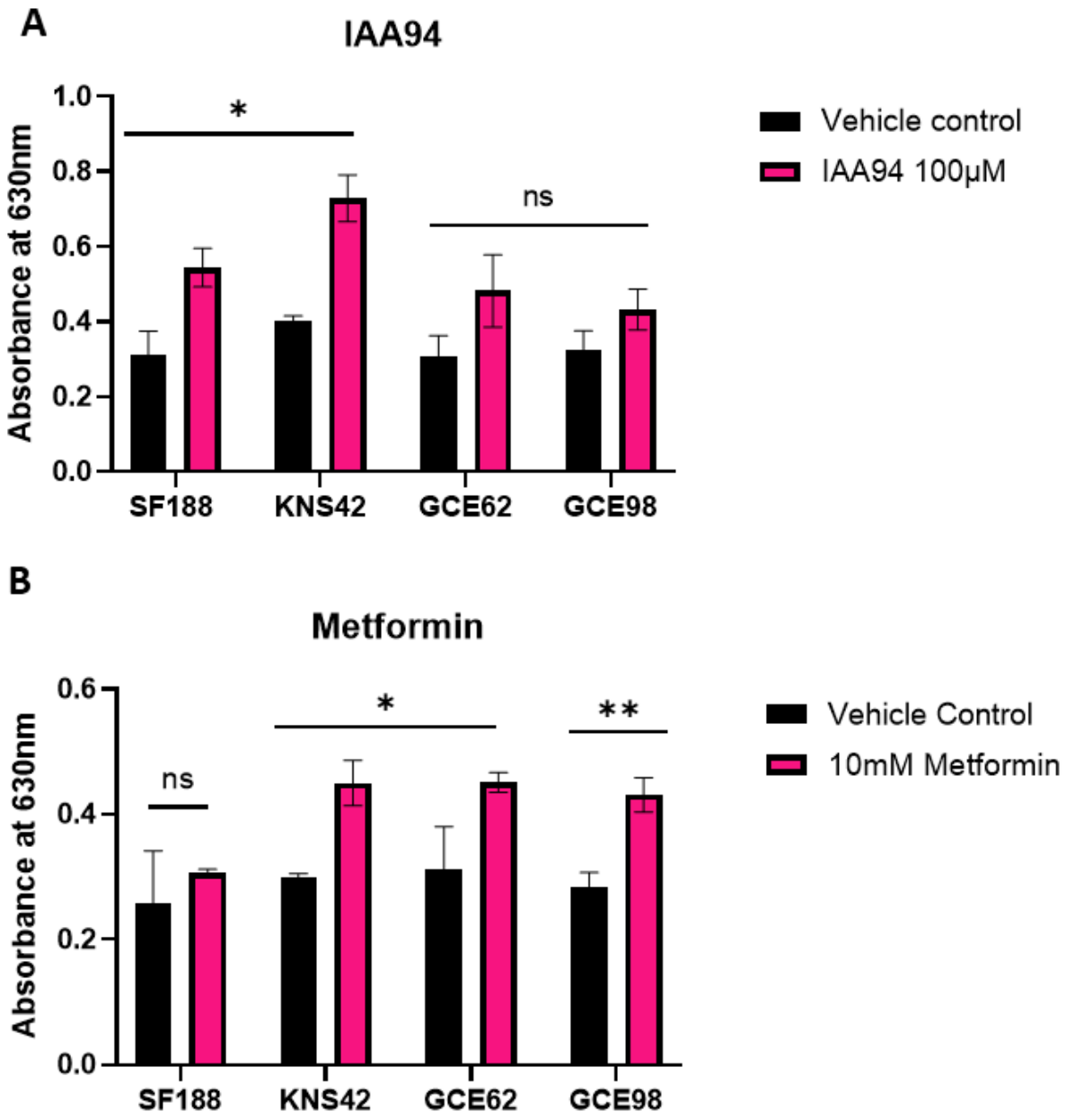

Figure 5.3 CLIC pharmacological targeting reduces Cl- efflux across cells A) CLIC1 specific blocking via IAA94 causes significant reduction in chloride efflux in SF188 and KNS42 cells. B) Pharmacological inhibition via metformin causes reduced Cl- ion flux across pHGG cells with significant channel blockage observed in KNS42, GCE62 and GCE98 cells. N=3. Statistical testing by ANOVA. Error bars represent mean +/- SD.

5.2.1.2 Transient knock down of CLIC1 and CLIC4 via siRNA decreased Cl- ion efflux in pHGG.

To specifically interrogate the role that CLIC1 and CLIC4 have in the movement of chloride ions across the membrane, the chloride efflux assay was performed on CLIC1 and CLIC4 deficient HGG cells.

Figure 5.4A demonstrates that CLIC4 deficiency produces a significant reduction in chloride efflux in KNS42 (p=0.007) and GCE62 (0.0397) cells, mirroring the data found when exposing cells to metformin. This may be indicative of a CLIC4 specific inhibitory effect of metformin. Whereas CLIC1 knock down provided sufficient to cause alterations in the chloride efflux across all cells, with significant reduction seen SF188 (p= 0.0059), KNS42 (p=0.0028), GCE62 (p=0.0189) (figure 5.4). These data remain consistent with result found in call viability assays, whereby CLIC1 deficiency produces a more pronounced reduction on cell viability. Thus, these data indicate that there is a link between the movement of chloride ions across the cell and the viability. Similarly, cell cycle analysis (section 4.4.3) data revealed significant alterations in cell cycling following CLIC1 knock down, data which confirms that the observed decreased in chloride efflux may be contributing to the aberrant cell cycling of pHGG cells.

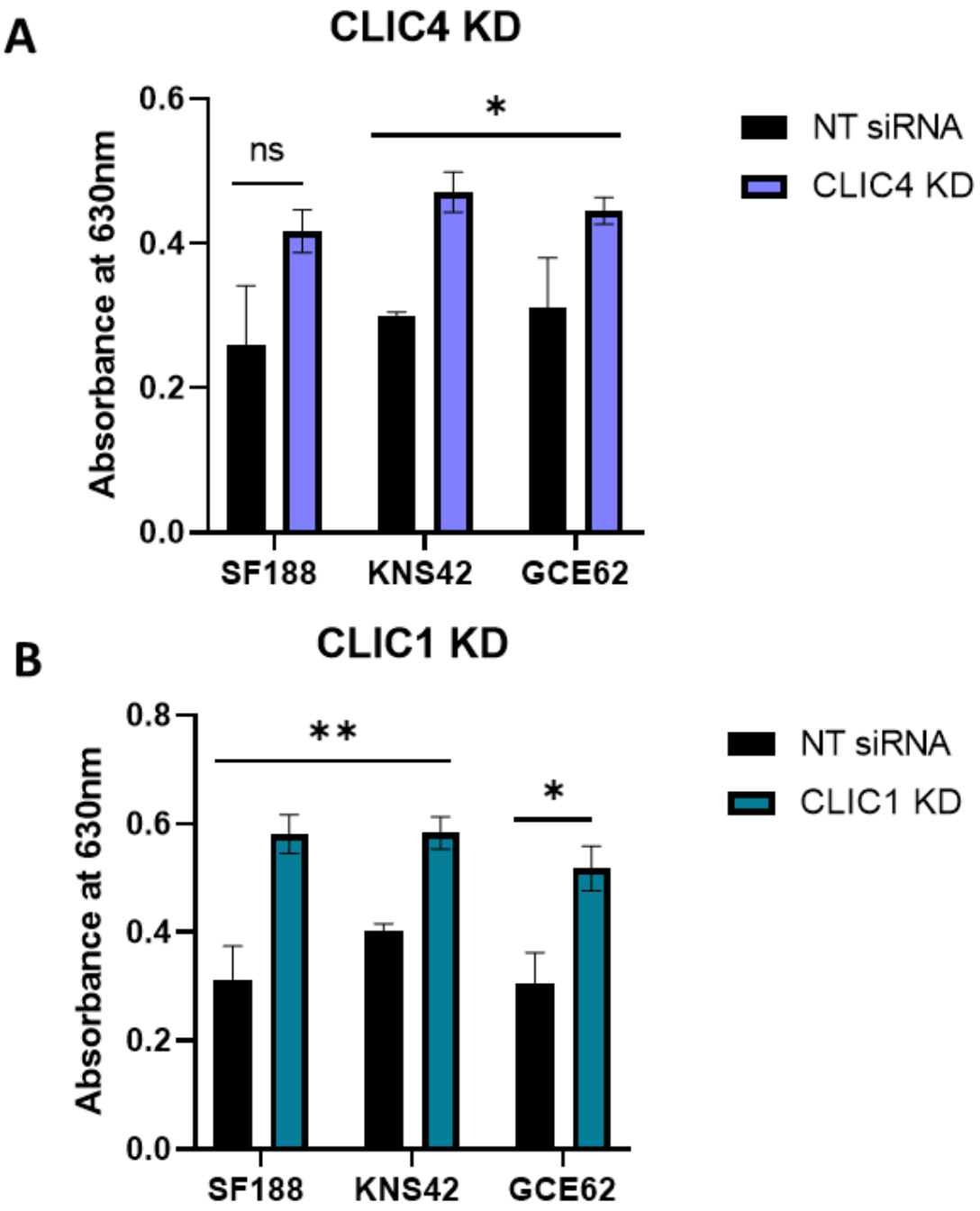

Figure 5.4 siRNA targeting of CLIC1 and CLIC4 reduces chloride efflux. A) KNS42 and GCE62 cells targeted with CLIC4 siRNA have reduced Cl- ion efflux. B) CLIC1 siRNA targeting reduces Cl- ion efflux across all cells. N=3, statistical analysis by 1-way ANOVA. Error bars represent mean +/- SEM.

5.2.2 Flexstation membrane potential assay

As previously mentioned, the membrane potential is one of the key mechanistic drivers of the cell cycle and cell proliferation. Therefore, we sought to assess the membrane potential of these cells via high through put assays combined with drug, genetic and electrical targeting of CLICs.

A Flexstation membrane potential assay was employed whereby cells are seed, loaded with an FMP dye (Molecular devices), treated with a drug, and fluorescence values read using a Flexstation plate reader (Figure 5.5). The dye utilised in this assay is a lipophilic, anionic, bis-oxonol dye that can partition across the cytoplasmic membrane of live cells (Molecular devices). Its fluorescence intensity increases when the dye is bound to cytosolic proteins. When the cells are depolarized, the permeability of the membrane increases, and more dye is able to enter the cells (204). Consequently, the increased intracellular concentration of dye leads to an increase in binding to cytosolic proteins and subsequently, an increase in fluorescence signal.

It is important to note that blocking Cl- channels has been suggested to prevent the G2-M (112) phase progression via preventing the depolarisation of the membrane, suggesting that chloride channel movement is essential in the depolarization of cells. When blocking the efflux of Cl^- the membrane potential of the cell becomes more hyperpolarised. As previously explained, depolarisation is seen via an increase in fluorescent signal, therefore hyperpolarisation linked to chloride channel blocking would indeed produce a reduction in relative fluorescent units (RFU). Whilst RFU is not directly translatable to a membrane potential value, however experimental research has suggested that a change in 5% RFU is relative to around a 10mV change in membrane potential (204).

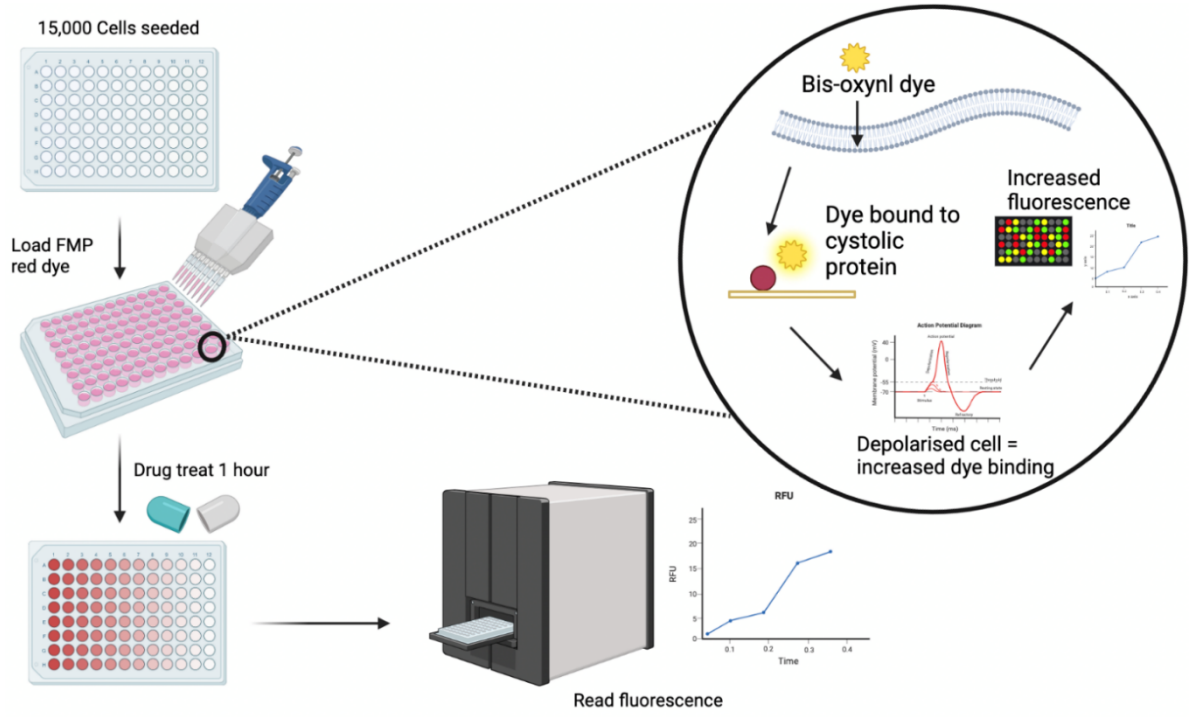

Figure 5.5 Workflow schematic of Flexstation membrane potential assay for high throughput measurement of membrane potential using fluorescence. The FLIPR membrane potential assay (Molecular Devices) was used as a high through put method of assessing the membrane potential of cells in a 96 well format.

To analyse the data gained via FLIPR membrane potential assays read on the Flexstation, SoftMax Pro software was utilised. Figure 5.6 demonstrates and example of a representative trace of an untreated astrocyte. Each trace is taken from a reading of an individual well of a 96 well plate, and each data point represents an individual read. To process the data, the trace was reduced to remove background and normalised within the software, and the 'area under curve' function was used to analyse the change in RFU. At 15 seconds wells were 'spiked' with 1M KCl to trigger ion channel activity and cellular activity as expressed as RFU was measured post KCl spike. An average read was taken from the 'area under curve' and treated samples were processed as a maximum percentage change of the control condition compared to basal levels. Untreated controls were normalised to the pre-spike values.

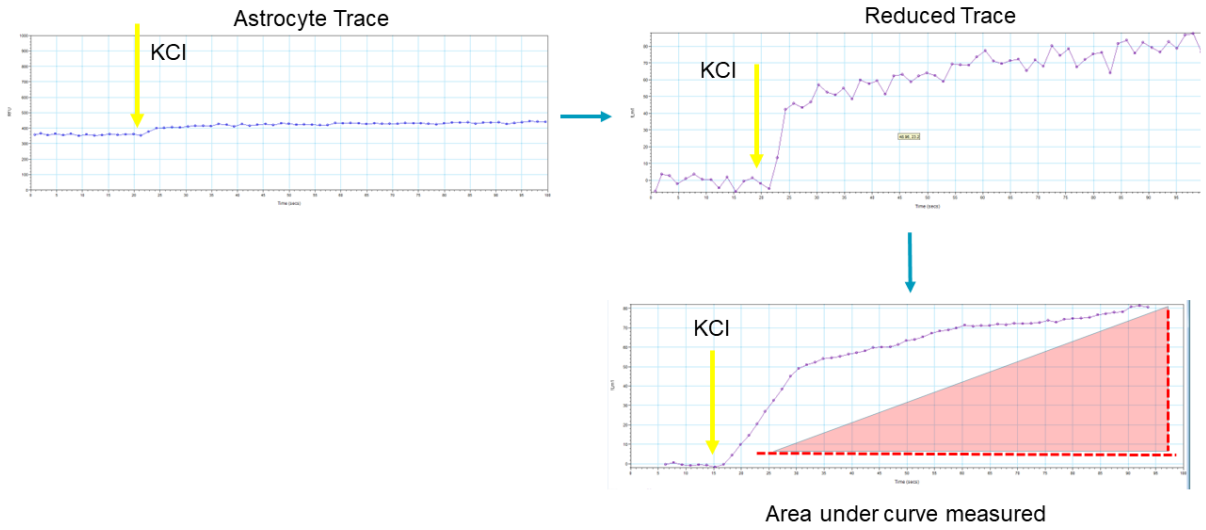

Figure 5.6 Example trace analysis from data gained via FLIPR membrane potential assay. Representative trace from Astrocyte cell line. Each trace is taken from one well of a 96 well plate and each data point represents a single read. 8 wells per cell line per condition were read in triplicate.

Initial experiments aimed to interrogate the baseline resting membrane potential in the panel of HGG cell lines and normal human astrocytes. All cell lines tested elicited a response to KCl at 15 seconds and demonstrate membrane potential change in response to external stimuli. Surprisingly, there were no significant differences found between the HGG cell lines (figure 5.7), with relative RFU % change post KCl challenge being consistent across the three paediatric cell lines (SF188, KNS42, GCE62) and adult HGG cell lines (GIN98 and GCE98). Via previous experimentation, differences in the CLIC channel activity were found as demonstrated by protein and gene expression, response to inhibitors and chloride efflux levels, so it is unexpected that there were no baseline differences in Vm observed.

The differences in RFU between normal astrocytes and HGG cell lines was also assessed. We found that on average normal astrocyte cells were more hyperpolarised (as reflected by a reduced RFU) than the panel of HGG cell lines. The paediatric glioma cell lines SF188

and GCE62 were significantly depolarised (following KCl exposure) compared to normal human astrocytes ($p=<0.05$), whereas no significant changes in KNS42 Vm was observed. Intriguingly, the adult GBM cell line GIN98, that has had previous exposure to TTFields, had the most significant difference in RFU ($p=<0.01$) and therefore increasingly depolarised resting membrane potential compared to normal astrocytes (figure 5.7). This is interesting, particularly as the matched cell line GCE98 from the core region of the same tumour sample did not exhibit significant differences and therefore this may provide some mechanistic insight into the effect of TTFields on the membrane potential of cells in the invasive margins of GBM tumours. It is worth noting that the percentage response will vary depending on the cell lines relative permeability of K^+ and Cl^- and further validation should be assessed using electrophysiology techniques. Similarly, an osmotic control such as NaCl would be beneficial here, as KCl may lead to cell shrinkage (205), and less dye uptake.

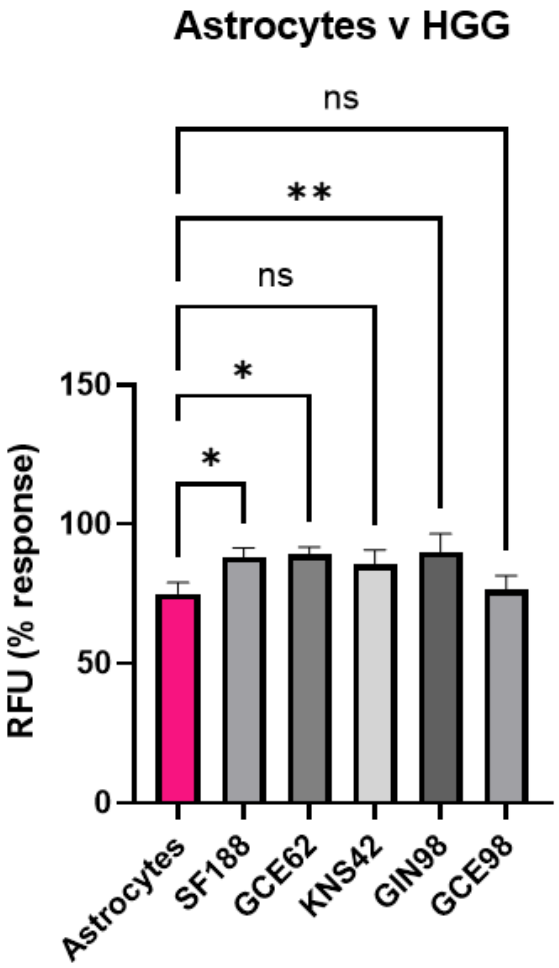

Figure 5.7 Differences in membrane potential between HGG cells and astrocytes measured via membrane potential fluorescence assay. Data is represented as the total percentage response when normalised to a control (100%). Astrocytes have a significantly increased RFU % change when compared to SF188, GCE62 and GIN98 cells. N=3, statistical testing via 1 way ANOVA with multiple comparisons. Means +/- SD.

5.2.2.1 IAA94 and metformin treatment cause membrane potential changes in pHGG

In the pursuit of further understanding the role of membrane potential, and after determining baseline readings of resting membrane potential values, we undertook a series of experiments to ascertain the effect of CLIC inhibition on the membrane potential of pHGG cells.

Earlier we demonstrated that pharmacological inhibition of CLIC1 and CLIC4 result in a reduction in cell viability, and in chloride efflux across the cell, therefore we sought to assess if this change was linked to alterations in membrane potential. Treatment with IAA94 at 50 and 100µM is sufficient to cause alterations in the membrane potential across SF188, GCE62 and KNS42 cells. Hyperpolarisation, as demonstrated by a reduction in RFU % (relative to control conditions), was seen across all cell lines, with the most significant reduction in RFU in the primary cell line, GCE62. The overall reduction in RFU for SF188 cells was 13%, GCE62 was 16% compared to a 10% reduction in KNS42 cells. Previous literature has cited that a reduction in 5% is relative to a -10mV change (Molecular Devices (204)), and as such this may be representative of a -26mV, -32mV and -20mV change in membrane potential in the cells, respectively. These changes in Vm are sufficient to induce changes in downstream cellular function but it is not yet possible to link these to specific mechanisms.

SF188 cells seemed to possess the most linear relationship between concentration of IAA94 and overall RFU, with GCE62 seeing the largest change in Vm (figure 5.8a). Interestingly, this data conflicts previous findings as GCE62 are evidenced to be the least sensitive cell line to IAA94 in both viability assays and Cl- efflux assays. This may be a result of compensation mechanisms via alternate chloride channels that do not have significant contribution to membrane potential control.

In addition to exploring the effect of IAA94 of Vm, the broad Cl- channel blocker metformin was assessed (figure 5.8b). Treatment was carried out at 100µM, 10mM and 50mM to assess if any concentration dependant changes occur. When treating cells with 100µM (to simulate clinically feasible treatment range) no effect on membrane potential in any of the cell lines was observed. However, there is significant reduction in % RFU seen in both the 10mM and 50mM treatment conditions. As expected, the 50mM treatment condition elicited the most significant cellular hyperpolarisation. In order to maintain comparability, the 10mM condition was assessed. Analogously to the data gained from IAA94 experiments, KNS42 cells appear to be the least sensitive cell line, with a decrease of 8% at when treated with 10mM (~ -16mV). SF188 exhibited the highest level of sensitivity, with a 12% reduction (~ -26mV) and GCE62 showing a 10% decrease (~-20mV).

These data suggest that pharmacological targeting of CLIC1 and CLIC4 via IAA94 or metformin may be sufficient to cause hyperpolarisation of the membrane, and as such, more reflective of the Vm observed in astrocytes.

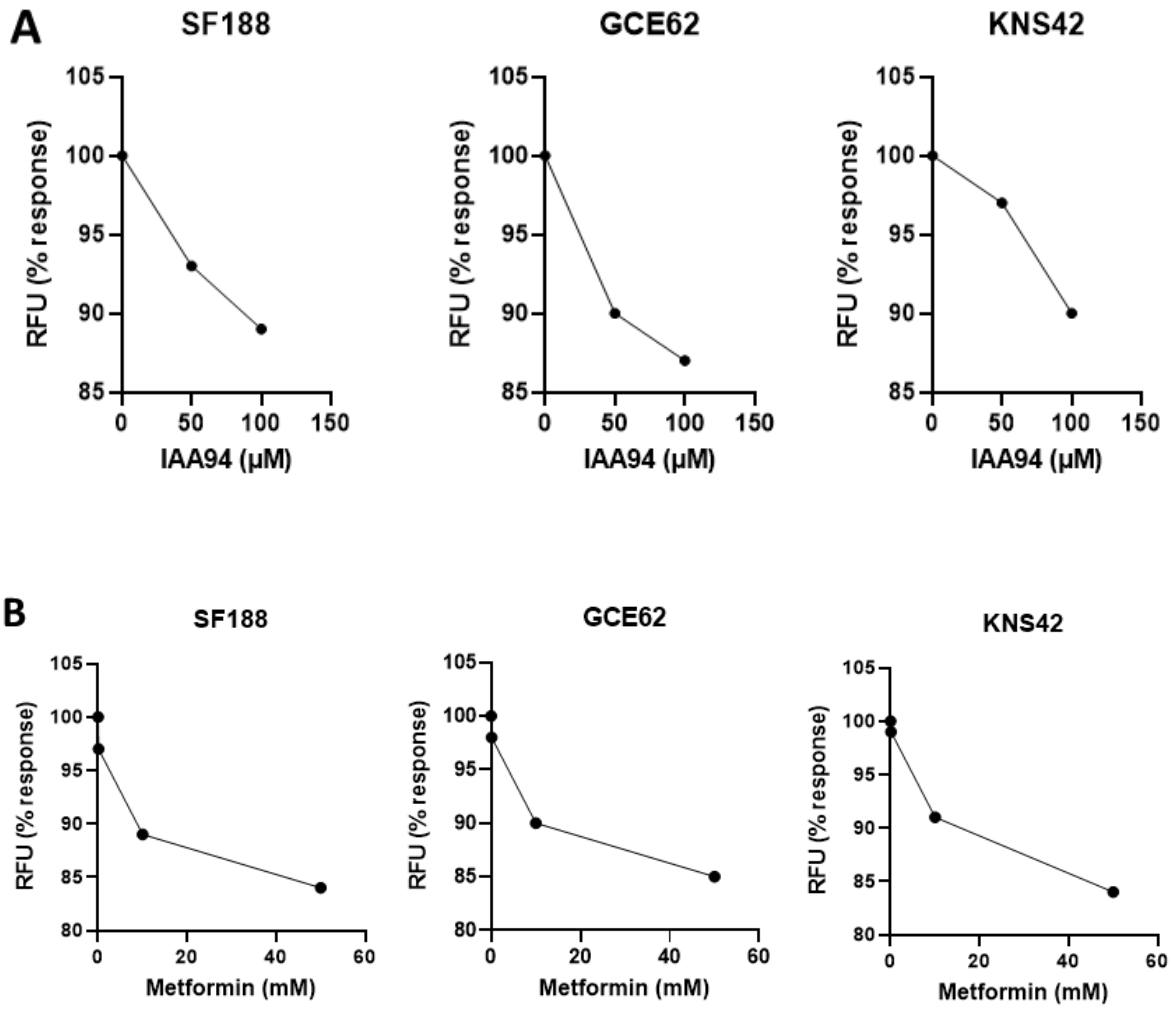
A
SF188
GCE62
KNS42
RFU (% response)
105
100
95
90
85
0
50
100
150
IAA94 (μM)
B
SF188
GCE62
KNS42
RFU (% response)
105
100
95
90
85
80
0
20
40
60
Metformin (mM)

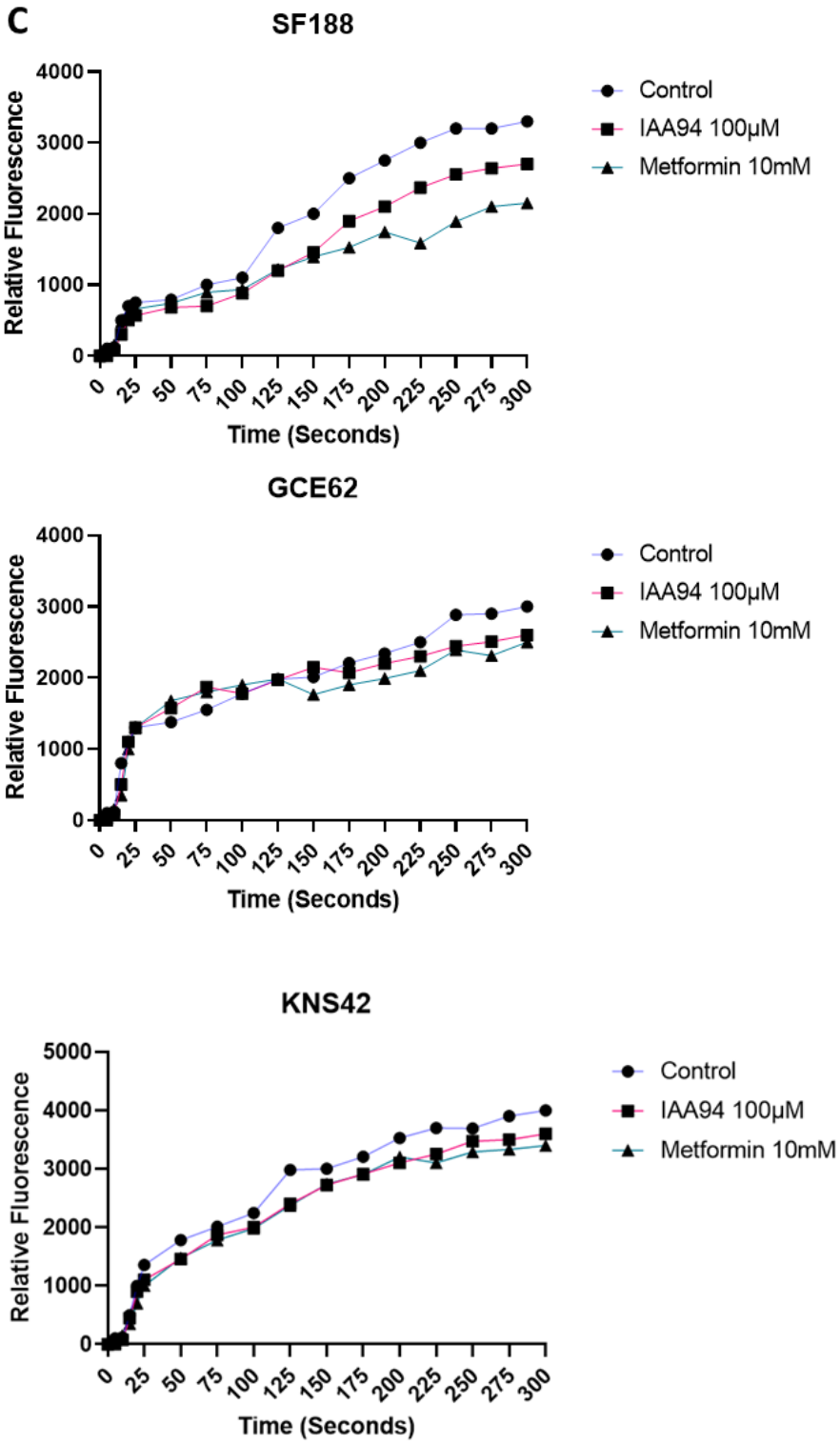

Figure 5.8 Changes in membrane potential as measured via fluorescence in pHGG in response to pharmacological treatment. Relative fluorescent units as measured as a percentage of the total response seen in control conditions (100%). Traces analysed via using the area under curve function on SoftMax Pro software. A) IAA94 alters membrane potential in HGG cells in a dose dependant manner. B) Metformin treatment at 100Um has no effect on membrane potential, but treatment at 10mM causes reduction in RFU count. C) Representative reduced traces of cells treated with IAA94 or metformin.

5.2.2.2 *Membrane potential changes following CLIC1 or CLIC4 knock down in pHGG.*

To explore CLIC1 and CLIC4 specific roles in the membrane potential of cells we combined siRNA targeting with FLIPR membrane potential assays. Figure 5.9A shows that CLIC1 deficient KNS42 cells exhibited no significant differences in membrane potential when compared to NT cells. Despite this, there was significant cellular hyperpolarisation seen in SF188 (11%) and GCE62 cells (15%) on CLIC1 KD. CLIC4 targeting was sufficient to cause membrane potential alterations across all cell lines, with an average hyperpolarisation of 10%, 11%, and 8% in SF188, KNS42 and GCE62 respectively (figure 5.9B).

Interestingly there appears to be less of an effect on membrane potential following siRNA knock down of CLIC1 and CLIC4. This may be due to a myriad of reasons, the first being any off target affects associated with drug treatment, and an immediate effect of drug spiking during the experiment. These elements should be further explored.

All together, these data confirm that targeting of CLIC1 and CLIC4 via pharmacological inhibitor or siRNA results in varying degrees of membrane hyperpolarisation. As such, this hyperpolarisation is the likely cause of the cell cycle alterations and reduced invasive and proliferative capacity of the cells explored in chapter 4. It is well understood that membrane potential is essential in cell cycle control, proliferation, and invasion (104), with cell membrane alterations being specifically implicated in glioma pathology (189,199,200).

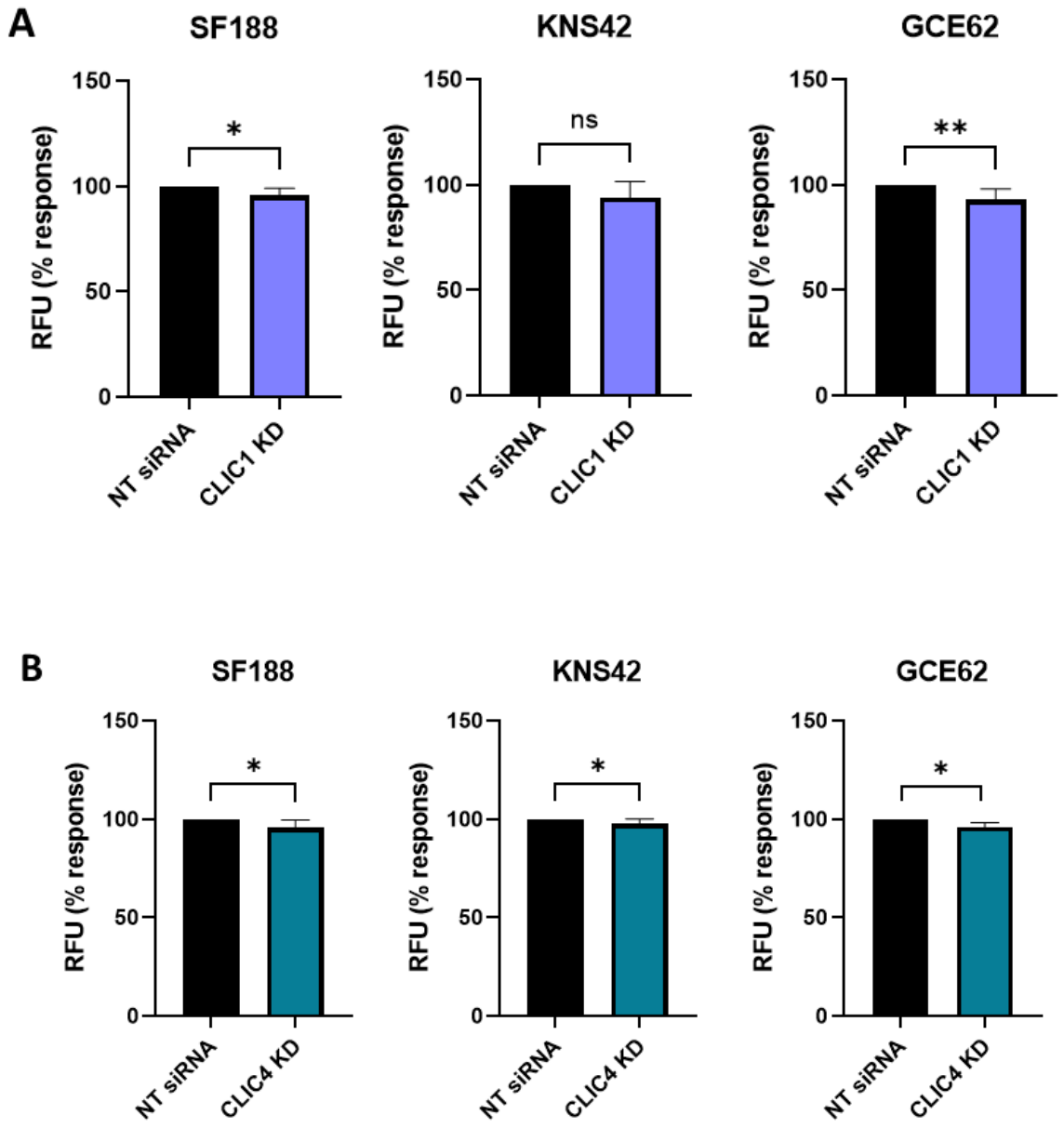

Figure 5.9 siRNA targeting of CLIC1 and CLIC4 causes significant alterations in membrane potential. A) knock down of CLIC1 results in a significant percentage change in RFU when compared to control siRNA in SF188 and GCE62 cells. B) CLIC4 knock down results in significant increase in RFU response when compared to normalised control (100%). N=3, unpaired t-test.

5.2.3 Electrophysiology of pHGG cells.

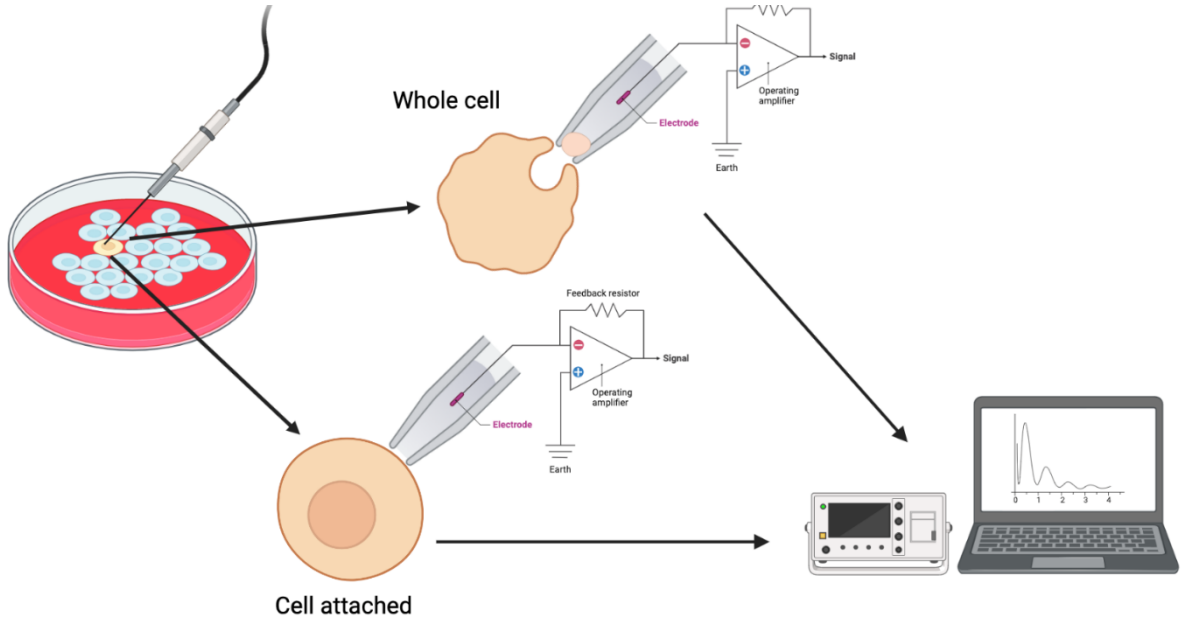

Figure 5.10 Workflow schematic of whole cell and cell attached patch clamping experiments.

5.2.3.1 Cell attached experiments.

To assess channel activity cell attached (CA) electrophysiological experiments were performed. This methodology as shown in figure 5.10 is completed by attaching an electrode to the membrane of a cell and forming a gigaohm seal without breaking the membrane. This methodology preserves intracellular integrity and can be used to both measure single channel activity and properties, as well as estimate cellular RVM in situ. The membrane potential of the cell-attached patch (Vpatch) is a function of the membrane potential of the cell (Vcell) and the potential applied via the patch pipette (Vpipette), and is defined by the formula: (Vpatch) = (Vcell)-(Vpipette).

Figure 5.11 demonstrates representative single-channel current records made with the cell-attached configuration. The pipette holding potential was 0mV so that the channel activity observed is typical of that at the resting membrane potential of the cell with the peaks on the oscilloscope trace representing ion channel activity. Using the cell attached

configuration we saw that SF188 cells often possesses two main types of ion channel: the large amplitude BK (confirmed via experimentation not included in this thesis) and a smaller one, with single-channel conductance's of ~ 160 pS and ~50pS, respectively. Conversely, GCE62 cells appear to possess the small amplitude channel, likely chloride due to the composition of the bath solution.

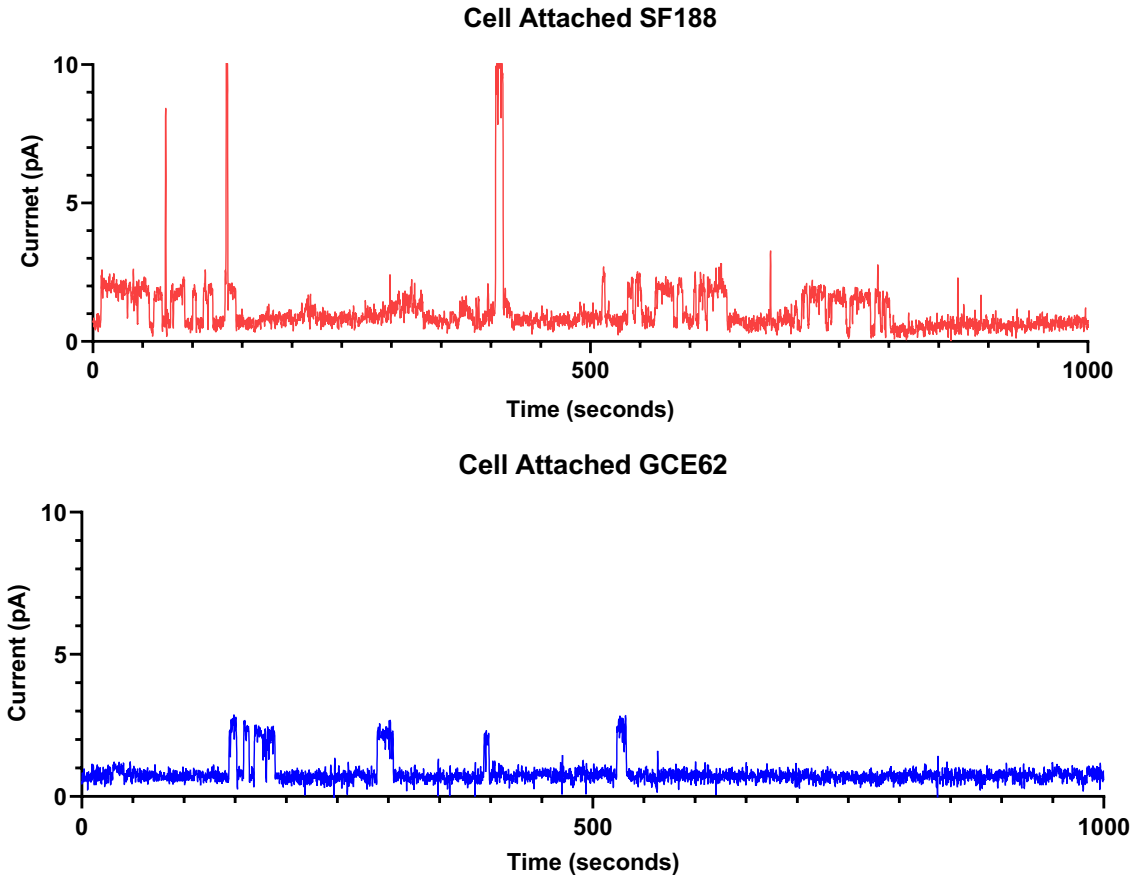

Figure 5.11 representative traces of SF188 and GCE62 cells in the cell attached configuration. Measurement of current against time in cell attached configuration. Upward deflections in the current trace represent single channel opening. Note two types of channels in SF188 and one type in GCE62**.**

5.2.3.2 Whole cell experiments

To assess the activity of multiple channels across the cell membrane as a whole, whole cell (WC) patch clamp configuration was employed. As shown in figure 5.10 whole cell

experiments measure channel activity in the form of macroscopic current across a large region of the cell by rupturing the cell membrane. This provides access to the intracellular region of the cell, and provides a means to study the effect of drugs etc. on the action of ion channels intracellularly.

Figure 5.12 shows representative whole-cell current records made with the whole-cell configuration. Currents were elicited in response to voltage steps from -50 to + 80 mV in 10 mV increments from a holding potential of -60 mV.

SF188 cell possessed both linear and voltage-sensitive currents (figure 5.12), the latter were activated at positive membrane potentials (positive to -50mV), indicative of the voltage sensitive BK channels observed in cell attached experiments. Conversely, the GCE62 cells only possessed linear currents. The linear component is probably carried by the small amplitude channel seen in the cell-attached experiments. These data indicate to us how these cells respond to changes in Vm, therefore alteration in membrane potential result in BK channel activity in SF188 cells. However, without pharmacology we cannot confirm that these channels are indeed BK. On-going experiments with the BK channel inhibitor paxilline suggest that these currents are indeed BK (data not shown in thesis).

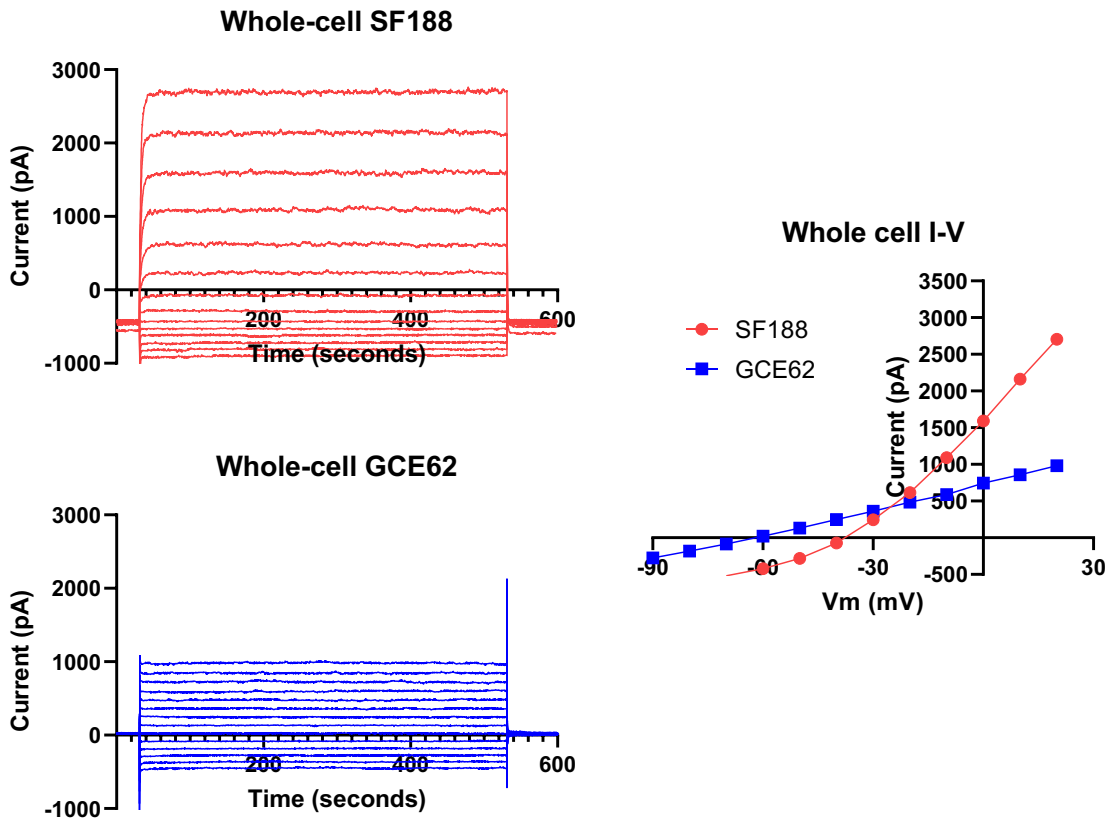

Figure 5.12 representative traces of SF188 and GCE62 in whole-cell configuration. SF188 and GCE62 ion channel activity was assessed using whole cell patch clamping using a voltage step method and a holding potential of -60mV.

5.2.3.3 SF188 cells have spontaneous BK channel activity.

Recordings show that 21 out of 26 patches had large inward currents >4pA at Vp=0 that are indicative of BK channels. This is consistent with data that has been previously published on glioma cell lines. (161,206,207). Single channel current-voltage analyses indicated a voltage activation with a median slope conductance of around 210pS (figure 5.13). Several patches had smaller single-channel current amplitude, although these cannot be soundly identified without further experimentation. Figure 5.13a shows that that Vm measured in SF188 cells with high [Ca^{2+}] pipette solution (2.5mM) (Vm1) was 14.9 mv more negative (p=0.0043) than that measured with low [Ca^{2+}] (45nM) (Vm0) suggestive of K^+ channel activation by elevation of intracellular [Ca^{2+}]. Figure 5.13b show that the

input in high [Ca^{2+}] resistance (Rm1) was 240 MΩ smaller (p=0.0443) relative to that measured with low [Ca^{2+}] (Rm0). Data is also indicative of greater channel activity with elevation of intracellular [Ca^{2+}] in this condition, and that SF188 possess BK channels that can be activated by elevations in intracellular [Ca^{2+}] and Vm depolarisation. As such, suggesting that SF188 cells are significantly electrically active cells. This is consistent with data that has been previously published on glioma cell lines, suggesting that BK channels are over expressed in GBM cell lines (161,207).

From the single-channel current-voltage analyses of Bk it is possible to estimate the membrane potential Vmr of the cell from the pipette potential, Vp, when the electrochemical driving force is zero and the single-channel amplitude i = 0 pA.

If it is assumed that Bk is predominantly permeable to K^+ then its single channel current amplitude, i , is given by $^{i=slope\ conductance\ x\ (Vmr-Vp-EK)}$ where EK is the Nernst equilibrium potential for K^+.

If it is assumed that the pipette solution has a similar [K^+] to that of the cytosol, ~140mM, then the Nernst equilibrium potential for K^+ , EK, is 0 mV. Such that, when $^{i = 0\ pA.\ Vp = Vmr}$.

When Vmr was estimated this way it was almost identical to Vm0 subsequently measured in the same cell under whole-cell conditions with a low [Ca^{2+}] pipette solution (p=0.9221, Paired t test)(Figure 5.15); data that consolidates Vm0 as a reliable measure, free from effects of the pipette solution formulation. This confirms that the constituents of the pipette solution has no direct effect on the membrane potential readings for SF188 cells.

Taken together this data indicates that SF188 cells exhibit spontaneous channel activity of BK at rest in cell-attached mode, and that going whole cell with a high [Ca^{2+}] activates Bk to decrease Rm and hyperpolarize Vm. The presence of high [Ca^{2+}] in the whole-cell pipette

solution was also associated with an outwardly rectifying current-voltage relationship ($p=0.002$, Fisher's exact test) (not shown).

To further explore the electrical activity of CLIC1 channels in SF188 cells, the CLIC1 specific antagonist IAA94 was used. Figures 5.14 demonstrated that 72-hour incubation in 100 μM IAA94 neither affected Vm nor Rm in SF188 cells, respectively. This combined with the data finding elevated BK channel activity indicate that CLIC channels are not the predominant channel type acting in SF188 cells and therefore are not driving the Vm of the cell.

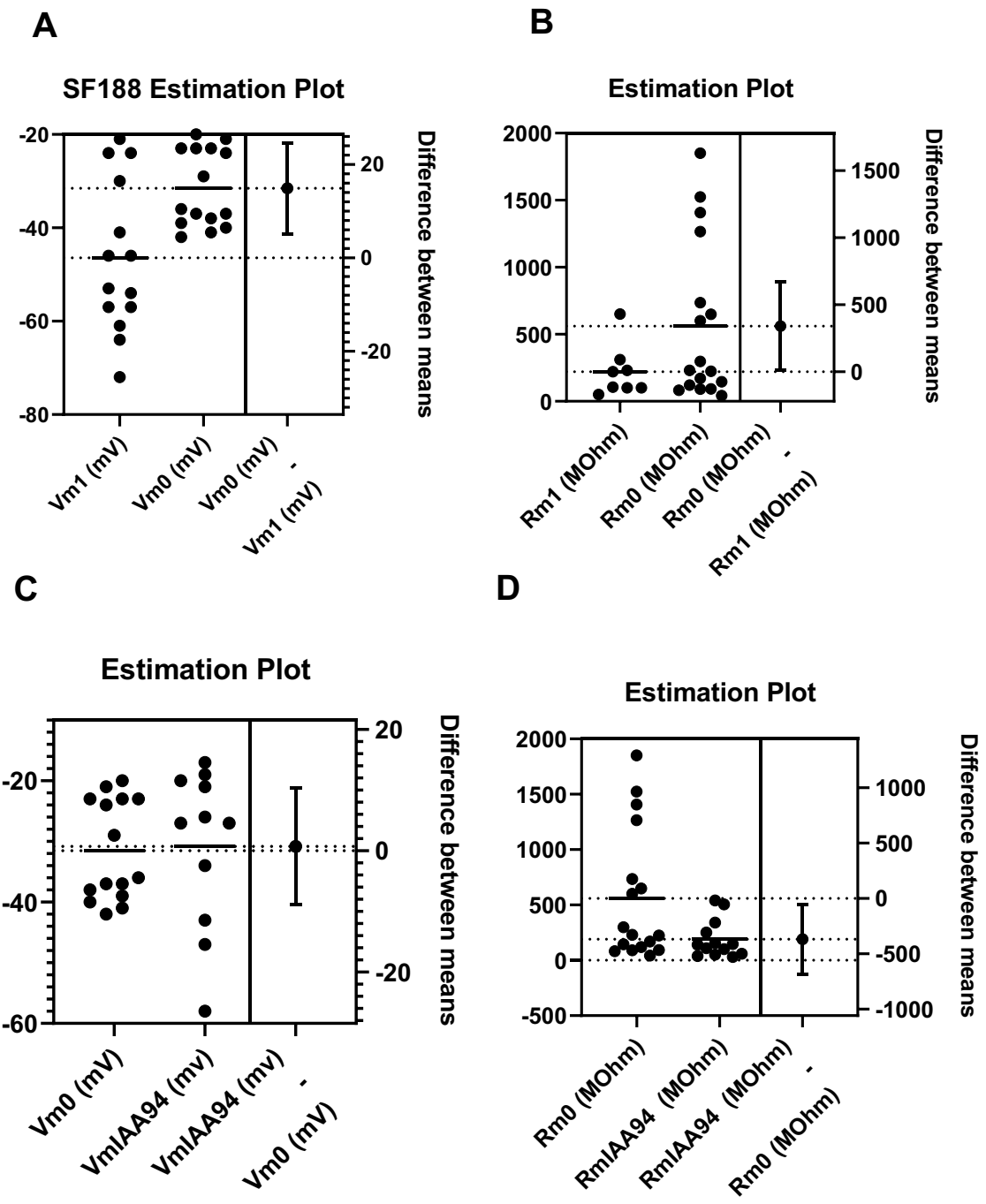

Figure 5.13 Comparison of membrane potential and input resistance of SF188 under a variety of conditions. A) Comparison of membrane potential measured from different cells with high (Vm1) and low (Vm0) [Ca2+] in the pipette solution. B) Comparison of input resistance measured from different cells with high (Rm1) and low (Rm0) [Ca2+] in the pipette solution. C) Comparison of membrane potential measured from different cells all with low [Ca2+] in the pipette solution under control conditions (Vm0) and after 72 hr incubation in 100 µM IAA94 (VmIAA94). D) Comparison of input resistance measured from different cells all with low [Ca2+] in the pipette solution under control conditions (Rm0) and after 72 hr incubation in 100 µM IAA94 (RmIAA94). Each point is measured from a different cell. Differences are indicated as mean ± S.D.

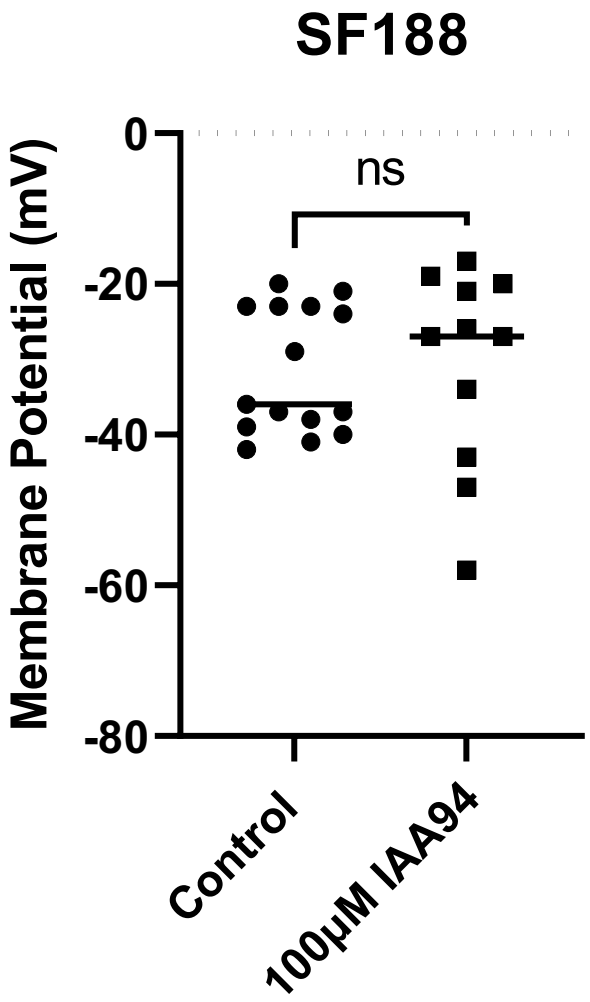

Figure 5.14 Treatment with IAA94 does not cause significant changes to SF188 membrane potential. The membrane potential of IAA94 treated and control SF188 cells was measured**.** Cells were pre-treated with 100µM IAA94 for 72 hours. Each point is measured from a different cell. Differences are indicated as mean ± S.D. Statistical analysis via paired t-test. Repeated data from figure 5.13 shown for clarity of point.

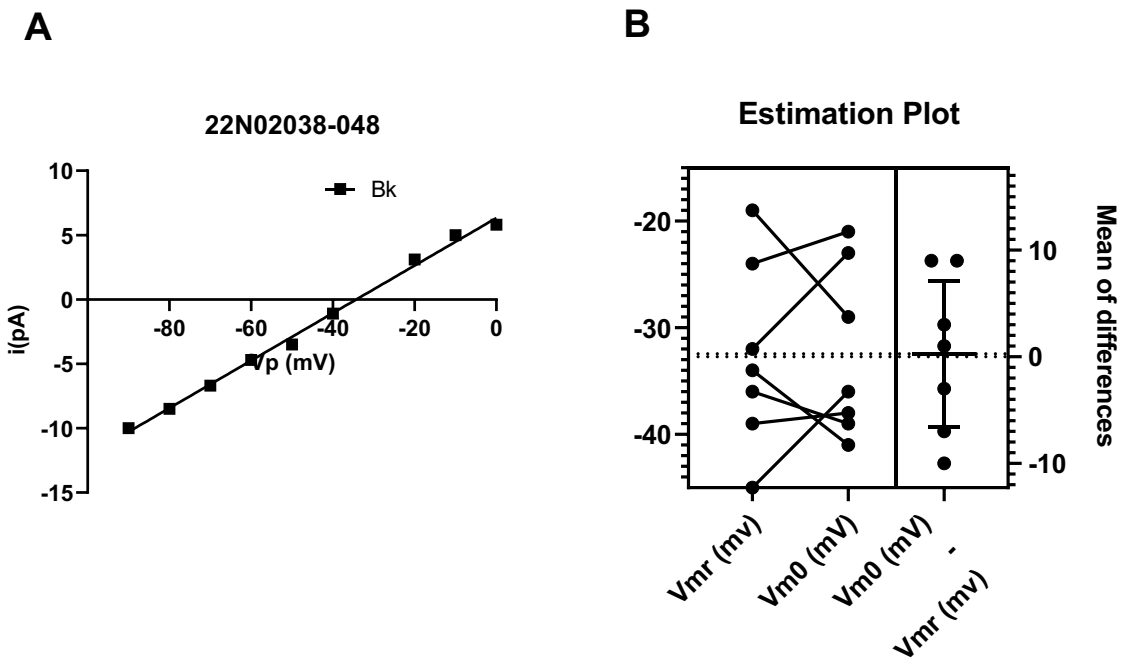

Figure 5.15 Representative single-channel current voltage relationship of Bk channel measured on a SF188 cell. Each point is the median of 5 individual amplitude determinations. Solid line is fit by linear regression. In this case the slope is 185 pS and Vmr is -34 mV. B) Pairwise comparison of membrane potential estimated from the single-channel current voltage reversal potential (Vmr) and that measured in the same cell (Vm0) on whole-cell with low [Ca^{2+}] in the pipette solution .

5.2.3.4 GCE62 cells lack large outward currents but have CLIC1 activity.

To explore the differences in ion channel activity between SF188 (commercial line) and in-house primary line GCE62, the above experiments were repeated. In cell–attached mode 1 out of 30 GCE62 cells had a large inward current >4pA at Vp=0 indicative of BK channels. This is different to the dominating presence of BK channels found in SF188 cells. Figure 5.16 shows when using the whole cell configuration, the presence or absence of [Ca^{2+}] in the pipette solution had no significant effect on the magnitude of the resting membrane potential, Vm, input resistance, Rm, or the presence of outward rectification.

To further explain, Figure 5.16a shows that Vm measured with high [Ca^{2+}] pipette solution (Vm1) was not significantly different (p=0.5426) to that measured with low [Ca^{2+}] (Vm0). Similarly, Figure 5.16b demonstrates that the input resistance Rm was also not different

(p=0.87, Unpaired t-test) in high [Ca^{2+}] (Rm1) relative to that measured with low [Ca^{2+}] (Rm0). Taken together this data indicates that GCE62 cells possess little activity of BK channels, and that using a whole cell configuration with a high [Ca^{2+}] is insufficient to activate any Bk to decrease Rm and hyperpolarize Vm. An outwardly rectifying whole-cell current-voltage relationship was not observed in these cells.

The resting membrane potential of GCE62 cells was 10 mV more hyperpolarized (p=0.035, Unpaired t-test) than that of SF188 when measured whole-cell with a low [Ca^{2+}] pipette solution (Figure 5.16).

In order to assess the CLIC1 channel activity in GCE62 cells, the CLIC1 specific inhibitor was used to block CLIC1 chloride currents. Figures 5.16c and 5.17 demonstrated that 72-hour incubation in 100 μM IAA94, a selective CLIC1 antagonist significantly depolarized Vm by 12.8 mV (p=0.0297) however Rm was unaffected (p=0.1377). This data confirms that CLIC1 channels are active in GCE62 cells.

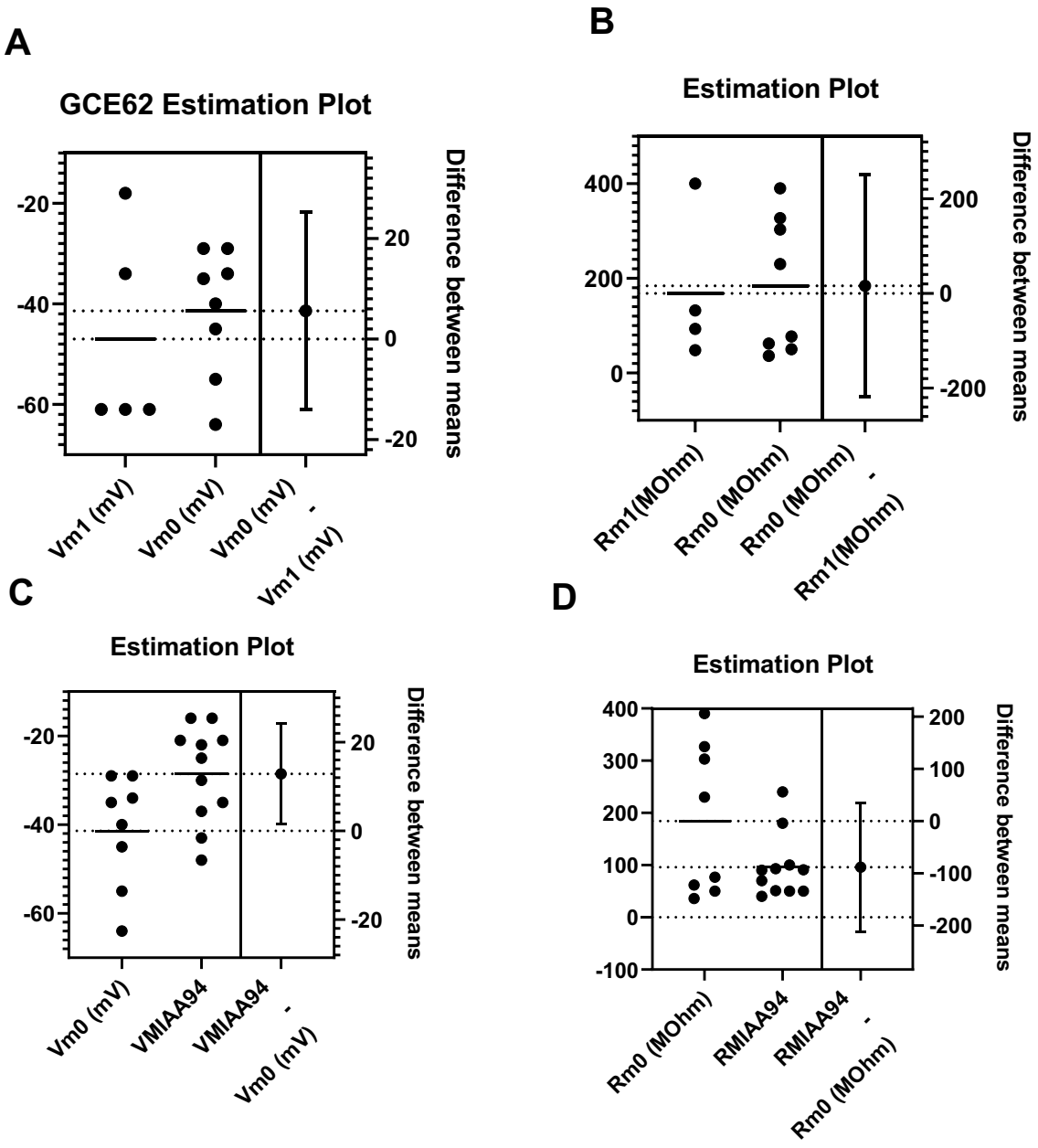

Figure 5.16 Comparison of membrane potential and input resistance of GCE62 under a variety of conditions. A) Comparison of membrane potential measured from different cells with high (Vm1) and low (Vm0) [Ca2+] in the pipette solution. B) Comparison of input resistance measured from different cells with high (Rm1) and low (Rm0) [Ca2+] in the pipette solution. C) Comparison of membrane potential measured from different cells with low [Ca2+] in the pipette solution under control conditions (Vm0) and after 72 hr incubation in 100 µM IAA94 (VmIAA94). D) Comparison of input resistance measured from different cells with low [Ca2+] in the pipette solution under control conditions (Rm0) and after 72 hr incubation in 100 µM IAA94 (RmIAA94). Each point is measured from a different cell. Differences are indicated as mean ± S.D.

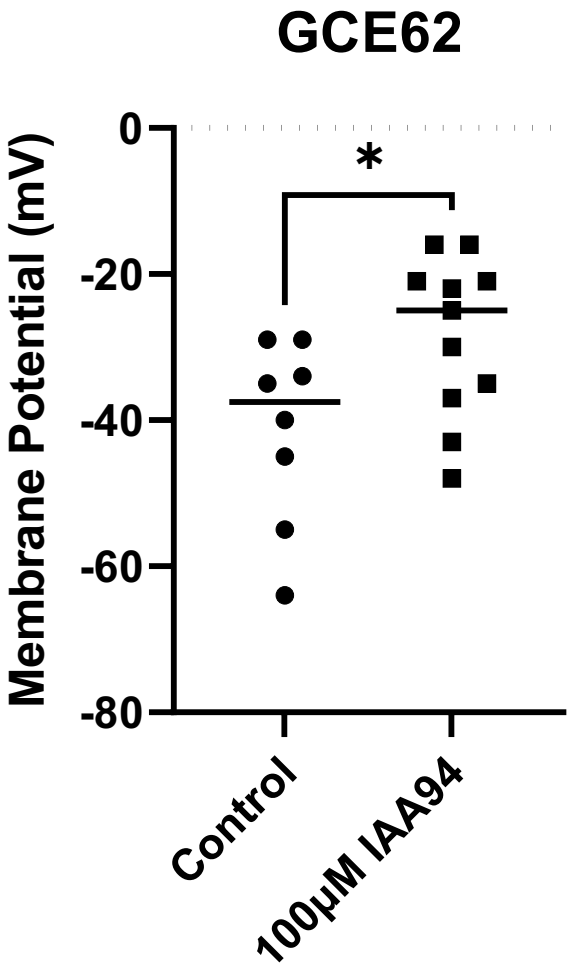

Figure 5.17 Treatment with IAA94 causes significant changes to GCE62 membrane potential. The membrane potential of IAA94 and control GCS62 cells was measured**,** Cells were pre-treated with 100µM IAA94 for 72 hours. Each point is measured from a different cell. Differences are indicated as mean ± S.D. Statistical analysis via paired t-test. Figure repeated from data in figure 5.16 to show clarity.

5.2.3.5 *The membrane potential of pHGG cells is not significantly different to normal astrocytes.*

Comparison of the membrane potential of SF188, GCE62 and normal human astrocyte cells was carried out. Figure 5.18 shows that there is a significant difference in the membrane potential between SF188 and GCE62 cells. The average membrane potential of SF188 cells was significantly more depolarised than GCE62 cells. Interestingly, there was no significant differences in the membrane potential seen in normal human astrocytes when compared to pHGG GCE62 cells. Here we see high levels of variability in the average membrane potential reading of astrocytes, with a range of -18mV to -59mV. Despite the variability, these data were significantly different to the suggested membrane potential readings that have been described in the literature (208–210). Several studies have found that astrocytes have a highly negative membrane potential, being significantly more hyperpolarised than other brain cells (104). Not only does an average Vm reading of -30mV conflict with the literature, it also conflicts with findings from high through put assessment of membrane potential found previously in this chapter, whereby astrocytes were notably more hyperpolarised than HGG cell lines. To gain further insight into the resting membrane potential of astrocyte further experiments should include assessment of astrocytes derived from neural stem cells. Although not transformed, the astrocyte line use in this work is not

post mitotic, as such; this retention of replicative capacity may mean it is not wholly reflective of normal human astrocytes *in vivo*.

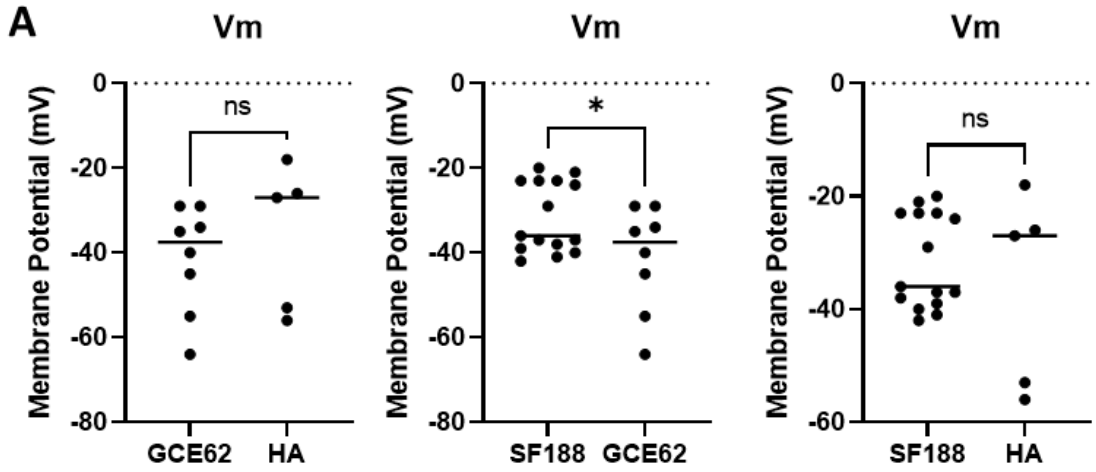

Figure 5.18 Comparison between the membrane potential measured from Human astrocytes, SF188 and GCE62 with low [Ca^{2+}] in the pipette solution. Each point is measured from a different cell. Differences are indicated as mean ± S.D.

5.2.4 CLIC1 and CLIC4 have bioelectrical capacity in pHGG.

As demonstrated via electrophysiology, voltage dye and fluorescent assays above, CLIC1 and CLIC4 harness an electrical capacity in pHGG cells, and therefore present as valuable bioelectric targets for candidacy in therapy. These data give us an overall idea as to whether the CLIC channels are functioning as their integral membrane protein form, and therefore whether CLIC activity is acting to potentiate the cell cycle and aid proliferation of these cells. Inhibition of these proteins results in a reduction of channel activity, indicating that CLICs are acting in their ion channel form.

Despite this we cannot conclusively say that CLIC1 and CLIC4 are acting solely in their ion channel form, and that they are exclusively exerting an ion channel role. It is likely that CLIC1 and CLIC4 insert themselves into the membranes of glioma cells when experiencing specific pressures, as demonstrated by our exploration of the role of hypoxia and acidosis on the localisation of CLIC1 and CLIC4. The contribution of CLIC1 and CLIC4 to the tumorigenesis and invasive properties of glioma cells is likely due to a combination of the myriad of roles they perform. As such, targeting CLIC channels will enable us to target a multitude of functions, as well as manipulating the electrical properties of the cell, and cell cycle.

To further investigate the role of CLIC channels more in-depth electrophysiology experiments will be performed, whereby a myriad of channel blocking experiments will aim to elucidate the key ion channel activity across the cells. Additionally, the role of CLIC channels could be further explored by performing pull down experiments, and assays to explore the enzymatic function of CLIC1 by substrate specific targeting.

5.3 Electrotherapies in the treatment of pHGG

5.3.1 Tumour Treating Fields

Tumour treating fields therapy was applied directly to cells via the Inovitro *in vitro* TTFields generator (Optune, Haifa). Previous work by Dr Branter optimised the frequency of treatment on panel of aHGG cell lines (152), and along with the literature suitable treatment range is suggested to be between 100-500kHz (72). As such, treatment parameters were set at 200kHz alternating electrical fields (1-3v/cm) for 72 hours.

5.3.1.1 Treatment with TTFields reduces cell viability and count.

A panel of pHGG cells (SF188, KNS42 and GCE62) cells were exposed to TTFields at 200kHz for 48 and 72 hours. We found that all cell lines were sensitive to TTFields and that there was a significant decrease in cell count observed in a time dependant manner (figure 5.19). SF188 and KNS42 cells were the most sensitive to TTFields with an average overall reduction in cell viability of 51% and 61% respectively ($p = <0.0001$). This was mirrored with a decrease in cell count by 55% (SF188) and 60% (KNS42) when taken as a percentage of control cells. However, KNS42 cells demonstrated the most variable effects, with remaining viable cells ranging from 20% to 50% across four experimental replicates. Importantly variability across wells (internal replicates) was limited. The overall decrease in viability of the primary GCE62 cells was 47%, being the least sensitive of the cell lines in the panel ($p=<0.001$).

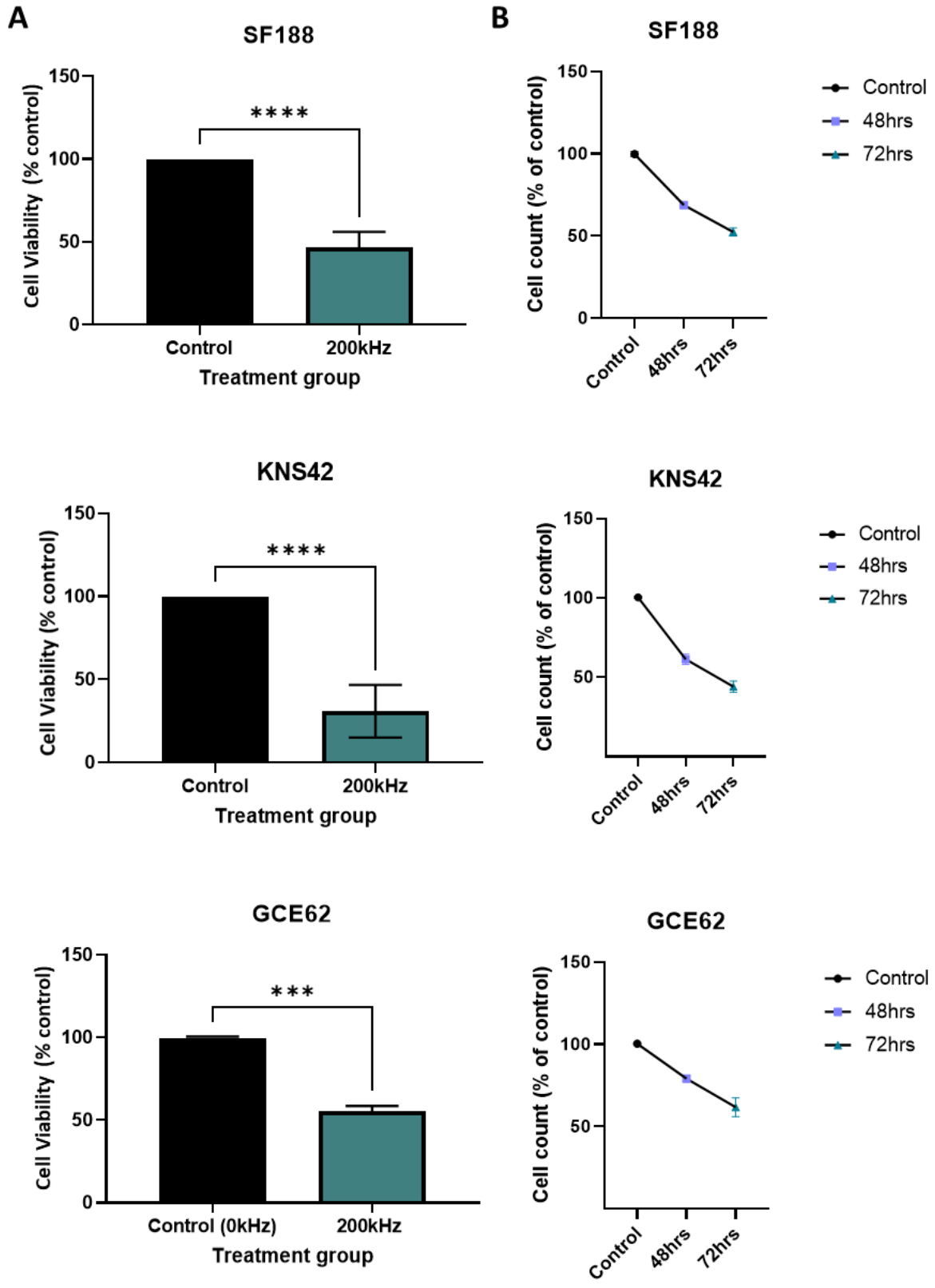

Figure 5.19 Treatment with TTFields significantly reduces cell viability and cell count. A) Cell viability of SF188, KNS42 and GCE62 cells following TTFields exposure via Inovitro *in vitro* TTFields device at 200kHz for 72 hours. B) cell count of cells treated with TTFields at 48- and 72-hours treatment. N=4, statistical testing by paired t-test.

5.3.1.2 *Neurospheres are significantly more resistant to TTFields than 2D monolayer cells.*

As 3D culture is well known to be a more biologically appropriate model of investigating cancers, we sought to assess the effect of TTFields on neurosphere culture. A plethora of studies have identified that 3D culture confers treatment resistance in a variety of settings such as in chemotherapeutic and radiosensitivity assays, when compared to monolayer culture. In order to recapitulate a tumour representative model and assess the sensitivity to TTFields, neurospheres were grown for three days until maturity, trypsinised, re-seeded into non-adherent wells for 24 hours at low confluency and allowed to reform neurospheres. Once spheres had formed, cells were transferred to the Inovitro device, and treated for 72 hours, and their size and viability measured.

Previous experiments used to assess the viability of pHGG neurospheres failed due to poor penetration of the PrestoBlue reagent into the sphere. However, following a method alteration which included dissociating the neurospheres with a pipette prior to PrestoBlue assay, we found consistent results, with biological and technical replicates being within a consistent range of each other. As such, these data have been included as they are deemed acceptable and reliable.

We have found that TTFields treatment is successful at significantly reducing the viability of KNS42, SF188 and GCE62 neurospheres following exposure for 72 hours. SF188 and GCE62 neurospheres were found to be overall more sensitive to TTFields than KNS42 neurospheres, with an average reduction in viability of 45% and 41% respectively, compared to an 18% reduction in viability observed in KNS42 neurospheres.

An explanation to this may be due to the size of the KNS42 neurospheres. Experiments detailed in chapter 4 found that KNS42 cells form the largest and most consistent neurospheres. This may result in reduced penetration of the alternating electrical fields

generated by the Inovitro device, thus imposing a diminished overall therapeutic effect across the spheres. Additionally, larger spheres ten to upregulate resistance genes that are associated with chemo and radio-resistance and as such, the same may be true for TTFields.

Subsequently, we wanted to further scrutinise the data, and assess any differences in treatment efficacy observed between 2D and 3D culture. As hypothesised, we find that SF188 and KNS42 pHGG cells that are cultured as neurospheres are significantly more viable following TTFields exposure. SF188 cells are 20% more viable, whereas KNS42 neurospheres are 38% more viable than their 2D counterparts are. GCE62 neurospheres did not show any significant resistance to TTFields.

Interestingly, we have previously found that neurospheres overexpress both CLIC1 and CLIC4 when compared to their monolayer standard culture. For ease of comparison (figure 5.20c) is repeated here. These data, in combination with the CLIC1 inhibition studies presented later in this chapter suggest that there may be a correlation between CLIC1 and CLIC4 levels and the efficacy of TTFields, and that an over expression of CLIC1 and CLIC4 as seen in the neurospheres may be protective to the HGG cells, and thus conferring resistance to TTFields treatment.

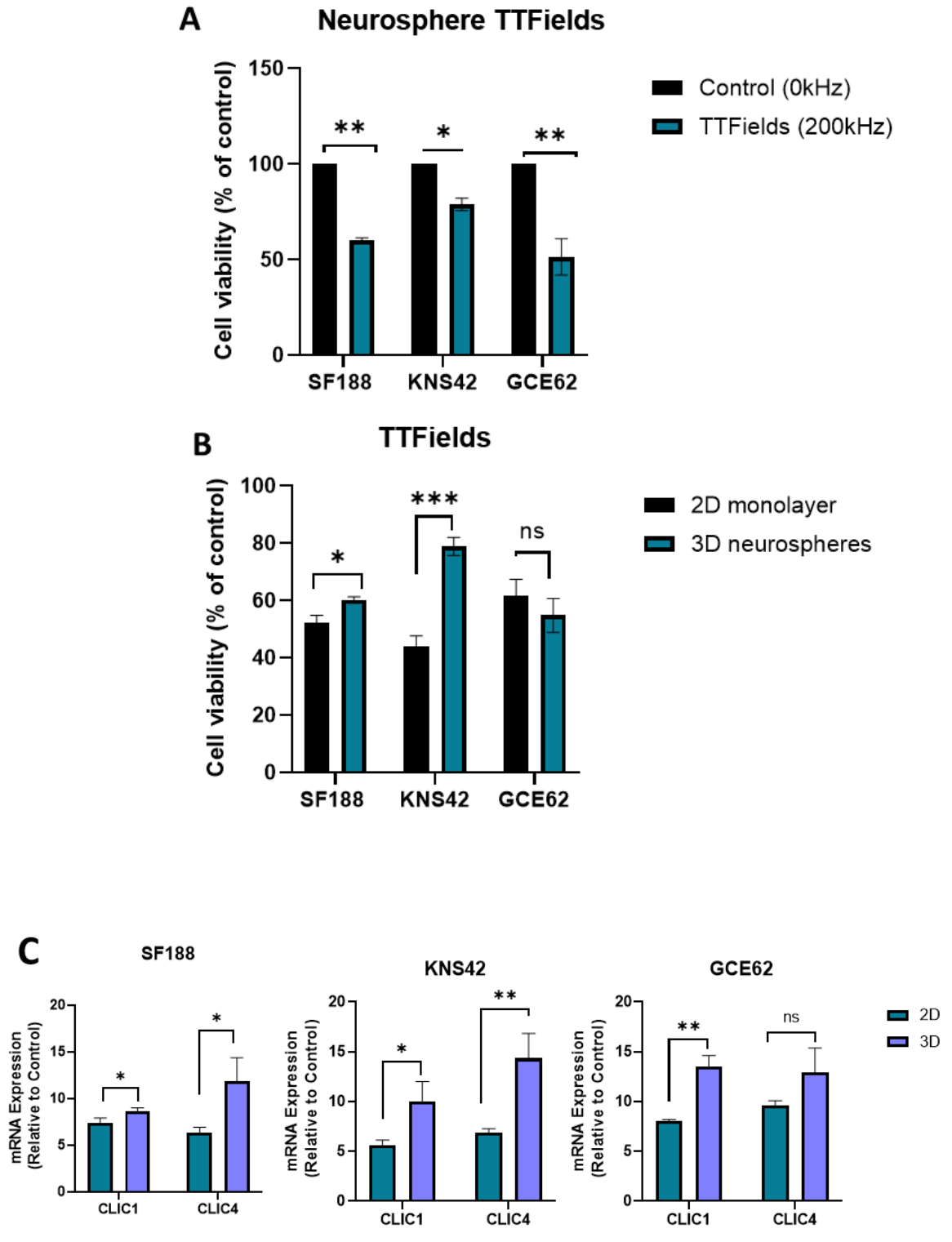

Figure 5.20 Neurospheres are more resistant to TTFields than pHGG monolayer culture. A) Cell viability of KNS42, SF188, GCE62 neurospheres exposed to TTFields (200kHz, 72 hours). Data presented at % viability of control neurospheres (0kHz, sham dish). B) Comparison of the viability (as shown as percentage of control) of 3D neurospheres and 2D monolayer culture of pHGG cells exposed to TTFields. C) Replicate image of the expression of CLIC1 and CLIC4 in 2D vs 3D culture of pHGG. N=3, statistical testing by T-test. P <0.05*, p <0.01 **, p <0.001 ***.

5.3.1.3 TTFields exposure does not prevent SF188 and KNS42 from forming neurospheres.

Further to the above work, we sought to assess if treatment with TTFields could prevent the formation of neurospheres post exposure to 200kHz alternating electric fields for 72 hours. The formation of neurospheres is suggestive of a clinically aggressive subset of cells with 'stem-like' properties, and as such we interrogated the effect of TTFields on the formation of these spheres. Cells were trypsinised following TTFields exposure and re-plated in neurosphere media in non-adherent plates for 72 hours, following which their size was measured.

As there is a significant decrease in both the viability and cell number of cells treated with TTFields, it would be appropriate to expect that there would be a reduction in the number of neurospheres forming, or a cessation neurosphere formation all together.

Unexpectedly, SF188 and KNS42 cells still form neurospheres following TTFields exposure, however there were fewer and smaller spheres formed when compared to controls and SF188 were very delicate, falling apart with slight agitation i.e., removing from incubator. The representative images in figure 5.21 show a large number of debris in the wells following TTFields treatment, which may be a result of unviable cells. Similarly, as observable in the representative images, a dark necrotic core was common in the KNS42 neurospheres that had been exposed to TTFields treatment.

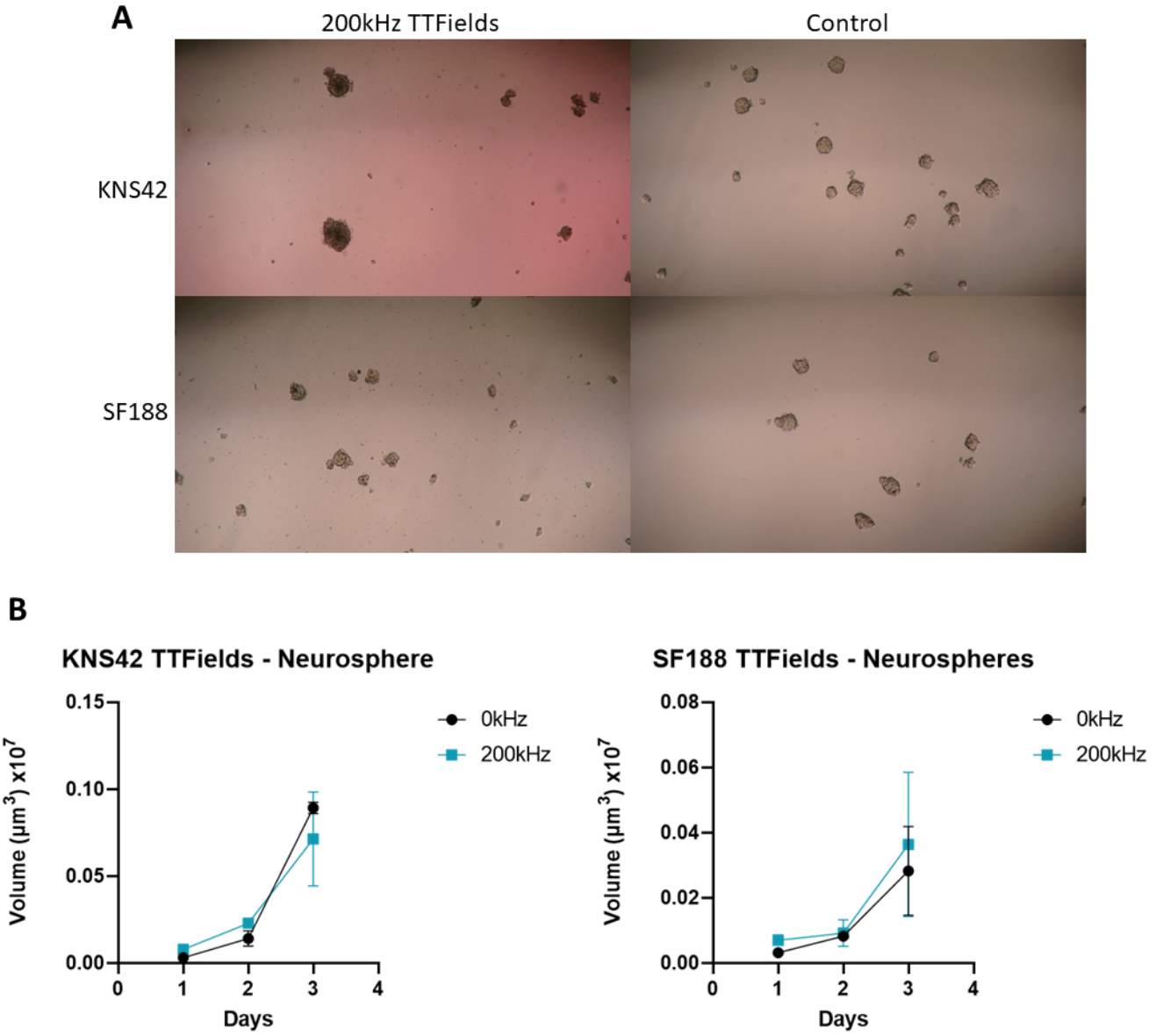

Figure 5.21 SF188 and KNS42 retain the ability to form neurospheres post TTFields. A) representative images of neurospheres exposed to TTFields treatment at 200kHz for 72 hours compared to control neurospheres. B) Quantification of the size of neurospheres across three days of growth. Magnification 10x Cells were cultured in non-adherent flasks in stem cell media for 4 days. Average neurosphere size was imaged daily and measured using ImageJ. N= 3**.** Scale bar = 250uM.

5.3.2 Deep brain stimulation

In order to deliver DBS treatment to cells, a panel of pHGG cells were plated in to t25 flasks and left to adhere overnight. To begin treatment electrodes were inserted into the filter cap of the flask and connected to a Neurostimulator. The optimum parameters for DBS electric fields were previously optimised by Dr Branter (152) via running a panel of voltages across a number of adult and paediatric brain tumour cell lines.

Cells were treated at a constant 10v, 130hz, 450µs pulse width continuously for 7 days. Flasks were filled with 20ml of media to ensure that the wire was completely covered, resistance across the flask was measured daily to ensure no unwanted spikes.

5.3.2.1 Treatment with DBS reduces cell viability and count.

Paediatric high-grade glioma cell lines KNS42, SF188 and GCE62 were exposed to DBS treatment for 7 days continuously, following this their viability was measured and cell count performed. We found that DBS electric fields demonstrate efficacy across all of the cell lines in the panel (figure 5.22). SF188 cell had the most significant decrease in viability at both day 5 and day 7, with over 60% reduction in viability and 50% reduction in cell count. KNS42 was the least sensitive at day 5, with only 47% reduction in viability, but was comparable to both GCE62 and SF188 at day 7 with 57% reduction compared to 60% and 65% in SF188 and GCE62, respectively.

It is worth noting that the treatment time for DBS (7 days) far exceeds that of TTFields (72 hours) with differences in the voltage that the cells were exposed to in DBS (10v) therapy vs TTFields (1-3v/cm). Two time points were selected to assess if the duration of treatment could be made more comparable. It was found in previous experiments that DBS treatment of aHGG cell lines have no significant effect on the viability at 3 days (the same treatment length as TTFields), so we sought to assess the viability of the cells at day 5 and day 7 time points.

DBS treatment appears to be comparable to TTFields treatment of pHGG cells, and in fact, more efficacious at day 7 with reduction in viability being greater in DBS treatment than TTFields. Despite the overall reduction in viability being greater, we found significant variability between each experimental repeat and biological repeats. This may be a direct result of the positioning of the wire in the flask, as previous work has identified that DBS

electric fields have diminishing intensity the further the cells are away from the wire. TTFields *in vitro* is well contained, with cells sitting in a small 24mm dish, and thus cells are exposed to more consistent intensities of treatment.

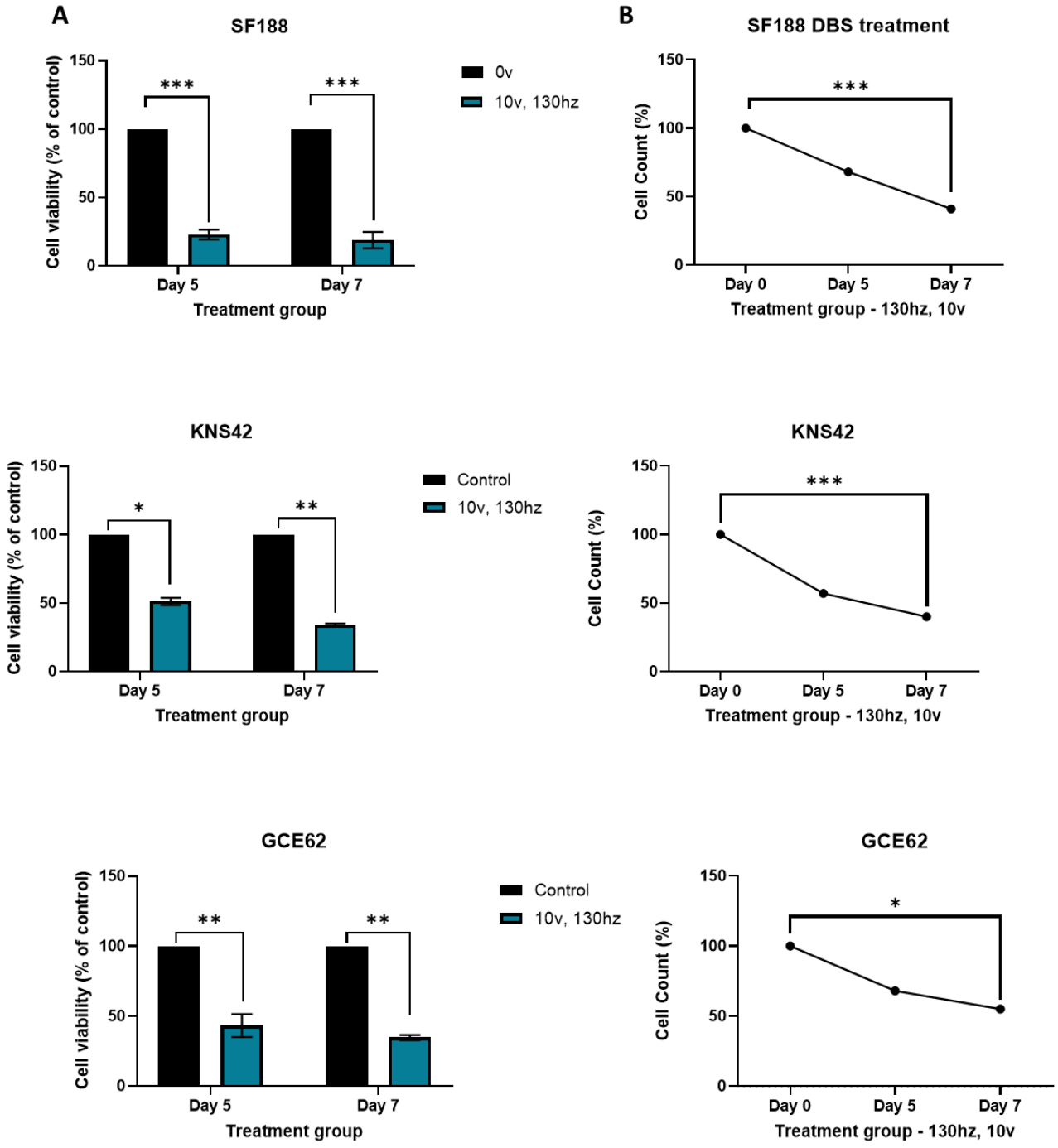

Figure 5.22 Treatment DBS significantly reduces cell viability and cell count. Cell treated at 130hz and 10v continuously. A) Analysis via presto blue assay reveals a significant reduction in cell viability across cells lines with deep brain stimulation at day 5 and day 7. B) Cell count is significantly reduced in a time dependant manner. N=4. Statistical analysis by paired t-test.

5.3.3 Electrotherapy does not decrease astrocyte cell viability.

We have shown the efficacy of DBS and TTFields treatment on a panel of paediatric high-grade glioma cell lines. To interrogate the clinical feasibility of these therapies, we assessed the effect of TTFields treatment at 200kHz for 72 hours, or DBS treatment at 10v for 5 days on a human astrocyte cell line. Viability was assessed via a presto blue assay, and cells were counted manually using a haemocytometer following treatment, and normalised to a non-treatment control.

Both the cell count and viability assay via presto blue revealed that neither TTFields nor DBS therapies exhibit a cytotoxic effect on normal astrocytes (p = ns) as show in figure 5.23. It is important to note that this cell line is not post mitotic and still possesses replicative capabilities. Previous work by Dr Branter confirms that the lack of cytotoxicity is replicated in non-dividing astrocytes derived from H1-hESC cells (152). Previous reports have found that actively and rapidly dividing cells are the target of electrotherapies, and as such, these treatments will have little to no effect on non-dividing cells (72). Although the astrocyte lines used maintain their replicative ability, they are limited to around 7 population doublings, have very limited metabolic activity and growth kinetics when compared to the panel of pHGG cell lines. Here these data confirm that rapidly diving cells such as cancer cells are the target of electrotherapies, thus suggesting there is limited potential toxicity on the normal brain.

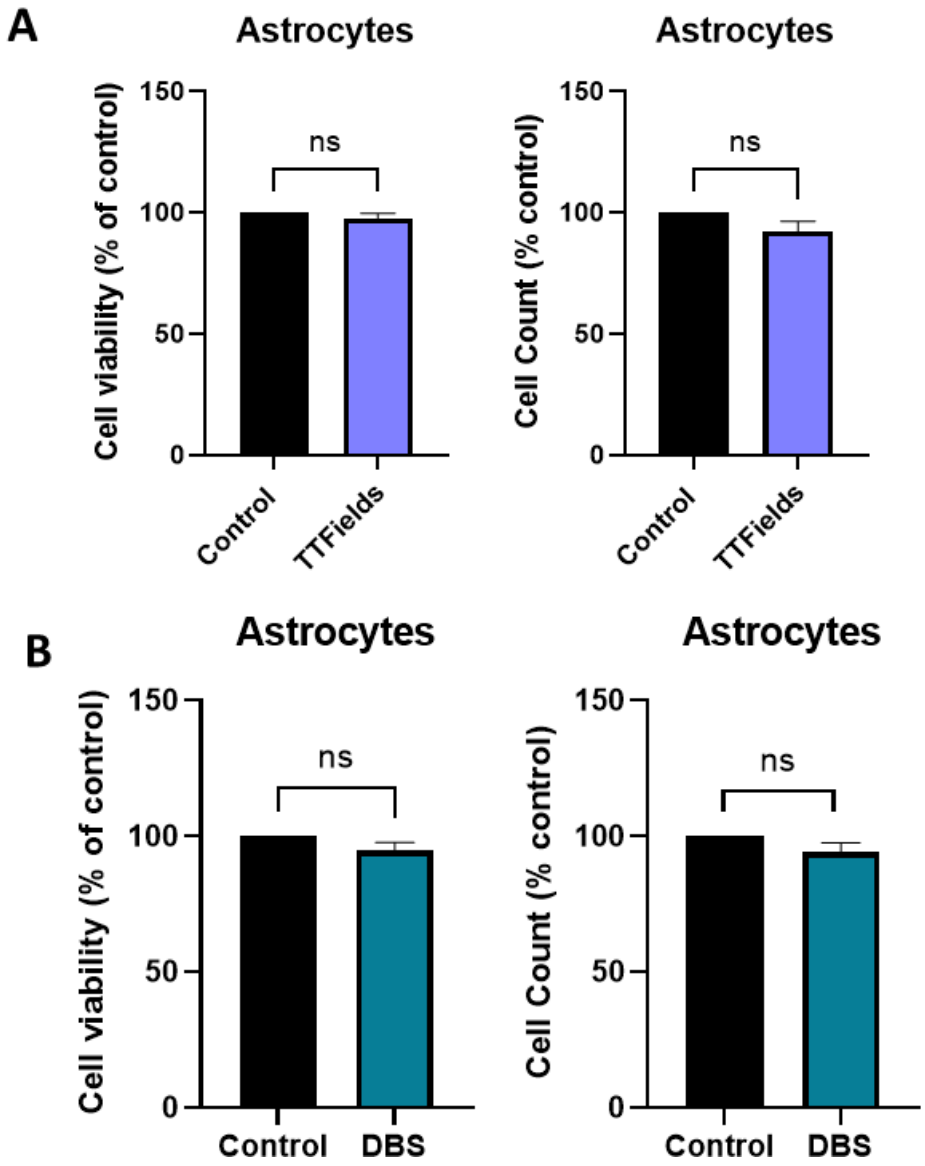

Figure 5.23 Treatment with TTFields or DBS does not reduce astrocyte cell viability. A) Astrocytes treating for 72 hours with TTFields at 200kHz do not exhibit reduced viability or cell count. B) Astrocytes treated with DBS for 5 days do not exhibit reduced viability or cell count. N=3, statistical testing via paired t-test.

5.3.4 Electrotherapy treatment is linked to unique ion channel expression.

5.3.4.1 CLIC1 and CLIC4 mRNA is downregulated following TTFields and DBS

Previous research by Dr Branter was carried out to assess the differential gene expression and genome wide analysis of cells treated with TTFields and DBS (152). The Human Clariom S Array (Thermofisher) was used for an unbiased whole transcriptome gene expression analysis with microarray processing performed by Dr Castellenos, University of

Nottingham. This data was then re-analysed and enriched to look at ion channel specific genes.

Genome wide analysis of KNS42 cells treated with TTFields and DBS reveals a unique ion channel expression compared to untreated cells. Hierarchical clustering analysis was performed using Partek, with the criteria for significant genes being: false discovery rate (Bonferroni correction) and p-value <0.05 with a fold change of <-2.0 and >2.0. Supervised clustering was performed on ion channel genes previously identified in chapter 3, and is displayed as a heat map figure 5.24. We found that there was clear clustering of cells untreated (yellow), and cells treated with TTFields or DBS (red and orange). Several ion channel genes were identified to be differentially expressed following TTFields therapy, with CLIC1 and CLIC4 having significant down regulation, and up regulation of the aquaporin channels AQP1 and AQP4 and the ENaC channels SCNN1a and SCNN1d.

In order to validate these findings, rtPCR analysis was used to determine KNS42, GCE62 and SF188 mRNA expression levels of ion channel genes found to be differentially expressed following electrotherapy treatment of KNS42 cells. rtPCR data emulated the results found in gene array analysis, whereby TTFields treatment of KNS42, SF188 and GCE62 cells resulted in a significant reduction of CLIC4, along with a significant reduction of CLIC1 expression in KNS42 and SF188 (p=<0.05). Interestingly there was no significant changes in the expression of P2RX7 across the cell lines following TTFields exposure, despite gene array data suggesting an up regulation of P2RX7 in KNS42 cells in treatment conditions. P2RX7 was found to be significantly down regulated (p=<0.05) in GCE62 cells following TTFields, aligning with data shown in gene array analysis.

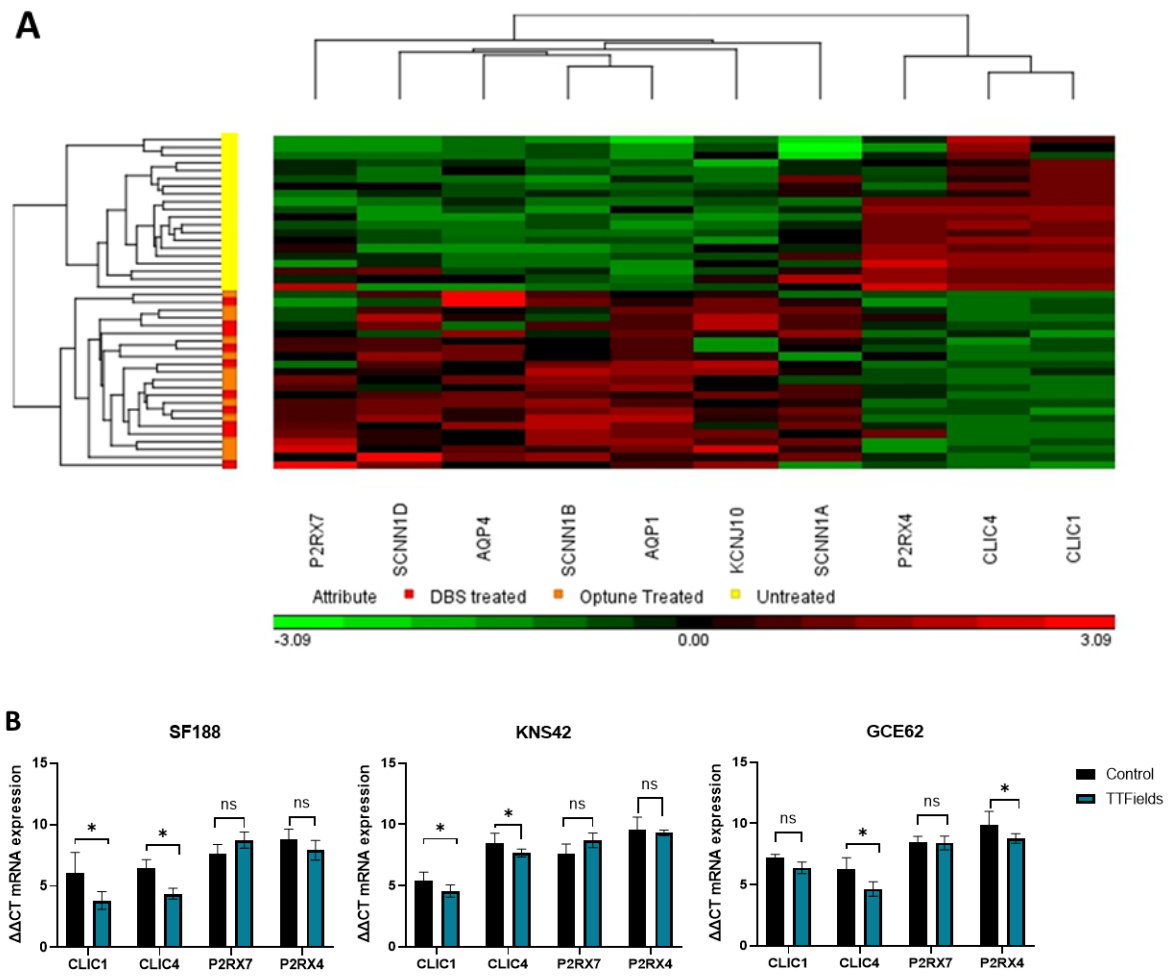

Figure 5.24 TTFields treatment is associated with a down regulation of CLIC1 and CLIC4 A) Gene array analysis reveals a down regulation in the expression of CLIC1 and CLIC4 following treatment with TTFields in KNS42 cells when compared to untreated cells. A unique ion channel expression pattern is observed. *Fold change of +2 to -2 P= <0.01* B) rtPCR analysis of TTFields treated cells shows a down regulation of CLIC1 and CLIC4. T-test.

5.3.4.2 Cells treated with electrotherapies cluster independently.

To further visualise the clustering of cells exposed to electrotherapies a PCA plot was generated. These data were not enriched to assess ion channel genes and are representative of unsupervised differential gene expression. Here we find that TTFields (Optune) treated cells cluster independently from control cells. These data are echoed when further stratifying to look at the clustering of individual cell lines in each treatment condition.

All cells treated with TTFields cluster together, independent of the cell line. These data are indicative of fundamental genetic changes occurring in cells treated with TTFields.

Key: G= GIN28, U= U87, K= KNS42. 10 = DBS treatment, 200 = TTFields treatment.

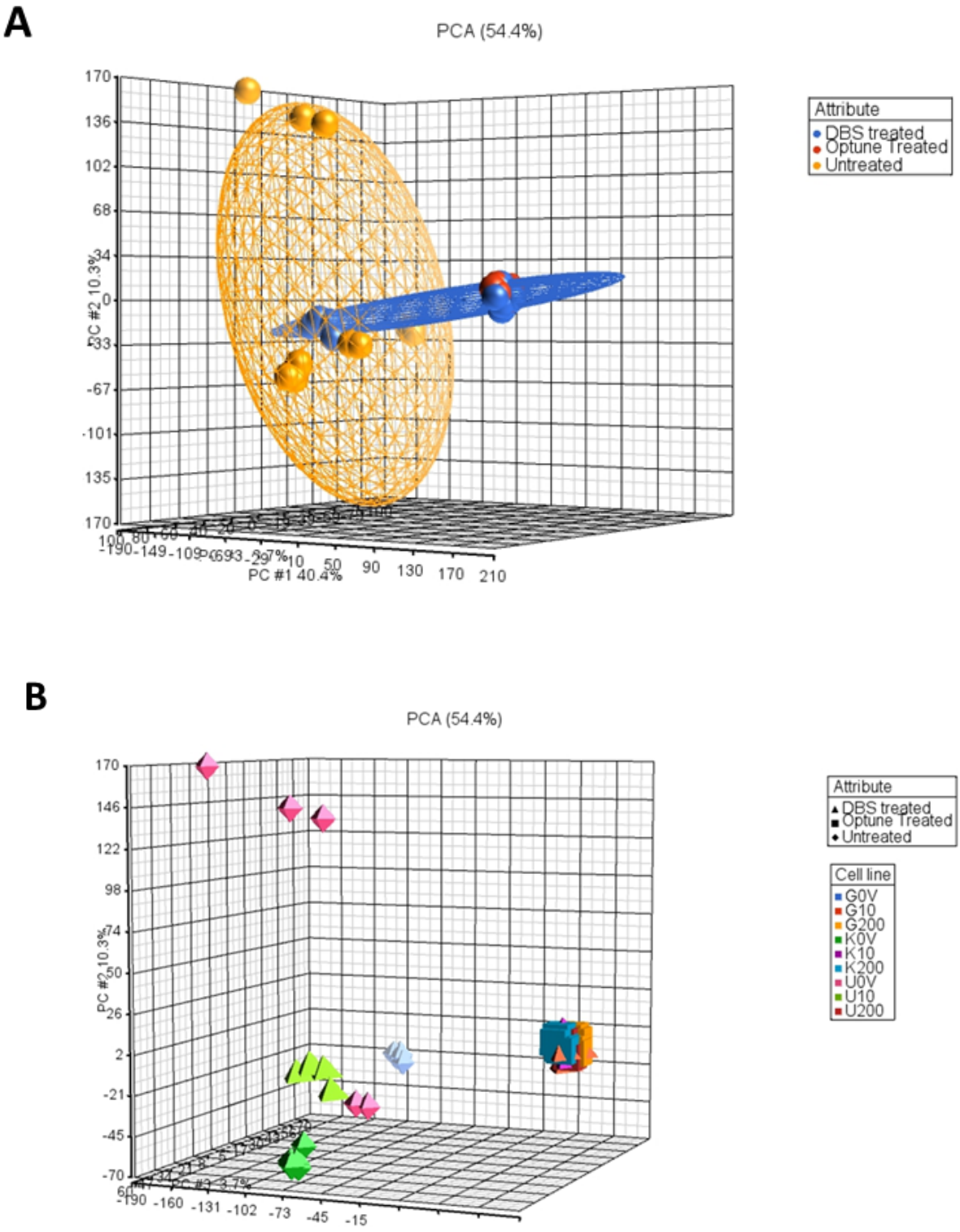

Figure 5.25 Cells treated with electrotherapy cluster independently. Gene array data (Affymetrix) from cells treated with either DBS or TTFields (Optune) performed by Dr Joshua Branter was re-analysed using Partek by Dr Marcos Costellanos.

A) PCA plot representation of the clustering of DBS treated, TTFields treated or untreated cells. B) PCA plot of all conditions including adult and paediatric cell lines treated with TTFields.

5.4 Targeting CLIC1 and CLIC4 in combination with electrotherapies

Despite efficacy demonstrated at both pre-clinical and clinical level, TTFields is not widely available, with only limited clinical trials and private clinics providing Optune treatment to patients in the UK. Further to this, the use of Optune therapy in paediatrics is not yet FDA approved. With a £20,000 a month price tag, TTFields therapy far exceeds the NICE willingness to pay scale with a cost per QALY of approximately 300 thousand pounds, and as such severely limits the availability to patients across the UK. TTFields is approved as a dual therapy with Temozolomide, but combination with other chemotherapeutics to date has failed to show an increase in overall survival. We seek to assess whether a dual therapy approach using novel bioelectrical targeting of ion channels in combination with TTFields may hold a key to extended survival, and therefore increased accessibility of this therapy. As such, we aim to explore the combination of CLIC inhibition with electrotherapies and the effect on cell viability.

5.4.1 TTFields treatment reduces chloride efflux across cells.

Initially, due to the electrical nature of TTFields and DBS therapy, we wanted to assess whether electrotherapies had the capacity to alter Cl- channel flux using the Abcam colorimetric assay.

Exposure to TTFields for 72 hours resulted in a significant reduction in the chloride efflux (as seen by an increase in fluorescence) in KNS42 and GCE98 cell lines ($p=<0.05$). There were no significant differences found in SF188 reflecting findings seen in the metformin treatment conditions and CLCIC4 knock down. This may indicate that the reduction in chloride efflux seen in TTFields treatment is a CLIC4 associated reduction (figure 5.26a).

We found that treatment with DBS for 7 days had no significant effect on the efflux of chloride across the membrane in any of the cell lines (5.26b).

These data indicate that electrotherapeutics delivered in the form of TTFields is sufficient to cause alterations in the efflux of chloride across the cell membrane, with significant reductions suggesting inhibition of chloride channels. DBS treatment did not alter chloride efflux, and as such, this may indicate that there is no direct effect on chloride channels.

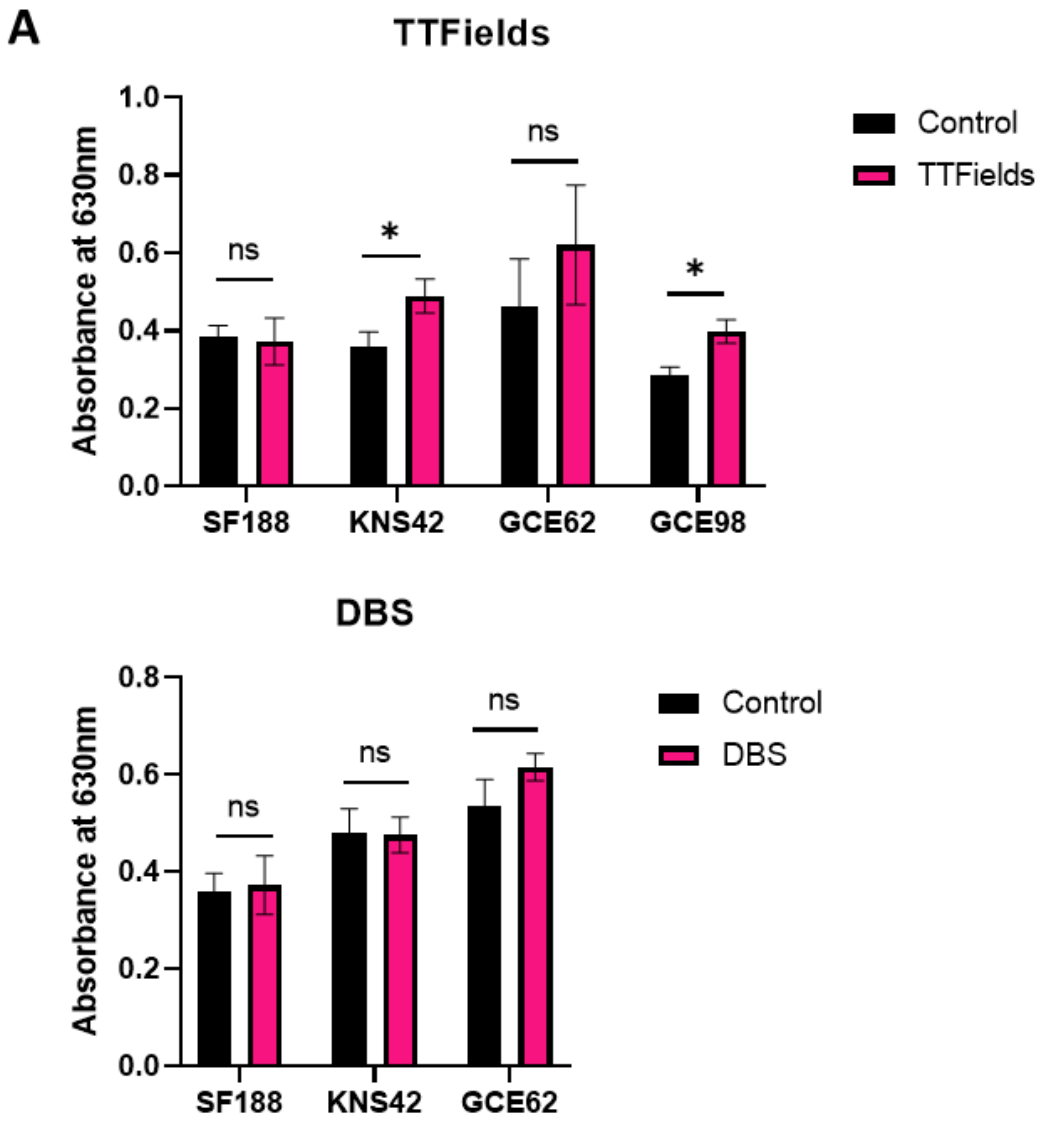

Figure 5.26 Measurement of Cl- efflux across HGG following electrotherapy exposure. A) Treatment with TTFields for 72 hours results in significant differences in Cl- efflux in KNS42 and GCE98 cells. However, there are no significant differences observed in Cl- efflux in cells treated with DBS. N=3, Statistical analysis by paired t-test.

5.4.2 Targeting of CLIC1 and CLIC4 in combination with DBS reduces cell proliferation.

Deep brain stimulation treatment cells at 130hz and 10v significantly reduces the capacity of pHGG cell to proliferate and divide, reducing viability of cells by as much as 40%. To explore whether we could potentiate the anti-proliferative effects of DBS therapy with CLIC1 and CLIC4 specific targeting, SF188 and KNS42 cells transfected with CLIC1 or CLIC4 siRNA prior to DBS treatment. Technical replicates of SF188 cells transfected with CLIC4 siRNA exhibited no differences in viability compared to wild type SF188 treated cells (Figure 5.27). However, CLIC1 deficient SF188 cells were more sensitive to DBS therapy in technical replicates, with a 10% reduction in viability observed. Knock down of either CLIC1 or CLIC4 in combination with DBS therapy reduced the viability of KNS42 cells compared to DBS treatment alone. CLIC4 deficient cells were more sensitive to DBS than CLIC1 deficient KNS42 cells. Importantly there were no differences observed between DBS treated wild type cell and DBS treated NT siRNA cells (figure 5.27).

Following this, we then interrogated the effect combining inhibition of CLIC channels via IAA94 and DBS therapy. We found that treatment with 100µM of IAA94 was not sufficient to further sensitise KNS42 or SF188 cells to DBS, and therefore had no effect on increasing efficacy.

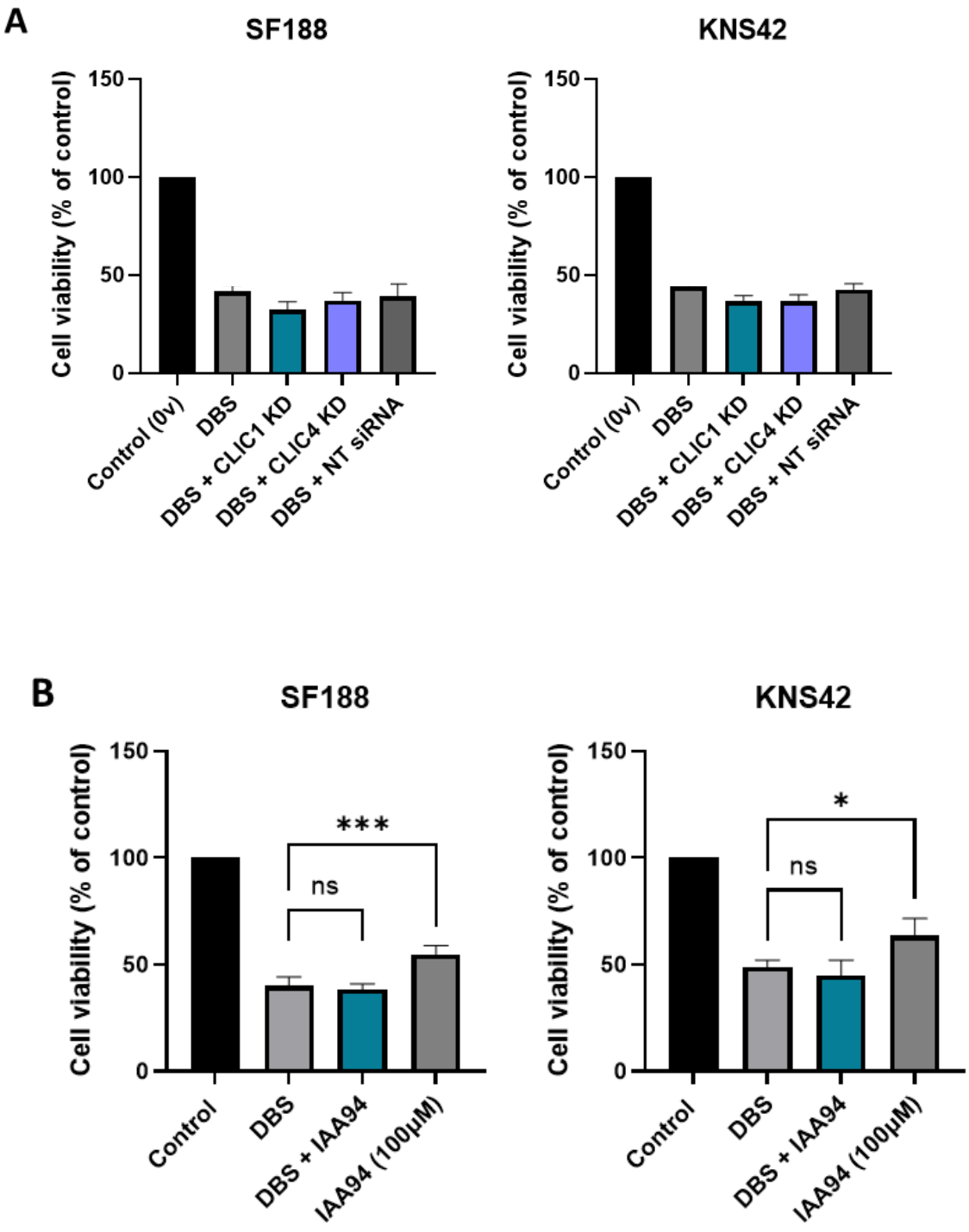

Figure 5.27 CLIC targeting in combination with DBS therapy has variable effects A) CLIC1 and CLIC4 KD in pHGG cells in combination with DBS treatment for 5 days n= 2 shown as technical replicates. CLIC1 sensitise cells to DBS in KNS42 and SF188 cells B) Treatment with 100uM IAA94 has no effect on DBS efficacy. N=3. Statistical testing by 2-way ANOVA with multiple comparisons.

5.4.3 CLIC inhibition and TTFields as a dual therapeutic approach

We have identified that both DBS and TTFields hold promise as therapeutic outputs in pHGG, and that clinical repurposing of DBS therapy may be an appropriate treatment of pHGG. Despite promising results in DBS experiments in combination with CLIC1 or CLIC4 siRNA, drug targeting in combination with DBS did not significantly sensitise the cells.

It was decided to only pursue experimental work with TTFields. The rationale for this decision is that TTFields is an already FDA approved device for the treatment of adult glioma, and as such, repurposing of the treatment for paediatric patients would likely be faster. Similarly, Optune therapy currently costs ~£20,000 per month in the UK, therefore research into combination or dual therapies, such as with ion channels, may be the key to unlocking more life years gained and therefore deeming this treatment appropriate to provide on the NHS, and therefore be an option for paediatric patients. This work may hold potential as a proof of concept, and future rationale to take these studies further, with an end goal of clinical trials, and thus, translatability of the approach is imperative.

5.4.3.1 IAA94 treatment increased the efficacy of TTFields in pHGG.

To assess the potential of combining pharmacological inhibition with TTFields, we exposure cells to 100µM IAA94 and TTFields simultaneously for 72 hours. Combination of therapies significantly reduced the viability of SF188 and GCE62 cells. Furthermore, colony forming assay revealed a significant reduction in the proliferative capacity of SF188 cells following dual treatment with TTFields and IAA94. This suggesting feasibility of CLIC in inhibition in combination with TTFields therapy.

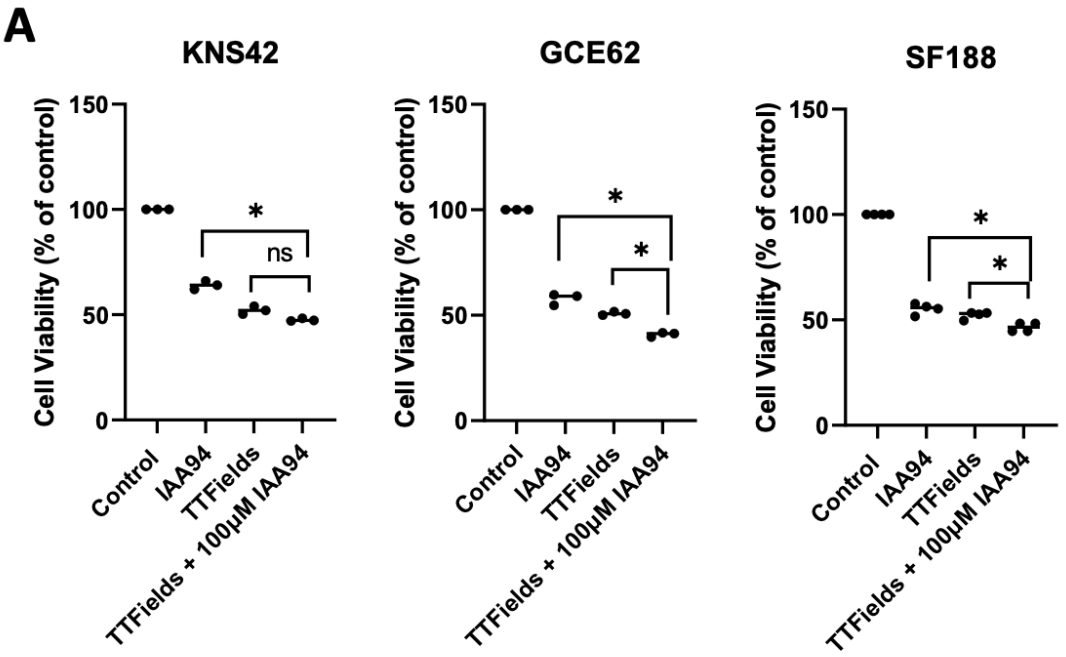
A
KNS42
GCE62
SF188
Cell Viability (% of control)
150
100
50
0
*
ns
*
*
*
Control
IAA94
TTFields
TTFields + 100μM IAA94

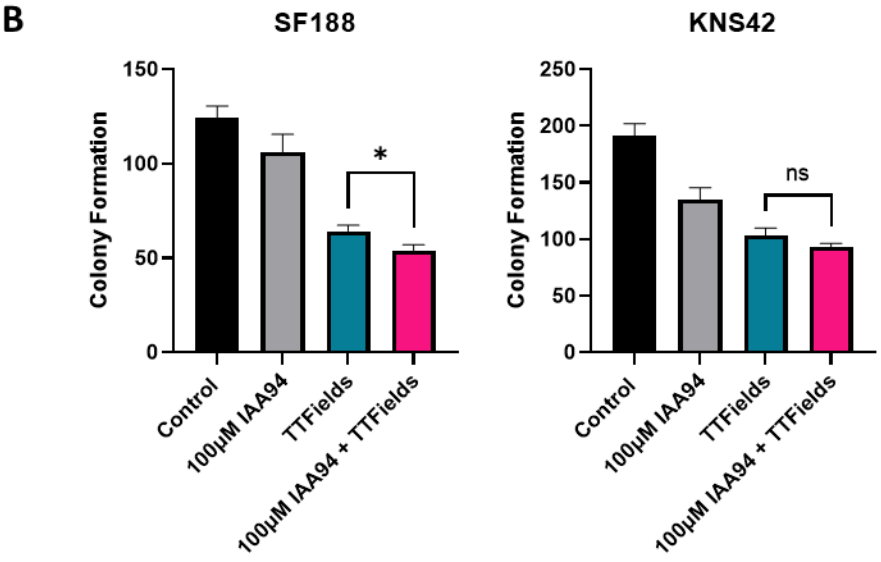
B
SF188
KNS42
Colony Formation
150
100
50
0
250
200
150
100
50
0
*
ns
Control
100μM IAA94
TTFields
100μM IAA94 + TTFields

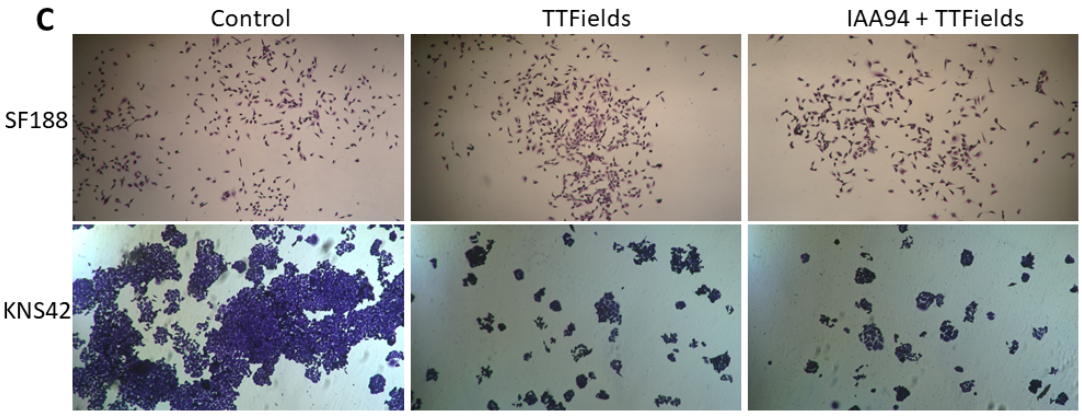
C
Control
TTFields
IAA94 + TTFields
SF188
KNS42

Figure 5.28 CLIC inhibition via 100µM of IAA94 sensitises cells to TTFields. A) Cells were treated with 100µM IAA94 for 72 hours in combination with TTFields and compared to TTFields treatment alone. Combination of IAA94 and TTFields significantly reduces cell viability (as measured by presto blue assay) when compared to TTFields alone. B) Quantification of staining intensity from cells stained with crystal violet reveals significant reduction in viable cells when combining TTFields and IAA94 when compared to TTFields treatment alone. C) Representative images of colonies. 10x magnification inverted light microscope.

5.4.3.2 Metformin acts synergistically with TTFields.

Further to analysis with the experimental drug IAA94, we wanted to understand if there was a clinically feasible route to combination of CLIC1 inhibition and TTFields therapy. As metformin is widely available, FDA approved, well tolerated, and has understood safety profiles it is of high interest as a candidate for repurposing in the treatment of brain tumours.

Cells were treated with 10mM metformin for 72 hours during the exposure to TTFields (figure 5.29b). We found that there was a significant reduction in the cell count across all cell lines ($p=<0.05$) when comparing metformin + TTFields, to TTFields monotherapy. Similarly, there was a significant reduction in the viability of SF188 cells ($p=0.0056$) and KNS42 cells ($p=0.037$) treated with metformin and TTFields, with overall viability being 15% and 10% lower in the cell lines respectively (figure 5.29).

This indicates that metformin and TTFields may be acting synergistically, resulting in reduced viability of pHGG and increased efficacy to TTFields. As such, providing proof of concept that repurposing of clinically available drugs may increase TTFields success, and sensitise cells to treatment.

Treatment at 10mM is outside of a clinically feasible range of treatment, and as such we repeated the experiments with 100µM metformin. Each cell line was plated 8 times, therefore providing 8 technical repeats, however biological repeats were not completed.

We found that treatment with 100μM metformin (replenished daily for 72 hours) was able to sensitise SF188 cells to TTFields.

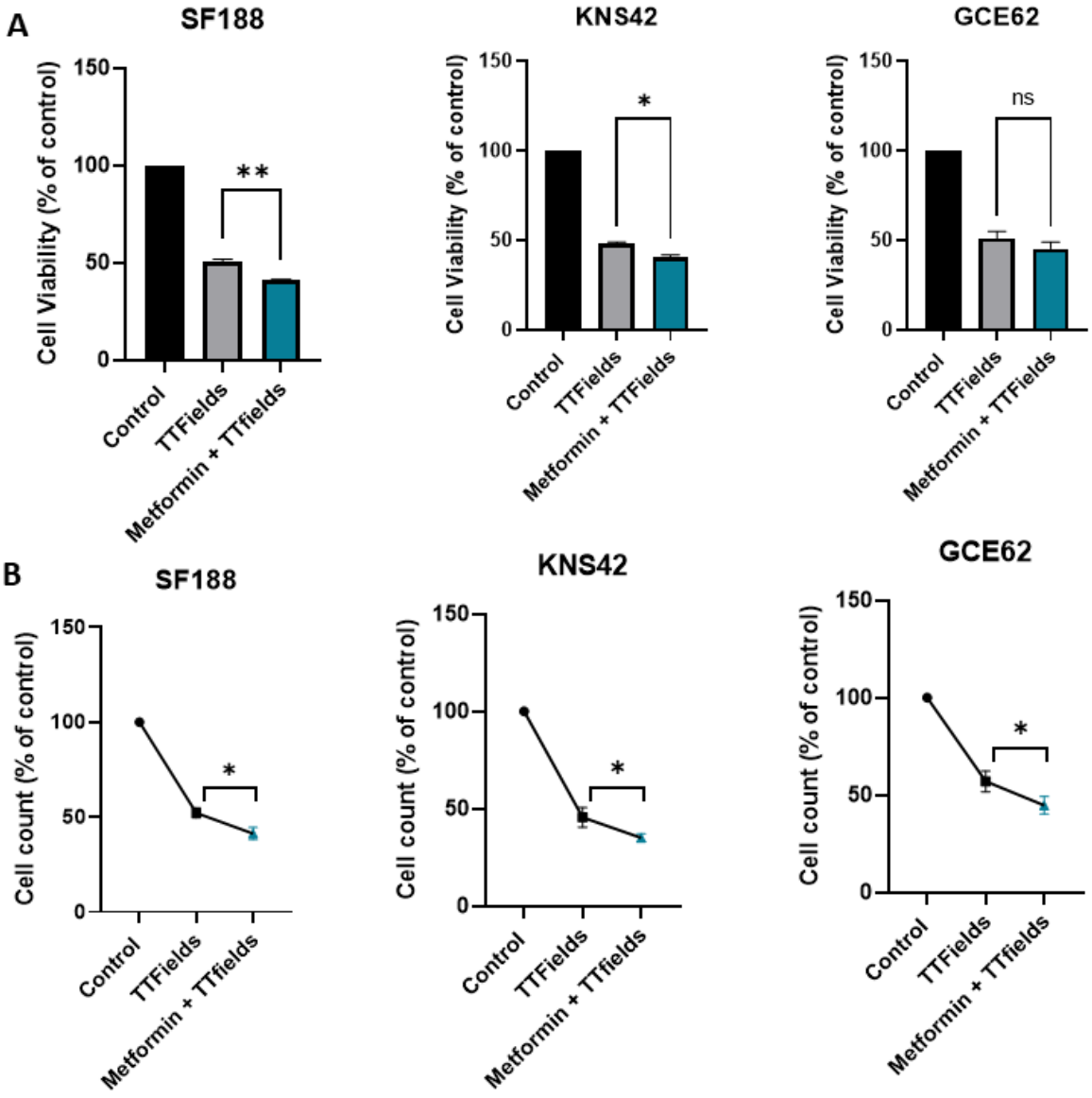
A
SF188
KNS42
GCE62
Cell Viability (% of control)
150
100
50
0
**
*
ns
Control
TTFields
Metformin + TTfields
B
SF188
KNS42
GCE62
Cell count (% of control)
150
100
50
0
*
*
*
Control
TTFields
Metformin + TTfields

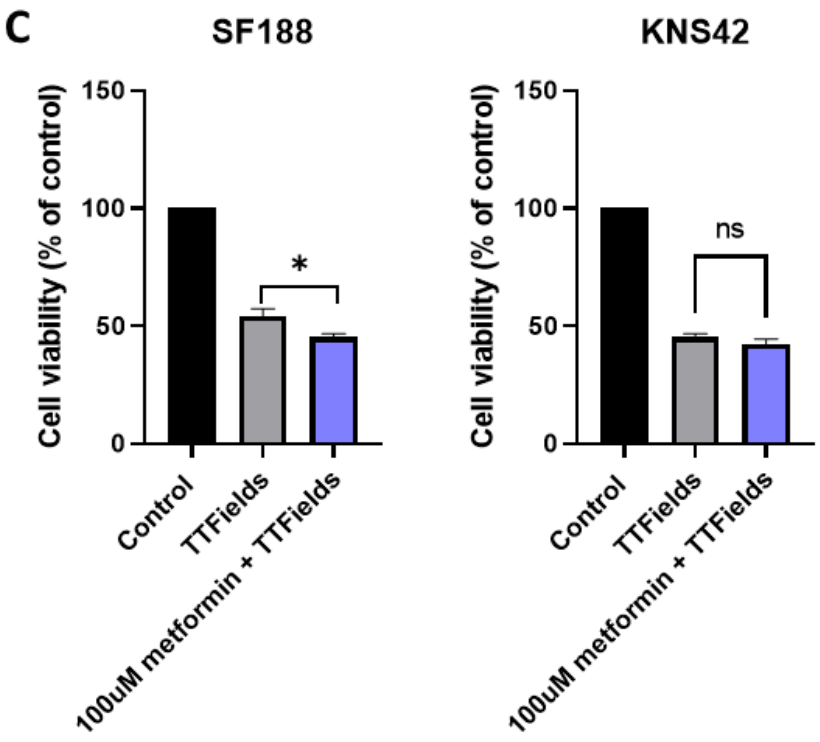

Figure 5.29 Combination of metformin and TTFields significantly reduces cell viability and cell count. A) Cell viability readings of SF188, KNS42 and GCE62 cells following exposure to TTFields and 10mM metformin for 72 hours. B) Cell count performed following 72hours exposure to TTFields and Metformin. Data represented as percentage of control values. N=3, statistical testing by paired t-test. C) Cells viability measurement of cells treated 100uM metformin and exposed to TTFields for 72 hours. Technical replicates = 8 n=1. T-test.

5.4.3.3 siRNA targeting of CLIC1 and CLIC4 in combination with TTFields.

We have found that CLIC1 and CLIC4 deficient pHGG cells have a reduced capacity to proliferate and invade, and therefore seek to assess the effect of genetic targeting of CLIC1 and CLIC4 in combination with TTFields therapy.

A combination of TTFields and knock down of CLIC1 significantly reduced the viability of KNS42 ($p=<0.01$) and SF188 ($p=<0.001$) cells compared to TTFields treatment alone. A decrease in viability of an additional 15% and 10% was seen in SF188 and KNS42 cells, respectively. However, CLIC4 siRNA targeting failed to sensitise SF188 cells to TTFields, with no significant decrease in viability observed. Despite this, CLIC4 targeting in KNS42 did

indeed increase the efficacy of TTFields treatment compared to TTFields monotherapy ($p=<0.05$) (figure 5.30).

Unexpectedly, CLIC4 knock down in combination with TTFields did not significantly inhibit the clonogenic capacity of KNS42 cells following treatment, but did however, reduce clonogenicity of SF188 cells ($p=<0.05$). As seen in viability assays, the combination of CLIC1 knock down and TTFields treatment for 72 hours influences significant sensitivity in both KNS42 and SF188 cells, with a decrease in the colony forming units when compared to TTFields alone.

Importantly, we find that CLIC1 or CLIC4 knock down alone is not significantly more cytotoxic to cells, and as such, we can confirm that these results are due to a combination of CLIC1 and CLI4 knock down with TTFields. To further this research a dual knock down of CLIC1 and CLIC4 would be performed to enhance understanding of the mechanistic implication of CLIC1 and CLIC4 on TTFields sensitivity.

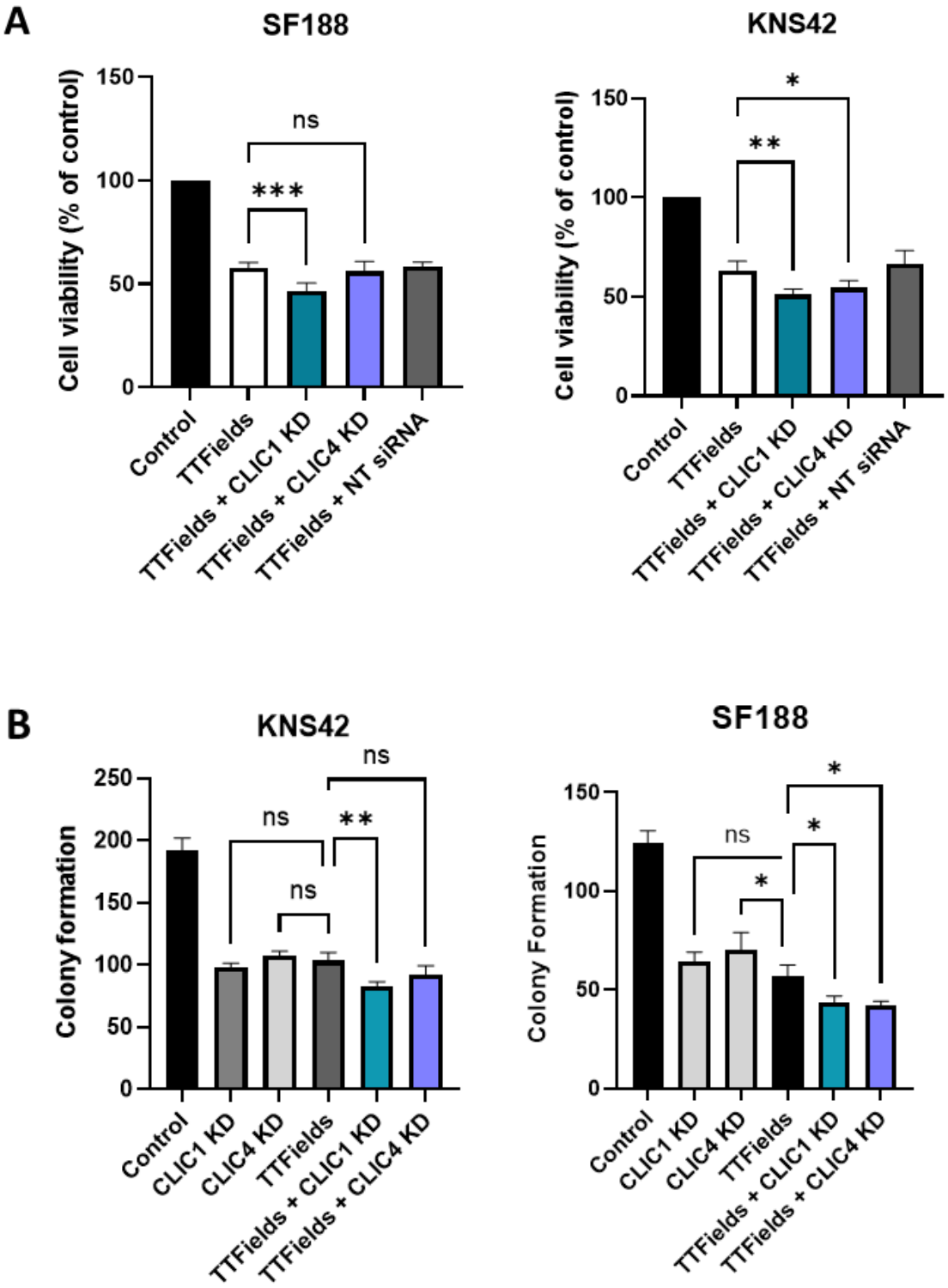

Figure 5.30 CLIC KD sensitises cells to TTFields. A) Cell proliferation as measured by presto blue is significantly reduced when combining CLIC1 and CLIC4 KD with TTFields compared to TTFields alone. B) Colony assay reveals a reduction in colony forming units following siRNA targeting of CLIC1 and CLIC4 combined with TTFields. N=4, Statistical testing by 2-way ANOVA with multiple comparisons.

5.4.3.4 TTFields treatment causes alternation in the membrane potential of pHGG cells.

Throughout this chapter, we have identified that CLIC1 and CLIC4 are bioelectrically active in pHGG cell lines, and that manipulation of CLIC channels in combination with TTFields therapy is sufficient to increase cell death. We sought to further elucidate the mechanism behind this apparent synergy, and therefore determine if changes to membrane potential, associated with CLIC activity may be linked to dysregulation or changes in membrane potential.

Cells were exposed to TTFields for 24 and 72 hours in order to assess membrane potential changes over a time course. Cells were trypsinised on ice and the FLIPR membrane potential assay was immediately completed. Interestingly, we find similar patterns in membrane potential fluctuations when treating with TTFields and when drug or siRNA targeting CLIC1 and CLIC4. All cell lines experience significant hyper-polarisation following TTFields treatment when compared to controls (100%), with significant differences seen in the membrane potential of SF188 and GCE62 cells between 24 and 72 hours. This suggests that increasing exposure to TTFields causes significant alterations in the membrane potential of SF188 and GCE62 cells (figure 5.31).

The hyperpolarisation observed following TTFields is significantly more pronounced than that seen when manipulating chloride channels.

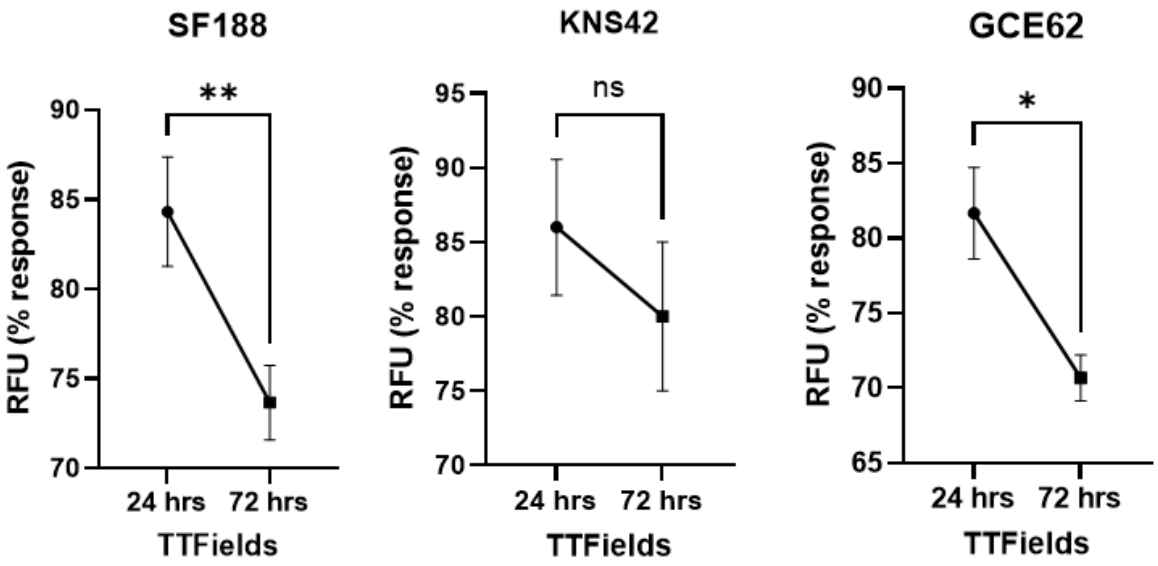

Figure 5.31 exposure to TTFields caused alterations in the membrane potential of SF188 and GCE62 cells. Cells were treated with TTFields for either 24 hours or 72 hours prior to membrane potential assay. Statistical testing by paired t-test.

5.4.3.5 Long term TTFields treatment is associated with tolerance and recovery of CLIC1 and CLIC4

To better recapitulate TTFields in the clinical setting, we sought to assess the effect of long-term exposure to TTFields and potential routes to tolerance of TTFields therapy. Following optimisation of long-term studies by Novocure™ an exposure period of 13 days was selected to mimic continuous alternating electric fields therapy. Cells were plated at significantly lower seeding densities than previously described to avoid over-confluency having an effect on the overall results. SF188 cells were seeded at a density of 1,000 cells/well, KNS42 2,000 cells/well and GCE62 2,000 cells/well.

Cells were plated, exposed to TTFields and their viability measured as previously described. We found that there were no significant differences in the viability of SF188 or GCE62 cells when comparing standard treatment at 3 days to long term treatment for 13 days (figure 5.32). Interestingly, we found that there was a significant increase in the percentage of

surviving SF188 cells following 13 days treatment, however presto blue assay results reveal that the additional surviving fraction of cells were likely unviable.

Unexpectedly, we found that following long term exposure to TTFields, KNS42 cells were significantly more viable when compared to standard treatment for 3 days. The average cell viability was 63% at day 13 when compared to 50% at day 3. These results were paralleled upon performing cell counts whereby the surviving fraction of cells (as normalised to a percentage of untreated control) was significantly higher in the long-term treatment group when compared to standard treatment.

To rule out any technical issues the well settings were investigated to ensure adequate functioning throughout, with no discrepancies observed. It is important to note that the Inovitro device has an 8 well format, with 4 replicates of KNS42 and 4 replicates of GCE62 being plated on the same base plate for each experimental repeat. As such we can rule out baseplate malfunctions causing reduced treatment efficacy as we do not observe any significant differences in the GCE62 cells. This data is particularly interesting, as Flexstation assessment of membrane potential revealed that there were no significant differences between the Vm of KNS42 cell treated for 24 hours vs 72 hours. This may be indicative of KNS42 cells being able to retain a relatively stable Vm under long term exposure to TTFields, and thus not experiencing cell cycle changes related to long term Vm alteration potentiated by TTFields.

To further interrogate this result, we carried out a rtPCR on the cells treated with TTFields for 13 days (5.23C/D). We have previously found that exposure to TTFields results in a down regulation of both CLIC1 and CLIC4 across all cell lines, and wanted to explore whether this apparent tolerance to long-term exposure of TTFields in KNS42 cells was linked to the expression of CLIC1 or CLIC4. Following treatment with TTFields for 13 days

CLIC4 and CLIC1 mRNA expression was significantly higher than expression values observed at day 3 in KNS42 cells. Despite an increase in CLIC mRNA expression, there was not a full recovery of CLIC expression to baseline levels seen in the controls. These data suggest that in KNS42 cells tolerance to TTFields treatment may be linked to the expression of CLIC1 and CLIC4, and that these ion channels may hold mechanistic insight.

In GCE62 cells there were no significant changes in either CLIC1 or CLIC4 expression observed. Interestingly, despite no significant increase in viability at day 13, there was an increase in CLIC1 expression in SF188 cells following long-term exposure to TTFields. This increase was lower than the increase seen in KNS42 CLIC1 expression, and therefore may not be high enough to translate to therapy tolerance.

It is interesting that tolerance is only observed in one cell line in our panel, and that KNS42 cells typically show a consistent level of sensitive to TTFields. This may be in part due to the baseline expression levels of CLIC1 and CLIC4 in KNS42 cells. rtPCR experiments have shown that KNS42 harbours the highest expression levels of both CLIC1 and CLIC4, and as such may become protective to the cells upon long term exposure to TTFields.

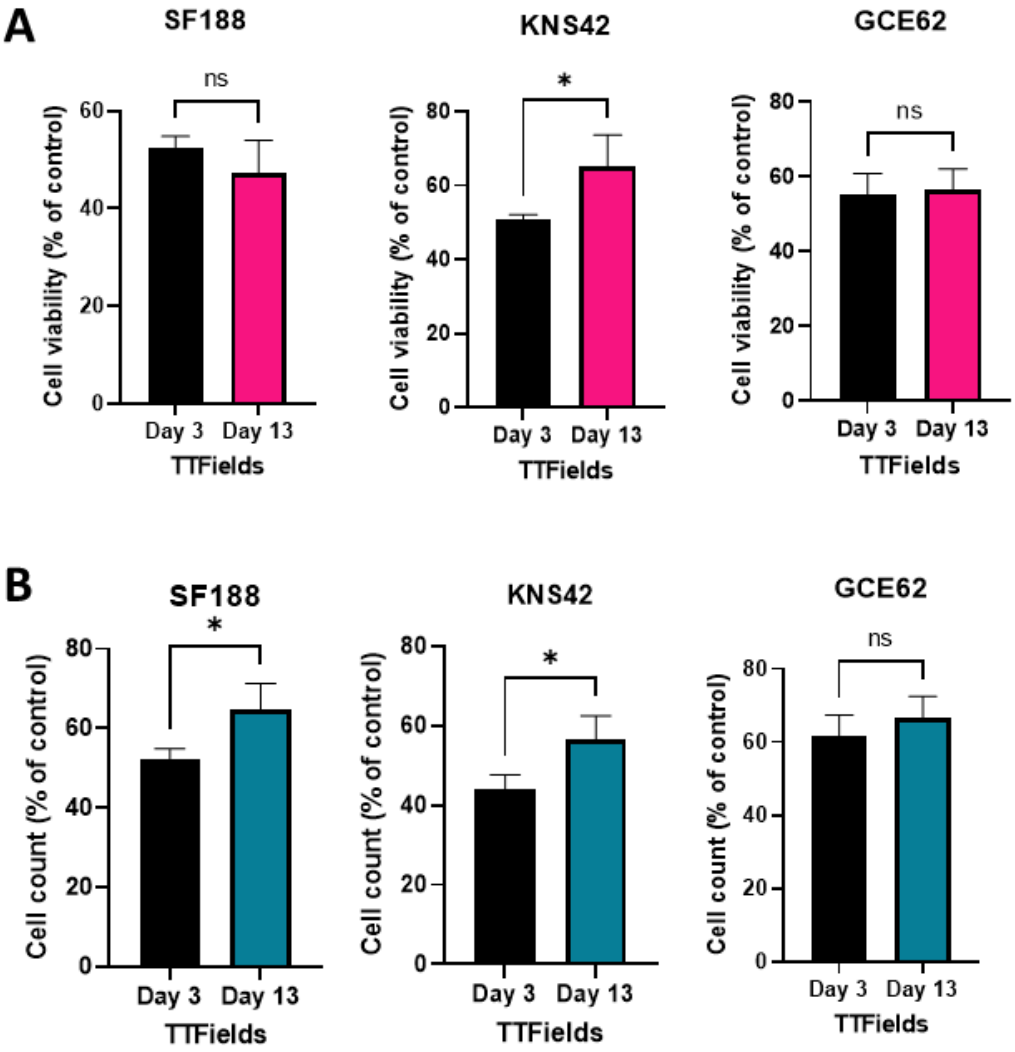
A
SF188
KNS42
GCE62
ns
*
ns
Cell viability (% of control)
0
20
40
60
80
Day 3
Day 13
TTFields
B
SF188
KNS42
GCE62
*
*
ns
Cell count (% of control)
0
20
40
60
80
Day 3
Day 13
TTFields

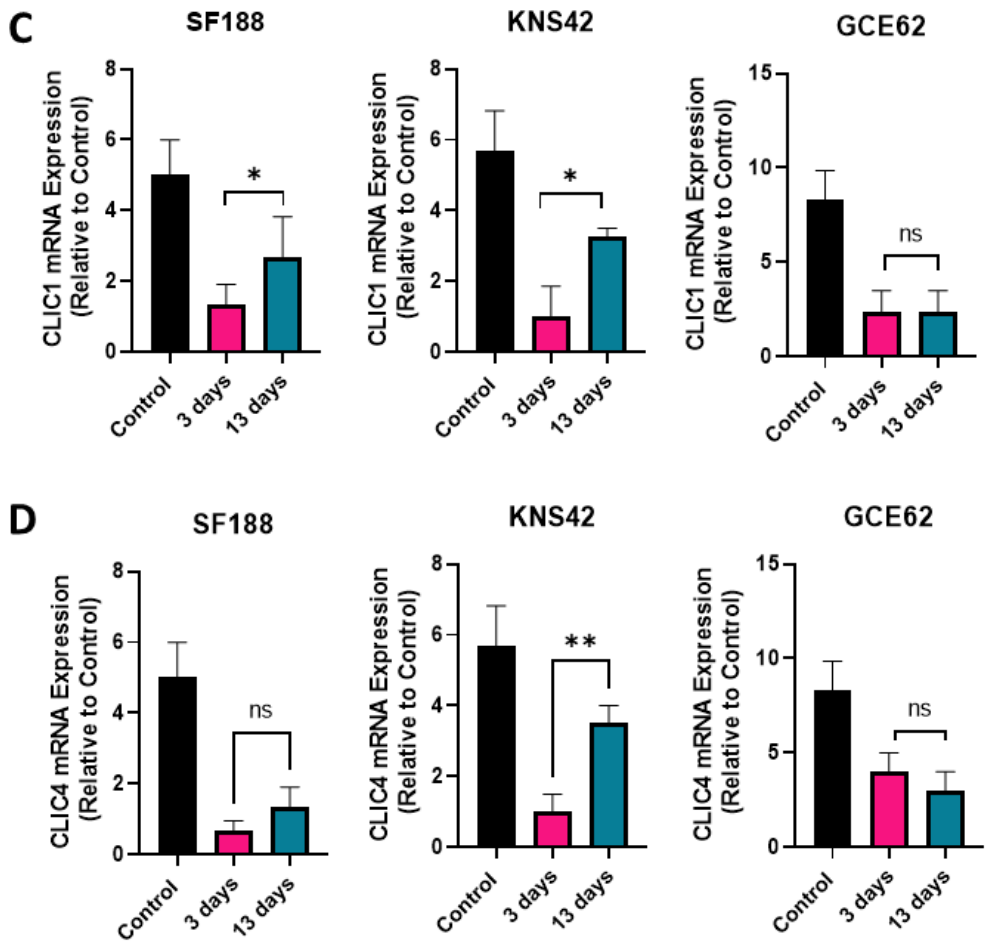

Figure 5.32 Long term exposure to TTFields results in treatment tolerance in KNS42 associated with increased CLIC1 and CLIC4 expression. Cells were treated with TTFields at 200kHz for standard treatment of 72 hours (3 days) or 13 days to deliver long term treatment. A) Cell viability in KNS42 cells is significantly increased following long-term treatment with TTFields. B) Cell count is significantly increased in SF188 and KNS42 following long term exposure to TTFields when compared to standard treatment time. C) rtPCR analysis of CLIC1 expression following standard (72hrs) or long term (13 day) exposure to TTFields. CLIC1 expression is significantly upregulated in SF188 and KNS42 cells exposed to long term TTFields when compared to standard treatment. D) CLIC4 expression is significantly upregulated in KNS42 cells following long term exposure to TTFields when compared to standard treatment. N=3 , statistical analysis via paired t-test.

5.4.3.6 siRNA targeting prevents long term tolerance to TTFields in KNS42 cells.

We then sought to further interrogate the protective role that CLIC1 and CLIC4 appear to hold in establishing tolerance to TTFields in KNS42 cells. We used siRNA targeting to assess if CLIC1 and CLIC4 deficient KNS42 cells would retain the ability to exhibit tolerance to long-term treatment with TTFields. Following CLIC1 knock down we found that there was a significant difference in both the viability and cell count found between CLIC1 deficient cells treated for 13 days when compared to NT siRNA, with CLIC1 KD cells exhibiting significantly reduced viability (figure 5.33a). Importantly, there were no significant differences found between the viability or cell CLIC1 deficient cells treated for 13 days, and NT siRNA KNS42 cells treated for 3 days. These findings suggest that CLIC1 knock down is able to return cells to their native state of sensitivity to TTFields.

Conversely, when targeting CLIC4 there were no significant differences in viability or cell count found at the 13-day treatment time point when comparing KD to non-targeting cells. However, there were also no significant differences found between treatment at day 3 and long-term treatment in combination with CLIC4 KD. Thus, suggesting that although CLIC4 KD does not significantly reduce the viability of cells treated for 13 days, there was no significant differences with the cells treated for 3 days, suggesting that these two groups (13 days + CLIC4 KD and 3 days) are comparable in efficacy.

This experiment is flawed because of the transient nature of siRNA, with most siRNAs demonstrating efficient knock down until day 7. To ensure some element of knock down was still present at day 7 and day 13 we performed rtPCR analyses of KNS42 cells transfected with CLIC1 or CLIC4 siRNA. Here we found that at day 7 CLIC1 transfection remained 77% efficient, and at day 13 30% gene knock down was still observed. Similarly, 73% CLIC4 gene knock down was seen at 7 days post transfection, with 27% gene knock

down remaining at day 13. Whilst these efficiencies would not typically be considered successful or appropriate for knock down experimentation, we accepted this for the purpose of assessing if CLIC knock down (in any capacity) could affect tolerance, as for 50% of the treatment duration there would be 75% knock down of the genes. To move these studies, forward these experiments would be repeated with a stable CLIC1 or CLIC4 knock out cell line.

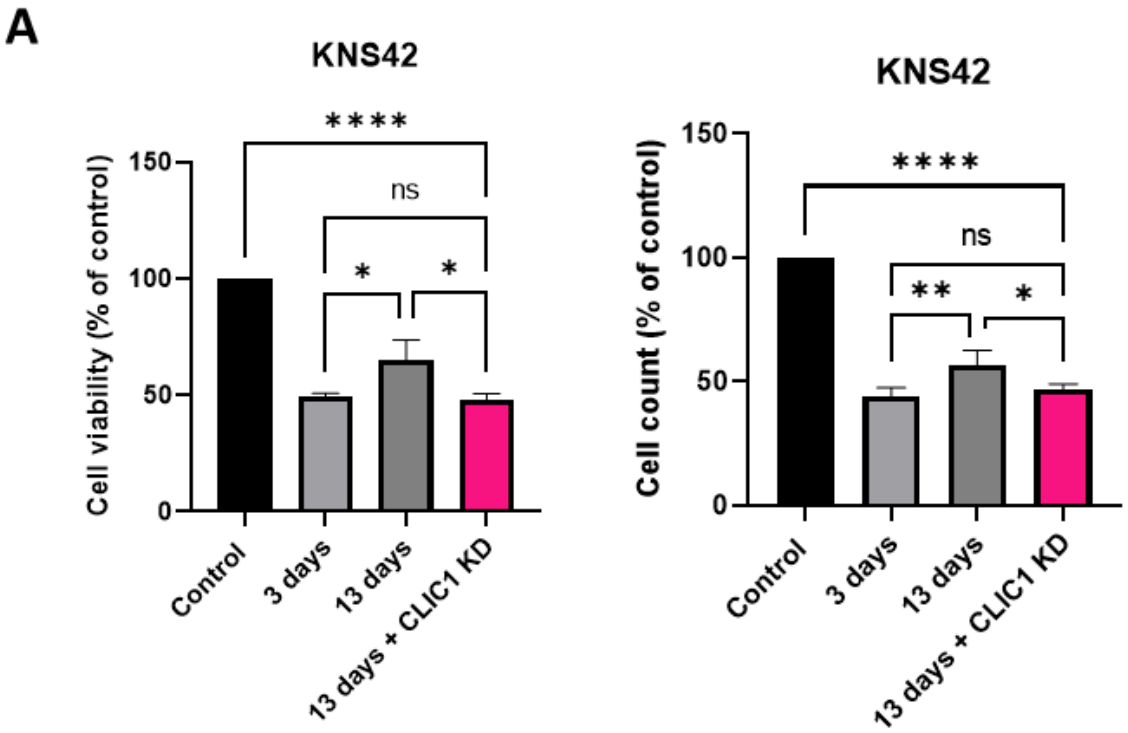

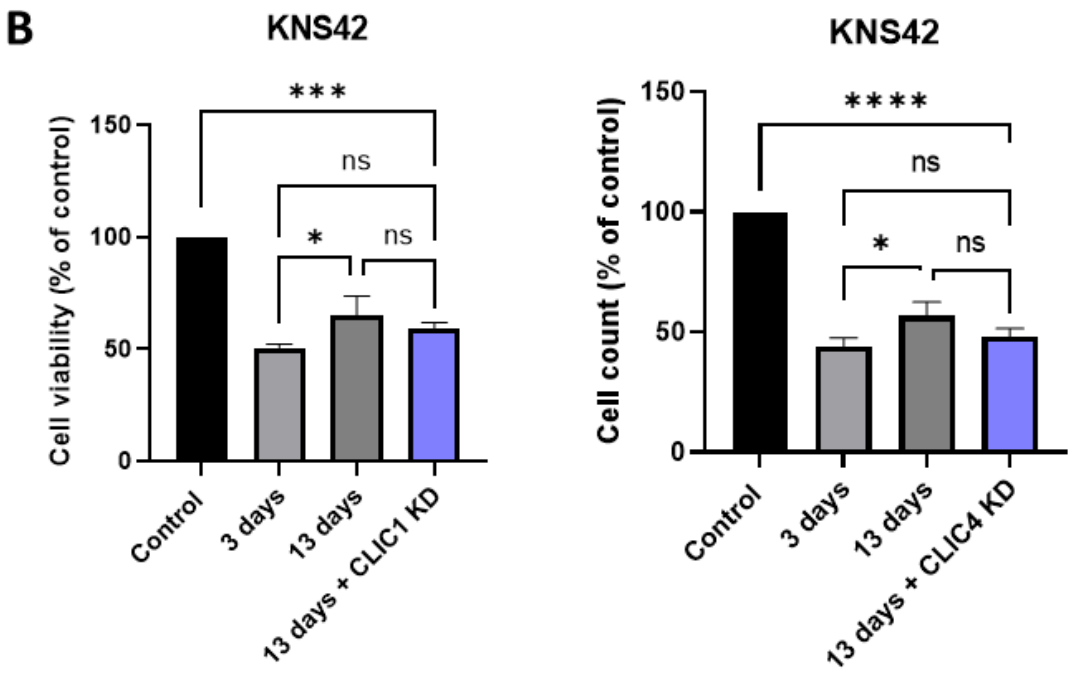

Figure 5.33 CLIC1 siRNA targeting prevents tolerance to TTFields in KNS42 cells. A) KNS42 cells were transfected with CLIC1 siRNA and exposed to TTFields for 13 days to simulate long-term exposure. Viability assay and cell count were performed post treatment. B) CLIC4 knock down KNS42 cells were exposed to TTFields for 13 days and cell viability and count calculated. N=3. Statistical testing via ordinary 2-way ANOVA with multiple comparisons.

5.5 Chapter summary

In this chapter, we have explored the role of CLIC1 and CLIC4 as bioelectrical targets in high-grade glioma, and whether their electrical activity can be exploited in combination with electrotherapy as a novel therapeutic route. We have interrogated the electrical activity of CLIC1 and CLIC4 in pHGG via high throughput voltage dye-based assays, and via electrophysiology experiments. We have identified that treatment with electrotherapies results in a unique panel of differentially expressed ion channels, and that TTFields results in a down regulation of CLIC1 and CLIC4. We have explored the potential for the translation of TTFields treatment into a paediatric population, and the combination of CLIC1 and CLIC4 targeting with TTFields. We have assessed the effect of long-term TTFields treatment and the effect that CLIC targeting has to long-term tolerance of TTFields.

We have found that CLIC1 and CLIC4 are electrically active in our panel of HGG cell lines, and that exploitation of this electrical activity can sensitise cells to TTFields treatment. We have identified that long-term tolerance to TTFields in KNS42 cells is associated with a recovery of CLIC1 and CLIC4 levels, and that siRNA targeting of CLIC1 is sufficient to re-sensitise cells to TTFields treatment. These data may provide mechanistic evidence into the success of TTFields treatment and elucidate a role in aberrant CLIC1 and CLIC4 ion channel function in the success of TTFields.

Chapter outcomes:

1) CLIC1 and CLIC4 ion channels have electrical activity in pHGG cell lines.
    - There are no significant differences in the chloride efflux observed across untreated pHGG cell lines. However, when treating cells with IAA94 or metformin there is a significant reduction in Cl- efflux in the cell. Targeting of CLIC1 via siRNA reduces Cl- efflux across all cell lines, whereas CLIC4 targeting only reduces Cl- efflux in KNS42 and GCE62 cells.
    - High throughput membrane potential assays demonstrate that astrocytes are significantly more hyperpolarised than pHGG cells. Targeting of CLIC1 and CLIC4 via IAA94, metformin or siRNA significantly hyperpolarises pHGG cells, and as such targeting of CLICs is sufficient to return pHGG to a membrane potential reminiscent of astrocytes.
    - Electrophysiology experiments found that the membrane potential of SF188 cells is associated with BK channel activity but is not significantly different to normal human astrocytes. IAA94 targeting in SF188 cells does not lead to significant changes in Vm.

- GCE62 cells treated with IAA94 have significantly altered membrane potential, and as such, CLIC1 may be key in membrane potential maintenance of GCE62 cells.

2) TTFields and DBS treatment are efficacious in pHGG.
   - Treatment with DBS and TTFields significantly reduces the viability and cell count in all cell lines in our panel.
   - Cells treated with electrotherapy cluster independently, and gene array analysis reveals that CLIC1 and CLIC4 are significantly down regulated following treatment.
3) CLIC1 and CLIC4 ion channels may elucidate the mechanism behind TTFields success.
   - Treatment with IAA94 and metformin shows synergy with TTFields, significantly increase the efficacy in SF188 and GCE62 cells.
   - CLIC1 deficient KNS42 and SF188 cells are significantly more sensitive to TTFields than nt controls. CLIC4 deficient KNS42 cells have favourable treatment response to TTFields.
   - Long-term exposure to TTFields results in tolerance in KNS42 cells. This tolerance is associated with a recovery of CLIC1 and CLIC4 mRNA expression. A combination of siRNA knock down and TTFields is sufficient to re-sensitise tolerant cells to TTFields.

6 A case study into TTFields in the patient: the mechanism of GBM recurrence following TTFields therapy.

6.1 Introduction

Optune™ therapy (TTFields) has demonstrated success in phase 3 clinical trials and is slowly becoming more widely available across Europe and the US. Unfortunately, its availability is limited in the UK with only 40 of the 25,000 Optune™ patients worldwide being UK citizens (Novocure, March 2022). This is namely a result of the significant treatment cost failing to meet NICE willingness to pay criteria and as such, preventing NHS funding. Consequently, TTFields therapy in treating in UK glioblastoma patients is rare. This, combined with the rarity of second and third tumour resections of recurrent disease, means that studying the *in vivo* effects of TTFields in the patient is unfeasible in most contexts, unless studies are conducted postmortem. Indeed, post-mortem analysis of tumour genetics harbours with its only issues, particularly because of biochemical changes related to the dying process.

Several studies have explored the effect of *in vitro* TTFields on the genome, but *in vivo* studies are severely lacking. A publication by Branter *et al* analysed the genome-wide expression effects of TTFields treatment across adult and paediatric HGG cell lines. This study found that genes associated with mitochondrial and ER functioning, including, electron transport, metabolism, ion signalling, and protein folding were implicated post TTFields exposure (152). Additionally, studies utilising proteomic and transcriptomic analyses indicated that *in vitro* TTFields treatment mainly affected nuclear proteins and interrupt cell mitosis-related events (211) and can activate STING and AIM2

inflammasomes (212). Furthermore, molecular analyses of a recurrent GBM controlled using TTFields demonstrated differentially expressed genes compared to the primary tumour. Following progression on TTFields, the resected lesion was found to possess a deep deletion of CDK2NA and an activating mutation in mTOR (V2006I)(213). These studies demonstrate that further interrogation into the effects of TTFields may help further elucidate its mechanism and expose therapeutic windows for additional pathway targeting. Here we present with a unique opportunity to study the *in vivo* effects of TTFields in three matched recurrent samples from a single patient, referred to as patient 98 here on out. We submit this case study as an analysis into the genetic and mechanistic effect that TTFields exerts on patient tissue and its derivative cell lines. This will enable increased global understanding of the mechanism of TTFields in glioblastoma recurrence and identify further therapeutic windows.

RNA sequencing analysis was employed explore the effect exerted by short term and prolonged TTFields exposure on gene expression over recurrent glioblastoma tumours from an adult male patient. These analyses will provide a mechanistic insight into the genetic changes occurring over time, and potential mechanisms into acquired resistance to TTFields. Furthermore, cell lines derived from tumour samples exposed to *in vivo* TTFields were used to better model the clinical effects of electric field therapy, and its associations to chloride intracellular channels. As such, this study aids in the validation of findings from *in vitro* TTFields experiments carried out in this project.

Chapter aims:

1) To explore differential gene expression across recurrent tumours following exposure to TTFields compared to the primary untreated tumour.
2) To use differential gene expression to uncover pathways that may exposure GBM vulnerabilities and treatment windows.
3) To validate pathways or gene targets identified from differential gene analysis of RNA sequencing data.
4) We aim to characterise cell lines derived from tumour tissue exposed to *in vivo* TTFields, including expression profiling and functional analyses of CLIC1 and CLIC4.
5) To assess the *in vitro* effect of TTFields on cell lines derived from tumour tissue exposed to *in vivo* TTFields.

6.2 Patient 98 clinical history

Here we present a unique opportunity for a case study assessing the genome specific effects of TTFields exposure in the primary lesion and two recurrent lesions in an adult

male patient (patient 98) with histologically diagnosed glioblastoma (IV). The brief clinical history is outlined in figure 6.2 with molecular characterisation of the tumour detailed in table 6.2. Patient 98 underwent surgery for the gross total resection of the temporal lobe lesion, and subsequent histological analyses confirmed diagnosis of a glioblastoma (WHO grade IV astrocytoma), IDH wildtype. A specimen was collected and preserved via fixing and FFPE embedding for histological analyses (specimen GBM98(a)). The patient was treatment naïve and had experienced no prior radio or chemotherapy exposure. The patient then underwent standard of care therapy including Temozolomide treatment and radiotherapy (60Gy), with subsequent additional treatment via Optune^{TM} TTFields therapy. Twenty-six months later, a secondary recurrent tumour was identified, and macroscopic total resection was again carried out. The specimen was then collected and FFPE embedded (specimen GBM98(b)). The respective specimen was no longer treatment naïve, with Temozolomide and radiotherapy exposure as well as intermediate exposure to TTFields. The patient then continued TTFields therapy for another 15 months until a tertiary presentation. Patient 98 underwent maximal resection of a tertiary recurrence of a histologically diagnosed glioblastoma, at NUH, Queens Medical Centre. Tumour specimen collection was performed under full ethical approval (chapter 3), with collection of distinct neuroanatomical regions under 5ALA guided surgery. The samples GBM98.1, GBM98.2, GBM98.3, GBM98.4 and GBM.95 were collected, and preserved as FFPE embedded tissue samples, or frozen for future use. The specific spatial regions are described in table 6.2. Additionally, samples GBM98.5 (invasive margin) and GBM98.2 (core enhanced) underwent dissociation into cell lines respectively know as known as GIN98 and GCE98 (described in figure 6.2). The sample known as GBM98(c), and the sample used for comparison to previous tumour tissues is the sample derived from the medial fluorescence

region (GBM98.3). This region was selected as it is the most representative of the tumour as a whole and is free of excessive necrotic regions. Unfortunately, the tumour has since recurred, and the patient has sadly died. We would like to specifically acknowledge patient 98 and express our sincere gratitude for allowing collection of their sample for research purposes and allowing this unique and rare study to be a possibility.

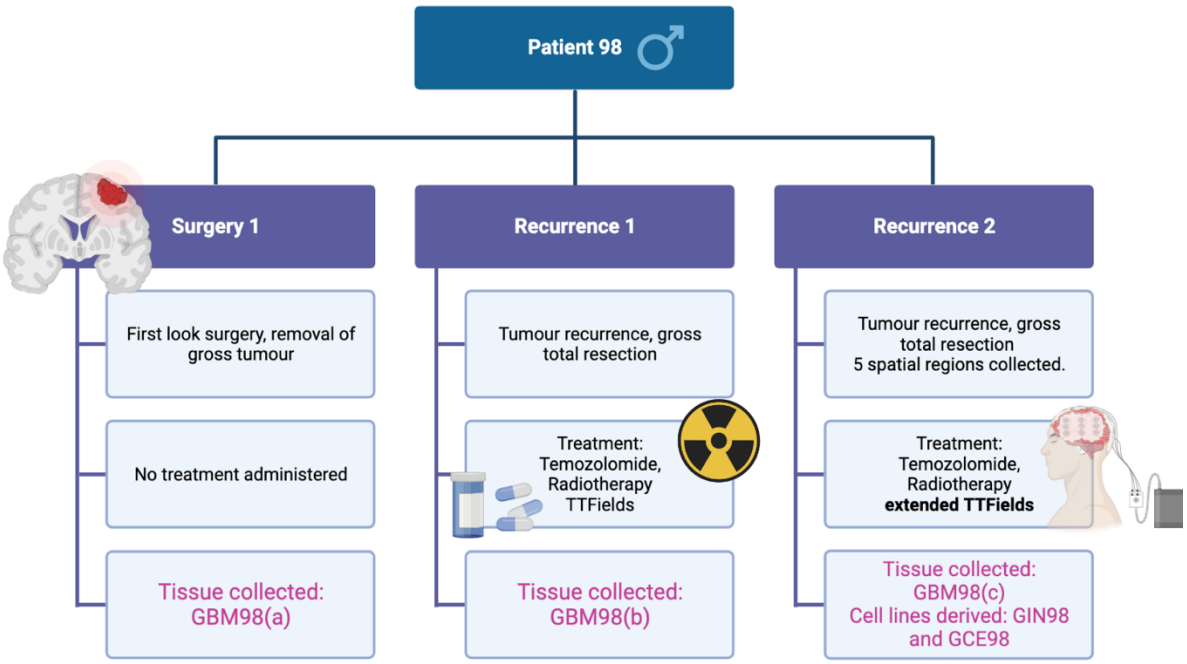

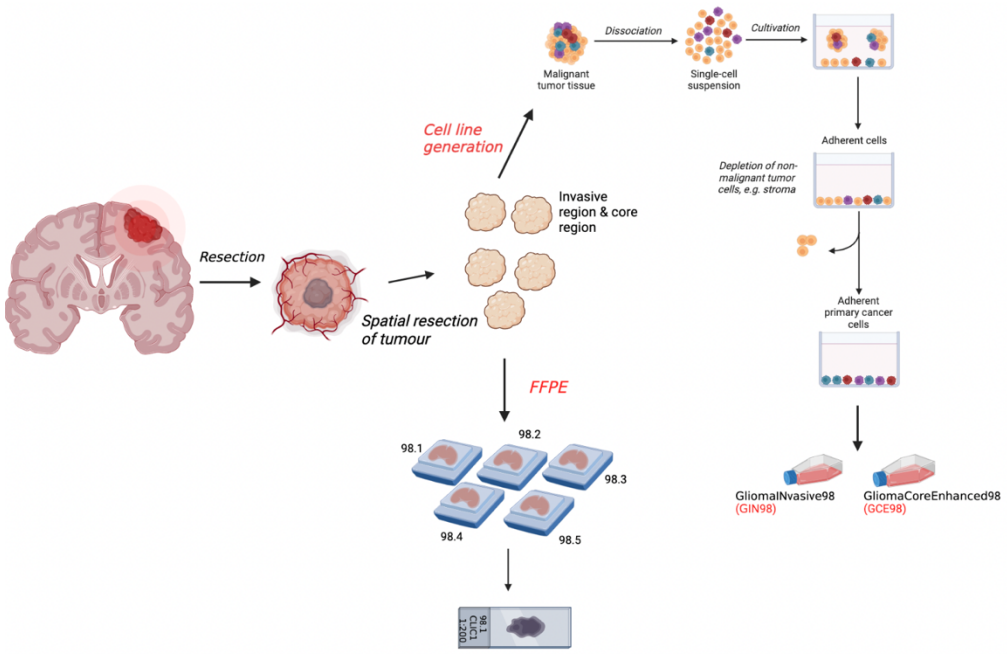

Figure 6.1 Treatment and surgery details for patient 98. A) Schematic demonstrating the clinical history of patient 98 and as such the individual specimens and treatments that the tumour samples had been exposed to. B) **Schematic representing the collection of tumour tissue GBM98(c) and the downstream uses.** Gross total resection of GBM98(c) was carried out with collection of distinct spatial regions. The invasive margin (98.5) and core region (98.32) of the tumour were dissociated into cell lines GIN98 and GCE98. Additionally, the five spatial regions were FFPE embedded for downstream staining analyses.

Table 6.1 Molecular biology of GBM98(c). A diagnostic screen of the molecular biology of patient 98 specimen GBM98a,b and c were carried out revealing a IDH wildtype status, confirming glioblastoma diagnosis.

Patient 98 Molecular Biology (GBM98c)	
IDH	Wild type
ATRX	Wild type
MGMT promoter methylation	Low (5-10%)
Chromosome 7	Gain
Chromosome 10	Loss
EGFR	Amplification
CDKN2A/B	Homozygous deletion

Table 6.2 Neuroanatomical region of spatial samples collected from tumour specimen GBM98(c). During 5ALA guided surgical resection of the tumour, five distinct neuro anatomical regions were collected.

Spatial regions collected from tissue sample GBM98(c)	
GBM 98.1	Superficial
GBM 98.2	Central Fluorescence
GBM 98.3	Medial Fluorescence
GBM 98.4	Inframedial
GBM 98.5	Invasive margin

6.3 RNA sequencing characterisation of differentially expressed genes across recurrent adult GBM associated with TTFields treatment.

To attempt to understand the complexities of glioblastoma disease progression, and the molecular alterations associated with exposure to standard of care chemo-irradiation, and further treatment with TTFields, 3' mRNA sequencing was performed. RNA was extracted in triplicate from FFPE embedded tissue from GBM98(a), GBM98(b) and GBM98(c)as described in section 2.11.4. Throughout sections 6.3-6.5 GBM98(a) will be referred to as 2018, GBM98(b) will be referred to a 2020, and GBM98(c) will be referred to as 2021. Not only will this study reveal mechanistic factors associated with the life span of recurrent tumours, it will also give us an insight into any potential pathways mediating TTFields resistance in this patient.

In order to perform NGS of recurrent GBM tissues it was essential to extract high quality RNA for library preparation and sequencing. However, RNA isolation from FFPE embedded tissue is particularly difficult due to the low yields of RNA obtained. As such, 3' mRNA

sequencing was selected, a method used for low input samples that sequences the 3' end of RNA near the poly-A tail.

Library preparation and 3’ mRNA sequencing was carried out by Deep Seq, University of Nottingham following the Lexogen pipeline as described in section 2.12.2. Initial bioinformatic analyses were carried out by Dr Sonal Henderson (Deep Seq, University of Nottingham), with further analyses carried out by the author. Quality assurance for this project is described in appendix A6.

There is disparity in the naming of samples between RNA sequencing and other laboratory techniques performed in this chapter. For clarity, the below key describes the samples under both nomenclatures.

Key:

Tumour tissue ID	RNAseq ID
GBM98(a)	(P98_)2018
GBM98(b)	(P98_)2020
GBM98(c)	(P98_)2021

The library preparation TapeStation report showed that whilst the RNA profiles for each replicate group were consistent, there was a noticeable difference in the DV200 scores between the 3 conditions, the 2021 group having the lowest percentage DV200 scores, followed by 2020 and then 2018. Electronic gel image generated by Agilent 4200 TapeStation showing the RNA profile of each sample is provided in the appendices. On average, 7.8M 75 bp single-end reads were obtained per sample, ranging between 4.2M and 10.8M reads (appendix A6). Of these, on average 89% of reads were retained after trimming. The remaining reads were aligned to the reference GRCh38 release 107. On

average, 71% of reads aligned uniquely. Unique reads were quantified by gene. Differential expression for the three contrasts between each timepoint were calculated using gene abundance values using DESeq2. No batch effect control was applied. PCA analysis of normalised counts showed distinct grouping by timepoint. Samples from timepoint 2021 were more variable than those from other timepoints. The reference has 61,920 genes. Of these, 32,796 had zero read counts in all nine samples, as such were filtered out. Differential expression at p-adjusted value < 0.1 and fold-change above and below 2 was calculated between the contrasts for the remaining 29,124 genes. Where indicated the p value is stated as the adjusted pvalue for Benjamini-Hochberg FDR testing. The adjusted p-values for the genes which do not pass the filter threshold are set to NA.

6.3.1 Tumours cluster independently related to recurrence and treatment status.

Initial bioinformatic analysis was carried out to assess the clustering of independent replicates of each tumour sample. Quantification of the number of reads that map to each gene sequence allows an estimate of gene expression, which is normalised using the trimmed mean of M values (TMM) normalisation technique to allow for comparison between samples (214). Prior to statistical analysis, Principal Component Analyses (PCA) was first undertaken to explore sample clusters and variation between samples. On the PCA plot shown, the data points representing individual replicates were projected onto the 2D plane such that they spread out in the two directions that demonstrate the greatest variance in the data.

Here we find that the 2018 (red), 2020 (green) and 2021 (blue) tumours cluster completely independently. The PCA plot presented below (figure 6.4) defines a stark difference between each group. The individual replicates in the treatment naïve primary (2018) tumour and the secondary (2020) tumour cluster tightly, with minimal variance. However,

the tertiary tumour (2021) demonstrates a noted level of variance, with individual replicates showing a maximum of 20% variance between samples. It is worth noting that the tumour collection and processing for the 2018 and 2020 samples were carried out at a different site to 2021 and thus this variance may be due to the processing and preservation of the tumour.

Interestingly, the 2021 sample clusters significantly differently than the 2018 and 2020 samples. Whilst this is partially expected due to the extended nature of therapy exposure, which may be imperative in causing DNA damage, and transcriptional alterations, it is interesting that the tertiary tumour reflects significant genetic differences compared to the primary tumour. This is confirmatory of the evolving heterogeneity of the tumour across its life span, and such is reflected in the molecular landscape. Furthermore, gene expression is visualised on the below MA plot (figure 6.4). The plot visualizes the differences between measurements taken by transforming the data onto M (log ratio) and A (mean average) scales, then plotting these values. These data allow visualisation of differentially expressed genes in the cohort. Differentially expressed genes are plotted in red, where red triangles at the top and bottom of the plots indicate a log fold changes greater and lower than -2, respectively. Analysis of the 2020 vs 2021 comparison reveals are greater distribution of differentially expressed genes when compared to 2018 vs 2020. Overall, there are fewer significantly differentially down regulated genes across all three comparisons when compared to gene upregulation, suggesting that tumour progression and recurrence is associated with an upregulation of pathways which will be explored further.

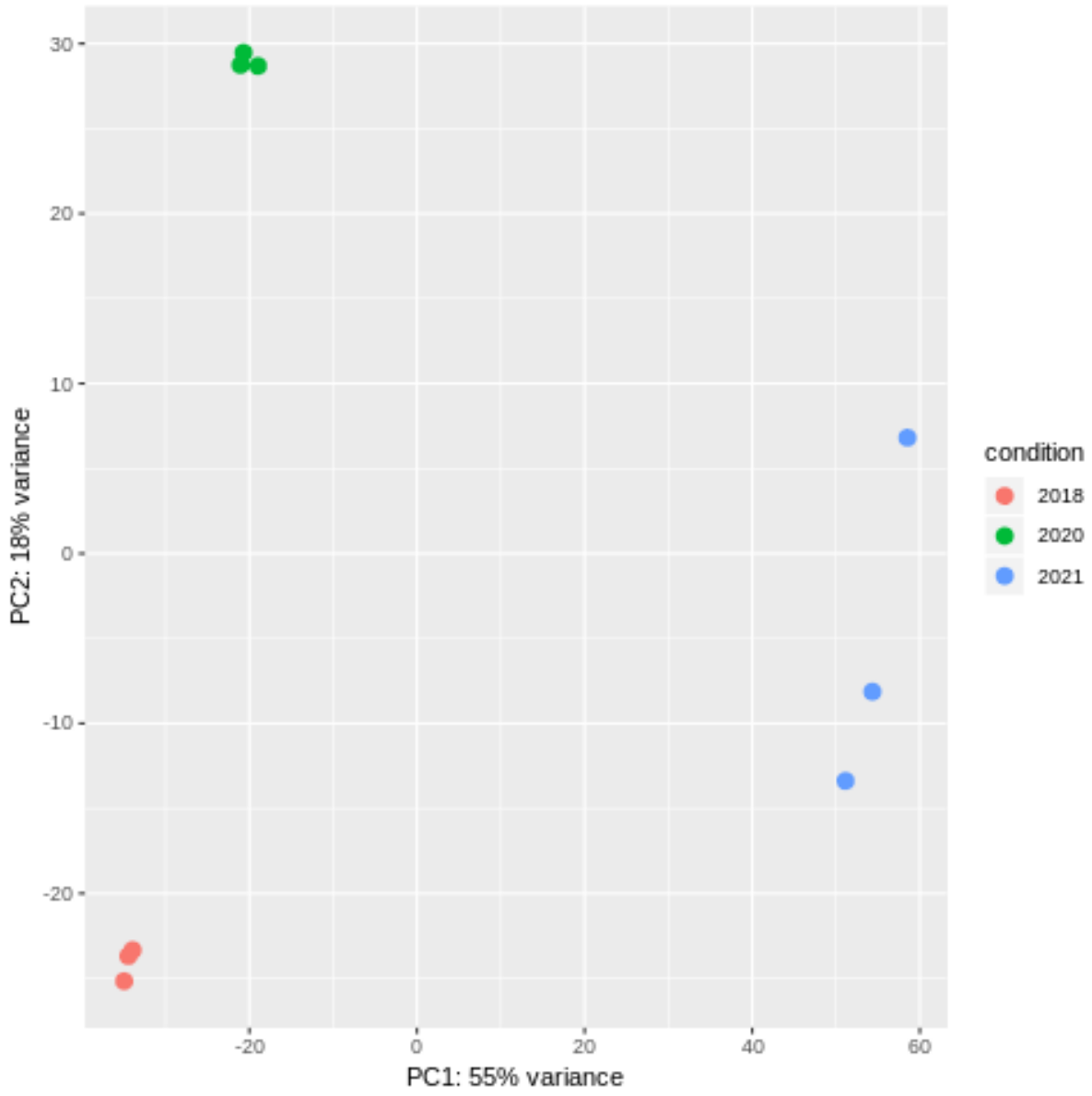

Figure 6.2 Primary, secondary and tertiary tumours cluster independently. Principal component analysis plot shows how the expression of samples relates to each other. Analysis and figure by S.H

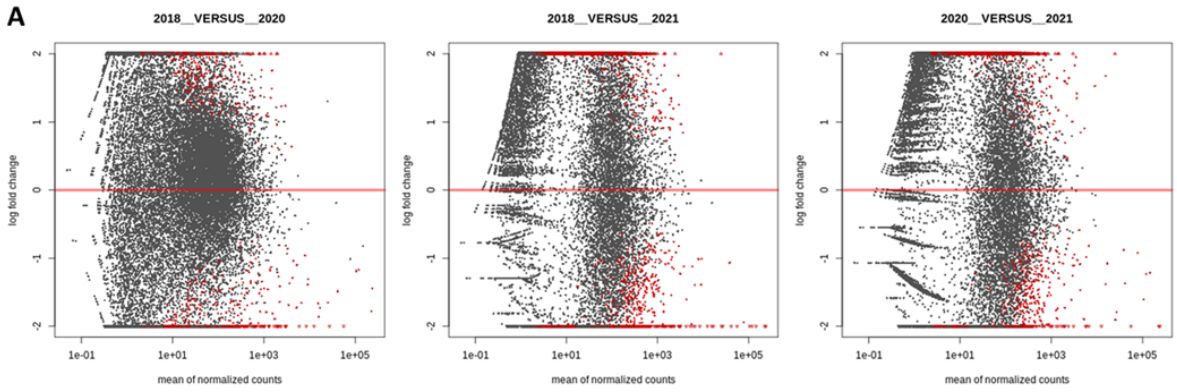

Figure 6.3 MA plots for each contrast comparing log fold change to mean normalised counts for each gene. Differentially expressed genes are plotted in red. Red triangles at the top and bottom of the plots indicate log fold changes greater and lower than -2, respectively. Analysis and figure by S.H

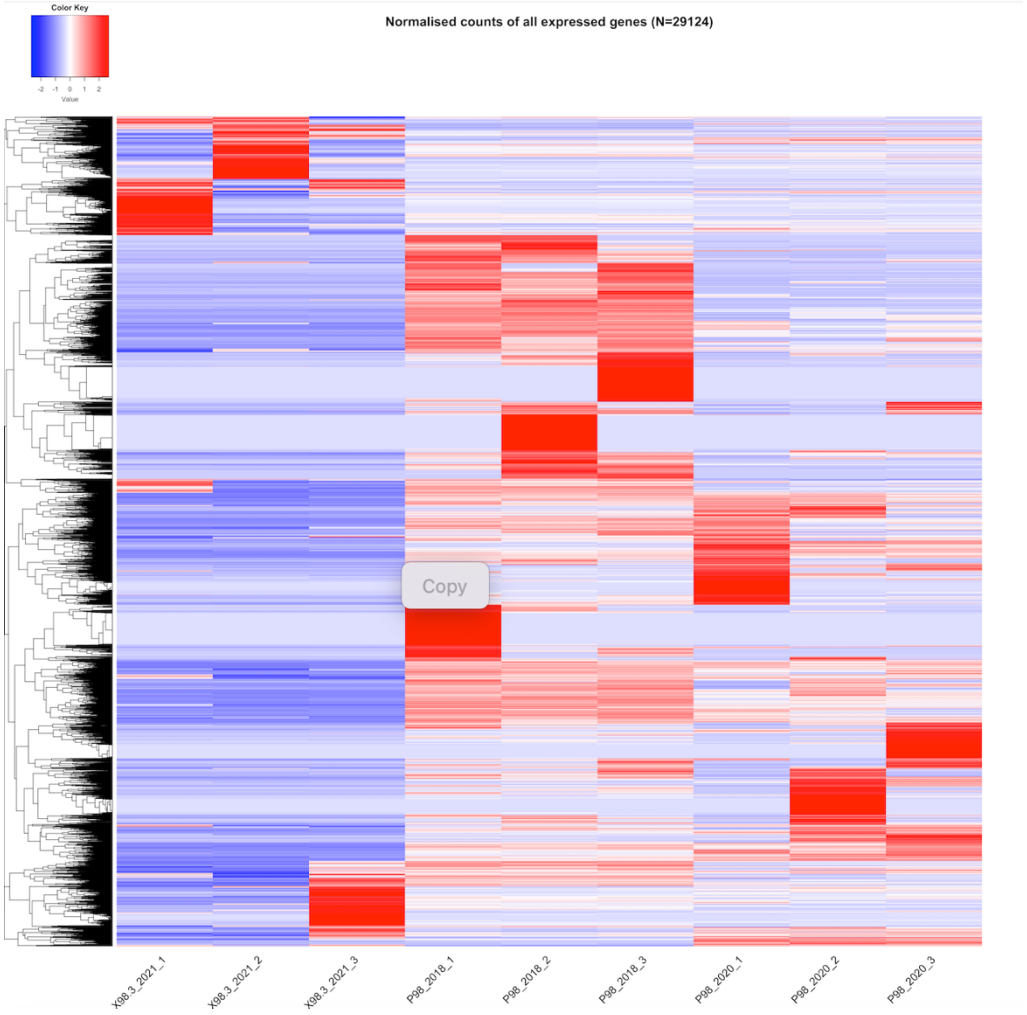

Figure 6.4 Heat map representing all significantly expressed genes across the replicates. Heatmap representing the logfold change of significantly expressed genes in triplicate across each sample.

6.3.2 Differential expression analysis

6.3.2.1 Differentially expressed genes in 2018 vs 2020

Unsupervised hierarchical clustering was carried out using the differentially expressed genes (DEGs) found across triplicate samples of each tumour (figure6.7), here we compare the DEGs in 2018 vs 2020. Figure 6.7A represents the differentially upregulated genes, and figure 6.7B represents the differentially down regulated genes between the 2018 and 2020 sample. Lowly expressed genes were filtered out of normalised gene expression datasets prior to heatmap generation, significantly differentially expressed genes were filtered based on fold change (Log2 ≥1) and FPKM value (≥20). Each column represents one sample, and each row represents a singular gene. The variance in colour represents the normalised gene expression compared to the total row mean, comparatively across the cohort of samples, represented as a Z score. Supporting observations from PCA (Principal Component Analyses) plot analyses, we see differences in gene expression widely visible across the cohort, with triplicates of each sample clustering consistently. As expected from PCA analysis, 2021 samples have a less distinctive clustering pattern and as such, show a less distinctive gene expression signature.

When comparing the primary tumour to the secondary tumour, we see several genes of interest that are up or down regulated. Table 6.3a details the 20 topmost differentially upregulated genes and Table 6.3b details the 20 top most differentially down regulated genes in 2020 vs 2018. Notably, several of the significantly upregulated genes in the 2018 sample compared to the 2020 sample are non-protein coding RNA sequences, and as such have missing gene names.

Analysis reveals that the 2020 tumour has a significant downregulation of genes associated with cell adhesion (215), growth factor binding (7), gene expression regulation, RNA methylation and mitochondrial function when compared to 2018. Whereas genes

associated with immune statue, metastasis, and tumour initiation (216), calcium binding and GABA synaptic activity are significantly upregulated in the 2020 sample compared to 2018. Importantly IGFN1, IGHG1, NODAL and CALB1 have all been implicated in glioma (215–219).

BTNL9 has been implicated in response to TTFields exposure in previous work by the group (152), finding that *in vitro* exposure to TTFields results in an up regulation of the gene as seen in the comparison between 2018 and 2020.

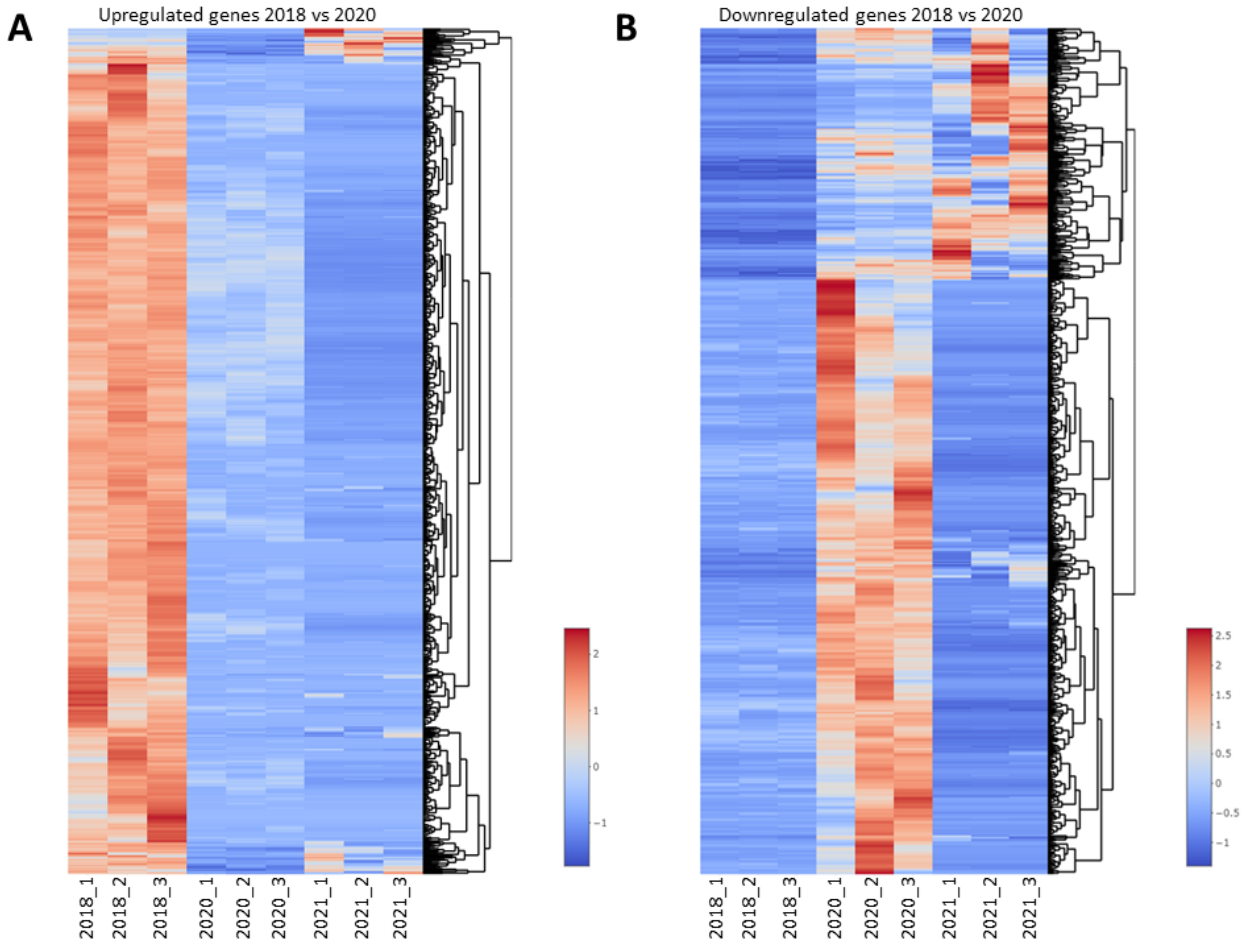

Figure 6.5 Heatmap representing normalised counts of up and down regulated genes in 2018 vs 2020. A) Heatmap of upregulated genes in 2018 compared to 2020. B) Heatmap of downregulated genes in 2018 compared to 2020. Analysis and figure by S.H

Table 6.3 Summary table of the top 20 differentially expressed genes in 2018 vs 2020 A) Top 20 differentially up regulated in 2018 genes. B) Top 20 differentially down regulated in 2018 genes. Analysis by S.H. Gene functions via STRING network analysis

A. Gene ID	Gene Name	Gene function	baseMean	log2FoldChange	padj
Upregulated in 2018 vs 2020					
ENSG00000163395	IGFN1	Immunoglobulin-like and fibronectin type iii domain-containing protein 1;.	11.15002537	7.414819251	2.66E-06
ENSG00000128713	HOXD11	Homeobox protein Hox-D11; Sequence-specific transcription factor which is part of a developmental regulatory system	10.58364879	7.347565281	9.41E-06
ENSG00000236494			10.291686	7.283270952	1.79E-05
ENSG00000156574	NODAL	Nodal growth differentiation factor; Nodal homolog;	10.09980103	7.25821593	1.95E-05
ENSG00000106133	NSUN5P2	Pseudo-gene linked to methylation.	8.914806039	7.0398905	7.27E-05
ENSG00000184414	IRS3P	Insulin receptor substrate 3.	10.95258307	6.622351039	3.07E-05
ENSG00000165810	BTNL9	Butyrophilin-like protein 9;	18.85650461	6.48740789	2.10E-05
ENSG00000287867			16.61365166	6.463532814	4.85E-06
ENSG00000164107	HAND2	Heart- and neural crest derivatives-expressed protein 2. Upstream regulator of sonic hedgehog (SHH) induction in the limb bud.	5.538190841	6.364332693	0.00079359
ENSG00000279425			5.447862197	6.337903163	0.00088769
ENSG00000232104	RFX3-DT	RFX3 Divergent Transcript	5.1008783	6.259218032	0.00099991
ENSG00000223969			5.079235557	6.209276181	0.00159899
ENSG00000125538	IL1B	Interleukin-1 beta; Potent proinflammatory cytokine.	7.725146675	6.072207016	0.00048231
ENSG00000234104			4.408043393	6.00693761	0.00292576
ENSG00000163126	ANKRD23	Ankyrin repeat domain-containing protein 23;.	4.335735339	5.988086245	0.00299359
ENSG00000241157	RPL32P32	Ribosomal Protein L32 Pseudogene 32	4.186377604	5.929872004	0.00364493
ENSG00000289128			4.105252174	5.924253299	0.00329197
ENSG00000169856	ONECUT1	Hepatocyte nuclear factor 6;	4.011673799	5.837563732	0.00554466
ENSG00000035499	DEPDC1B	Dep domain-containing protein 1b; DEP domain containing 1B	4.013032382	5.833854278	0.00571876
ENSG00000207032	Y_RNA	Small non-coding RNA	3.865405654	5.806065946	0.00545037

B. Gene ID	Gene Name	Gene function	baseMean	log2FoldChange	padj
Down regulated in 2018 vs 2020					
ENSG00000165309	ARMC3	Armadillo repeat-containing protein 3	14.0121258	-8.0898916	5.63E-07
ENSG00000132465	JCHAIN	Joining chain of multimeric iga and igm; Immunoglobulin J chain; Serves to link two monomer units of either IgM or IgA.	11.5244899	-7.7389069	7.51E-06
ENSG00000100362	PVALB	Parvalbumin alpha; In muscle, parvalbumin is thought to be involved in relaxation after contraction. It binds two calcium ions.	30.8365033	-7.6110428	4.36E-05
ENSG00000136750	GAD2	Glutamate decarboxylase 2; Catalyses the production of GABA	76.5421992	-7.4084185	6.84E-05
ENSG00000104327	CALB1	Calbindin; Buffers cytosolic calcium. May stimulate a membrane Ca(2+)-ATPase	7.97990471	-7.2681892	3.24E-05
ENSG00000168748	CA7	Carbonic anhydrase 7; Reversible hydration of carbon dioxide;	6.70642978	-6.9697538	0.00016577
ENSG00000211592	IGKC	Immunoglobin kappa constant.	91.5130057	-6.9650065	2.68E-12
ENSG00000211677	IGLC2	Immunoglobin lambda constant.	44.9608932	-6.8765556	4.85E-06
ENSG00000248485	PCP4L1	Purkinje cell protein 4 like 1; Belongs to the PCP4 family	23.0212561	-6.7639419	9.73E-09
ENSG00000206172	HBA1	Haemoglobin subunit alpha.	1271.85039	-6.7225886	8.75E-44
ENSG00000185274	GALNT17	Encodes an N-acetylglucosaminyltransferases	174.526534	-6.6276028	9.45E-18
ENSG00000090659	CD209	CD209 antigen; Pathogen-recognition receptor	8.09275657	-6.5476338	6.97E-05
ENSG00000244734	HBB	Haemoglobin subunit beta	8427.12903	-6.4484486	5.91E-89
ENSG00000152822	GRM1	Metabotropic glutamate receptor 1; G-protein coupled receptor for glutamate	4.63505431	-6.4477021	0.0009217
ENSG00000166863	TAC3	Tachykinin-3; Tachykinins are active peptides which excite neurons.	4.71356841	-6.423001	0.00135986
ENSG00000211897	IGHG3	Immunoglobin heavy constant 3.	22.9378782	-6.3881197	0.0006
ENSG00000147655	RSPO2	R-spondin-2; Activator of the canonical Wnt signalling pathway.	25.8328189	-6.3750739	5.07E-11
ENSG00000099715	PCDH11Y	Protocadherin-11 X-linked; Potential calcium-dependent cell-adhesion protein.	5.27154463	-6.3632707	0.00455521
ENSG00000101327	PDYN	Proenkephalin-B; Leu-enkephalins;	12.4947001	-6.3449621	1.98E-06

6.3.2.2 Differentially expressed genes in 2018 vs 2021

Differential gene expression analysis was also carried out on the primary tumour vs the tertiary tumour to explore the genes associated with advanced tumour progression and long-term exposure to TTFields treatment via Optune^{TM} therapy. Here we find clear differences in the expression patterns of down regulated genes in the 2021 tumour when compared to both 2018 and 2020. Interestingly replicates across both 2018 and 2021 cluster closely when compared to 2020 replicates. Furthermore, when assessing gene expression distribution, there is distinct variability in the clusters of overexpressed genes in the 2021 one sample, with almost distinct gene expression signatures observed across the three replicates.

Further to this, the top 20 most differentially up and down regulated genes stratified from this comparison are shown (Table 6.4). As previously noted, these genes were selected based on significance via adjusted p-value. Analysis reveals that the 2021 tumour has significant down regulation of genes associated with transporting cellular cargo, angiogenesis (220), microtubule formation (221), chromatin organisation (222) and DNA methylation (223)when compared to 2018.

Whereas significantly up regulated genes in the 2021 tumour primarily include those functioning in integral membrane transport and solute carrying, specifically functioning in GABA uptake (224). As such, reflecting a changing genetic landscape, favouring an overexpression of solute carriers in the 2021 recurrent tumour.

Interestingly ANGPT2 is noted as a prognostic marker in glioblastoma, inducing angiogenesis and tumorigenesis (220). Furthermore, SMARCC1 has been found to harbour tumour suppressor capacity, inhibiting glioma cell proliferation (225).

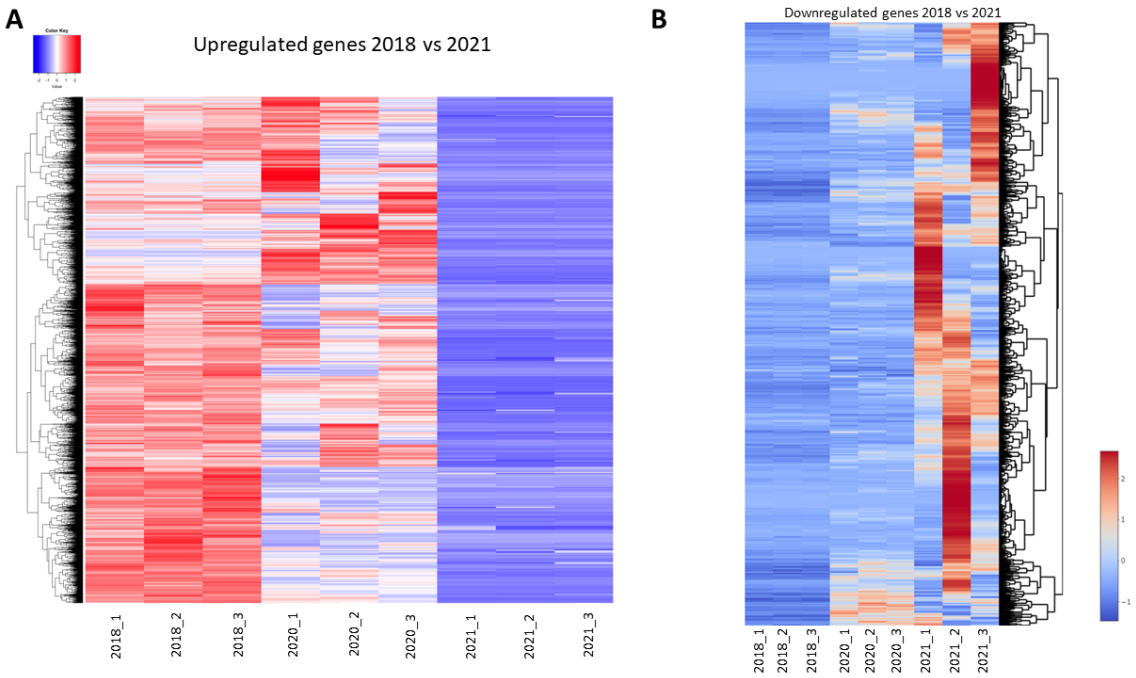

Figure 6.6 Heat map representing normalised counts of up and down regulated genes in 2018 vs 2021. A) Heatmap of upregulated genes in P98_2018 compared to P98_2021. B) Heatmap of downregulated genes in P98_2018 compared to P98_2021. Analysis and figure by S.H

Table 6.4 Summary table of the top 20 differentially genes in 2018 v 2021 A) top 2020 differentially up regulated genes. B) Top 20 differentially down regulated genes. Analysis by S.H. – Gene functions via STRING network analysis.

A. Gene ID	Gene Name	Gene function	baseMean	log2FoldChange	padj
Upregulated in 2018 vs 2021					
ENSG00000091879	ANGPT2	Angiopoietin-2; Binds to TEK/TIE2, competing for the ANGPT1 binding site, and modulating ANGPT1 signalling.	194.926808	9.07313939	1.82E-12
ENSG00000174501	ANKRD36C	Ankyrin repeat domain-containing protein 36C	139.499379	8.69474495	2.51E-12
ENSG00000146425	DYNLT1	Dynein light chain Tctex-type 1; Acts as accessory components of the cytoplasmic dynein 1 complex.	175.802371	8.67320412	1.87E-12
ENSG00000135837	CEP350	Centrosome-associated protein 350; Plays an essential role in centriole growth.	170.577478	8.6634884	5.77E-12
ENSG00000130816	DNMT1	DNA (cytosine-5)-methyltransferase 1; Methylates CpG residues. Preferentially methylates hemi methylated DNA.	135.128392	8.65112771	5.77E-12
ENSG00000009694	TENM1	Teneurin transmembrane protein 1; Teneurin-1; Involved in neural development.	109.62259	8.56286296	5.77E-12
ENSG00000141582	CBX4	E3 SUMO-protein ligase CBX4; E3 SUMO-protein ligase which facilitates SUMO1 conjugation by UBE2I.	143.355999	8.50766087	5.32E-12
ENSG00000149212	SESN3	Sestrin 1/3; Sestrin-3; May function as an intracellular leucine sensor that negatively regulates the TORC1 signaling pathway.	215.376652	8.41018257	2.00E-11
ENSG00000186432	KPNA4	Karyopherin subunit alpha 4; Importin subunit alpha-3; Functions in nuclear protein import	149.966273	8.2434331	1.97E-11
ENSG00000173473	SMARCC1	Swi/snf related, matrix associated, actin dependent regulator of chromatin subfamily c member 1; SWI/SNF complex subunit SMARCC1; Involved in transcriptional activation and repression of select genes by chromatin remodelling.	114.07513	8.2080013	4.10E-11
ENSG00000146938	NLGN4X	Neuroligin-4, X-linked; Putative neuronal cell surface protein involved in cell- cell-interactions.	102.212717	8.17926639	2.49E-10
ENSG00000241743	XACT	Produces a spliced long non-coding RNA that is thought to play a role in the control of X-chromosome inactivation	84.5481187	8.14576866	3.11E-08
ENSG00000105928	GSDME	Gasdermin E.	91.6753608	8.14312744	1.21E-10
ENSG00000112769	LAMA4	Laminin subunit alpha-4; Binding to cells via a high affinity receptor	98.7417641	8.13670863	1.48E-10
ENSG00000171634	BPTF	Nucleosome-remodelling factor subunit BPTF; Histone-binding component of NURF	308.042253	8.12815249	8.31E-18
ENSG00000164199	ADGRV1	G-coupled protein receptor V1	81.4099351	8.1183315	6.36E-11
ENSG00000087448	KLHL42	Kelch-like protein 42; Substrate-specific adapter of a BCR	122.40384	8.11248472	4.43E-11

B. Gene ID	Gene Name	Gene function	baseMean	log2FoldChange	padj
Down regulated in 2018 vs 2021					
ENSG00000206172	HBA1	Haemoglobin subunit alpha.	1271.85039	-8.4869636	6.22E-71
ENSG00000101438	SLC32A1	Vesicular inhibitory amino acid transporter; Involved in the uptake of GABA and glycine into the synaptic vesicles; Solute carriers	46.4992918	-8.3447041	1.46E-09
ENSG00000210176	MT-TH	Mitochondrially encoded tRNA histidine, also known as MT-TH, is a transfer RNA .	1973.26192	-8.1357045	9.00E-49
ENSG00000122012	SV2C	Synaptic vesicle glycoprotein 2C; Plays a role in the control of regulated secretion in neural and endocrine cells	135.101978	-8.1001068	4.83E-07
ENSG00000270350	MTND4LP5	Mitochondrially Encoded NADH:Ubiquinone Oxidoreductase Core Subunit 4L Pseudogene 5	61.2227689	-8.0109509	2.20E-10
ENSG00000136750	GAD2	Glutamate decarboxylase 2; Catalyzes the production of GABA	76.5421992	-7.8639309	1.26E-06
ENSG00000122585	NPY	Pro-neuropeptide Y; NPY is implicated in the control of feeding and in secretion of gonadotrophin-release hormone	219.61712	-7.8082326	1.84E-15
ENSG00000133392	MYH11	Myosin heavy chain11	34.3901934	-7.702864	2.49E-06
ENSG00000185761	ADAMTSL5	ADAMTS-like protein 5; May play a role in modulation of fibrillin microfibrils in the extracellular matrix	37.1063858	-7.6658722	3.90E-05
ENSG00000185274	GALNT17	Encodes an N-acetylglucosaminyltransferases	174.526534	-7.6019341	4.36E-24
ENSG00000123612	ACVR1C	Activin receptor type-1C; Serine/threonine protein kinase which forms a receptor complex on ligand binding	171.26208	-7.5933021	9.78E-07
ENSG00000251385	MTCYBP16	Mitochondrially Encoded Cytochrome B Pseudogene 16	23.4948086	-7.5856179	1.16E-06
ENSG00000197106	SLC6A17	Sodium-dependent neutral amino acid transporter SLC6A17	211.924657	-7.4445109	1.38E-17
ENSG00000104888	SLC17A7	Solute carrier family 17 (sodium-dependent inorganic phosphate cotransporter)	920.460528	-7.4319261	7.45E-40
ENSG00000210144	MT-TY	Mitochondrially encoded tRNA tyrosine.	1273.76645	-7.1739682	3.07E-44
ENSG00000169271	HSPB3	Heat shock protein beta-3;	43.2547584	-7.0410837	0.00027431
ENSG00000270388	MTCO3P22	Mitochondrially Encoded Cytochrome C Oxidase III Pseudogene 22	28.6312469	-6.9448327	3.72E-09
ENSG00000184672	RALYL	RNA-binding Raly-like protein	61.7644433	-6.932808	2.60E-06
ENSG00000229031	MTCO1P25	Mitochondrially Encoded Cytochrome C Oxidase I Pseudogene 25.	11.6234674	-6.9207239	0.00048604

6.3.2.3 Differentially expressed genes in 2020 vs 2021

To provide a comparison between the primary and tertiary tumour, differential gene analysis was carried out between the secondary and tertiary tumour to identify and potentially overlapping pathways, and as such allow for stratification of unique pathways between secondary and tertiary specimens associated with prolonged TTFields exposure.

In this comparison there is a clear preferential over-expression of genes in the 2018 tumour. There is a defined clustering of over expressed genes (figure 6.7) in the 2020 (secondary) sample that are down regulated in both the primary and tertiary tumours.

Table 6.5 demonstrates the top 20 up and down regulated genes in this comparison.

Interestingly genes associated with programmed cell death (226), EGFR degradation (217), mitochondrial function (227), NFKB regulation and P53 activation (228) are significantly downregulated in the 2021 secondary tumour when compared to the 2020 tertiary tumour. Furthermore, genes associated with cell cycle control (at G2/M) (229,230), opening of acetyl choline ion channels (230), ECM formation, and DNA-Damage induced apoptosis (231) are significantly upregulated in the 2021 tumour.

Interestingly, CCNB2 has been implicated in a variety of tumours, and has been founded to be linked to TTFields treatment in adult brain tumours (232).

MTND5 has been implicated in response to TTFields exposure in previous work by the group (152), finding that *in vitro* exposure to TTFields results in a down regulation of the gene.

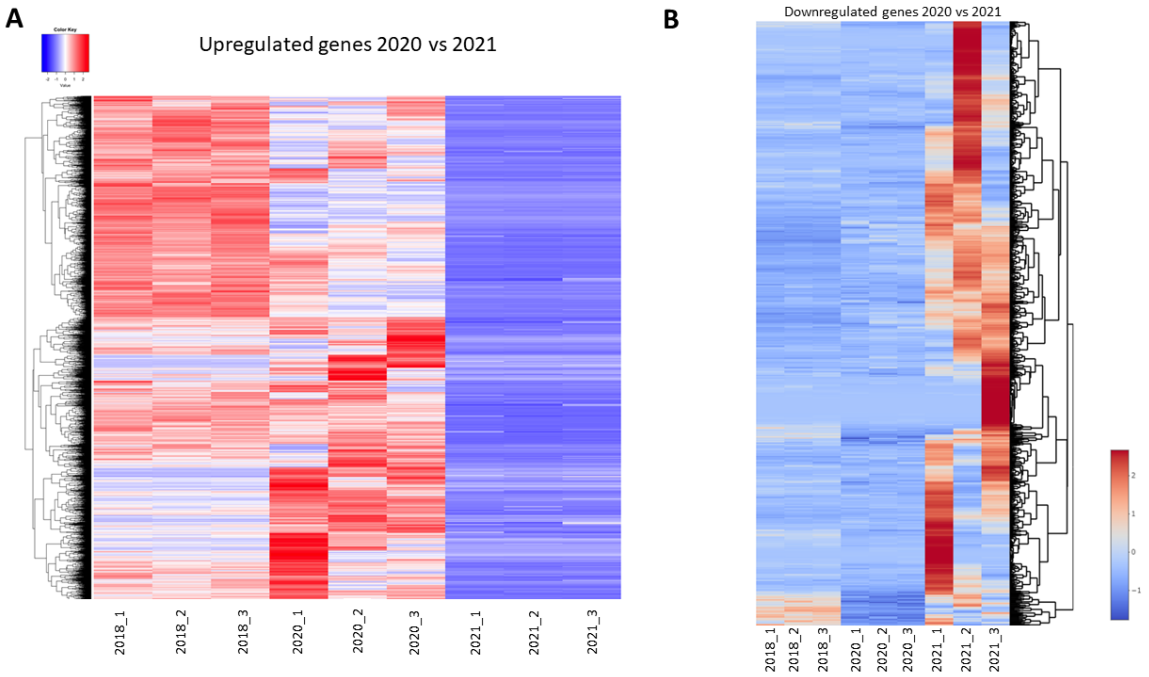

Figure 6.7 Heat map representing normalised counts of up and down regulated genes in 2020 vs 2021. A) Heatmap of upregulated genes in P98_2020 compared to P98_2021. B) Heatmap of downregulated genes in P98_2020 compared to P98_2021. Analysis and figure by S.H

Table 6.5 Summary table of the top 20 differentially genes in 2020 v 2021 A) top 20 differentially up regulated genes. B) Top 20 differentially down regulated genes. Analysis by S.H.

A. Gene ID	Gene Name	Gene function	baseMean	log2FoldChange	padj
Upregulated in 2020 vs 2021					
ENSG00000100600	LGMN	Legumain; Has a strict specificity for hydrolysis of asparaginyl bonds.	172.985774	8.94381814	4.24E-12
ENSG00000149212	SESN3	Sestrin 1/3; Sestrin-3; May function as an intracellular leucine sensor	215.376652	8.74905155	8.60E-12
ENSG00000211592	IGKC	Immunoglobin kappa chain constant.	91.5130057	8.48272139	4.79E-09
ENSG00000196743	GM2A	Ganglioside GM2 activator	152.84156	8.44112937	2.61E-11
ENSG00000131018	SYNE1	Nesprin-1; Multi-isomeric modular protein which forms a linking network between organelles and the actin cytoskeleton to maintain the subcellular spatial organization.	137.405199	8.37214962	1.01E-10
ENSG00000107798	LIPA	Lysosomal acid lipase/cholesteryl ester hydrolase.	128.599484	8.31180887	6.98E-11
ENSG00000183023	SLC8A1	Sodium/calcium exchanger 1; Mediates the exchange of one Ca(2+) ion against three to four Na(+) ions across the cell membrane.	122.055743	8.16621529	1.36E-10
ENSG00000165672	PRDX3	Thioredoxin-dependent peroxide reductase, mitochondrial.	117.977688	8.14035602	7.55E-10
ENSG00000113269	RNF130	E3 ubiquitin-protein ligase RNF130;	111.224044	8.12487071	5.35E-10
ENSG00000140022	STON2	Stonin-1/2; Stonin-2; Adapter protein involved in endocytic machinery	94.9838717	8.11399628	8.62E-10
ENSG00000121691	CAT	Catalase; serves to protect cells from the toxic effects of hydrogen peroxide.	125.150834	8.10715425	2.27E-10
ENSG00000124920	MYRF	Myelin regulatory factor	93.3172135	8.08050938	3.17E-10
ENSG00000095970	TREM2	Triggering receptor expressed on myeloid cells 2;	202.237242	8.05557728	8.21E-12
ENSG00000186432	KPNA4	Karyopherin subunit alpha 4; Importin subunit alpha-3; Functions in nuclear protein import	149.966273	8.03504997	2.07E-10
ENSG00000211896	IGHG1	Immunoglobin heavy chain 1	153.936488	8.02312469	5.67E-07
ENSG00000143514	TP53BP2	Apoptosis-stimulating of p53 protein 2; Regulator that plays a central role in regulation of apoptosis and cell growth via its interactions	104.338933	7.97423209	4.14E-10
ENSG00000129003	VPS13C	Vacuolar protein sorting-associated protein 13C; mitochondrial transmembrane potential	114.374067	7.9518531	4.73E-10
ENSG00000204136	GGTA1	Glycoprotein, Alpha-Galactosyltransferase 1	93.6831798	7.95031196	5.44E-10
ENSG00000172461	FUT9	4-galactosyl-N-acetylglucosaminide 3-alpha-L-fucosyltransferase	100.392109	7.94344579	1.46E-09

B. Gene ID	Gene Name	Gene function	baseMean	log2FoldChange	padj
Down regulated in 2020 vs 2021					
ENSG00000229503	RPL21P37	Ribosomal Protein L21 Pseudogene 37	11.5831808	-6.6915549	6.76E-04
ENSG00000270350	MTND4LP5	MT-ND4L Pseudogene 5	61.2227689	-6.6437477	2.45E-08
ENSG00000185761	ADAMTSL5	ADAMTS-like protein 5; May play a role in modulation of fibrillin microfibrils in the extracellular matrix	37.1063858	-6.3632644	5.17E-04
ENSG00000250169	MTND5P13	Mitochondrially Encoded NADH:Ubiquinone Oxidoreductase Core Subunit 5 Pseudogene 13	10.9429944	-6.179654	9.89E-03
ENSG00000245857	GS1-24F4.2	Uncharacterised	8.29644566	-6.1646019	1.41E-03
ENSG00000262095	MTATP6P25	Mitochondrially Encoded ATP Synthase 6 Pseudogene 25	16.5390648	-6.1163293	5.97E-05
ENSG00000165490	DDIAS	DNA damage-induced apoptosis suppressor protein; May be an anti-apoptotic protein involved in DNA repair or cell survival	71.6660134	-6.1092085	2.15E-04
ENSG00000221923	ZNF880	Zinc finger protein 880	167.252431	-6.0621081	6.61E-06
ENSG00000260420	LINC02182	Long Intergenic Non-Protein Coding RNA 2182	8.45184176	-6.0398758	4.97E-03
ENSG00000286681			8.84310952	-5.9174982	5.22E-03
ENSG00000247624	CPEB2-DT	CPEB2-DT (CPEB2 Divergent Transcript) is an RNA Gene, and is affiliated with the lncRNA class	8.20236831	-5.9015714	5.42E-03
ENSG00000157456	CCNB2	G2/mitotic-specific cyclin-B2; Essential for the control of the cell cycle at the G2/M (mitosis) transition; Belongs to the cyclin family	26.3647054	-5.826682	5.42E-05
ENSG00000108556	CHRNE	Acetylcholine receptor subunit epsilon	7.17364244	-5.6257556	7.18E-03
ENSG00000200153	RNU6-23P	RNA, U6 Small Nuclear 23, Pseudogene	9.35998638	-5.535958	2.44E-02
ENSG00000236483	MTND2P40	Mitochondrially Encoded NADH:Ubiquinone Oxidoreductase Core Subunit 2 Pseudogene 40	9.10854005	-5.5157639	2.50E-02
ENSG00000261325	LINC02192	Long Intergenic Non-Protein Coding RNA 2192	7.39380383	-5.4735479	0.01946841
ENSG00000286950			6.70111717	-5.4602895	1.88E-02
ENSG00000272848			11.216222	-5.4408044	8.82E-03
ENSG00000135898	GPR55	G protein-coupled receptor 55; G-protein coupled receptor 55; May be involved in hyperalgesia associated with inflammatory and neuropathic pain	5.03722517	-5.4247724	0.01149391

6.3.3 Genes significantly differentially expressed in multiple analyses

The greatest overlap of genes was observed when comparing the total number of differentially expressed genes between 2018 vs 2020 and 2018 vs 2021 with a total of 1088 overlapping genes present. Whereas the smallest number of overlapping genes was found when comparing the overlapping differentially down regulated genes in the 2018 vs 2020 analysis and 2018 vs 2021.

There are 636 similarly over expressed genes when comparing the 2018 vs 2020 tumour differential analysis, to the 2018 vs 2021 DEGs. The majority of the differentially expressed genes are upregulated. Interestingly, when assessing the top 20 differentially expressed genes in each comparison, there were no overlapping genes present in the up-regulated group (figure 6.8). However, there were three common down regulated genes when comparing 2020 vs 2021 and 2020 vs 2018, suggesting that these genes are consistently down regulated in the 2020 compared to the 2018 and 2021 tumour. These genes were GAD2, HBA1 and GALNT17. Similarly, ADAMTSL5 and MTND4LP5 were commonly down regulated between the 2018 vs 2021 and 2020 vs 2021 grouping, again suggesting unique expression of these genes in the 2021 tumour.

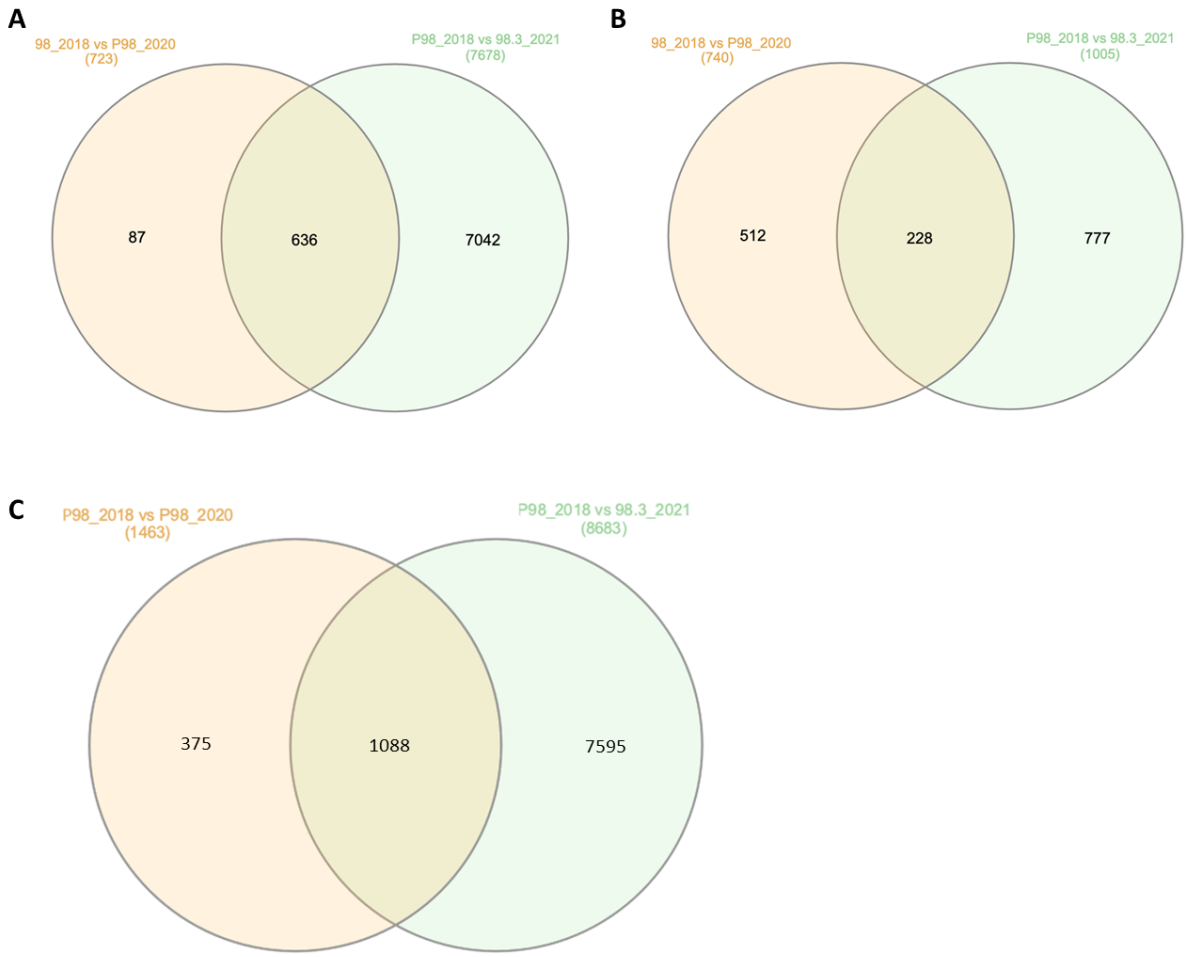

Figure 6.8 Venn diagrams showing the number of differentially expressed genes (up and down regulated) found commonly in the two contrasts – 2018 vs 2020 and 2018 vs 2021 and as a whole. A) Presents the overlap of differentially upregulated expressed genes between the two contrasts 2018 vs 2020 and 2018 vs 2021. B) Presents the differentially down regulated genes in 2018 vs 2020 and 2018 vs 2021. C) Overlap of total genes in the cohorts. 1088 DEGs were common between the two contrasts. 636 genes upregulated were common in both while 228 down-regulated genes were common in both contrasts. Analysis and figure by S.H

Table 6.6 Number of differentially expressed genes between groups. P-adjusted threshold of 0.10 for FDR and genes with greater than or less than zero log2 fold change are considered as differentially expressed.

Contrast	Upregulated	Down-regulated
2018 VS 2020	723	740
2018 VS 2021	7678	1005
2020 VS 2021	7155	713

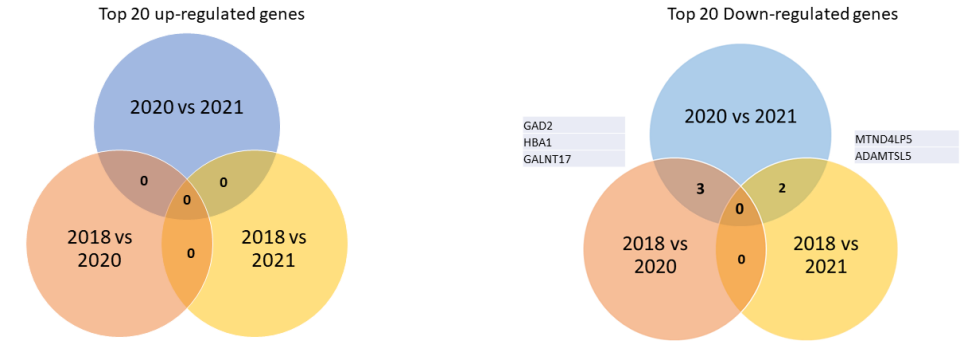

Figure 6.9 Venn diagram of overlapping top differentially expressed genes. The top differentially up regulated genes have no overlap, whereas the top 20 down regulated genes overlap between samples.

6.4 Pathway analysis and gene ontology

Given that any gene is likely to be part of a more complex biological process, it was next of interest to see if any cellular functions or pathways were commonly disrupted in the process of disease recurrence and therapy exposure. As such, differential gene expression patterns were utilised to carry out gene ontology analysis of cellular function and pathway analysis (KEGG).

6.4.1 Recurrent tumours are associated with loss of cell functions related to the cell of origin.

Gene ontology analysis by Dr S.H was carried out to assess cellular functions associated with significantly differentially expressed genes with the highest fold changes. We then further validated this using the cellular functions tool via the Gene ontology website (http://geneontology.org/). Gene Ontology describes a gene/gene product in detail, considering three main aspects: its molecular function, the biological process in which it participates, and its cellular location. Here we explore the cellular component of the up and down regulated genes across the life span of the tumour.

Interestingly in all comparisons, the primary tumour appears to be significantly enriched for cellular functions related to neurogenesis, neuronal function, synaptic control, and brain development. As demonstrated in table 6.7 the entirety of the top 20 most differentially upregulated cellular functions in the primary tumour are associated with synapse function or formation (35%), neuronal and axonal morphology (50%) or cytoplasm and vesicle formation (15%), with similar figures presented in the 2018 vs 2020 comparison (table 6.7). This apparent down regulation of these mechanisms in the secondary and tertiary tumours indicates a loss of the normal functions of the cells, as they become more dysregulated, primitive, and less like their astrocytic cells of origin. Thus, the progression

from primary, to secondary and tertiary recurrence is associated with loss of normal function of the cells as they evolve. Undoubtedly the 2018 primary tumour harbours a significant mutational burden, with substantial genetic and molecular alterations compared to somatic cells. Despite this, it remains clear that when assessing the mRNA landscape of the primary tumour, there are still significant links to the primary function of the cell of origin. Across the lifespan of the glioblastoma these functions become less expressed, and may be evidence for clonal selection with tumour progression for treatment resistant clones.

Conversely, when assessing the up regulated genes in the 2020 tumour compared to 2021 tumour, the signature of neuronal and astrocytic function is lost. Instead, we see a signature of biosynthetic processed and protein binding. Thus, suggesting that the cells harbouring these cellular functions are the treatment sensitive cohort and as such are subject to rapid selection, allowing for expansion of treatment resistant clonal populations, and loss of these primary functions.

The 2021 tumour is endowed with an enhanced preference for biosynthetic and metabolic processes, perhaps relating to the microenvironmental pressures of the tumour. The enhanced metabolic requirements of an actively invading and progressing tumour are demonstrated clearly. Tumours have an inherent capacity to reprogram pathways of nutrient acquisition and metabolism in order to meet the sizeable bioenergetic, biosynthetic, and redox demands of a malignant cell. These features as described in table 6.9 may signify aggressive and recurrent disease, and act as a potential biomarker for glioblastoma progression. Interestingly, this is recapitulated in the 2020 vs 2021 comparison, whereby the 2021 tumour has a significant upregulation and an enhanced network of genes associated with cell metabolism and energy demands. Furthermore, in

this comparison we find upregulation of ion binding capacity in the 2021 tumour. As discussed throughout the duration of this thesis, ion channel activity and binding is a key regulator of the cell cycle and thus the proliferative and invasive capacity of malignant cells. As such, an enriched ion binding phenotype is favourable to the glioblastoma, allowing for progression and recurrence.

Another particularly interesting observation comes from the comparison between the 2018 and 2020 tumour (table 6.9). There is a significant upregulation of cellular functions associated with DNA repair and replication in the 2020 tumour when compared to the primary. This augmented capacity to repair DNA signifies a direct response to DNA damaging therapies such a TMZ and radiotherapy. Equally, increased levels of DNA and RNA binding suggest an actively replicative and proliferative phenotype.

Table 6.7 Differentially expressed cellular functions in 2018 vs 2021 tumours.

Cellular function	P-value	Number of Genes
Upregulated in 2018 vs 2021		
synapse	1.07E-33	150
neuron projection	3.65E-33	152
cell junction	8.93E-33	194
somatodendritic compartment	1.31E-32	115
cytoplasm	1.46E-32	610
vesicle	4.58E-28	276
anterograde trans-synaptic signalling	1.52E-26	98
chemical synaptic transmission	1.52E-26	98
trans-synaptic signalling	2.22E-26	98
synaptic signalling	5.61E-26	99
cell projection	2.23E-25	192
postsynapse	2.44E-25	84
axon	2.07E-24	87
plasma membrane bounded cell projection	2.73E-23	181
modulation of chemical synaptic transmission	8.22E-22	70
regulation of trans-synaptic signalling	8.22E-22	70
neuronal cell body	1.22E-21	72
cell body	1.40E-21	77
nervous system development	1.83E-21	192
cytoplasmic vesicle membrane	2.99E-21	116
Down regulated in 2018 vs 2021		
cytoplasm	6.14E-108	3967
protein binding	3.52E-85	4819
cellular biosynthetic process	1.36E-82	2108
biosynthetic process	2.54E-81	2155
organic substance biosynthetic process	2.64E-81	2129
macromolecule biosynthetic process	4.57E-78	1803
regulation of cellular metabolic process	2.17E-73	2032
regulation of nitrogen compound metabolic process	7.83E-70	2039
regulation of primary metabolic process	7.83E-70	2085
nucleoplasm	4.56E-67	1574
regulation of cellular process	1.43E-64	3501
cellular nitrogen compound biosynthetic process	1.89E-63	1770
kidney	2.54E-62	3065
regulation of nucleobase-containing compound metabolic process	3.07E-62	1528
regulation of biosynthetic process	7.22E-61	1551
fallopian tube	2.00E-60	2835
regulation of cellular biosynthetic process	4.62E-60	1528
regulation of macromolecule biosynthetic process	1.40E-59	1478
colon	1.40E-59	3085
gallbladder	7.40E-59	2888

Table 6.8 Differentially expressed cellular functions in 2020 vs 2021 tumours.

Cellular function	P-value	Number of Genes
Upregulated in 2020 vs 2021		
cytoplasm	1.50E-19	415
Factor: ZF5; motif: GSGCGCGR; match class: 1	3.42E-13	482
protein binding	1.22E-12	467
multicellular organism development	1.91E-12	195
biosynthetic process	1.91E-12	235
organic substance biosynthetic process	1.91E-12	232
cellular biosynthetic process	2.73E-12	228
Factor: ZF5; motif: GGSGCGCGS; match class: 1	4.21E-12	495
cellular nitrogen compound biosynthetic process	4.44E-12	201
Factor: E2F-2; motif: GCGCGCGCGYW; match class: 1	9.76E-12	435
Factor: ZF5; motif: GSGCGCGR	1.28E-11	518
cerebral cortex	1.97E-11	336
Factor: E2F-2; motif: GCGCGCGCNCS; match class: 1	2.11E-11	484
Factor: E2F-1:HES-7; motif: GGCRCGTGSYNNWNGGCGCSM; match class: 1	3.08E-11	500
Factor: ETF; motif: CCCCGCCCCYN; match class: 1	3.08E-11	463
Factor: Egr-1; motif: GCGCATGCG	3.08E-11	404
Factor: Sp1; motif: GGNDGGRGGCGGGG	4.81E-11	333
Factor: ZF5; motif: NRNGNGCGCGCWN	7.15E-11	494
Factor: E2F-2; motif: GCGCGCGCNCS	7.15E-11	519
Factor: Egr-1; motif: GCGCATGCG; match class: 1	7.15E-11	376
Down regulated in 2020 vs 2021		
cytoplasm	6.36E-109	3870
protein binding	5.12E-90	4691
regulation of cellular process	1.36E-56	3365
cellular biosynthetic process	3.82E-53	1938
biosynthetic process	1.36E-51	1980
organic substance biosynthetic process	1.36E-51	1956
cytosol	1.17E-49	1826
regulation of cellular metabolic process	2.79E-45	1863
macromolecule biosynthetic process	8.45E-45	1628
regulation of primary metabolic process	1.05E-44	1923
regulation of nitrogen compound metabolic process	4.95E-44	1876
bronchus	2.36E-43	2726
nasopharynx	2.36E-43	2657
fallopian tube	2.51E-43	2736
biological regulation	9.05E-42	3734
ion binding	8.11E-41	2110
nucleoplasm	4.83E-40	1432
kidney	1.34E-39	2948
gallbladder; glandular cells	1.45E-36	2769
gallbladder	1.45E-36	2769

Table 6.9 Differentially expressed cellular functions in 2018 vs 2020 tumours.

Cellular function	P-value	Number of Genes
Upregulated in 2018 vs 2020		
synapse	1.12E-46	148
anterograde trans-synaptic signalling	2.39E-41	104
chemical synaptic transmission	2.39E-41	104
trans-synaptic signalling	2.39E-41	105
synaptic signalling	1.61E-40	105
cell junction	2.15E-37	173
cell-cell signalling	5.31E-32	143
neuron projection	1.23E-31	128
multicellular organismal process	2.82E-30	356
nervous system development	1.03E-29	177
plasma membrane bounded cell projection	5.79E-29	164
cell projection	5.79E-29	169
cell periphery	3.05E-28	305
system development	1.68E-26	226
multicellular organism development	2.04E-25	247
presynapse	6.65E-24	64
somatodendritic compartment	7.50E-24	87
plasma membrane	1.43E-23	277
modulation of chemical synaptic transmission	2.51E-23	63
regulation of trans-synaptic signalling	2.58E-23	63
Down regulated in 2018 vs 2020		
DNA binding	1.74E-17	134
sequence-specific double-stranded DNA binding	2.20E-17	99
sequence-specific DNA binding	4.42E-17	102
double-stranded DNA binding	8.88E-17	101
transcription cis-regulatory region binding	2.24E-16	94
transcription regulatory region nucleic acid binding	2.24E-16	94
RNA polymerase II transcription regulatory region sequence-specific DNA binding	8.52E-15	87
regulation of transcription by RNA polymerase II	1.39E-14	125
transcription by RNA polymerase II	5.91E-14	126
DNA-binding transcription factor activity	1.00E-13	85
regulation of cellular metabolic process	1.15E-13	207
regulation of nucleobase-containing compound metabolic process	1.95E-13	165
DNA-binding transcription factor activity, RNA polymerase II-specific	2.58E-13	82
regulation of cellular process	3.86E-13	330
regulation of macromolecule biosynthetic process	8.39E-13	159
regulation of RNA metabolic process	8.39E-13	154
cis-regulatory region sequence-specific DNA binding	1.11E-12	75
regulation of RNA biosynthetic process	1.39E-12	145
regulation of DNA-templated transcription	3.54E-12	143
regulation of nucleic acid-templated transcription	3.54E-12	143

6.4.2 KEGG pathway analysis

To further interrogate the data set, KEGG pathway analysis was performed using the DAVID bioinformatics database (https://david.ncifcrf.gov/). Here we present the top 20 up and down regulated pathways associated differential genes expressed in each comparison. Comparison between 2018 and 2021 (table 6.10) finds that genes associated with DNA repair, cancer pathways and glycan signalling are amongst the most common up regulated pathways. Whereas pathways associated with neurodegenerative disorders, diabetes, addiction, and ion channel signalling are down regulated in this comparison. Similarly, the comparison between 2020 vs 2021, and 20218 vs 2020 yielded comparable results (table 6.12 and 6.11). A clear signature of progression is demonstrated via these comparisons, revealing that recurrent disease in this patient is associated with a reduction in DNA repair capacity and glycan synthesis, and an increase in ion channel dependent pathways such as neurodegeneration and addiction.

Table 6.10 KEGG pathway analysis of differentially expressed genes in 2018 vs 2021. Green column heading represents upregulated pathways in the primary tumour compared to the tertiary tumour and red column headings represent down regulated pathways for the same group. Shaded boxes represent the non-significant pathway following FDR correction. Bold pathways indicate pathways of interest.

Up regulated KEGG pathway in 2018	p-Value	adjP-value	Down regulated KEGG pathway 2018	p-Value	adjP-value
Herpes simplex virus 1 infection	4.3E-22	1.5E-19	Retrograde endocannabinoid signalling	5.4E-12	1.7E-09
Fanconi anaemia pathway	5.6E-11	9.7E-09	**Parkinson disease**	1.7E-11	2.6E-09
DNA replication	0.000014	0.0017	Oxidative phosphorylation	3.3E-10	3.5E-08
Homologous recombination	0.00002	0.0017	**Neurodegeneration**	2.8E-09	2.1E-07
N-Glycan biosynthesis	0.00018	0.012	Diabetic cardiomyopathy	5.2E-09	3.2E-07
Amino sugar and nucleotide sugar metabolism	0.00034	0.02	Chemical carcinogenesis - reactive oxygen species	1.5E-08	7.8E-07
Pancreatic cancer	0.00051	0.024	Prion disease	2.2E-08	9.8E-07
Glycosylphosphatidylinositol (GPI)-anchor biosynthesis	0.00055	0.024	**Nicotine addiction**	3.5E-08	1.4E-06
Small cell lung cancer	0.001	0.04	**Huntington disease**	5E-08	1.7E-06
Epstein-Barr virus infection	0.0019	0.065	**Amphetamine addiction**	1.9E-07	5.8E-06
Inositol phosphate metabolism	0.0023	0.073	**GABAergic synapse**	3E-07	8.4E-06
Other types of O-glycan biosynthesis	0.003	0.087	**Dopaminergic synapse**	5.2E-07	0.000013
Other glycan degradation	0.0045	0.11	Aminoacyl-tRNA biosynthesis	6E-07	0.000014
Phospholipase D signalling pathway	0.0046	0.11	**Alzheimer disease**	1.1E-06	0.000024
Pathways in cancer	0.0049	0.11	**Amyotrophic lateral sclerosis**	1.8E-06	0.000037
Mismatch repair	0.0052	0.11	**Morphine addiction**	0.000002	0.00004
Colorectal cancer	0.0071	0.14	**Synaptic vesicle cycle**	5.6E-06	0.0001
Various types of N-glycan biosynthesis	0.0072	0.14	Thermogenesis	0.000012	0.0002
NF-kappa B signalling pathway	0.0081	0.14	**Glutamatergic synapse**	0.000012	0.0002
Metabolic pathways	0.0082	0.14	Vasopressin-regulated water reabsorption	0.000047	0.00072

Table 6.11 KEGG pathway analysis of differentially expressed genes in 2018 vs 2020. Green column heading represents upregulated pathways in the primary tumour compared to the secondary tumour and red column headings represent down regulated pathways for the same group. Shaded boxes represent the non-significant pathway following FDR correction. Bold pathways indicate pathways of interest.

Up regulated KEGG pathway in 2018	p-value	adjP-value	Down regulated KEGG pathway in 2018	p-value	adjP-value
Herpes simplex virus 1 infection	5.7E-26	2E-23	Metabolic pathways	2.4E-18	8.4E-16
Fanconi anaemia pathway	8.3E-06	0.0014	**Pathways of neurodegeneration - multiple diseases**	3.7E-14	6.4E-12
Cell cycle	0.000033	0.0038	Endocytosis	6.5E-14	7.6E-12
DNA replication	0.000064	0.0055	**Huntington disease**	4.4E-12	3.8E-10
Small cell lung cancer	0.00042	0.029	**Amyotrophic lateral sclerosis**	1.3E-11	9.3E-10
ECM-receptor interaction	0.0012	0.068	Ubiquitin mediated proteolysis	4E-11	2.4E-09
Focal adhesion	0.0014	0.071	**Parkinson disease**	6.8E-11	3.4E-09
p53 signalling pathway	0.0028	0.12	Salmonella infection	1.3E-10	5.9E-09
Mismatch repair	0.0032	0.12	**Alzheimer disease**	2.5E-10	9.7E-09
Homologous recombination	0.0038	0.13	Thermogenesis	7.7E-10	2.7E-08
Breast cancer	0.0056	0.17	Diabetic cardiomyopathy	2.3E-08	7.2E-07
Human papillomavirus infection	0.0076	0.22	Prion disease	3.5E-07	9.8E-06
Maturity onset diabetes of the young	0.0082	0.22	Oxidative phosphorylation	3.8E-07	9.8E-06
Signalling pathways regulating pluripotency of stem cells	0.012	0.29	Sphingolipid signalling pathway	3.9E-07	9.8E-06
One carbon pool by folate	0.018	0.41	Retrograde endocannabinoid signalling	4.2E-07	9.9E-06
Hypertrophic cardiomyopathy	0.03	0.63	Protein processing in endoplasmic reticulum	1.2E-06	0.000027
Nucleotide excision repair	0.032	0.63	Chemical carcinogenesis - reactive oxygen species	1.4E-06	0.000029
Nucleocytoplasmic transport	0.033	0.63	Axon guidance	0.000002	0.000039
GnRH secretion	0.036	0.65	Autophagy - animal	2.1E-06	0.000039
Notch signalling pathway	0.038	0.66	MAPK signalling pathway	2.9E-06	0.000052
Transcriptional mis regulation in cancer	0.041	0.66	Yersinia infection	5.1E-06	0.000085

Table 6.12 KEGG pathway analysis of differentially expressed genes in 2020 vs 2021. Green column heading represents upregulated pathways in the primary tumour compared to the tertiary tumour and red column headings represent down regulated pathways for the same group. Shaded boxes represent the non-significant pathway following FDR correction. Bold pathways indicate pathways of interest.

Upregulated KEGG pathway in 2020	**p-Value**	**adjP-value**	**Down regulated KEGG pathway in 2020**	**p-Value**	**adjP-value**
Herpes simplex virus 1 infection	8.5E-12	0.000000003	Oxidative phosphorylation	2.3E-14	8E-12
Fanconi anaemia pathway	4E-07	0.00007	**Alzheimer disease**	6.1E-13	7.8E-11
N-Glycan biosynthesis	0.00053	0.063	**Parkinson disease**	6.7E-13	7.8E-11
NF-kappa B signalling pathway	0.0016	0.1	Diabetic cardiomyopathy	1.8E-11	1.6E-09
Other types of O-glycan biosynthesis	0.0022	0.1	Prion disease	2.2E-10	0.000000015
Metabolic pathways	0.0023	0.1	Thermogenesis	6.5E-09	0.00000038
Glycosylphosphatidylinositol (GPI)-anchor biosynthesis	0.0025	0.1	Non-alcoholic fatty liver disease	0.00000001	0.00000052
Epstein-Barr virus infection	0.0025	0.1	Chemical carcinogenesis - ROS (Reactive Oxygen Species)	0.000000017	0.00000076
Toxoplasmosis	0.0026	0.1	**Huntington disease**	0.000000073	0.0000029
DNA replication	0.0033	0.12	**Pathways of neurodegeneration - multiple diseases**	0.00000023	0.000008
Inositol phosphate metabolism	0.0039	0.12	Retrograde endocannabinoid signalling	0.0000024	0.000072
Hematopoietic cell lineage	0.0045	0.13	Amyotrophic lateral sclerosis	0.0000025	0.000072
Various types of N-glycan biosynthesis	0.0055	0.14	Spliceosome	0.0000077	0.00021
Homologous recombination	0.0055	0.14	Ribosome	0.000057	0.0014
Other glycan degradation	0.0059	0.14	Bacterial invasion of epithelial cells	0.00016	0.0035
Calcium signalling pathway	0.011	0.24	HIF-1 signalling pathway	0.00016	0.0035
Amino sugar and nucleotide sugar metabolism	0.012	0.24	Cardiac muscle contraction	0.00022	0.0045
Pathways in cancer	0.016	0.32	Endocytosis	0.00024	0.0045
Cell adhesion molecules	0.021	0.35	Salmonella infection	0.00024	0.0045
Measles	0.021	0.35	**Synaptic vesicle cycle**	0.00025	0.0045

6.4.2.1 Recurrent tumours are associated with a down regulation of DNA repair mechanisms.

KEGG analysis of the significantly up and down regulated genes across each comparison has provided interesting insight into the dysregulated pathways associated with disease progression. Of these pathways there were several DNA replication and repair pathways found to be significantly upregulated in the primary tumour. The pathways include the Fanconi anaemia pathway, homologous recombination, missmatch repair and DNA replication. DNA repair is essential for the maintence of genome integrity, and has been explored thoroughly In the context of cancer. Through KEGG analysis of differentially expressed genes, we see a signature of down regulation of DNA repair pathways across the recurrent tumours (2020 and 2021), which via lack of repair, may contribute to enhanced mutational burden of the secondary and tertiary tumours.

STRING networking analysis was used to assess the interacting proteins present in each KEGG pathway, here we explored the Fanconi Anaemia (FA) (figure 6.10) and homologous recombination pathways (figure 6.11). Through this analysis we were able to identify overlapping protein-protein networks in each pathway to help elucidate targets.

We found that BRCA1 and BRCA2 had multiple protein interactions in each KEGG network, as well as RAD50, and RPA2.

Furthermore, the Venn diagram in figure 6.12 displays the overlapping genes present in each pathway that were found via differential genes expresion analysis. Of the genes found to be differentially upregulated in the 2018 tumour there were 3 overlapping between the FA and missmatch repair (MMR) pathways. The comparison with the most overlapping genes was between the FA and homologous recombination (HR) pathways, finding 10 differentailly up regulated genes in common, whereas only 4 genes overlapped between

MMR and HR. When comparing all pathways there was only one overlapping gene: replication protein A2 (RPA2) which functions across all three pathways and is differentially down regulated in the 2020 and 2021 tumours compared to 2018.

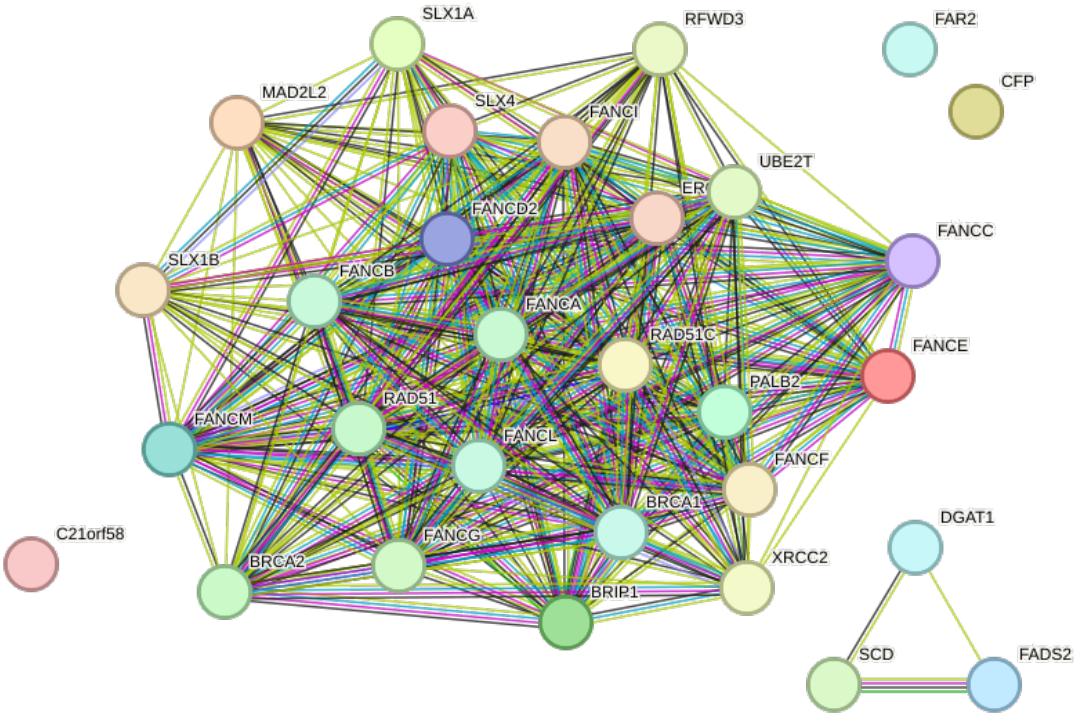

Figure 6.10 STRING network of the Fanconi anaemia pathway. Analysis of protein-protein interactions in the total protein population of the pathway. Spheres represent individuals proteins and lines between spheres represent interactions. https://string-db.org/cgi/my?sessionId=bvHjY4AFFjFQ

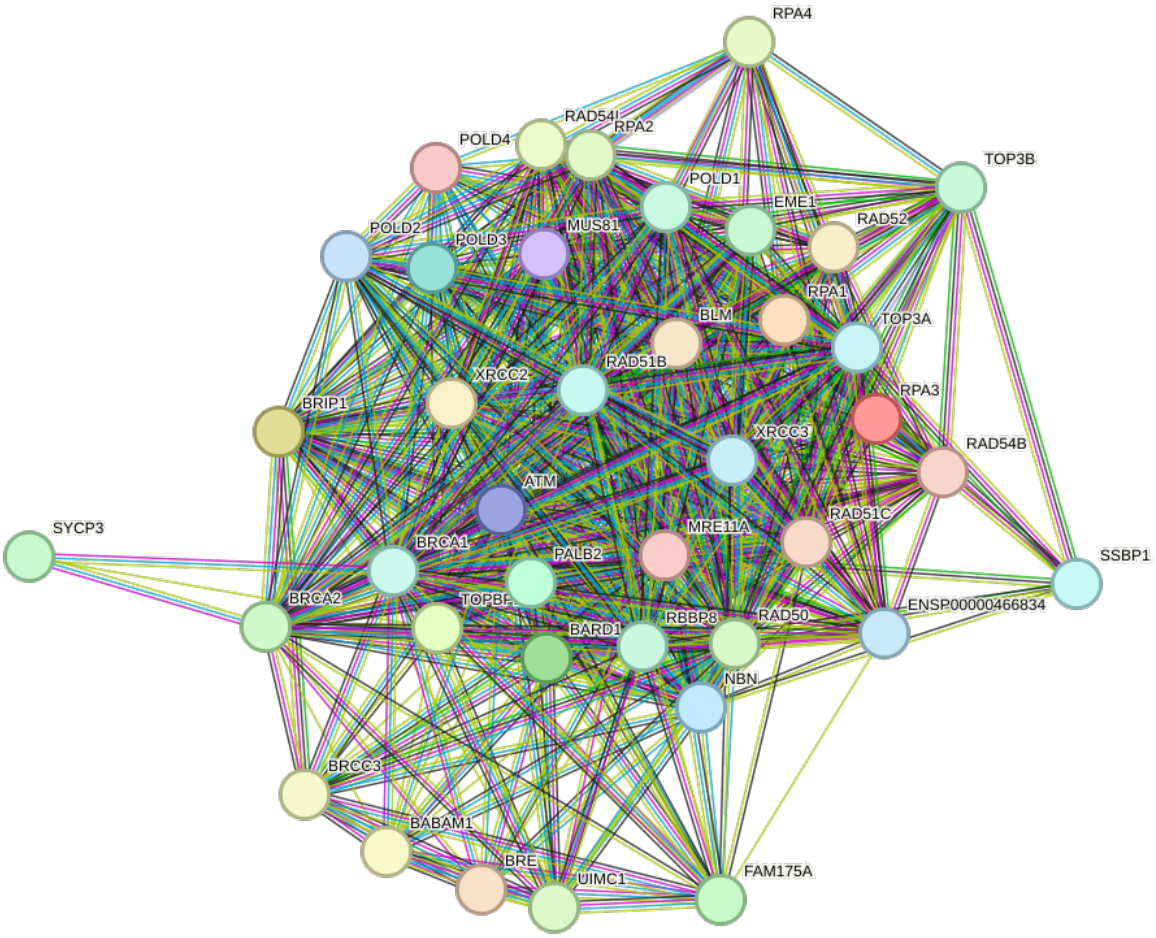

Figure 6.11 STRING network of the homologous recombination pathway. Analysis of protein-protein interactions in the total protein population of the pathway. Spheres represent individuals proteins and lines between spheres represent interactions. https://string-db.org/cgi/my?sessionId=bvHjY4AFFjFQ

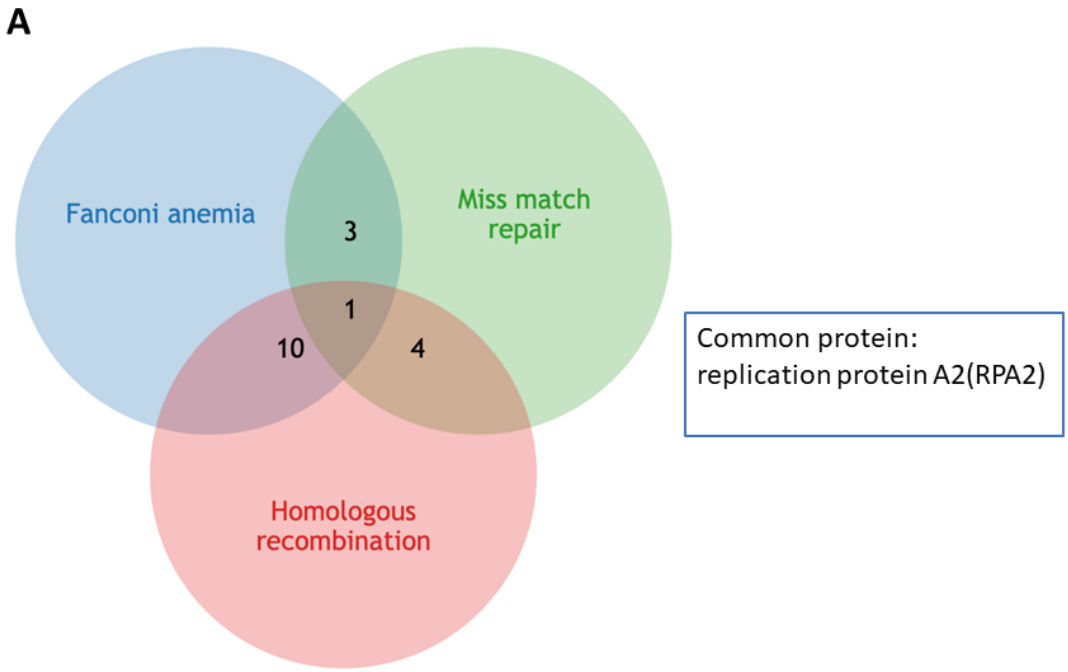

Figure 6.12 Venn diagram showing the overlap of proteins involved in each DNA repair pathway found to be downregulated in tertiary tumor (compared to primary and secondary).

As the single commonly expressed gene between the groups we sought to further explore these findings using replication protein A2 (RPA2). In the cellular response to DNA damage, the RPA complex controls the repair of damage DNA and checkpoint activation. RPA2 stabilises single-stranded DNA that form as a result of DNA replication or DNA stress. Upon binding to DNA, RPA2 prevents reannealing and activates proteins involved in DNA metabolism. Thereby, it plays an essential role both in DNA replication and the cellular response to DNA damage (233). Further assessment using publicly available data sets revealed that RPA2 is overexpressed in glioblastoma tissues when compared to normal healthy brain. Differential gene expression analysis reveals that RPA2 is significantly upregulated in the primary tumour, as such has lower expression values in the secondary and tertiary tumour, suggesting that a reduced expression is linked to recurrence of disease. To assess this the TCGA data set was explored on R2 using survival correlation

analysis. Progression free survival is significantly correlated with RPA expression (figure 6.13c), with a poor prognosis and reduced overall survival being associated with a low expression of RPA2. This supports the data found in this study, as recurrence is linked to poor overall survival.

Other interesting targets to investigate further are BRCA1, BRCA2 and RAD51 due to their significant implication in other cancers and overlap in multiple of the differentially expressed pathways.

The down regulation of DNA pathways repair following exposure to TTFields may be indicative that TTFields has a significant effect on the ability of GBM cells to repair damaged DNA. However, DNA repair activation may be more simply, an innate trend in tumour response to all treatment types. This reduction in repair capacity would significantly inhibit the cancer cell's ability to overcome chemo-irradiation induced DNA insults, and as such TTFields may be acting synergistically with standard of care therapy.

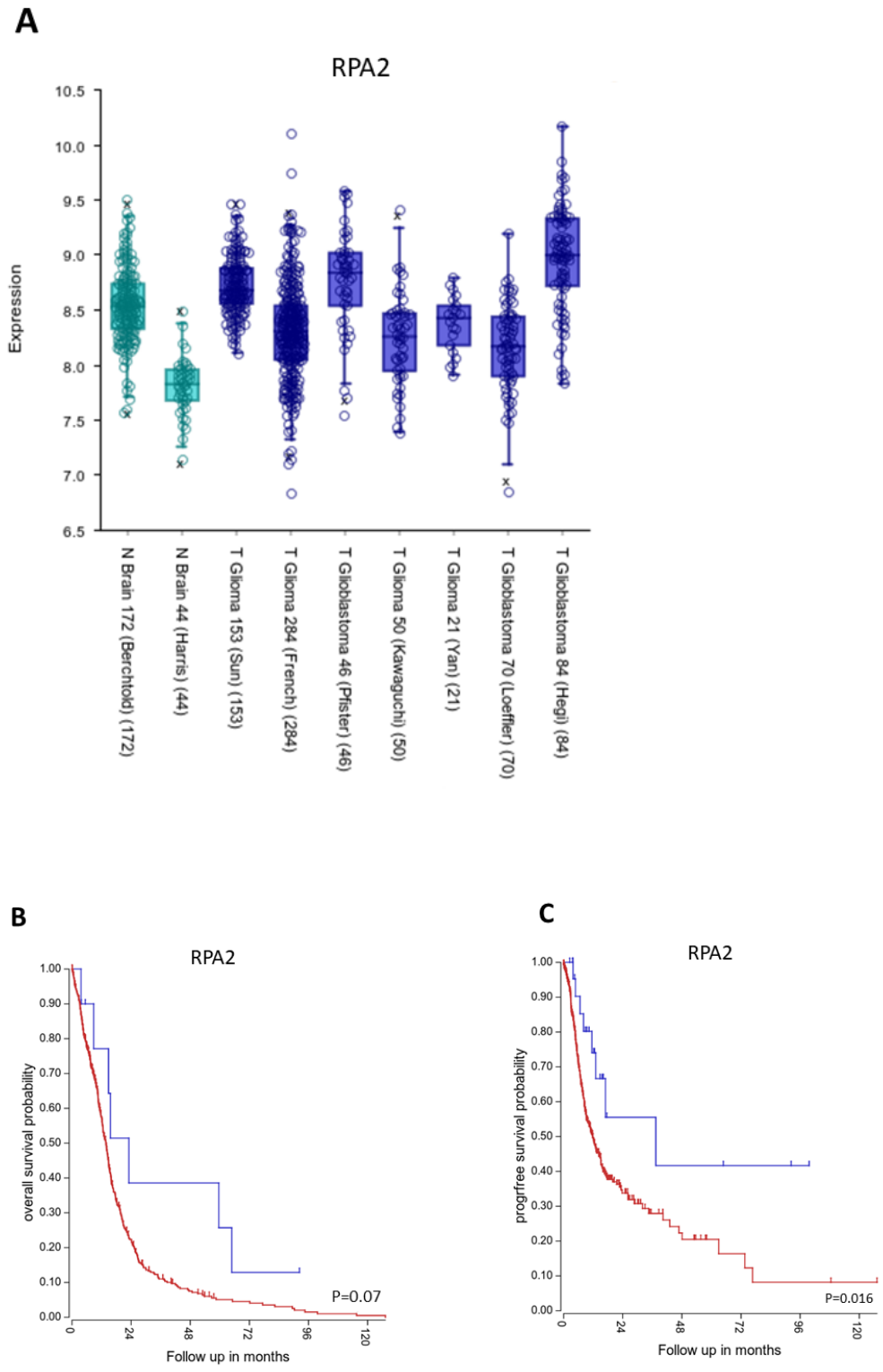

Figure 6.13 Expression and clinicopathological association of RPA2 in glioblastoma. A) Overall expression of RPA2 in glioblastoma data sets compared to normal brain data sets (turquoise). B) Kaplan Meier curve showing the overall survival correlated with RPA2 expression. C) Kaplan curve of progression free survival associated with RPA2 expression. Red = high expression, blue = low expression. Figures created using the R2 genomics platform as previously described. Kaplan Meier curves drawn from the TCGA data set.

6.4.2.2 *Recurrent tumours harness enhanced neurodegeneration and mitochondrial function pathways.*

Comparison of the 2018 tumour with 2020 and 2021 tumours revealed a signature of enhanced neurodegenerative pathways in the recurrent (2020 and 2021) tumours.

Of the proteins associated with these neurodegenerative pathways, genes associated with mitochondrial coding of NADP were significantly present in the cohort. Interestingly, these data align with that previously found in the group via gene array analysis of *in vitro* exposure to TTFields. MTND4 was found to be significantly differentially expressed in the treatment group compared to the untreated controls, furthermore neurodegeneration pathways were found to be amongst the top upregulated pathways . Of note, the Parkinson's, Huntington's, and Alzheimer's pathways were significantly differentially expressed in all comparisons.

STRING analysis of interacting proteins in each pathway is shown in figures 6.14 and 6.15, where solute carriers SLC30, SLC39 and MTND subunits are particularly of note, with many interacting partners.

There were 32 common differentially expressed genes found in our analyses that overlapped between the three pathways, with 32 overlapping between Huntington's and Parkinson's. Furthermore, there were 32 overlapping genes between Huntington's and Alzheimer's and 35 overlapping differentially expressed genes between Alzheimer's and Parkinson pathways (figure 6.17). Of note the MTND subunits were highly present as shown in table 6.13.

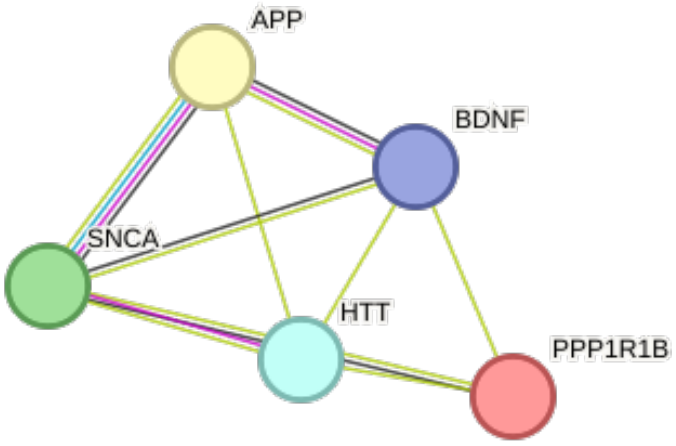

Figure 6.14 STRING network of the Huntingdon disease pathway. Analysis of protein-protein interactions in the total protein population of the pathway. Spheres represent individual proteins and lines between spheres represent interactions. https://string-db.org/cgi/my?sessionId=bvHjY4AFFjFQ

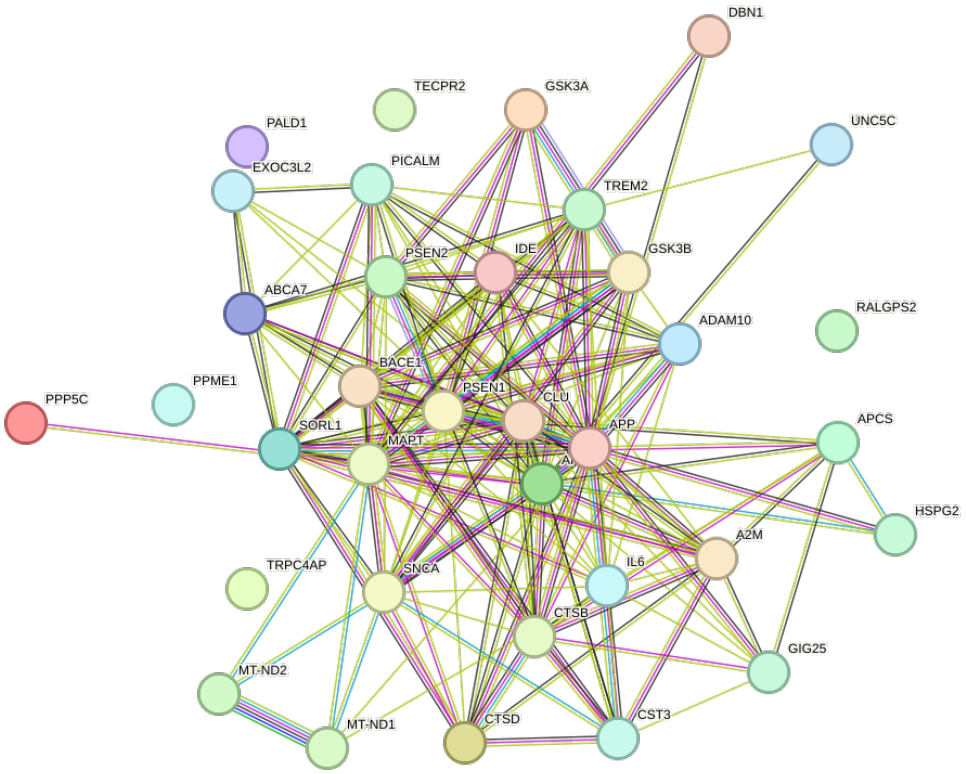

Figure 6.15 STRING network of the Alzheimer's disease pathway. Analysis of protein-protein interactions in the total protein population of the pathway. Spheres represent individual proteins and lines between spheres represent interactions. https://string-db.org/cgi/my?sessionId=bvHjY4AFFjFQ

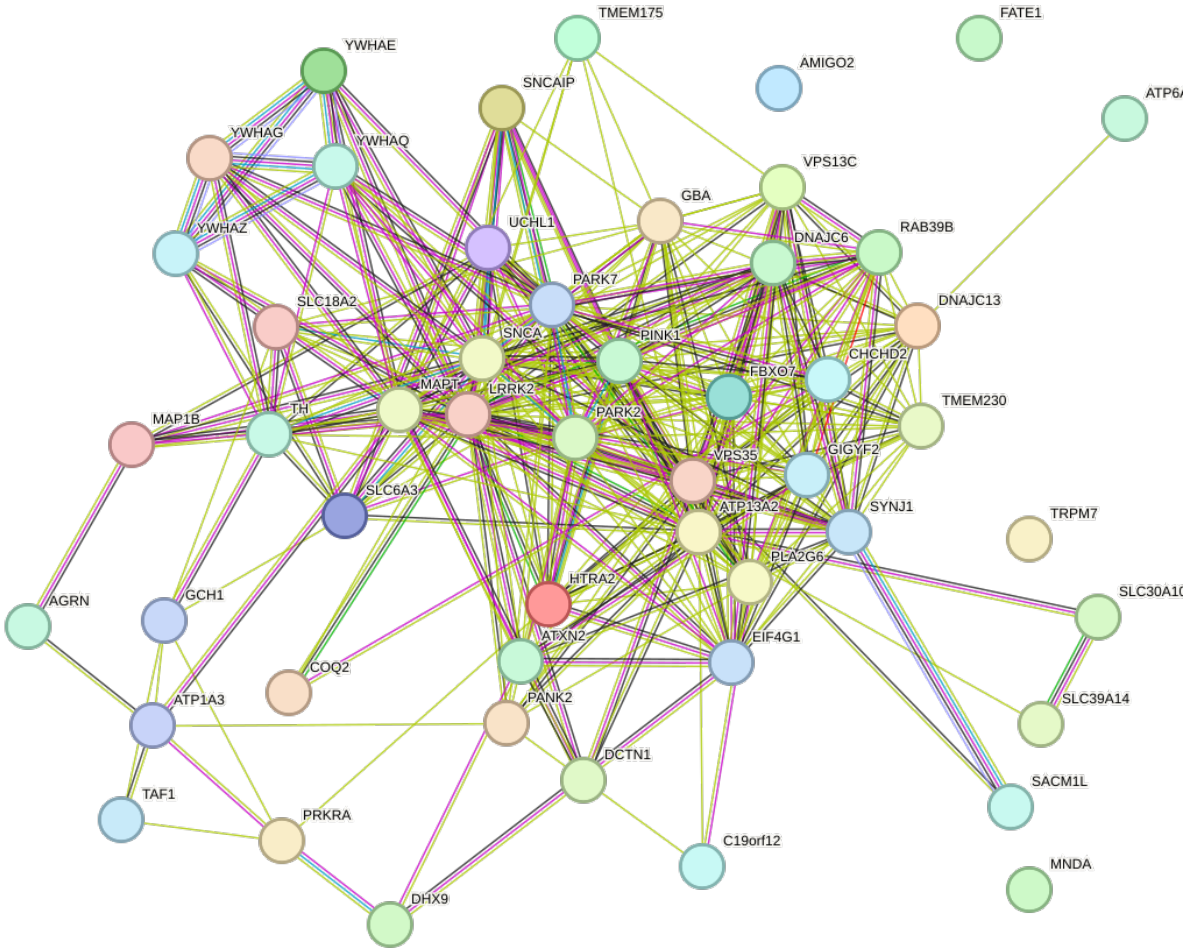

Figure 6.16 STRING network of the Parkinson's disease pathway. Analysis of protein-protein interactions in the total protein population of the pathway. Spheres represent individuals proteins and lines between spheres represent interactions. https://string-db.org/cgi/my?sessionId=bvHjY4AFFjFQ

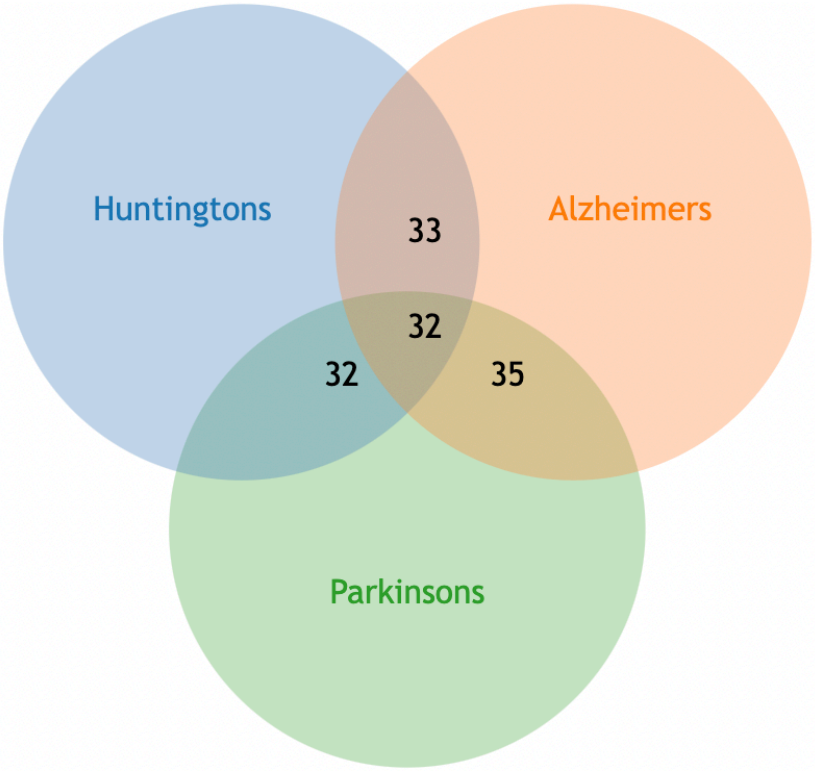

Figure 6.17. Venn diagram showing the overlap of proteins involved in each neurodegenerative pathway found to be upregulated in tertiary tumor (compared to primary and secondary).

Table 6.13 Table of the common differential down regulated proteins in all three pathways.

Differentially DR genes present in all 3 pathways
ADRM1 26S proteasome ubiquitin receptor(ADRM1)
ATP synthase F1 subunit delta(ATP5F1D)
ATP synthase F1 subunit gamma(ATP5F1C)
NADH:ubiquinone oxidoreductase subunit A13, A3, B11, B4, C1(NDUF)
NDUFA4 mitochondrial complex associated like 2(NDUFA4L2)
cytochrome c oxidase subunit 6B1(COX6B1), subunit 7C(COX7C)
cytochrome c1(CYC1)
kinesin family member 5A(KIF5A)
mitochondrially encoded ATP synthase 6(MT-ATP6), synthase 8(MT-ATP8)
cytochrome c oxidase subunit 6B1(COX6B1), subunit 7C(COX7C)
mitochondrially encoded NADH 4L dehydrogenase(MT-ND4L)
mitochondrially encoded NADH dehydrogenase 1(MT-ND1), 2(MT-ND2), 3(MT-ND3), 4(MT-ND4), 5(MT-ND5), 6(MT-ND6)
mitochondrially encoded cytochrome b(MT-CYB)
mitochondrially encoded cytochrome c oxidase I(MT-CO1), II(MT-CO2), III(MT-CO3)
proteasome 20S subunit beta 5(PSMB5)
solute carrier family 25 member 6(SLC25A6)
tubulin alpha 1b(TUBA1B)
tubulin alpha 1c(TUBA1C)
tubulin beta 4A class IVa(TUBB4A)
voltage dependent anion channel 2(VDAC2)

In order to interrogate findings and align with glioblastoma, the gene ADRM1 was assessed via publicly available data sets using the R2 genomics platform. We find that the expression of ADRM1 is variable across datasets, but tends to exhibit lower expression when compared to normal brain tissue. To further this, survival analysis was carried out via Kaplan Meier curves. Progression free survival is significantly associated with the expression of ADRM1 in glioblastoma patients (TCGA), whereby high expression confers a decrease in PFS. As such this may indicate that an upregulation in pathways expressing ADRM1 is associated with tumour progression, and may reveal an interesting biomarker for GBM recurrence and potentially treatment resistance.

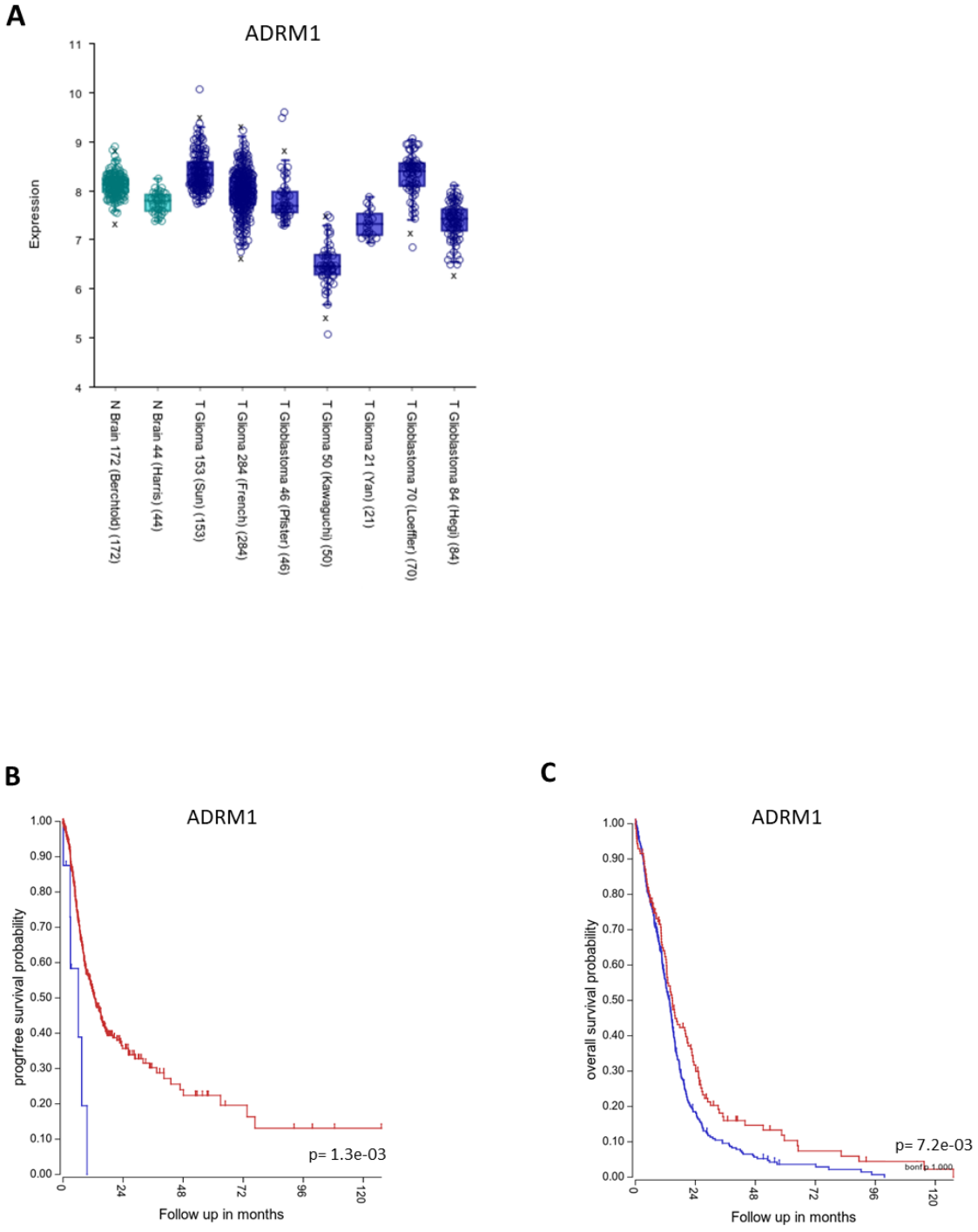

Figure 6.18 Expression and clinicopathological association of ADRM1 in glioblastoma. A) Overall expression of ADRM1 in glioblastoma data sets compared to normal brain data sets (turquoise). B) Kaplan Meier curve showing the PFS correlated with ADRM1 expression. C) Kaplan curve of OS associated with ADRM1 expression. Red = over expression, Blue = low expression. Figures created using the R2 genomics platform as previously described. Kaplan Meier curves drawn from the TCGA data set.

6.4.2.3 *Multiple pathways linked to ion channel control are dysregulated upon tumour progression.*

KEGG pathway analysis and gene ontology analysis have both revealed that there are multiple cellular processes and biological pathways involved with ion channel transport and function that are significantly dysregulated.

Several of the top 20 most differentially up or down regulated genes are solute carriers, suggesting a key role in ion movement in the progression of this tumour, and genetic alterations associated with TTFields treatment.

6.4.2.4 *Overlapping pathways*

KEGG pathway analysis revealed that there were several significantly altered pathways present throughout the lifespan of the tumour, and these may hold bearing in determining mechanistic insight into the genetic response of TTFields in vivo.

Here we find that there are 6 total overlapping pathways between the three comparisons. The highest number of overlapping pathways was found between the 2020 vs 2021 comparison and the 2018 vs 2021 comparison, with 18 KEGG pathways in common. The lowest number of overlapping pathways was found in the 2020 vs 2021 and 2018 vs 2020 comparison.

This provides evidence that the 2020 tumour is an intermediary for the genetic alterations observed tumour between the primary, treatment naïve tumour, and the tertiary tumour with heavy TTFields exposure. Thus, giving evidence for evolution of the tumours genetic landscape associated with TTFields exposure and recurrence.

We also found several unique pathways belong to each comparison. Further research into these may elucidate potential target mechanisms for disease recurrence.

A

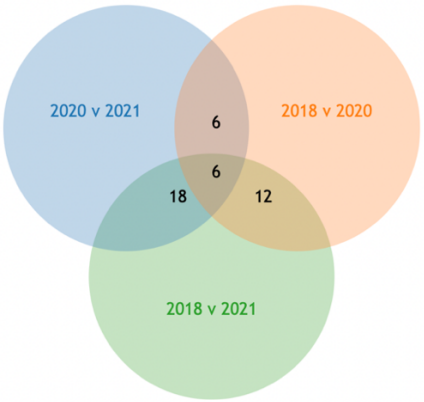

B

Unique to 2018 vs 2021	Unique to 2020 vs 2021	Unique to 2018 vs 2020
Lysine degradation	Hematopoietic cell lineage	ECM-receptor interaction
Chronic myeloid leukemia	Calcium signaling pathway	Focal adhesion
Colorectal cancer	Cell adhesion molecules	p53 signaling pathway
Pancreatic cancer	Phosphatidylinositol signaling system	Breast cancer
Inflammatory mediator regulation of TRP channels	Ubiquitin mediated proteolysis	Human papillomavirus infection
Hedgehog signaling pathway	PPAR signaling pathway	Maturity onset diabetes of the young
	Peroxisome	Signaling pathways regulating pluripotency of stem cells
	PD-L1 expression and PD-1 checkpoint pathway in cancer	One carbon pool by folate
	Axon guidance	Hypertrophic cardiomyopathy
	Chemokine signaling pathway	Nucleotide excision repair
	Glycosphingolipid biosynthesis - globo and isoglobo series	GnRH secretion
	Glycosphingolipid biosynthesis - lacto and neolacto series	Notch signaling pathway
		Amoebiasis
		Antifolate resistance
		PI3K-Akt signaling pathway
		Arrhythmogenic right ventricular cardiomyopathy
		Dilated cardiomyopathy
		Progesterone-mediated oocyte maturation

Figure 6.19 Overlapping KEGG pathways between the three comparisons.

6.5 Extended *in vivo* TTFields treatment confers a unique ion channel signature.

We then sought to further assess the genetic landscape in the three tumour samples, and enriched our analyses to assess expression patterns of ion channels genes of interest throughout this project.

Excitingly, upon enriching our analyses for ion channel genes we observed the unique ion channel expression pattern in the patient tissue as we observed in cell line experiments. When comparing CLIC1 and CLIC4 ion channel expression we see a significantly reduced expression of both genes in the 2021 samples when compared to 2018 sample, and 2020. This marked decrease mirrors the expression pattern observed in cell lines following TTFields exposure, confirming that *in vitro* findings are recapitulated in an *in vivo* setting. Similarly, SCNN1D, TRPM7, KCNNA4, P2RX7 reveal a downregulation in expression across the recurrent tumours, with a significant decrease observed in 2021 samples. Importantly, all three replicates possess the same signature of reduction. Interestingly, the primary tumour harbours a low expression of KCNB1 and KCNJ10, which is significantly upregulated

following recurrence and initial exposure to chemo-irradiation and TTFields therapy. This upregulation this then followed by a down regulation in the tertiary tumour, suggesting the tumour entering an altered state associated with the movement of potassium ions. Whilst we cannot confirm that these genetic changes are solely due to TTFields exposure due to the myriad of contributing factors, we can use these data to support lab-based findings. Here the primary (2018) tumour acts as a 'control' giving insight into the mutational and base line expression status of ion channels in a glioblastoma sample. By comparing the secondary (2020) tumour to the primary tumour we are able to elucidate genetic changes happening in association with TMZ, RXT and minimal TTFields exposure, as well as the initial mechanisms of recurrence and potential tumour resistance. Comparing the 2020 and 2021 tumour gives an indication of what is occurring following extended TTFields treatment, with no further TMZ or RXT. Furthermore, comparison of the primary and tertiary tumours reveals evolutionary insight and mechanistic understanding of extended TTFields exposure compared to a treatment naïve state.

Furthermore, we assessed the overall expression of the ion channel panel across the total cohort, finding that CLIC1 was significantly up regulated in the primary tumour compared to the secondary tumour, and that KCNJ10 was significantly down regulated. Additionally, SLC2A13 was significantly upregulated in the 2018 tumour vs 20201, and SCNN1D was significantly upregulated in the secondary tumour (2020) vs the tertiary tumour (2021). These data suggest that although expression differences are clear when performing supervised hierarchical clustering, these expression patterns may not be significantly different in the whole cohort.

Interestingly, multiple levels of analysis have revealed a dysregulation of ion channel expression throughout the recurrence of the tumour. Ion channel mediated pathways such

as ion binding, addiction and synaptic control have been found to be significantly differentially expressed when comparing the primary tumour to the secondar and tertiary tumour. These data support the feasibility studies carried out through the duration of this project, supporting findings indicating that ion channels may provide mechanistic insight into the success of TTFields therapy.

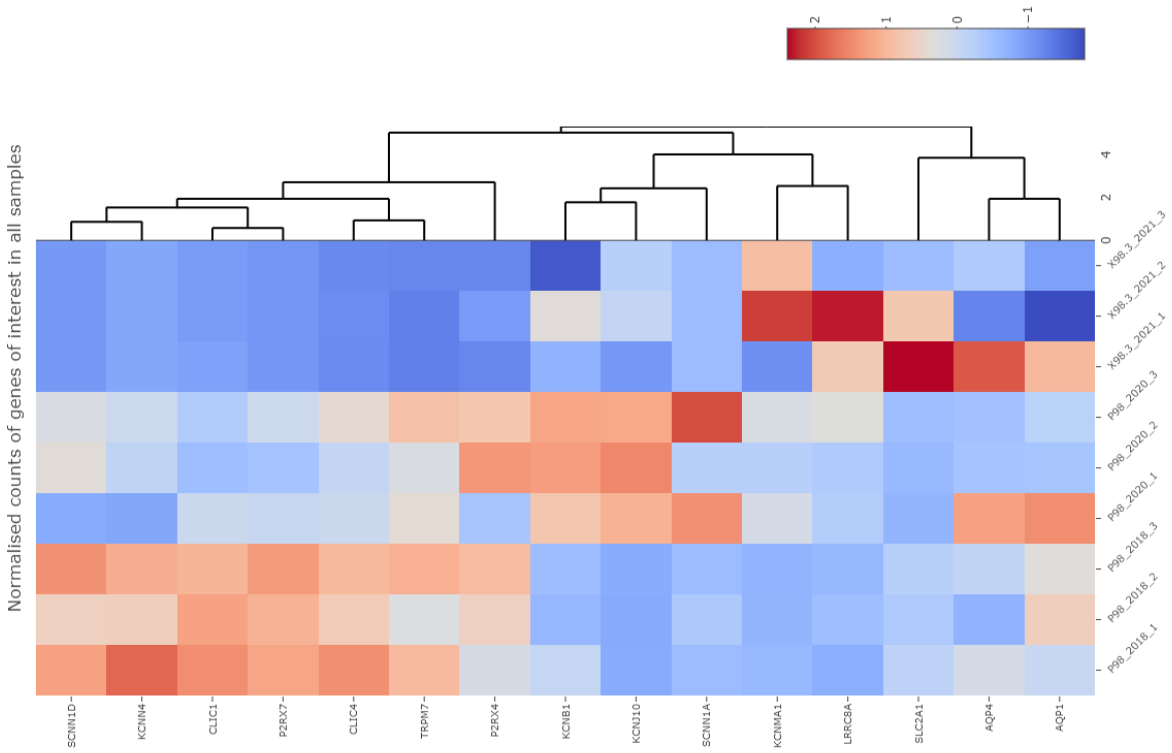

Figure 6.20 Heatmap of the normalised counts of the genes of interest in all samples. Clustering is seen for CLIC1, CLIC4, SCNN1A, SCNN1D, P2RX7, P2RX4, KCNMA1, KCNN4, AQP1, AQP4 ,TRPM7 ,KCNB1 ,KCNJ10, SLC2A1, LRRC8A. Analysis and figure by S.H

Table 6.14 Significantly differentially expressed ion channel genes in the whole cohort. (cut off adjusted P-values <0.05)

Differential expression 2018 vs 2020		
Gene name	**Log fold change**	**pAdj**
CLIC1	1.63092	0.047224
KCNJ10	-1.754267472	0.003010441
Differential expression 2018 vs 2021		
Gene name	**Log fold change**	**pAdj**
SLC2A13	5.819508641	3.22E-06
Differential expression 2020 vs 2021		
Gene name	**Log fold change**	**pAdj**
SCNN1D	4.187467061	0.004616992

6.6 Expression of CLIC1 and CLIC4 tumour tissue exposed to TTFields *in vivo*.

This project has sought to elucidate the role of CLIC1 and CLIC4 ion channels in glioma pathology, and as potential targets for TTFields therapy. As such, patient 98 tissues were used as patient model and a mechanism to validate our candidate targets in the *in vivo* exposure of TTFields. Following promising findings from RNA sequencing analysis, we sought to validate the expression profiles of CLIC1 and CLIC4.

Initial experiments were conducted to understand the overall expression levels of CLIC1 and CLIC4 across the primary lesion (GBM98a) compared to the recurrent TTFields exposed tumour specimens (GBM98b and GBM98c). Immunohistochemistry analysis staining against CLIC1 and CLIC4 was firstly used to determine the expression patterns and protein localisation (figure 6.21) across the three matched samples. CLIC1 and CLIC4 were predominantly localised to the cytoplasm, however the distribution of cytoplasmic staining was not as markedly elevated as that observed in other patient tissues (figure 6.21). Interestingly the nuclear expression was of CLIC1 significantly higher than the cytoplasmic expression in the primary tumour. This observation is noteworthy as CLIC1 localises to the membrane and cytoplasm in its functionally active form. Additionally, comparisons were drawn between TTFields exposed tissue and primary adult and paediatric HGGs, with overall staining intensity in the primary tissue being comparable across patient 98 and other HGG tissues used in microarrays in this study.

To further this, we sought to assess the protein expression of CLIC1 and CLIC4 across the primary and subsequent recurrent tumours (figure 6.21b). CLIC1 was significantly down regulated in GBM98(c) when compared to the to primary tumour (GBM98(a)) $p= <0.01$ and first recurrence (GBM98(b)) $p=<0.001$. Conversely, despite GBM98(c) demonstrating lower average overall CLIC4 staining, there were no significant differences found in the

primary lesion compared to recurrent lesions. Thus, validating the down regulation of CLIC1 and CLIC4 mRNA observed in RNA sequencing analysis.

This is interesting as this research has identified that CLIC overexpression is linked to increasingly aggressive disease including higher WHO grade. As such, one may expect that recurrent tumours would exhibit and increased expression of CLIC proteins, as these are the aggressive and resistant subclone populations. However, previous experiments in this study have identified that there is an overexpression of CLICs in the core region of the tumour when compared to the invasive region. Theoretically, it is the cells in the invasive margin that remain, and cause tumour recurrence, and therefore exhibiting lower levels of CLIC expression. Another explanation for this may be the result of TTFields exposure. Genome wide expression analysis found that CLIC1 and CLIC4 were both down regulated following TTFields exposure in KNS42 cells, and this effect may be being recapitulated *in vivo*.

Research including this study, has previously noted that high expression of CLIC1 and CLIC4 are prognostic indicators of poor or reduced overall survival. As of February 2023, Patient 98 was 5 years post diagnosis, with only 5% of patients falling into the >5 year survival category. The relatively reduced expression of CLIC1 and CLIC4 in the recurrent tumour samples may be contributing to the more favourable prognosis and overall survival of patient 98.

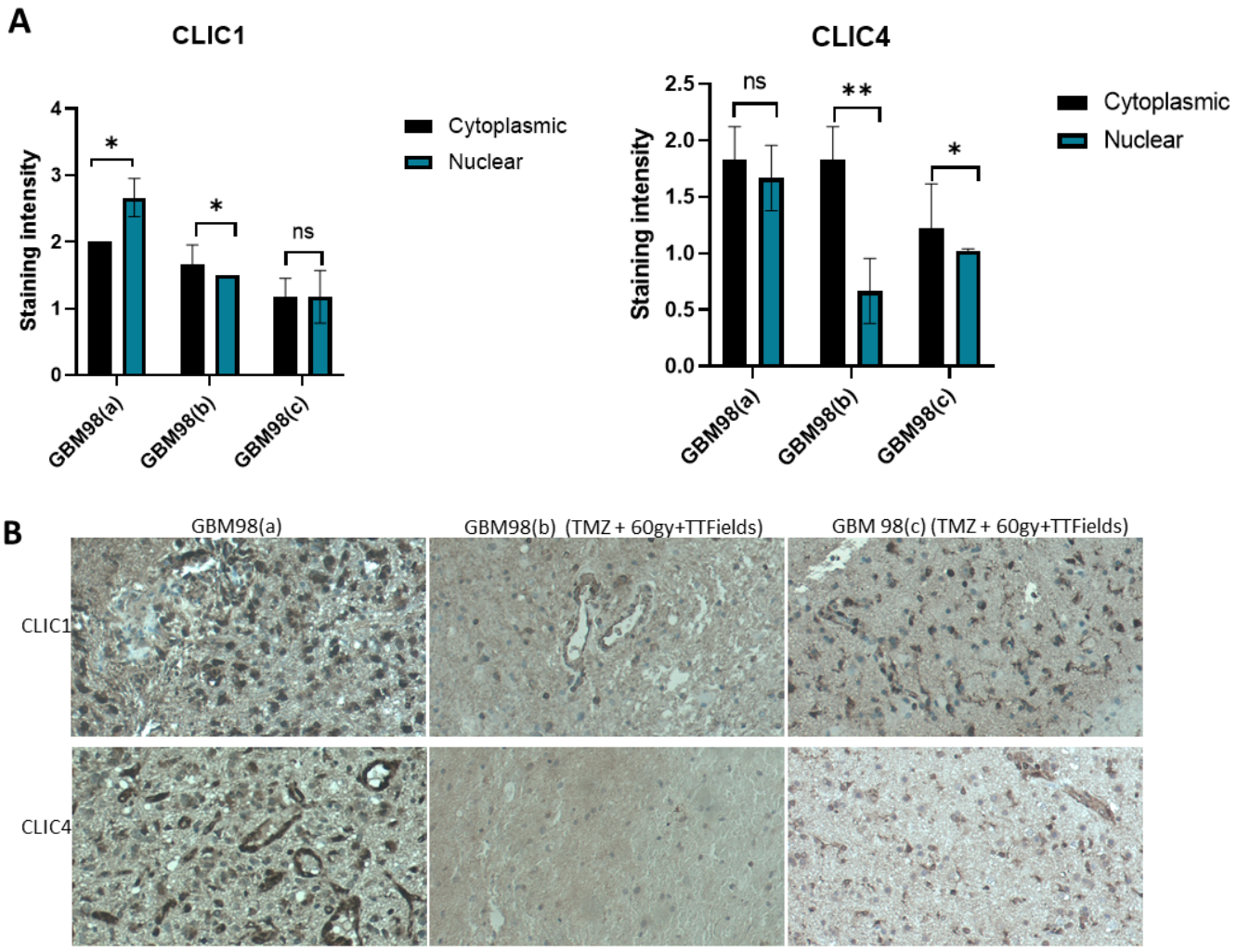
A
CLIC1
Staining intensity
4
3
2
1
0
*
*
ns
GBM98(a)
GBM98(b)
GBM98(c)
Cytoplasmic
Nuclear
CLIC4
Staining intensity
2.5
2.0
1.5
1.0
0.5
0.0
ns
**
*
GBM98(a)
GBM98(b)
GBM98(c)
Cytoplasmic
Nuclear
B
GBM98(a)
GBM98(b) (TMZ + 60gy+TTFields)
GBM 98(c) (TMZ + 60gy+TTFields)
CLIC1
CLIC4

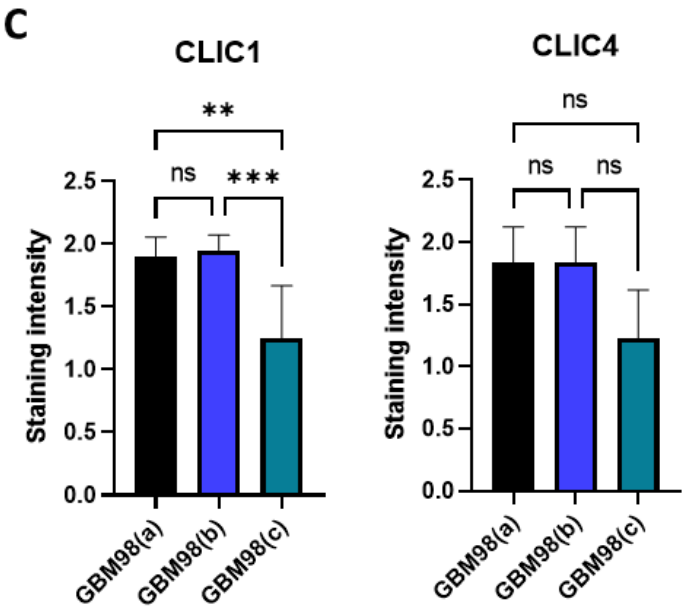

Figure 6.21. CLIC1 is significantly down regulated in recurrent tumour samples. Analysis via immunohistochemistry was carried out on tissue sections from patient 98. Key: GBM98(a): first look surgery, no treatment; GBM98(b) recurrent tumour 1, treatment with TMZ, 60gy and TTFields; GBM(c) recurrent tumour 2, treatment with TMZ, 60gy and TTFields. Each section was stained in triplicate, and scoring carried out across 4 independent and randomly selected areas of each tissue specimen. A) Relative protein expression of CLIC1 and CLIC4 as shown by staining intensity of cytoplasmic and nuclear compartments. B) Representative images of tissues sections stained for CLIC1 and CLIC4. Magnification 20x. C) Comparison of the cytoplasmic expression of CLIC1 and CLIC4 across all three tumour samples.

6.6.1 Spatial analysis of CLIC1 and CLIC4 expression in GBM98(c) tissue

Sequencing studies performed by our group have shown that the cells present in the invasive margin are more similar to recurrent disease than the central region of the primary tumour (234,235). To test the hypothesis that the down regulation of CLIC1 observed in GBM98(c) was a result of cells from the invasive margin of the primary tumour making up a significant portion of the recurrent tumour, spatial analyses was carried out on distinct regions of GBM98(c). There were no significant differences in the expression of CLIC4 across distinct neuroanatomical regions of the tumour specimen.

There were, however, significant differences in the expression of CLIC1 in 98.2 vs 98.5 – the core and invasive regions respectively ($p=<0.05$). Unexpectedly, these data directly conflict previous findings and our hypothesis. Here we find that CLIC1 is significantly over expressed in the invasive region (98.5) of GBM98(c) when compared to the core region (98.2). Previously, the study confirmed across adult glioblastoma TMAs that there is a significant upregulation of CLIC1 in the core compared to the invasive region. Although not anticipated, this result is likely due to sample bias as a direct result of a n=1. Additionally, 98.5 remains very cellular, so may not represent the true invasive edge.

Unfortunately, analyses on GBM98(a) and GBM98(b) was not possible as the centre that collected the tumours did not separate into distinct regions.

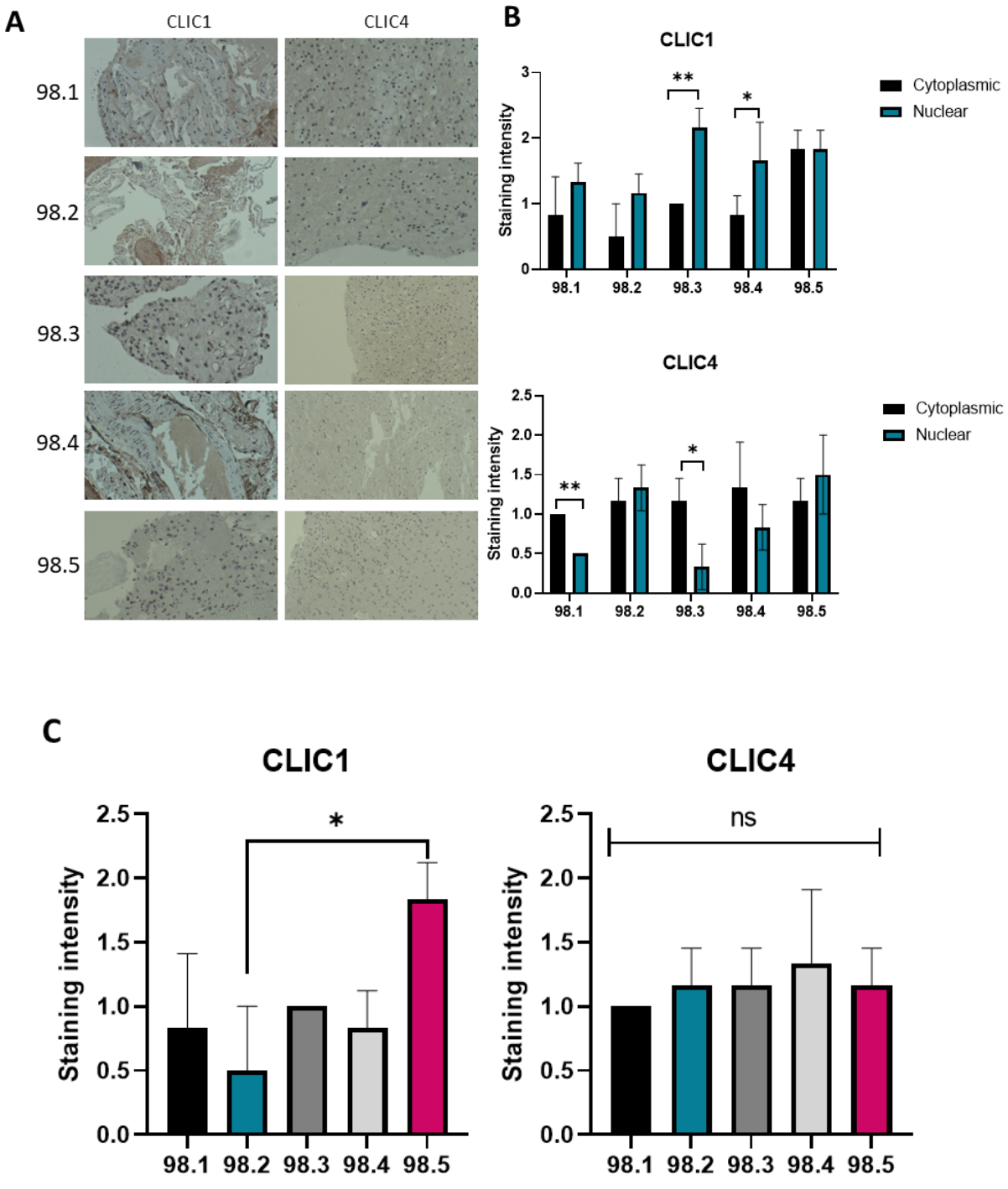

Figure 6.22 Spatial expression of CLIC1 and CLIC4 in GBM98(c). A) Representative image of the staining intensity of CLIC1 and CLIC4 expression across different neuroanatomical regions of the tumour. Magnification x10 B) Quantification of the relative staining intensity in nuclear and cytoplasmic regions. C) Comparison of the cytoplasmic expression of CLIC1 and CLIC4 in different neuroanatomical regions.

6.7 Characterisation of cell lines derived from GCE98(c)

6.7.1 GIN98 and GCE98 cell morphology and behaviour

GCE98 and GIN98 were both derived from GBM98(c) – specifically the core and invasive regions, respectively. Low passage patient derived cell lines are essential in maintain biological validity and retaining inherent properties that are representative of the original tumour. Despite being derived from the same tumour, GIN98 and GCE98 cells behave very distinctly. As shown in figure 6.23 they two cell lines have very distinct morphologies, with GIN98 showing a spindly like morphology, with cells forming long projections and filling the space independently. Conversely, GCE98 cells are more compact with shorter cell bodies, opting to grow in clusters across the culture vessel. This is matched with distinct growth kinetics observed between the two. The average doubling time for GIN98 is around 30 hours, whereas GCE98 take longer at 40 hours, with PrestoBlue readings on control GIN98 cells being around 1.25x that of GCE98, indicating increased metabolic activity.

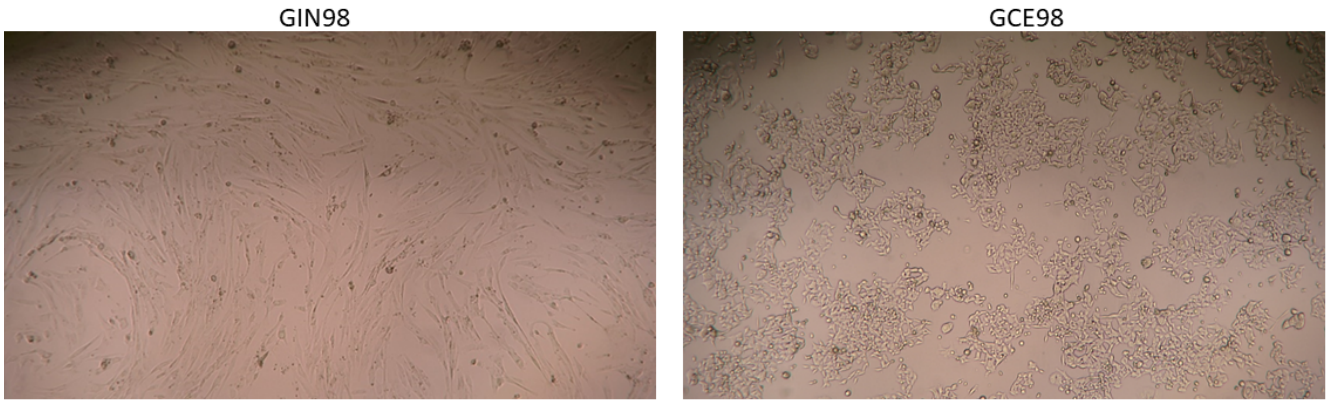

Figure 6.23 Representative image of GCE98 and GIN98 cells. Cell morphology captured by inverted light microscopy at 10x magnification.

6.7.1.1 GIN98 cells fail to form neurospheres.

The ability of cells to form neurospheres demonstrates an ability to proliferate indefinitely, is associated with stem cell like behaviour, and as such can measure tumour forming capacity of cell lines. Through this the neurosphere forming capacity of cells derived from the core and invasive region of the recurrent tumour GBM98(c) was characterised.

It was hypothesised that the inability of GIN98 to form neurospheres may be a result of epithelial-mesenchymal-transition, resulting in a reduction in overall stemness. As such, GBM98a,b,c tissue was stained to explore the expression of Zeb1, a marker associated with EMT. Results found that the cytoplasmic expression of ZEB1 in GBM98(c) (both the core and invasive regions) was higher than both the temporal lobe, and primary glioma tissue from a matched patient. Interestingly, the nuclear expression in all GBM98 specimens was significantly elevated compared to the nuclear expression of ZEB1 in GBM28. High expression of ZEB1 may link to EMT but this needs much further analysis to validate findings. Research has suggested that Zeb1 is cytoplasmic in central tumour regions (reminiscent of our core samples), transitioning to the nucleus in the invasive regions of tumours (28). The highest overall expression of ZEB1 was seen in GBM98c core region, the tissue specimen that GCE98 was derived from. If the lack of neurosphere formation in GIN98 was in fact due to EMT, one would expect an over expression in the GBM98c invasive region tissue, however this is not the case.

It can be assumed that *in vivo* exposure to TTFields is not the reason for the inability of GIN98 to form neurospheres as we have demonstrated that KNS42 and SF188 cells exposed to invitro TTFields do form neurospheres. However, the effects of *in vivo* TTFields may be more pertinent, exhibiting a more pronounced effect on tumour biology and as

such cell line behaviour. Equally, the expression level of CLIC1 and CLIC4 is unlikely to be the cause, as GIN98 expresses both at mRNA level, albeit less so than the primary tumour.

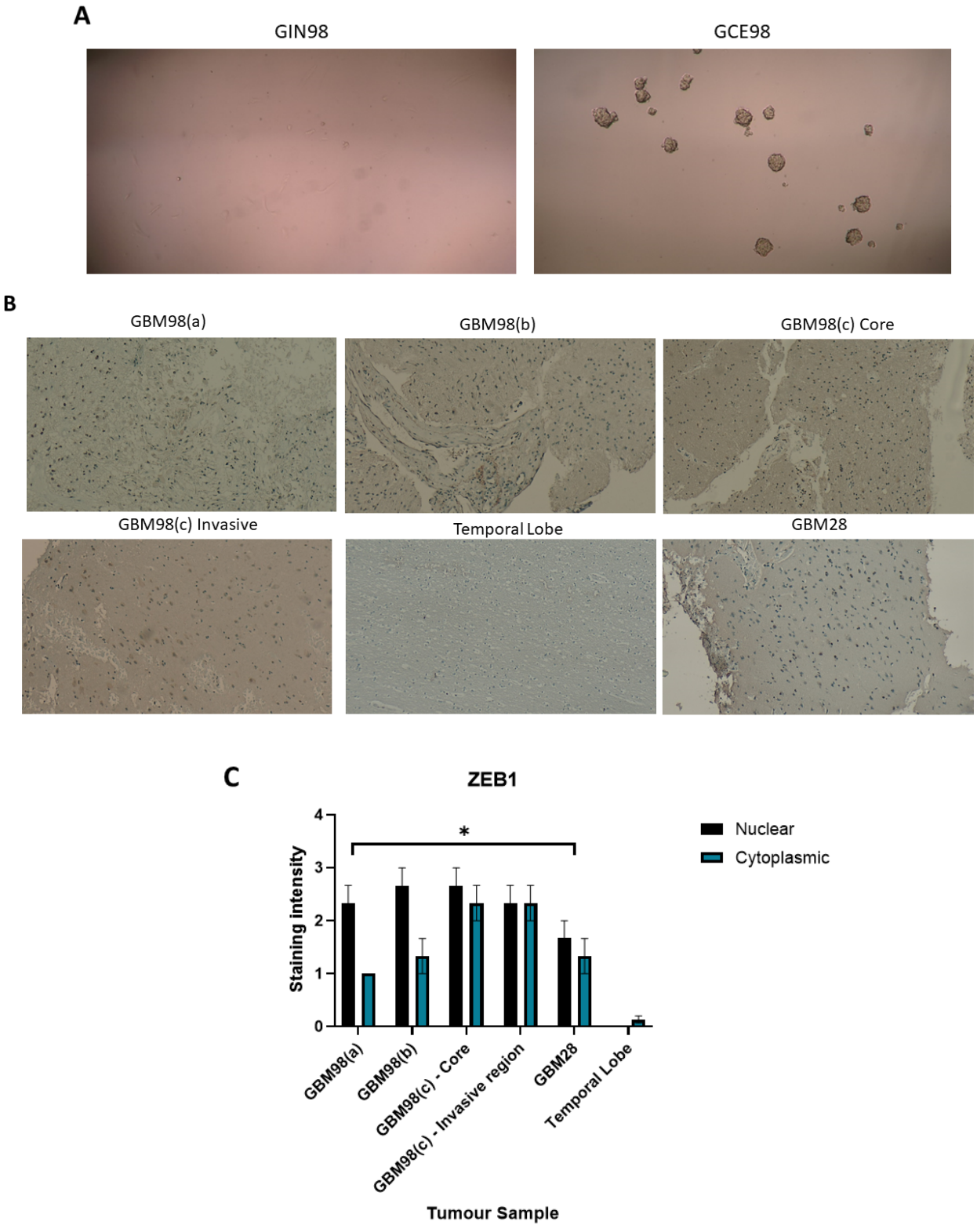

Figure 6.24 Gin98 is unable to form sufficient neurospheres. A) representative images of the neurosphere forming capacity of GIN98 and GCE98 at day 3. 10x magnification. B) patient 98 tumour tissue was stained with ZEB1 a recognised EMT marker to assess whether the inability to form neurospheres, and therefore reflect stemness associated with EMT. C) quantification of the staining intensity of ZEB1 in patient 98 tumour tissues compared to temporal lobe and GBM28. Statistical analysis via t-test.

6.7.2 Patient 98 has lower overall expression of CLIC1 and CLIC4 compared to pHGG cell lines.

To expand the studies, the patient derived cell lines GIN98 and GCE98 were compared to the panel of pHGG cell lines – SF188, KNS42 and GCE62. Firstly, this allowed exploration of the expression of ion channels in these adult derived cell lines, but also to aid identification of any expression changes seen following *in vivo* TTFields in order to validate *in vitro* TTFields experiments. The panel of ion channel candidates explored in chapter 3 were assessed at mRNA level in GIN98 and GCE98 cells. Here its shown (figure 6.25) that all of the ion channel genes identified as implicated in gliomagenesis are expressed in both cell lines. Further work sought to stratify these results and compare the CLIC1 and CLIC4 specific expression in GIN98 and GCE98 cells compared to pHGG cell lines.

Firstly, rtPCR identified that GCE98 significantly over expresses CLIC1 compared to GIN98 ($p=<0.05$), conflicting findings at the protein level from IHC experiments on distinct spatial regions. Interestingly, CLIC1 expression in the primary paediatric line GCE62 was also significantly over expressed when compared to GIN98 cells ($p=<0.01$). Furthermore, analysis of CLIC4 expression revealed that GCE98 ($p=<0.01$), SF188 ($p=<0.05$) and GCE62 ($p=<0.01$) significantly overexpress CLIC4 when compared to GIN98. Here a clear down regulation of CLIC1 and CLIC4 is observed in the invasive region of recurrent GBM treated with TTFields when compared to non-TTFields exposed cell lines.

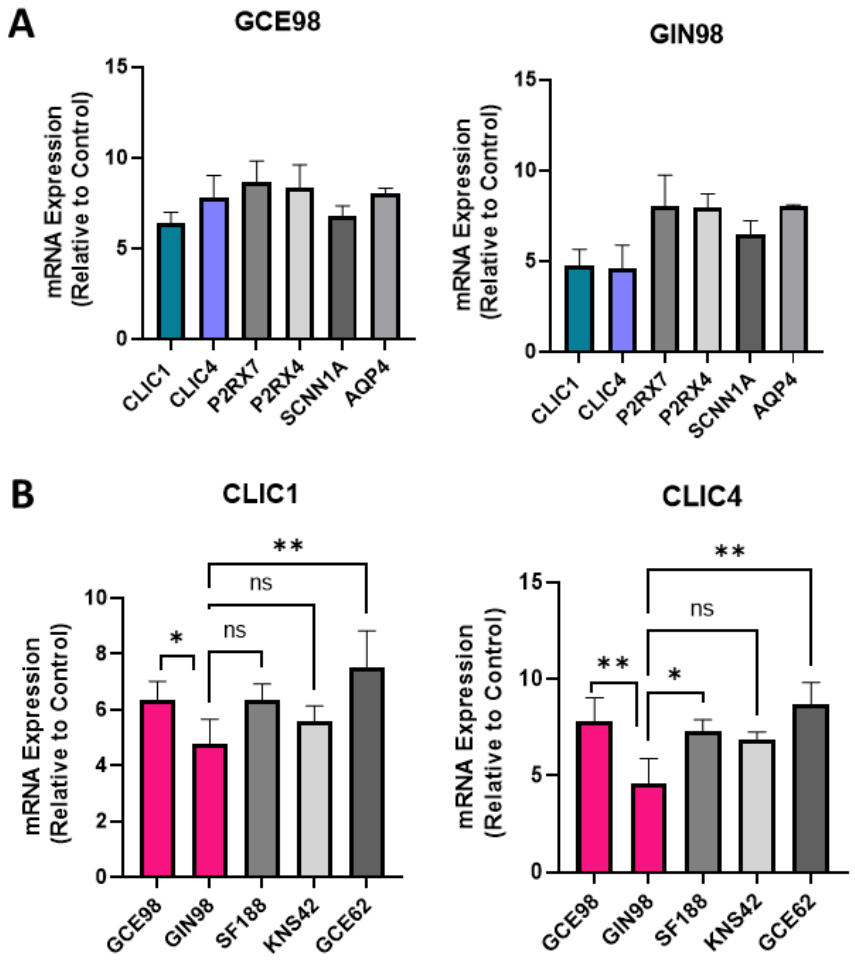

Figure 6.25 CLIC1 and CLIC4 expression are downregulated in GIN98 cells compared to pHGG. A) rtPCR was used to assess the expression levels of a panel of ion channel genes in GCE98 and GIN98. Expression of CLIC1 and CLIC4 is significantly lower in the GIN98 cell line. B) Comparison of rtPCR vales for CLIC1 and CLIC4 expression across pHGG and GCE98 and GIN98 cell lines. A significantly lower expression of CLIC1 and CLIC4 is seen in GIN98 compared to pHGG. (One way ANOVA, multiple comparisons)

6.7.2.1 CLIC1 and CLIC4 targeting in GIN98 and GCE98

To further identify any potential mechanistic insights into the role of CLIC1 and CLIC4 in the response to TTFields, siRNA targeting of CLIC1 and CLIC4 was carried out on GIN98 and GCE98. As previously observed, the overall mRNA expression levels of CLIC4 were significantly lower in the GIN98 cell line that has previous *in vivo* exposure to TTFields.

6.7.2.2 CLIC1 and CLIC4 knock down significant reduced cell viability and GCE98 colony count.

Deficiency of CLIC1 and CLIC4 was explored via siRNA targeting of GIN98 and GCE98 cells (figure 6.26). Knock down of CLIC1 and CLIC4 resulted in a significant reduction in viability ($p=<0.01$) in GIN98 cells, with overall efficacy observed being less than CLIC knock down in pHGG cell lines. However, only CLIC4 knock down resulted in a reduction in viability in GCE98 cells ($p=<0.05$), with significantly less of an effect observed when compared to pHGG cells.

To further explore this, clonogenic assays were carried out to assess the effect of CLIC1 and CLIC4 knock down in the colony forming capacity of GIN98 and GCE98. Recurrent disease is often assumed to be more 'aggressive' due to the inherent selection of treatment resistant subclones; as such, it could be assumed that cells derived from recurrent disease would have an increased colony forming capacity. Cells may lose proliferative drive and become more invasive due to the selection pressures of treatment, aligning to the 'Go or Grow' hypothesis. Interestingly GIN98 fails to form both neurospheres and colonies. These two assays in particular are measures of tumorigenicity, and as such aggressiveness of the cells. This would suggest that GIN98 is a less 'aggressive' and due to extensive tumour heterogeneity, the subclones that were present in this region may lack tumour sphere forming capabilities. Indeed, this may not be the case at all, and the observed results may merely be an artefact of the spindle morphology of the cells.

CLIC1 and CLIC4 knock down resulted in a 50% reduction in the ability of GCE98 cells to form colonies (p=<0.001).

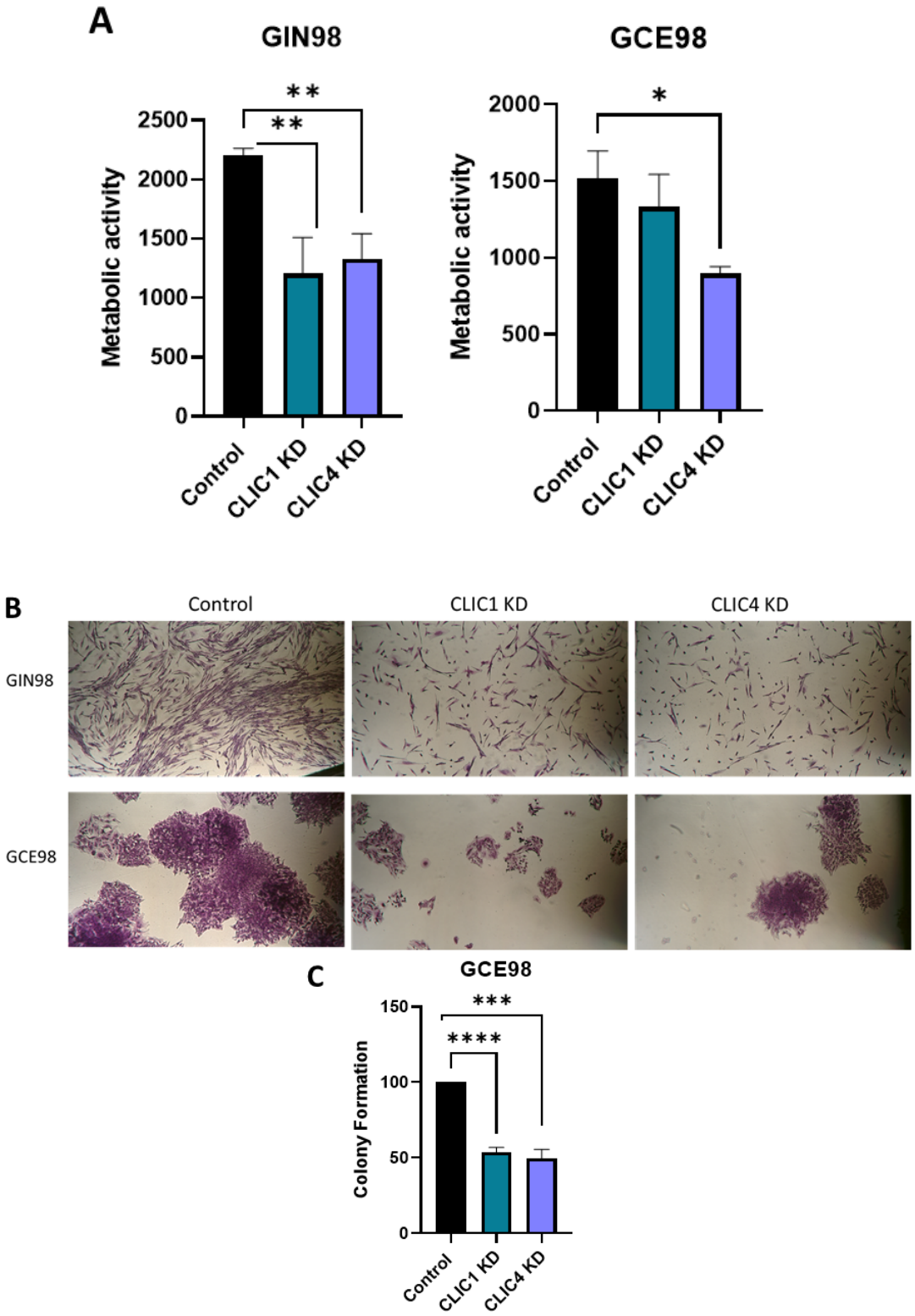

Figure 6.26 CLIC1 and CLIC4 knock down reduces proliferation in patient 98 cell lines. A) siRNA targeting of CLIC1 and CLIC4 in GIN98 cells reveals a significant reduction in cell viability as measured by presto blue, however only CLIC4 knock down resulted in a significant reduction in viability in GCE98 cells. B) proliferation as measured by clonogenic assay

analysis reveals as significant reduction in the proliferative capacity of GIN98 and GCE98. GIN98 failed to form colonies, however staining of the cells with crystal violet revels a significant reduction in proliferation following CLIC1 and CLIC4 knock down. Knock down of both CLCI1 and CLIC4 resulted in a significant reduction in colony forming units in GCE98 cells.

6.7.3 Assessment of the invasive capacity of recurrent GBM cell line vs pHGG cell lines

We have previously hypothesised that CLIC1 and CLIC4 are key drivers of invasion in HGG cell lines, with CLIC targeting via pharmacology or siRNA resulting in a significant reduction in invasive capacity.

Firstly, the inherent invasive capacity of GIN98 and GCE98 was assessed. A modified Boyden chamber (coated with collagen IV) assay was used. A chemotactic gradient was created in which serum starved cells invade towards 10% FBS. Both GIN98 and GCE98 have invasive capacity, with over 60% of cells invading towards the FBS gradient ($p=<0.01$). Following confirmation of the invasive ability of GIN and GCE98, we sought to compare the invasiveness of these cells to pHGG cell lines (figure 6.27). The overall percentage of invading GIN98 and GCE98 cells was found to be significantly lower than SF188 and KNS42 cell lines under control conditions. These findings are interesting as the overall level of CLIC1 and CLIC4 expression in GIN98 was significantly lower than pHGG cells. This may suggest that lower levels of CLIC1 and CLIC4 are linked to the cell lines reduced invasive capacity, confirming the hypothesis that CLIC proteins contribute to the mechanism of invasion in pHGG cells.

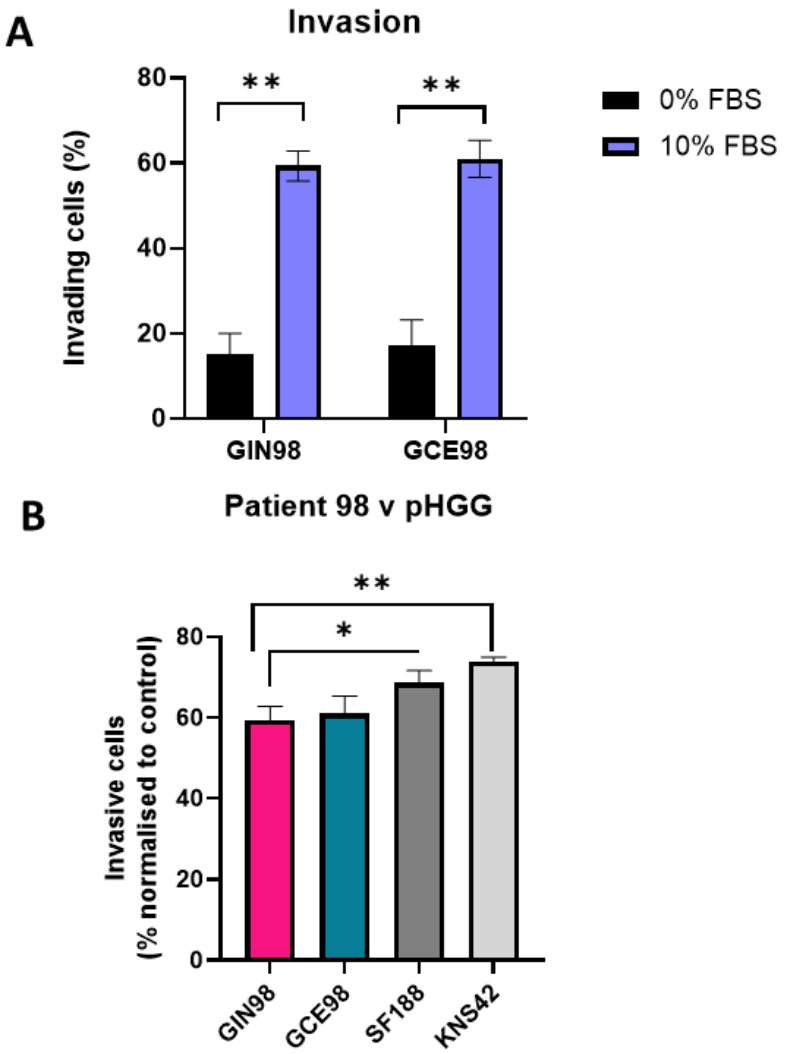

Figure 6.27 Patient 98 cells have invasive capacity but are significantly less invasive than pHGG cells. A) Invasive capacity of GIN98 and GCE98 was measured using a modified boyden chamber assay coated in in collagen IV. A FBS gradient was used to create a chemo attractant whereby cells seeded in 0% FBS media either invaded towards 10% FBS media, or 0% FBS media. GIN98 and GCE98 invaded significantly more towards the 10% FBS gradient. B) invasive capacity of GIN98 and GCE98 was compared to pHGG cells, and reveals a significantly reduced capacity for patient 98 to invade.

6.7.3.1 CLIC1 and CLIC4 siRNA reduced invasive capacity of GIN98 and GCE98

In order to further pursue the investigation into CLIC channels and invasion, siRNA targeting was used to assess CLIC deficiency in GIN98 and GCE98 cells. It was found that CLIC1 and CLIC4 knock down significantly reduced the invasive capacity of GIN98 cells ($p=<0.01$) with an average decrease in invasion of 41 and 45% seen in CLIC1 and CLIC4 deficient GIN98 cells respectively. Comparably, the invasion of GCE98 cells was significantly reduced by 35% following CLIC1 knock down, and 30% following CLIC4 knock down ($p=<0.01$) as shown in figure 6.28.

The overall invasive capacity of pHGG cell lines SF188 and KNS42 was found to be significantly elevated compared to patient 98 derived cells. Interestingly, knock down of CLIC1 and CLIC4 had markedly more of an effect on the reduction of invasion in SF188 cells when compared to GIN98.

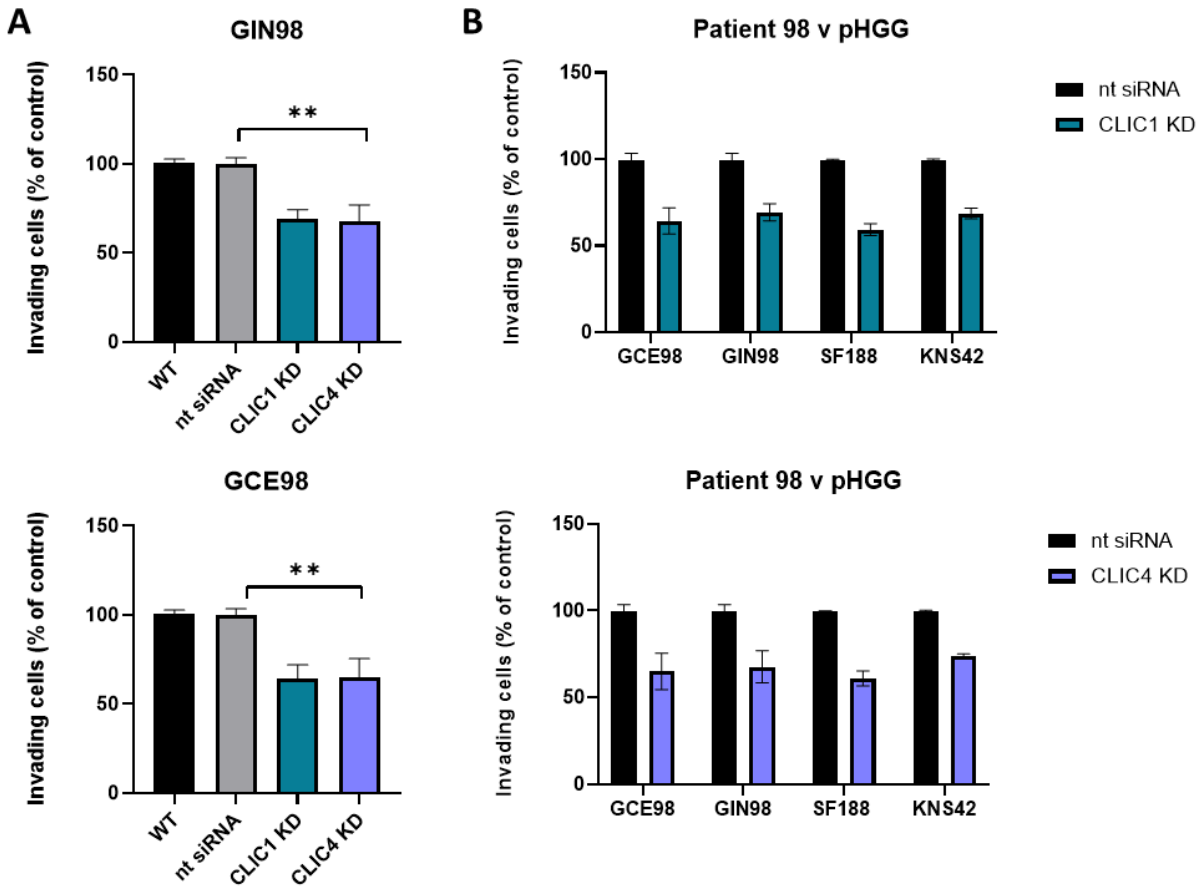
A
GIN98
Invading cells (% of control)
150
100
50
0
**
WT
nt siRNA
CLIC1 KD
CLIC4 KD
GCE98
Invading cells (% of control)
150
100
50
0
**
WT
nt siRNA
CLIC1 KD
CLIC4 KD
B
Patient 98 v pHGG
Invading cells (% of control)
150
100
50
0
GCE98
GIN98
SF188
KNS42
nt siRNA
CLIC1 KD
Patient 98 v pHGG
Invading cells (% of control)
150
100
50
0
GCE98
GIN98
SF188
KNS42
nt siRNA
CLIC4 KD

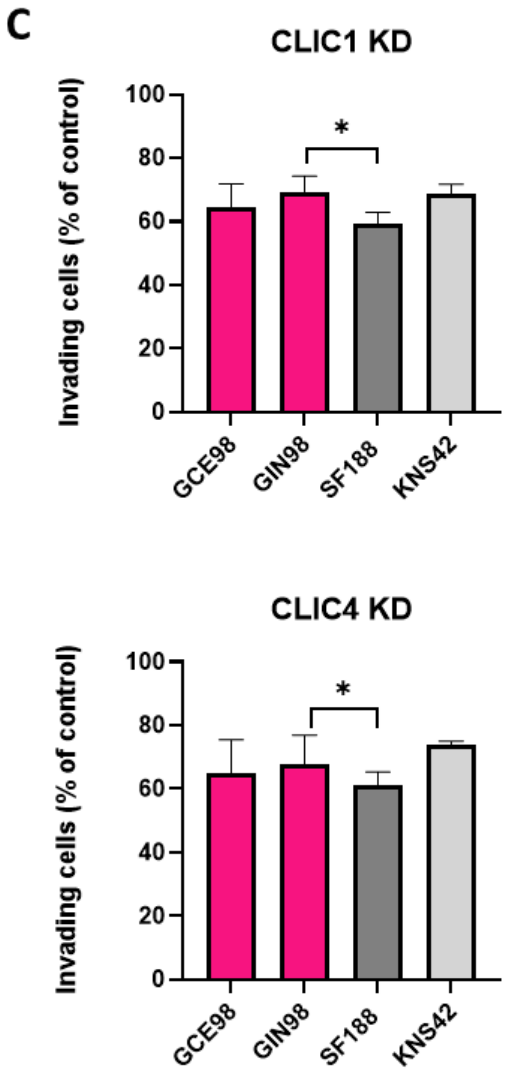

Figure 6.28 CLIC1 and CLIC4 knock down significantly reduces invasive capacity of patient 98 cells, but results in less inhibition of invasion than in pHGG. A) siRNA targeting of CLIC1 and CLIC4 results in a significant reduction in invasion of GCE98 and GIN98 cells. B) Comparison of the invasive capacity of cell lines following CLIC1 knock down. GIN98 has significantly increased ability to invade compared to pHGG. C) Comparison of the invasive capacity of cell lines following CLIC4 knock down. GIN98 has significantly increased ability to invade compared to pHGG.

6.7.4 The effect of invitro TTFields on GIN98 and GCE98 cell lines exposed to *in vivo* TTFields.

It is widely accepted and understood that TTFields treatment of adult HGG shows efficacy and treatment response both *in vivo* and *in vitro*. Previous work in this study has confirmed that TTFields demonstrates efficacy as a treatment for pHGG cell lines with no prior exposure to TTFields. We sought to interrogate the effect of *in vitro* TTFields treatment on adult GBM cell lines that had been exposed to *in vivo* TTFields. The literature has widely discussed that recurrent disease is likely a result of remaining treatment resistant sub clones that retain the ability to proliferate and infiltrate even following treatment. GIN98 and GCE98 cells were derived from a tertiary tumour (second recurrence) that had previously exposed to TTFields, temozolomide and radiotherapy *in vivo* for multiple treatment rounds. It is feasible to hypothesise that as surviving subclones, GIN98 and GCE98 may harness an inherent resistance to TTFields.

6.7.4.1 GCE98 is more tolerant to TTFields than pHGG.

GCE98 and GIN98 cells were exposed to *in vitro* TTFields for 72 hours at a treatment frequency of 200kHz. Following TTFields exposure, GIN98 and GCE98 exhibited a significant reduction in the viability and cell count (figure 6.29). Interestingly, when comparing to pHGG cell lines, GCE98 was significantly less sensitive to TTFields, with an average reduction in viability of 25% compared to 50% reduction in SF188 ($p=<0.01$), 53% reduction in KNS42 ($p=<0.01$) and 40% in GCE62 cells ($p=<0.05$). GIN98 demonstrated a comparable overall treatment efficacy to pHGG cell lines. As discussed, GCE98 cells have an increased expression of CLIC1 and CLIC4 compared to GIN98, and show an increased invasive capacity. These data suggest that increased expression of CLIC1 and CLIC4 may be protective to the tumour, and result in treatment resistance to TTFields. Despite this, the overall expression level of CLIC1 and CLIC4 is reduced in patient 98 derived cell lines when

compared to pHGG, yet shows increased tolerance to TTFields *in vitro*. Further assessment into the mechanism of sensitivity TTFields would provide valuable insight into the role ion channels in determining treatment efficacy.

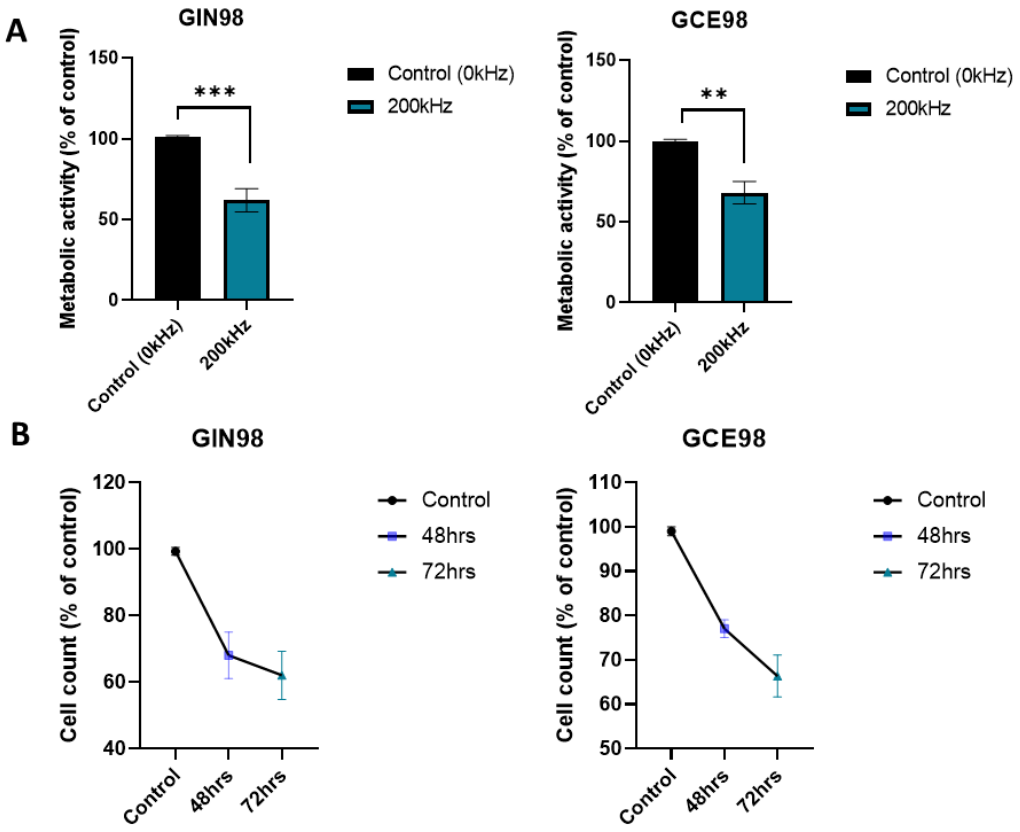

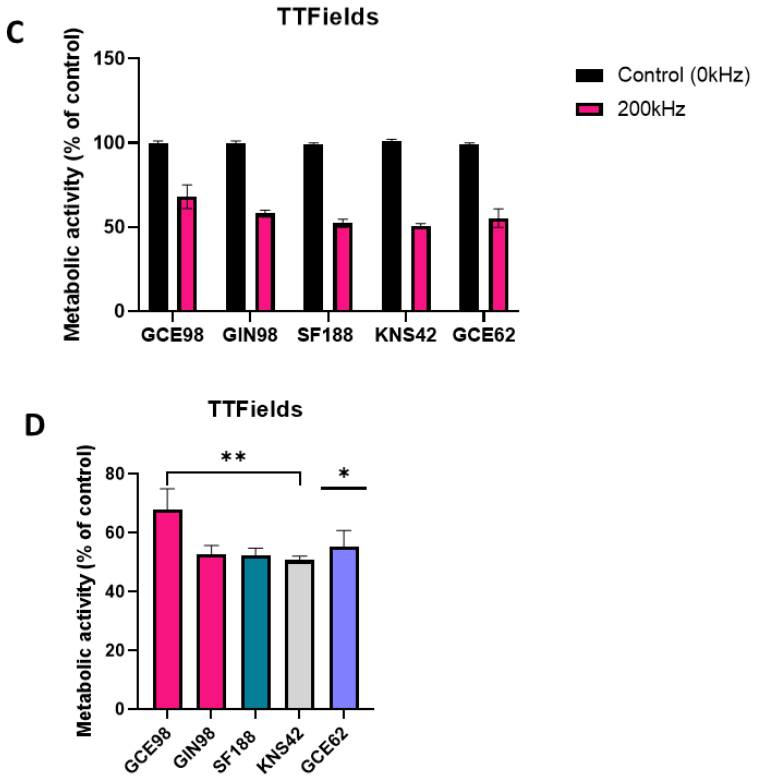

Figure 6.29 Patient derived cells with previous exposure to TTFields have higher tolerance to *in vitro* TTFields than pHGG cell lines. A) Treatment of GIN98 and GCE98 with TTFields at 200kHz for 72hrs results in significant reduction in cell viability as measured by presto blue assay normalised to untreated cells. B) Cell count measured as a percentage of control, untreated cells, is significantly reduced following TTFields and 48 and 72 hours. C) GCE98 cells have a higher tolerance to TTFields compared to pHGG.

6.7.5 Long term treatment confers increased tolerance in GIN98 and GCE98 cells.

Cells derived from the core region of patient tumour exposed to *in vivo* TTFields show an increased tolerance to short term *in vitro* treatment. To further assess tolerance to TTFields, GIN98 and GCE98 cells were exposed to long term TTFields treatment for 13 days. GIN98 and GCE98 cells exposed to TTFields for 13 days were significantly more viable at day 13 ($p=<0.05$) when compared to day 3 (figure 6.30).

Tolerance in KNS42 cell lines appeared to be associated with an increased expression of CLIC1, suggesting a role of CLIC1 in the mechanism of treatment sensitivity. To assess this in patient 98 derive cells, rtPCR analyses of CLIC1 and CLIC4 levels was performed on control cells and long vs short term treatment. Similarly, to pHGG, there was a significant

decrease in CLIC1 and CLIC4 expression in GIN98 and GCE98 following 3 days exposure to TTFields. Furthermore, long term exposure to TTFields resulted in a significant recovery of CLIC1 expression in both GIN98 and GCE98 cell lines.

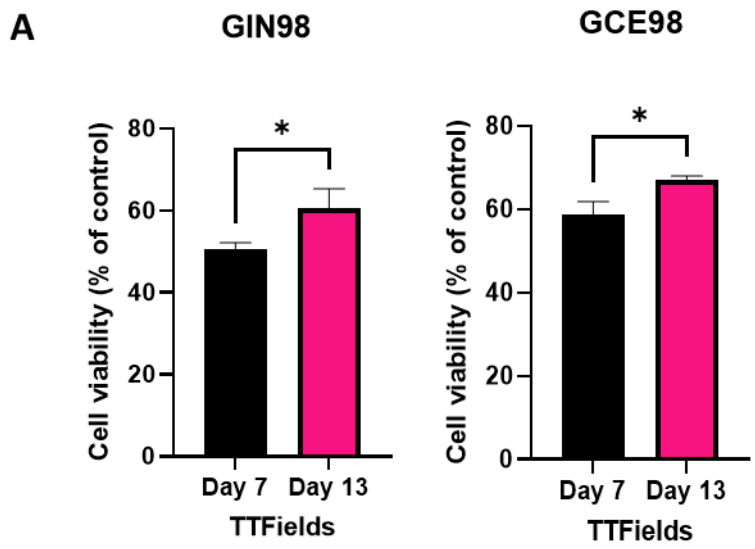

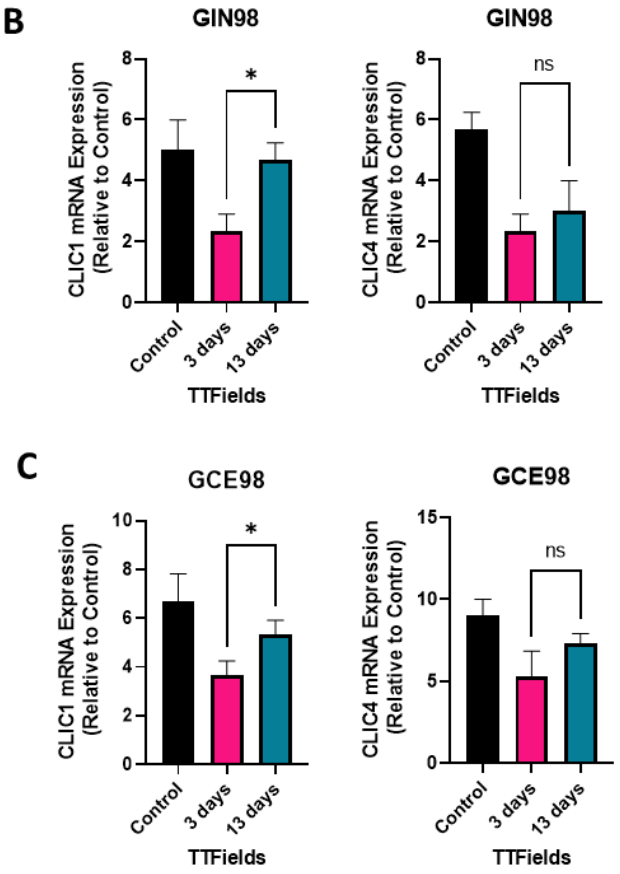

Figure 6.30 GIN98 and GCE98 demonstrate tolerance to Long-term exposure to tumour treating fields. A) GCE98 and GIN98 demonstrate increased viability following long term exposure of TTFields when compared to standard 3-day treatment. B) rtPCR experiments found GIN98 tolerance to TTFields is associated with an increase in CLIC1 mRNA. C) rtPCR of GCE98 cells treated with TTFields for 13 days have increased expression of CLIC1 mRNA compared to 3-day treatment.

6.8 Chapter summary

This chapter aimed to provide mechanistic insight into the *in vivo* effects of TTFields in recurrent patient samples. We used RNA sequencing analysis to explore a unique opportunity to assess the genetic effects of TTFields treatment in recurrent glioblastoma samples. We have interrogated findings to reveal significantly up and down regulated genes across the life span of the tumour, and divulge the significantly altered pathways associated with GBM disease recurrence, and genetic effects associated with TTFields therapy. Through this we have cross examined previous findings in the project, to assess the effect of TTFields on ion channel expression in a patient model, concluding that *in vitro* is indeed, recapitulated in the patient. Thus, these data confirm that CLIC1 and CLIC4 may hold

mechanistic insight into the action of TTFields, and further confirm their status biomarkers for HGG.

We have validated the findings from RNA sequencing analysis at both the protein and mRNA level via IHC staining and rtPCR of recurrent tissue and cell lines. Further to this we have explored the malignant capacity of cell lines generated from the tertiary TTFields exposed tumour, evaluated the effects of CLIC channel inhibition in a model of recurrent GBM. Finally, the *in vitro* effect TTFields following prior *in vivo* exposure was analysed, revealing that recurrent GBM cells acquire tolerance to TTFields.

These data confirm the imperative nature of tackling GBM progression and support our findings that ion channels are viable targets to prevent disease relapse and treatment resistance.

Chapter outputs:

1) RNA sequencing analysis reveals that recurrent GBM tumours have unique genetic landscapes.
    - Primary, secondary, and tertiary tumours cluster independently and exhibit unique genetic profiles.
    - There is minimal overlap in the top 20 up and down regulated genes between the primary, secondary, and tertiary tumour, revealing genetic evolution across the lifespan of the tumour.
    - Gene ontology assessing cellular function reveals that recurrent tumours evolve away from their primary astrocytic function, which is reflective of tumour cells becoming more primitive and losing glial features. Furthermore, the primary

tumour has an upregulation of DNA and RNA replicative activity indicating enhanced mitotic activity.

- KEGG analysis reveals downregulation of DNA repair mechanisms is found in the secondary and tertiary tumours, suggesting that TTFields exposure may be driving dysregulation of DNA repair mechanisms. Additionally, an upregulation of neurodegenerative pathways in the tertiary tumour aligns with previous invitro work and may identify new biomarkers for GBM.

2) *In vivo* exposure to TTFields results in a down regulation of CLIC1 and CLIC4 and a unique ion channel signature compared to the primary tumour.
    - Pathways associated with ion channel functioning and control are significantly differentially expressed when comparing primary and recurrent tumours highlighting the imperative nature of ion channel function in tumour progression and response to TTFields.
3) CLIC1 and CLIC4 staining is significantly reduced in the recurrent tumour GBM98(c) compared to the primary (GBM98(a)).
    - Spatial analyses via IHC reveals that CLIC1 is significantly overexpressed in the invasive region of the GBM98(c)
4) Cell lines derived from GBM98(c) have significantly different morphologies and characteristics compared to pHGG.
    - GIN98 cells fail to form neurospheres and this is associated with an upregulation of ZEB1, suggestive of EMT.
    - rtPCR reveals that CLIC1 and CLIC4 mRNA expression is significantly lower in GCE98 and GIN98 compared to pHGG cells.
    - The invasive capacity of GIN98 is significantly lower than pHGG.

5) CLIC1 or CLIC4 knock down significantly reduces the capacity for GIN98 and GCE98 to proliferate and invade.

6) Cells exposed to *in vivo* TTFields are significantly less sensitive to *in vitro* TTFields.
   - GCE98 is significantly more tolerant to TTFields than pHGG.
   - Long term treatment confers increased tolerance in GIN98 and GCE98 cells.
   - Tolerance to TTFields is associated with an increase of CLIC1 mRNA expression.

7 Discussion

This thesis has identified CLIC1 and CLIC4 ion channels as prognostic indicators for survival in patients with high-grade gliomas. Through a combination of *in vitro* assays and clinical analyses, we have explored the expression profile of CLIC channels in pHGG glioma and the functional and clinicopathological implications associated with CLIC1 and CLIC4 expression in patient data sets and cell lines.

We present evidence to suggest that CLIC1 and CLIC4 expression mediates the malignant response of pHGG, and that targeting these channels can reduce the capacity of pHGG to proliferate and invade. We have explored the role of bioelectricity in HGG tumorigenesis; confirming that CLIC and CLIC4 affect the bioelectrical properties of pHGG, and that inhibition of these channels alters chloride flux, membrane potential and cell cycling. We have interrogated *in vitro* TTFields treatment for pHGG, identifying that TTFields treatment exposure results in dysregulation of the expression of CLIC1 and CLIC4 ion channels and down regulation at mRNA and gene level. We find that, long term exposure to TTFields can lead to treatment tolerance, and that sensitivity to TTFields may be mediated by expression of CLIC1 and CLIC4. A combination of CLIC inhibition and TTFields has synergistic effects, sensitising cells to treatment. Patient derived cell lines from tumours exposed to *in vivo* TTFields are inherently more tolerant to *in vitro* TTFields, and exhibit reduced invasive and proliferative capacity.

We present a unique case study into the genome wide effects of TTFields in recurrent glioblastoma tissue. Cell lines from the core region and invasive zone derived from an adult patient exposed to *in vivo* TTFields were assessed for expression of CLIC proteins, invasive capacity and sensitivity to TTFields. We find that CLIC1 and CLIC4 are down regulated, suggesting that cell data is recapitulated in the patient setting. We interrogated the effect

of *in vitro* TTFields following previous *in vivo* exposure of the native tissue, finding that cell lines derived from said tissue are significantly less sensitive to TTFields than pHGG cells. Using 3' mRNA sequencing we have identified that tumour progression is associated with a down regulation of cell-of-origin features such as neurogenesis and synaptogenesis. Furthermore, recurrent tumours and exposure to TTFields therapy confers a reduced expression of DNA-repair associated genes, that is associated with an upregulation of neurodegenerative pathways associated with mitochondrial function. We have identified potential therapeutic vulnerabilities in recurrent glioblastoma that may hold promise as future targets for HGG treatment alone, or in combination with TTFields.

7.1 The structure and function of chloride intracellular channels

The primary aim of this research project was to identify ion channels that held prognostic significance in HGG, and to perform expression profiling to confirm the promise of exploiting these channels therapeutically. Following assessment of the literature and publicly available datasets, as well as in-house 3' mRNA sequencing data from adult glioma tissue, CLIC1 and CLIC4 were determined as valuable and interesting targets to pursue throughout this study. Chloride intracellular channels are a family of structurally and functionally diverse channels that can act as monomeric soluble proteins, or integral membrane proteins (180). The channels are uniquely distinguished from other chloride channel types by their dimorphic existence. Whilst the crystal structure of CLIC channels has yet to be fully elucidated, the cystolic structure of most of the CLIC family of proteins is known. Cromer et al found that the cystolic form of CLIC channels is identical to the glutathione S-transferase super family (236) giving rise to metabolic isoenzyme function. Furthermore, CLIC1 has been noted to possess latrotoxin-like enzymatic activity, possessing a key role in redox signalling across

cells (237). As previously discussed, reactive oxygen species are crucial in controlling cellular stability, bearing regulatory roles on a multitude of signalling pathways. Under homeostatic conditions, redox systems prevent cellular oxidative damage; however, in gliomagenesis, redox mechanisms may give rise to drug resistance and metabolic adaption (238). Electrophysiological studies have revealed CLIC proteins are associated with Cl- selective channel activity with single-channel conductance that ranges from ∼6–120 pS for CLIC1 and ∼1–86 pS for CLIC4 with consistent Cl–-selective channel activity which was sensitive to IAA-94 (239,240).

A key outstanding question in understanding the structure of the CLIC family of proteins is assessing by which mechanism soluble protein unfolds and inserts into the membrane to form a functional ion channel (179), and as such further research will reveal mechanistic insight into the physiological function, and guide future research into the malignant capacity of CLIC channels. Indeed, recent studies have provided insight into this, suggesting that pH is a central mediator of CLIC membrane insertion, whereby acidic conditions such as encountered in HGG, prime the transmembrane region in the N-domain, lowering the energy barrier for the conversion of soluble CLICs to their membrane-inserted forms (241). As such, this reveals noteworthy considerations into the microenvironmental influence in the tumorigenic capacity of CLIC1 and CLIC4. The chloride intracellular family of proteins are known to interact with cytoskeletal filaments, and other intracellular proteins, sharing regulatory roles. The CLIC family of proteins localise to various organelles throughout the cell, with CLIC1 and CLIC4 favouring endosomes and the plasma membrane (figure 7.1). All six family members localise to the cytoplasm with high abundance (179). Furthermore, intracellular chloride channels have been implicated in a myriad of diseases and disorders. Namely, the role of CLICs is well established in both tubulogenesis and angiogenesis (176).

Removal of CLIC4 in mice gave rise to stunted vascular development, additionally CLIC4 is implicated in endothelial cell proliferation and regulation of morphogenesis (83). Data which suggests the important implications for the role of CLIC4 in angiogenesis of brain tumours.

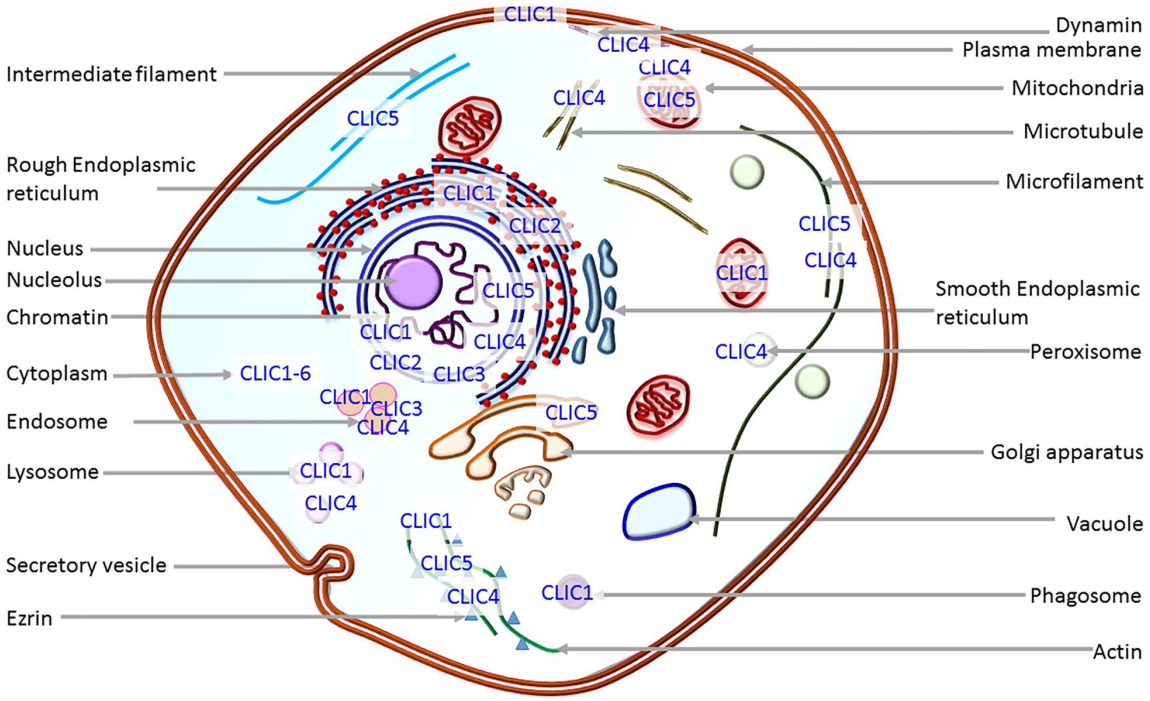

Figure 7.1 Schematic representing the localisation of CLIC proteins. All CLIC proteins localise to organelles, except for CLIC1 which localises to the plasma membrane upon overexpression. (179)

7.2 CLIC1 and CLIC4 ion channels have oncogenic implications in adult and paediatric high-grade glioma.

High-grade gliomas are one of the most aggressive forms of brain tumours with high morbidity and mortality rates. Despite a myriad of research, this thesis has highlighted the dire need for new treatment options for high-grade gliomas. Ion channels have been implicated in several solid cancers (169–171), and have been found to play a crucial role in the growth and invasion of glioma cells (120). Despite the innate electrical capacity of the brain, ion channels are relatively under-studied in brain tumours.

Chloride intracellular channels are ubiquitously expressed in different cell types, and have been reported to be overexpressed in adult glioblastoma and high-grade gliomas (142,242). Despite this, the role of CLIC4 in glioblastoma is poorly research in adult HGG with just two dedicated studies assessing CLIC4 in aHGG (243,244).

Furthermore, less is known about the function of these ion channels in paediatric cohorts, with database searches revealing no relevant literature focussing on CLIC1 or CLIC4 expression in paediatric patient tissues or cell lines, or any other CLIC channel for that matter. Further work beyond that presented in this thesis is needed to validate this interesting preliminary data into the functional significance of CLIC1 and CLIC4 in HGG.

7.2.1 Gliomas overexpress CLIC1 and CLIC4 with increased cytoplasmic localisation.

Assessment via both R2 genomic analysis and inhouse patient cohorts has found the expression of both CLIC1 and CLIC4 to be significantly higher in patient tissues and cell lines when compared to normal frontal lobe or astrocytes (chapter 3). We found that higher grade gliomas (grade IV) possessed the most significant increase in CLIC1 expression, which serves as an interesting result given the propensity for recurrence and aggressive disease.

This is found in agreement with Setti *et al* and Peretti *et al* whereby elevated levels of CLIC1 and CLIC4 are found across patient tissues and cell lines when comparing to anatomically relevant tissue (142,242).

In this study universal expression of both CLIC1 and CLIC4 was observed across cell lines and patient tissue, with high and ubiquitous protein expression seen in both pHGG and aHGG tissues and cells alike. However, significant heterogeneity in CLIC1 expression across distinct patient derived 2D cell cultures has been observed, defining variable CLIC1 expression across a cohort of GBM derived cell lines (245).

The multi-organelle localisation of the CLIC family of proteins has been defined by multiple studies, finding that CLIC1 and CLIC4 accumulate in cytoplasm (202).

We find a preferential expression pattern of CLIC1 and CLIC4 in the cytoplasmic region of SF188, KNS42 and GCE62; a novel study into the subcellular localisation of these proteins in primary paediatric TMAS. Furthermore, assessment via immunofluorescence indicated an accumulation of CLIC1 expression in the plasma membranous compartment of GCE62 cells. The cellular localisation of CLIC1 and CLIC4 is indicative of its functional state, with CLIC1 being the predominant CLIC channel of the two that demonstrates membrane insertion (180).

CLICs have been previously found to display ubiquitous expression, with each member exhibiting specific subcellular localisation; all CLICs except CLIC3, exhibit a highly conserved putative nuclear localisation sequence (246). Although not absent, immunohistochemistry staining in this study found minimal CLIC1 and CLIC4 expression in the nuclear compartment. These findings should be further interrogated via subcellular protein extraction and western blotting to further elucidate the compartmentalisation of CLIC1 and CLIC4. Preliminary data in this study indicates both membrane insertion and

cytoplasmic accumulation of CLIC1 and as such, a bi-functional capacity between monomeric soluble protein and integral membrane protein can be concluded.

7.2.2 High expression of CLIC1 and CLIC4 correlates with poor overall survival in adult and paediatric cohorts.

Studies have previously identified CLIC4 as a prognostic marker for other solid cancers (TCGA), but little research has assessed the prognostic significance of CLIC4 in brain cancers. However, we have shown for the first time, that CLIC4 has prognostic significance in HGG, whereby a high expression of CLIC4 confers poor overall survival in both adult and paediatric cohorts. Alongside this, we have confirmed results found by Wang *et al* finding that elevated CLIC1 expression is correlated with poor prognosis in glioma patients, with a significant reduction in overall survival of adult and paediatric glioma patients reported in this work (247). These data align with interrogation into the prognostic significant of CLIC1 in other solid cancers, CLIC1 expression in pancreatic cancer patients have a worse overall survival compared to the CLIC1 null group (248), additionally CLIC1 upregulation is correlated with treatment resistance and reduced survival in epithelial ovarian cancers (167).

CLIC1 and CLIC4 expression did not have a significant influence on the prognosis of low-grade gliomas, potentially indicating a lesser role of these channels in the less aggressive disease. These data signify that CLIC1 is an emerging biomarker for survival and treatment response in several solid cancers, including high grade gliomas. Furthermore, we have identified CLIC1 and CLIC4 as a novel marker of prognosis in pHGG.

7.2.3 CLIC1 and CLIC4 expression is heterogenous in adult HGG tissue.

The exploration of intra-tumour heterogeneity is a developing and imperative factor in understanding glioma pathophysiology. The fundamental importance of this research is highlighted by the lack of successful glioma treatment strategies.

As such, we sought to assess the expression patterns of CLIC1 and CLIC4 protein and mRNA across spatially distinct patient tumour regions. In this study we find that there is a preferential accumulation of both CLIC1 and CLIC4 in the core region compared to the invasive front of the patient tumour tissue when assessed by both rtPCR and IHC. Studies confirm that gliomas are highly heterogenous tumours, with spatial and temporal analyses revealing significant molecular differences, histopathological subtypes, and dynamic spatial transcriptomic signatures across tumours (151,249,250).

Despite this emerging foundation in glioma biology, the spatial expression of ion channels is yet to be defined. For the first time, we explore the spatial temporal expression of chloride channels in glioma patient tissues, defining a signature of protein and mRNA accumulation in the core of adult GBM tissues. This heterogeneity may be a major limiting factor in glioma treatment efficacy, with populations of treatment resistant and treatment sensitive cells residing throughout the tumour and therefore drive glioma recurrence, thus rendering CLIC1 and CLIC4 valuable in exposing therapeutic windows.

Recent studies have identified that tumour cells originating from the invasive front of the tumour, are biologically distinct from those in the core region of the tumour; instead, closely resembling the molecular biology of recurrent tumours. As such, exploring the invasive front of glioma cells may reveal a signature of infiltrative disease, and mechanisms for recurrence that provide therapeutic vulnerabilities (251). Therefore, the reduction of

CLIC1 and CLIC4 expression that we observe in this invasive region may reveal a marker for recurrence, despite an increase expression being associated with aggressive primary disease.

Intriguingly the accumulation of CLIC1 in the core region was unexpected due to the association between chloride channels and glioma invasion, as such we would expect an overexpression of CLIC1 and CLIC4 on the invasive front (252). In support of this, there is mounting evidence supporting the role of CLIC1 in cancer cell proliferation, Thus, these data may be indicative of an accumulation of CLIC1 acting in combination with other signalling pathways to promote the active proliferation of cells into the invasive margin (170). Although it may be expected that the cells residing in the invasive margin would have the higher expression of CLIC proteins as they are actively invading, it may be the case that the functional protein is not being cycled as the initial drive towards resources has been complete, thus resulting in higher overall expression in the core region. The invasive zone may be less acidotic and therefore, may lead to less membrane accumulation of CLIC proteins.

Assessment of spatially distinct transcriptional programs and subclonal architecture is to forward glioma research and this study aids in elucidating part of the molecular ion channel landscape of gliomas. Additionally, single cell sequencing methodologies may help to resolve this further.

7.2.4 Tumour microenvironmental factors affect CLIC expression.

Interactions between the components of the HGG microenvironment enhance the well know diversity observed in these tumours, presenting as a challenging and interesting therapeutic avenue. The microenvironment of HGG is, like the molecular landscape, heterogenous, and in certain areas is significantly hypoxic, with a rich supply of growth stimulating factors in the invasive front (253).

We report that SF188 cells exposed to hypoxia harboured a significant reduction in the relative CLIC1 expression. However, despite the overall reduction in staining intensity, image analysis found a significantly higher accumulation of CLIC1 in the membranous region of the cells. Similarly, we note that acidosis appears to be associated with re-localisation of CLIC1 and CLIC4, with an accumulation in the nuclear region post exposure to acidotic media. Conversely, the induction of hypoxia in KNS42 resulted in a significant increase in CLIC1 expression and granular accumulation in the cytoplasm. In support of these findings, CLIC1 membrane insertion is well established to be regulated by pH (242), with its unfolding reliant on acidic conditions (241). Studies into other solid cancers confirm that CLIC1 is upregulated with significant membrane insertion in gastric cancer (GC) cells under hypoxic stress (254), and that CLIC1 participates in the metastasis and invasion of GC cells by regulating hypoxia-reoxygenation-induced intracellular ROS (255) with this regulation being reliant on overexpression. Furthermore, CLIC1 deficient cell lines show excessive ROS production, confirming the role of CLIC1 in the maintenance of the tumour microenvironment (256). Although there is limited literature into the association between CLIC channels and hypoxia in brain cancers. Chloride channels are shown to be

essential for brain tumour cells to undergo regulatory volume decrease as a survival mechanism in response to exposure to hypoxia (257).

As such, in this study we demonstrate a network of associations owing to a pro-malignant phenotype perpetrated by CLIC1 and CLIC4. The very nature of the insertion of CLIC proteins into the membrane is reliant on an acidic microenvironment (258), this along with the accumulation of CLIC1 and CLIC4 in the hypoxic and necrotic core of the tumour highlights the association of CLIC function and tumour microenvironment. Furthermore, this central role of pH in the dimorphic nature of CLIC1 and CLIC4 further perpetuates the theory that chloride channels are critical in glioma cell invasion. As discussed, glioma cell invasion occurs concomitantly with microenvironmental changes associated with pH and hypoxia(259); driving the migratory and invasive phenotype observed in HGG. Here we have shown that exposure to hypoxia significantly upregulates CLIC1 expression, rendering cells primed for invasion, with functionally active membrane accumulation of CLIC1 and CLIC4 in acidic and hypoxic environments. As such, this concomitant occurrence of CLIC elevation and hypoxia results in an increased invasive capacity and malignant phenotype.

7.2.5 CLIC expression is associated with an increase in stem markers in 3D culture.

Section 4.2 assessed the capacity of pHGG to form neurospheres to better recapitulate a physiologically appropriate setting and to assess the inherent malignant capacity of the cell lines. Glioma stem cells (GSCs) refer to a population of tumour originating cells that harness the capacity to undergo self-renewal and differentiation. Evidence suggests that these GSCs are linked to resistance to treatment, a debated and controversial across the literature. A stem-like cell enriched population is associated extended capacity for proliferation and self-renewal, giving rise to an aggressive phenotype (191,260).

This study confirms that commercial cell lines SF188 and KNS42 as well as primary cell line GCE62 readily form neurospheres that can be maintained over several passages. The ability of KNS42 and SF188 cells to form neurospheres has been shown across several other studies, confirming the ability to generate a stem-like precursor population in these commercial lines (261–263). GCE62 formed the largest neurospheres, which was to be expected due to its status as an early passage primary cell line as primary cell lines are associated with an increased capacity for stemness and ability to form free forming neurospheres (264).

Chloride intracellular channel expression levels have previously been linked to a pro-stem phenotype (198) therefore, the expression of CLIC1 and CLIC4 along with stem markers SOX2 and NESTIN were assessed. We report that the mRNA expression of CLIC1 and CLIC4 is significantly increased in 3D cell culture compared to 2D monolayer culture, and this upregulation is associated with a dual increase in stem-cell markers.

Setti *et al* found that the expression of CLIC is variable in patient derived neurospheres, however there was a significant increase in expression in the stem compartment (142). Furthermore, agreement comes from characterisation of CLIC1 levels via RNA-seq, whereby the progenitor cells derived from GBM neurospheres reflect an overall increased expression than 2D monolayer culture. Heterogeneity across distinct patient derived cultures has also been observed (245).

Despite rtPCR linking CLIC1 and CLIC4 expression to the glioma stem cell population in the culture, the results observed via IF were variable in the present study. This may be a result of several factors, firstly although the spheres were assessed for a necrotic core, merely using light microscopy is not sufficient for this, and a live dead stain would have provided

more accurate data(264). As such, the lack of staining in the core areas of the neurospheres may be due to a higher percentage of non-viable cells leading to poor antibody penetrance. On the other hand, this may be an indication of increasing expression of CLIC1 and CLIC4 in the actively recruiting areas of the sphere. A possible explanation could be that the margins of the neurospheres consist of the cells that have most recently migrated to join the sphere, and as such, maintain high CLIC protein expression levels needed for this.

Figure 7.2 highlights the key findings from the chapter 3 of this thesis.

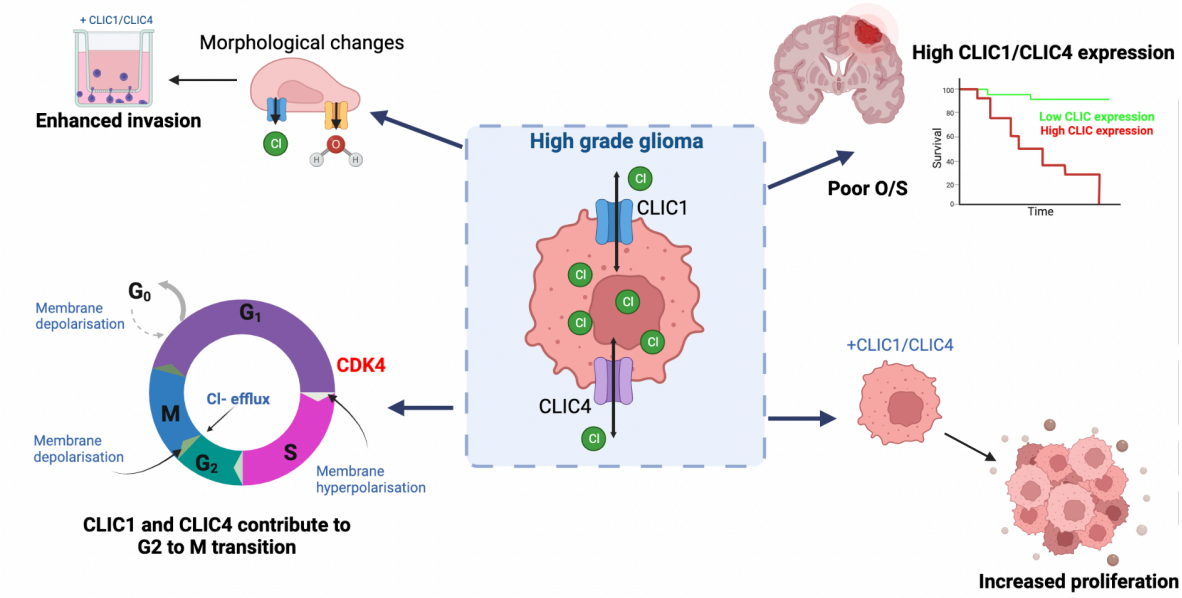

Figure 7.2 Graphical summary of the malignant associations of CLIC1 and CLIC4 in pHGG. Image created using bio render.

7.3 Targeting CLIC channels reduces malignant capacity of pHGG cells.

In this study we sought to assess pharmacological and genetic targeting of pHGG to determine the viability of chloride intracellular channels as therapeutic targets. Ion channel inhibiting drugs make up one of the largest classes of drugs on the market to date (155), and as such their repurposing would be clinically feasible, with potentially fast translation to the clinic.

7.3.1 Pharmacological inhibition of CLIC1 and CLIC4 is clinically feasible and results in significant reduction in viability and invasion of HGG cells.

IAA94 is a potent and selective inhibitor of the chloride intracellular channel protein family of ion channels, including CLIC1 and CLIC4 (265) . In preclinical studies, IAA94 has been shown to have anticancer properties and to inhibit the proliferation, migration, and invasion of cancer cells, including glioblastoma cells (266). In this study, we were unable to produce a completely cytotoxic effect of either IAA94 or metformin, failing to reach 100% reduction in viability upon IC50 analyses for both 2D and 3D culture. As such, a combination of literature and experimental data were used to select inhibition concentrations. A concentration of 100μM was selected for IAA94 as this has been previously shown to abolish CLIC currents in electrophysiology experiments (142,203,267,268). The IC50 of metformin was found to fall within the range of 9-11mM, with incomplete cytotoxic effect observed up to 50mM. In contrast to our findings, other studies have identified the IC50 of metformin to be in the range of 2.1mM to 7.5mM in a glioblastoma stem cell population (269–271). The most likely cause of this difference is due to the sensitivity of an enriched stem cell cohort, and biological selection because of stem

cell media. However, agreement come from Sesen *et al* (271) finding that treatment with 10mM of metformin significantly reduced cell viability and enhances therapeutic response to main stay therapies. It is very common to see a wide range of IC50s across different cell lines, methodologies, and laboratory settings, despite this disparity, IC50s in the millimolar range are not clinically feasible.

Findings in this study revealed that both the treatment with 100μM IAA94 and 10mM metformin is sufficient to reduce the capacity of paediatric glioma to proliferate and invade, with a substantial decrease in cell viability, cell count and clonogenic capacity. SF188 and GCE62 cells were sensitive to CLIC inhibition via IAA94, however KNS42 has no significant reduction in overall viability. Furthermore, metformin treatment did not significantly affect GCE62 clonogenic capacity, but did reduce the viability and cell count of all cell lines. Importantly, there were no significant reductions in the viability of normal astrocyte cells when treated with either metformin or IAA94, suggesting that these drugs would be therapeutically viable in patients due to lack of toxicity to normal tissues. However, it would be of benefit to assess the toxicity on other native brain cells such as neurones.

Despite promising results, treatment with metformin at 10mM is unfeasible within clinical range, therefore we assessed the feasibility of 100μM treatment. We only found a significant decrease viability in the SF188 cell line with an average decrease in viability and cell count of 15 and 20% respectively. These results indicate that metformin may not be suitable for a monotherapy in HGG as it fails to be effective in reducing viability in a clinically achievable range. Metformin has a less significant effect on the viability of cells at the same concentration of the CLIC1 specific inhibitor, IAA94, with mean reduction in viability of SF188 being significantly less when treated with metformin. This is not to say

that metformin is not still an attractive candidate in the treatment of gliomas, and it may hold promise as a dual therapy. Often brain tumours require prolonged exposure to chemotherapeutics for efficacy of treatment to be seen. Further analysis would look to explore the effect of long-term exposure to metformin on the viability of pHGG cells. Some pre-clinical studies have described the efficacy of IAA94 as a monotherapy (142,167,169,171,198,203,242,272)or as a combination therapy with standard of care TMZ or mTOR inhibitor everolimus in solid tumours. The studies found that showed that the combination therapy had clinical activity, however the off-target effects were not fully elucidated (263). Furthermore, the possible promise of metformin in a combination therapy is supported by its ability to act synergistically with temozolomide in glioma neurospheres (273).

Gritti *et al* have shown that CLIC1 is a direct target for metformin, and that exposure to the drug can induce antiproliferative effects in an enriched human glioblastoma stem cell population (198). Furthermore, Barbieri *et al* find that CLIC1 channel activity is not required for glioblastoma development but its inhibition dictates glioma stem cell responsivity to novel biguanide derivatives (265). Although studies are identifying CLIC1 as a mechanistic target for Metformin, its functional mechanism has not yet been elucidated, with a broad chloride ion channel inhibiting effect noted, as well as glucose transporter (GLUT4) targeting. Furthermore, the success of CLIC1 channel inhibition has been demonstrated in other brain tumours (274), finding that CLIC1 promotes medulloblastoma growth and that selective inhibition via metformin or IAA94 significantly reduced the growth capacity of these cells.

As far as novel HGG treatments are concerned, time to translation from bench to bedside is essential. Metformin is a widely used, FDA approved drug with well-known safety profiles, thus is a strong candidate for drug repurposing for the treatment of HGGs.

IAA94 has shown promising results in preclinical studies, but despite this there is limited evidence on the potential for using IAA94 *in vivo*. Despite these promising results the use of IAA94 in clinical trials is limited by a lack of well-defined treatment window, and potential toxicity. Studies report off target effects and some significant cardia toxicities(194). Further research is needed to fully understand the potential for clinical used of IAA94, including safety profiles, optimal dosage, and off target effects such as cardiac toxicity. The development of selective CLIC inhibitors will fully exploit the potential for targeting these channels to prevent glioma progression. This study provides a proof of concept that developing these inhibitors is worthwhile and may provide major contributions to brain tumour treatment. On the other hand, metformin is clinically well tolerated and has a known safety profile. This study has found that metformin does not act significantly on pHGG cells in a clinically tolerable range, however, gives justification for the use of other novel, more potent biguanide derivatives. Several clinical studies are already assessing the effects of metformin, or other biguanide derivatives in the treatment of HGGs. One open label trial (NCT02780024) is currently assessing the combination of metformin with TMZ with the aim of assessing toxicity of the dual therapy, another phase II trial (NCT02496741) is assessing the combination of metformin and chloroquine in IDH mutated gliomas (275). Table 7.1 represents all of the current clinical trials assessing metformin in brain cancer treatment. Adeberg *et al* found that in a cohort of 276 GBM patients, longer PFS (Progression Free Survival) was found in diabetic patients treated with

metformin (276). Similarly, Seliger *et al* assessed 1093 HGG patients, finding that metformin treatment was associated with increased OS (Overall Survival) and PFS. However, there are significant methodological issues occurring with studies such as these, due to the co-morbidities of the patient, and lack of true control. Interestingly, a significant relationship was only observed in WHO IV tumours (277), confirming the relationship between CLIC1 expression and increased tumour grade that we have previously reported in this study.

Table 7.1 Current clinical trials assessing metformin in brain tumour treatment.

NCT Number	Title of the study	Disease	Interventions	Clinical Phase
NCT02780024	Metformin, Neo-adjuvant Temozolomide and Hypo-Accelerated Radiotherapy Followed by Adjuvant TMZ in Patients With GBM	GBM	•Drug: Metformin	Phase 2
NCT03151772	Bioavailability of Disulfiram and Metformin in Glioblastomas	GBM	•Drug: Disulfiram •Drug: Metformin	Early Phase 1
NCT01430351	Phase I Factorial Trial of Temozolomide, Memantine, Mefloquine, and Metformin for Post-Radiation Therapy (RT) Glioblastoma Multiforme (GBM)	Brain Cancer	•Drug: Temozolomide •Drug: Memantine •Drug: Mefloquine •Drug: Metformin	Phase 1
NCT02149459	Treatment of Recurrent Brain Tumors: Metabolic Manipulation Combined with Radiotherapy	Brain Neoplasms	•Radiation: Partial brain reirradiation. •Drug: Metformin•Behavioral: low carbohydrate diet	Phase 1
NCT03151772	Bioavailability of Disulfiram and Metformin in Glioblastomas	GBM	•Drug: Disulfiram •Drug: Metformin	Early Phase 1

7.3.2 CLIC1 and CLIC4 deficiency reduces pHGG invasion.

One of the pathological hallmarks of any cancer is the ability for malignant cells to invade outside of the local tumour environment. Brain tumours are unique in that they are anatomically constrained by the CNS; tumours such as HGG rarely metastasise outside of the brain. Instead, HGG harbour a diffuse phenotype, with projections of cells invading the surrounding brain parenchyma. To do this, CLIC channels endow glioma cells with an enhanced capacity to alter their morphology, promoting the dual efflux of water and chloride ions to reduce cell volume (257).

This study reports that KNS42, SF188, GCE62, GIN98 and GCE98 all have an inherent invasive capacity, allowing for invasion across transwell coated with collagen IV. This invasion is successfully inhibited by siRNA knock down of either CLIC1 or CLIC4, resulting in up to 45% reduction in the invasive capacity in all of these cell lines. Furthermore, treatment with IAA94 found a significant reduction in invasive capacity of SF188 and KNS42 cells. Interestingly GCE62 invasion was not significantly inhibited by IAA94, despite the primary nature of the cell line. This may be a direct consequence of the cell line retaining inherent characteristic associated with the primary tumour, and as such, overcoming CLIC inhibition and maintaining invasive capacity. Here we report novel findings on the association of CLIC1 and CLIC4 in the ability of pHGG cells to invade through ECM like coating. These findings indicate that CLIC1 or CLIC4 may contribute to the invasive ability of pHGG cells.

Previous studies into adult HGG cell lines confirm our findings, noting that CLIC1 deficient (shRNA or siRNA KD) cells had reduced invasion (142,266) linked to reduction in cell

viability. Furthermore, treatment with both metformin and IAA94 have previously been shown to reduce invasive capacity in glioma cells (142,198,242,252,265).

CLIC4 overexpression is associated with an increase in the expression of matrix metallopeptidase MMP9, and therefore potentiated invasion (278). One of the ways in which CLIC1 and CLIC4 promote glioma progression is by modulating the tumour microenvironment (186). CLIC1 and CLIC4 can regulate the pH of the extracellular environment, which affects the activity of different enzymes and proteins involved in tumour invasion and migration (259). Local hypoxia triggers cell migration and invasion throughout the parenchyma, with HIF1A induced production of invasive molecules and degradation of the surrounding extracellular matrix (279). Through this process astrocytes and microglia become tumour associated, further promoting invasion, with interacting factors actively promoting infiltration (259). Similarly, another mechanism associated with glioma progression is the CLIC1 mediated regulation of signalling pathways. CLIC1 has been found to associate with epidermal growth factor receptor (EGFR), activating proliferation and invasive capacity of glioma cells (67,280). Additionally, CLIC1 and CLIC4 have been implicated in the MAPK/ERK pathway; regulating cellular survival and proliferation, thus contributing to malignancy in glioma cells (170). Similarly, CLIC1 recruits PIP5K1A/C to induce cell-matrix adhesions for tumour metastasis in hepatocellular carcinoma cells (196), clearly defining a role for CLIC1 in cancer cell invasion.

The outcome of this study confirms that CLIC1 has a fundamental role in the invasive capacity of HGG cells, and as such may reveal a mechanism of glioma pathogenesis. This is supported by a myriad of literature sources confirming several pathway links between glioma cell invasion and CLIC1 expression, implicating several well-known cancer associated pathways.

7.3.3 Targeting CLIC channels causes aberrant cell cycling.

We have identified the effect of CLIC1 inhibition via IAA94 on the cell cycle of paediatric HGG cells. We show that treatment with IAA94 results in aberrant cell cycling associated with accumulation in G1 and reduction in S-phase. Furthermore, we find that CLIC1 deficiency via siRNA KD is associated with a significant increase in the percentage of cells present in G1 phase accompanied by a significant decrease in S phase. Both CLIC1 and CLIC4 KD results in a higher percentage of cells present in G2/M. The results for the cell cycle experiments were variable, demonstrating a multitude of changes associated with s-phase, G2/M and G1 (sections 4.3.6 and 4.4.2.3).

Pharmacological targeting of CLIC1 has been shown to induce G1 arrest in a time dependent manner (281). Conversely, CLIC1 and CLIC4 have also been implicated in G2/M phase progression associated with chloride-mediated depolarisation of the cell (258). However, other studies have shown that CLIC1 and CLIC4 are not necessary for cell cycle progression at all (270,282). Peretti *et al* find that CLIC1 inhibition has a pronounced effect on G1 transition time, resulting in an accumulation in G1 phase. With CLIC1 inhibition resulting in cells needing around 8 more hours to reach the same percentage of cells in S-phase as control conditions (242). Furthermore, CLIC1 had been found to interact with cyclin dependent kinase 4 (CDK4), a key regulator of the cell cycle. CDK4 regulates the transition from G1 to S phase, promoting DNA synthesis (283) . What this demonstrates is that although the role of CLIC proteins in the cell cycle have been explored, the literature is controversial, and a conclusive answer has not been found.

CLIC4 has also been shown to play a role in the G2/M transition, which is the point in the cell cycle when the cell prepares to divide. CLIC4 has been shown to interact with and regulate the activity of the checkpoint kinase 1 (Chk1), which is a key regulator of the G2/M transition. Knockdown of CLIC4 has been shown to cause defects in the G2/M transition and to lead to cell cycle arrest in cancer cells (112,132).

The precise mechanisms by which CLIC1 and CLIC4 regulate the cell cycle are not fully understood and require further investigation. However, these findings suggest that CLIC1 and CLIC4 may be important targets for the development of cancer therapies that target the cell cycle. To further assess the effect of CLIC1 inhibition on the cell cycle, cells should be subject to cell cycle synchronisation by inhibition of CDK4, arresting cells in G1 phase for a 24-hour period, and then released prior to treatment with either IAA94 or metformin.

Figure 7.3 provides a graphical summary of the findings of chapter 4.

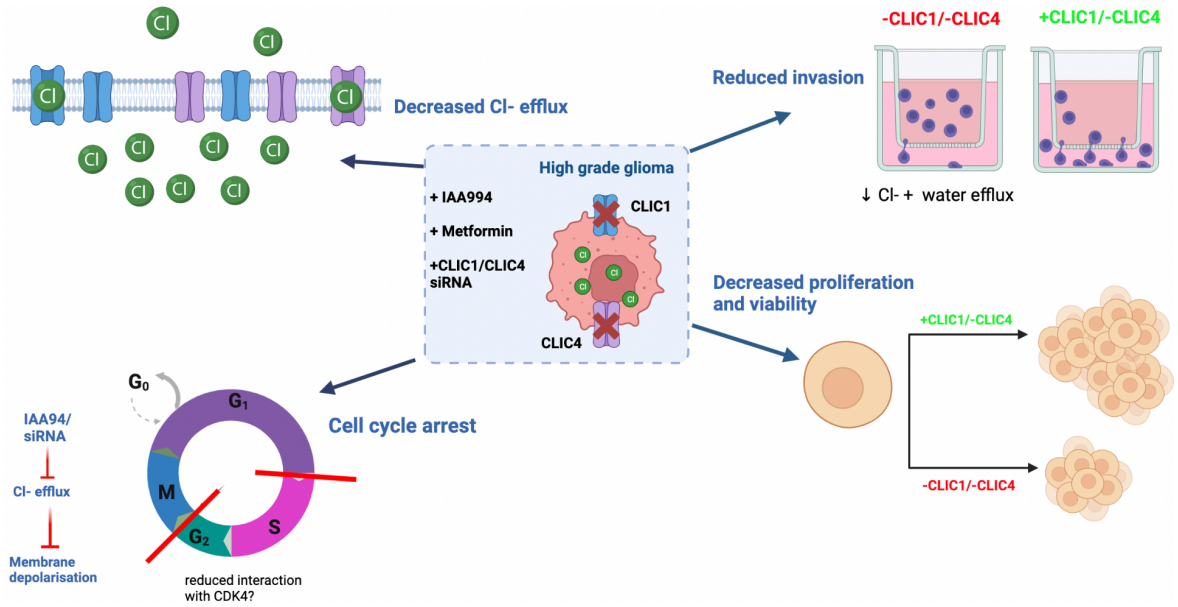

Figure 7.3 Graphical summary of targeting CLIC channels in pHGG.

7.4 Bioelectricity: a novel avenue for pHGG treatment?

7.4.1 CLIC1 and CLIC4 are electrically active targets in pHGG.

In the present work, we have interrogated the functional bioelectric role of CLIC1 and CLIC4 ion channels. We find that inhibiting CLIC channels via metformin, IAA94 or siRNA resulted in aberrant chloride efflux and changes to membrane potential. As with other work presented in this thesis, this presents as a unique study into the movement of Cl- ions across the membranes of pHGG cells. As discussed previously, CLIC channels have been assessed in a limited number of adult glioma studies, but are yet to be explored in paediatric HGG.

By inhibiting chloride channels, we have shown that there are significant changes in the flux of chloride ions across the cell.

Although we find no significant difference in the chloride efflux across astrocyte membranes when compared to pHGG, we do see significant changes in Cl- efflux when targeting CLIC channels. siRNA knock down of CLIC1 significantly inhibits the movement of chloride ions across KNS42, GCE62 and SF188 cells. However, the effects of both metformin and IAA94 treatment were variable across cell lines.

7.4.2 Exploring the membrane potential in pHGG malignancy

To further assess the role of ion channels in glioma malignancy, we sought to interrogate the resting membrane potential of glioma cells compared to normal human astrocytes. As previously discusses, membrane potential is instructive for the functional nature of cells, including cell replication and invasion, and as such presents as an interesting therapeutic target.

A high throughput voltage dye-based assay was used to measure membrane potential. This study revealed that astrocytes are significantly more hyperpolarised than pHGG cell lines (SF188, KNS42 and GCE62) by on average ~-20mV. This is found in agreement with studies

noting that astrocytes have a highly negative membrane potential of around -90mV (104,208).

However, this method lacks the sensitivity and specificity needed to define the exact membrane potential of these cells. To address this, we employed whole cell patch clamping to measure resting membrane potential across GCE62, SF188 and astrocytes. Electrophysiology experiments demonstrate that the membrane potential of astrocytes and pHGG cells lines are comparable, an unexpected result as cancers cells have been shown, on average a more depolarised membrane potential when compared to their somatic counterparts (104). However, this may be due to the fact that the astrocytes used in this study were not terminally differentiated, and as such possess mitotic and replicative capacity, and are therefore more representative of tumour cells than normal post mitotic astrocytes. The present study found the average resting membrane potential of GCE62 cells to be -35mV and -37mV for SF188. Here we see high levels of variability in the average membrane potential reading of astrocytes, with a range of -18mV to -59mV, with no significant difference between astrocytes and HGG cells.

GCE62 is a primary in-house cell line and as such recording the membrane potential of these cells presents a novel finding, similarly, although the mitochondrial membrane potential has been measured in SF188 cells, there appears to be no assessment into the resting membrane potential of these paediatric HGG cells. Our data is consistent with the assessment of adult glioma cells, which have been characterised *in vitro* and in situ by a resting membrane potential of -20mV to -40mV (102).

7.4.3 IAA94 successfully blocks Cl- currents in GCE62 cells.

In the present study, we find that treatment with 100μM of IAA94 does not significantly affect the membrane potential of SF188 cells. However, IAA94 has a pronounced effect of the resting membrane potential of GCE62 cells, resulting in an overall depolarisation of Vm. This confirms CLIC1 activity in the membranes of GCE62 cells, and as such, these chloride channels may be acting as key drivers of membrane potential in the primary cell line. Interestingly, electrophysiology studies report wide-ranging success in using IAA94 to disrupt Vm via CLIC1 mediated currents. Setti *et al* were able to isolate CLIC1 specific currents via perforated patch clamp techniques in GBM cells using IAA94 (142) with a significant depolarisation in membrane potential in IAA94 treated cells.

CLIC1 is known to have a role in modulating membrane potential when acting as a membrane protein, and this is suggested to be via regulating the activity of voltage gated potassium and chloride channels. CLIC1 conductance during ROS overproduction is key in mediating the resting membrane potential, allowing electrogenic activity of enzymes and ensuring further ROS production (177). Importantly we have measured the resting membrane potential of normal human astrocytes. Here we see that the Vm is not significantly more hyperpolarised than the pHGG, despite defined hyperpolarisation observed in high through put voltage dye-based assay measuring Vm. Studies were not carried out to assess the electrophysiological effect of IAA94 on normal human astrocytes, but will be part of ongoing work in this project.

7.4.4 CLIC proteins may reveal mechanistic insight into TTFields.

In this thesis, we present novel data on the expression profiling of ion channels following TTFields treatment. Gene array analysis demonstrated that TTFields treatment confers a unique ion channel signature, significantly down regulating the expression of CLIC1 and

CLIC4. We validated this using rtPCR across pHGG cell lines. Further to this we found differential expression of other ion channel targets, namely epithelial sodium channels (ENaC/SCNN channels), purine receptors and aquaporin. Interestingly aquaporins AQP1 and AQP4 were found to be upregulated following TTFields exposure. These channels have been implicated in the invasive capacity of glioma cells (284) with an upregulation of AQP1 promoting a pro-invasive phenotype. The working model of the 'go or grow' hypothesis denotes that tumour cells fall into one of two phenotypes: invasive, or proliferative. These data may indicate that although TTFields significantly reduced the proliferative capacity of cells (as demonstrated in chapter 5), there may be a drive towards an invasive phenotype. Additional research should be carried out to assess the invasive capacity of HGG cells following TTFields exposure. Only one other study reports the association between TTFields and ion channel expression, identifying CaV1.2 calcium channels as targets for TTFields (285).

Interestingly, voltage dye-based assays reveal that TTFields produces a significant dysregulation of the membrane potential of cells, potentiating a significant depolarisation of membrane potential. This significant decrease in negative state of the cell membrane suggests that there is an accumulation of positive ions in the membrane; which may be reflected via a prevention of the movement of Cl- ions. Additionally, when assessing chloride efflux, we found that TTFields significantly reduced the movement of chloride ions across the membrane of KNS42 and GCE62 cells. These data further support our findings that the success of TTFields may be mediated by ion channel specific changes at the plasma membrane level, more specifically by aberrant CLIC1 and CLIC4 function. Unfortunately, due to time and technical constraints we were unable to use patch clamping to measure the

membrane potential of cells exposed to TTFields. To further pursue the role of CLIC proteins in TTFields, electrophysiological techniques should be used to further elucidate the functional significance of these channels. It would be of interest to assess the membrane potential changes associated with TTFields treatment; and as such, this may reveal other mechanistic targets to pursue.

7.4.4.1 Combination CLIC inhibition is synergistic with TTFields.

It is now widely understood that one of the main mechanisms of TTFields is the interaction of the electric fields with highly polar molecules known as dipoles. When a cancer cell is exposed to TTFields, these dipoles, such as tubulin subunits, fail to align correctly, instead aligning with the alternating electrical fields causing aberrant tubulin alignment and metaphase arrest (286).

To elucidate the role of chloride channels in TTFields success and to understand if CLIC channels are viable targets in combination with TTFields, the present study assessed CLIC inhibition and TTFields as a combination therapy. Here we report novel findings on the combination of ion channel inhibition and TTFields as a dual therapeutic approach. Combination of IAA94 and TTFields results in a significant reduction in the cell viability and colony forming capacity of SF188 cells, and a significant reduction in the viability of GCE62 cells. Similarly, treatment with metformin and TTFields significantly reduced the cell count of SF188, KNS42 and GCE62 cells, with a reduction in viability of SF188 and KNS42 when compared to either treatment as a monotherapy. Furthermore, these results were repeated when using siRNA targeting of CLIC1 and CLIC4 in SF188 and KNS42 cells whereby knock down significantly sensitised cells to TTFields.

We report that chloride intracellular channel inhibition can successfully sensitise pHGG cells to TTFields, and as such may open a clinical avenue for increasing life years gained, and thus bring this non-invasive therapy to children.

The clinical benefit of TTFields and TMZ has already been well-explored (287–289) with multiple clinical trials demonstrating the efficacy of TTFields in combination with TMZ. Other studies have explored augmenting TTFields with drugs such as anti-angiogenics (290), alkylating agents (288), mitotic inhibitors (291) and immune therapeutics (153) giving a clear foundation of evidence in using TTFields in combination with chemotherapeutics.

It is important to note that the apparent synergy observed when using IAA94/metformin in combination with TTFields may in fact be due to an increased drug uptake caused by the alternating electric fields. There is evidence that suggests TTFields can affect the drug uptake in HGG cells, with one study finding that TTFields significantly increased uptake of membrane penetrating compounds such as dextran-FITC (292). Furthermore, TTFields can increase the levels of 5-aminolevulinic acid uptake by GBM cells (293).

7.4.4.2 TTFields tolerance is associated with CLIC expression recovery.

As it stands, no ion channels have been implicated in the potential mechanism to resistance of TTFields therapy. As previously discussed, the calcium ion channels Cav1.2 and Cav1.3 have been implicated in the mechanism of TTFields. rtPCR data (294) and transcriptome (295) data reveal an overexpression of these channels associated with TTFields treatment, but no link to resistance has been found.

In this thesis we report that KNS42 cells can become tolerant to TTFields following extended treatment; with an increase in both cell viability and cell count following 13-day exposure.

Additionally, this tolerance was associated with a recovery of CLIC1 and CLIC4 expression, that was previously seen to be downregulated at day 3 of treatment. Interestingly, siRNA knock down of CLIC1 was sufficient to reverse tolerance to TTFields, re-sensitising KNS42 cells to TTFields treatment. The link between CLIC channels has not been previously explored, and as such, there is little previous evidence to suggest why there is an apparent synergy and mechanistic link between CLIC channels and TTFields.

A study by Wang *et al* has suggested that TTFields resistance may be mediated by AMPK activation leading to an induction of autophagy or alternatively through mutations of CDK2NA and mTOR (292). This may provide some insight into the results found in the present study. CLIC1 is a known interactor of CDK2 (283) and mTOR (296), with CLIC1 knock down resulting in a reduction of mTOR protein , with further studies finding that CLIC1 inhibition prevents mTOR downstream signalling (297). Further to this, CLIC1 can interact with AMPK, further inhibiting mTOR (265).

These data have very important implications, not only for the mechanistic properties of CLIC channels in TTFields, but also on avenues to treatment resistance, suggesting CLIC1 as a key target for TTFields.

7.5 RNA sequencing of recurrent GBM patient tissue reveals key pathways associated with GBM recurrence and TTFields treatment.

To build a comprehensive picture of the global genomic status of patient tissues exposed to TTFields, we employed 3' mRNA sequencing across three recurrent tumours from one patient. Although a case study of an individual patient, as far as the authors are aware, there are no similar studies documenting the effect of TTFields and tumour recurrence across the primary, secondary, and tertiary tumours of a patient. As such, we present novel findings into the genetic alterations associated with TTFields treatment in recurrent

tumours. A wide scale assessment of the effect of TTFields in GBM cell lines has been previously carried out using whole transcriptome and proteome analysis (211) and within the group we have assessed the genome wide expression of *in vitro* TTFields using gene microarrays (152), however little work has been carried out in recurrent patient tissues.

As expected, the 2018, 2020 and 2021 tumours all cluster independently, with clear stratification and differential gene expression apparent between groups. Previous assessment into cell lines exposed to TTFields reflect a very similar genetic pattern of significantly altered genes when compared to untreated cells (298). Furthermore, it is well understood that glioblastomas evolve over their lifespan, acquiring significant mutational burdens, differing greatly from the primary tumour; with clonal evolution following therapy (299–301).

In this study we find a host of genetic alterations across the life span of the tumour, with over 3,000 DEGs in the 2018 vs 2020 comparison, over 7,000 DEGS in the 2020 vs 20201 comparison, and over 12,000 significantly differentially expressed genes between 2018 and 2021 tumour. Indeed, this increasing number of differentially expressed genes across the comparisons, with the highest number in the 2018 vs 2021 comparison, highlights the additional mutational load and evolutionary landscape of genetic aberrations following TTFields and recurrence.

Interestingly, assessment of dysregulated cellular functions revealed that there was a significant downregulation of functions associated with neurogenesis as the tumour recurred.

7.5.1 TTFields treatment leads to dysregulation of ion channel regulated cellular processes and pathways.

It is noteworthy that of the significantly DEGs, several were associated with cellular functions such as synaptogenesis and solute transport. Assessment of cellular function reveals that the primary tumour is significantly enriched for functions related to neurogenesis, neuronal function, synaptic control, and brain development. This translates to a down regulation of these functions upon tumour progression and recurrence. As cancer progresses, the cells because more primitive, losing their primary function and glial features. Undoubtedly there is a significant mutational burden across the life span of the tumour, altering the genetic landscape and promoting the malignant state. This primitive undifferentiated state appears to coincide with tumour recurrence, and may provide valuable insight into disease resistance. Further to this, there was a signature of increased protein biosynthesis in the recurrent samples.

KEGG pathway enrichment highlighted that pathways with heavy ion channel involvement such as addiction, development of synapses; dopamine and pain pathways were implicated following TTFields treatment. Ion channels are notably prominent in the development of addiction pathways; drugs bind to ionotropic receptors and ion channels, with ion channels in turn regulating neuronal activity (302). Studies have previously identified links between gliomagenesis and addiction pathways, with drugs such a disulfiram (a drug used in alcohol addiction) being explored in clinical trials (303).

This upregulation of ion channel associated pathways, and synaptic formation supports the role of ion channels in glioma development, and the emerging field of cancer neuroscience (200). Landmark research by the Monje group found that gliomas can integrate into the neural circuitry, forming synapses with the surrounding healthy brain (199). As such, these

data provide further evidence to support the expanding field of bioelectric in HGG and cancer neuroscience.

7.5.1.1 *CLIC1 and CLIC4 are down regulated following* in vivo *TTFields exposure.*

To validate *in vitro* findings, we enriched our analysis to look at an ion channel specific subset. Here we recapitulate the unique ion channel signature seen in HGG cell lines following *in vitro* exposure to TTFields. Importantly, we find that both CLIC1 and CLIC4 are significantly down regulated in the 2020 and 2021 tumour when compared to 2018. Furthermore, this down regulation occurs in a time dependent manner, with expression in the 2021 tumour markedly reduced compared to the 2020 tumour. This study is the first of its kind to assess the *in vivo* association between ion channel expression and TTFields treatment in a recurrent patient sample. This data combined with *in vitro* experiments confirms previous findings in this study identifying CLIC1 and CLIC4 as biomarkers for HGG; CLIC channels may be prognostic indicators for the success of TTFields, as well as revealing insight into its mechanism of action. We confirm via *in vivo* and *in vitro* assessment that TTFields treatment is associated with a down regulation of CLIC1 and CLIC4 as shown by RNA sequencing, rtPCR and IHC.

7.5.2 *In vivo* TTFields exposure is associated with a reduction in DNA repair associated genes.

Our NGS studies reveal that recurrent glioblastoma is associated with a downregulation in pathways associated with DNA repair. Of note, the Fanconi anaemia and homologous recombination pathways were highlighted in all three comparisons.

DNA damage has been long recognised as causal factor for cancer development. Erroneous DNA repair can lead to mutations or chromosomal aberrations affecting oncogenes and tumour suppressor genes, leading to malignant transformation (304). DNA damage not only comprises a root cause for cancer development but also continues to provide an important avenue for chemo- and radiotherapy (304,305). Whilst inefficient DNA repair may be a driver for cancers, an enhanced capacity to perform DNA repair is actually protective for cancer cells; allowing them to repair DNA insults from targeted chemo or radiotherapy (306).

Multiple studies have cited the significance of DNA repair in cancer. Importantly, the pan cancer atlas identified that DNA damage repair alterations were found across 33 human cancer types. It found that multiple genes across multiple DDR pathways aberrantly expressed and linked to malignancy. Importantly 48 of these DDR genes were identified as cancer drivers (65).

Indeed, it is interesting that the tumour appears to lose its capacity to repair damage DNA across recurrent samples, suggesting a hypermutated phenotype and an enhanced DNA repair network present in the primary tumour. Multiple studies have cited the significance of DNA repair in glioblastoma/HGG (307–309). It is well known that the main stay treatment for GBM is temozolomide, an alkylating agent that forms alkyl adducts on the DNA via the addition of methyl groups at N7 and O6 sites on guanines and the N3 site on adenines (310). TMZ-induced DNA damage is efficiently repaired by the BER repair

pathway or by the MGMT pathway. Therefore, it has been hypothesized that combining TMZ with novel small molecule inhibitors of these pathways may improve patient survival. Studies have found that combining PARP inhibitors with TMZ can enhance the latter's anticancer effects (310), sensitising GBM to TMZ treatment (311). Other than surgery, radiotherapy is the main predictor of glioma prognosis. Radiotherapy exerts cellular damage by inducing a wide range of DNA lesions, but it is particularly associated with the generation of large amounts of SSBs and DSBs. Poly (ADP-ribose) polymerase-1 (PARP1) plays a pivotal role in detection of SSBs, facilitating the colocalisation of the single-strand break repair mechanisms. Studies have identified that PARP inhibition can lead to radio-sensitisation in resistant GBM (312).

A study by Gobin *et al* found a 27 DDR gene signature associated with recurrent glioblastoma implicating BER, NHEJ and NER in glioma recurrence (313). There are several on-going clinical trials at various phases assessing targeted DDR therapies. These studies primarily focus on targeting ATM/ATR, CHK1 and 2 and DNA-PK and PARP pathways (314), highlighting the emerging focus on DNA repair in HGG and clinical feasibility.

Studies such as the GLASS consortium have sought to use wide scale cohorts to define glioma tumour evolution and to expose its therapeutic vulnerabilities, they have found that the DNA in GBM recurrent samples is hyper-mutated across many repair pathways (315). And as such these patient tissue directed studies of recurrent are the key future in glioma research and may further help to elucidate DDR mechanism in a wide scale manner. As well as elucidating the genetic changes associated with tumour recurrence, this study also reveals mechanistic insight into the genetic changes occurring following TTFields exposure. The Fanconi anaemia pathway is assumed to be a key mediator in the co-ordination of enlisting DNA repair pathways: nucleotide excision repair, homologous

recombination, and mutagenic translesion synthesis (316). The Fanconi anaemia pathway has been found contribute to gliomagenesis and radio-resistance (317), agreeing with the data found in the present NGS study, but has also been implicated in the mechanism of TTFields response (87). Data has shown that TTFields regulates DNA damage repair mechanisms and drug resistance via the Fanconi-anaemia-BRCA pathway (318). An increasing level of genomic instability is observed, with the FA-BRCA pathway being a key mediator in the repair of DSBs and interstrand cross-links via the homologous recombination repair pathway (319). BRCA1, TP53 and GADD45 were observed to increase following TTFields treatment, associated with G2/M phase cell cycle arrest (320) implicating FA-BRCA associated proteins in TTFields response.

TTFields have been found to enhance chemo-sensitivity in GBM cells via the down regulation of the FA-BRCA pathway (88) and increased replication stress via impaired replication fork dynamics. Karanam *et al* found that when combining TTFields with radiotherapy, BRCA1 expression was significantly down regulated, inhibiting the repair of DSBs and sufficiently sensitising cells to radiotherapy (89).

Additionally, TTFields has been shown to downregulate the Fanconi Anaemia-BRCA pathway and increase the efficacy of chemotherapy in malignant pleural mesothelioma preclinical models (321). Differential gene expression analysis in NSCLC (Non-Small Cell Lung Carcinoma) finds that TTFields is associated with a down regulation of MRE11A, FANCM, FANCD2 and BRCA1, with downregulation correlation with TTFields sensitivity.

In this study, we provide *in vivo* evidence to support cell-based studies, demonstrating that TTFields leads to a reduction in DNA repair genes, with dysregulation in the FA and HR pathways. These findings validate the significant of DNA repair proteins as therapeutic targets alone, or in combination with TTFields.

7.5.3 Neurodegenerative pathways associated with mitochondrial function are upregulated in recurrent GBM.

KEGG analysis revealed that recurrent tumours significantly upregulate pathways associated with neurodegeneration. Interestingly, the neurodegenerative actions of gliomas resemble the mechanisms that are also found in many neurodegenerative diseases such as Alzheimer's disease, Parkinson's disease, and amyotrophic lateral sclerosis (322), with autophagy being highly implicated in both processes (323). Interestingly, the disease pathways were consistently differentially upregulated in recurrent samples across all comparisons. These *in vivo* findings support previous work performed by the group, where Branter et al show that *in vitro* TTFields results in the upregulation of DEGs associated with neurodegeneration pathways (152).

Emerging research has stated that the age-associated changes such as chronic neuro-inflammation are potential contributors to the reduced overall survival observed in adult GBM patients aged 65+ years (324). Recent data has shown that glioma's take advantage of neuronal glutamate signalling, using them to potentiate their own growth. This is associated with an excessive glutamate release that produces a microenvironment that is toxic for neurones, leading to a neuro degenerative effect (325). Interestingly, ion channels are crucial in this process, providing additional evidence for the role of ion channels in glioma progression. The WNT pathway has also been implicated in glioma-associated neurodegeneration. Glioma cells can leach WNT from surrounding neurons, triggering and JNK/MMP signalling loop, causing neurodegenerative effects (326). Alternatively, Jarabo *et al* have shown that insulin signalling is a key mediator of the neurodegenerative effects observed in glioma (327) .

The major contributor to the over expression of the neurodegenerative pathways was the subunits of MTND; genes of the mitochondrial genome coding for the NADH-ubiquinone oxidoreductase chain proteins. This indicates a dysfunction of mitochondrial bioenergetics in recurrent GBM. Importantly, metabolic mapping has shown that NADH fluxes are associated with glioblastoma phenotype, with elevation of NADH associated with decreased overall survival (328). Inhibition of the NADH complex 5 significantly reduces glioma cell proliferation, and sensitised radio-resistant u87 cells (329). These genes have been previously found to be aberrantly expressed following TTFields, with MTND5 showing differential upregulation following TTFields (152). Additionally, MTND5 has previously been implicated in gastric cancer, with SNV and point mutations across patient tissue (330). These data provide evidence for a novel research avenue into mitochondrial bioenergetics in glioma, which may provide exciting insights for further therapeutic targets.

7.6 *In vitro* assessment of TTFields treated recurrent patient derived GBM cell lines.

Following a wealth of data produced via NGS analysis of recurrent GBM tissues we sought to validate our findings. As the primary focus of this research was to assess the importance of CLIC1 and CLIC4 in HGG, we pursued validation of these targets, following the promising *in vivo* data confirming our previous *in vitro* TTFields experiments. The primary, secondary, and tertiary tumours were stained for both CLIC1 and CLIC4, whereby a marked down-regulation of these proteins was seen in the recurrent tumour when compared to the primary tumour, supporting DEG (differentially expressed genes) analysis shown in section 6.5. Furthermore, rt-PCR was performed on cell lines derived from the 2021 tumour (GIN98 and GCE98), we found that these cell lines exhibited a significantly reduced expression of CLIC1 and CLIC4 when compared to pHGG. Further analysis revealed that the cell lines were significantly less sensitive to *in vitro* TTFields, suggesting a developing inherent resistance to TTFields therapy. Very few studies have assessed TTFields resistance; largely due to the difficulty with data stratification as patients often receive a myriad of treatments, all of which instigate genetic alterations in the tumour. Excitingly, together these data support our hypothesis that CLIC channels are implicated in the mechanism of TTFields treatment, proving as viable and attractive targets, and are pivotal in glioma progression. Figure 7.4 provides a graphical summary of the findings associated with TTFields treatment presented in chapters 5 and 6 of this thesis.

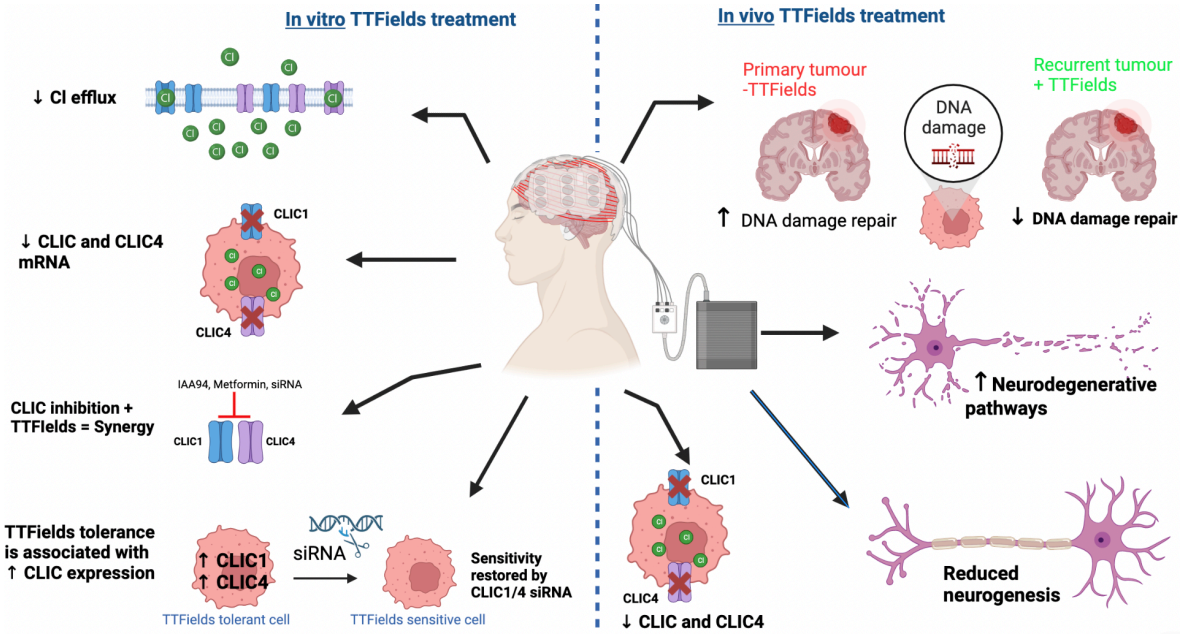

Figure 7.4 Graphical summary of the *in vitro* and *in vivo* findings from TTFields experiments.

7.7 Future work

The next steps in this research would be two-fold. Firstly, electrophysiological techniques such as whole cell and cell attached patch clamping to further assess the functionality of CLIC channels in glioblastoma cells. This would include the screening of a range of chloride channel inhibitors and CLIC deficient cells to assess changes in Vm, with single channel recordings to isolate CLIC channels. Furthermore, generation of a stable knock out of CLIC1 in pHGG cells and further NGS analysis would reveal further mechanistic insight into the role that CLIC1 and CLIC4 hold in gliomagenesis. Electrophysiology should be exploited to explore the functional bioelectric effects of TTFields, and further interrogate the dysregulation of membrane potential associated with alternating electric field exposure.

Secondly, validation of 3' mRNA sequencing data would provide important information and insights into GBM recurrence associated with TTFields therapy. These data should be validated across the original patient tissue, which unfortunately due to time constraints was not feasible within the time frame of this project. DNA repair in response to TTFields

treatment in HGG is currently being explored, however, novel insight may be offered by assessing some lesser-explored candidates highlighted in this study. It would be interesting to establish whether this signature of increased neurodegenerative pathways holds any bearing on the development of a wider cohort of GBM samples, as such, publicly available datasets could be used to assess this. The investigation of how perturbation of the TTFields treatment signature impacts HGG cell viability and response to mainstay therapies will also be vital in expanding our knowledge. Rather than targeting individual genes that are differentially expressed following TTFields, it may be of benefit to target the pathway signatures as a whole. To do this a screening approach may be of benefit, whereby publicly available platforms can be used to assess genetic signatures alongside compound libraries. This will be essential in identifying novel inhibitors of glioma recurrence and treatment resistance.

8 Concluding statement

Brain tumours are the biggest killer of children and adults under the age of 40, with the survival statistics being dismal in most patient cohorts. Our research programme focussed on paediatric high-grade gliomas (WHO grade IV) and IDH wild type adult glioblastoma, for which patient prognosis remains invariably poor worldwide, despite multimodal treatment.

Importantly, there are no curative treatment for these high-grade gliomas. No therapies, other than TTFields have shown efficacy in significantly prolonging overall survival in phase 3 clinical trials since the landmark trials on TMZ; which we know, for many patients, has no clinical effect. We are faced with a significant unmet clinical need and as such, we sought to identify therapeutically actionable signatures of ion channel expression in HGG.

In this thesis, we have presented a feasibility study assessing whether ion channels are viable targets in paediatric high-grade gliomas. Here we provide proof of concept that targeting CLIC1 and CLIC4 *in vitro* will significantly reduce the capacity for pHGG to proliferate and invade. Furthermore, we have characterised the bioelectrical properties of CLIC1 and CLIC4 in SF188, KNS42 and GCE62 cells, finding that disrupting the innate bioelectricity of these cell causes aberrant cell cycling and altered chloride flux.

Additionally, we have shown that TTFields shows efficacy in pHGG, identifying that chloride intracellular channels may reveal mechanistic insight into the success of TTFields. We have identified that treatment with TTFields confers a down regulation of CLIC1 and CLIC4 mRNA expression, and further targeting of CLIC1 and CLIC4 via siRNA or pharmacologically targeting significantly sensitised pHGG cells to TTFields. We explore tolerance to TTFields, finding that KNS42 cells harness an enhanced capacity to withstand TTFields anti-

proliferative effects following long-term treatment when compared to short-term treatment. Further to this, tolerance was associated with a recovery of CLIC1 and CLIC4 expression, that with induce deficiency via siRNA knock down, re-sensitised cells to TTFields.

The wealth of data provided by 3'mRNA sequencing has provided a multitude of additional research avenues to follow, further implicating CLIC channels in the biological response to TTFields and validating out *in vitro* findings. DNA repair and neurodegenerative pathways have been highlighted as significantly altered in response to TTFields and GBM recurrence, and present as particularly interesting pathway targets for future work.

The studies provide valuable insight into the role that chloride intracellular channels play in pHGG, and the sensitivity to TTFields. Thus, unlocking a potential mechanism for TTFields success, and providing a defined targetable ion channel signature that is highly translational and feasible for clinical pursuit. This project has identified new therapeutic targets for HGG, a disease with a high mortality rate and few treatment options. By investigating the role of ion channels in HGG tumorigenesis and response to therapy, we share new therapeutic strategies that can improve patient outcomes. Feasibility studies such as this are essential in the common goal to improve clinical practice by advancing our understanding of the processes and mechanisms involved in the formation and spread of aggressive, treatment-resistant brain cancers.

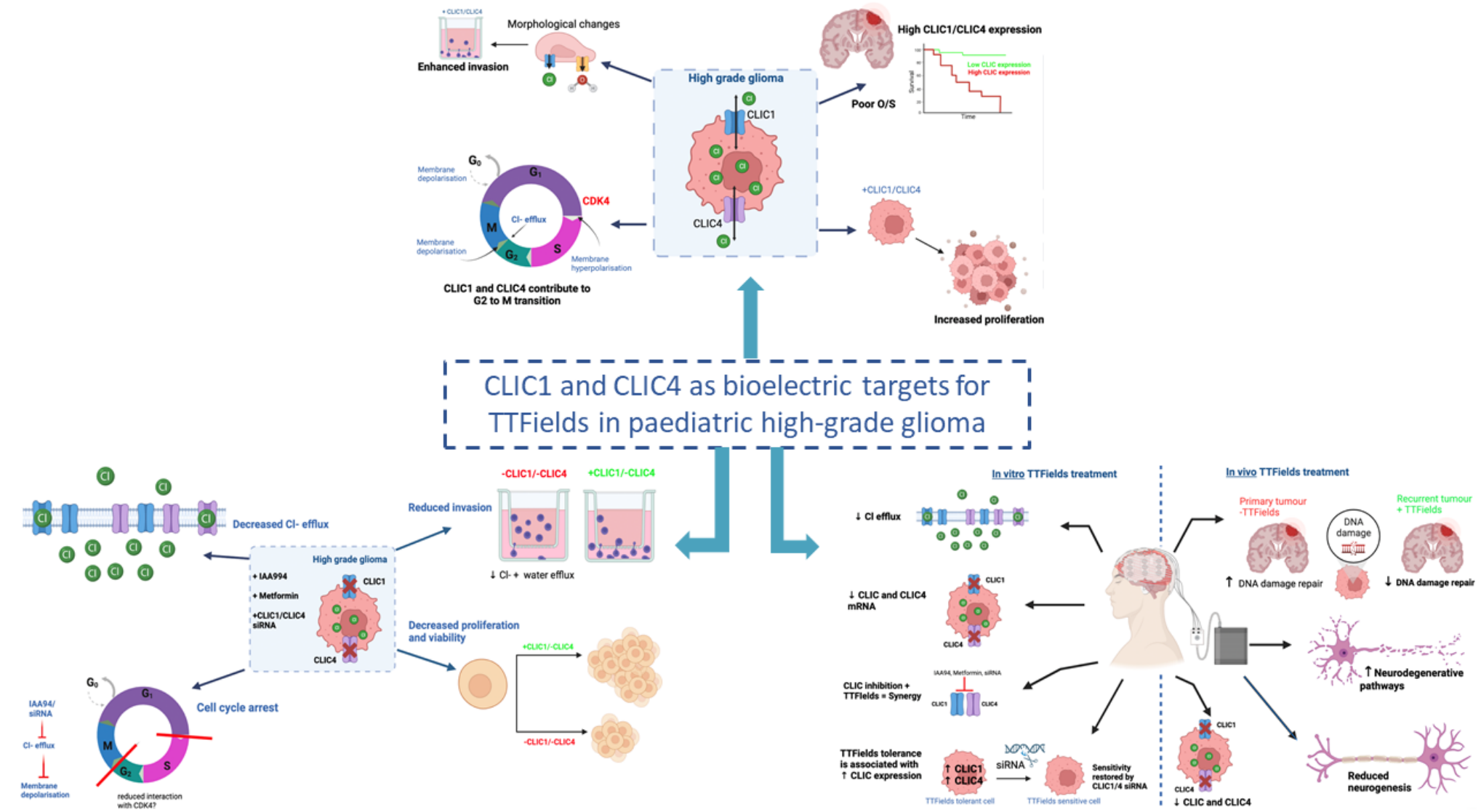
+ CLIC1/CLIC4
Morphological changes
Enhanced invasion
High grade glioma
CLIC1
CLIC4
High CLIC1/CLIC4 expression
Low CLIC expression
High CLIC expression
Survival
Time
Poor O/S
+CLIC1/CLIC4
Increased proliferation
Membrane depolarisation
Cl- efflux
Membrane hyperpolarisation
CDK4
CLIC1 and CLIC4 contribute to G2 to M transition
CLIC1 and CLIC4 as bioelectric targets for TTFields in paediatric high-grade glioma
Decreased Cl- efflux
High grade glioma
+ IAA994
+ Metformin
+CLIC1/CLIC4 siRNA
Reduced invasion
-CLIC1/-CLIC4
+CLIC1/-CLIC4
↓ Cl- + water efflux
Decreased proliferation and viability
Cell cycle arrest
IAA94/ siRNA
Cl- efflux
Membrane depolarisation
reduced interaction with CDK4?
In vitro TTFields treatment
↓ Cl efflux
↓ CLIC and CLIC4 mRNA
CLIC inhibition + TTFields = Synergy
IAA94, Metformin, siRNA
TTFields tolerance is associated with ↑ CLIC expression
↑ CLIC1 ↑ CLIC4
siRNA
Sensitivity restored by CLIC1/4 siRNA
TTFields tolerant cell
TTFields sensitive cell
In vivo TTFields treatment
Primary tumour -TTFields
Recurrent tumour + TTFields
DNA damage
↑ DNA damage repair
↓ DNA damage repair
↑ Neurodegenerative pathways
Reduced neurogenesis
↓ CLIC and CLIC4

9 References

1. Public Health England. Childhood Cancer Statistics, England Annual Report 2018. Public Health England. 2018;31.
2. UK CR. Cancer Research UK. Cancer incidence by age. [Internet]. Cancer Research UK. (2020). Cancer incidence by age. [online] Available at: https://www.cancerresearchuk.org/health-professional/cancer-statistics/incidence/age#heading-Two [Accessed 27 Feb. 2020]. 2020. Available from: Cancer Research UK. (2020). Cancer incidence by age. [onlinwww.cancerresearchuk.org/health-professional/cancer-statistics/incidence/age#heading-Two
3. Steliarova-Foucher E, Colombet M, Ries LAG, Moreno F, Dolya A, Bray F, et al. International incidence of childhood cancer, 2001–10: a population-based registry study. Lancet Oncol. 2017;
4. Cancer.org C with. Childhood cancer: facts and figures [Internet]. 2020 [cited 2020 Sep 21]. Available from: https://www.childrenwithcancer.org.uk/childhood-cancer-info/childhood-cancer-facts-figures
5. Coleman C, Stoller S, Grotzer M, Stucklin AG, Nazarian J, Mueller S. Pediatric hemispheric high-grade glioma: targeting the future. Cancer and Metastasis Reviews. 2020.
6. Donahue B. Short- and long-term complications of radiation therapy for pediatric brain tumors. Pediatric Neurosurgery. 1992.

7. Willard VW, Berlin KS, Conklin HM, Merchant TE. Trajectories of psychosocial and cognitive functioning in pediatric patients with brain tumors treated with radiation therapy. Neuro Oncol. 2019;
8. Wilne S, Collier J, Kennedy C, Koller K, Grundy R, Walker D. Presentation of childhood CNS tumours: a systematic review and meta-analysis. Lancet Oncology. 2007;
9. Shen CJ, Terezakis SA. The Evolving Role of Radiotherapy for Pediatric Cancers With Advancements in Molecular Tumor Characterization and Targeted Therapies. Front Oncol. 2021 Sep 16;11.
10. Louis DN, Perry A, Wesseling P, Brat DJ, Cree IA, Figarella-Branger D, et al. The 2021 WHO Classification of Tumors of the Central Nervous System: a summary. Neuro Oncol. 2021 Aug 2;23(8):1231–51.
11. RALLIS KS, GEORGE AM, WOZNIAK AM, BIGOGNO CM, CHOW B, HANRAHAN JG, et al. Molecular Genetics and Targeted Therapies for Paediatric High-grade Glioma. Cancer Genomics - Proteomics. 2022 Jun 22;19(4):390–414.
12. Reilly KM. Brain Tumor Susceptibility: the Role of Genetic Factors and Uses of Mouse Models to Unravel Risk. Brain Pathology. 2009 Jan;19(1):121–31.
13. Ostrom QT, Fahmideh MA, Cote DJ, Muskens IS, Schraw JM, Scheurer ME, et al. Risk factors for childhood and adult primary brain tumors. Neuro Oncol. 2019 Nov 4;21(11):1357–75.
14. Malbari F, Lindsay H. Genetics of Common Pediatric Brain Tumors. Pediatr Neurol. 2020 Mar;104:3–12.
15. KANTI DAS K, KUMAR R. Pediatric Glioblastoma. In: Glioblastoma. 2017.

16. Konar SK, Bir SC, Maiti TK, Nanda A. A systematic review of overall survival in pediatric primary glioblastoma multiforme of the spinal cord. Journal of Neurosurgery: Pediatrics. 2017.

17. Subramanian S and A. Childhood Brain Tumors. In: Cancer [Internet]. StatPearls Publishinh; 2020. Available from: https://www.ncbi.nlm.nih.gov/books/NBK535415/

18. Shanmugavadivel D, Liu JF, Murphy L, Wilne S, Walker D. Accelerating diagnosis for childhood brain tumours: An analysis of the HeadSmart UK population data. Arch Dis Child. 2020;

19. Zong H, Verhaak RGW, Canolk P. The cellular origin for malignant glioma and prospects for clinical advancements. Expert Review of Molecular Diagnostics. 2012.

20. Laug D, Glasgow SM, Deneen B. A glial blueprint for gliomagenesis. Nature Reviews Neuroscience. 2018.

21. Torp SH, Solheim O, Skjulsvik AJ. The WHO 2021 Classification of Central Nervous System tumours: a practical update on what neurosurgeons need to know—a minireview. Acta Neurochir (Wien). 2022 Jul 26;164(9):2453–64.

22. Walker C, Baborie A, Crooks D, Wilkins S, Jenkinson MD. Biology, genetics, and imaging of glial cell tumours. British Journal of Radiology. 2011;

23. Blionas A, Giakoumettis D, Klonou A, Neromyliotis E, Karydakis P, Themistocleous MS. Paediatric gliomas: diagnosis, molecular biology, and management. Ann Transl Med. 2018;

24. Silantyev AS, Falzone L, Libra M, Gurina OI, Kardashova KS, Nikolouzakis TK, et al. Current and Future Trends on Diagnosis and Prognosis of Glioblastoma: From Molecular Biology to Proteomics. Cells. 2019.

25. Ostrom QT, Price M, Neff C, Cioffi G, Waite KA, Kruchko C, et al. CBTRUS Statistical Report: Primary Brain and Other Central Nervous System Tumors Diagnosed in the United States in 2015–2019. Neuro Oncol. 2022 Oct 5;24(Supplement_5):v1–95.

26. Liu M, Thakkar JP, Garcia CR, Dolecek TA, Wagner LM, Dressler EVM, et al. National cancer database analysis of outcomes in pediatric glioblastoma. Cancer Med. 2018;

27. Himes BT, Zhang L, Daniels DJ. Treatment Strategies in Diffuse Midline Gliomas With the H3K27M Mutation: The Role of Convection-Enhanced Delivery in Overcoming Anatomic Challenges. Front Oncol. 2019 Feb 8;9.

28. Haizel-Cobbina J, Spector LG, Moertel C, Parsons HM. Racial and ethnic disparities in survival of children with brain and central nervous tumors in the United States. Pediatr Blood Cancer. 2021 Jan 24;68(1).

29. Merchant TE, Pollack IF, Loeffler JS. Brain Tumors Across the Age Spectrum: Biology, Therapy, and Late Effects. Semin Radiat Oncol. 2010 Jan;20(1):58–66.

30. Muskens IS, Feng Q, Francis SS, Walsh KM, Mckean-Cowdin R, Gauderman WJ, et al. Pediatric glioma and medulloblastoma risk and population demographics: a Poisson regression analysis. Neurooncol Adv. 2020 Jan 1;2(1).

31. Korshunov A, Schrimpf D, Ryzhova M, Sturm D, Chavez L, Hovestadt V, et al. H3-/IDH-wild type pediatric glioblastoma is comprised of molecularly and prognostically distinct subtypes with associated oncogenic drivers. Acta Neuropathol. 2017;

32. Sturm D, Witt H, Hovestadt V, Khuong-Quang DA, Jones DTW, Konermann C, et al. Hotspot Mutations in H3F3A and IDH1 Define Distinct Epigenetic and Biological Subgroups of Glioblastoma. Cancer Cell. 2012;

33. Andreiuolo F, Lisner T, Zlocha J, Kramm C, Koch A, Bison B, et al. H3F3A-G34R mutant high grade neuroepithelial neoplasms with glial and dysplastic ganglion cell components. Acta Neuropathol Commun. 2019;

34. Lee JH. Somatic mutations in disorders with disrupted brain connectivity. Exp Mol Med. 2016 Jun 10;48(6):e239–e239.

35. Louis DN, Perry A, Reifenberger G, von Deimling A, Figarella-Branger D, Cavenee WK, et al. The 2016 World Health Organization Classification of Tumors of the Central Nervous System: a summary. Acta Neuropathologica. 2016.

36. Hauser P. Classification and Treatment of Pediatric Gliomas in the Molecular Era. Children. 2021 Aug 27;8(9):739.

37. Cai X, Sughrue ME. Glioblastoma: New therapeutic strategies to address cellular and genomic complexity. Oncotarget. 2018.

38. Buccoliero AM, Giunti L, Moscardi S, Castiglione F, Provenzano A, Sardi I, et al. Pediatric High Grade Glioma Classification Criteria and Molecular Features of a Case Series. Genes (Basel). 2022 Mar 31;13(4):624.

39. Smith SJ, Long A, Barrow JH, Macarthur DC, Coyle B, Grundy RG. Pediatric high-grade glioma: Identification of Poly(ADP-ribose) polymerase as a potential therapeutic target. Neuro Oncol. 2011;

40. Lewis PW, Müller MM, Koletsky MS, Cordero F, Lin S, Banaszynski LA, et al. Inhibition of PRC2 Activity by a Gain-of-Function H3 Mutation Found in Pediatric Glioblastoma. Science (1979). 2013 May 17;340(6134):857–61.

41. Lim KY, Won JK, Park CK, Kim SK, Choi SH, Kim T, et al. H3 G34-mutant high-grade glioma. Brain Tumor Pathol. 2021 Jan 29;38(1):4–13.

42. Davies H, Bignell GR, Cox C, Stephens P, Edkins S, Clegg S, et al. Mutations of the BRAF gene in human cancer. Nature. 2002 Jun 9;417(6892):949–54.

43. Gielen GH, Baugh JN, van Vuurden DG, Veldhuijzen van Zanten SEM, Hargrave D, Massimino M, et al. Pediatric high-grade gliomas, and the WHO CNS Tumor Classification—Perspectives of pediatric neuro-oncologists and neuropathologists in light of recent updates. Neurooncol Adv. 2022 Jan 1;4(1).

44. Buczkowicz P, Bartels U, Bouffet E, Becher O, Hawkins C. Histopathological spectrum of paediatric diffuse intrinsic pontine glioma: diagnostic and therapeutic implications. Acta Neuropathol. 2014 Oct 22;128(4):573–81.

45. YOSHIMURA J, ONDA K, TANAKA R, TAKAHASHI H. Clinicopathological Study of Diffuse Type Brainstem Gliomas: Analysis of 40 Autopsy Cases. Neurol Med Chir (Tokyo). 2003;43(8):375–82.

46. Wesseling P, van den Bent M, Perry A. Oligodendroglioma: pathology, molecular mechanisms, and markers. Acta Neuropathol. 2015 Jun 6;129(6):809–27.

47. Ceglie G, Del Baldo G, Agolini E, Rinelli M, Cacchione A, Del Bufalo F, et al. Cancer Predisposition Syndromes Associated With Pediatric High-Grade Gliomas. Front Pediatr. 2020 Nov 12;8.

48. Bougeard G, Renaux-Petel M, Flaman JM, Charbonnier C, Fermey P, Belotti M, et al. Revisiting Li-Fraumeni Syndrome From *TP53* Mutation Carriers. Journal of Clinical Oncology. 2015 Jul 20;33(21):2345–52.

49. Jett K, Friedman JM. Clinical and genetic aspects of neurofibromatosis 1. Genetics in Medicine. 2010 Jan;12(1):1–11.

50. Kim J, Kim J, Bae JS. ROS homeostasis and metabolism: a critical liaison for cancer therapy. Exp Mol Med. 2016 Nov 4;48(11):e269–e269.

51. Kim B, Tabori U, Hawkins C. An update on the CNS manifestations of brain tumor polyposis syndromes. Acta Neuropathol. 2020 Apr 22;139(4):703–15.

52. Kyritsis AP, Bondy ML, Rao JS, Sioka C. Inherited predisposition to glioma. Neuro Oncol. 2010 Jan 1;12(1):104–13.

53. Malmer B, Adatto P, Armstrong G, Barnholtz-Sloan J, Bernstein JL, Claus E, et al. GLIOGENE—an International Consortium to Understand Familial Glioma. Cancer Epidemiology, Biomarkers & Prevention. 2007 Sep 1;16(9):1730–4.

54. Malmer B, Haraldsson S, Einarsdottir E, Lindgren P, Holmberg D. Homozygosity mapping of familial glioma in Northern Sweden. Acta Oncol (Madr). 2005 Mar 8;44(2):114–9.

55. Braganza MZ, Kitahara CM, Berrington de Gonzalez A, Inskip PD, Johnson KJ, Rajaraman P. Ionizing radiation and the risk of brain and central nervous system tumors: a systematic review. Neuro Oncol. 2012 Nov 1;14(11):1316–24.

56. Chatwin H V., Cruz J, Green AL. Pediatric high-grade glioma: moving toward subtype-specific multimodal therapy. FEBS J. 2021 Nov 11;288(21):6127–41.

57. Sontheimer H. An unexpected role for ion channels in brain tumor metastasis. Experimental Biology and Medicine. 2008.

58. Weaver AK, Liu X, Sontheimer H. Role for calcium-activated potassium channels (BK) in growth control of human malignant glioma cells. J Neurosci Res. 2004;

59. Weaver AK, Bomben VC, Sontheimer H. Expression and function of calcium-activated potassium channels in human glioma cells. Glia. 2006;

60. Sánchez Fernández I, Loddenkemper T. Seizures caused by brain tumors in children. Seizure. 2017.

61. El-Ayadi M, Ansari M, Sturm D, Gielen GH, Warmuth-Metz M, Kramm CM, et al. High-grade glioma in very young children: A rare and particular patient population. Oncotarget. 2017.

62. Patel V, McNinch NL, Rush S. Diagnostic delay and morbidity of central nervous system tumors in children and young adults: a pediatric hospital experience. J Neurooncol. 2019;

63. Dhurgshaarna, Shanmugavadivel; David, Walker; Jo-Fen, Liu; Sophie W. HeadSmart: are you brain tumour aware? Paediatr Child Health. 2016;6(2):81–6.

64. Kline C, Felton E, Allen IE, Tahir P, Mueller S. Survival outcomes in pediatric recurrent high-grade glioma: results of a 20-year systematic review and meta-analysis. J Neurooncol. 2018;

65. Knijnenburg TA, Wang L, Zimmermann MT, Chambwe N, Gao GF, Cherniack AD, et al. Genomic and Molecular Landscape of DNA Damage Repair Deficiency across The Cancer Genome Atlas. Cell Rep. 2018 Apr;23(1):239-254.e6.

66. Grill J, Massimino M, Bouffet E, Azizi AA, McCowage G, Cañete A, et al. Phase II, open-label, randomized, multicenter trial (HERBY) of bevacizumab in pediatric patients with newly diagnosed high-grade glioma. Journal of Clinical Oncology. 2018;

67. Weller M, Butowski N, Tran DD, Recht LD, Lim M, Hirte H, et al. Rindopepimut with temozolomide for patients with newly diagnosed, EGFRvIII-expressing glioblastoma (ACT IV): a randomised, double-blind, international phase 3 trial. Lancet Oncol. 2017;

68. Reardon DA, Brandes AA, Omuro A, Mulholland P, Lim M, Wick A, et al. Effect of Nivolumab vs Bevacizumab in Patients with Recurrent Glioblastoma: The CheckMate 143 Phase 3 Randomized Clinical Trial. JAMA Oncol. 2020;

69. Kinzel A, Ambrogi M, Varshaver M, Kirson ED. Tumor Treating Fields for Glioblastoma Treatment: Patient Satisfaction and Compliance With the Second-Generation Optune ® System. Clin Med Insights Oncol. 2019;

70. Stupp R, Taillibert S, Kanner A, Read W, Steinberg DM, Lhermitte B, et al. Effect of tumor-treating fields plus maintenance temozolomide vs maintenance temozolomide alone on survival in patients with glioblastoma a randomized clinical trial. JAMA - Journal of the American Medical Association. 2017;

71. Connelly J, Hormigo A, Mohilie N, Hu J, Chaudhry A, Blondin N. Planning TTFields treatment using the NovoTAL system-clinical case series beyond the use of MRI contrast enhancement. BMC Cancer. 2016;

72. Kirson ED, Gurvich Z, Schneiderman R, Dekel E, Itzhaki A, Wasserman Y, et al. Disruption of Cancer Cell Replication by Alternating Electric Fields. Cancer Res. 2004;

73. Wenger C, Salvador R, Basser PJ, Miranda PC. The electric field distribution in the brain during TTFields therapy and its dependence on tissue dielectric properties and anatomy: A computational study. Phys Med Biol. 2015;

74. Wenger C, Giladi M, Bomzon Z, Salvador R, Basser PJ, Miranda PC. Modeling Tumor Treating Fields (TTFields) application in single cells during metaphase and telophase. In: 2015 37th Annual International Conference of the IEEE Engineering in Medicine and Biology Society (EMBC). IEEE; 2015. p. 6892–5.

75. Lacouture ME, Elizabeth Davis M, Elzinga G, Butowski N, Tran D, Villano JL, et al. Characterization and Management of Dermatologic Adverse Events With the NovoTTF-100A System, a Novel Anti-mitotic Electric Field Device for the Treatment of Recurrent Glioblastoma. Semin Oncol. 2014 Jun;41:S1–14.

76. Jain A, Jobson I, Griffin M, Rahman R, Smith S, Rawson FJ. Electric field responsive nanotransducers for glioblastoma. Bioelectron Med. 2022 Oct 19;8(1):17.

77. Gera N, Yang A, Holtzman TS, Lee SX, Wong ET, Swanson KD. Tumor treating fields perturb the localization of septins and cause aberrant mitotic exit. PLoS One. 2015;

78. Kirson ED, Dbalý V, Tovaryš F, Vymazal J, Soustiel JF, Itzhaki A, et al. Alternating electric fields arrest cell proliferation in animal tumor models and human brain tumors. Proc Natl Acad Sci U S A. 2007;

79. Kops GJPL, Shah J V. Connecting up and clearing out: How kinetochore attachment silences the spindle assembly checkpoint. Chromosoma. 2012.

80. Pines J. Cubism and the cell cycle: the many faces of the APC/C. Nat Rev Mol Cell Biol. 2011;12:427–38.

81. Giladi M, Schneiderman RS, Voloshin T, Porat Y, Munster M, Blat R, et al. Mitotic Spindle Disruption by Alternating Electric Fields Leads to Improper Chromosome Segregation and Mitotic Catastrophe in Cancer Cells. Sci Rep. 2015;

82. Hayashi MT, Karlseder J. DNA damage associated with mitosis and cytokinesis failure. Oncogene. 2013.

83. Tung JJ, Tattersall IW, Kitajewski J. Tips, Stalks, Tubes: Notch-Mediated Cell Fate Determination and Mechanisms of Tubulogenesis during Angiogenesis. Cold Spring Harb Perspect Med. 2012 Feb 1;2(2):a006601–a006601.

84. Mun EJ, Babiker HM, Weinberg U, Kirson ED, Von Hoff DD. Tumor-treating fields: A fourth modality in cancer treatment. Clinical Cancer Research. 2018.

85. Giladi M, Munster M, Schneiderman RS, Voloshin T, Porat Y, Blat R, et al. Tumor treating fields (TTFields) delay DNA damage repair following radiation treatment of glioma cells. Radiation Oncology. 2017 Dec 29;12(1):206.

86. Branter J, Basu S, Smith S. Tumour treating fields in a combinational therapeutic approach. Oncotarget. 2018.

87. Rominiyi O, Vanderlinden A, Clenton SJ, Bridgewater C, Al-Tamimi Y, Collis SJ. Tumour treating fields therapy for glioblastoma: current advances and future directions. Br J Cancer. 2021 Feb 16;124(4):697–709.

88. Mumblat H, Martinez-Conde A, Braten O, Munster M, Dor-On E, Schneiderman RS, et al. Tumor Treating Fields (TTFields) downregulate the Fanconi Anemia-BRCA pathway and increase the efficacy of chemotherapy in malignant pleural mesothelioma preclinical models. Lung Cancer. 2021 Oct;160:99–110.

89. Karanam NK, Srinivasan K, Ding L, Sishc B, Saha D, Story MD. Tumor-treating fields elicit a conditional vulnerability to ionizing radiation via the downregulation of BRCA1 signaling and reduced DNA double-strand break repair capacity in non-small cell lung cancer cell lines. Cell Death Dis. 2017 Mar 30;8(3):e2711–e2711.

90. Chang E, Patel CB, Pohling C, Young C, Song J, Flores TA, et al. Tumor treating fields increases membrane permeability in glioblastoma cells. Cell Death Discov. 2018 Dec 5;4(1):113.

91. Prager BC, Bhargava S, Mahadev V, Hubert CG, Rich JN. Glioblastoma Stem Cells: Driving Resilience through Chaos. Trends Cancer. 2020 Mar;6(3):223–35.

92. Stupp R, Wong ET, Kanner AA, Steinberg D, Engelhard H, Heidecke V, et al. NovoTTF-100A versus physician's choice chemotherapy in recurrent glioblastoma: A randomised phase III trial of a novel treatment modality. Eur J Cancer. 2012;

93. Goldman S, Margol A, Hwang EI, Tanaka K, Suchorska B, Crawford JR, et al. Safety of Tumor Treating Fields (TTFields) therapy in pediatric patients with malignant brain tumors: Post-marketing surveillance data. Front Oncol. 2022 Jul 29;12.

94. Goldman S, Hwang E, Lai JS, Kocak M, Lulla R, Dhall G, et al. PDCT-07. FEASIBILITY TRIAL OF TTFIELDS (TUMOR TREATING FIELDS) FOR CHILDREN WITH RECURRENT OR PROGRESSIVE SUPRATENTORIAL HIGH-GRADE GLIOMA (HGG) AND EPENDYMOMA: A PEDIATRIC BRAIN TUMOR CONSORTIUM STUDY: PBTC-048. Neuro Oncol. 2018 Nov 5;20(suppl_6):vi201–2.

95. Crawford J, Saria MG, Dhall G, Margol A, Kesari S. Feasibility of Treating High Grade Gliomas in Children with Tumor-Treating Fields: A Case Series. Cureus. 2020 Oct 5;

96. Williams A, Gill S, Varma T, Jenkinson C, Quinn N, Mitchell R, et al. Deep brain stimulation plus best medical therapy versus best medical therapy alone for advanced Parkinson's disease (PD SURG trial): a randomised, open-label trial. Lancet Neurol. 2010;

97. Coubes P, Cif L, El Fertit H, Hemm S, Vayssiere N, Serrat S, et al. Electrical stimulation of the globus pallidus internus in patients with primary generalized dystonia: Long-term results. J Neurosurg. 2004;

98. Miocinovic S, Somayajula S, Chitnis S, Vitek JL. History, applications, and mechanisms of deep brain stimulation. JAMA Neurology. 2013.

99. Hartmann CJ, Wojtecki L, Vesper J, Volkmann J, Groiss SJ, Schnitzler A, et al. Long-term evaluation of impedance levels and clinical development in subthalamic deep brain stimulation for Parkinson's disease. Parkinsonism Relat Disord. 2015;

100. Amon A, Alesch F. Systems for deep brain stimulation: review of technical features. Journal of Neural Transmission. 2017.

101. M.O. A, A. S, H.E. H, E.J. H, J.K. K. Glial tumors and deep brain stimulation: An increasingly recognized association? Journal of Clinical Neuroscience. 2019;

102. Bordey A, Sontheimer H. Electrophysiological Properties of Human Astrocytic Tumor Cells In Situ: Enigma of Spiking Glial Cells. J Neurophysiol. 1998 May 1;79(5):2782–93.

103. Deweyert A, Iredale E, Xu H, Wong E, Schmid S, Hebb MO. Diffuse intrinsic pontine glioma cells are vulnerable to low intensity electric fields delivered by intratumoral modulation therapy. J Neurooncol. 2019;

104. Yang M, Brackenbury WJ. Membrane potential and cancer progression. Frontiers in Physiology. 2013.

105. Goñi FM. The basic structure and dynamics of cell membranes: An update of the Singer-Nicolson model. Biochimica et Biophysica Acta - Biomembranes. 2014.

106. Wright SH. Generation of resting membrane potential. American Journal of Physiology - Advances in Physiology Education. 2004;

107. Pirahanchi Y, Jessu R AN. Physiology, Sodium Potassium Pump (Na+ K+ Pump) [Internet]. Available from: www.ncbi.nlm.nih.gov/books/NBK537088/%0A

108. Chen H, Chatelain FC, Lesage F. Altered and dynamic ion selectivity of K+ channels in cell development and excitability. Trends in pharmacological sciences. 2014.

109. Goldman DE. Potential, impedance, and rectification in membranes. Journal of General Physiology. 1943;

110. Hodgkin AL, Katz B. The effect of sodium ions on the electrical activity of the giant axon of the squid. J Physiol. 1949;

111. Urrego D, Tomczak AP, Zahed F, Stühmer W, Pardo LA. Potassium channels in cell cycle and cell proliferation. Philosophical Transactions of the Royal Society B: Biological Sciences. 2014.

112. Blackiston DJ, McLaughlin KA, Levin M. Bioelectric controls of cell proliferation: Ion channels, membrane voltage and the cell cycle. Cell Cycle. 2009.

113. Cone CD. Variation of the transmembrane potential level as a basic mechanism of mitosis control. Oncology. 1970;

114. Cone CD. Unified theory on the basic mechanism of normal mitotic control and oncogenesis. J Theor Biol. 1971;

115. Cone CD. Electroosmotic interactions accompanying mitosis initation in sarcoma cells *in vitro*. Trans N Y Acad Sci. 1969;

116. Levin M. Large-scale biophysics: ion flows and regeneration. Trends in Cell Biology. 2007.

117. Marino AA, Morris DM, Schwalke MA, Iliev IG, Rogers S. Electrical potential measurements in human breast cancer and benign lesions. Tumor Biology. 1994;

118. Stevenson D, Binggeli R, Weinstein RC, Keck JG, Lai MC, Tong MJ. Relationship between Cell Membrane Potential and Natural Killer Cell Cytolysis in Human Hepatocellular Carcinoma Cells. Cancer Res. 1989;

119. Chubinskiy-Nadezhdin VI, Sudarikova A V., Shilina MA, Vasileva VY, Grinchuk TM, Lyublinskaya OG, et al. Cell Cycle-Dependent Expression of Bk Channels in Human Mesenchymal Endometrial Stem Cells. Sci Rep. 2019;

120. Griffin M, Khan R, Basu S, Smith S. Ion Channels as Therapeutic Targets in High Grade Gliomas. Cancers (Basel). 2020 Oct 21;12(10):3068.

121. Hanahan D, Weinberg RA. The hallmarks of cancer. Cell. 2000.

122. Hanahan D, Weinberg RA. Hallmarks of cancer: The next generation. Cell. 2011.

123. Prevarskaya N, Skryma R, Shuba Y. Ion channels in cancer: Are cancer hallmarks oncochannelopathies? Physiological Reviews. 2018.

124. Pancrazio JJ, Viglione MP, Tabbara IA, Kim YI. Voltage-dependent Ion Channels in Small-Cell Lung Cancer Cells. Cancer Res. 1989;

125. Ogata E, Tsuruo T. Enhancement of Voltage-Gated Na+ Channel Current Associated with Multidrug Resistance in Human Leukemia Cells. Cancer Res. 1987;

126. Rao VR, Perez-Neut M, Kaja S, Gentile S. Voltage-gated ion channels in cancer cell proliferation. Cancers. 2015.

127. Humeau J, Bravo-San Pedro JM, Vitale I, Nuñez L, Villalobos C, Kroemer G, et al. Calcium signaling and cell cycle: Progression or death. Cell Calcium. 2018.

128. Payne SL, Levin M, Oudin MJ. Bioelectric Control of Metastasis in Solid Tumors. Bioelectricity. 2019;

129. Nilius B, Owsianik G, Voets T, Peters JA. Transient receptor potential cation channels in disease. Physiological Reviews. 2007.

130. Jagirdar R, Molyvdas PA, Gourgoulianis K, Hatzoglou C, Zarogiannis S. The role of amiloride sensitive epithelial sodium channel (ENaC) in cell migration of mesothelioma cells is dependent on the cell type and the extracellular matrix. In 2016.

131. He M, Liu S, Gallolu Kankanamalage S, Borromeo MD, Girard L, Gazdar AF, et al. The Epithelial Sodium Channel (αENaC) Is a Downstream Therapeutic Target of ASCL1 in Pulmonary Neuroendocrine Tumors. Transl Oncol. 2018;

132. Rooj AK, McNicholas CM, Bartoszewski R, Bebok Z, Benos DJ, Fuller CM. Glioma-specific cation conductance regulates migration and cell cycle progression. Journal of Biological Chemistry. 2012;

133. Bubien JK, Keeton DA, Fuller CM, Gillespie GY, Reddy AT, Mapstone TB, et al. Malignant human gliomas express an amiloride-sensitive Na+ conductance. Am J Physiol Cell Physiol. 1999;

134. B.K. B, J. X, L.A. M, J.M. M, G.Y. G, T.B. M, et al. Acid-sensing ion channels in malignant gliomas. Journal of Biological Chemistry. 2003;

135. Joshi AD, Parsons DW, Velculescu VE, Riggins GJ. Sodium ion channel mutations in glioblastoma patients correlate with shorter survival. Mol Cancer. 2011;

136. Pollak J, Rai KG, Funk CC, Arora S, Lee E, Zhu J, et al. Ion channel expression patterns in glioblastoma stem cells with functional and therapeutic implications for malignancy. PLoS One. 2017;

137. Serrano-Novillo C, Capera J, Colomer-Molera M, Condom E, Ferreres JC, Felipe A. Implication of voltage-gated potassium channels in neoplastic cell proliferation. Cancers. 2019.

138. Wang HY, Li JY, Liu X, Yan XY, Wang W, Wu F, et al. A three ion channel genes-based signature predicts prognosis of primary glioblastoma patients and reveals a chemotherapy sensitive subtype. Oncotarget. 2016;

139. Bertolesi GE, Shi C, Elbaum L, Jollimore C, Rozenberg G, Barnes S, et al. The Ca2+ channel antagonists mibefradil and pimozide inhibit cell growth via different cytotoxic mechanisms. Mol Pharmacol. 2002;

140. Olsen ML, Schade S, Lyons SA, Amaral MD, Sontheimer H. Expression of voltage-gated chloride channels in human glioma cells. Journal of Neuroscience. 2003;

141. Wang R, Gurguis CI, Gu W, Ko EA, Lim I, Bang H, et al. Ion channel gene expression predicts survival in glioma patients. Sci Rep. 2015;

142. Setti M, Savalli N, Osti D, Richichi C, Angelini M, Brescia P, et al. Functional role of CLIC1 ion channel in glioblastoma-derived stem/progenitor cells. J Natl Cancer Inst. 2013;

143. Habela CW, Olsen ML, Sontheimer H. ClC3 is a critical regulator of the cell cycle in normal and malignant glial cells. Journal of Neuroscience. 2008;

144. Hoffmann EK, Lambe IH. Ion channels and transporters in the development of drug resistance in cancer cells. Philosophical Transactions of the Royal Society B: Biological Sciences. 2014.

145. Bomben VC, Sontheimer H. Disruption of transient receptor potential canonical channel 1 causes incomplete cytokinesis and slows the growth of human malignant gliomas. Glia. 2010;

146. Bomben VC, Turner KL, Barclay TTC, Sontheimer H. Transient receptor potential canonical channels are essential for chemotactic migration of human malignant gliomas. J Cell Physiol. 2011;

147. Tajeddine N, Gailly P. TRPC1 protein channel is major regulator of epidermal growth factor receptor signaling. Journal of Biological Chemistry. 2012;

148. Bagal SK, Brown AD, Cox PJ, Omoto K, Owen RM, Pryde DC, et al. Ion channels as therapeutic targets: A drug discovery perspective. Journal of Medicinal Chemistry. 2013.

149. Kale VP, Amin SG, Pandey MK. Targeting ion channels for cancer therapy by repurposing the approved drugs. Biochimica et Biophysica Acta - Biomembranes. 2015.

150. Arvanitis CD, Ferraro GB, Jain RK. The blood–brain barrier and blood–tumour barrier in brain tumours and metastases. Nature Reviews Cancer. 2020.

151. Smith SJ, Rowlinson J, Estevez-Cebrero M, Onion D, Ritchie A, Clarke P, et al. Metabolism-based isolation of invasive glioblastoma cells with specific gene signatures and tumorigenic potential. Neurooncol Adv. 2020 Jan 1;2(1).

152. Branter J, Estevez-Cebrero M, Diksin M, Griffin M, Castellanos-Uribe M, May S, et al. Genome-Wide Expression and Anti-Proliferative Effects of Electric Field Therapy on Pediatric and Adult Brain Tumors. Int J Mol Sci. 2022 Feb 11;23(4):1982.

153. Wong ET, Lok E, Gautam S, Swanson KD. Dexamethasone exerts profound immunologic interference on treatment efficacy for recurrent glioblastoma. Br J Cancer. 2015 Jul 14;113(2):232–41.

154. Panyi G, Beeton C, Felipe A. Ion channels and anti-cancer immunity. Philosophical Transactions of the Royal Society B: Biological Sciences. 2014 Mar 19;369(1638):20130106.

155. Hutchings CJ, Colussi P, Clark TG. Ion channels as therapeutic antibody targets. MAbs. 2019 Feb 17;11(2):265–96.

156. Catacuzzeno L, Sforna L, Esposito V, Limatola C, Franciolini F. Ion Channels in Glioma Malignancy. In 2020. p. 223–67.

157. Takayasu T, Kurisu K, Esquenazi Y, Ballester LY. Ion Channels and Their Role in the Pathophysiology of Gliomas. Mol Cancer Ther. 2020 Oct 1;19(10):1959–69.

158. Guan X, Luo L, Begum G, Kohanbash G, Song Q, Rao A, et al. Elevated Na/H exchanger 1 (SLC9A1) emerges as a marker for tumorigenesis and prognosis in gliomas. Journal of Experimental & Clinical Cancer Research. 2018;

159. Brackenbury WJ. Voltage-gated sodium channels and metastatic disease. Channels. 2012.

160. Hemmerlein B, Weseloh RM, de Queiroz FM, Knötgen H, Sánchez A, Rubio ME, et al. Overexpression of Eag1 potassium channels in clinical tumours. Mol Cancer. 2006;

161. Kraft R, Krause P, Jung S, Basrai D, Liebmann L, Bolz J, et al. BK channel openers inhibit migration of human glioma cells. Pflugers Arch. 2003 May 15;446(2):248–55.

162. Xia Ding, Zhuohao He, Kechun Zhou, Ju Cheng, Hailan Yao, Dongliang Lu, Rong Cai, Yening Jin, Bin Dong, Yinghui Xu YW. Essential Role of TRPC6 Channels in G2/M Phase Transition and Development of Human Glioma. J Natl Cancer Inst. 2010;14(102):1052–68.

163. Paugh BS, Qu C, Jones C, Liu Z, Adamowicz-Brice M, Zhang J, et al. Integrated Molecular Genetic Profiling of Pediatric High-Grade Gliomas Reveals Key Differences With the Adult Disease. Journal of Clinical Oncology. 2010 Jun 20;28(18):3061–8.

164. Rigau V, Zouaoui S, Mathieu-Daudé H, Darlix A, Maran A, Trétarre B, et al. French Brain Tumor DataBase: 5-Year Histological Results on 25 756 Cases. Brain Pathology. 2011 Nov;21(6):633–44.

165. Kawaguchi A, Yajima N, Tsuchiya N, Homma J, Sano M, Natsumeda M, et al. Gene expression signature-based prognostic risk score in patients with glioblastoma. Cancer Sci. 2013 Sep;104(9):1205–10.

166. Berchtold NC, Cribbs DH, Coleman PD, Rogers J, Head E, Kim R, et al. Gene expression changes in the course of normal brain aging are sexually dimorphic. Proceedings of the National Academy of Sciences. 2008 Oct 7;105(40):15605–10.

167. Yu W, Cui R, Qu H, Liu C, Deng H, Zhang Z. Expression, and prognostic value of CLIC1 in epithelial ovarian cancer. Exp Ther Med. 2018 Mar 28;

168. Moriconi C, Civita P, Neto C, Pilkington GJ, Gumbleton M. Caveolin-1, a Key Mediator Across Multiple Pathways in Glioblastoma and an Independent Negative Biomarker of Patient Survival. Front Oncol. 2021 Aug 20;11.

169. Yu W, Cui R, Qu H, Liu C, Deng H, Zhang Z. Expression, and prognostic value of CLIC1 in epithelial ovarian cancer. Exp Ther Med. 2018 Mar 28;

170. Li B pei, Mao Y tian, Wang Z, Chen Y yang, Wang Y, Zhai C yu, et al. CLIC1 Promotes the Progression of Gastric Cancer by Regulating the MAPK/AKT Pathways. Cellular Physiology and Biochemistry. 2018;46(3):907–24.

171. Peng JM, Lin SH, Yu MC, Hsieh SY. CLIC1 recruits PIP5K1A/C to induce cell-matrix adhesions for tumor metastasis. Journal of Clinical Investigation. 2021 Jan 4;131(1).

172. Zhong J, Kong X, Zhang H, Yu C, Xu Y, Kang J, et al. Inhibition of CLIC4 Enhances Autophagy and Triggers Mitochondrial and ER Stress-Induced Apoptosis in Human Glioma U251 Cells under Starvation. PLoS One. 2012 Jun 25;7(6):e39378.

173. Hayashi Y, Edwards NA, Proescholdt MA, Oldfield EH, Merrill MJ. Regulation and Function of Aquaporin-1 in Glioma Cells. Neoplasia. 2007 Sep;9(9):777–87.

174. Simone L, Pisani F, Binda E, Frigeri A, Vescovi AL, Svelto M, et al. AQP4-dependent glioma cell features affect the phenotype of surrounding cells via extracellular vesicles. Cell Biosci. 2022 Sep 7;12(1):150.

175. Lan YL, Wang X, Lou JC, Ma XC, Zhang B. The potential roles of aquaporin 4 in malignant gliomas. Oncotarget. 2017 May 9;8(19):32345–55.

176. Verkman AS, Galietta LJ V. Chloride channels as drug targets. Nat Rev Drug Discov. 2009 Feb 19;8(2):153–71.

177. Cianci F, Verduci I. Transmembrane Chloride Intracellular Channel 1 (tmCLIC1) as a Potential Biomarker for Personalized Medicine. J Pers Med. 2021 Jul 5;11(7):635.

178. Tulk BM, Kapadia S, Edwards JC. CLIC1 inserts from the aqueous phase into phospholipid membranes, where it functions as an anion channel. American Journal of Physiology-Cell Physiology. 2002 May 1;282(5):C1103–12.

179. Gururaja Rao S, Patel NJ, Singh H. Intracellular Chloride Channels: Novel Biomarkers in Diseases. Front Physiol. 2020 Feb 14;11.

180. Gururaja Rao S, Ponnalagu D, Patel NJ, Singh H. Three Decades of Chloride Intracellular Channel Proteins: From Organelle to Organ Physiology. Curr Protoc Pharmacol. 2018 Mar;80(1):11.21.1-11.21.17.

181. Carrano A, Juarez JJ, Incontri D, Ibarra A, Guerrero Cazares H. Sex-Specific Differences in Glioblastoma. Cells. 2021 Jul 14;10(7):1783.

182. Do DT, Yang MR, Lam LHT, Le NQK, Wu YW. Improving MGMT methylation status prediction of glioblastoma through optimizing radiomics features using genetic algorithm-based machine learning approach. Sci Rep. 2022 Aug 4;12(1):13412.

183. Comba A, Faisal SM, Dunn PJ, Argento AE, Hollon TC, Al-Holou WN, et al. Spatiotemporal analysis of glioma heterogeneity reveals COL1A1 as an actionable target to disrupt tumor progression. Nat Commun. 2022 Jun 24;13(1):3606.

184. Dinevska M, Widodo SS, Furst L, Cuzcano L, Fang Y, Mangiola S, et al. Cell signaling activation and extracellular matrix remodeling underpin glioma tumor microenvironment heterogeneity and organization. Cellular Oncology. 2022 Dec 26;

185. Ozaki S, Mikami K, Kunieda T, Tanaka J. Chloride Intracellular Channel Proteins (CLICs) and Malignant Tumor Progression: A Focus on the Preventive Role of CLIC2 in Invasion and Metastasis. Cancers (Basel). 2022 Oct 6;14(19):4890.

186. Gao F, Wang Z, Gu J, Zhang X, Wang H. A Hypoxia-Associated Prognostic Gene Signature Risk Model and Prognosis Predictors in Gliomas. Front Oncol. 2021 Nov 12;11.

187. Smith SJ, Wilson M, Ward JH, Rahman C V., Peet AC, Macarthur DC, et al. Recapitulation of Tumor Heterogeneity and Molecular Signatures in a 3D Brain Cancer Model with Decreased Sensitivity to Histone Deacetylase Inhibition. PLoS One. 2012 Dec 18;7(12):e52335.

188. Kadry H, Noorani B, Cucullo L. A blood–brain barrier overview on structure, function, impairment, and biomarkers of integrity. Fluids Barriers CNS. 2020 Dec 18;17(1):69.

189. Venkatesh HS, Morishita W, Geraghty AC, Silverbush D, Gillespie SM, Arzt M, et al. Electrical and synaptic integration of glioma into neural circuits. Nature. 2019 Sep 26;573(7775):539–45.

190. Yang Y, Schubert MC, Kuner T, Wick W, Winkler F, Venkataramani V. Brain Tumor Networks in Diffuse Glioma. Neurotherapeutics. 2022 Oct 10;19(6):1832–43.

191. C. Jayakrishnan P, H. Venkat E, M. Ramachandran G, K. Kesavapisharady K, N. Nair S, Bharathan B, et al. *In vitro* neurosphere formation correlates with poor survival in glioma. IUBMB Life. 2019 Feb;71(2):244–53.

192. Corsaro A, Bajetto A, Thellung S, Begani G, Villa V, Nizzari M, et al. Cellular prion protein controls stem cell-like properties of human glioblastoma tumor-initiating cells. Oncotarget. 2016 Jun 21;7(25):38638–57.

193. Luzak B, Siarkiewicz P, Boncler M. An evaluation of a new high-sensitivity PrestoBlue assay for measuring cell viability and drug cytotoxicity using EA.hy926 endothelial cells. Toxicology *in Vitro*. 2022 Sep;83:105407.

194. Lee JR, Lee JY, Kim HJ, Hahn MJ, Kang JS, Cho H. The inhibition of chloride intracellular channel 1 enhances Ca2+ and reactive oxygen species signaling in A549 human lung cancer cells. Exp Mol Med. 2019 Jul 17;51(7):1–11.

195. Barbieri F, Würth R, Pattarozzi A, Verduci I, Mazzola C, Cattaneo MG, et al. Inhibition of chloride intracellular channel 1 (CLIC1) as biguanide class-effect to impair human glioblastoma stem cell viability. Front Pharmacol. 2018;

196. Peng JM, Lin SH, Yu MC, Hsieh SY. CLIC1 recruits PIP5K1A/C to induce cell-matrix adhesions for tumor metastasis. Journal of Clinical Investigation. 2021 Jan 4;131(1).

197. He L, Wondisford FE. Metformin Action: Concentrations Matter. Cell Metab. 2015 Feb;21(2):159–62.

198. Gritti M, Würth R, Angelini M, Barbieri F, Peretti M, Pizzi E, et al. Metformin repositioning as antitumoral agent: selective antiproliferative effects in human glioblastoma stem cells, via inhibition of CLIC1-mediated ion current. Oncotarget. 2014 Nov 30;5(22):11252–68.

199. Venkatesh HS, Morishita W, Geraghty AC, Silverbush D, Gillespie SM, Arzt M, et al. Electrical and synaptic integration of glioma into neural circuits. Nature. 2019;

200. Monje M, Borniger JC, D'Silva NJ, Deneen B, Dirks PB, Fattahi F, et al. Roadmap for the Emerging Field of Cancer Neuroscience. Cell. 2020;

201. Perlmutter JS, Mink JW. Deep brain stimulation. Annual Review of Neuroscience. 2006.

202. Ulmasov B, Bruno J, Woost PG, Edwards JC. Tissue and subcellular distribution of CLIC1. BMC Cell Biol. 2007 Dec 27;8(1):8.

203. Jiang L, Salao K, Li H, Rybicka JM, Yates RM, Luo XW, et al. Intracellular chloride channel protein CLIC1 regulates macrophage functions via modulation of phagosomal acidification. J Cell Sci. 2012 Jan 1;

204. Wolff C, Fuks B, Chatelain P. Comparative Study of Membrane Potential-Sensitive Fluorescent Probes, and their Use in Ion Channel Screening Assays. SLAS Discovery. 2003 Oct;8(5):533–43.

205. Jentsch TJ. VRACs and other ion channels and transporters in the regulation of cell volume and beyond. Nature Reviews Molecular Cell Biology. 2016.

206. Yang H, Zhang G, Cui J. BK channels: Multiple sensors, one activation gate. Frontiers in Physiology. 2015.

207. Bordey A, Sontheimer H, Trouslard J. Muscarinic Activation of BK Channels Induces Membrane Oscillations in Glioma Cells and Leads to Inhibition of Cell Migration. J Membr Biol. 2000 Jul;176(1):31–40.

208. McKhann GM, D'Ambrosio R, Janigro D. Heterogeneity of Astrocyte Resting Membrane Potentials, and Intercellular Coupling Revealed by Whole-Cell and Gramicidin-Perforated Patch Recordings from Cultured Neocortical and Hippocampal Slice Astrocytes. The Journal of Neuroscience. 1997 Sep 15;17(18):6850–63.

209. McNeill J, Rudyk C, Hildebrand ME, Salmaso N. Ion Channels and Electrophysiological Properties of Astrocytes: Implications for Emergent Stimulation Technologies. Front Cell Neurosci. 2021 May 20;15.

210. Kimelberg HK, Kettenmann H. Swelling-induced changes in electrophysiological properties of cultured astrocytes and oligodendrocytes. I. Effects on membrane

potentials, input impedance and cell-cell coupling. Brain Res. 1990 Oct;529(1–2):255–61.

211. Xu S, Luo C, Chen D, Tang L, Chen L, Liu Z. Whole transcriptome, and proteome analyses identify potential targets and mechanisms underlying tumor treating fields against glioblastoma. Cell Death Dis. 2022 Aug 18;13(8):721.

212. Lee J, Grabowski MM, Lathia JD. Tumor Treating Fields: killing two birds with one stone. Journal of Clinical Investigation. 2022 Apr 15;132(8).

213. Robins HI, Nguyen HN, Field A, Howard S, Salamat S, Deming DA. Molecular Evolution of a Glioblastoma Controlled With Tumor Treating Fields and Concomitant Temozolomide. Front Oncol. 2018 Oct 15;8.

214. Robinson MD, Oshlack A. A scaling normalization method for differential expression analysis of RNA-seq data. Genome Biol. 2010;11(3):R25.

215. Lu CH, Wei ST, Liu JJ, Chang YJ, Lin YF, Yu CS, et al. Recognition of a Novel Gene Signature for Human Glioblastoma. Int J Mol Sci. 2022 Apr 9;23(8):4157.

216. Lu W cheng, Xie H, Yuan C, Li J jiang, Li Z yang, Wu A hua. Identification of potential biomarkers and candidate small molecule drugs in glioblastoma. Cancer Cell Int. 2020 Dec 28;20(1):419.

217. Khan SU, Khan IM, Khan MU, Ud Din MA, Khan MZ, Khan NM, et al. Role of LGMN in tumor development and its progression and connection with the tumor microenvironment. Front Mol Biosci. 2023 Feb 7;10.

218. Khan I, Baeesa S, Bangash M, Schulten HJ, Alghamdi F, Qashqari H, et al. Pleomorphism and drug resistant cancer stem cells are characteristic of aggressive primary meningioma cell lines. Cancer Cell Int. 2017 Dec 21;17(1):72.

219. Zhong S, Wu B, Han Y, Cao Y, Yang L, Luo SX, et al. Identification of Driver Genes and Key Pathways of Pediatric Brain Tumors and Comparison of Molecular Pathogenesis Based on Pathologic Types. World Neurosurg. 2017 Nov;107:990–1000.

220. Sie M, Wagemakers M, Molema G, Mooij JJA, de Bont ESJM, den Dunnen WFA. The angiopoietin 1/angiopoietin 2 balance as a prognostic marker in primary glioblastoma multiforme. J Neurosurg. 2009 Jan;110(1):147–55.

221. Dumitru CA, Brouwer E, Stelzer T, Nocerino S, Rading S, Wilkens L, et al. Dynein Light Chain Protein Tctex1: A Novel Prognostic Marker and Molecular Mediator in Glioblastoma. Cancers (Basel). 2021 May 27;13(11):2624.

222. Gonçalves AB, Hasselbalch SK, Joensen BB, Patzke S, Martens P, Ohlsen SK, et al. CEP78 functions downstream of CEP350 to control biogenesis of primary cilia by negatively regulating CP110 levels. Elife. 2021 Jul 14;10.

223. Hervouet E, Peixoto P, Delage-Mourroux R, Boyer-Guittaut M, Cartron PF. Specific or not specific recruitment of DNMTs for DNA methylation, an epigenetic dilemma. Clin Epigenetics. 2018 Dec 9;10(1):17.

224. Schiöth HB, Roshanbin S, Hägglund MGA, Fredriksson R. Evolutionary origin of amino acid transporter families SLC32, SLC36 and SLC38 and physiological, pathological, and therapeutic aspects. Mol Aspects Med. 2013 Apr;34(2–3):571–85.

225. Li C, Wang T, Gu J, Qi S, Li J, Chen L, et al. SMARCC2 mediates the regulation of DKK1 by the transcription factor EGR1 through chromatin remodeling to reduce the proliferative capacity of glioblastoma. Cell Death Dis. 2022 Nov 23;13(11):990.

226. Jin X, Cheng H, Chen J, Zhu D. RNF13: an emerging RING finger ubiquitin ligase important in cell proliferation. FEBS Journal. 2011 Jan;278(1):78–84.

227. Leonzino M, Reinisch KM, De Camilli P. Insights into VPS13 properties and function reveal a new mechanism of eukaryotic lipid transport. Biochimica et Biophysica Acta (BBA) - Molecular and Cell Biology of Lipids. 2021 Oct;1866(10):159003.

228. Huo Y, Cao K, Kou B, Chai M, Dou S, Chen D, et al. TP53BP2: Roles in suppressing tumorigenesis and therapeutic opportunities. Genes Dis. 2022 Sep;

229. Yang K, Cheng H, Yuan F, Meng L, Yin R, Zhang Y, et al. CHRNE compound heterozygous mutations in congenital myasthenic syndrome. Medicine. 2018 Apr;97(17):e0347.

230. Li MJ, Yan SB, Chen G, Li GS, Yang Y, Wei T, et al. Upregulation of CCNB2 and Its Perspective Mechanisms in Cerebral Ischemic Stroke and All Subtypes of Lung Cancer: A Comprehensive Study. Front Integr Neurosci. 2022 Jul 19;16.

231. Im JY, Kim BK, Lee JY, Park SH, Ban HS, Jung KE, et al. DDIAS suppresses TRAIL-mediated apoptosis by inhibiting DISC formation and destabilizing caspase-8 in cancer cells. Oncogene. 2018 Mar 15;37(9):1251–62.

232. Kabir F, Apu MNH. Multi-omics analysis predicts fibronectin 1 as a prognostic biomarker in glioblastoma multiforme. Genomics. 2022 May;114(3):110378.

233. Shi W, Feng Z, Zhang J, Gonzalez-Suarez I, Vanderwaal RP, Wu X, et al. The role of RPA2 phosphorylation in homologous recombination in response to replication arrest. Carcinogenesis. 2010 Jun;31(6):994–1002.

234. Smith S, Diksin M, Chhaya S, Sairam S, Estevez-Cebrero M, Rahman R. The Invasive Region of Glioblastoma Defined by 5ALA Guided Surgery Has an Altered Cancer Stem Cell Marker Profile Compared to Central Tumour. Int J Mol Sci. 2017 Nov 18;18(11):2452.

235. Smith SJ, Rowlinson J, Estevez-Cebrero M, Onion D, Ritchie A, Clarke P, et al. Metabolism-based isolation of invasive glioblastoma cells with specific gene signatures and tumorigenic potential. Neurooncol Adv. 2020 Jan 1;2(1).

236. Cromer B, Morton C, Board P, Parker M. From glutathione transferase to pore in a CLIC. European Biophysics Journal. 2002 Aug 1;31(5):356–64.

237. Al Khamici H, Brown LJ, Hossain KR, Hudson AL, Sinclair-Burton AA, Ng JPM, et al. Members of the Chloride Intracellular Ion Channel Protein Family Demonstrate Glutaredoxin-Like Enzymatic Activity. PLoS One. 2015 Jan 12;10(1):e115699.

238. Olivier C, Oliver L, Lalier L, Vallette FM. Drug Resistance in Glioblastoma: The Two Faces of Oxidative Stress. Front Mol Biosci. 2021 Jan 27;7.

239. Sepuri NB V., Tammineni P, Mohammed F, Paripati A. Nuclear Transcription Factors in the Mitochondria: A New Paradigm in Fine-Tuning Mitochondrial Metabolism. In 2016. p. 3–20.

240. Ponnalagu D, Singh H. Anion Channels of Mitochondria. In 2016. p. 71–101.

241. Fanucchi S, Adamson RJ, Dirr HW. Formation of an Unfolding Intermediate State of Soluble Chloride Intracellular Channel Protein CLIC1 at Acidic pH. Biochemistry. 2008 Nov 4;47(44):11674–81.

242. Peretti M, Raciti FM, Carlini V, Verduci I, Sertic S, Barozzi S, et al. Mutual Influence of ROS, pH, and CLIC1 Membrane Protein in the Regulation of G1–S Phase Progression in Human Glioblastoma Stem Cells. Mol Cancer Ther. 2018 Nov 1;17(11):2451–61.

243. XU Y, KANG J, YUAN Z, LI H, SU J, LI Y, et al. Suppression of CLIC4/mtCLIC enhances hydrogen peroxide-induced apoptosis in C6 glioma cells. Oncol Rep. 2013 Apr;29(4):1483–91.

244. Zhong J, Kong X, Zhang H, Yu C, Xu Y, Kang J, et al. Inhibition of CLIC4 Enhances Autophagy and Triggers Mitochondrial and ER Stress-Induced Apoptosis in Human Glioma U251 Cells under Starvation. PLoS One. 2012 Jun 25;7(6):e39378.

245. Barbieri F, Bosio AG, Pattarozzi A, Tonelli M, Bajetto A, Verduci I, et al. Chloride intracellular channel 1 activity is not required for glioblastoma development but its inhibition dictates glioma stem cell responsivity to novel biguanide derivatives. Journal of Experimental & Clinical Cancer Research. 2022 Feb 8;41(1):53.

246. Færch O, Worth R, Achilonu I, Dirr H. Nuclear localisation sequences of chloride intracellular channels 1 and 4 facilitate nuclear import via interactions with import mediator importin-α: An empirical and theoretical perspective. Journal of Molecular Recognition. 2023 Feb 10;36(2).

247. Wang L, He S, TU Y, Ji P, Zong J, Zhang J, et al. Elevated expression of chloride intracellular channel 1 is correlated with poor prognosis in human gliomas. Journal of Experimental & Clinical Cancer Research. 2012 Dec 11;31(1):44.

248. Lu J, Dong Q, Zhang B, Wang X, Ye B, Zhang F, et al. Chloride intracellular channel 1 (CLIC1) is activated and functions as an oncogene in pancreatic cancer. Medical Oncology. 2015 Jun 26;32(6):171.

249. Smith S, Diksin M, Chhaya S, Sairam S, Estevez-Cebrero M, Rahman R. The Invasive Region of Glioblastoma Defined by 5ALA Guided Surgery Has an Altered Cancer Stem Cell Marker Profile Compared to Central Tumour. Int J Mol Sci. 2017 Nov 18;18(11):2452.

250. Romero-Garcia R, Mandal AS, Bethlehem RAI, Crespo-Facorro B, Hart MG, Suckling J. Transcriptomic and connectomic correlates of differential spatial patterning among gliomas. Brain. 2023 Mar 1;146(3):1200–11.

251. Andrieux Geoffroy, TDas, GMichaela, SStuart, CSajib. Spatial-transcriptomics reveals unique defining molecular features of 5-aminolevulinic acid+ infiltrative tumor cells associated with glioblastoma recurrence and poor survival.

252. Soroceanu L, Manning TJ, Sontheimer H. Modulation of glioma cell migration and invasion using Cl- and K+ ion channel blockers. Journal of Neuroscience. 1999;

253. Dahlberg D, Rummel J, Distante S, De Souza GA, Stensland ME, Mariussen E, et al. Glioblastoma microenvironment contains multiple hormonal and non-hormonal growth-stimulating factors. Fluids Barriers CNS. 2022 Dec 4;19(1):45.

254. Wang P. Chloride intracellular channel 1 regulates colon cancer cell migration and invasion through ROS/ERK pathway. World J Gastroenterol. 2014;20(8):2071.

255. Chen J, Zhang M, Ma Z, Yuan D, Zhu J, Tuo B, et al. Alteration and dysfunction of ion channels/transporters in a hypoxic microenvironment results in the development and progression of gastric cancer. Cellular Oncology. 2021 Aug 15;44(4):739–49.

256. Lee JR, Lee JY, Kim HJ, Hahn MJ, Kang JS, Cho H. The inhibition of chloride intracellular channel 1 enhances Ca2+ and reactive oxygen species signaling in A549 human lung cancer cells. Exp Mol Med. 2019 Jul 17;51(7):1–11.

257. Saberbaghi T, Wong R, Rutka JT, Wang GL, Feng ZP, Sun HS. Role of Cl− channels in primary brain tumour. Cell Calcium. 2019 Jul;81:1–11.

258. Averaimo S, Milton RH, Duchen MR, Mazzanti M. Chloride intracellular channel 1 (CLIC1): Sensor and effector during oxidative stress. FEBS Lett. 2010 May 17;584(10):2076–84.

259. Tamai S, Ichinose T, Tsutsui T, Tanaka S, Garaeva F, Sabit H, et al. Tumor Microenvironment in Glioma Invasion. Brain Sci. 2022 Apr 15;12(4):505.

260. C. Jayakrishnan P, H. Venkat E, M. Ramachandran G, K. Kesavapisharady K, N. Nair S, Bharathan B, et al. *In vitro* neurosphere formation correlates with poor survival in glioma. IUBMB Life. 2019 Feb;71(2):244–53.

261. Josupeit R, Bender S, Kern S, Leuchs B, Hielscher T, Herold-Mende C, et al. Pediatric and Adult High-Grade Glioma Stem Cell Culture Models Are Permissive to Lytic Infection with Parvovirus H-1. Viruses. 2016 May 19;8(5):138.

262. Gaspar N, Marshall L, Perryman L, Bax DA, Little SE, Viana-Pereira M, et al. MGMT-Independent Temozolomide Resistance in Pediatric Glioblastoma Cells Associated with a PI3-Kinase–Mediated *HOX* /Stem Cell Gene Signature. Cancer Res. 2010 Nov 15;70(22):9243–52.

263. Nguyen A, Moussallieh FM, Mackay A, Cicek AE, Coca A, Chenard MP, et al. Characterization of the transcriptional and metabolic responses of pediatric high grade gliomas to mTOR-HIF-1α axis inhibition. Oncotarget. 2017 Sep 22;8(42):71597–617.

264. Rahman M, Reyner K, Deleyrolle L, Millette S, Azari H, Day BW, et al. Neurosphere and adherent culture conditions are equivalent for malignant glioma stem cell lines. Anat Cell Biol. 2015;48(1):25.

265. Barbieri F, Bosio AG, Pattarozzi A, Tonelli M, Bajetto A, Verduci I, et al. Chloride intracellular channel 1 activity is not required for glioblastoma development but its inhibition dictates glioma stem cell responsivity to novel biguanide derivatives. Journal of Experimental & Clinical Cancer Research. 2022 Feb 8;41(1):53.

266. Thuringer D, Chanteloup G, Winckler P, Garrido C. The vesicular transfer of CLIC1 from glioblastoma to microvascular endothelial cells requires TRPM7. Oncotarget. 2018 Sep 7;9(70):33302–11.

267. Averaimo S, Abeti R, Savalli N, Brown LJ, Curmi PMG, Breit SN, et al. Point Mutations in the Transmembrane Region of the Clic1 Ion Channel Selectively Modify Its Biophysical Properties. PLoS One. 2013 Sep 18;8(9):e74523.

268. Ponnalagu D, Hussain AT, Thanawala R, Meka J, Bednarczyk P, Feng Y, et al. Chloride channel blocker IAA-94 increases myocardial infarction by reducing calcium retention capacity of the cardiac mitochondria. Life Sci. 2019 Oct;235:116841.

269. Yang SH, Li S, Lu G, Xue H, Kim DH, Zhu JJ, et al. Metformin treatment reduces temozolomide resistance of glioblastoma cells. Oncotarget. 2016;

270. Würth R, Pattarozzi A, Gatti M, Bajetto A, Corsaro A, Parodi A, et al. Metformin selectively affects human glioblastoma tumor-initiating cell viability. Cell Cycle. 2013 Jan 1;12(1):145–56.

271. Sesen J, Dahan P, Scotland SJ, Saland E, Dang VT, Lemarié A, et al. Metformin inhibits growth of human glioblastoma cells and enhances therapeutic response. PLoS One. 2015;

272. Griffin M, Smith S, Basu S, Khan R. HGG-28. CLIC1 and CLIC4 ion channel deficiency confers increased sensitivity to tumour treating fields and improved survival in paediatric glioblastoma. Neuro Oncol. 2022 Jun 3;24(Supplement_1):i66–7.

273. Choi J, Lee JH, Koh I, Shim JK, Park J, Jeon JY, et al. Inhibiting stemness and invasive properties of glioblastoma tumorsphere by combined treatment with temozolomide and a newly designed biguanide (HL156A). Oncotarget. 2016 Oct 4;7(40):65643–59.

274. Francisco MA, Wanggou S, Fan JJ, Dong W, Chen X, Momin A, et al. Chloride intracellular channel 1 cooperates with potassium channel EAG2 to promote medulloblastoma growth. Journal of Experimental Medicine. 2020 May 4;217(5).

275. Molenaar RJ, Coelen RJ, Khurshed M, Roos E, Caan MW, van Linde ME, et al. Study protocol of a phase IB/II clinical trial of metformin and chloroquine in patients with *IDH1* -mutated or *IDH2* -mutated solid tumours. BMJ Open. 2017 Jun 10;7(6):e014961.

276. Adeberg S, Bernhardt D, Harrabi S Ben, Bostel T, Mohr A, Koelsche C, et al. Metformin influences progression in diabetic glioblastoma patients. Strahlentherapie und Onkologie. 2015 Dec 2;191(12):928–35.

277. Seliger C, Genbrugge E, Gorlia T, Chinot O, Stupp R, Nabors B, et al. Use of metformin and outcome of patients with newly diagnosed glioblastoma: Pooled analysis. Int J Cancer. 2020 Feb 29;146(3):803–9.

278. Chiang PC, Chou RH, Chien HF, Tsai T, Chen CT. Chloride intracellular channel 4 involves in the reduced invasiveness of cancer cells treated by photodynamic therapy. Lasers Surg Med. 2013 Jan;45(1):38–47.

279. Leng TD, Li MH, Shen JF, Liu ML, Li XB, Sun HW, et al. Suppression of TRPM7 Inhibits Proliferation, Migration, and Invasion of Malignant Human Glioma Cells. CNS Neurosci Ther. 2015;

280. Britschgi A, Bill A, Brinkhaus H, Rothwell C, Clay I, Duss S, et al. Calcium-activated chloride channel ANO1 promotes breast cancer progression by activating EGFR and CAMK signaling. Proc Natl Acad Sci U S A. 2013;

281. Lee JR, Lee JY, Kim HJ, Hahn MJ, Kang JS, Cho H. The inhibition of chloride intracellular channel 1 enhances Ca2+ and reactive oxygen species signaling in A549 human lung cancer cells. Exp Mol Med. 2019 Jul 17;51(7):1–11.

282. Würth R, Barbieri F, Florio T. New Molecules and Old Drugs as Emerging Approaches to Selectively Target Human Glioblastoma Cancer Stem Cells. Biomed Res Int. 2014;2014:1–11.

283. Sheppard KE, McArthur GA. The Cell-Cycle Regulator CDK4: An Emerging Therapeutic Target in Melanoma. Clinical Cancer Research. 2013 Oct 1;19(19):5320–8.

284. Yang W, Tan Z, Dong D, Ding Y, Meng H, Zhao Y, et al. Association of aquaporin-1 with tumor migration, invasion and vasculogenic mimicry in glioblastoma multiforme. Mol Med Rep. 2017 Dec 12;

285. Neuhaus E, Zirjacks L, Ganser K, Klumpp L, Schüler U, Zips D, et al. Alternating Electric Fields (TTFields) Activate Cav1.2 Channels in Human Glioblastoma Cells. Cancers (Basel). 2019 Jan 18;11(1):110.

286. Berkelmann L, Bader A, Meshksar S, Dierks A, Majernik GH, Krauss JK, et al. Tumour-treating fields (TTFields): Investigations on the mechanism of action by electromagnetic exposure of cells in telophase/cytokinesis. Sci Rep. 2019;9(7362).

287. Shi P, Tian J, Ulm BS, Mallinger JC, Khoshbouei H, Deleyrolle LP, et al. Tumor Treating Fields Suppression of Ciliogenesis Enhances Temozolomide Toxicity. Front Oncol. 2022 Mar 11;12.

288. Stupp R, Taillibert S, Kanner A, Read W, Steinberg DM, Lhermitte B, et al. Effect of Tumor-Treating Fields Plus Maintenance Temozolomide vs Maintenance Temozolomide Alone on Survival in Patients With Glioblastoma. JAMA. 2017 Dec 19;318(23):2306.

289. Bokstein F, Blumenthal D, Limon D, Harosh C Ben, Ram Z, Grossman R. Concurrent Tumor Treating Fields (TTFields) and Radiation Therapy for Newly Diagnosed

Glioblastoma: A Prospective Safety and Feasibility Study. Front Oncol. 2020 Apr 21;10.

290. Friedman HS, Prados MD, Wen PY, Mikkelsen T, Schiff D, Abrey LE, et al. Bevacizumab Alone and in Combination With Irinotecan in Recurrent Glioblastoma. Journal of Clinical Oncology. 2009 Oct 1;27(28):4733–40.

291. Kessler AF, Frömbling GE, Gross F, Hahn M, Dzokou W, Ernestus RI, et al. Effects of tumor treating fields (TTFields) on glioblastoma cells are augmented by mitotic checkpoint inhibition. Cell Death Discov. 2018 Jul 16;4(1):77.

292. Wang M, Zhang C, Wang X, Yu H, Zhang H, Xu J, et al. Tumor-treating fields (TTFields)-based cocktail therapy: a novel blueprint for glioblastoma treatment. Am J Cancer Res. 2021;11(4):1069–86.

293. Guo X, Yang X, Wu J, Yang H, Li Y, Li J, et al. Tumor-Treating Fields in Glioblastomas: Past, Present, and Future. Cancers (Basel). 2022 Jul 28;14(15):3669.

294. Vatter T, Klumpp L, Ganser K, Stransky N, Zips D, Eckert F, et al. Against Repurposing Methadone for Glioblastoma Therapy. Biomolecules. 2020 Jun 17;10(6):917.

295. Neuhaus E, Zirjacks L, Ganser K, Klumpp L, Schüler U, Zips D, et al. Alternating Electric Fields (TTFields) Activate Cav1.2 Channels in Human Glioblastoma Cells. Cancers (Basel). 2019 Jan 18;11(1):110.

296. Geng H, Feng C, Sun Z, Fan X, Xie Y, Gu J, et al. Chloride intracellular channel 1 promotes esophageal squamous cell carcinoma proliferation via mTOR signalling. Transl Oncol. 2023 Jan;27:101560.

297. Barbieri F, Verduci I, Carlini V, Zona G, Pagano A, Mazzanti M, et al. Repurposed biguanide drugs in glioblastoma exert antiproliferative effects via the inhibition of intracellular chloride channel 1 activity. Frontiers in Oncology. 2019.

298. Lee YJ, Seo HW, Baek JH, Lim SH, Hwang SG, Kim EH. Gene expression profiling of glioblastoma cell lines depending on TP53 status after tumor-treating fields (TTFields) treatment. Sci Rep. 2020 Jul 23;10(1):12272.

299. Georgescu MM, Olar A. Genetic and histologic spatiotemporal evolution of recurrent, multifocal, multicentric and metastatic glioblastoma. Acta Neuropathol Commun. 2020 Dec 3;8(1):10.

300. Wang J, Cazzato E, Ladewig E, Frattini V, Rosenbloom DIS, Zairis S, et al. Clonal evolution of glioblastoma under therapy. Nat Genet. 2016 Jul 6;48(7):768–76.

301. Johnson BE, Mazor T, Hong C, Barnes M, Aihara K, McLean CY, et al. Mutational Analysis Reveals the Origin and Therapy-Driven Evolution of Recurrent Glioma. Science (1979). 2014 Jan 10;343(6167):189–93.

302. Leslie FM, Mojica CY, Reynaga DD. Nicotinic Receptors in Addiction Pathways. Mol Pharmacol. 2013 Apr;83(4):753–8.

303. Huang J, DeWees T, Campian JL, Chheda MG, Ansstas G, Tsien C, et al. A TITE-CRM phase I/II study of disulfiram and copper with concurrent radiation therapy and temozolomide for newly diagnosed glioblastoma. Journal of Clinical Oncology. 2019 May 20;37(15_suppl):2033–2033.

304. Huang R, Zhou PK. DNA damage repair: historical perspectives, mechanistic pathways, and clinical translation for targeted cancer therapy. Signal Transduct Target Ther. 2021 Jul 9;6(1):254.

305. Alhmoud JF, Woolley JF, Al Moustafa AE, Malki MI. DNA Damage/Repair Management in Cancers. Cancers (Basel). 2020 Apr 23;12(4):1050.

306. Hakem R. DNA-damage repair; the good, the bad, and the ugly. EMBO J. 2008 Feb 20;27(4):589–605.

307. Bonm A, Kesari S. DNA Damage Response in Glioblastoma. The Cancer Journal. 2021 Sep;27(5):379–85.

308. Ferri A, Stagni V, Barilà D. Targeting the DNA Damage Response to Overcome Cancer Drug Resistance in Glioblastoma. Int J Mol Sci. 2020 Jul 11;21(14):4910.

309. Morás AM, Henn JG, Steffens Reinhardt L, Lenz G, Moura DJ. Recent developments in drug delivery strategies for targeting DNA damage response in glioblastoma. Life Sci. 2021 Dec;287:120128.

310. Wu S, Li X, Gao F, de Groot JF, Koul D, Yung WKA. PARP-mediated PARylation of MGMT is critical to promote repair of temozolomide-induced O6-methylguanine DNA damage in glioblastoma. Neuro Oncol. 2021 Jun 1;23(6):920–31.

311. Montaldi A, Lima S, Godoy P, Xavier D, Sakamoto-Hojo E. PARP-1 inhibition sensitizes temozolomide-treated glioblastoma cell lines and decreases drug resistance independent of MGMT activity and PTEN proficiency. Oncol Rep. 2020 Sep 7;

312. Jannetti SA, Zeglis BM, Zalutsky MR, Reiner T. Poly(ADP-Ribose)Polymerase (PARP) Inhibitors and Radiation Therapy. Front Pharmacol. 2020 Mar 3;11.

313. Gobin M, Nazarov P V., Warta R, Timmer M, Reifenberger G, Felsberg J, et al. A DNA Repair and Cell-Cycle Gene Expression Signature in Primary and Recurrent Glioblastoma: Prognostic Value and Clinical Implications. Cancer Res. 2019 Mar 15;79(6):1226–38.

314. Everix L, Nair S, Driver CHS, Goethals I, Sathekge MM, Ebenhan T, et al. Perspective on the Use of DNA Repair Inhibitors as a Tool for Imaging and Radionuclide Therapy of Glioblastoma. Cancers (Basel). 2022 Apr 3;14(7):1821.

315. Aldape K, Amin SB, Ashley DM, Barnholtz-Sloan JS, Bates AJ, Beroukhim R, et al. Glioma through the looking GLASS: molecular evolution of diffuse gliomas and the Glioma Longitudinal Analysis Consortium. Neuro Oncol. 2018 Jun 18;20(7):873–84.

316. Ceccaldi R, Sarangi P, D'Andrea AD. The Fanconi anaemia pathway: new players and new functions. Nat Rev Mol Cell Biol. 2016 Jun 5;17(6):337–49.

317. Rominiyi O, Collis SJ. DDRugging glioblastoma: understanding and targeting the DNA damage response to improve future therapies. Mol Oncol. 2022 Jan 11;16(1):11–41.

318. Kim H, D'Andrea AD. Regulation of DNA cross-link repair by the Fanconi anemia/BRCA pathway. Genes Dev. 2012 Jul 1;26(13):1393–408.

319. Stecklein SR, Jensen RA. Identifying and exploiting defects in the Fanconi anemia/BRCA pathway in oncology. Translational Research. 2012 Sep;160(3):178–97.

320. Jeong H, Sung J, Oh S ick, Jeong S, Koh EK, Hong S, et al. Inhibition of brain tumor cell proliferation by alternating electric fields. Appl Phys Lett. 2014 Nov 17;105(20):203703.

321. Mumblat H, Martinez-Conde A, Braten O, Munster M, Dor-On E, Schneiderman RS, et al. Tumor Treating Fields (TTFields) downregulate the Fanconi Anemia-BRCA pathway and increase the efficacy of chemotherapy in malignant pleural mesothelioma preclinical models. Lung Cancer. 2021 Oct;160:99–110.

322. Savaskan N, Fan Z, Broggini T, Buchfelder M, Eyupoglu I. Neurodegeneration in the Brain Tumor Microenvironment: Glutamate in the Limelight. Curr Neuropharmacol. 2015 May 25;13(2):258–65.

323. Hombach-Klonisch S, Mehrpour M, Shojaei S, Harlos C, Pitz M, Hamai A, et al. Glioblastoma and chemoresistance to alkylating agents: Involvement of apoptosis, autophagy, and unfolded protein response. Pharmacol Ther. 2018 Apr;184:13–41.

324. Kim M, Ladomersky E, Mozny A, Kocherginsky M, O'Shea K, Reinstein ZZ, et al. Glioblastoma as an age-related neurological disorder in adults. Neurooncol Adv. 2021 Jan 1;3(1).

325. Savaskan N, Fan Z, Broggini T, Buchfelder M, Eyupoglu I. Neurodegeneration in the Brain Tumor Microenvironment: Glutamate in the Limelight. Curr Neuropharmacol. 2015 May 25;13(2):258–65.

326. Portela M, Venkataramani V, Fahey-Lozano N, Seco E, Losada-Perez M, Winkler F, et al. Glioblastoma cells vampirize WNT from neurons and trigger a JNK/MMP signaling loop that enhances glioblastoma progression and neurodegeneration. PLoS Biol. 2019 Dec 17;17(12):e3000545.

327. Jarabo P, de Pablo C, Herranz H, Martín FA, Casas-Tintó S. Insulin signaling mediates neurodegeneration in glioma. Life Sci Alliance. 2021 Mar 1;4(3):e202000693.

328. Schroeder AB, Pointer KB, Clark PA, Datta R, Kuo JS, Eliceiri KW. Metabolic mapping of glioblastoma stem cells reveals NADH fluxes associated with glioblastoma phenotype and survival. J Biomed Opt. 2020 Mar 25;25(03):1.

329. Gao X, Yang Y, Wang J, Zhang L, Sun C, Wang Y, et al. Inhibition of mitochondria NADH–Ubiquinone oxidoreductase (complex I) sensitizes the radioresistant glioma U87MG cells to radiation. Biomedicine & Pharmacotherapy. 2020 Sep;129:110460.

330. Li L, Xing R, Cui J, Li W, Lu Y. Investigation of frequent somatic mutations of MTND5 gene in gastric cancer cell lines and tissues. Mitochondrial DNA Part B. 2018 Jul 3;3(2):1002–8.

10 Appendix

10.1 A1 – Growth curves

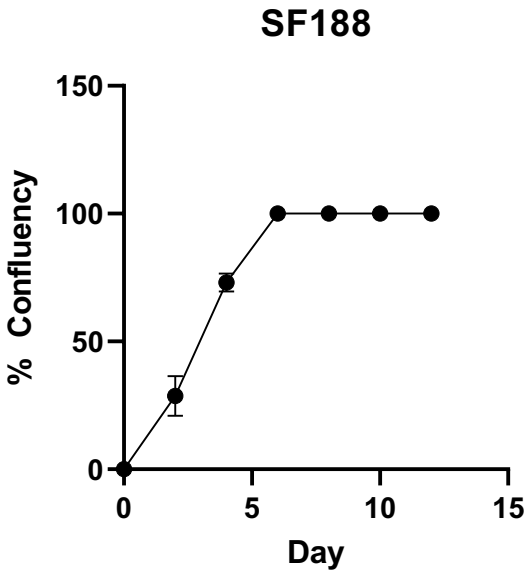

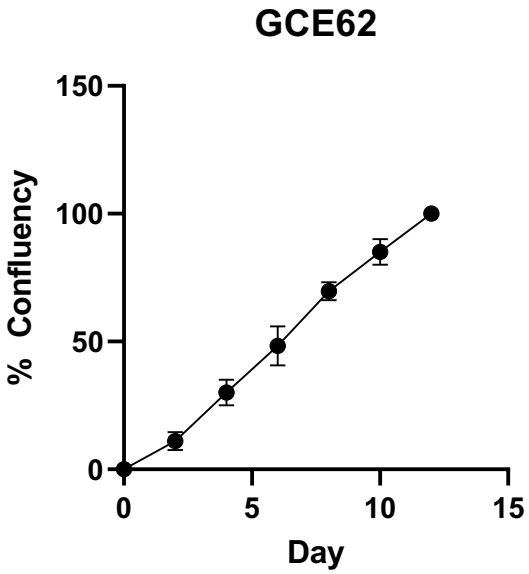

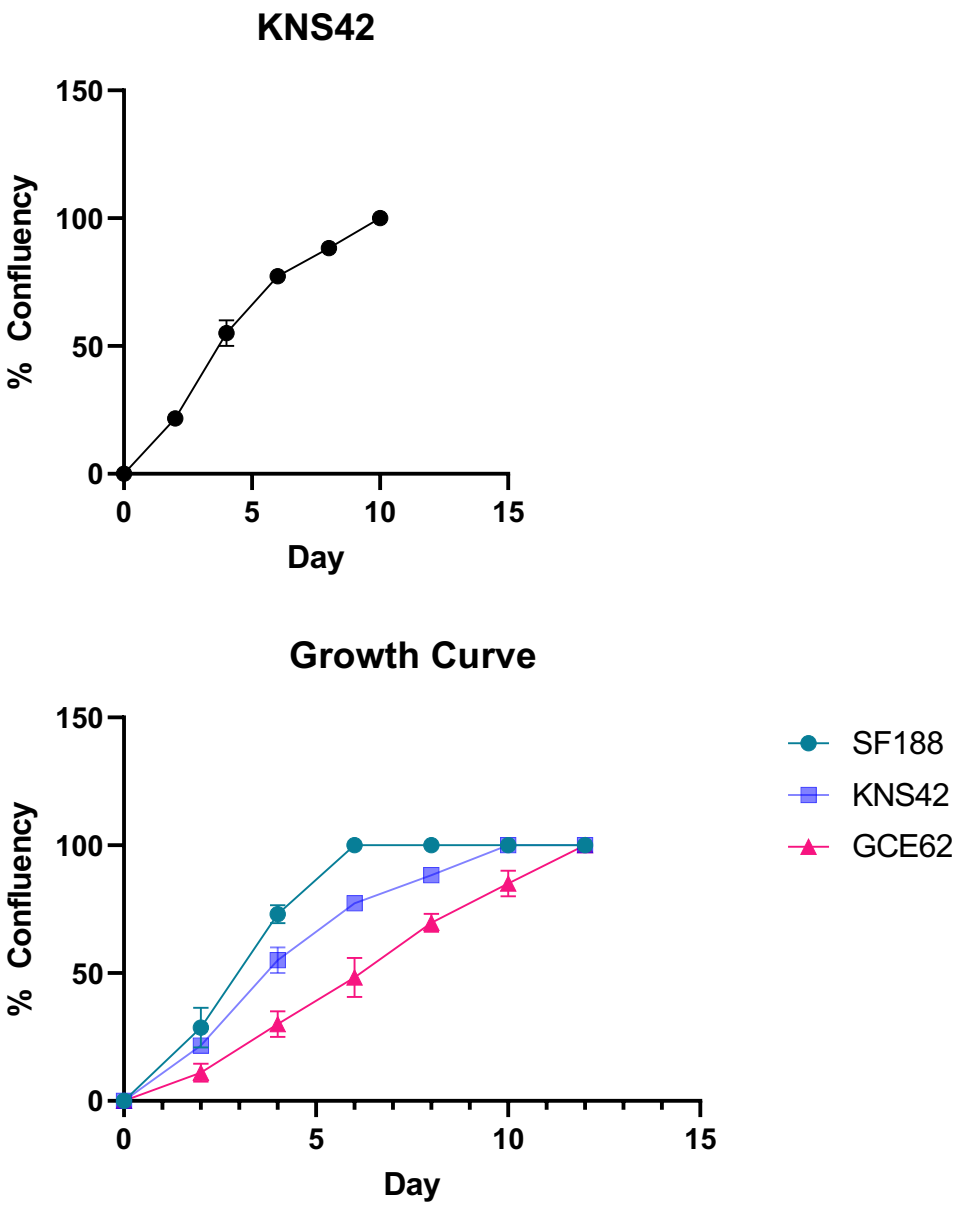

Figure 10.1 Growth curves for SF188, KNS42 and GCE62 cells. Cell growth curves give the % of confluency (surface of plate covered) measured across three flasks at three independent time points as a function of time in days.

10.2 A2- IHC controls

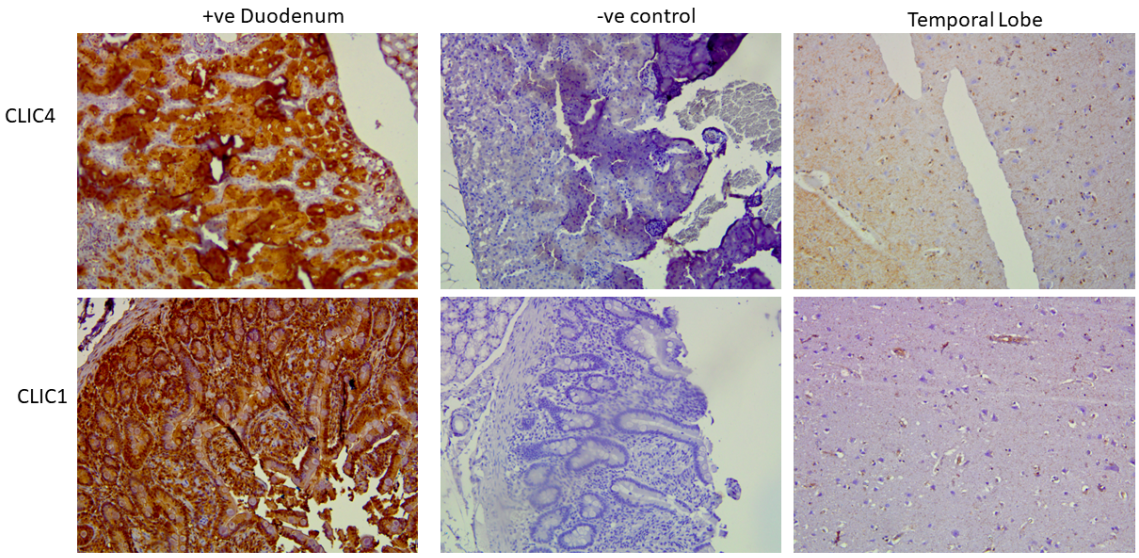

Figure 10.2 Control tissue used for IHC staining. Duodenum was used as appositive control for both CLIC1 and CLIC4 staining. Representative images shown include a -ve antibody control where tissues sections were incubated without antibody, and a temporal lobe normal brain control. 20x magnification.

10.3 A3- Clonogenic optimisation

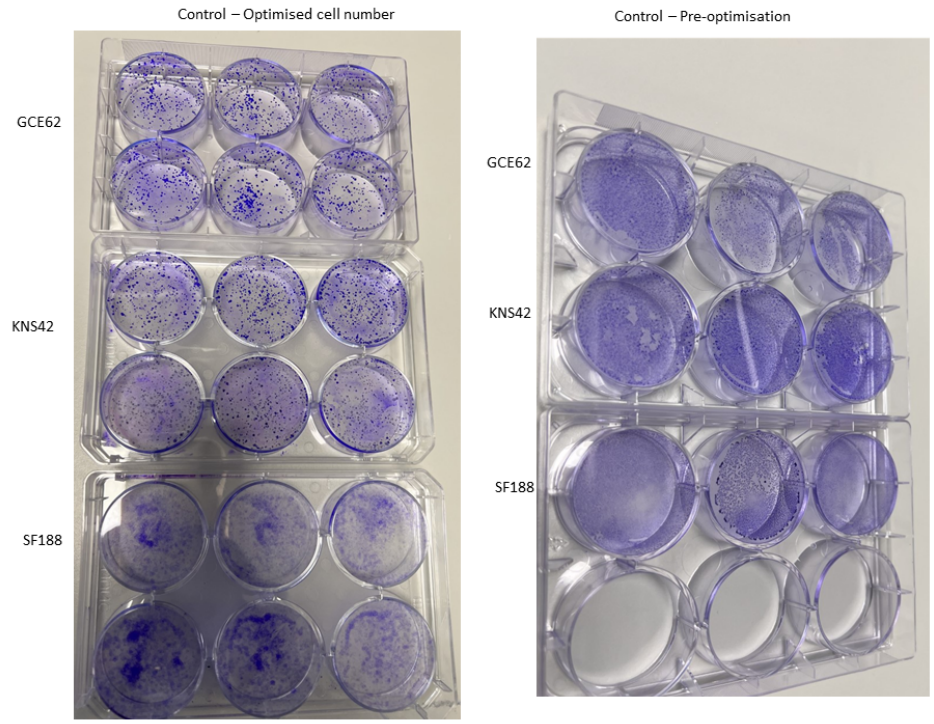

Figure 10.3 Representative images of colony forming units pre and post optimisation.

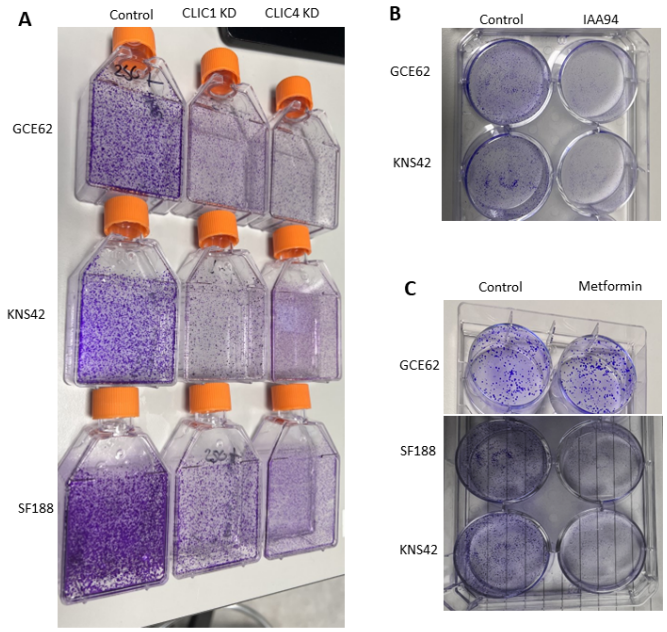

Figure 10.4 Representative images of colony formation following CLIC inhibition. A) Representative whole images of CLIC1 and CLIC4 knock down clonogenic. B) representative image of IAA94 treatment of KNS42 and GCE62 cells. C) Colony forming units following metformin treatment.

10.4 A4 – Invasion assay optimisation

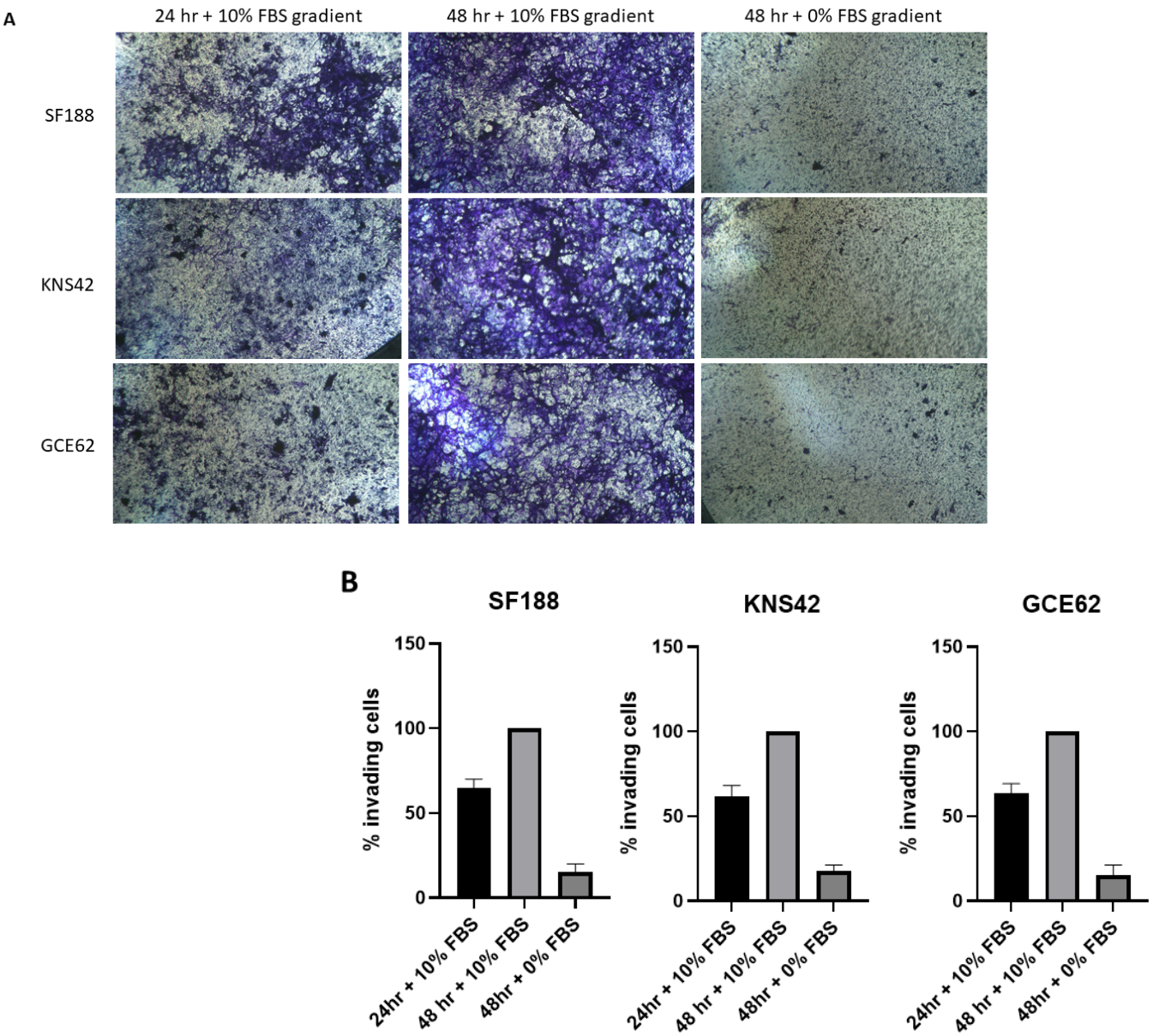

Figure 10.5 Optimisation of invasion assay. Example optimisation figure of SF188, KNS42 and GCE62 cells. Cell seeding density was pre-determined via assessment of growth curves and previous work in the group. Invasion was optimised across a 10% FBS gradient. A 24hour invasion period was selected as the data gained at the 48 hours' time point was uninterpretable due to too many cells invading.

10.5 A6 - RNA sequencing

10.5.1 A6.1 Quality control

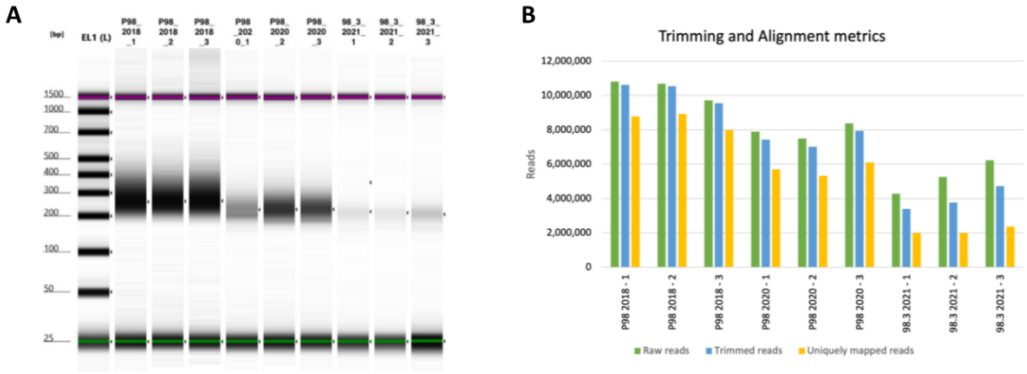

Figure 10.6 A) Electronic gel image generated by Agilent 4200 TapeStation showing the RNA profile of each sample. **B).** Bar chart comparing number of reads filtered and aligned uniquely to reference genome for each sample.

Table 10.1 Input reads for library prep.

Parameter	MIN	MEDIAN	MAX
Number of input reads [Million]	3.39 98.3_2021_1	7.43	10.63 P98_2018_1
Number of uniquely mapped reads [Million]	2.00 98.3_2021_1	5.70	8.93 P98_2018_2

Table 10.2 Basic statistics for alignment reads. The STAR aligner (Spliced Transcripts Alignment to a Reference) is Lexogens aligner of choice for aligning reads which were generated in a Corall experiment.

Sample	Number of input reads	Uniquely mapped reads number	Uniquely mapped reads %	Average input read length
98.3_2021_1	3393817	2000566	58.95	55
98.3_2021_2	3775613	2003979	53.08	52
98.3_2021_3	4722328	2371650	50.22	51
P98_2018_1	10628080	8780668	82.62	69
P98_2018_2	10548371	8930057	84.66	69
P98_2018_3	9542186	7994843	83.78	69
P98_2020_1	7426595	5699591	76.75	62
P98_2020_2	7012600	5329573	76.00	62
P98_2020_3	7948217	6101800	76.77	63

Table 10.3 Summary of the FASTQC numerical results for all sample reads.

Sample Read	Duplicates %	GC Content %	Average Sequence Length	Total Sequences	Fails %
98.3_2021_1_R1	71.67	38.0	76.00	4293790	18.18
98.3_2021_2_R1	65.64	41.0	76.00	5270924	18.18
98.3_2021_3_R1	66.79	38.0	76.00	6228026	18.18
P98_2018_1_R1	38.83	41.0	76.00	10804348	9.09
P98_2018_2_R1	30.73	41.0	76.00	10682816	9.09
P98_2018_3_R1	29.94	41.0	76.00	9717756	9.09
P98_2020_1_R1	74.06	37.0	76.00	7900493	18.18
P98_2020_2_R1	62.44	36.0	76.00	7494811	18.18
P98_2020_3_R1	64.29	37.0	76.00	8377157	18.18

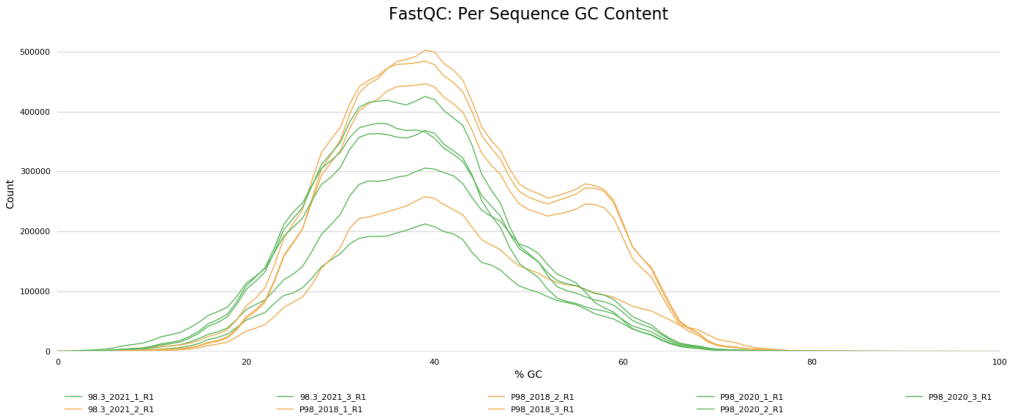

Figure 10.7 Per-sequence GC content plot (counts)

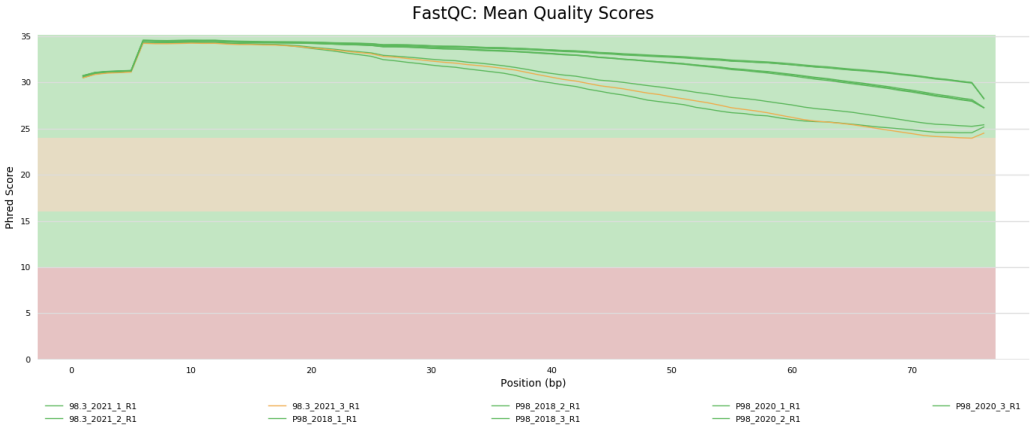

Figure 10.8 Per base sequence quality plot.

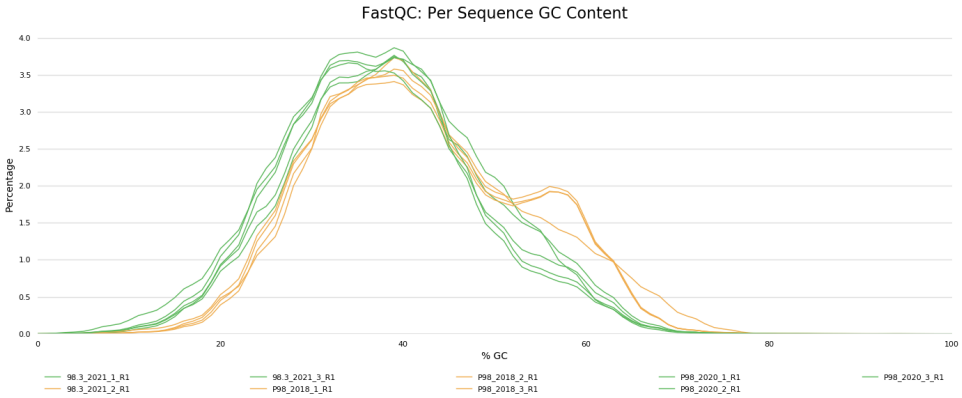

Figure 10.9 Per-sequence GC content plot (percentages)

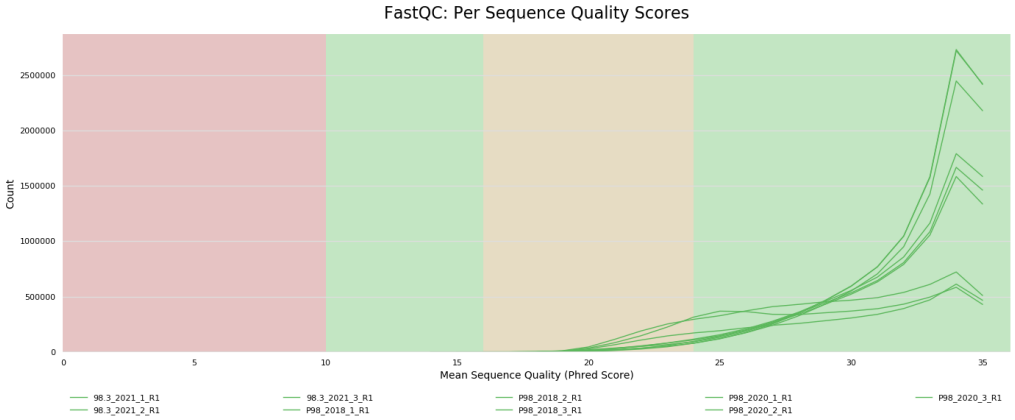

Figure 10.10 Per-sequence Quality scores plot

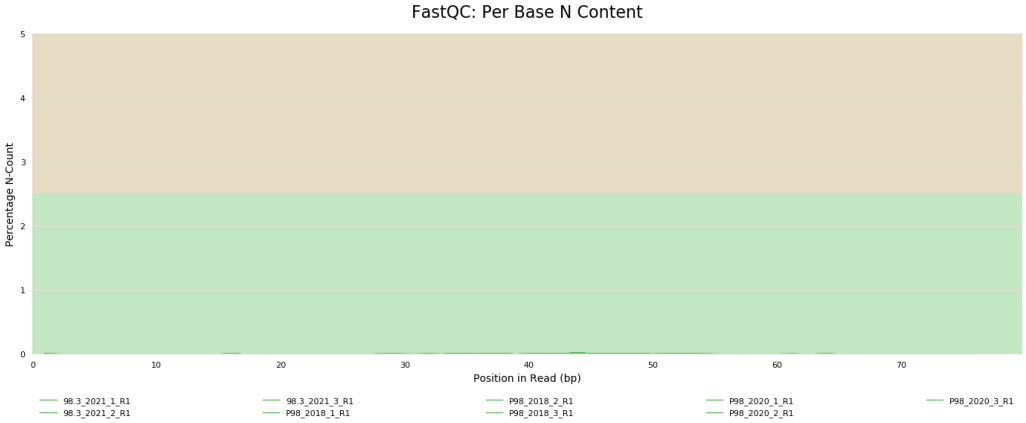

Figure 10.11 Per-base N content plot

10.5.2 A6.2 Differential gene expression analysis summary

Table 10.4 Summary of differential gene analysis performed.

Gene **Expression**	Gene **Count**	**% of Total**	**Comment**
Total	29124	100.00	nonzero total read count
LFC > 0 (up)	723	2.48	adjusted p-value < 0.10
LFC < 0 (down)	740	2.54	adjusted p-value < 0.10
Outliers	2072	7.11	
Low counts	10092	34.65	mean count < 1

Table 10.5 Contrast of 2018 vs 2021. DESeq2 provides a summary of the results of the differential expression analysis for all genes and all samples

Gene **Expression**	Gene **Count**	**% of Total**	**Comment**
Total	29124	100.00	nonzero total read count
LFC > 0 (up)	7678	26.36	adjusted p-value < 0.10
LFC < 0 (down)	1005	3.45	adjusted p-value < 0.10
Outliers	2072	7.11	
Low counts	11155	38.30	mean count < 1

Table 10.6 Contrast of 2020 vs 2021. DESeq2 provides a summary of the results of the differential expression analysis for all genes and all samples

Gene **Expression**	Gene **Count**	**% of Total**	**Comment**
Total	29124	100.00	nonzero total read count
LFC > 0 (up)	7155	24.57	adjusted p-value < 0.10
LFC < 0 (down)	713	2.45	adjusted p-value < 0.10
Outliers	2072	7.11	
Low counts	11155	38.30	mean count < 1